2001

MAGNETIC DATING OF VESUVIAN LAVAS

Tiano, Pasquale

http://hdl.handle.net/10026.1/2045

http://dx.doi.org/10.24382/4154
University of Plymouth

MAGNETIC DATING OF VESUVIAN LAVAS

by

Pasquale Tiano

A thesis submitted to the University of Plymouth
in partial fulfilment for the degree of

DOCTOR OF PHILOSOPHY

Department of Geological Sciences
Faculty of Science

In collaboration with

Dipartimento di Scienze della Terra
Universita' degli Studi di Napoli "Federico II"

( )

August 2001

MAGNETIC DATING OF VESUVIAN LAVAS

Pasquale Tiano

Abstract

A palaeomagnetic study has been carried out on Vesuvian lava flows emplaced since 79 AD. This involved both palaeodirection and palaeointensity investigations of samples from sites on the W, S and SE slopes of the volcano. Thermal demagnetization of 3 component IRMs, susceptibility measurements and coercivity analyses have been carried out on one pilot specimen per site in order to identify the magnetic carriers and to estimate the magnetic grain size. The identification of the primary direction of TRM was carried out following very stringent criteria (Incoronato, 1996). Palaeointensities were evaluated using both a modification of the Modified Thellier & Thellier method (McClelland et al., 1996) and the innovative microwave technique (Shaw et al., 1999). This study has shown that establishing whether or not different exposures or flows are contemporaneous can be established and, in most, but not all, cases can be undertaken successfully using magnetic information recorded by Vesuvian lavas to define the geomagnetic field direction and intensity at the time of their eruption. It is shown that numerous lava flows, outcropping on the W to S slopes of the volcano, must be associated to a large eruption in AD 1631, confirming some previous studies. A new age for a lava flow, ascribed in literature to the 1697 event, is suggested on the basis of both palaeodirection and palaeointensity investigations. Significantly different properties have been found between microwave and thermal experiments although they showed an exceptional level of agreement for the AD 1631 lava flow. In general the trend the palaeointensity variations was similar to that obtained by thermal processes for the last few centuries from other European, Mediterranean and Near East regions (Aitken et al., 1989).

List of Contents

List of Illustrations

List of Tables

Acknowledgements

Author's Declaration

This is to certify that:

At no time during the registration for the degree of Doctor of Philosophy has the author

been registered for any other University award.

This study was financed with the aid of a studentship from the European Community and

carried out in collaboration with the Dipartimento di Scienze della Terra, Universita' degli

Studi di Napoli "Federico II", Italy.

Relevant scientific seminars and conferences were regularly attended at which work was

often presented and some papers prepared for publication.

Presentation and Conferences Attended:

Angelino A., Cacciapuoti S., Incoronato A., Sauna R. & **Tiano P. (1998)** - Indagini di "Palaeo-& Rock -Magnetism" in aree vulcaniche: un esempio di applicazione all'Etna. - *XIV Convegno GNV, Catania 2-4 Marzo, Poster.*

Angelino A., Ferrante A., Incoronato A., **Tiano P,** & Vanacore G. **(1999)** – Southern italian archaeomagnetic record of Mount Arso, Etna and Vesuvius lavas. – *XXIV General Assembly EGS, SE47 Geophysics for Archaeology, 2 Dating for Archaeology. The Haughe, 17,23 Aprile.*

Tiano P., Incoronato A. & Tarling D. H. **(2000)** - Palaeomagnetic study on Vesuvius lava flows. – *VIII Workshop on Geo-Electromagnetism, Maratea (Pz) 12-14 Ottobre.*

Tiano P., Tarling D.H. & Incoronato A. **(2000)** - Palaeointensity determinations on Vesuvius lava flow specimen. – *VIII Workshop on Geo-Electromagnetism, Maratea (Pz) 12-14 Ottobre.*

Tiano P. & Incoronato A. **(2000).-** Determinazione delle paleodirezioni e delle paleointensità del Campo Magnetico Terrestre al Vesuvio da indagini paleomagnetiche condotte su flussi lavici. - *XIX Convegno GNGTS 7-9 Novembre 2000.*

Tiano P., Tarling D.H., Incoronato A. & Taylor, G.K. **(2001)** - Palaeointensity and palaeodirection determinations of the E'sMF from palaeomagnetic study on Vesuvian lava flows. – *EGS XXVI General Assembly, Nice, France, 25-30 March 2001, Poster*

Pasquale Tiano

Date 27 August 2001

Chapter I

INTRODUCTION AND THE EARTH'S MAGNETIC FIELD

1.1 Introduction

Vesuvius is one of the most famous volcanoes in the world because of its dramatic explosive eruption in 79 AD which entirely destroyed the Roman city of Pompeii. Equally important, to a wide range of scientific aspects, are the age and nature of all the effusive events that have occurred during the last few centuries until the 1944 AD eruption, since which the volcano seems to be in a dormant state. In palaeomagnetism, lava flows are highly important as geomagnetic field recorders. Since observed records of geomagnetic directions (Gilbert, 1600) and intensity (Gauss, 1835) go back only a few hundreds years, to obtain information over more remote times it is necessary to look to the record that is contained in rocks, sediments or artefacts.

Generally, it is assumed that when a lava is cooling down it acquires a natural remanent magnetization (NRM) with both direction and intensity reflecting the geomagnetic field that was present at the time of the extrusion. It is also assumed that most of the NRM held in lava is of thermal origin (e.g. Thermo-Remanent Magnetization, TRM), with a relatively small VRM (Viscous Remanent Magnetisation). Although these simple assumptions are the basis of the magnetic recording mechanism in lava, there are still questions as to whether the magnetic field measured in a lava is truly representative of the geomagnetic field at the time of extrusion. Geochemical and geophysical changes can occur during and/or after a lava has been emplaced and such changes could distort or mask the original TRM. One of the purposes of this study is to establish how well historic Vesuvian lava flows can record and retain both palaeodirections and palaeointensities information.

As all laboratory experiments, palaeomagnetic experiments on lavas try to duplicate what really happened in nature, and therefore are, in general, based on thermal mechanisms. One

1

of the major problems is that mineralogical changes due to heating effects can occur during the experiments, particularly as laboratory experiments are normally in an oxidising atmosphere, while the interior of a lava, when emplaced, is commonly in a reducing environment. Monitoring of sensitive parameters, such as susceptibility, and checking on their repeatability during and after the experiments are regularly performed to avoid or identify mineralogical alterations affecting the magnetic minerals. For palaeointensity determination performed with the Thellier-type experiment (Section 3.4a), repeated checks are necessary, but they are very time-consuming which is also a reason for the limited palaeointensity data currently available. However, a new technique based on microwave mechanisms has been developed (Section 3.4b) that should avoid the risk of mineralogical changes and also reduce significantly the duration of experiments since the samples will be subjected to microwave power for no more than 10 sec. Both the Modified Thellier & Thellier (MTT) and the microwave techniques for palaeointensity determinations will be used and compared in the present work.

Lava flows erupted at different time should record different geomagnetic fields and, if the age of the eruption is known, should provide information on long term changes in direction and intensity of the Earth's magnetic field. Although it is known that geomagnetic directions and intensities can re-occur, they are unlikely to be identical at any one time. Therefore, correlation and discriminations between different lava flows can be made even when either the directions or the intensities of the geomagnetic fields are very similar. When a secular variation curve has been established it can be also usefully used as absolute dating tools. All this information about different lava flows can converge in a better understanding of the frequency and nature of eruptive events. This could play an important role in assessing the geo-hazard of a volcanic area such around Vesuvius, considering that about a million of people live around and some actual "on" the volcano.

1.2 The Present geomagnetic field

The magnetic field at every point on the Earth's surface is described (fig. 1.1) by a

vector F, which can be divided in to a horizontal component, H,:

$$H = F \cos I$$

and a vertical component, Z:

$$Z = F \sin I$$

where I is the inclination which varies between +90° and –90°. The inclination is

positive when the vector points downward (unlike Cartesian co-ordinates).
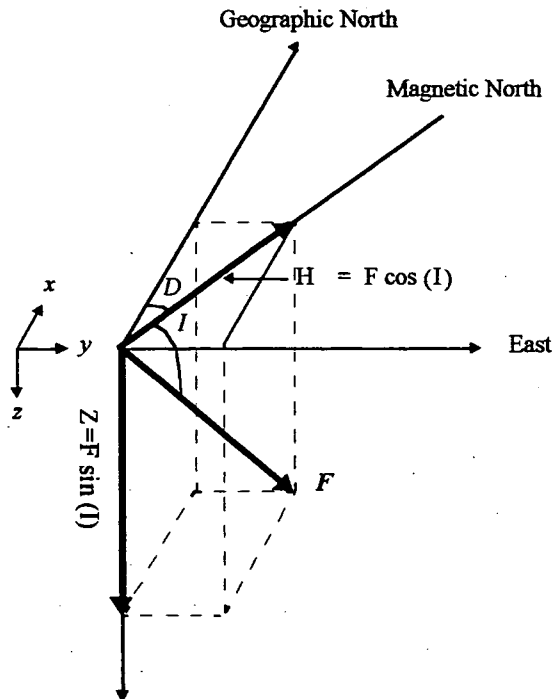
Figure 1.1. Description of the Earth's magnetic field direction.
Declination, D, is the azimuthal angle between the horizontal component ,H, of F and geographic north.
Inclination, I, is the vertical angle between the horizontal and F.

The north component, defined on the x axes, and east component, defined on the y

axes, are the geographic components of the earth magnetic field and are respectively;

$$X = F \cos I \cos D$$

$$Y = F \cos I \sin D$$

where D is declination, the angle from geographic north to the horizontal component, ranging from 0° to 360°, positive clockwise.

For the *geocentric axial dipole* model (GAD), the declination (D) will be 0° at all points on the Earth's surface, while the inclination (I) is related to latitude (λ) by:

$$\tan I = 2 \tan \lambda.$$

In 1832 Gauss applied the techniques of potential theory to a detailed analysis of the Earth's magnetic field. He determined the first four coefficients of the spherical harmonics of the field in which the first-order coefficient described the geocentric dipolar nature of the majority of the field. The present geomagnetic field is obviously more complex than a GAD field, and is better described by an *inclined geocentric dipole* model where the dipole is inclined at ~11.5° to the Earth's rotational axis. The current dipole moment is some 8.75×10^{25} G cm^3 (8.75×10^{22} Am^2). This dipole provides the best-fit that can be achieved using a single dipole model, and can account for 90% of the observed field. At any given time, the direction of the surface geomagnetic field varies spatially. Such variations are described by the higher order terms of the spherical harmonic expansions. Such local complexities in the magnetic field are referred to as the *non-dipole field*, which is calculated by removing the dipole field from the observed geomagnetic field. This non-dipole field change with time and its variation can be substantial even over historical time periods. The field also varies with time in both intensity and direction. Over shorter periods of time, <10 kyr, these changes are termed *secular variations*.

1.3 Geomagnetic Secular Variation

a - Directions

Changes with periods dominantly between 1 and 10^5 years constitute geomagnetic secular variation. Geomagnetic observations during the last few 100 years show that

4

over sub-continental regions, the patterns of the secular variation can be very similar. This is certainly the case for the secular variation patterns observed in London (Fig.1.2), Paris, and south of Italy. From one continent to another, however, the patterns of secular variation can be very different. This observation probably reflects the changes in the size of the non-dipole sources of geomagnetic field within the Earth's core. There is no long-term information about the time changes of this non-dipole field but during the last hundred years it has shown a characteristic change well known as *westward drift*. It is, however, also thought that the non-dipole field contains stationary components and it has been suggested that eastward drift may also occur.

One of the main objectives of palaeomagnetic investigations is to obtain records of such geomagnetic secular variation. In fact most of the information about it during the last 10 ka has been provided by the palaeomagnetism of archaeological artefacts (archaeomagnetism), Holocene volcanic rocks, and postglacial lake sediments.
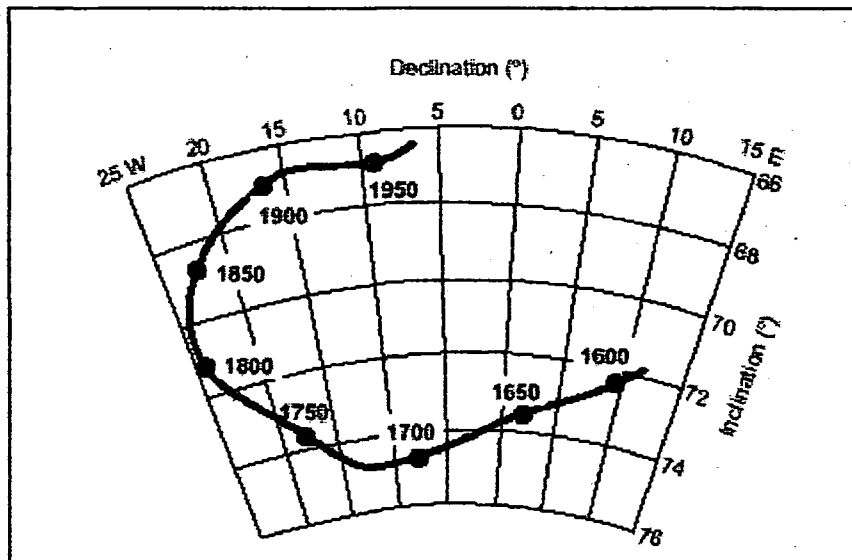
Figure 1.2 Historic records of geomagnetic field direction at Greenwich, England. Redrawn after Malin and Bullard.

5

b - Intensities

The magnitude of the geomagnetic dipole also changes with time (Fig. 1.3) but the available laboratory geomagnetic records span only the last 170 years. As for directional studies, however, records of the ancient field strength can be obtained from archaeological materials and volcanic rocks. For the purpose of comparing such data from sampling sites at different latitudes it is necessary if possible to calculate the equivalent dipole moment for each determination. Such a dipole moment is called a Virtual Dipole Moment (VDM) or Virtual Axial Dipole Moment (VADM). If no knowledge of the magnetic inclination is available then the dipole axis is assumed to be the axis of rotation during historical times. Such studies suggest that oscillations of up to ±50% of the mean value of the dipole moment appear to have occurred during the last 10 ka with a possible period of roughly 10^4 yr.
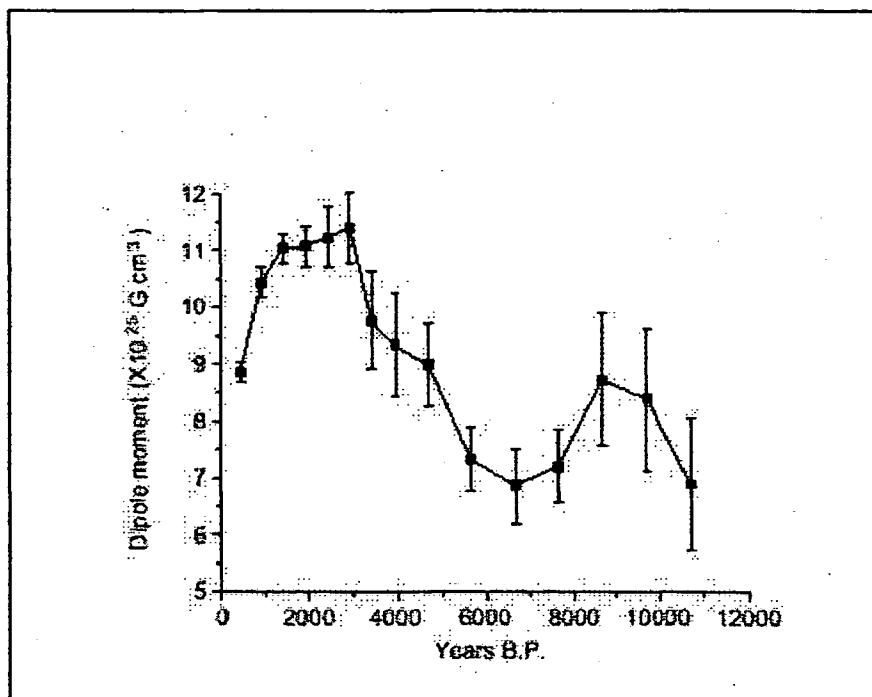
Figure 1.3. Geomagnetic dipole moment over the past 10,000 years.
Error bars are the 95% confidence limits. Redrawn after Merrill and McElhinny (1983).

6

1.4 Thesis Organisation

In **chapter II** the basic magnetic properties of relevant magnetic minerals are described, followed by a brief description of the ways in which rocks acquire their remanence. In **chapter III** all the techniques used in this thesis are described; including methodology and instruments used for palaeodirections, palaeointensities, magneto-mineralogical and grain size investigations. A brief description of the software used for interpreting data and of the main statistical parameters is also given. The geological background of the volcano, with a complete description of the eruptive history from 79 to 1944 AD, is given in **chapter IV**. In **chapters V, VI, VII** all the palaeodirection, palaeointensity and magnetic properties of the lavas are analysed using the techniques described in chapter III. In **chapter VIII** the magnetic properties are also discussed and interpreted. In **chapter IX** all the site and sample results, both palaeodirections and palaeointensities, are combined and discussed at a lava flow level. Results are presented in terms of mean values using the statistical parameters and criteria described in chapter III. All the mean magnetic values obtained from both thermal and microwave experiments are also compared with rock magnetic properties. Finally, a palaeosecular variation curve and a time-dependent curve are presented for palaeodirections and palaeointensities results. The conclusions together with some indications for further work, are given in **chapter X**. A summary of the entire work of the present study is shown in fig. 1.4.

Magnetic Dating of Vesuvian Lavas

8

```
                          ┌─────────────────────────┐
                          │     Work organisation    │
                          └─────────────────────────┘
        ┌────────────────────────────┼────────────────────────────┐
┌───────────────────────────────┐ ┌──────────────┐ ┌──────────────┐
│     Bibliographic search      │ │ Measurements │ │   Results    │
│ Sampling of 420 specimens from│ │              │ │ Conclusions  │
│      21 different sites       │ │              │ │              │
│ Preparation of standard-sized │ │              │ │              │
│          specimens            │ │              │ │              │
│ Preparation of special-sized  │ │              │ │              │
│   specimens (5mm x 3mm)       │ │              │ │              │
└───────────────────────────────┘ └──────────────┘ └──────────────┘
```

| Thermal and magnetic calibration experiment | Magneto-mineralogic investigations | Palaeointensity | Palaeodirections |

- Magneto-mineralogic investigations
  - Irm & Irm 3 axes
  - Susceptibility
  - Grain size
  - Coercivity of remanence
  - KArm/K
- Palaeointensity
  - Modified Thellier&Thellier
  - Microwave
- Palaeodirections
  - Progressive Thermal Demagnetization

Fig.1.4 Thesis' work organisation

Chapter II

BASIC MAGNETIC PROPERTIES

2.1 Introduction

In this chapter the basic magnetic properties of relevant magnetic minerals are described, followed by a brief description of the ways in which rocks acquire their remanence. More detailed discussions, based on these general comments, are given when interpreting the results (Chapter 8).

2.2 The Main Magnetic Minerals

The magnetic carriers of rocks are mainly iron and titanium oxides such as magnetite, titanomagnetite, haematite and maghaemite. Although these oxides make up only a few percent of the volume of rocks the rock magnetic properties largely depend on them. Iron sulphides or manganese oxides may also become important when oxides of iron and titanium are unusually scarce. The weak paramagnetism of silicate or hydroxide minerals containing Fe^{2+} and Fe^{3+} ions is generally swamped by the stronger magnetism of the less abundant iron oxides.

2.2.a - Iron and Titanium oxides

The most important ferrimagnetic minerals are iron (Fe) and titanium (Ti). These minerals are usually plotted using a ternary diagram $TiO_2 - FeO - Fe_2O_3$ (Fig. 2.1). Moving from the left to the right the amount of ferric iron (Fe^{3+}) increases compared to the ferrous one (Fe^{2+}) (or non-magnetic ions), while moving from the bottom to the top the increasing amount of titanium (Ti) can be seen.

9
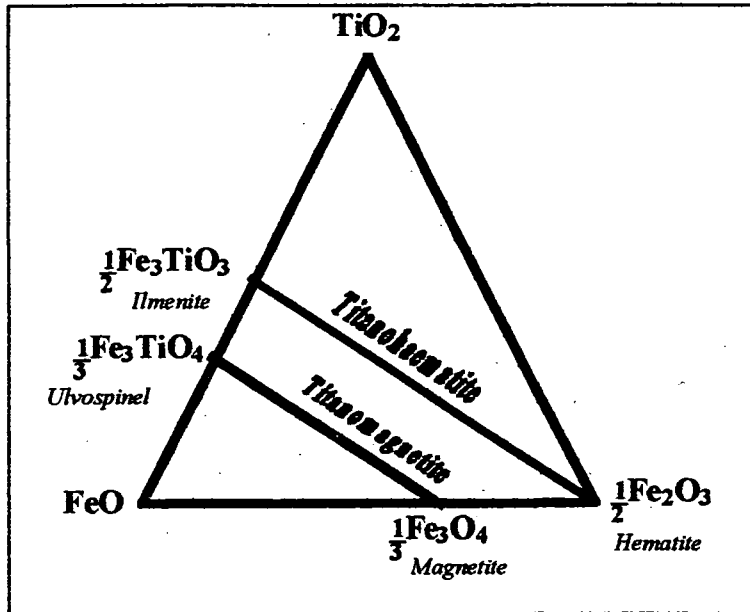
Fig 2.1 Fe and Ti oxides plotted on the ternary diagram $TiO_2 - FeO - 1/2Fe_2O_3$

i) *Titanomagnetites*

The titanomagnetites are opaque, cubic minerals with compositions between end members magnetite (Fe_3O_4) and ulvospinel (Fe_2TiO_4). The crystal structure of titanomagnetites is the spinel structure. The spinel crystal structure produces a preferred direction of magnetization (= magnetocrystalline easy direction) along the cube diagonal [111]. The resulting saturation magnetization of magnetite is 4.8×10^5 A/m, and the Curie temperature is 580°C. In the titanomagnetite series, Ti^{4+} substitutes for Fe^{3+} as Ti content increases. The generalized chemical formula for titanomagnetite is $Fe_{3-x}Ti_xO_4$, where x ranges from 0.0 for magnetite to 1.0 for ulvospinel. The ionic substitution is $2Fe_{3+} \rightarrow Fe_{2+} + Ti_{4+}$, indicating that a remaining Fe cation must change valence from Fe_{3+} to Fe_{2+} for each Ti_{4+} introduced. The convenient approximation that Fe_{2+} and Fe_{3+} are equally distributed between the sublattices can be used for rapidly cooled titanomagnetites. This gives a linear dependence of saturation magnetization upon the composition. So the addition of Ti_{4+} into the magnetite structure

10

progressively decreases saturation magnetization M_S. Equally important is the observed dependence of Curie temperature, T_C, upon Ti content. Both T_C and M_S are functions of the titanomagnetite compositional parameter, x. Any titanomagnetite with x > 0.8 will be paramagnetic at room temperature or above.

MAGNETITE (Fe_3O_4)

Magnetite is a very common magnetic mineral. It is found in the vast majority of igneous rocks and many metamorphic and sedimentary rocks. It has the cubic inverse spinel structure and is ferrimagnetic (Néel 1948). The magnetite Curie temperature of 580°C corresponds to a transition from ferrimagnetic ordering to disorder. At low temperatures, near -155°C, magnetite undergoes another magnetic transition (Verwey & Haayman 1941) involving a decrease in crystallographic symmetry and an associated change in electrical conductivity.

ii) *Titanohaematites*

In most basic igneous rocks, titanohaematites and their oxidation products constitute a lesser portion of ferro-magnetic minerals than do titanomagnetites. Haematite can be, however the dominant ferromagnetic mineral especially for highly silicic and highly oxidized igneous rocks. The titanohaematites are generally opaque minerals with a magnetic structure most easily described by using the hexagonal system. Ionic substitution in the titanohaematite series is exactly as in titanomagnetites, with Ti^{4+} substituting for Fe^{3+} and one remaining Fe cation, changing the valence from Fe^{3+} to Fe^{2+}. The generalized formula is $Fe_{2-x}Ti_xO_3$, where x ranges from 0.0 for haematite to 1.0 for ilmenite. The "Curie" temperature has a simple linear dependence on composition, but saturation magnetization can vary in a complex fashion.

HAEMATITE (αFe_2O_3)

Haematite is a significant magnetic mineral in oxidised igneous rocks and sediments formed in oxidising conditions. When present as fine grains haematite has a distinctive blood-red colour. For pure haematite all cations are Fe^{3+} and occur in layers alternating with layers of O^{2-} anions. The net magnetization lies in the basal plane nearly perpendicular to magnetic moments of the Fe^{3+} layers. Haematite is referred to as a canted antiferromagnetic and has a saturation magnetization of $\sim 2 \times 10^3$ A/m. It is also very strongly anisotropic, with an easy direction within its basal plane and is very difficult to magnetize along its c axis. Some naturally occurring haematite has additional magnetization referred to as defect ferromagnetism, probably due to lattice defects or nonmagnetic impurity cations. These two contributions to net magnetization give haematite a weak ferromagnetism with M_S of about 2-3 $\times 10^3$ A/m. The temperature at which exchange coupling within the haematite disappears, the Néel temperature, is 680°C.

iii) *Exsolution*

Titanomagnetites and titanohaematites start to crystallize at ~1300°C and solid solution of both is complete at high temperatures. Although all compositions are possible at high temperature, compositional gaps develop at lower temperatures (Fig. 2.2). Intermediate compositions normally exsolve into Ti-rich regions and Ti-poor regions by solid state diffusion of Fe and Ti cations. Titanomagnetites unmix at fairly low temperature (~600°C), hence exsolution is slow and is generally observed only in slowly cooled plutonic rocks. In the titanohaematite series compositional gaps develop at higher temperatures, hence exsolution is more rapid.
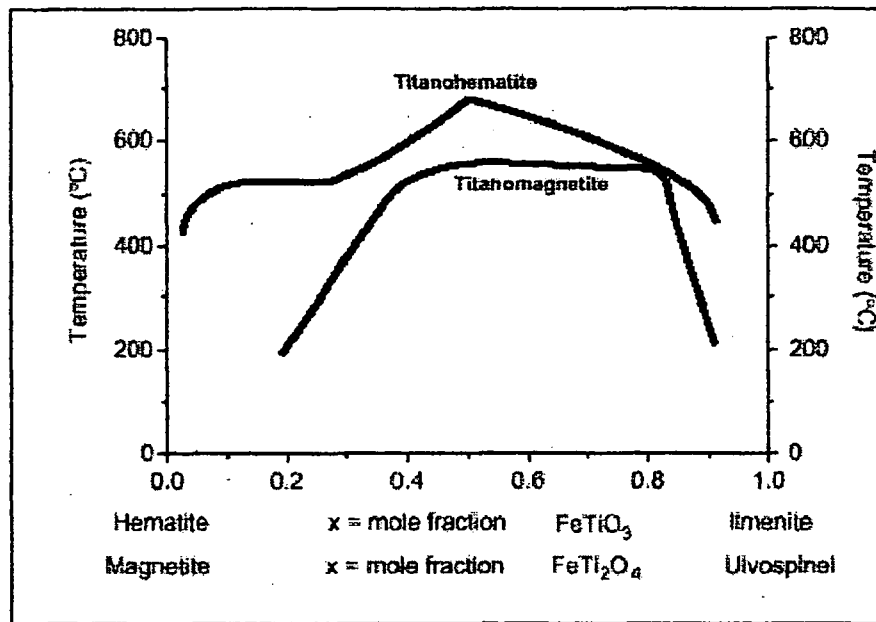
Fig.2.2: - Compositional gaps for titanohaematite and titanomagnetite. Nagata (1961)

Exsolution is very important for altering magnetic properties such as M_S and T_c, and for increasing or decreasing effective grain size. In fact by exsolution, a large homogeneous grain can be transformed into a composite grain of much smaller Ti-poor (Fe-rich) regions and complementary Ti-rich (Fe-poor) regions.

iv) *Low-temperature oxidation*

Weathering of titanomagnetites at ambient surface temperatures, or hydrothermal alteration at T < 200°C, can cause the production of cation deficient spinels. Maghemite (γFe_2O_3) is the classic example of oxidation of magnetite. Its saturation magnetization is 4.2 $\times 10^5$ A/m and it is usually physically metastable and irreversibly changes to a hexagonal crystal structure (αFe_2O_3) on heating to 300°–500°C. Similar low-temperature oxidation of titanomagnetites produces cation-deficient titanomaghemites.

2.2.b - Iron sulphides

PYRRHOTITE (FeS)

The most magnetic of iron sulphides, the next most important magnetic mineral after the iron oxides, is pyrrhotite. It is ferrimagnetic with a monoclinic structure. The majority of natural pyrrhotites have compositions within the range Fe_7S_8 to Fe_9S_{10}. The former has a Curie temperature of 320°C while the latter has a slightly lower Curie temperature of 290°C. Addition of impurities, such as nickel, into the pyrrhotite lattice causes the Curie temperature to be further lowered. In absence of stronger magnetic minerals, pyrrhotite can carry a useful palaeomagnetic record of the ancient geomagnetic field in some igneous rocks and sediments. It also has a high susceptibility (Clark, 1984).

2.2.c - *Iron hydroxides*

GOETHITE (αFeOOH)

Goethite has an orthorhombic structure. It is a very common mineral, particularly as a weathering product. Although most goethites are antiferromagnetic, because of uncompensated spins produced by oxygen ion vacancies, some are weakly magnetic, with a Néel temperature of 120°C. They can acquire a thermoremanent magnetisation of low intensity but very high coercivity on cooling through its Néel temperature. It is chemically unstable and is generally destroyed at about 120°C.

2.3 - Magnetic domains and hysteresis loop

Many of the simple magnetic properties can be described and better understood in terms of hysteresis loops (Fig. 2.3). These describe the field dependence of magnetization plotting the magnetization M on the vertical axis against magnetic field H on the horizontal axis. Saturation magnetization, M_S, is the magnetization induced in the presence of a large (> 1 T) magnetic field. The saturation remanent magnetization, M_{RS} is the remaining magnetization when the field is removed. By the application of a field, in the opposite direction to that first

used, the induced magnetization can be reduced to zero. The reverse field which makes the magnetization zero is called the coercivity -Hc. If this reverse field is reduced to zero at this stage, then there would still be a positive magnetization.
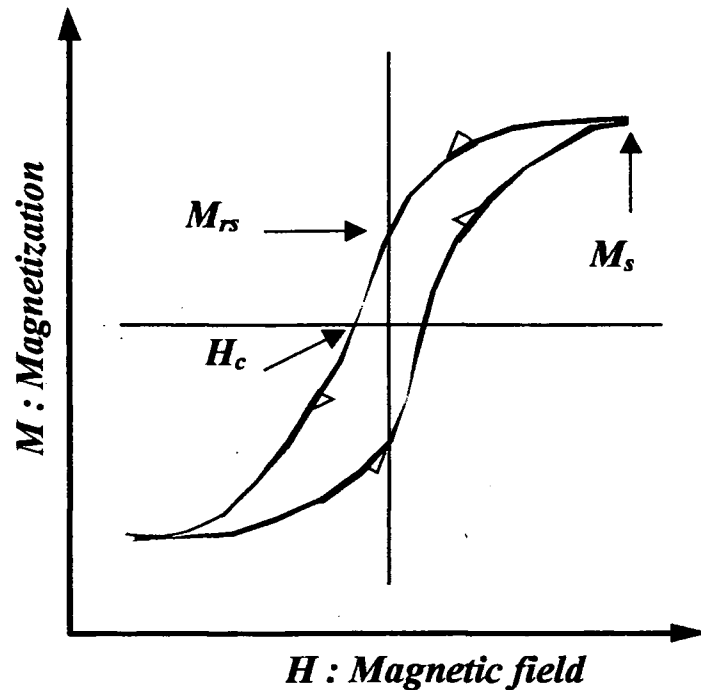
Fig.2.3 : Magnetic hysteresis loop.
Ms = saturation magnetization: Mrs = saturation remanence: Hc = coercivity force

This happen because the zero magnetization at -Hc consists of two components which cancel; an in-field negative magnetization and a remanent positive magnetization In order to effectively reduce the remanent magnetization to zero, after the subsequent withdrawal of the -Hc, the hysteresis loop must reach a larger reverse field. This reverse field is called the coercivity of remanence, -H$_{CR}$. The gradient of the initial magnetization curve (low field reversible changes) is the initial susceptibility, K. A complete hysteresis loop is obtained by cycling the magnetic field from an extreme applied field in one direction to an extreme in the opposite direction and back again.

2.3a - Domains and domain walls

The hysteresis properties of ferromagnets are largely related to the arrangements of magnetic domains. The material can be split up into many regions, called domains, (Weiss, 1907), each spontaneously magnetized in one direction. These domains can be magnetized in different directions so that the sum of each domain magnetization can be zero. The magnetic domains are separated by zones of finite thickness known as domain or Bloch walls (Bloch, 1930). The formation of magnetic domains produces a state of low total energy, establishing a balance between various competing energies.

2.3b - Single-domain (SD) behaviour

The shape of the loop of an individual single-domain grain depends on the orientation of the grain with respect to the applied field. A single-domain grain with its easy magnetization direction (long axis) parallel to the applied field will give a rectangular shape. In this case the magnetization simply flips through 180° when applying a coercive force. When the easy magnetization direction is perpendicular to the applied field the hysteresis loop has three linear segments that pass trough zero. On application of a field the magnetization turns towards the field direction, but it returns to its original 'easy' axis direction perpendicular to the field direction on removal of the field. Obviously things in nature are not so schematic. Most natural samples contain assemblages of single-domain grains that have random orientations of their easy axes. The net hysteresis loop hence, will result from the answer of such random assemblages.

2.3c - Multi-domain (MD) behaviour

The main effect of the application of an external field to a large multidomain grain is the movement of domain walls that will produce the growth of domains with a magnetization component in the direction of the applied field. On removal of the external field the boundary walls may be blocked as they return towards their initial locations at local minimum energy. In this way a multidomain grain can retain a remanent magnetization. When these

domain wall movements are irreversible, a sufficiently strong field is needed to jumps out of the local "traps". This phenomenon is known as Barkhausen jumps. A multidomain grain is completely saturated when all the domain magnetizations are aligned in the applied field direction. The magnetic remanence of multi-domain grain assemblages is much lower and less stable than that of single-domain grain assemblages.

2.3d -Pseudo-single-domain (PSD) behaviour

The grains that behave in this way play an important role in understanding magnetization of rocks containing magnetite or titanomagnetite. These grains cover an interval between large SD grains and small multi-domains grains and show intermediate Mr/Ms and intermediate Hc. The PSD grain-size interval for magnetite is approximately 1–10 μm. Grains in this size range contain a small number of domains and can have substantial magnetic moment. They can also exhibit significant coercivity and time stability of remanent magnetism.

2.3e -Magnetic relaxation

It describes how the remanent magnetization of an assemblage of SD grains decays with time. It is defined by

$$M_r(t) = M_{ro} \exp(-t/\tau)$$

where M_{ro} is the initial remanent magnetization; t, the time and τ the *characteristic relaxation time*. The latter is defined by

$$\tau = \frac{1}{C} \exp\left(\frac{v h_c M_s}{2kT}\right)$$

or more simply

$$\log \tau \propto \frac{v}{T}$$

17

where v is the volume of the grain and T the absolute temperature. Therefore, single domain particles, on cooling, show a logarithmic increase in its relaxation time as it cools from a temperature at or below its Curie temperature. The relationship between temperature, volume and relaxation time for the case of a magnetic remanence acquired by cooling in a magnetic field over temperature ranges below the Curie point (*thermoremanent magnetization*) is clearly described by the graph in fig. 2.4. The temperature at which the remanence, acquired during cooling in a magnetic field, becomes blocked within it for the duration of the experiment, is called *blocking temperature*, Tb (or *unblocking temperature*, Tub when, heating up, the remanence is lost). The Tb of any individual domain depends, hence, on its size and composition and also on the strengths and duration of the magnetic field.
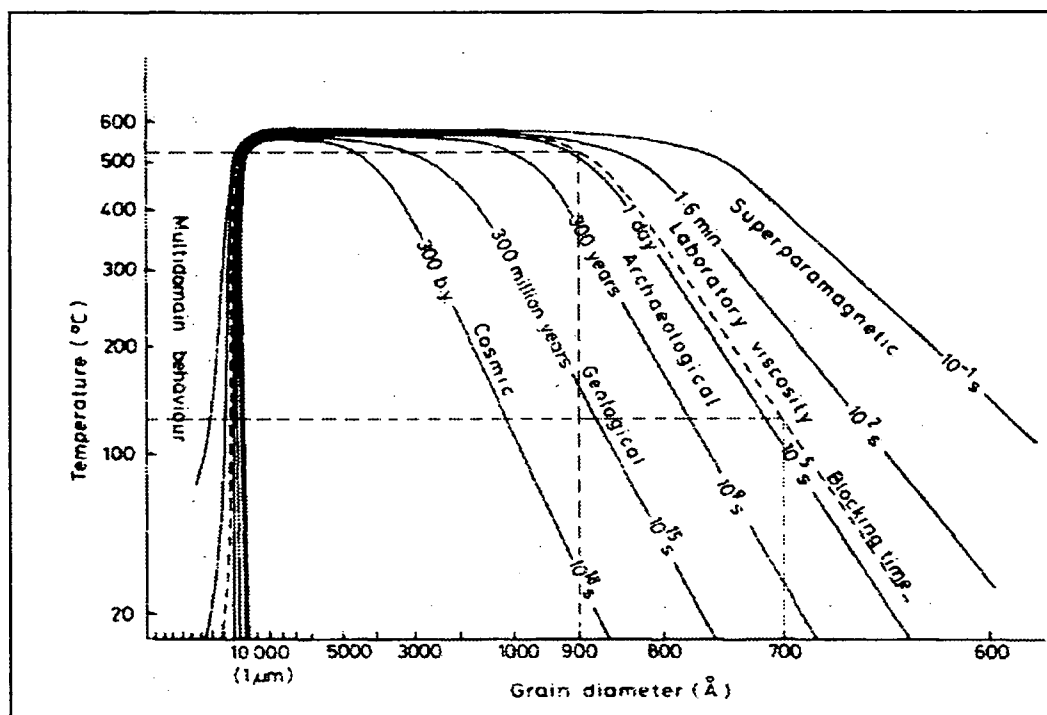
Fig.2.4 General behaviour of a single domain grain of titanomagnetite in relation with temperature, volume and relaxation time.
Note that the Tb of a larger SD grain (900 Å) is much higher than a smaller one (700 Å) (dashed line). Redrawn after Tarling, 1983

2.4 - Acquisition of Magnetization

The magnetization acquired at the time of rock formation should be ideally the same, in terms of directions, as the prevailing geomagnetic field acting at that time. Its intensity is also directly proportional to the strength of the field. Such magnetization is the *primary component of magnetization* and in igneous rocks, is generally a *thermal remanent magnetization (TRM)*. The magnetic minerals acquire this magnetization when they cool below their characteristic Curie temperatures. In sedimentary rocks the main process of acquisition is the *detrital remanent magnetization (DRM)* and it can be *depositional* or *post-depositional*. In the last case it is the result of the aligning force of the magnetic field on a magnetic grain at the sediment-water interface. Another type of remanence acquisition, most common in sediments, is the *chemical remanent magnetization (CRM)*.

In some case a magnetization may not have been acquired at the time of rock formation. In fact, it is very common that a rock contains *secondary components of magnetization*. These are acquired by partial remagnetization after formation of the rock due to heating, lightning strikes, fluid or chemical alteration, or by influence of the geomagnetic field in a different direction to that of the primary magnetization. For this reason most rocks are referred to as *multi-components*. Whereby, they carry a primary component and a mix of secondary components. The resulting total magnetization is called *natural remanent magnetization (NRM)*. The identification of all the components constituting the NRM is not always possible and in many cases the primary magnetization cannot be recovered. Furthermore, the common characteristic magnetic direction recovered from the majority of samples in a rock, the *characteristic remanent magnetization (ChRM)*, may not necessarily represent the primary magnetization because it is possible that a rock will be completely remagnetized with no trace of its original primary magnetization remaining.

2.5 - Thermal remanent magnetization (TRM)

TRM is the form of remanent magnetism acquired by most igneous rocks. As described in section 2.2e, magnetic moments of ferromagnetic grains will be stable to time decay at or below the respective blocking temperatures. As temperature decreases through Tb of an individual SD grain, that grain has a dramatic increase in relaxation time, t, and changes behaviour from superparamagnetic to stable single domain. The total TRM can be broken into portions acquired within windows of blocking temperatures from Tc = 580°C down to 20°C. These portions of TRM, referred to as "partial TRM," (pTRM), are related to the TRM by the law of additivity of **pTRM**;

$$TRM = \sum_{n}^{1} TRM(Tbn)$$

The law describes that individual pTRMs depend only on the magnetic field during cooling through their respective Tb intervals. This is fundamental for the application of the thermal demagnetization technique. In fact it is based on the ability to remove components of magnetization held by grains with low Tb while leaving the higher Tb grains unaffected.

It is important to remember that the model of TRM acquisition considers only single-domain grains and, unfortunately, only a small percentage of grains in a typical igneous rock are truly SD. Most grains are PSD or MD. It has been noticed that efficiency of TRM acquisition drops off dramatically in the PSD grain-size range from 1 μm to about 10 μm while it seems that for grains of d>10 μm, the acquisition of TRM is inefficient. However, PSD grains do acquire TRM that can be stable against time decay and against demagnetization by later magnetic fields, SD and PSD grains are the effective carriers of TRM, while larger MD grains are likely to carry a component of magnetization acquired long after original cooling. However, it has been observed that rapidly cooled volcanic rocks generally have grain-size distributions peaking at d<10 μm, with a major portion of

the distribution within SD and PSD ranges. Thus, volcanic rocks are commonly observed to possess fairly strong and stable TRM and minimal secondary components of magnetization carried by MD grains.

2.5 - Thermal demagnetization

A specimen can be demagnetized by heating to progressively higher temperatures and cooling in zero magnetic field between measurement steps. All grains with unblocking temperatures below the maximum applied temperature at each demagnetization step will have their contribution to the specimen NRM removed. This technique of demagnetization, usually referred to as *progressive thermal demagnetization* (PTD), is the main one used for the present work and its modality will be more fully described in the section 3.3.

Chapter III

INSTRUMENTS, TECHNIQUES AND STATISTICS

3.1 Introduction

In this chapter, all the techniques used in this thesis are described; methodology and instruments used for palaeodirection and palaeointensity determination and for magneto-mineralogical and grain size investigations. It is also given a brief description of the software used for interpreting data and of the main statistic parameters used. Most experiments were carried out at the Laboratory of Palaeomagnetism of the Plymouth University. In addition some other equipment was used at the Laboratorio di Palaeomagnetismo e Magnetismo delle Rocce of the University of Naples "Federico II" and at the Laboratory of Geomagnetism of the Liverpool University. In all laboratories, the remanences were measured with a Molspin Minispin with similar noise-levels of about 0.03mA/m, with the exception of the microwave palaeointensities (section 3.4b).

3.2 Thermal and magnetic calibration experiment

The MMTD1 is a sophisticated programmable thermal demagnetiser that can heat and cool palaeomagnetic samples fully automatically. To apply correctly the PTD (section 3.3a) and the Thellier's method (section 3.4a), a long and meticulous thermal calibration to check the temperature inside the oven has been required to establish the internal properties of the equipment. Nine pilot samples were used and were subjected to heating and cooling cycles from room temperature up to 500° C, on steps of 50 and from 500° C up to 700°C on steps of 20. To determine the correct temperature for each position inside the oven and for every step of measurements, high-temperature thermo-couples in silicon oil, were put inside holes drilled into each specimen and connected to voltmeters outside the oven. The output values, in mV, were converted to °C using a conversion table obtained from experimental values (Fig. 3.1). The 9 specimens were placed in the

oven always in the same place with a thermocouple in alternate specimens, starting at specimen 1. Once the oven had reached its set temperature, the voltages indicated by the voltmeters were recorded every 2 minutes until it stabilised (Fig. 3.2).
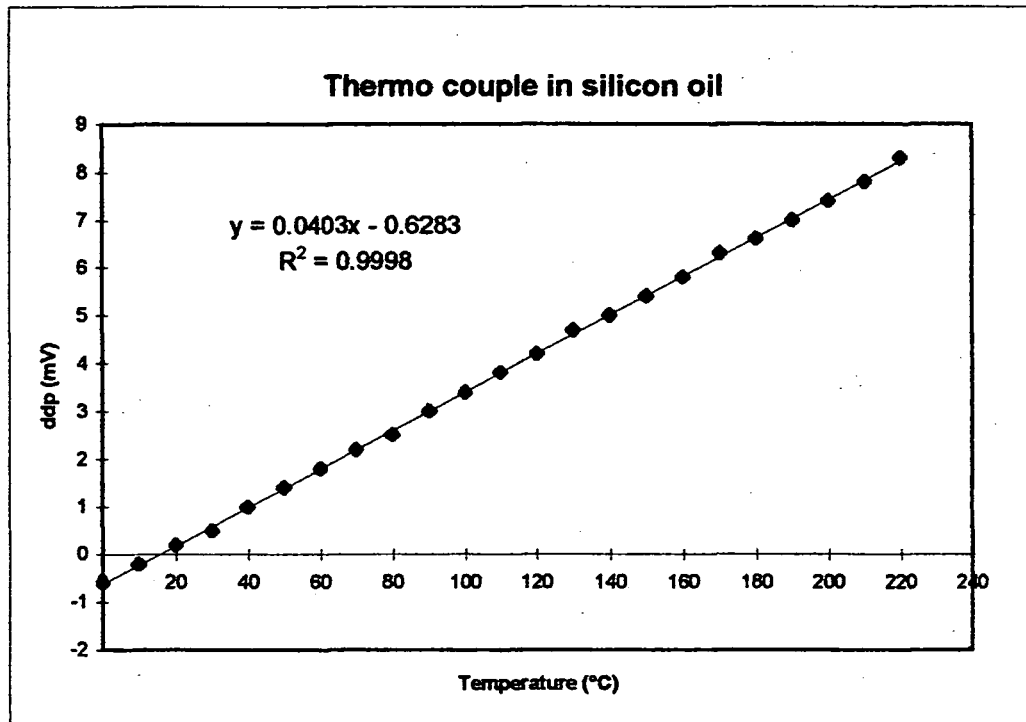
Fig. 3.1 Experimental linear relation between the potential difference (ddp) and the temperature. At higher temperatures values were extrapolated using the same gradient.
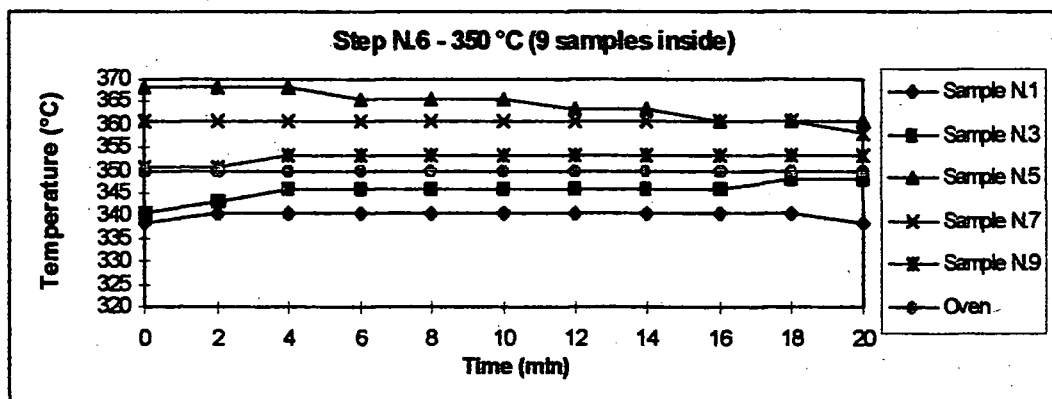
Fig. 3.2 Example of recorded data while the oven set temperature was kept for 20 minutes.

The result of this experiment was that, up to 250°C, the specimens reached slowly the temperature set for the oven (Fig.3.3a) but at the end of the process, the heating chamber failed to reach the set temperature by some 5-8°C especially for the more external

specimens. The results obtained between 300 and 500°C were completely different. In fact in this range the specimens nearest the door opening (1,3) gave always the lower values while those in the middle (5,7) gave values higher then the set temperature. The far specimen (9) gave the closest value to the set temperature. In general, the heating chamber failed to reach or overstepped the set temperature by ~10°C (Fig.3.3b). Over 500°C, all the specimens gave a higher value of about 25°C (Fig.3.3c) and the middle position (5) seemed to be the closest to the set value. While these results indicate that the heating chamber may be failing to uniformly reach the set temperature, the problem of heat affecting the resistance of the wires connecting the thermocouple to the voltmeter is unquantified as also how well the wires were connected to the specimens. In addition, each specimen had a different mineralogy and magnetic properties and therefore they could be heated to the same temperature yet give different results. This experiment suggested that some consideration must be made when interpreting specimen magnetization/demagnetization temperatures. The strength of the field that could be applied during cooling was also tested. Two terminals, on the front panel of MMTD1, were connected to a long close-wound solenoid. Passing a constant current through the solenoid via the terminals creates a uniform constant magnetic field inside the oven. The calibration factor for the oven, 0.44 μT/mA, was tested along with the uniformity of a 50μT field inside the oven at room temperature.

a)

24
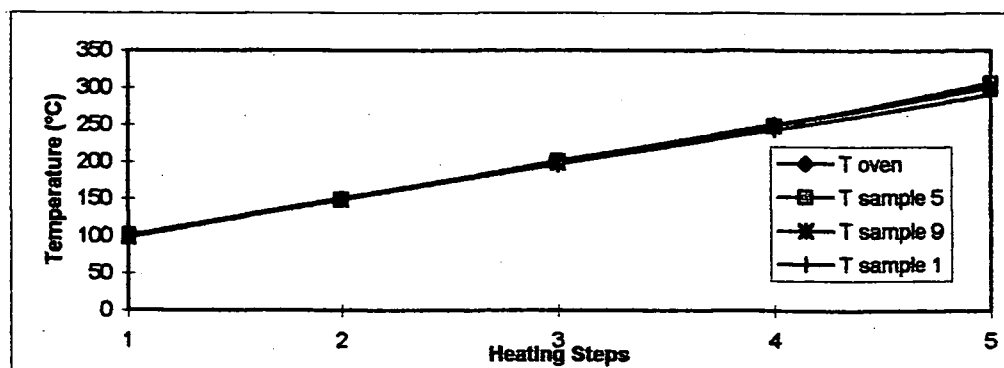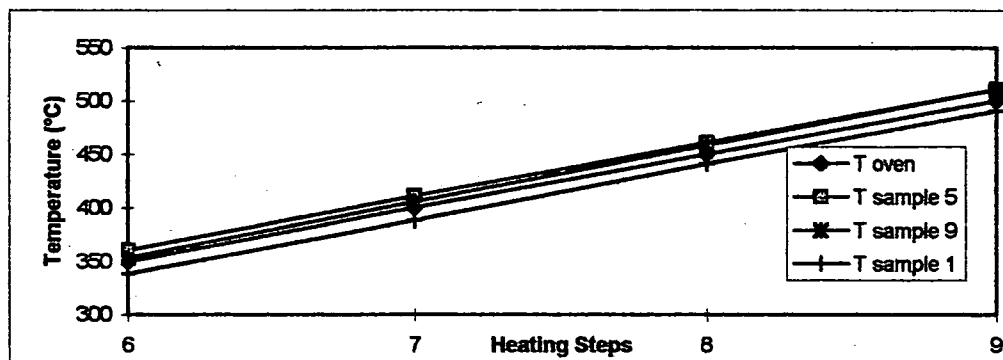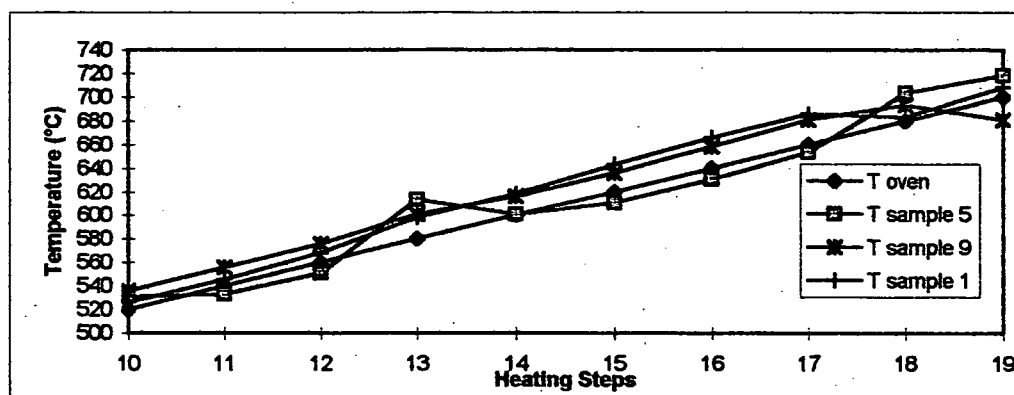
Fig. 3.3 Behaviour at different temperature range at the internal, middle and external position.
a) 100-250°C; b) 300-500°C; c) 520-700°

3.3 Palaeodirections

a - Progressive Thermal Demagnetization (PTD)

The procedure for PTD involves cycles of heating specimens, up to a certain temperature (T_{demag}), and cooling down to room temperature in zero magnetic field. This causes all grains with blocking temperature (T_B) $\leq T_{demag}$ to acquire a random "thermoremanent magnetization" in F = 0, thereby erasing the NRM carried by these grains. In other words, for each step of temperature, the magnetization of all grains for which (T_B) $\leq T_{demag}$ is randomized.

The PTD were carried out using a Schonstedt thermal demagnetizer (which is not automatic as was the MTTD1) but allows work to be done with two set of specimens at the same time. For this experiment, sets of 6 specimens were used and subjected to a complete demagnetization starting from 100°C. Steps of 50° were used up to 300°, then 30° until 500° and finally 15° until the NRM was considered negligible. Dealing with Vesuvian lava flows specimens (commonly characterized by titano-magnetite carrier), smaller steps at higher temperature were chosen to get more detailed information when approaching the Curie temperature of the constituent ferromagnetic minerals.

3.4 Palaeointesities

The original Thellier (1937,38) method of palaeointensity estimation depended on comparison of thermal demagnetization characteristics of the natural remanence and a laboratory-imposed TRM. If the NRM was of thermoremanent origin, the NRM and TRM demagnetization curves should be the same shape, scaled in proportion to the geomagnetic field in which they were acquired. Acceptance of results was reliant on internal consistency because the method allowed no checks on alteration during heating. This is a major uncertainty in this type of method and the original method was therefore superseded by an incremental method of demagnetizing NRM and imposing partial TRMs (pTRMs) at increasing temperatures (Thellier and Thellier, 1959). This allowed the determination of palaeointensity from low temperature measurements before the onset of alteration. The ratio of NRM lost to pTRM gained is then the estimated relative strength of the ancient and laboratory fields. Once magnetic alteration began, the experiment was abandoned. Thellier and Thellier (1959) and subsequently, others (Briden, 1966; Coe, 1967) developed repeat measurements at lower temperatures (pTRM checks) to identify the onset of alteration. These further developments of Thellier and Thellier (1959)

method are commonly referred in the literature as the modified Thellier- Thellier methods (MTT).

Limitations imposed by multidomain grains

An important aspect to consider for paleointensity studies is linked to the behaviour of multidomain grains. These are very common in most lavas and may have important consequences. Multidomain grains do not necessarily obey the experimental law of additivity of partial TRMs such as acquired in non-overlapping temperature intervals by SD grains. A direct consequence is the common existence of two different slopes (or a concave shape) in the NRM-TRM plots between low and high temperatures. Such behaviour is commonly ascribed to the difference between the blocking (Tb) and the unblocking (Tub) temperatures of MD grains.

In theory the presence of multidomain grains should be detected by examining the thermal demagnetisation of the NRM. If a TRM is given first by heating to temperature, Ti, the magnetization will not be removed completely by subsequent re-heating at the same temperature if it is carried by MD grains. A direct consequence is that the NRM derived from these two successive heatings will be affected and biased towards the direction of the applied field.

a - The Modified Thellier & Thellier (MTT)

Taking in account the limitations discussed above, the follow experimental procedure has been applied:

1. Thermal demagnetisation to temperature Tj (*DEMAG 1*).

2. Re-magnetisation from Tj to room temperature in a 50 μT field to add a pTRM (*pTRM*).

3. A second thermal de-magnetisation again at Tj, to check for MD remanence or CRM remanence growth, comparing the NRM intensity and direction with those obtained after DEMAG1 (*DEMAG 2*).

4. PTRM check by repetition of operation (2) at the previous temperature step Tj-1 to check for alteration with blocking temperature (Tb) below Tj-1. (*pTRMck*).

To allow a further check on the NRM behaviour, the temperature steps used were the same as in PTD with the only difference that DEMAG2 and pTRMck started at 150°C instead of 100°C.

b - The Microwave method

Using microwaves instead of the conventional thermal demagnetisation, the first steps of heating are bypassed. Magnons, which are spin waves created by the exchange of energy between phonons (lattice vibrations) and the surrounding system (Walton et al. 1992, 1993) are directly excited with the use of high-frequency microwaves. This should, in theory, eliminate the need to heat the bulk sample. However, some heating does occur due to the generation of phonons. Since the alteration is both time and temperature dependent (Tanguy 1975; Walton 1988), the alteration obtained during the microwave application can be considered negligible, taking in to account that each microwave application is only for 10 sec.

An automated 8.2 GHz frequency microwave source and SQUID magnetometer system (Fig. 3.4) has been developed at the Geomagnetism Laboratory of Liverpool University. This microwave system can be used to carry out a Thellier type experiment, although the physical processes involved are very different. The microwave power is applied in incremental steps (up to a maximum of around 200 W) for no more then 10 sec on samples sized 5mm by 3 mm. A forward power meter controls the amount of power

28

Pneumatic control

Pneumatic Sample Movement

Waveguide

Klystron

Sample

Microwave cavity

TWT Amplifier

SQUID Magnetometer

8 GHz Signal generator

Measure position

Mu-metal shield

Computer
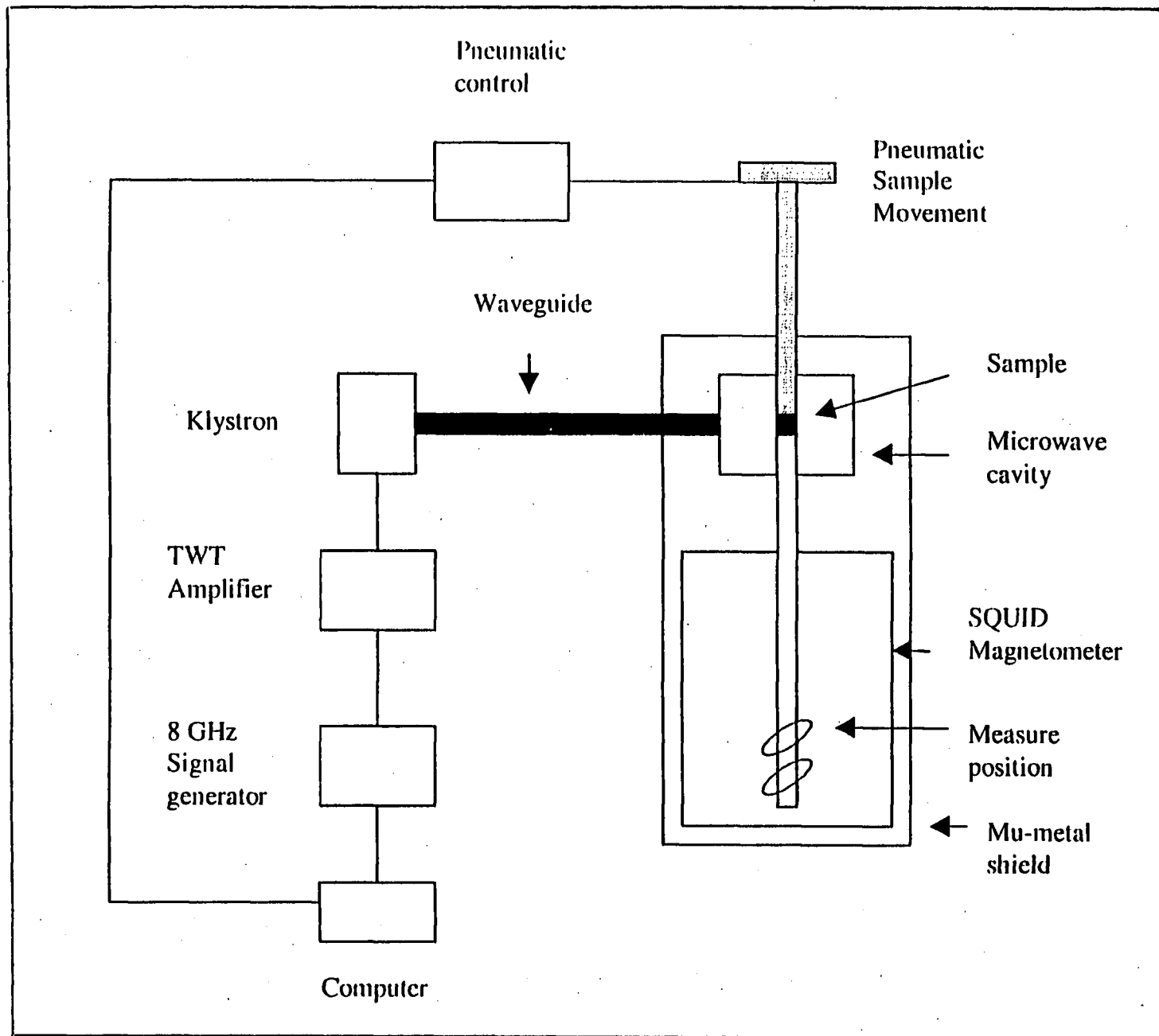
Fig. 3.4 Schematic diagram of the microwave and SQUID magnetometer system.

29

to be used. It is also necessary to measure and minimise the amount of power reflected back. The power is inputted using an increasing percentage of the maximum power available within the selected range. It is important to underline that there is no set power range to be used. Each sample is different and the effectivity of the method also strongly depends on its size and position of the sample within the microwave cavity. In general it is best to start with low powers and to perform some very small demagnetizing steps to get a stable NRM. Once this state has been established, microwaves can then be applied perpendicular (in the xy plane)to the stable NRM direction. The resulting vector intensity should not change drastically while the directions should show a gradually change. In particular the declination should change to 90° greater than its original value while the inclination should reduce to zero. Monitoring the evolution of the declination is therefore required to establish that equal demagnetisation steps had been applied throughout the experiment.

3.5 Magneto-mineralogical investigations

Magnetic mineralogy was investigated both observing the behaviour of specimens during demagnetization, which also involved monitoring of the bulk susceptibility, and by conducting rock magnetic experiments, in particular IRMs.

a - Bulk Susceptibility (K)

Low field susceptibility is a measure of how easy a material can be magnetised. Any change in susceptibility implies a change in magnetic properties. On this basis measurement of K during experiments were regularly carried out as a first order monitor of changes in mineralogy and to check the beginning of alterations in the magnetic mineralogy. For the present work, K was measured at the end of each step of the PTD and MTT experiments, and also during all the experiments to examine magneto-

mineralogical and grain-size information. The equipment used was the Agico Kappabridge KLY3.

b - 3 axes IRM (Lowrie experiment)

The analysis of the acquisition of isothermal remanent magnetisation (IRM) is a useful but ambiguous diagnostic technique when used on its own. For more conclusive interpretations, IRM acquisition can be combined with subsequent thermal demagnetisation of the IRM (Lowrie, 1990). In this method, different coercivity fractions of IRM were re-magnetized in successively smaller fields along three orthogonal directions. In these studies, 800mT was applied along the x-axis, referred to as "*hard*", 300mT along y-axis, "*medium*" and 50mT along z-axis, "*soft*". A larger field is desirable for this technique (ideally >2 T), but 800 mT is the maximum field that can be applied in the Plymouth laboratory and is considered adequate for samples in which haematite is not a major component. The remaining intensities of each orthogonal component, after successive thermal demagnetizations, were then plotted separately. Low-field susceptibility was also measure for every step of temperature.

The aim of a three-component IRM is to determine the dominant coercivity fraction by comparing the hard, medium and soft, and also assess what is the predominant magnetic carrier. For example, an intermediate value of 300 mT can be used to discriminate between magnetite and pyrrhotite; pyrrhotite has a maximum coercivity of 500-1000 mT, and is therefore less likely to saturate in a 300 mT field. The 50 mT field was the last applied and can be used to identify, for example, low coercivity multi-domain magnetite.

3.6 Grain size investigations

a - Coercivity of remanence (Hcr)

In this experiment, an unmagnetized specimen was firstly subjected to a stepwise IRM along its z-axes, which magnetized it in progressive fields up to 800 mT. On removal of

the specimen from each applied field, its remaining remanence was measured. Then the specimen was placed in reversed fields. (In practise, the IRM was applied along the negative z-axes) Increasing field strengths were then applied, with the new remanence measured after each increment. The reverse field, H_{CR}, required to reduce the saturation to zero remanence was found from inspection of the 'coercivity' curve. This whole process of assessing hysteresis properties through remanence measurements was performed quite quickly as each magnetization step took only a fraction of a second and each remanence measurement occupies less than a minute.

b - Anhysteretic Susceptibility (K_{ARM}) versus bulk Susceptibility

The K_{ARM}/K ratio has been used as parameter to discriminate between SD, PSD and MD (King, et al., 1982). The susceptibility was firstly measured, then the specimen was demagnetized up to 100 mT (in alternating field, AF) to remove any secondary remanence. In order to apply an anhysteretic magnetization to the specimen, the AMU-1 Anhysteretic Magnetiser (which is an option to the LDA-3 AF Demagnetizer) was used. This equipment produces a weak direct magnetic field ($50\mu T$), which is superimposed on a relatively strong alternating magnetic field (90mT). Both fields are coaxial and affect the specimen simultaneously.

c - Anisotropy

In some rocks, the direction of magnetization can deviate from that of the magnetizing field. Such rocks are magnetically anisotropic, i.e. their magnetic properties vary with the direction. There are two kinds of magnetic anisotropy:

1. anisotropy of magnetic susceptibility (AMS), in which susceptibility is a function of direction of the applied field; and

2. anisotropy of remanent magnetization, in which acquired remanent magnetization deviates from the direction of the magnetic field at the time of remanence acquisition.

In the case of magnetite-bearing rocks, AMS seems to be dominated by multidomain grains while single-domain and pseudo-single-domain grains are the main paleomagnetic recorders. Hence AMS might not be closely related to anisotropy of remanent magnetization (Stephenson et al., 1986).

As significant anisotropy of remanent magnetization in Vesuvian lavas flows specimens has been considered negligible, no anisotropy experiments were carried out. However, this seemed a very important point that will certainly need further investigations.

3.7 Data interpretation and statistics

a - Linear analyses and Fisher's statistics

The palaeomagnetic remanence directions were analysed using the integrated software packages of Randy Enkin. These packages allow visual presentation and analysis of results as Zijderveld diagrams (Zijderveld, 1967), stereonets and intensity plots. Directions were selected by considering all plots in field corrected co-ordinates. The best-fit directions were calculated using principal component analysis (Kirschvink, 1980). The acceptance criteria for these components are that they are defined by an absolute minimum of three consecutive points. All the possible components for each sample were reported and classified on the base of their Maximum Angular Deviation (MAD). In particular, components that showed MAD less then 2 were referred to as *well defined*, while components with values between 2 and 5 and greater than 5 were respectively referred to as *less* and *poorly defined*. In order to define the site mean direction all the components identified within each sample were considered only after their repeatability had been checked within the site. At least three similar components were required. Components were considered similar if their relative declination and inclination did not differ by more then 4/5°. To define the lava flow mean direction, the choice of the site

mean directions was based on their similarity (as for the site mean value) and/or better statistical parameters. Two Fisherian statistical parameters were calculated for each mean direction (Fisher, 1953). These were the estimate, k, of the true precision parameter, K. This is a measure of the concentration of the individual data points around the mean direction and is given by

$$k = (N-1)/(N-R)$$

where N is the number of individual unit vectors and R is the length of the resultant vector. The value of k ranges from 0 where the points are distributed uniformly over the sphere and approaches ∞ as the directions concentrate to a point. The second statistical parameter is the confidence limit on the mean direction. This is the semi-angle of the cone of confidence surrounding the calculated mean direction. This confidence limit is conventionally for a probability level of 95% (P = 0.95) and is referred to as α_{95}. This is given by

$$\cos^{(1-P)} = N-R/R\{(1/P)^{1/n-1}-1\}$$

where N is the number of individual unit vectors and R is the length of the resultant vector. This statistical parameter suggests that there is a 95% probability (20:1) that the true mean direction will lie within the cone of confidence calculated around the calculated mean direction. The α_{95} value, on equal angle stereographic projection, is represented by the radius of a circle of confidence. On plate carrée graphs (declination, inclination) the error in declination and inclination (δDec, δInc) can be calculated by:

$$\delta Dec = \frac{\alpha_{95}}{\cos Inc}$$

$$\delta Inc = \alpha_{95}$$

b - Palaeointensity analyses

A TRM formed by cooling in the geomagnetic field (TRM$_{paleo}$) theoretically depends linearly on the strength (F$_{paleo}$) of the magnetic field through a proportionally constant (A), which includes grain-size and shape distribution, blocking temperature and ferromagnetic properties of the material. This constant, A, should be determined by giving to the same specimen a new TRM (TRM$_{lab}$) in a known field, F$_{lab}$. If the TRM$_{paleo}$ is an uncomplicated, single-component TRM, the palaeointensity can be obtained by

$$Fpalaeo = \left(\frac{TRMpaleo}{TRMlab}\right) Flab$$

or more simply

$$F_{palaeo} = (b) \, F_{lab}$$

where (b) is the slope obtained by the common NRM-TRM plot.

As the number of samples measured for each site was small (1 for MTT experiment and 2 for microwaves), mean values were only determined at lava flow level. In order to define the lava flow mean intensity, the choice of the best representative value for a site was based on the consistency of sample values, at least three similar per site, and on improved statistical parameters. In general the parameter **q** (see next section) was used as a first order discriminator of the quality of the palaeointensity determinations, while **g** and **σb** were used as second order discriminators.

Coe Statistics

What follows is a brief description of Coe's parameters (Coe, 1978) and their means.

The **standard error of the slope** is calculated by:

$$\sigma_b = \left[\frac{2\sum_i (y_i - \bar{y})^2 - 2b\sum_i (x_i - \bar{x})(y_i - \bar{y})}{(N-2)\sum_i (x_i - \bar{x})^2}\right]^{1/2}$$

where N is the number of points being used (at least 4). This standard error, divided by the slope, is a useful measure of uncertainty and is often quoted with results.

The **f (fraction) value** is simply the fraction of total NRM used in calculating the palaeointensity. It is calculated using the equation below:

$$f = \Delta y_T / NRM_{tot}$$

where:

$$\Delta y_T = NRM_{max} - NRM_{min}$$

To look at a decent amount of total NRM, for this study **f** will be considered acceptable when greater than 0.15

The **g (gap) value** is a measure of the uniformity, along the NRM axis, of the spacing (Δy) between each point perpendicular projection onto the best fit straight line. This is calculated using the following equation.

$$g = 1 - \overline{\Delta y} / \Delta y_T$$

where:

$$\overline{\Delta y} = (1 / \Delta y_T) \Sigma_{i=1}^{N-1} \Delta y_i^2$$

The value of g increases with uniformity of spacing; it is 1 for perfectly even spacing of points along the NRM axis.

The **q value** is the index of quality of a palaeointensity determination. It is calculated using the equation:

$$q = | b | f g / \sigma_b$$

It is usually a matter of course for q values to be quoted alongside any palaeointensity determination. The reciprocal of q is a measure of the *relative uncertainty* of a palaeointensity measurement. Multiplying this by H_{pal} is it possible to determine an *absolute uncertainty*, but assuming that no other remanence or magnetic alterations have parameters that are linear functions of temperature.

Chapter IV

Geological Background

4.1 - General Introduction

During the Quaternary central and southern Italy were characterized by the strong development of the potash-rich volcanoes that form the so-called Roman Comagmatic Province (Washington, 1906). This volcanic activity started about 2.0 Ma ago and has lasted until the present day with the historical eruptions of Vesuvius, Phlegrean Fields and Ischia. The volcanism extends for more than 350 km along the Tyrrhenian coast from northern Latium (the Vulsini area) to Vesuvius; only one isolated alkalic Quaternary volcano (Vulture) is located on the Adriatic side of the Italian peninsula, east of the Apennine main axis (Fig. 4.1).

The Roman Province includes several eruptive centres, which generally present complex evolutionary histories. Large central volcanoes, mostly with summit calderas, occur as well as monogenic vents and regional calderas. The great variety of apparata reflects the nature of the products, ranging from extremely viscous lava domes to flood basalts and from ignimbrites to phreatic breccias.

The tectonic significance of this volcanism has been alternately interpreted in terms of either a shoshonitic member of an orogenic association related to converging plates (Ninkovich et al, 1972; Di Girolamo, 1978) or as the alkaline products of the initial stages of continental rifting (Cundari, 1979: Cundari et al, 1970). In practice the Quaternary potassic volcanoes of central and southern Italy are related to extensive vertical faulting displaying two main trends, respectively parallel (NW-SE) and perpendicular (NE-SW) to the main axis of the Apennines. Such a tectonic arrangement seems to be connected with the opening, since Miocene times, of the Tyrrhenian Sea abyssal plain, following the anticlockwise rotation of the Italian peninsula
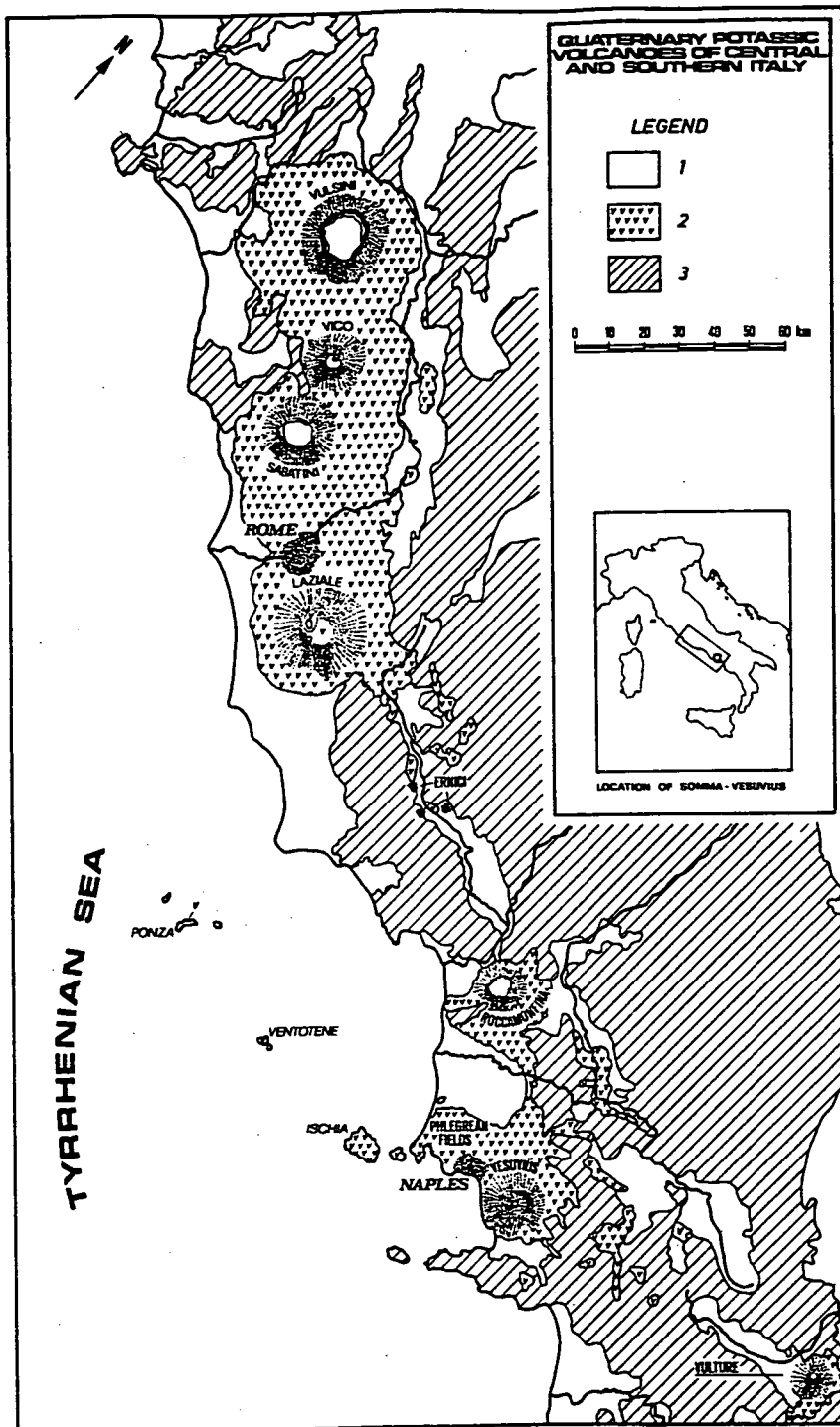
Fig. 4.1 The Roman Comagmatic Province.
1 = Recent alluvium; 2 = Quaternary potassic volcanoes; 3 = Tertiary and Mesozoic sedimentary formations. Redrawn after Marinelli (1979)

(Scandone, 1978). Within such a picture the Quaternary volcanoes are located over a variably thinned continental crust at the intersection of NW-SE perpendicular faults (responsible for the thinning) and NE-SW transverse related to the torsion of the Apennine range during the rotation.

4.2 - Geological setting of the Campanian Volcanic Area.

A schematic representation of the main stratigraphic and structural units of the Campanian region (Fig. 4.2) shows that the Campanian Apennines consist of a pile of nappes emplaced during the Miocene, with the more external ones overthrust towards the east (D'Argenio et al, 1973; Pescatore et al, 1973). The region is affected by intensive vertical tectonics of Plio-Quaternary age related to conjugate, respectively Apenninic and anti-Apenninic fracture systems which generally obliterate the older (Miocene) tectonic lineaments. Recent tectonics are related to the general uplift of the central part of the Apennine range and to the sinking of its western side. The Quaternary potassic volcanism of Campania occurred on a plain corresponding structurally to a basin, bordered on the NE by NW-SE Apenninic faults, on the south and on the north by horsts limited by NE-SW anti-Apenninic faults (Monti Lattari, Capri island and Monte Massico).

Some important faults revealed by seismic surveys (Finetti et al, 1974) in the Gulf of Naples extend up to the mainland (Fig. 4.2). The faults crossing Vesuvius are probably located at the intersection of conjugate NW-SE and NE-SW faults. Other important tectonic lines cut the western and the northern side of the Gulf of Pozzuoli.
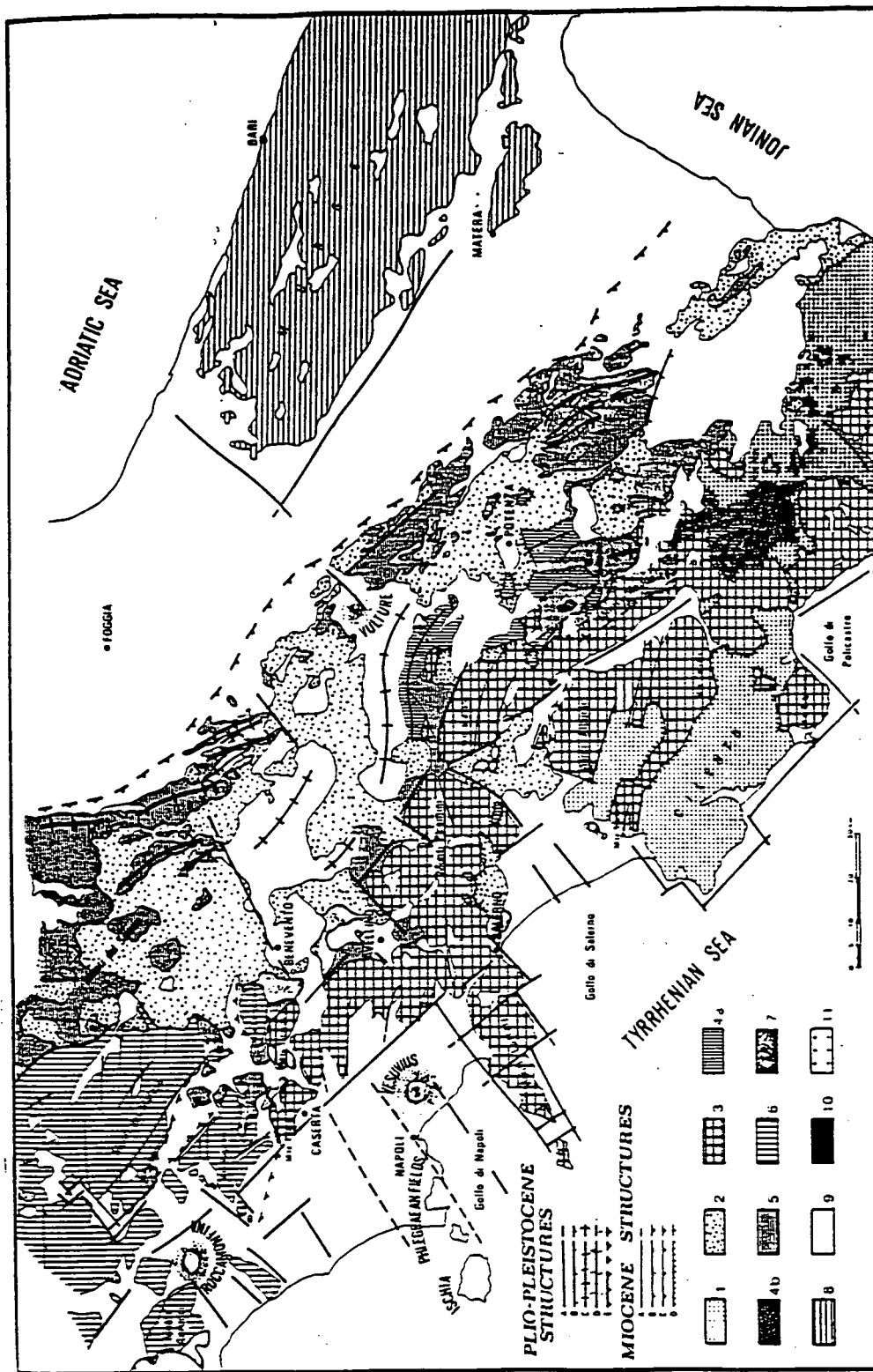
Fig. 4.2 Geological sketch map of the Campanian volcanic area.

PLIO-PLEISTOCENE STRUCTURES: A= normal faults; B= reverse faults; C= axes of synclines; D= axes of anticlines; E= subsurface boundary of nappes within the Bradanic fore deep.

MIOCENE STRUCTURES: A= normal faults; B= reverse faults; C= Tortonian overthrusts; D= Langhian overthrusts. Units: 1=Silentina and Frido; 2=Sicilide; 3= Monte Foraporta, Monte della Maddalena, Alburno-Cervati and Monte Bulgheria-Verbicaro; 4a Upper Lagonegro; 4b Lower Lagonegro; 5= Irpinia; 60 Frosolone, Matese, Monte Maggiore and Monte Croce; 7= Altavilla; Apulo-Gargano; 9= Quaternary sediments; 10= serpentine, gabbro and diabase; 11= granitic gneiss.After Ippolito et al., (1973)

40

4.3 - Stratigraphic outline of the potassic Quaternary volcanism of Campania.

Five volcanic complexes erupted potassic products during the Quaternary in the Campanian area: Ventotene-S. Stefano (Pontine islands), Roccamonfina, the Ischia and Procida islands, the Phlegrean Fields and Somma-Vesuvius. According to the available radiometric ages, the activity started between 1.5 and 1.0 Ma ago at Roccamonfina (Giannetti et al, 1979) and the Pontine islands (Barberi et al, 1967; Capaldi et al, 1985). However, no radiometric data are available on the beginning of volcanic activity in the Phlegrean Fields, where undatable pyroclastics covered by other volcanic products dated back to about 50,000 y.B.P. were intersected by deep geothermal wells. The date of the beginning of activity is also uncertain at Vesuvius and Ischia. For Vesuvius, in fact, K-Ar ages of about 0.3 Ma, obtained from a core near the bottom of the volcanic sequence encountered by the deep well Trecase 1 correlate badly with nanno-plankton ages (0.5-1.0 Ma) from silty interbeds (Bernasconi et al, 1981). Controversy also exists in Ischia where the oldest volcanic products were first dated back to about 700,000 y.B.P. (Capaldi et al, 1976) but ages no greater than 130,000 y.B.P were provided by Gillot et al. (1982). In spite of the complexity of the geochronological framework, a period of contemporaneous activity of all five complexes possibly occurred within a time interval between 200,000 and 100,000 years ago.

Eruptions are recorded historically for three volcanoes: Ischia in 1301 (Arso lava flow), the Phlegrean Fields in 1538 (Monte Nuovo explosive eruption) and, possibly, in 1198 (Solfatara phreatic explosion), and Vesuvius from A.D.79 to 1944.

4.4 - The Somma-Vesuvius volcanic complex.

As is well known, Somma-Vesuvius is a composite central volcano consisting of an older strato-volcano, Monte Somma, whose activity ended with a summit caldera collapse, and of a more recent

41

cone, Vesuvius, built inside the caldera. The main feature of the complex is represented by the sharp morphological contrast between the deeply eroded arched rampart of Monte Somma and the regular Vesuvius cone. The two structures join along the Valle del Gigante, a narrow semicircle whose floor is formed by the lava flows of several eruptions. The presence of a secondary high (roughly corresponding to Colle Margherita, formed during the 1891-1894 eruption) permits the distinction of the Atrio del Cavallo, dipping gently westwards, and, to the east, the Valle dell'Inferno, draining southwards. Somma Vesuvius is certainly one of the most famous volcanoes in the world. Hundreds of papers have been written about its eruptive history and its products, although geo-volcanological mapping is surprisingly scarce. The only complete document of this type is the excellent 1/10,000 map published in 1891 by Johnston-Lavis. After this date the Ufficio Geologico d'Italia, in 1910, and the Servizio Geologico d'Italia, in 1971, produced two editions of the 1/100,000 sheets of the Geological Map of Italy (sheets 184 Napoli and 185 Salerno), consisting substantially of a reduction and simplification of the Johnston-Lavis map. Major revisions were introduced by Rittmann in the Napoli-Ischia sheet of 1971, but these mainly related to the chronology of Somma-Vesuvius activity rather than to the mapping itself.

The newest 1:25,000 Geological Map of Somma-Vesuvius Complex introduced many significant modifications with respect to the previous documents. This work was executed in 1987 in the context of the basic research for the volcanic hazard zoning of the Vesuvius area (Operative Unit 3.3.1 of the Italian Geodynamic Project, under Roberto Santacroce). The significant modifications mainly consisted of a new general stratigraphy that is better defined, from a chronological viewpoint, and of a revision of historical sources for the definition of the recent (A.D. 1631-1944) period. This map (Fig. 4.3) has been used as a guide for the present work. The mapped area lies

Fig. 4.3

GEOLOGICAL MAP OF SOMMA-VESUVIUS VOLCANIC COMPLEX

Scale 1: 70.000

Redrawn after Santacroce, 1987

Legend:

1 — Undifferentiated, frequently reworked, pyroclastic products of the lower Vesuvius and Mt. Somma slopes. Air-fall deposits and distal facies of the pyroclastic flows, surges and lahar deposits left by the Somma-Vesuvius and Phlegrean Fields explosive events after 17.000 y.b.p.

2 — Undifferentiated pyroclastic products of the Vesuvius and Mt. Somma slopes, generally underlying air-fall ash, sand and lapilli of the recent activity. Air-fall deposits and pyroclastic flows, surges and lahar deposits younger than 17.000 years.

3 — Pyroclastic products (ash, sand, lapilli, bombs and blocks) of the Vesuvius cone and welded scoriae of 1944.

4 — Hot pyroclastic landslides occurring during the 1944 eruption.

5 — 1944 - 1913
6 — 1906 - 1875
7 — 1872 - 1855
8 — 1850 - 1824
9 — 1822 - 1798
10 — 1794 - 1744
11 — 1737 - 1637

La vas of the period 1637 - 1944; flows and exogenous tholoids showing generally "aa" and ropy "pahoehoe" surfaces, where tumulus formation is a frequent phenomenon.
Rocks of the high potassium (HK) association ranging in composition between tephritic and phonolitic leucitites. On the various flow-units date of eruption is indicated.

12 — Main fragmental flow deposits (glowing clouds and associated ash clouds, lahars) of the A.D. 1631 eruption.

13 — Lava flows before 1631 and after A.D. 79 frequently covered by thick pyroclastic deposits (glowing clouds, ash clouds, lahars) of the A.D. 1631 eruption.

14 — Pyroclastic products of A.D. 472 "Pollena eruption".

15
16
17
18
19 — Volcanic products erupted during the Monte Somma caldera formation (A.D. 79 - 17.000 y.b.p.)

20 — Pre - Monte Somma caldera volcanic products

within sheets 184 II NE ("Vesuvio"), 184 I SE ("Pomigliano d'Arco"), 185 IV SW ("S. Giuseppe Vesuviano") and 185 III NW ("Boscoreale") of the Topographic Map of Italy at 1:25,000 scale. It extends over about 165 km² between 40°45'00" and 40°53'30" North and 14°19'38" and 14°33'38" East. Most of the area is covered by the relief of the Somma-Vesuvius volcanic complex that gently reaches down to the plain in a nearly complete ring surrounding the central vent. Only the south-southwestern sector slopes more steeply down to the sea.

4.5 - Eruptive history from 79 AD to 1944 AD

The recorded history of the volcano, handed down through oral traditions and the writings of historians and chroniclers, covers only a short fraction of its total life. Consequently the reconstruction of the eruptive history of Somma Vesuvius requires different approaches according to the presence (or absence) of direct documentation and also to its reliability. In spite of this, three "historic" periods can be distinguished.

- The oldest (and longest) period, which precedes the famous A.D. 79 "Pompei" plinian eruption, lacks any direct historic data. The reconstruction of activity can only be based on geological data.

- The middle period, covering the A.D. 79-1631 time-span, has largely incomplete, intermittent historical documentation.

- The youngest period (1631-1944) is, on the whole, well-documented. Reconstruction of the eruptive history of the volcano during this time span is mainly based on the collection, interpretation, and synthesis of historical data.

a - The A.D. 79 - 1631 period of activity.

The written history of volcanology began with the description by the Younger Pliny of the A.D.

44

79 event, which is the first well-documented eruption. Unfortunately the data available on Vesuvius before the XVIIth century are scarce, scattered and incomplete, with gaps in the documentation for long periods (Alfano,1924, 1929). From what little information is available, though, it seems that the patterns of eruptive activity differed considerably from those of the most recent active cycle, 1631 - 1944;

1) - eruptions occurred at longer intervals;

2) - the eruptions were more explosive;

3) - fairly large eruptions occurred during the cycle (in particular, that of A.D. 472);

4) - if the entire interval between A.D. 79 and 1139 (the date of the last certain eruption before 1631) is taken as one eruptive cycle, then it would be more than three times longer than the following one.

The following eruptions (Tab. 4.1) are historically recorded before A.D. 1631, together with occasional indications of minor activity at the summit crater (main events are in bold character).

Timing	Description of the event
5-6 November 472	*Subplinian- Flows and lahars products.*
8 July 512	*Subplinian(?)*
February(?)-March(?) 685	*Major eruption with big lava flows*
787	*Big eruption, mainly explosive – probably some lava flows*
November or December 968	*Big eruption with lava flows toward the sea*
1007	*Big eruption. Lava flows*
27 January 1037	*Large lava flows toward the sea*
1-9 June 1139	*Major explosive activity which obscured the sky for several days*

Tab. 4.1 Historical record of Vesuvian eruptions before A.D. 1631. From Nazzaro, 1997.

45

Questionable eruptions are further listed for 172, 203, 222 until 235, 379 until 395, 505, 536, 991, 999, 1049, 1073±5, 1150, 1270 and 1347. An eruption in 1500, is believed by many authors to have been a very minor event. A lava flow has been described by Daniele Barbaro (a philosopher, Vitruvio's student) in 1568, but this eruption was later considered not to exist by other authors (Palmieri, 1880).

Of these eruptions, only seven had unequivocally erupted lava; the first occurring in 968. At least two eruptions produced pyroclastic flows and surges. The average repose periods seem to be considerably longer than during the 1631-1944 cycle, but this may be an enhanced effect of poor reporting in that period. Possible smaller-scale, persistent Strombolian activity from the summit crater (that may have been lying somewhat hidden in the major caldera depression left by the A.D. 79 eruption) may have escaped recording because it did not significantly affect life around the volcano. Two longer eruptive periods, reminiscent of 1631-1944 eruptive sub-cycles, are reported for 222-235 and 379-395, but details are lacking about the sequence of events during those periods. There is also a notable increase in eruption frequency beginning in 1007, but this coincided with better reporting on eruptions in contemporaneous sources and may therefore be more apparent than real.

The imprecise time scale used in the description and notation of eruptions during this period generally prevents reliable field correlations. The scarcity of paleosoils, which mark significant pauses in the activity, make it very difficult to separate single eruptive events which are frequently characterized by similar kinds of products. Radiocarbon dating permitted the sure identification of two eruptions: 472 and 1631; the chronological position of the other deposits of this period is uncertain.

The severe A.D. 472 eruption, also called the "Pollena" eruption, ravaged the Vesuvian area.

In a quarry near the village of Ottaviano, the A.D. 472 products are covered by a 20 cm thick air-fall breccia (mainly lava clasts), possibly indicating a phreatic event. It grades upward into a thin humified level with a radio-carbon age of 1,550 ± 50 B.P. years probably correlating with the pause preceeding the A.D. 512 eruption. The descriptions of this event strongly suggest the presence of fragmental flows (ash streams rushing down the mountainside) and indicated its strongly explosive character (ash fall reported in Costantinople, as occurring in A.D. 472). At the Terzigno quarry a deposit some 20 cm thick, made up of white to greenish pumice set in a sandy matrix, could represent the A.D. 512 event; air fall deposits of dark sand and lapilli cover the thin humified level overlying the 512 deposit. This type of deposit frequently crops out in the north eastern sector of the volcano, interlayered between the practically ubiquitous and clearly recognisable 472 and 1631 sequences. Generally they are covered - with a paleosoil in between - by another fall bed characterized by the ochre color of the altered pumice. No radiocarbon date is available for the paleosoils beneath these two deposits. In the southern sector of the volcano at least three leucitic lava flows underlie the younger of these two eruptions after 472 A.D..

b - The A.D. 1631 eruption; an entirely explosive event?

Compared with the AD 79 eruption, the event of 1631 was of minor proportions regarding eruptive magnitude and erupted volumes, but, not in terms of destruction and fatalities. Beginning on 16 December 1631 and culminating the day after, it destroyed all towns and villages around the volcano and killed at least 3000 and maybe up to 6000 persons. It was thus the worst volcanic disaster in the Mediterranean during the past 1800 years. The eruption occurred after a repose period lasting at least 130 and probably almost 500 years. Very detailed, but in part confusing or even misleading information is available about the 1631 eruption from contemporaneous or near-contemporaneous sources. Only very recently (starting in the late

1980's) has there been modern volcanological and palaeomagnetic research on this important event that has significant implications for volcanic hazard assessments of the region. In fact, many (more or less) modern sources dealing with the 1631 eruption (starting with Le Hon 1865, 1866) state that one of the most destructive and lethal agents was unusually fluid lava. Principe et al., in Santacroce (1987), however, were among the first to exclude the occurrence of lava flows in 1631. In contrast, Rolandi et al. (1993a) and Gialanella et al. (1993) again attribute several lava flows to the eruption, while Rosi et al. (1984) and Carracedo et al. (1993) refute this view. Both parties rely on magnetic evidence but Rosi et al. further mention that contemporaneous descriptions of the 1631 flow phenomena differ considerably from those of lava flows in historical documents of the 1139 eruption. Rosi and Santacroce (1984) made a detailed reconstruction of the 1631 event based on historical (Braccini, 1632; Danza, 1632; Falcone, 1632; Giuliani, 1632; Masculi, 1633; Mormile, 1635; Recupito, 1632) and stratigraphic data. The first important point they underlined was the explosive character of the eruption. In fact they affirmed that no lavas connected with this event were recognized: all lava flows assigned to 1631 are older, having probably been erupted during the period 968-1037.

Air fall deposits (light greenish to dark grey pumice) belong to the first eruptive phase: they outcrop in the northeastern sector of the volcano, reaching a maximum observed thickness of 60 cm. Lithics are abundant and increase upwards in the deposit; they include lavas, skarn rocks, and cumulates. The collapse of the eruptive column and the subsequent formation of pyroclastic flows are revealed by the presence of unwelded ash-tuff deposits containing abundant lithic clasts and dark grey pumice. The ash flow deposits are mainly concentrated in the southern sector of the volcano, where they rarely cover the fall deposits. A pink ash horizon commonly occurs at the top of both flow and fall deposits. In distal outcrops this bed shows a lateral transition to

vesiculated tuff. The 1631 sequence generally ends with lahar deposits.

c - The recent activity: 1631-1944.

The most recent period of the volcano's history (Alfano, 1929; Imbo', 1949,84) is characterized by semi-persistent, relatively mild activity (lava fountains, gases and vapour emission from the crater) frequently interrupted by short quiet periods that never exceeded seven years. Rare minor eruptions that occurred during the semi-persistent, strombolian-like activity of the volcano mainly consisted of small lava flows emitted from the summit crater ("intermediate eruptions"). More important eruptions closed each of the short cycles interposed between quiescent periods ("final eruptions"). Pasty fluid blebs, spherical bombs and ash were violently ejected from the summit crater accompanying the effusion of moderately fluid lavas. Lavas were sometimes produced by lateral cinder cones on the flanks of the volcano. The emplacement of relatively small mudflows along stream valleys cutting the Monte Somma slopes was usual during these eruptions. This was especially true if the water gained access to the vent during a lateral eruption so that a large quantity of ash was produced. Likewise, hot pyroclastics sometimes slumped from the oversteepened cone to form the so-called "hot-avalanches" (Ferret, 1924) and/or landslides of hot scoria.

As a whole the 1631-1944 period reflects open chimney conditions within a periodically refilled eruptive system. Under these conditions the triggering of intermediate eruptions could be ascribed to pulses of deep basic magma, while the final eruptions have been interpreted (Barberi et al, 1967; Santacroce, 1983) as episodic events, probably resulting from external causes (e.g. earthquakes), provoked by moderate, discontinuous magma-groundwater interactions. The 1906 eruption can be taken as a type-example of this activity (Matteucci et al, 1906; Johnston Lavis, 1909; Lacroix, 1906; Ferret, 1924; Sabatini, 1906).

The eruption started on April 4th after a 36 year-long cycle of persistent activity interrupted by long quiet effusions (1881-85, 1885-86, 1891-94, 1895-99, 1903-04) resulting in the formation of the Colle Margherita and Colle Umberto lava-hills (Imbo', 1984, Matteucci, 1886, 94, 99, 1904, Palmieri, 1896). The 1906 paroxysmal event lasted 20 days being preceded by strong earthquakes and noticeable uplift. Lava-flows were emitted from a sub-summit NNW-SSE trending fissure, while the summit crater explosively erupted large amounts of ash, lapilli, scoria, blocks and bombs, mainly on April 8th and 9th. Abundant rainfall accompanied the whole eruption, provoking the flow of mud streams along the valleys cutting the northern and north-eastern Mt. Somma slopes.

These final eruptions resulted in the emptying of the eruptive system: the following short pauses (1-7 years) reflect the re-establishment of a near-surface lava column within the chimney and preceded the resumption of the strombolian-type activity, opening a new short cycle.

Critically since December 1944 Vesuvius has remained dormant. This long quiescent period departs from the 1631-1944 pattern of activity. The mode of the future renewal of activity cannot, therefore, be predicted.

4.6 - Lava flows samples; sites map.

A highly density of people surround the Somma-Vesuvius volcanic complex and the population has recently been climbing higher and higher. Almost half a million people live in a near-continuous belt of towns and villages built actually on lava flows of any age. While this increased the hazard, it also restricted the sampling strategy. Most of the time was spent "hunting" the lavas between buildings, vineyards and old quarries, following their identification on the volcanological map. Fortunately, after a long bureaucratic process a special permit was

obtained for sampling along the A3 Napoli-Salerno motorway. It passes through the SW

Vesuvius slope, between the cities of Naples and Pompei, and exposes numerous lava flows

(Fig. 4.4). Because of the high danger of sampling (there is always intense traffic on the A3

motorway), a special and constant support unit was needed. Specimens were directly cored in

the field, using a portable electric drill, and oriented with a solar compass prior to removal. At

each sampling site, about 15 cores were collected. The cores were later sliced into standard

specimens (2,5 cm diameter and 2,2 cm high) at the Laboratorio di Paleomagnetismo of the

Dipartimento di Scienze della Terra, Universita' degli Studi di Napoli "Federico II" and into

special-sized specimens (5mm diameter x3mm high) at the Geomagnetism Laboratory,

Department of Earth Sciences, University of Liverpool.
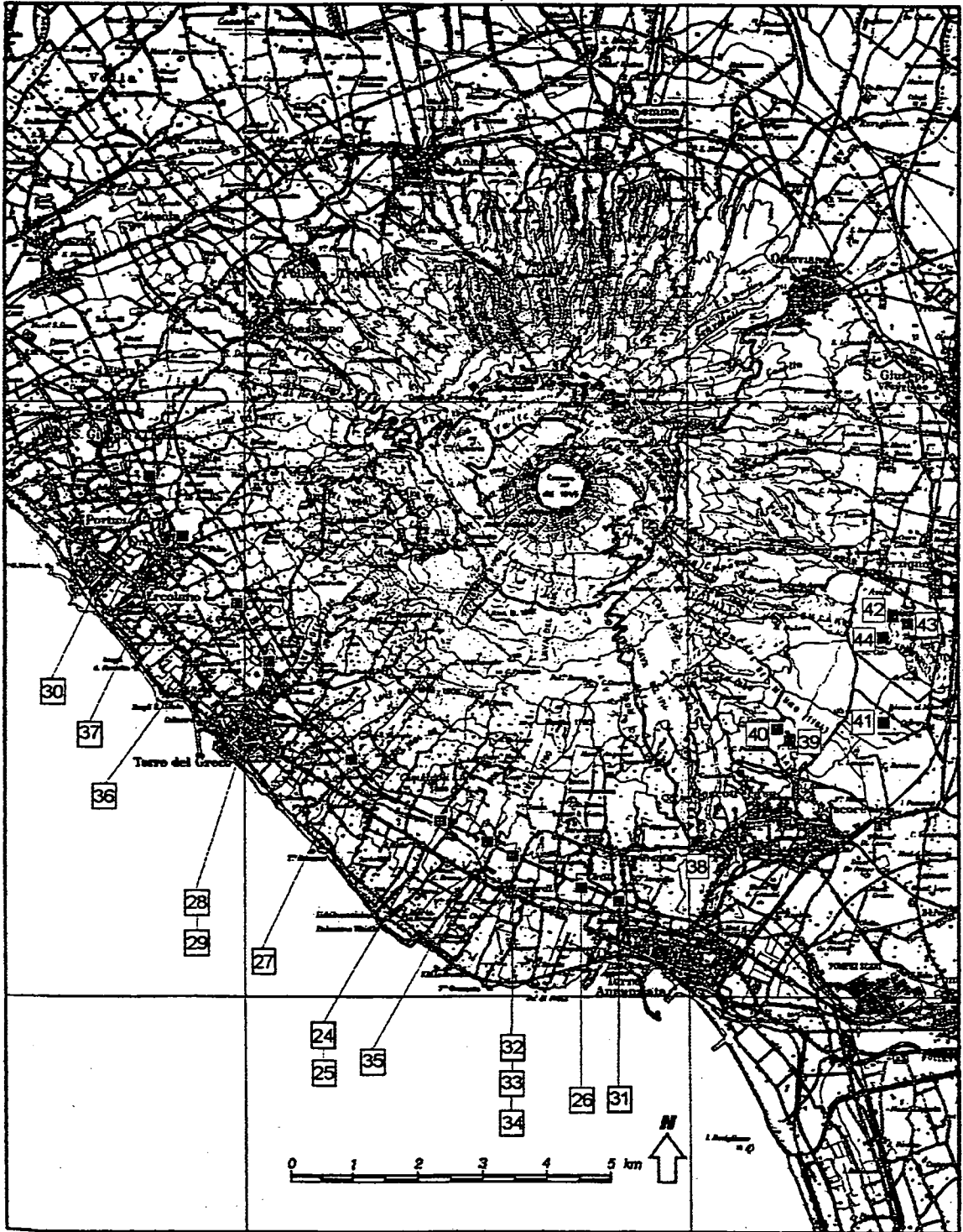
Fig. 4.4 Topograohic map of Somma-Vesuvius and location of sites investigated

52

Chapter V -

DIRECTIONAL PROPERTIES

5.1 - Introduction

In this chapter all the results obtained from the PTD experiment (section 3.3a) will be analysed and described using Zijderveld diagrams and Intensity plots.

Intensity - A complete description of its general behaviour throughout the experiments will be given together with the initial and final NRM values. Anomalies and significant T_{ub} will also be pointed out.

Directions - Both vertical and horizontal components will be peculiarly analysed in order to identify the best-defined component. However, at this stage all the possible results will be reported in tables with their relative temperature ranges and MAD following the criteria described in section 3.7. All break points and anomalies will be also outlined.

5.2 - AD 79 - AD 1631

5.2.1 - Site V30

a - Intensity Behaviour

These 6 samples had initial NRMs between 2570 and 4380 mA/m (Figs. 5.1, 5.2) and, by 620°-630°C, had been demagnetized almost completely. Most samples showed a smooth decrease in intensity, terminating with a small tail at 630°C, although sample P06 had a final steep decay, with no tail, and some 7% of the original remanence still remained. In all samples, the initial decrease of intensity was smooth, with no indication of a low blocking temperature component. At higher temperatures, there were very minor irregularities in the rate of decrease around 330°-360°C and 480°-500°C in 5 of the samples. Sample 03 showed a distinct inflection at about 330°C, followed by a decrease to 50% at 460°C,

indicating significant unblocking at this temperature. The intensity then dropped only slightly before recommencing a smooth fall to 292 mA/m (9%) at 630°C. In the other samples, the minor irregularities could be attributed to experimental error, but as they occur at slightly different temperatures in different samples, it is considered that these, though small, are likely to be real and may be related to mineralogical effects.

b – Directional Behaviour

The vectors for each sample comprised up to three apparently different components (Figs. 5.1, 5.2). These were separated by small irregularities, usually 1 or 2 successive measurements that simultaneously affected both the horizontal and vertical components. In all samples, the highest temperature component was the most well defined and the lowest temperature component, where present, was the least well defined (Tab. 5.1). For example, 03 showed components between 330° and 420°C, 480° and 565°C, and 580° and 630°C. However, when the irregular components were excluded then, for all samples, a single, very well defined vector was revealed, usually between 250-350° to 630°C. (This vector was slightly more precisely defined when the vector was anchored to the origin.) The irregularities observed in each sample vector coincided with the changes in curvature of intensity during demagnetisation (Section 5.2.1a).

5.2.2 - Site V36

a) - Intensity Behaviour

All 11 samples showed very similar behaviour (Figs. 5.3, 5.4, 5.5, 5.6). The initial NRM was about 6000 mA/m and, by 620°C, was almost completely demagnetized (< 2%). All curves showed an accelerating decrease in intensity with increasing temperature terminating with a small tail at 620°C. An anomalous inflection occurred at about 550°C for samples 03 and 05, indicating an unblocking temperature.

Sample 03

Mmax = 3260 mA/m

Scale = 1000 mA/m

Sample 06

Mmax = 3090 mA/m

Scale = 500 mA/m

Sample 09

Mmax = 2570 mA/m

Scale = 500 mA/m

Fig. 5.1 - Site V30: Zijderveld diagrams and Intensity plots.

Sample 11

Scale = 1000 mA/m

Mmax = 4380 mA/m

Sample 12

Scale = 500 mA/m

Mmax = 3540 mA/m

Sample 13

Scale = 500 mA/m

Mmax = 4420 mA/m
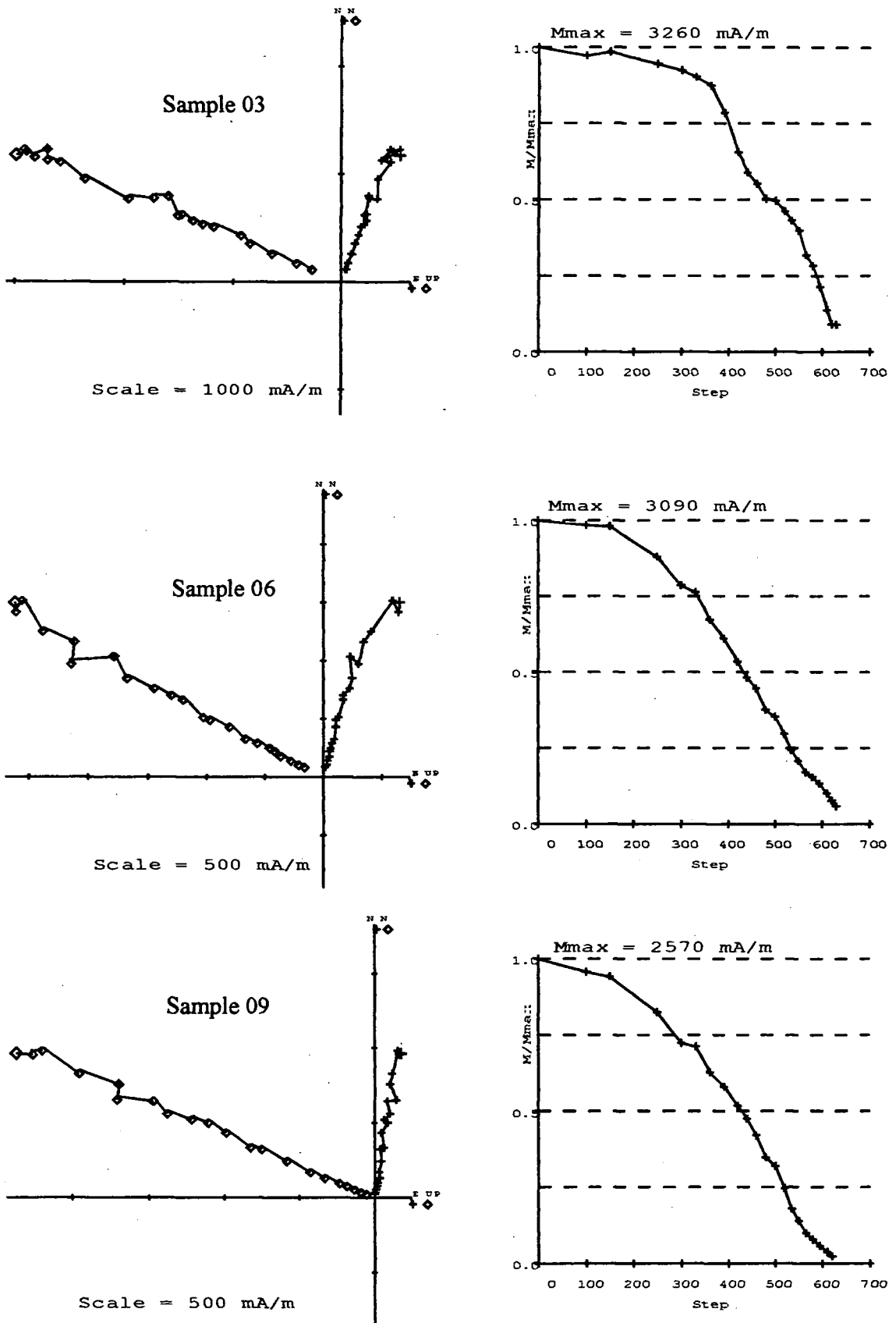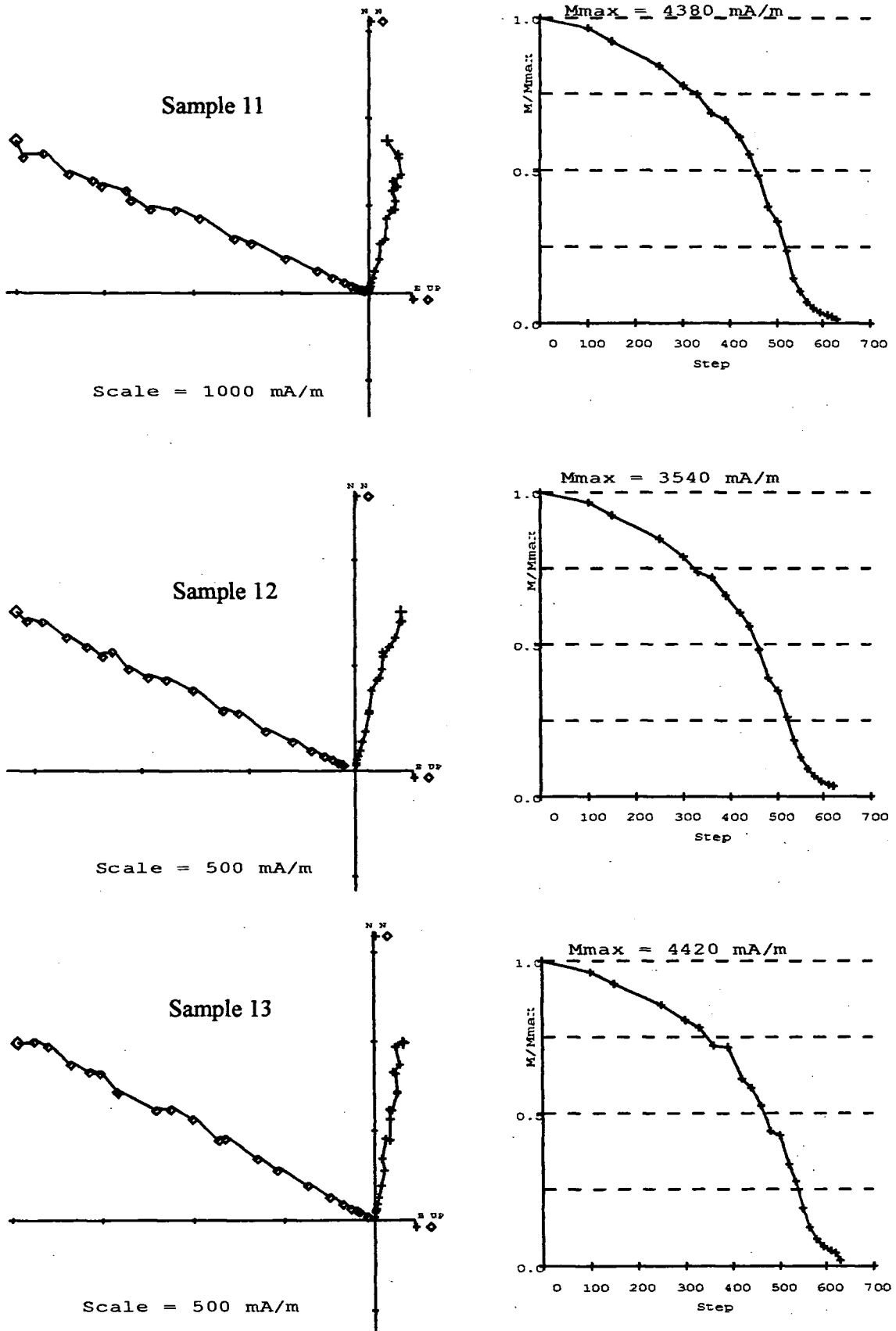
Fig. 5.2 - Site V30: Zijderveld diagrams and Intensity plots.

Sample03			
Steps	Dec	Inc	MAD
"D" 330/420	12.5	62.3	7.4
"D" 480/565	20.0	70.4	4.5
"D" 580/630	18.7	66.7	1.1
"D" 330/630 (*)	20.3	66.3	2.1
"O" 330/630 (*)	20.7	66.0	1.1

(*) erasing steps 440,460°C   (a)

Sample 11			
Steps	Dec	Inc	MAD
"D" 535/630	15.6	66.0	1.1
"O" 535/630	14.0	66.5	0.9
"D" 460/630 (*)	13.3	65.9	0.7
"O" 460/630 (*)	13.2	66.1	0.6

(*) erasing steps 480,520°C   (d)

Sample 06			
Steps	Dec	Inc	MAD
"D" 390/460	23.8	66.7	3.0
"D" 480/630	13.2	62.6	1.9
"O" 480/630	13.7	62.4	0.9
"D" 390/630 (*)	15.5	61.6	1.8
"O" 390/630 (*)	14.7	61.9	1.0

(*) erasing step 460°C   (b)

Sample12			
Steps	Dec	Inc	MAD
"D" 460/520	8.4	60.7	3.7
"D" 520/620	15.8	65.5	1.0
"O" 520/620	13.9	64.9	0.9
"D" 390/620 (*)	14.5	64.6	1.0
"O" 390/620 (*)	14.1	64.5	0.7

(*) erasing steps 460,500°C   (e)

Sample 09			
Steps	Dec	Inc	MAD
"D" 390/440	16.9	76.8	6.5
"D" 440/480	7.4	59.3	6.4
"D" 390/480	10.2	67.4	6.4
"D" 500/550	2.9	65.1	1.6
"D" 565/620	11.9	66.5	1.3
"O" 565/620	10.6	67.4	0.7
"D" 480/620 (*)	10.6	67.4	0.7
"O" 480/620 (*)	10.3	67.5	0.5

(*) erasing steps 500,550°C   (c)

Sample13			
Steps	Dec	Inc	MAD
"D" 440/535 (*)	6.6	59.3	1.8
"D" 535/630 (*)	11.3	62.4	0.9
"O" 535/630 (*)	10.5	62.2	0.6
"D" 360/630 (**)	9.8	62.9	0.7
"O" 360/630 (**)	9.7	62.7	0.5

(*) erasing step 480°C

(**) erasing steps 440,460,500°C   (f)

Tab. 5.1 - Site V30: Directional results calculated using principal component analysis (Kirschvink, 1980).
"D" = floating point; "O" = anchored to the origin

Some very minor irregularities occurred at the same steps of temperature in samples 01B, 03 & 05, which could be due to experimental error, although they occur in different samples at the slightly different temperatures.

b) - Directional Behaviour

In all 11 samples a high temperature component (usually between 520 - 620°C) was well defined. A medium temperature component, which was not always present, was less well defined but still statistically acceptable. The visual analyses of all the components showed sample 09 to have a very anomalous direction while all the remaining samples showed similar directions. In more detail (Tabs. 5.2, 5.3), the high temperature components analyses showed two possible groupings of declination values; an Easterly group (>20°E) and another between 10-20°E, while the inclination values were almost identical. The medium temperature component in samples 01B, 14, 17B and, although with a declination slightly different, in 05 & 06 was very similar to the Easterly high temperature group.

5.2.3 - Site V37

a) - Intensity Behaviour

The 10 samples had variable initial NRMs between 4250 and 8660 mA/m (Figs. 5.7, 5.8, 5.9, 5.10) and, by 620-630°C (in some samples 595°C), had been demagnetized almost completely. All the samples showed an accelerating decrease in intensity with increasing temperature starting from 150-250°C and terminating with a very anomalous tail. In fact, only samples 7A and 14B showed an ideal hyperbolic tail, while all the others showed a distinct inflection at about 535°C, indicating significant unblocking at this temperature.

Some minor irregularities were considered to be real as they occurred at different steps of temperature (within the range 420-520°C), although in some samples, (7B, 10B, 13B) the intensity behaviour was unclear.

b) – Directional Behaviour

All the samples showed a very well defined high temperature component between 520/550 and 595/635°C. The vertical vector, in all the spectra, showed a very linear trend for all the samples, while the horizontal one always had a zigzag behaviour at low and medium temperatures.

The high temperature component analyses showed two possible groupings of declination values; samples 06, 7A and 7B showed values around 0° while the others showed values around 14° (Tabs. 5.4, 5.5). The inclination was almost the same for all samples.

5.2.4 - Site V27

a) - Intensity Behaviour

These 6 samples had an initial NRM around 4000 mA/m and, by 620-630°C, had been completely demagnetized, generally with a final steep decay above 500°C (Figs. 5.11, 5.12). Samples 03, 04 and 06 showed an almost linear decrease in intensity with two clear breaks (360°C and 440°C) in the rate of decrease. Samples 07, 12, 13 had accelerating decreases in intensity with increasing temperature, although they showed minor deflections at the same temperatures as the above mentioned breaks. Same deflections occurred both in 07 and 12 around 550-565°C indicating a significant unblocking.

b) – Directional Behaviour

For all these samples only a high temperature component was well defined. They showed a very clear vertical component, while the horizontal was very unclear until 500°C. The analysis of the vectors showed similar directions for all the samples and with very low MAD values (Tab. 5.6).
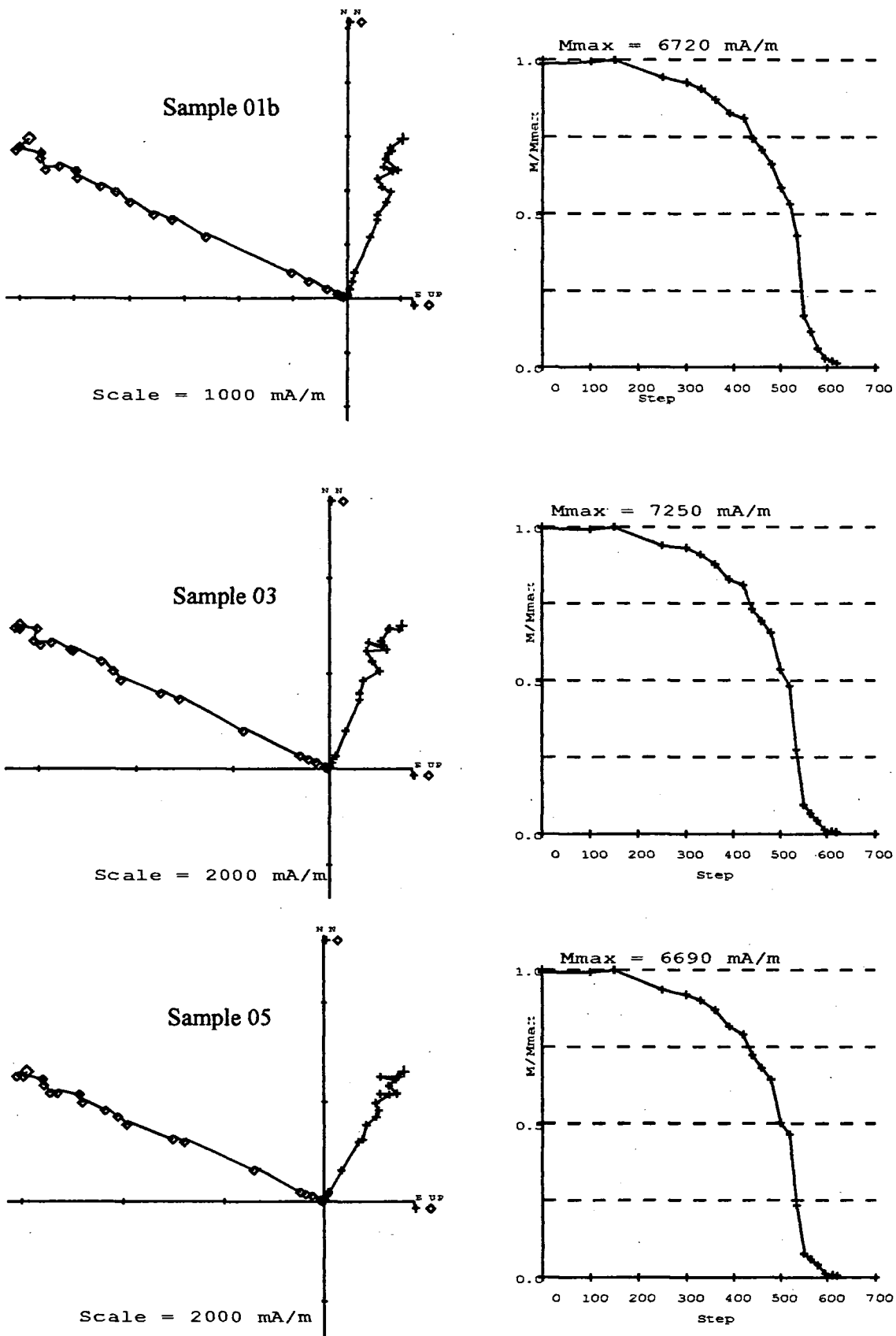
Sample 01b

Scale = 1000 mA/m

Mmax = 6720 mA/m

Sample 03

Scale = 2000 mA/m

Mmax = 7250 mA/m

Sample 05

Scale = 2000 mA/m

Mmax = 6690 mA/m

Fig. 5.3 - Site V36: Zijderveld diagrams and Intensity plots.

Sample 06

Mmax = 6190 mA/m

Scale = 1000 mA/m

Sample 07

Mmax = 5970 mA/m

Scale = 1000 mA/m

Sample 08

Mmax = 5240 mA/m

Scale = 1000 mA/m

Fig. 5.4 - Site V36: Zijderveld diagrams and Intensity plots.

Sample 09

Scale = 2000 mA/m

Mmax = 5560 mA/m

Sample 11

Scale = 1000 mA/m

Mmax = 6280 mA/m

Sample 14

Scale = 1000 mA/m

Mmax = 6720 mA/m
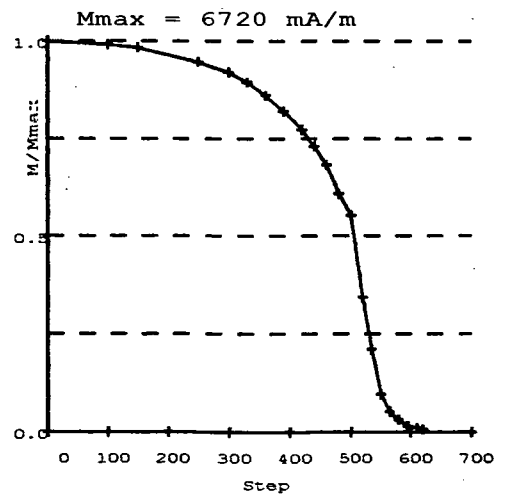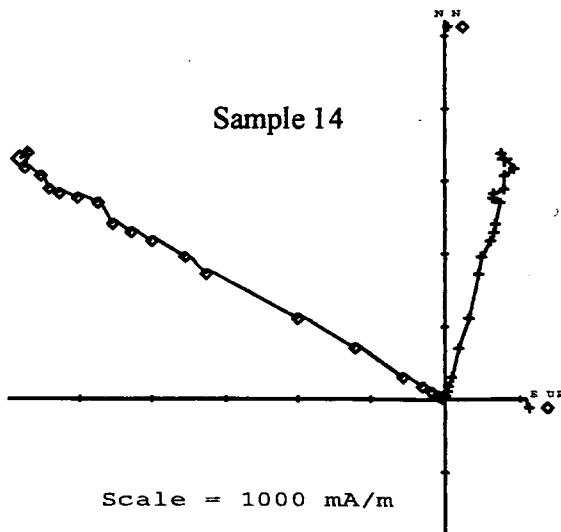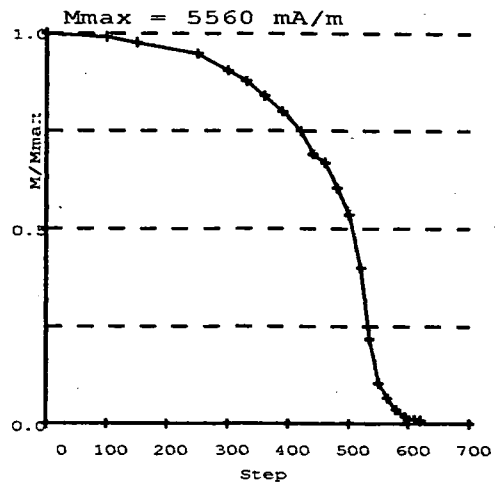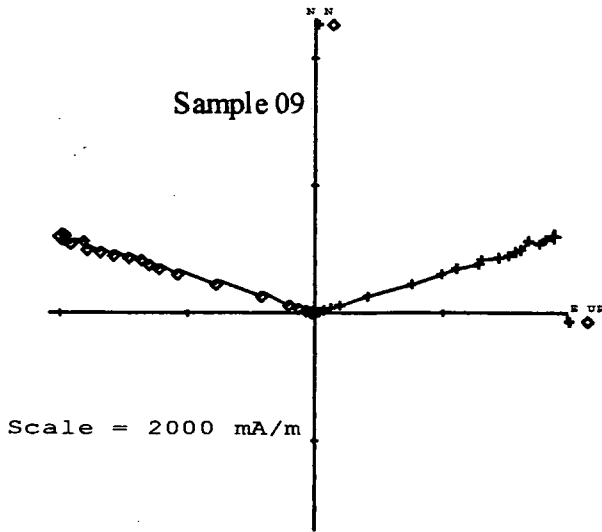
Fig. 5.5 - Site V36: Zijderveld diagrams and Intensity plots.

Sample 16

Scale = 1000 mA/m

Sample 17b

Fig. 5.6 - Site V36: Zijderveld diagrams and Intensity plots.

Sample 01B			
Steps	Dec	Inc	MAD
"D" 460/550	24.1	63.6	2.3 (*)
"D" 550/620	15.9	64.7	0.7
"O" 550/620	16.2	64.5	0.5
"D" 420/620	19.0	64.5	2.4
"O" 420/620	19.1	64.5	1.5

(*) visible only on H component   (a)

Sample 06			
Steps	Dec	Inc	MAD
"D" 525/580	31.3	62.4	1.3
"D" 580/620	23.1	62.0	0.9
"O" 580/620	24	62.3	0.7
"D" 460/620 (*)	30.8	62.4	1.3
"O" 460/620 (*)	30.4	62.6	1.0

(*) erasing steps 480°   (d)

Sample 03			
Steps	Dec	Inc	MAD
"D" 520/620	23.5	66.3	0.7
"D" 520/620	23.5	66.3	0.5
"D" 480/620 (*)	21.2	64.9	0.9
"O" 480/620 (*)	21.5	64.7	0.7

(*) erasing step 520°   (b)

Sample 07			
Steps	Dec	Inc	MAD
"D" 500/620	9.5	67.2	1.0
"O" 500/620	9.0	67.3	0.7
"D" 500/620 (*)	10	67.1	0.5
"O" 500/620 (*)	9.6	67.2	0.4
"D" 460/620 (**)	10.1	67.1	0.9
"O" 460/620 (**)	9.5	67.2	0.6

erasing steps (*) 535° and (**) 480°   (e)

Sample 05			
Steps	Dec	Inc	MAD
"D" 520/565	30.5	63.3	0.9
"D" 580/620	25.1	63.1	0.3
"O" 580/620	26.6	63.0	0.9
"D" 440/565 (*)	31.8	63.9	0.7
"D" 440/620 (*)	31.5	63.9	0.6
"O" 440/620 (*)	31.1	63.9	0.5

(*) erasing step 480°   (c)

Sample 08			
Steps	Dec	Inc	MAD
"D" 520/565	27.3	64.2	0.5
"D" 580/620	24.5	58.7	3.0
"O" 580/620	25.1	60.6	2.1
"D" 520/620	27.7	64.2	0.7
"O" 520/620	27.6	64	0.6
"D" 520/620 (*)	27.6	64.1	0.4
"O" 520/620 (*)	27.7	64.0	0.3

(*) erasing step 580°   (f)

Tab. 5.2 - Site V36: Directional results calculated using principal component analysis (Kirschvink, 1980).

AD 79 - 1631   site V36

Sample 09			
Steps	Dec	Inc	MAD
"D" 330/440	74.7	54.9	6.4
"D" 460/535	73.2	46.0	3.0
"D" 535/620	72.3	44.8	0.5
"O" 535/620	72.4	44.8	0.4

(a)

Sample16			
Steps	Dec	Inc	MAD
"D" 550/620	15.1	64.9	1.2
"O" 550/620	14.8	65.3	0.8
"D" 250/620	16.6	66.0	1.2
"O" 250/620	16.5	65.9	0.7

(d)

Sample 11			
Steps	Dec	Inc	MAD
"D" 595/620 (*)	27.8	66.9	0.6
"O" 595/620 (*)	27.5	66.9	0.4
"D" 390/620 (*)	28.1	67.4	0.8
"O" 390/620 (*)	28.1	67.4	0.6

(*) erasing steps 460, 480°   (b)

Sample 17B			
Steps	Dec	Inc	MAD
"D" 420/535	24.5	67.6	3.9
"D" 535/620	17.6	66.0	0.5
"O" 535/620	17.8	66.1	0.4

(e)

Sample 14			
Steps	Dec	Inc	MAD
"D" 420/480	22.7	63.7	2.6
"D" 500/620	15.0	61.2	1.0
"O" 500/620	15.1	60.9	0.9
"D" 420/620 (*)	15.5	61.1	0.6
"O" 420/620 (*)	15.5	60.9	0.5

(*) erasing step 500°   (d)

Tab. 5.3 - Site V36: Directional results calculated using principal component analysis (Kirschvink, 1980).

Fig. 5.7 - Site V37: Zijderveld diagrams and Intensity plots.

Sample 07a

Scale = 1000 mA/m

Mmax = 6650

Sample 07b

Scale = 1000 mA/m

Mmax = 5970 mA/m

Sample10a

Scale = 2000 mA/m

Mmax = 8350 mA/m

Fig. 5.8 - Site V37: Zijderveld diagrams and Intensity plots.

Sample 10b

(

Scale = 1000 mA/m

Mmax = 7950

Sample 11

Scale = 2000 mA/m

Mmax = 7550 mA/m

Fig. 5.9 - Site V37: Zijderveld diagrams and Intensity plots.

Sample 13b

Scale = 2000 mA/m

Mmax = 8660

Sample14b

Scale = 2000 mA/m

Mmax = 7600 mA/m
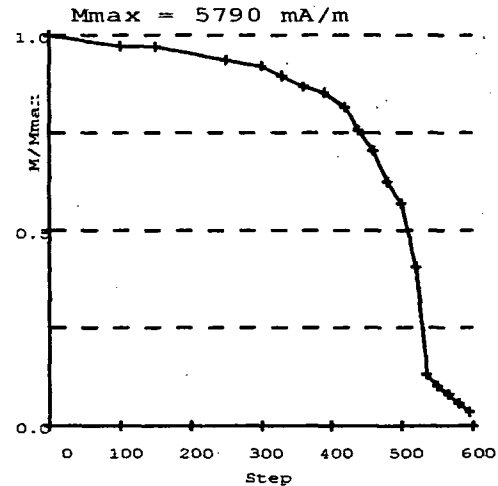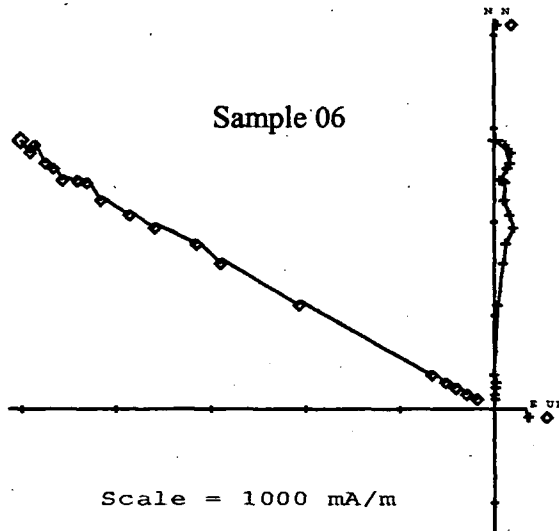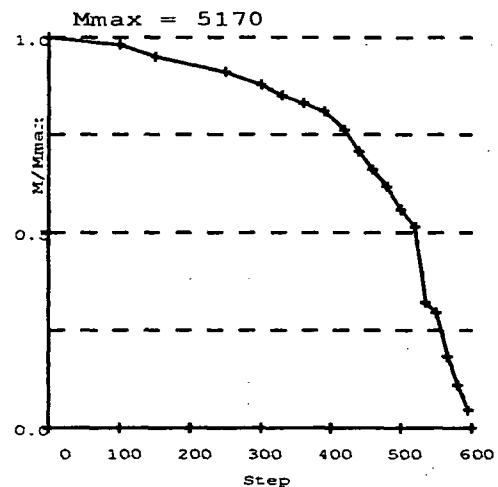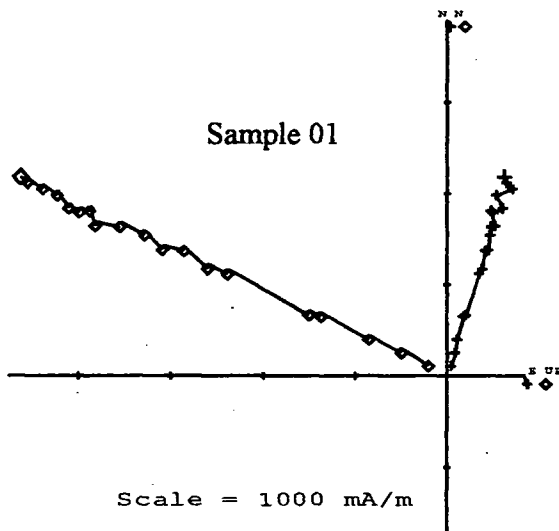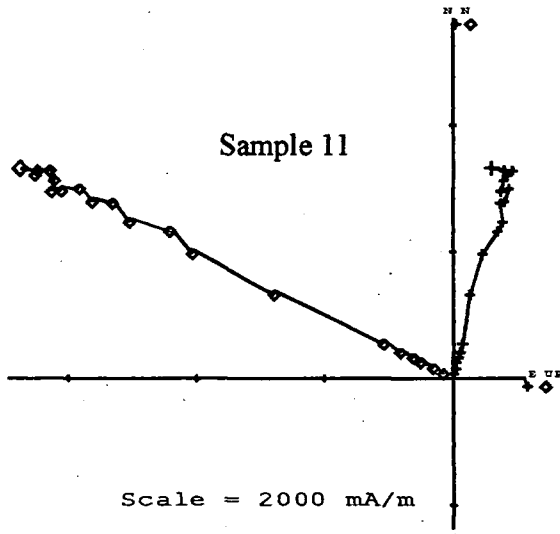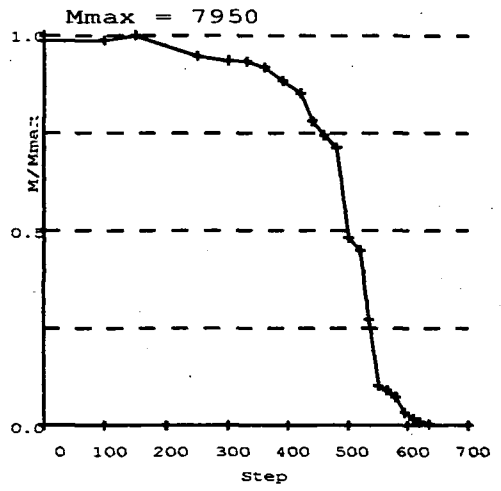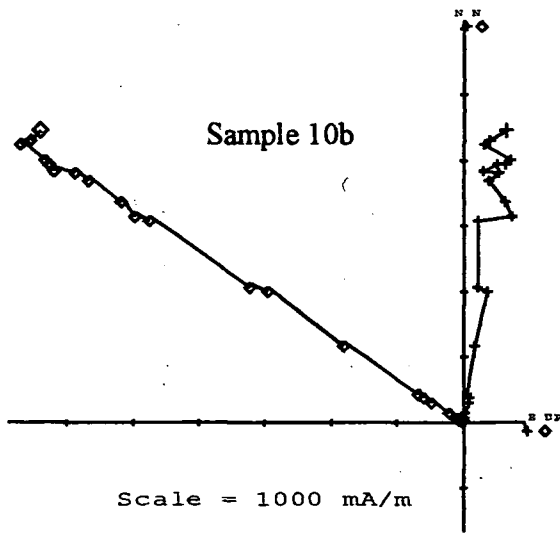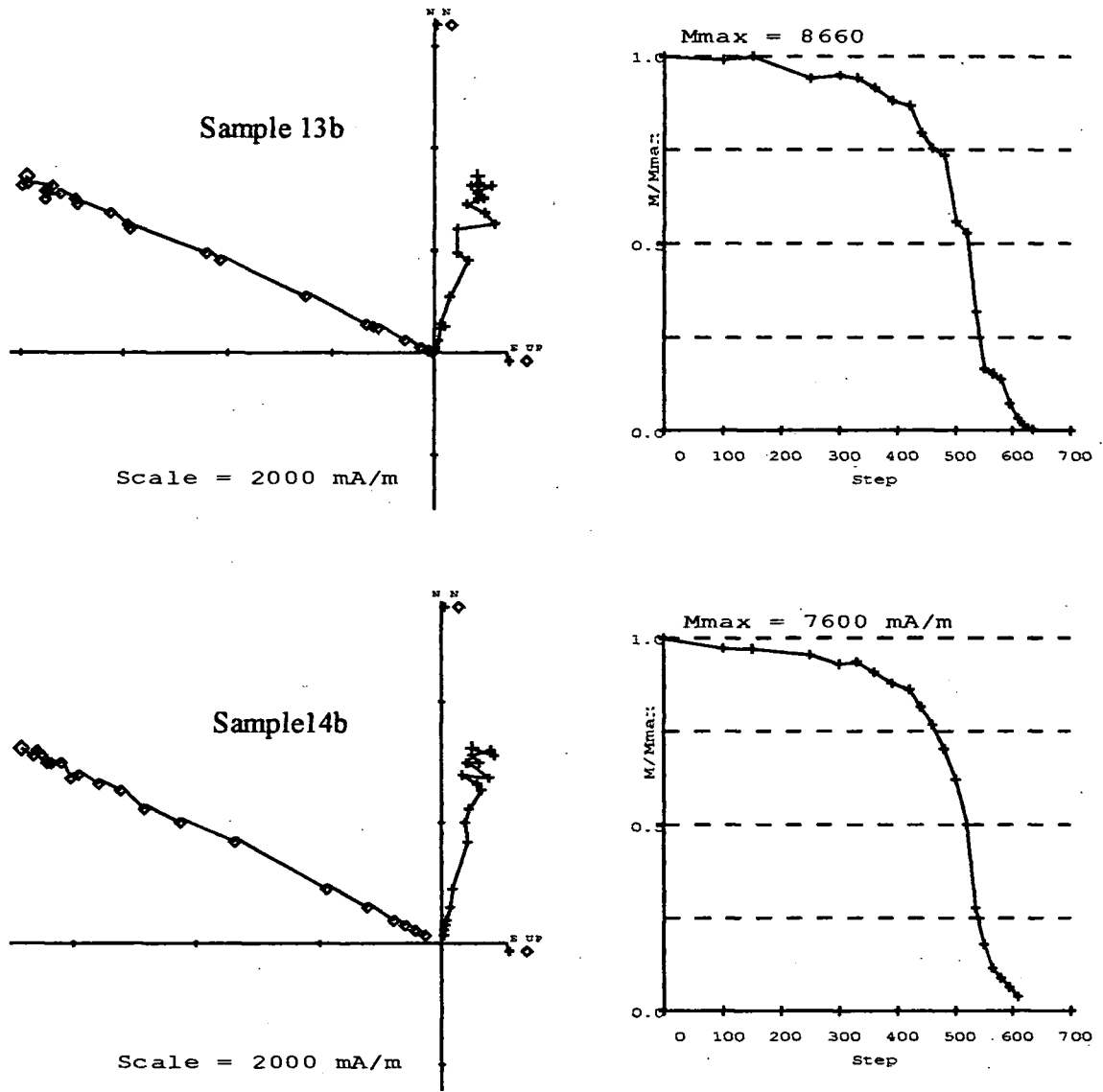
Fig. 5.10 - Site V37: Zijderveld diagrams and Intensity plots.

AD 79 - 1631 site V37

Sample P01

Steps	Dec	Inc	MAD
"D"420/595	16.7	64.4	1.3
"O"420/595	16.9	64.2	0.6
"D"550/595	13.5	64.9	1.0
"O"550/595	15.9	63.7	1.0

(a)

Sample P07A

Steps	Dec	Inc	MAD
"D"500/595	357.6	59.3	0.5
"O"500/595	357.5	59.4	0.4
"D"550/595	357.7	60.5	1
"O"550/595	357.7	59.7	0.6

(d)

Sample P05

Steps	Dec	Inc	MAD
"D"520/595	18.4	66.9	0.6
"D"520/595	18.5	66.5	0.5

(b)

Sample P07B

Steps	Dec	Inc	MAD
"D"480/550	354.6	59	0.9
"D"565/635	357.4	60.0	1.5
"O"565/635	357.8	58.8	1.5
"D"480/635 (*)	353.1	58.6	0.8
"O"480/635 (*)	353.3	58.4	0.6

(*) erasing steps 525,565°C   (e)

Sample P06

Steps	Dec	Inc	MAD
"D"520/595	1.5	61.9	0.6
"O"520/595	1.6	61.8	0.4

(c)

Sample P10A

Steps	Dec	Inc	MAD
"D"535/635	11.9	59.7	2.0
"O"535/635	11.4	60.4	1.6
"D"580/635	10.4	61.5	0.8
"O"580/635	9.7	61.5	0.6

(f)

Tab. 5.4 - Site V37: Directional results calculated using principal component analysis (Kirschvink, 1980).

AD 79 - 1631   site V37

Sample P10B			
Steps	Dec	Inc	MAD
"D"520/635	9.7	55.6	1.2
"O"520/635	9.5	55.9	1

(a)

Sample P13			
Steps	Dec	Inc	MAD
"D"580/635	14.0	65.5	0.9
"O"580/635	14.8	65.5	0.7
"D"535/635 (*)	14.7	65.6	1.0
"O"535/635 (*)	14.7	65.6	0.7

(*) erasing step 565°C   (c)

Sample P11			
Steps	Dec	Inc	MAD
"D"535/610	14.5	62.5	1.5
"O"535/610	14.2	62.8	0.7

(b)

Sample P14			
Steps	Dec	Inc	MAD
"D"550/610	12.2	63.6	1.2
"O"550/610	11.7	63.3	0.6
"D"480/610 (*)	11.0	64.9	0.4
"O"480/610 (*)	11.0	64.5	0.4

(*) erasing step 14(520)   (d)

Tab. 5.5 - Site V37: Directional results calculated using principal component analysis (Kirschvink, 1980).

Sample 03

Scale = 1000 mA/m

Mmax = 3660

Sample 04

Scale = 500 mA/m

Mmax = 3160 mA/m

Sample 06

Scale = 1000 mA/m

Mmax = 4050 mA/m
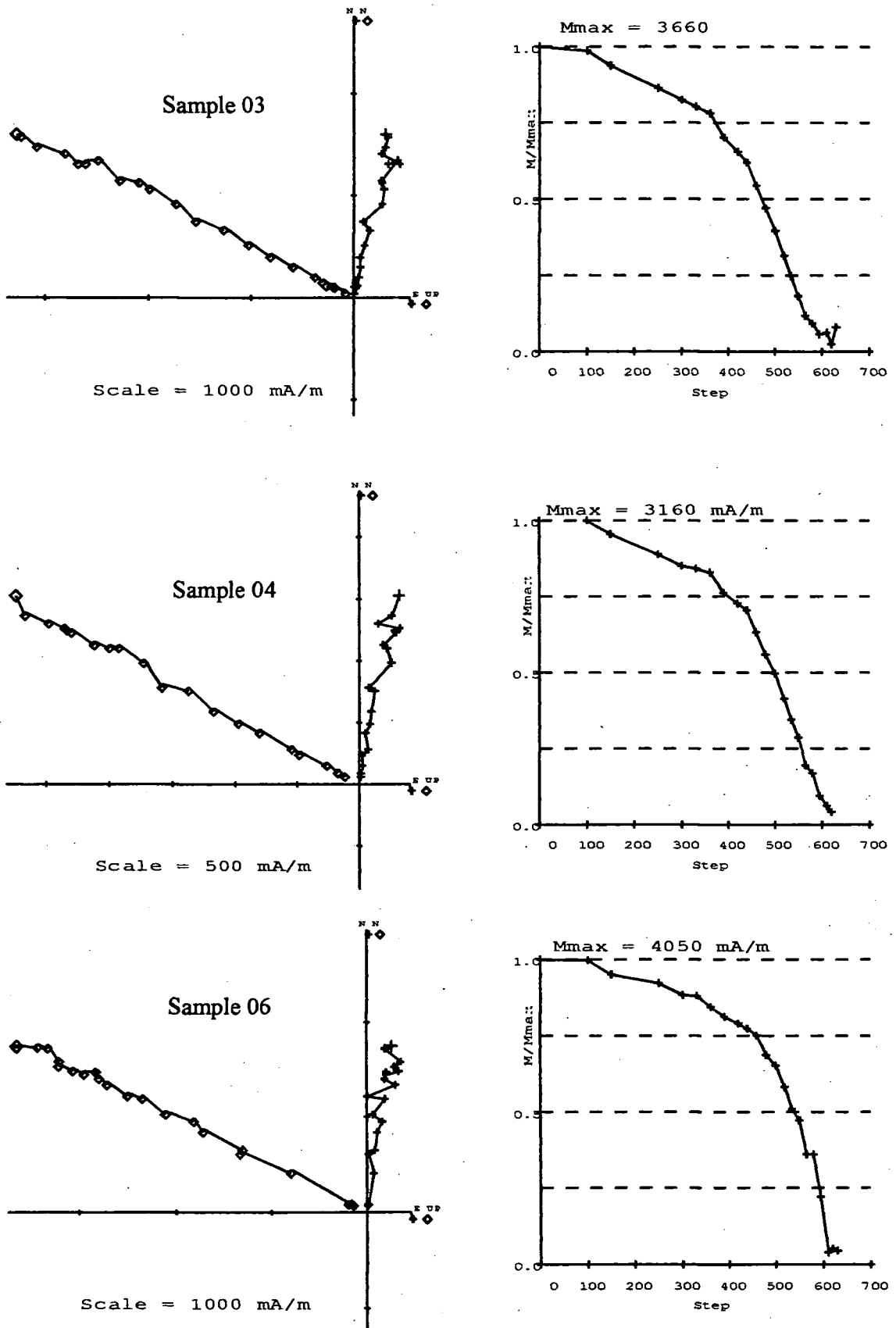
Fig. 5.11 - Site V27: Zijderveld diagrams and Intensity plots.

72

Sample 07

Scale = 1000 mA/m

Mmax = 5080

Sample 12

Scale = 1000 mA/m

Mmax = 5130 mA/m

Sample 13

Scale = 1000 mA/m

Mmax = 4050 mA/m
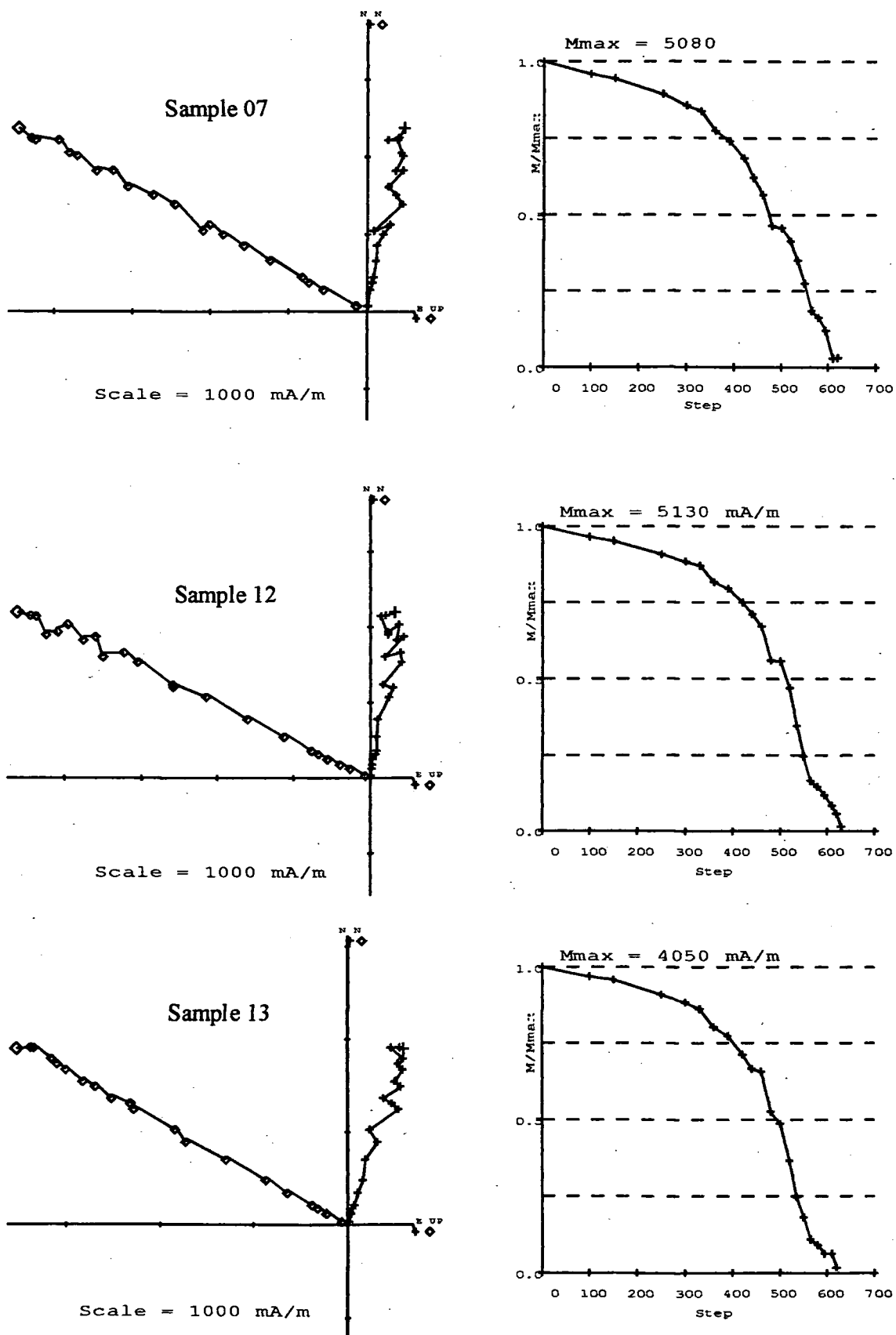
Fig. 5.12 - Site V27: Zijderveld diagrams and Intensity plots.

Sample P03			
Steps	Dec	Inc	MAD
"D" 500/620	13.0	62.4	1.8
"O" 500/620	12.3	62.5	1.1

(a)

Sample P07			
Steps	Dec	Inc	MAD
"D" 535/620	8.8	61.0	1.3
"O" 535/620	9.1	61.4	0.8

(d)

Sample P04			
Steps	Dec	Inc	MAD
"D" 520/620	9.1	63.3	2.0
"O" 520/620	9.3	62.8	1.1

(b)

Sample P12			
Steps	Dec	Inc	MAD
"D" 520/630	11.1	62.9	2.0
"O" 520/630	10.0	63.5	1.4

(e)

Sample P06			
Steps	Dec	Inc	MAD
"D" 550/630	6.9	63.5	1.0
"O" 550/630	7.7	63.4	0.7

(c)

Sample P13			
Steps	Dec	Inc	MAD
"D" 550/620	17.2	60.4	1.5
"O" 550/620	16.7	60.1	0.8

(f)

Tab. 5.6 - Site V27: Directional results calculated using principal component analysis (Kirschvink, 1980).

5.2.5 - Site V33

Premise

All 6 samples showed very anomalous behaviour during measurement. As it was observed that there was a little directional consistency, each measurement was repeated several times. Values were rejected when the measurement error was considered too high or when they started to behave randomly. This process did allow identification of some directions that had a similar direction. However, no consistency could be found above 500°C in most of the samples.

a) - Intensity Behaviour

Only sample 10 showed an unequivocal concave curve from 20 to 550°C, at which temperature the initial NRM (4110 mA/m) was completely demagnetized. All the other samples showed quite similar behaviour to each other and an initial NRM around 1800 mA/m (Fig. 5.13, 5.14). These showed a linear decrease, especially below 300°C, followed by an uncertain trend until the end, although a significant break point seemed to occur around 330-360°C in most samples.

b) – Directional Behaviour

Both the horizontal and vertical components showed a zigzag behaviour during demagnetization, especially at high temperature (> 400°C). Although some steps needed to be erased because of their poor definition, all samples showed a unique direction with a still acceptable value of MAD (< 5°). Sample 10 vectors had a curving trend. After detailed visual analysis, the vectors, showed a direction very similar to the others samples in the range 250-480°C (Tab. 5.7).

Sample 01

Scale = 200 mA/m

Mmax = 1710

Sample 02

Scale = 200 mA/m

Mmax = 1820 mA/m

Sample 03

Scale = 200 mA/m

Mmax = 1390 mA/m
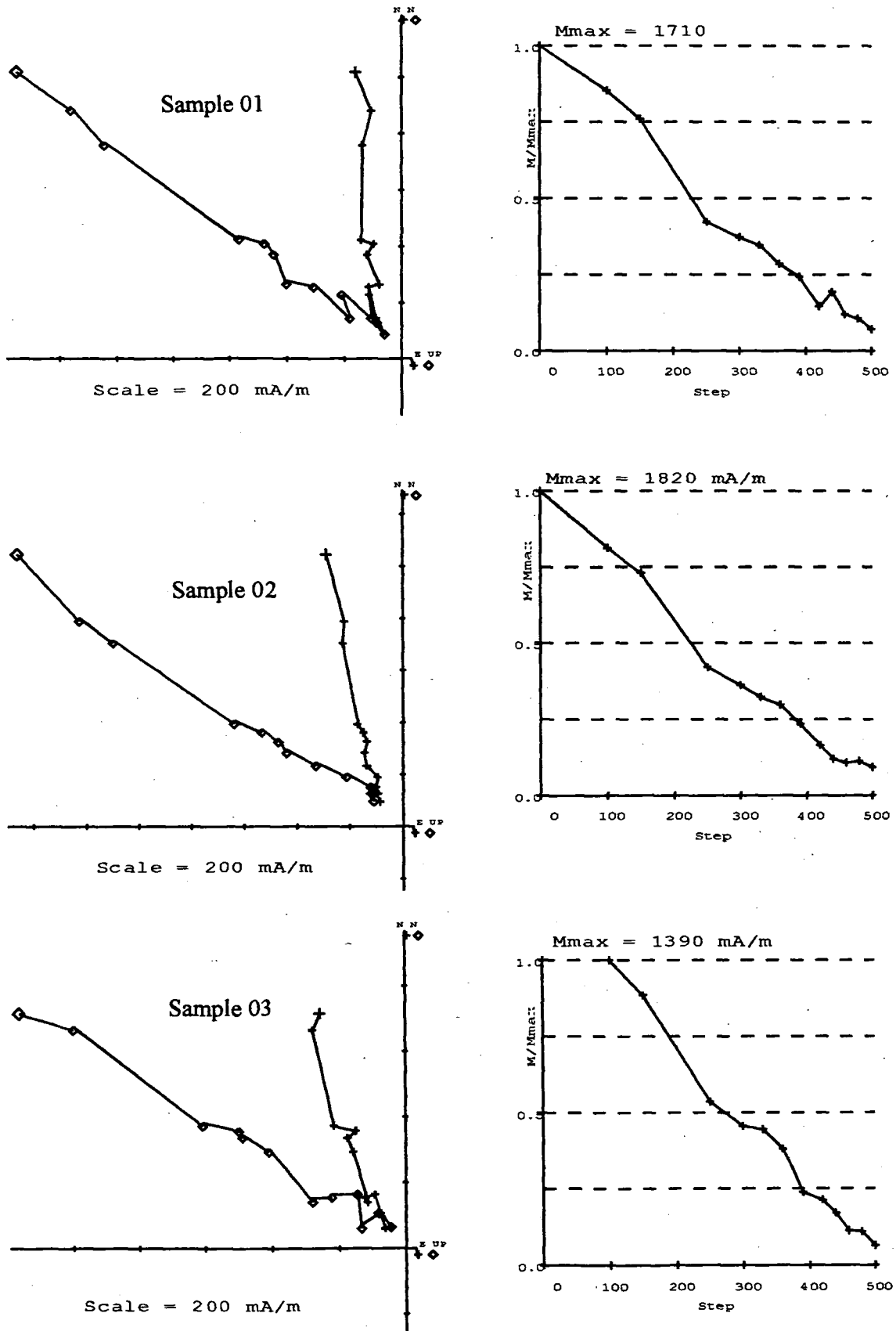
Fig. 5.13 - Site V33: Zijderveld diagrams and Intensity plots.
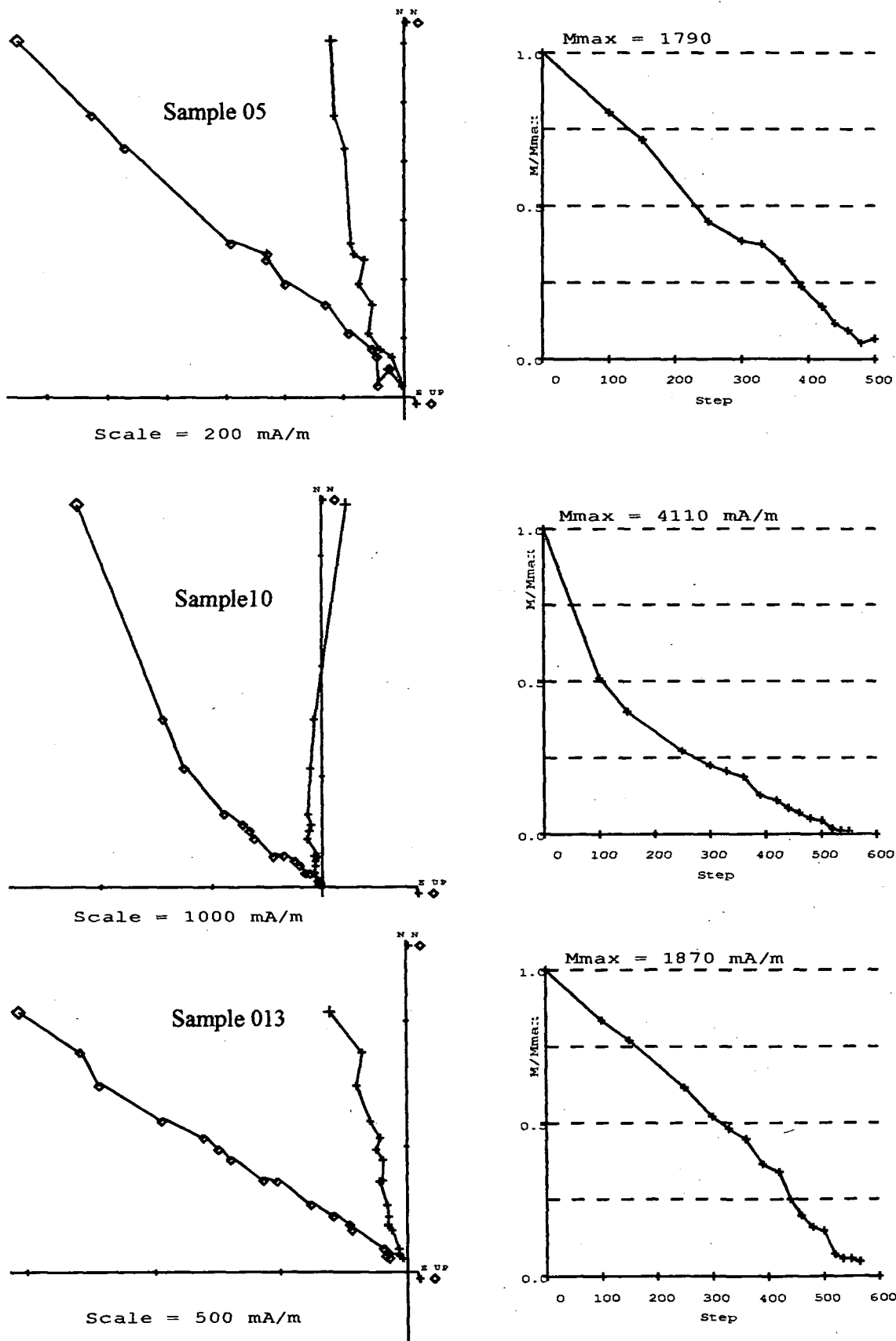
Fig. 5.14 - Site V33: Zijderveld diagrams and Intensity plots.

Sample P01			
Steps	Dec	Inc	MAD
"D" 20/420	356.8	53.6	3.2

(a)

Sample P05			
Steps	Dec	Inc	MAD
"D" 20/420	351.9	49.0	2.8

(d)

Sample P02			
Steps	Dec	Inc	MAD
"D" 100/440	348.5	59.0	2.6

(b)

Sample P10			
Steps	Dec	Inc	MAD
"D" 250/480	352.0	55.0	3.7

erasing step 390°C   (e)

Sample P03			
Steps	Dec	Inc	MAD
"D" 20/390	345.0	55.6	3.9

(c)

Sample P13			
Steps	Dec	Inc	MAD
"D" 300/565	349.5	57.9	2.9

(f)

Tab. 5.7 - Site V33: Directional results calculated using principal component analysis (Kirschvink, 1980).

5.2.6 - Site V26

a) - Intensity Behaviour

The initial NRM was around 2800 mA/m for all 6 samples. They showed the same behaviour over all the temperature spectra, except 07A, which had an increase in intensity between 20 and 100°C (Figs. 5.15, 5.16). A distinct convex curvature was always showed in the range 250-460°C followed by a quite linear decay until 565°C and terminating with a small tail at 580° where the initial remanence was completely demagnetized.

b) - Directional Behaviour

The 6 samples showed up to three different components. For example, sample 01 had a low temperature component in the range 100-360°C, a medium one between 390 and 460°C and the highest one between 460 and 560°C. All the other samples had the same high component while, the lowest one, was in the range 150 - 460°C.

The linear analyses of the vectors showed that the high temperature components did not always have the best definition but there was a good consistency between them. The same occurred for most of the medium components (Tab. 5.8).

5.2.7 - Site V31

a) - Intensity Behaviour

Sample 14 showed a very anomalous trend (Figs. 5.17, 5.18). A concave curve between 100 and 460°C and then, with increasing temperature, a linear decrease in intensity with a clear break at 520°C. At 620°C it was not completely demagnetized and showed a final steep decay, with no tail and some 7% of NRM still remained.

All the other samples showed a very similar behaviour to each other. Initial NRM was about 5000 mA/m and, by 620°C, was completely demagnetized. All the curves showed an accelerating decrease in intensity terminating with a small concave tail.

b) – Directional Behaviour

These 6 samples showed two completely different sets of behaviour. Samples 01, 06 and 08 had a quite clear single component that was very well defined, especially at high temperatures. The other 3 samples showed at least three different components, at different ranges of temperature, linked often with a curving trend.

The visual analyses of the vectors (Tab. 5.9) showed that the highest temperature component was almost identical to the one isolated from the first group of samples, but only in sample 11 was it well defined.

5.3 - AD 1697

5.3.1 - Site V28

a) - Intensity Behaviour

These 6 samples had an initial NRM around 8000 mA/m and, by 620°C, had been completely demagnetized, generally with a final small tail above 550°C (Figs. 5.19, 5.20). All the samples showed a very little decrease in intensity until 330°C followed by a rapid accelerating decrease with increasing temperature until the start of the final tail. A clear deflection occurred in the sample 02 at 480°C while, in samples 05 and 06, around the same temperature, it was poorly marked.

b) – Directional Behaviour

All the samples showed a very well defined high temperature component between 565 and 620°C. The vertical vector, in all the spectra, showed generally a better linear trend than the horizontal one which had a zigzag behaviour especially at low and medium temperatures.

The high temperature component analyses showed different groupings of declination values; samples 02, 05 and 06 showed declinations around 15°, 08 and 12 around 356° while

sample 11 declination had an intermediate value, 6°. The inclination was almost the same for all samples (Tab. 5.10).

5.3.2 - Site V29

Premise

For these 7 samples, slightly different steps of temperature were used than for other sites. It was the first site thermally demagnetized and therefore was used as a test. Later, in accordance with all the other experiments, different temperature settings were chosen.

a) - Intensity Behaviour

All the samples showed high initial NRM values of about 7500 mA/m and by 620°, were almost completely demagnetized. They showed an accelerating decrease in intensity starting from 150°C and terminating at 560°C, above which a little concave tail occurred. Minor deflections, at slightly different temperatures (425-460°C) were noticed in all the samples (Fig. 5.21, 5.22, 5.23).

b) – Directional Behaviour

Both vertical and horizontal vectors showed similar behaviour; a very linear trend throughout the medium and high temperatures and an unclear one at low temperatures. A more detailed analysis of the vectors showed a unique component for all the samples, except 03 that showed a slightly different component between 480-540°C.

The inclination value was almost identical for all the samples while the declination of the sample 13 was slightly different from all the others. It was noticed that the high temperature component of sample 13 was consistent with the medium one of the sample 03 (Tab. 5.11).

Sample 01

Mmax = 2550

Scale = 500 mA/m

Sample 03

Mmax = 3110 mA/m

Scale = 500 mA/m

Sample 04

Mmax = 2820 mA/m

Scale = 500 mA/m
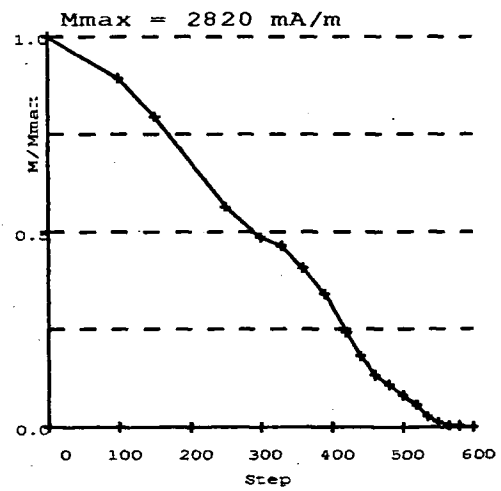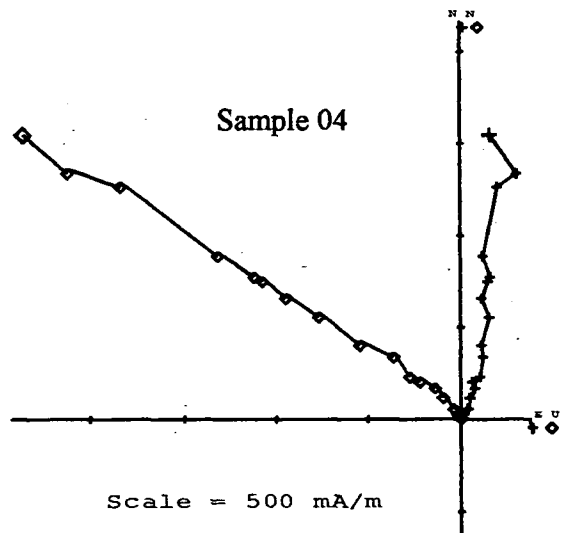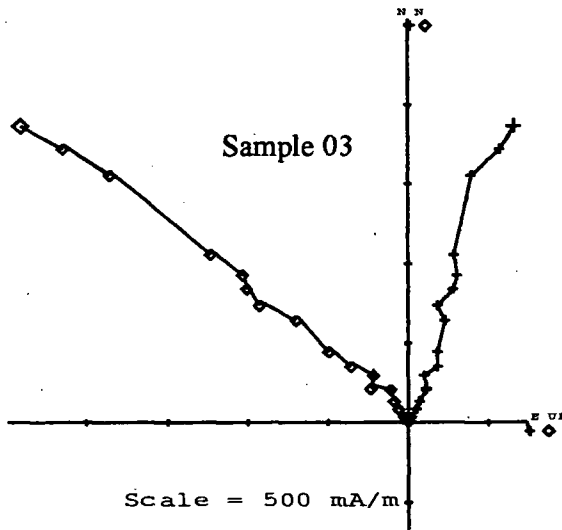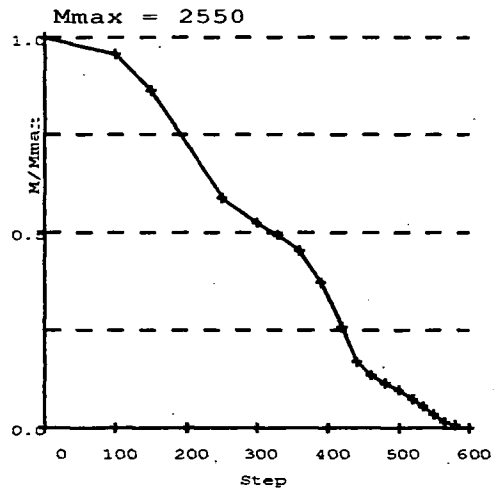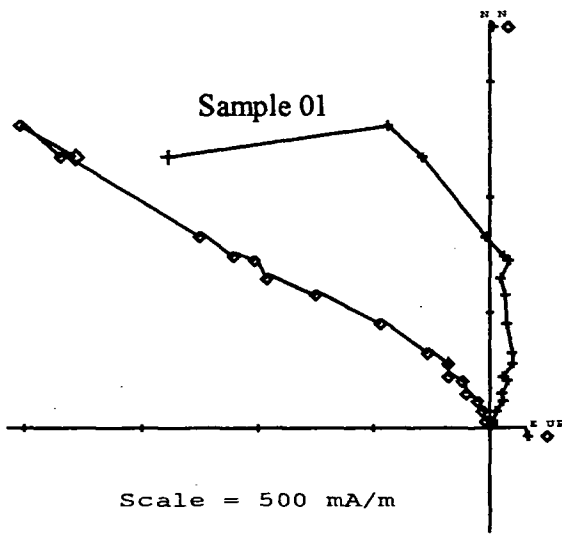
Fig. 5.15 - Site V26: Zijderveld diagrams and Intensity plots.

Sample 07a

Scale = 500 mA/m

Mmax = 2400

Sample 09a

Scale = 500 mA/m

Mmax = 2610 mA/m

Sample 10a

Scale = 500 mA/m

Mmax = 2820 mA/m
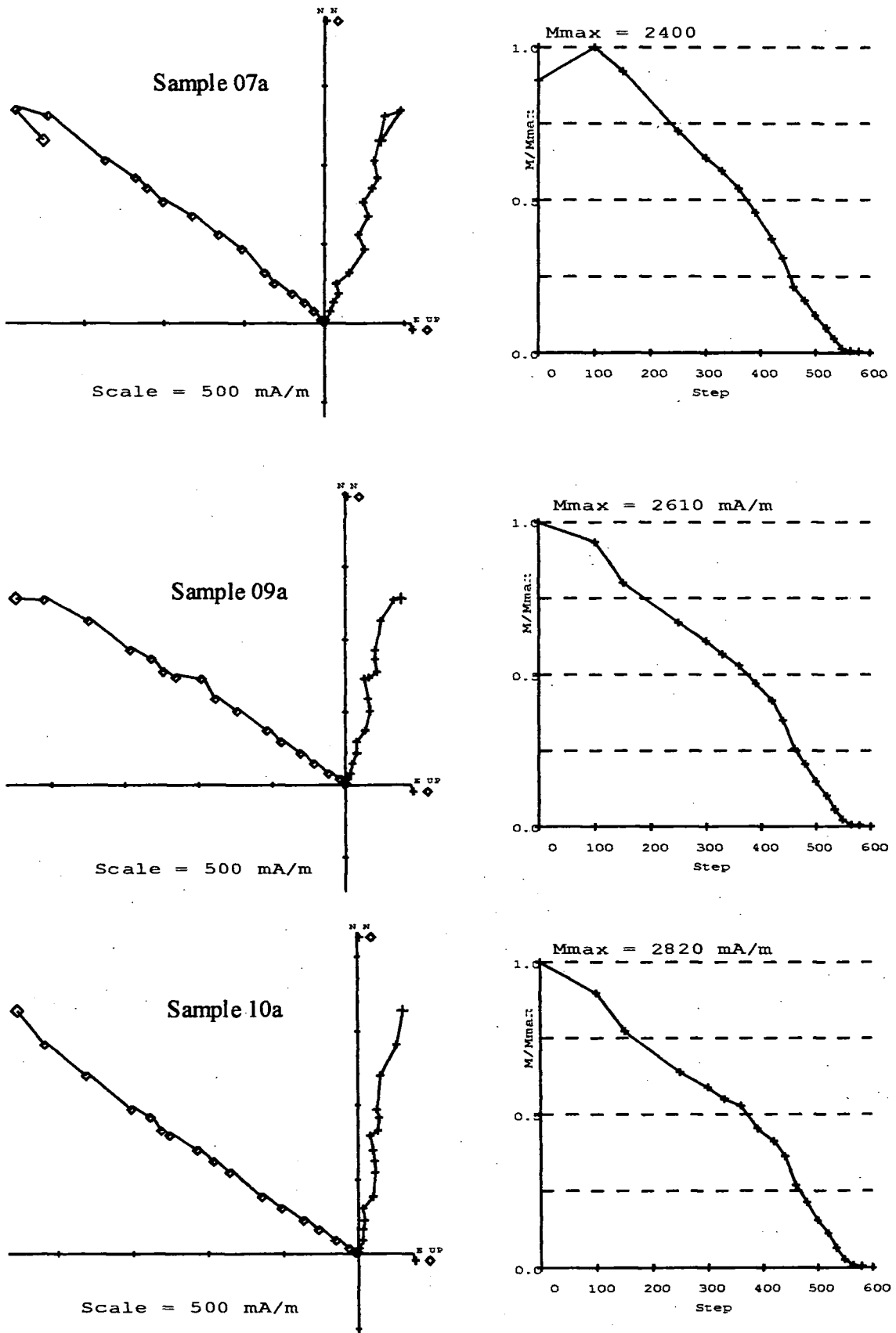
Fig. 5.16 - Site V26: Zijderveld diagrams and Intensity plots.

Sample 01			
Steps	Dec	Inc	MAD
"D" 460/565 (*)	18.4	32.2	5.8
"O" 460/565 (*)	19.8	29.9	3.3
"D" 390/460	353.5	62	2.1
"D" 100/360	321.5	52.6	3.7

(*) erasing steps 480,580°C   (a)

Sample 07A			
Steps	Dec	Inc	MAD
"D" 500/565 (*)	25.4	45	2.8
"O" 500/565 (*)	25.9	43	2.4
"D" 150/440	9.9	55.2	3.3

(*) erasing steps 580°C   (d)

Sample 03			
Steps	Dec	Inc	MAD
"D" 500/565 (*)	27.3	26.9	4.2
"O" 500/565 (*)	27.8	27.5	2.5
"D" 150/440 (**)	10.2	50.6	3.6

(*) erasing step 580°C   (b)
(**) erasing step 480°C

Sample 09A			
Steps	Dec	Inc	MAD
"D" 420/565 (*)	15.7	55.1	2.2
"O" 420/565 (*)	16.7	54.6	1.5
"D" 100/360	14.4	58	3.8
"D" 100/565 (**)	15	12.5	57.4
"O" 100/565 (**)	13.7	56.6	1.4

(*) erasing steps 580°C   (e)
(**) erasing steps 20,390,580°C

Sample 04			
Steps	Dec	Inc	MAD
"D" 500/565 (*)	21.5	39.1	3.8
"O" 500/565 (*)	24.2	36.8	3.4
"D" 150/500	11	5.5	57.3

(*) erasing steps 580°C   (c)

Sample 10A			
Steps	Dec	Inc	MAD
"D" 460/565 (*)	10.8	58.9	3.3
"O" 460/565 (*)	11.3	58.6	2
"D" 150/460	3.5	55.5	2.7

(*) erasing step 580°C   (f)

Tab. 5.8 - Site V26: Directional results calculated using principal component analysis (Kirschvink, 1980).

Sample 01

Mmax = 6070

Scale = 1000 mA/m

Sample 06

Mmax = 5100 mA/m

Scale = 1000 mA/m

Sample 08

Mmax = 5340 mA/m

Scale = 1000 mA/m

Fig. 5.17 - Site V31: Zijderveld diagrams and Intensity plots.

Sample 11

Scale = 1000 mA/m

Mmax = 4090

Sample 14

Scale = 1000 mA/m

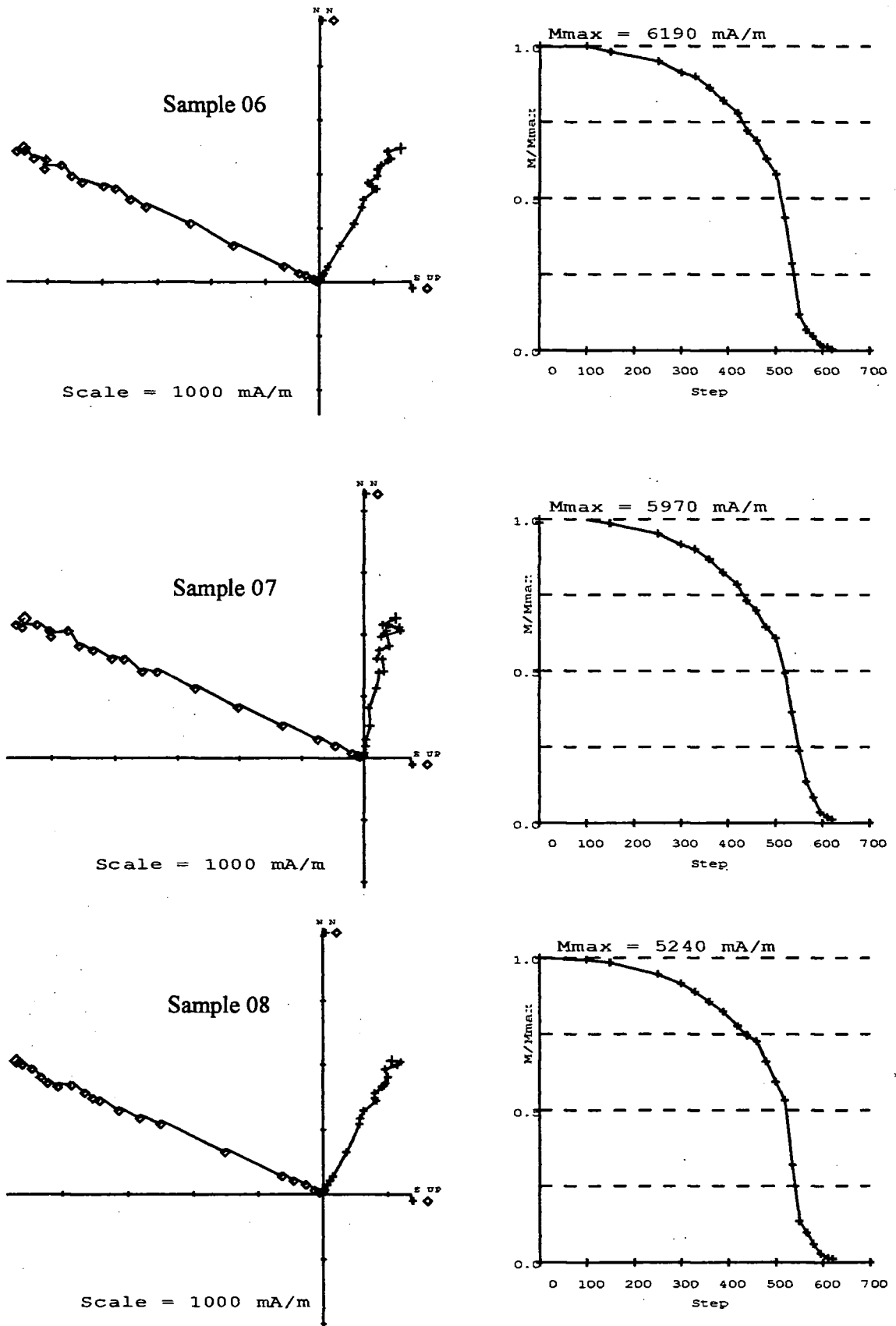Mmax = 6060 mA/m

Sample 16

Scale = 1000 mA/m

Mmax = 4470 mA/m
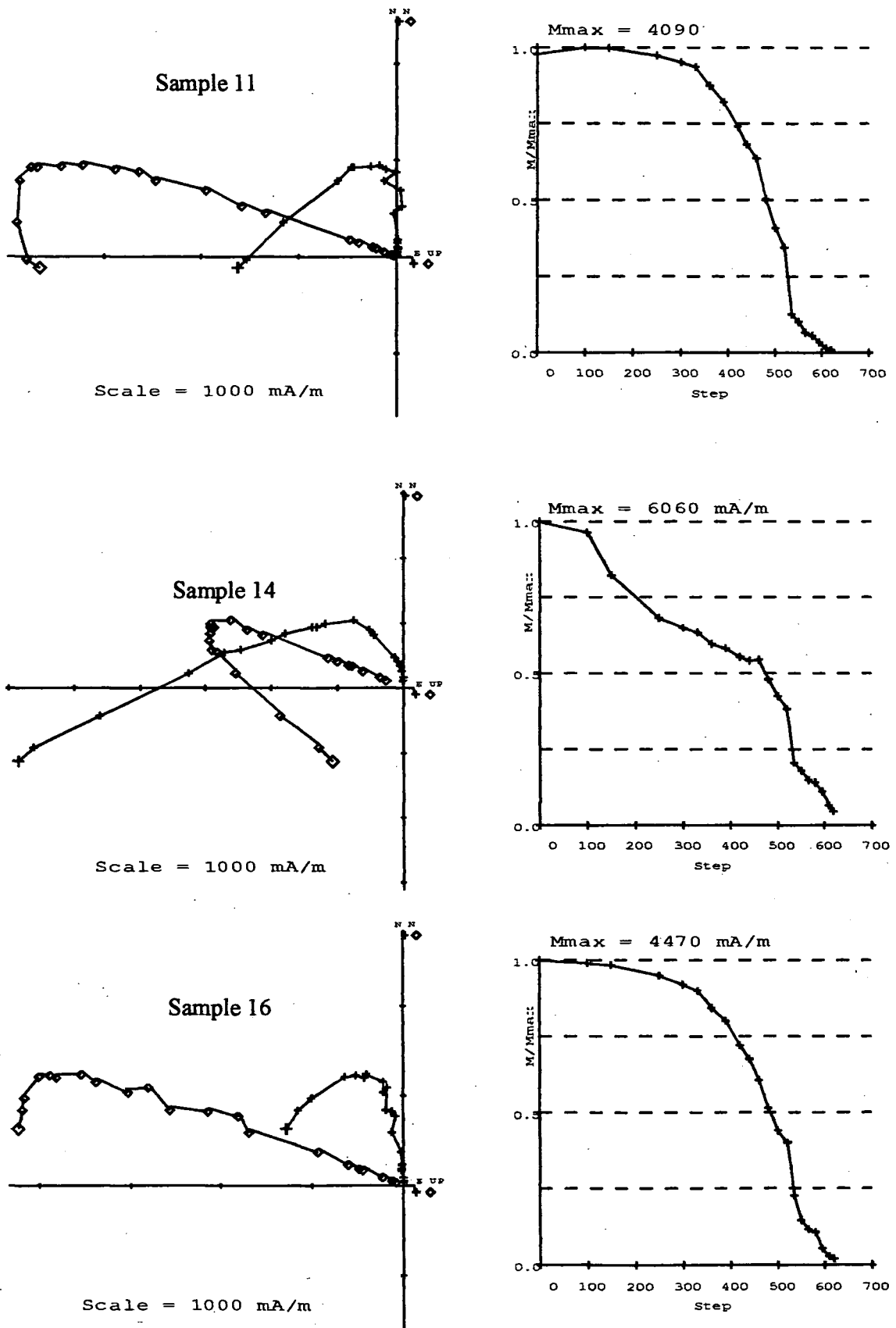
Fig. 5.18 - Site V31: Zijderveld diagrams and Intensity plots.

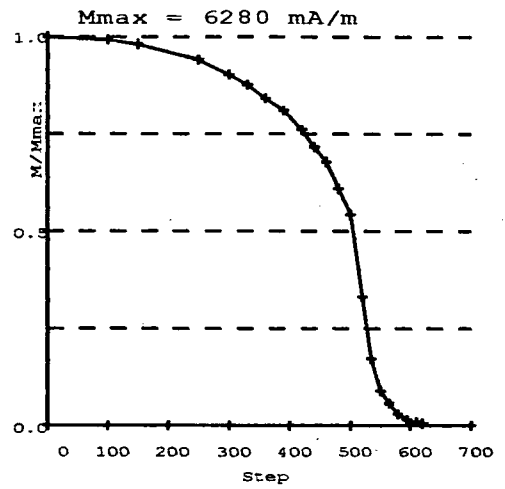| Sample 01			
Steps	Dec	Inc	MAD
"D" 535/620	17.8	65.7	0.6
"O" 535/620	17.8	65.4	0.5
"D" 330/440	8.9	59	2.5
"D" 300/620 (*)	14.6	65.1	1.6
"O" 300/620 (*)	15.3	65.2	1

(*) erasing steps 460°C   (a)

Sample 08			
Steps	Dec	Inc	MAD
"D" 520/620 (*)	9.8	64.4	0.4
"D" 330/620 (*)	9.5	64.1	1
"O" 330/620 (*)	9.8	64.1	0.6

(*) erasing steps 565°C   (c)

Sample 06			
Steps	Dec	Inc	MAD
"D" 520/620	13.1	61.9	0.6
"O" 520/620	14.2	61.3	1
"D" 360/620 (*)	13.9	60.8	1
"O" 360/620 (*)	14.2	60.7	0.7

(*) erasing step 500°C   (b)

Sample 11			
Steps	Dec	Inc	MAD
"D" 580/620	10.4	66.8	1
"O" 580/620	10.5	66	0.8

(d)

Tab. 5.9 - Site V31: Directional results calculated using principal component analysis (Kirschvink, 1980).

Fig. 5.19 - Site V28: Zijderveld diagrams and Intensity plots.

Sample 08
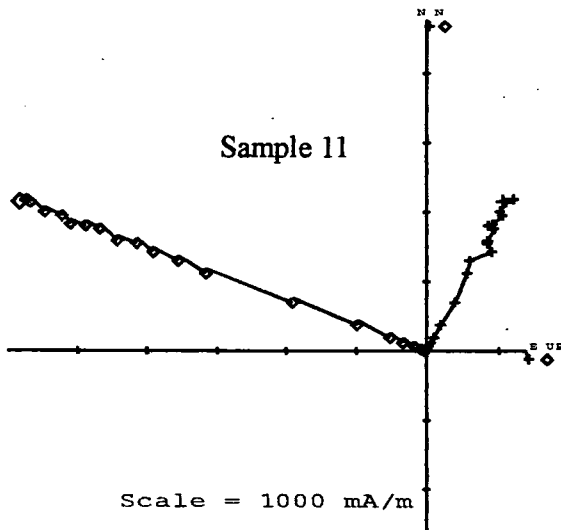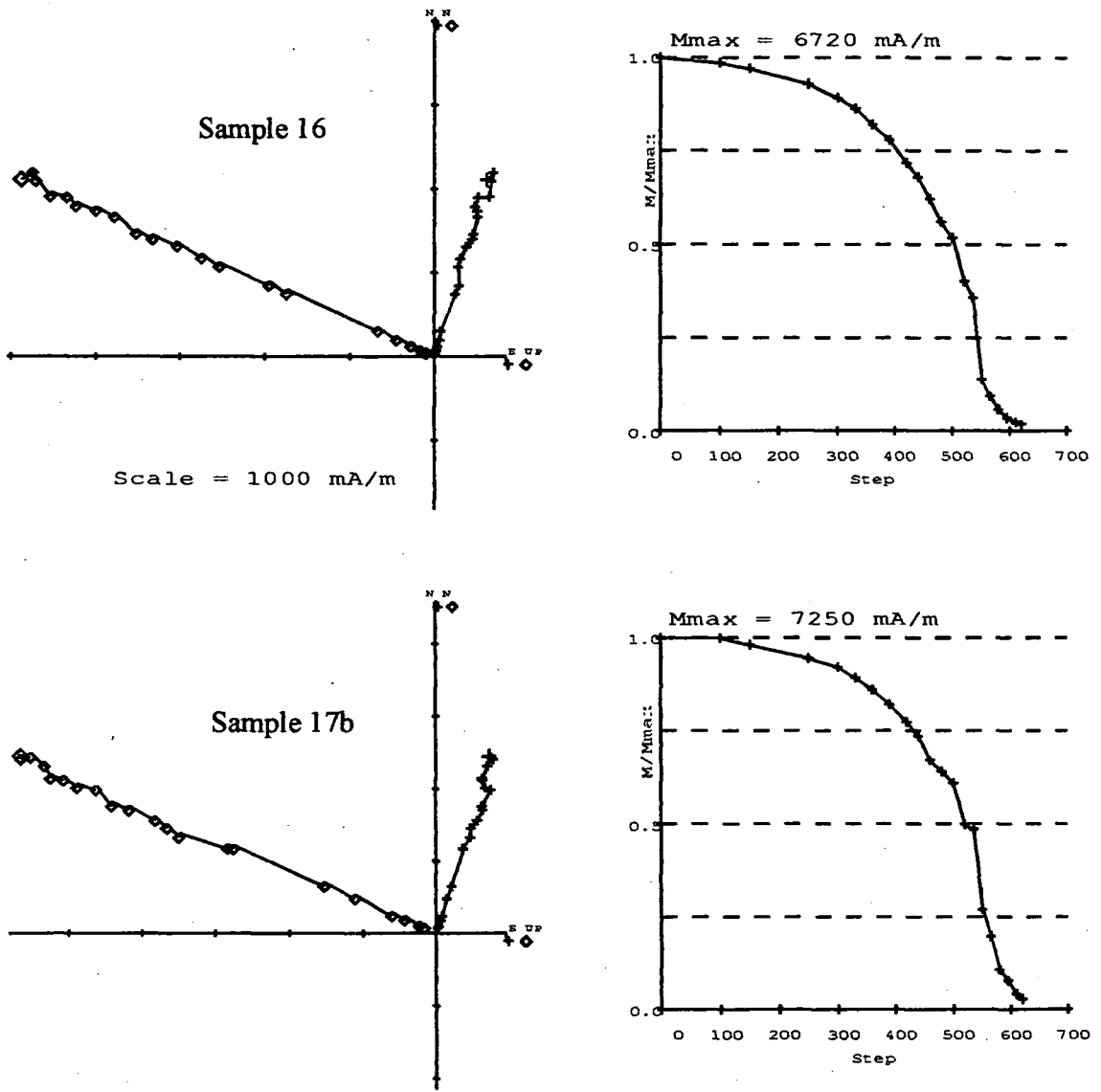
Scale = 2000 mA/m

Mmax = 7720 mA/m

Sample 11

Scale = 2000 mA/m

Mmax = 8620 mA/m

Sample 12

Scale = 1000 mA/m

Mmax = 8100 mA/m

Fig. 5.20 - Site V28: Zijderveld diagrams and Intensity plots.

AD 1697   site V28

Sample 02			
Steps	Dec	Inc	MAD
"D" 535/620	15.5	56.6	0.4
"O" 535/620	15.6	56.4	0.3
"D "250/535	16.8	54.4	7

(a)

Sample 08			
Steps	Dec	Inc	MAD
"D" 595/620	359.3	59.5	1.1
"O" 595/620	358.6	59.3	0.5
"D" 500/565	356	60.2	0.7

(d)

Sample 05			
Steps	Dec	Inc	MAD
"D" 580/620	18.3	62.2	0.4
"O" 580/620	18.9	61.6	0.5
"D" 440/535	16.6	59.9	4

(b)

Sample 11			
Steps	Dec	Inc	MAD
"D" 565/620	7	60	1
"O" 565/620	6.8	60	0.6
"D" 20/620	6	59.8	2.2
"O" 20/621	6	59.9	1.1

(e)

Sample 06			
Steps	Dec	Inc	MAD
"D" 580/620	11.2	62.7	1.2
"O" 580/620	12	61.9	0.8
"D" 480/550	12.7	61.2	1.5

(c)

Sample12			
Steps	Dec	Inc	MAD
"D"580/620	356.8	63.9	0.3
"D"580/620	356.6	63.6	0.2
"D"520/580	355.7	65.3	1
"D"520/620	355.7	65.1	0.8
"D"520/620	355.7	64.8	0.6

(f)

Tab. 5.10 - Site V28: Directional results calculated using principal component analysis (Kirschvink, 1980).

90

AD 1697 site V29

Sample 03

Scale = 1000 mA/m

Mmax = 7490 mA/m

Sample 04B

Scale = 1000 mA/m

Mmax = 6210 mA/m

Sample 05

Scale = 2000 mA/m

Mmax = 6040 mA/m

Fig. 5.21 - Site V29: Zijderveld diagrams and Intensity plots.

91

Sample 09

Scale = 2000 mA/m

Mmax = 8370 mA/m

Sample 13

Scale = 1000 mA/m

Mmax = 7730 mA/m

Fig. 5.22 - Site V29: Zijderveld diagrams and Intensity plots.

Sample 14

Scale = 1000 mA/m

Mmax = 7500 mA/m

Sample 15

Scale = 1000 mA/m

Mmax = 7700 mA/m

Fig. 5.23 - Site V29: Zijderveld diagrams and Intensity plots.

Sample03			
Steps	Dec	Inc	MAD
"D" 540/620	12.7	58.2	0.4
"O" 540/620	12.8	58.2	0.3
"D" 480/540	9.4	57.5	1.3
"D" 20/620	11.6	56.8	2
"O" 20/620	11.7	57.2	0.8

(a)

Sample 13			
Steps	Dec	Inc	MAD
"D" 500/620	8.2	53.3	0.7
"O" 500/620	8.2	53.5	0.5
"D" 440/620 (*)	7.9	53.6	0.6
"O" 440/620 (*)	8	53.7	0.4

(*) erasing steps 580°C   (e)

Sample 04			
Steps	Dec	Inc	MAD
"D" 400/620	15.2	56.7	0.6
"O" 400/620	15.3	56.7	0.3

(b)

Sample 14			
Steps	Dec	Inc	MAD
"D" 480/620	14.8	58	0.5
"O" 480/620	15	58.2	0.4
"D" 400/620 (*)	15.2	58.6	0.7
"O" 400/620 (*)	15.3	58.6	0.5

(*) erasing step 580°C   (f)

Sample 05			
Steps	Dec	Inc	MAD
"D" 500/620	14.3	56.1	0.5
"O" 500/620	14.5	56.2	0.4

(c)

Sample 09			
Steps	Dec	Inc	MAD
"D" 480/620 (*)	19	57.7	0.6
"O" 480/620 (*)	19.2	57.8	0.5
"D" 20/620	18.6	57.8	2.1
"O" 20/620	19	58	1

(*) erasing steps 610°C   (d)

Sample 15			
Steps	Dec	Inc	MAD
"D" 520/580	18.4	58.4	0.9
"O" 520/580	18.3	59.2	0.8
"D" 20/620	18.5	60.2	2.6
"O" 20/620	18.7	60.1	1

(g)

Tab. 5.11 - Site V29: Directional results calculated using principal component analysis (Kirschvink, 1980).

5.4 - AD 1714/(1906?)
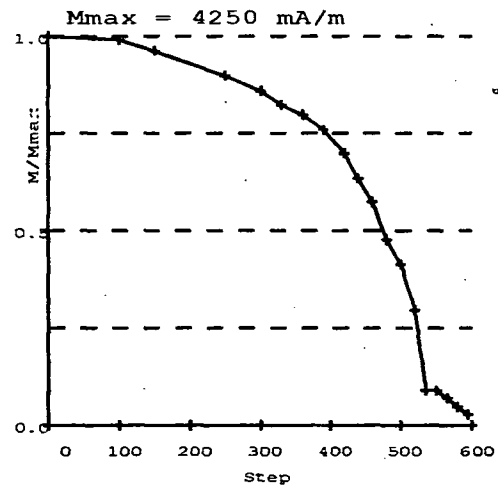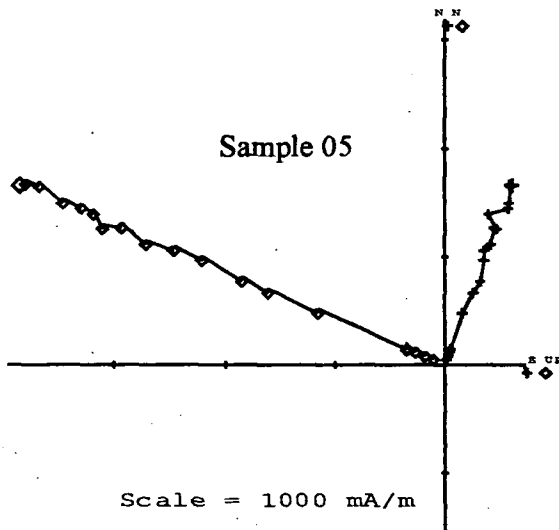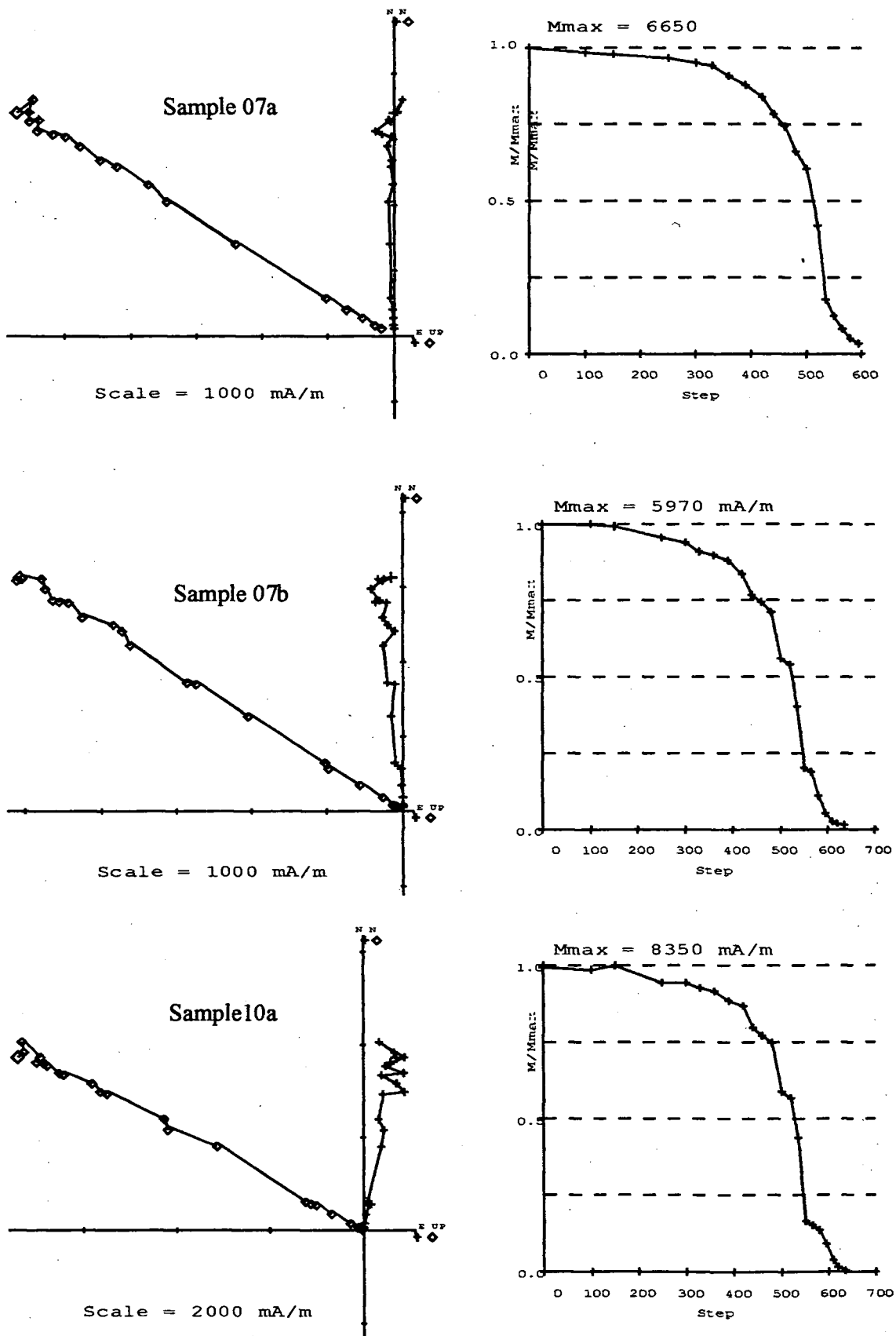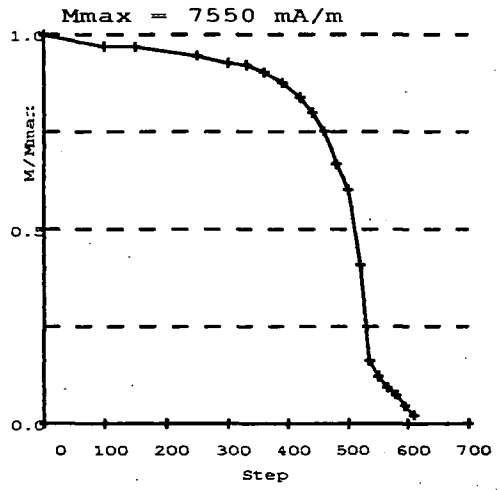
5.4.1 - Site V38

a) - Intensity Behaviour

All these 8 samples had an initial NRM around 5000mA/m and showed an accelerating decrease in intensity starting from 250-300°C, terminating around 580°C with an almost linear tail (except for samples 11A and 12B that showed a concave tail) until 620-630°C (Figs. 5.24, 5.25, 5.26).

Some samples showed minor irregularities around 330-360°C but all of them showed a clear deflection around 460-480°C. Sample 09A had an increase in intensity at 520°C.

b) – Directional Behaviour

Samples 09A and 07A had a very unclear trend, especially for the horizontal vector, and only a very high temperature component could be isolated by visual analyses. All the other sample vectors showed a similar behaviour to each other with a clear and unique component starting from 480-520°C.

Both declinations and inclinations were very consistent for all the samples (Tab. 5.12).

5.5 - AD 1754

5.5.1 - Site V39

a) - Intensity Behaviour

These 8 samples showed mainly a similar behaviour: an initial NRM around 5000 mA/m, an accelerating decrease in intensity starting around 300°C then, around 550°C, a tail with a generally linear trend, but sometimes concave.

Minor irregularities occurred in all the sample vectors around 360-420°C while a deflection occurred around 480°C for 04A, 05A and 06A (Figs. 5.27, 5.28, 5.29).

b) – *Directional Behaviour*

These samples showed two slightly different components, except sample 01A. A medium component between 440-500°C and 550-565°C, and a higher one between 565 and 610-630°C.

The linear analyses of the vectors showed that the high temperature component was not always the best defined but there was a good consistency between them. The same occurred for most of the medium components (Tab. 5.13).

At the highest temperature (610 to 630°C) all samples (except 05A and 06B) had both the declination and inclination values moving away from the main value.

5.5.2 - Site V40

a) - Intensity Behaviour

These 8 samples had an initial NRM around 4000 mA/m and, by 620-630°C, had been completely demagnetized, generally with a little final concave tail above 550°C (Figs. 5.30, 5.31, 5.32). All the samples (except 06A, 011A and 013A) showed an almost linear decrease in intensity with two clear breaks (420°C and 535°C) in the rate of decrease. The exceptional samples, mentioned above, had accelerating decreases in intensity with increasing temperature, starting around 300°C, although they showed minor deflections around the temperatures as the above mentioned breaks. The same deflections occurred in 06A and 12A around 565-580°C, probably indicating a significant unblocking.

b) – Directional Behaviour

In almost all the samples the horizontal vector showed a zigzag trend until 500-520°C, while the vertical vector was linear over all the temperature steps. Above 500-520°C, the visual analyses showed a quite well defined component with declination and declination values very similar for all the samples (Tab. 5.14).

At the highest temperature (620 to 640°C) all samples (except 06A and 11A) had both the declination and inclination values moving away from the main value.

5.5.3 - Site V41

a) - Intensity Behaviour

These 8 samples had an initial NRM around 6-7000 mA/m and, by 620°C, had been completely demagnetized, generally with a final little tail above 550°C (Figs. 5.33, 5.34, 5.35). All the samples showed a minor decrease in intensity until 330°C, followed by a rapid accelerating decrease until the start of the final tail.

A clear anomaly occurred in all the samples around 535-550°C, while minor irregularities occurred in different samples at different steps of temperature.

b) – Directional Behaviour

All the samples showed a very well defined high temperature component between 460/520 and 620°C. Both the vertical and the horizontal vector, showed a very linear trend for all the samples, whit a zigzag behaviour only at low temperatures. Samples 11A and 12A had the same clear irregularity at 550°C.

The high temperature component analyses showed a unique group of declination and inclination values with a very small MAD in all the samples (Tab. 5.15).

5.6 - AD 1760

5.6.1 - Site V32

a) - Intensity Behaviour

Samples 01 and 03 behaved quite differently from the other 4 samples. They had a lower initial NRM (4000 mA/m), two linear decreases in intensity with a clear break at 250°C and a

very significant deflection at 460°C indicating an important unblocking temperature. Neither showed a final tail and there was some NRM (~7%) remaining.

The other samples had a higher initial NRM (7000 mA/m). They showed a very small decrease in intensity until 300° followed by an accelerating decrease until 535°, from which temperature a little tail started (except 11 and 12 that had no evidence of it). Some minor irregularities occurred at 360, 460 and 550°C. (Figs. 5.36, 5.37)

b) – Directional Behaviour

All the samples behaved very similarly (Tab. 5.16). They showed a linear trend over the medium and high temperature range (especially the vertical vector) starting usually around 250-300°C. A few breaks in the trend occurred around the same temperatures as the above mentioned irregularities.

5.6.2 - Site V34

a) - Intensity Behaviour

Samples 01, 02, 03 and 04 showed a slightly different behaviour from the other two. In fact they had a higher initial NRM (3500 mA/m) and showed an accelerating decrease in intensity starting around 330°C with a clear deflection (especially 01 and 02) at 420°C.

Samples 06 and 11 had the initial NRM respectively of 3000 and 2500 mA/m. They showed a quite linear decay from 20°C and about 390°C showed a small accelerating decrease in intensity until 500°C. Minor irregularities occurred at 300 and 460°C.

All the samples showed a very small tail starting around 535-550°C. At highest temperature (550 to 580°C) samples (except 06, 11 and 04) had both the declination and inclination values moving slightly away from the main value (Figs. 5.38, 5.39).

b) – Directional Behaviour

Both vertical and horizontal vectors showed similar behaviour; a very linear trend throughout the medium and high temperatures, especially for the vertical component, and an unclear one at low temperatures. A detailed analysis of the vectors showed a unique component for all the samples with a very low MAD (Tab. 5.17).

5.6.3 - Site V35

a) - Intensity Behaviour

All these 11 samples showed a very similar behaviour (Figs. 5.40, 5.41, 5.42, 5.43). Starting from an initial NRM value of 3500 mA/m, by 620°C they had been almost completely demagnetized (<2°). No significant decrease in intensity was seen until 250°C, while an accelerating decrease started at that temperature until 535-550°. A final small linear tail was present.

Some minor irregularities occurred around 420 and 535°C in almost all the samples while an anomalous increase in intensity occurred at 500°C only in sample 05.

b) – Directional Behaviour

All the samples showed a very well defined high temperature component usually between 500 and 620°C. Both the vertical and horizontal vectors showed an unclear behaviour at lowest temperatures but a very linear trend above 500°C.

The high temperature component analyses showed a very good consistency in declination and inclination values with a MAD often below 1° in all the samples (Tab. 5.18).

99

Sample 01a

Scale = 1000 mA/m

Mmax = 4960 mA/m

Sample 03a

Scale = 1000 mA/m

Mmax = 5350 mA/m

Sample 05a

Scale = 1000 mA/m

Mmax = 5640 mA/m
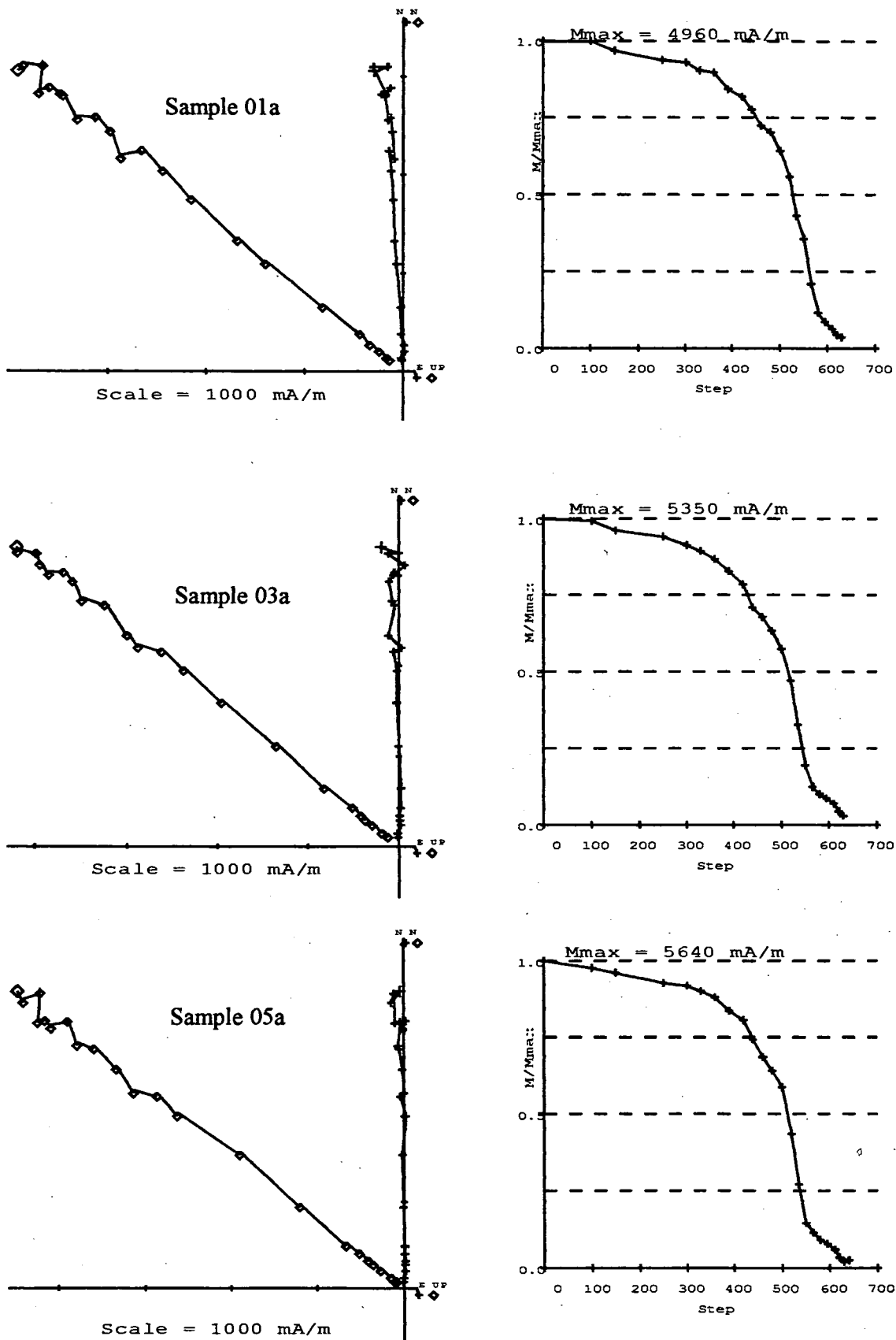
Fig. 5.24 - Site V38: Zijderveld diagrams and Intensity plots.

Fig. 5.25 - Site V38: Zijderveld diagrams and Intensity plots.

Mmax = 5630 mA/m

Sample 011b

Scale = 1000 mA/m

Mmax = 5420 mA/m

Sample 12b

Scale = 1000 mA/m
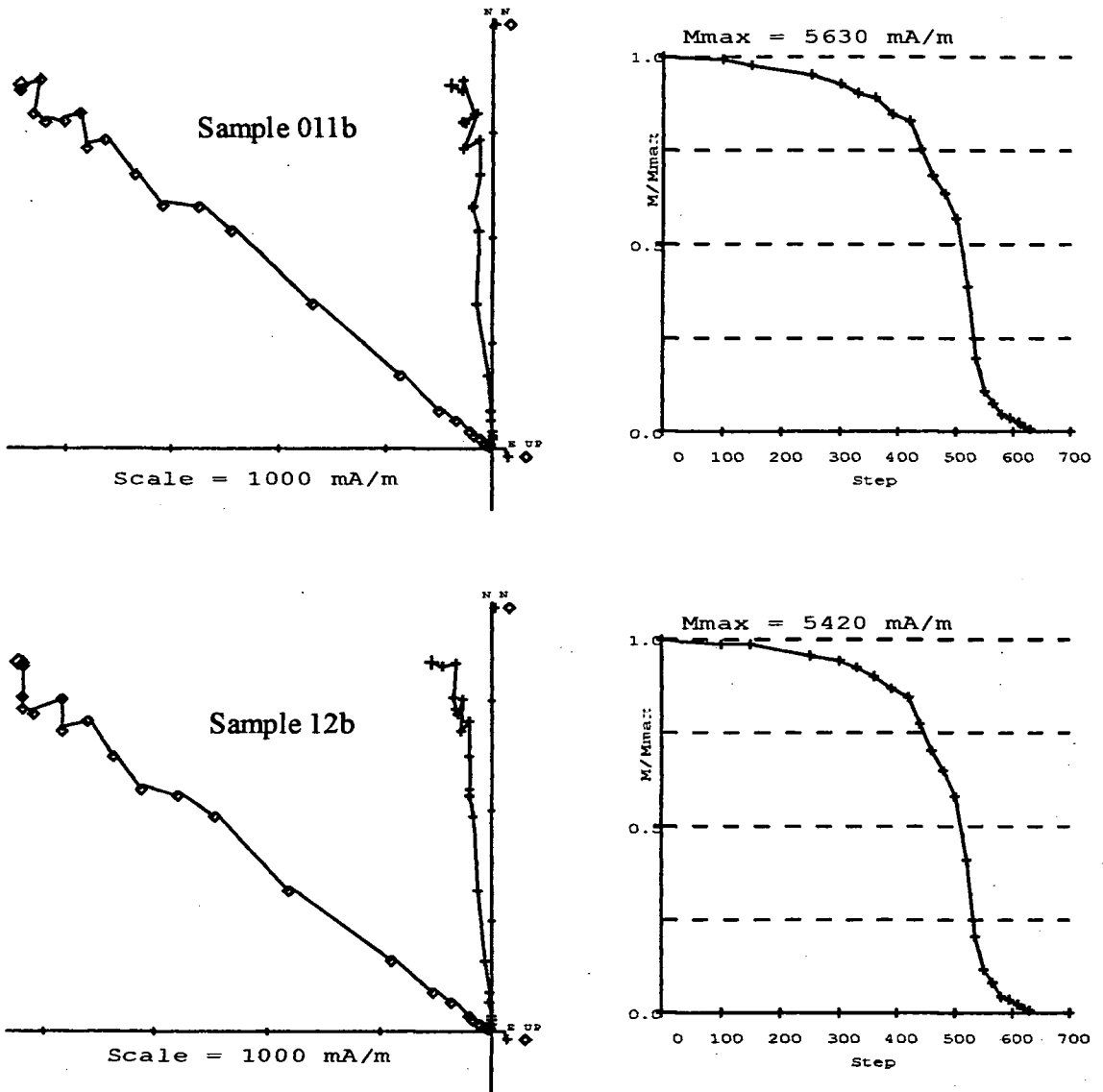
Fig. 5.26 - Site V38: Zijderveld diagrams and Intensity plots.

AD 1714(1906) site V38

Sample 01

Steps	Dec	Inc	MAD
"D" 20/630	356	51.2	2.2
"O" 20/630	356.4	51.2	1.1
"D" 480/535	356.5	46.8	1.1
"D" 535/580	355.8	52.8	0.9
"D" 480/630 (*)	356.6	50.3	1.3
"O" 480/630 (*)	356.6	50.6	0.8
"D" 550/630 (*)	357.2	52.2	1.3
"O" 550/630 (*)	356.8	51.6	1
"D" 480/630	356.3	50.3	1.3
"O" 480/630	356.6	50.6	0.9

(*) erasing steps 595,610°C　　　　　(a)

Sample 07

Steps	Dec	Inc	MAD
"D" 20/610	359.9	52	2.9
"O" 20/610	358.4	52.4	1.5
"D" 520/610 (*)	356.6	53.3	1
"O" 520/610 (*)	356.1	53	0.8

(*) erasing steps 535,565°C　　　　　(d)

Sample 08

Steps	Dec	Inc	MAD
"D" 565/630	359.3	51	2.4
"O" 565/630	357.5	51.3	1.4
"D" 500/565	354.2	48.9	1.7

(e)

Sample 03

Steps	Dec	Inc	MAD
"D" 20/630	358.5	51.5	1.9
"O" 20/630	358.9	51.4	1.1
"D" 480/630	358.7	50.6	0.9
"O" 480/630	359.2	50.7	0.7
"D" 480/550	357.5	50	0.7
"D" 565/610	358.6	48	3

(b)

Sample 09

Steps	Dec	Inc	MAD
"D" 565/620	352.6	52.2	0.7
"O" 565/620	352.5	52.1	0.5

(*) erasing steps 580°C　　　　　(f)

Sample 11

Steps	Dec	Inc	MAD
"D" 480/630	355.3	49.9	1.1
"O" 480/630	355.6	50.2	0.9
"D" 480/550	355.2	49.1	1.3

(g)

Sample 05

Steps	Dec	Inc	MAD
"D" 20/630	358.7	52.6	2
"O" 20/630	359.1	52.6	1.1
"D" 480/630	359.4	52.1	1.2
"O" 480/630	359.7	52.1	0.9

(c)

Sample 12

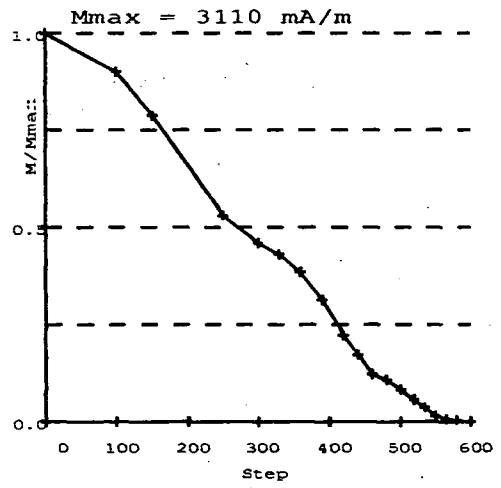| Steps	Dec	Inc	MAD
"D" 520/630	354.3	54.6	0.8
"O" 520/630	354.7	54.8	0.7
"D" 520/630 (*)	354.2	54.6	0.8
"O" 520/630 (*)	354.7	54.8	0.6

(*) erasing steps 610,620°C　　　　　(h)

Tab. 5.12 - Site V38: Directional results calculated using principal component analysis (Kirschvink, 1980).

Sample 01a

Mmax = 5150 mA/m

Scale = 1000 mA/m

Sample 04a

Mmax = 4280 mA/m

Scale = 1000 mA/m

Sample 05a

Mmax = 4140 mA/m

Scale = 1000 mA/m

Fig. 5.27 - Site V39: Zijderveld diagrams and Intensity plots.

Sample 06a

Mmax = 4760 mA/m

Scale = 1000 mA/m

Sample 06b

Mmax = 5590 mA/m

Scale = 1000 mA/m

Sample 09a

Mmax = 4920 mA/m

Scale = 1000 mA/m

Fig. 5.28 - Site V39: Zijderveld diagrams and Intensity plots.

Sample 011a

Mmax = 5200 mA/m

Scale = 1000 mA/m

Sample 014a

Mmax = 5150 mA/m

Scale = 1000 mA/m
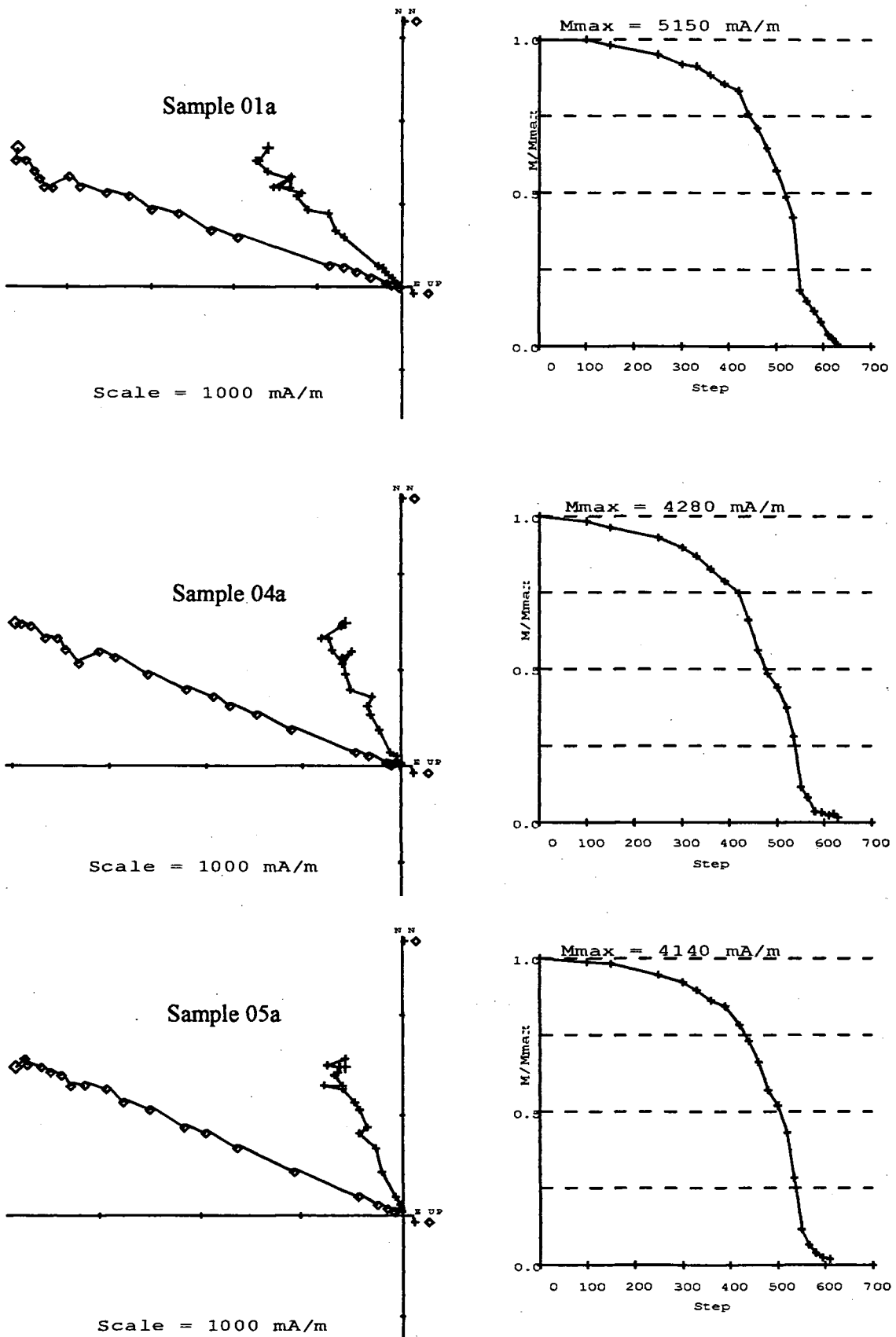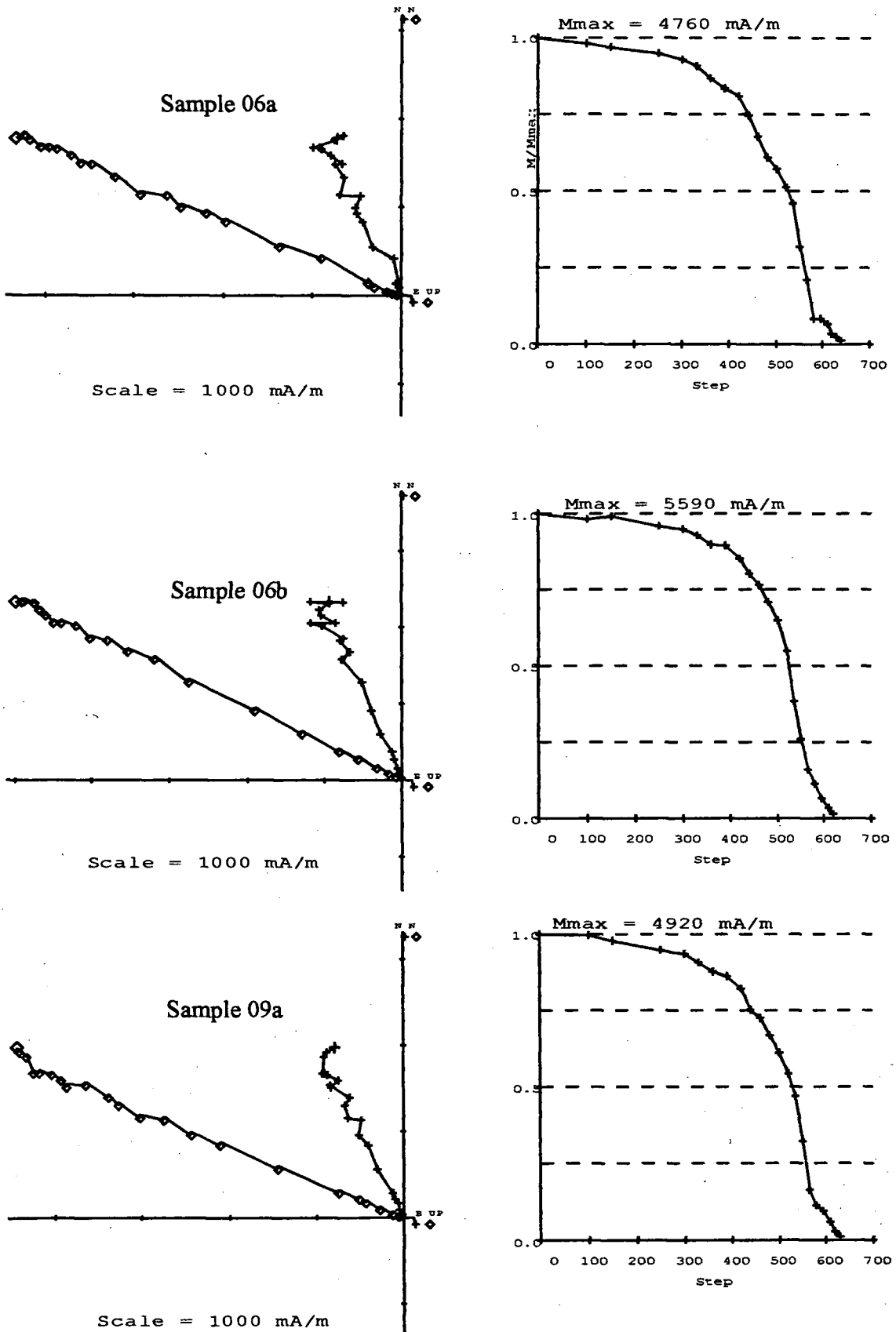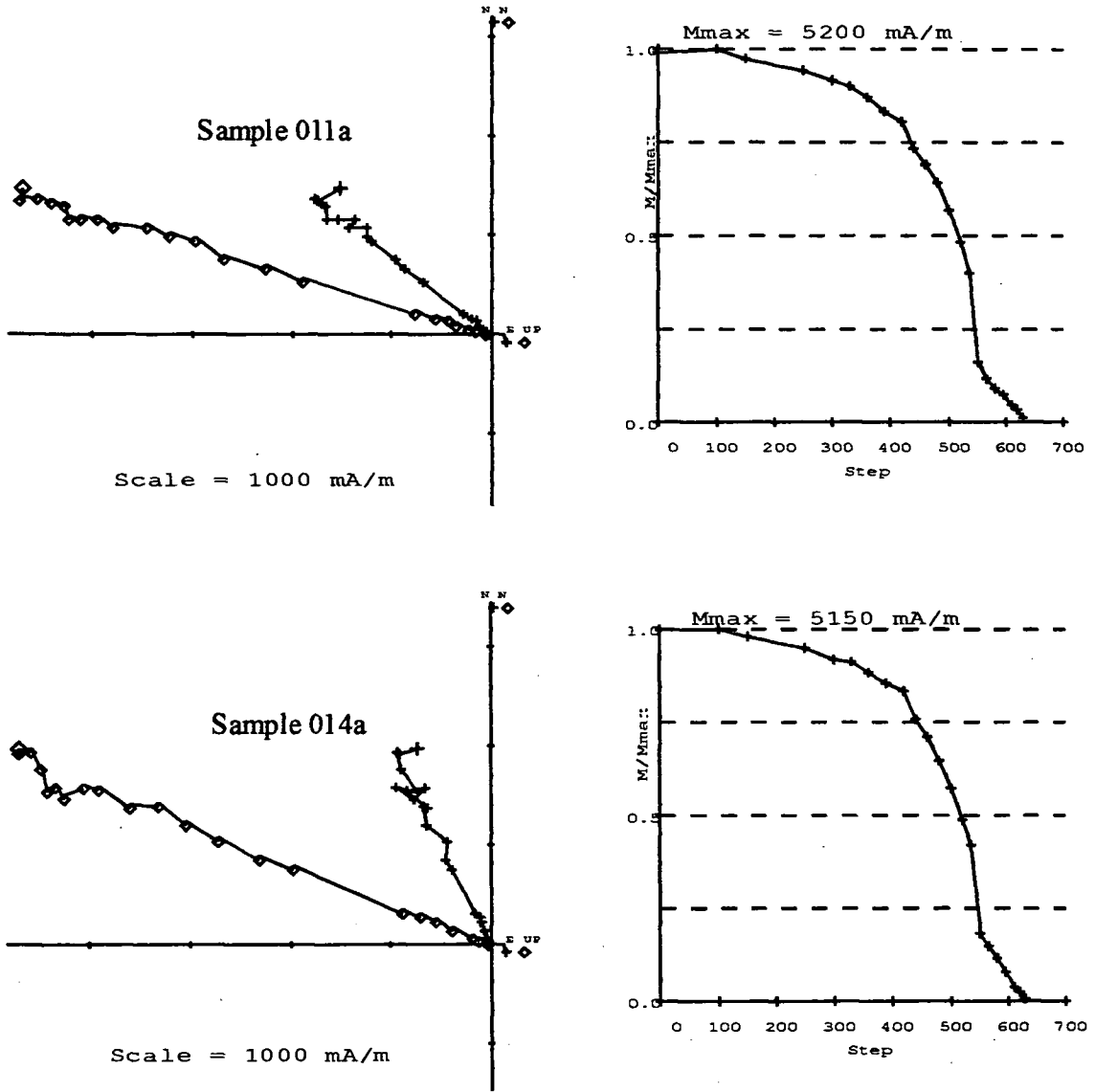
Fig. 5.29 - Site V39: Zijderveld diagrams and Intensity plots.

AD 1754 site V39

Sample 01			
Steps	Dec	Inc	MAD
"D" 520/595	309.8	65.4	1
"O" 520/595	311.3	65.4	0.7

(a)

Sample 06B			
Steps	Dec	Inc	MAD
"D" 565/620	341.1	64	1.3
"O" 565/620	340.7	63.5	0.8
"D" 520/565	337.7	63	1.6

(e)

Sample 04			
Steps	Dec	Inc	MAD
"D" 565/610	345.8	67.7	2.9
"D" 500/550	333.4	67.1	1.2
"D" 440/550 (*)	329.5	66.4	1.7

(*) erasing steps 480°C   (b)

Sample 09			
Steps	Dec	Inc	MAD
"D" 580/620	339.5	62.8	3.8
"D" 500/565	335.5	65.5	2.4
"D" 565/610	337.6	65.9	4.5
"O" 565/610	336.6	67.1	1.6

(f)

Sample 05			
Steps	Dec	Inc	MAD
"D" 565/610	346.2	67	1.3
"O" 565/610	345.8	65.7	0.8
"D" 440/565	337.7	66.1	1

(*) erasing step 500°C   (c)

Sample 11			
Steps	Dec	Inc	MAD
"D" 595/630	312.3	66.6	1.8
"D" 460/565	308.4	63.3	2.3
"D" 500/620	308.4	65.1	1.1
"O" 500/620	307.8	65.4	0.8

(g)

Sample 06A			
Steps	Dec	Inc	MAD
"D" 565/610	350.4	61.6	2.7
"D" 500/550	336.1	65.5	3.1

(d)

Sample 14			
Steps	Dec	Inc	MAD
"D" 565/630	340.9	65.6	1.7
"D" 480/565	330.8	65.8	1.3
"D" 565/620	341.1	65.2	1.9

(*) erasing step 500°C   (h)

Tab. 5.13 - Site V39: Directional results calculated using principal component analysis (Kirschvink, 1980).
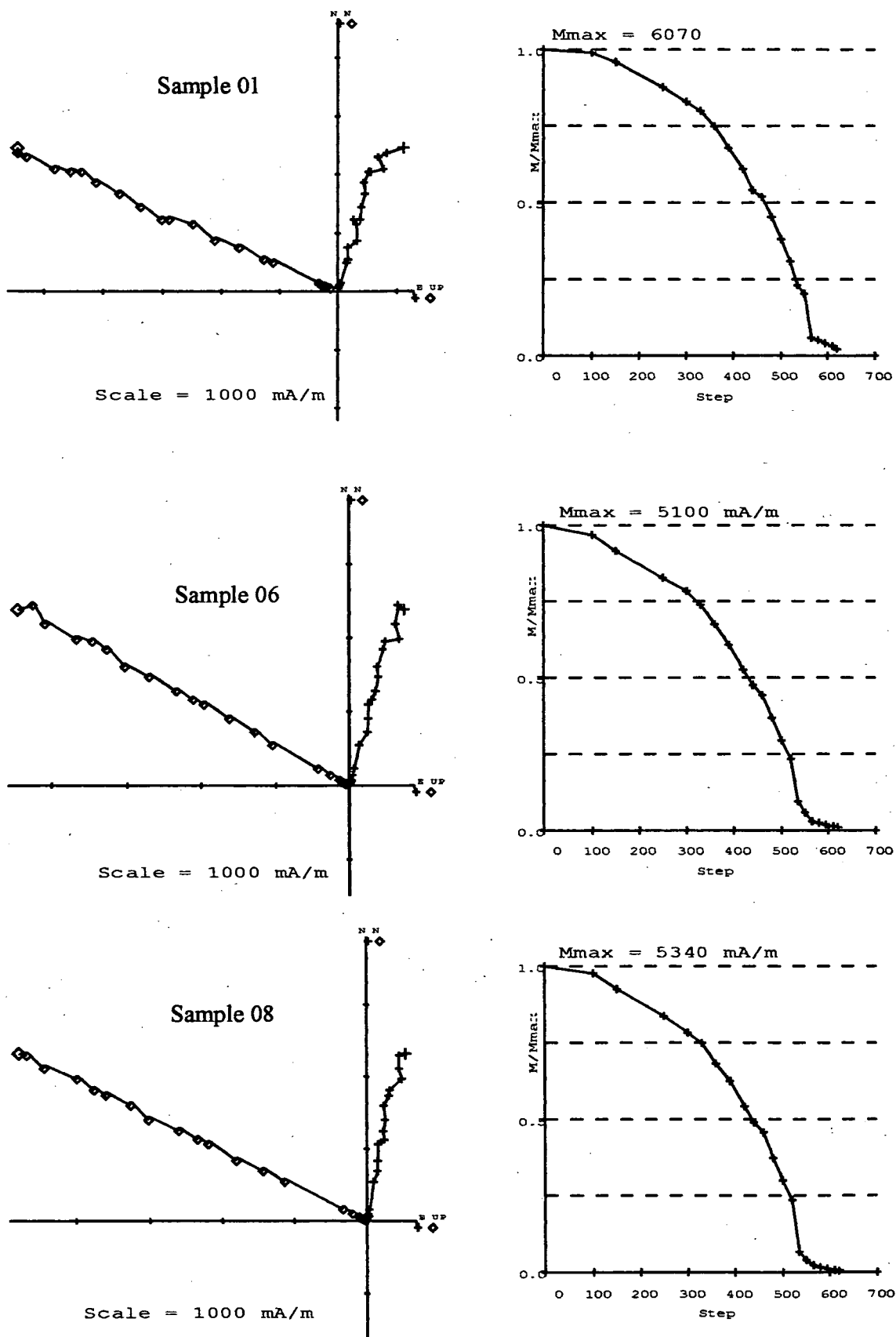
Sample 01a

Mmax = 3890 mA/m

Scale = 1000 mA/m

Sample 05a

Mmax = 4180 mA/m

Scale = 1000 mA/m

Sample 06a

Mmax = 4120 mA/m

Scale = 1000 mA/m
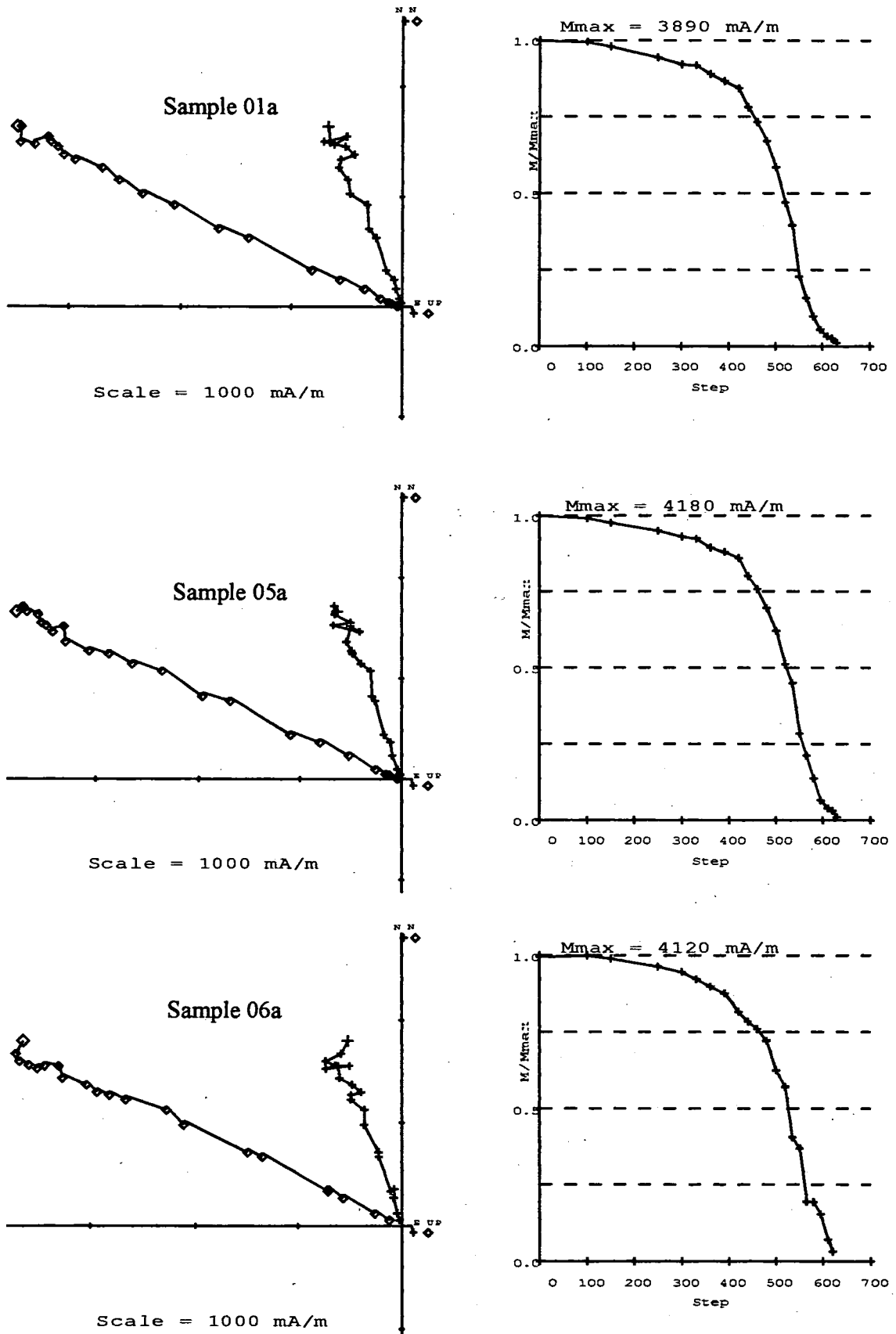
Fig. 5.30 - Site V40: Zijderveld diagrams and Intensity plots.

Sample 07a

Scale = 1000 mA/m

Mmax = 4120 mA/m

Sample 08a

Scale = 1000 mA/m

Mmax = 3850 mA/m

Sample 010a

Scale = 1000 mA/m

Mmax = 3820 mA/m
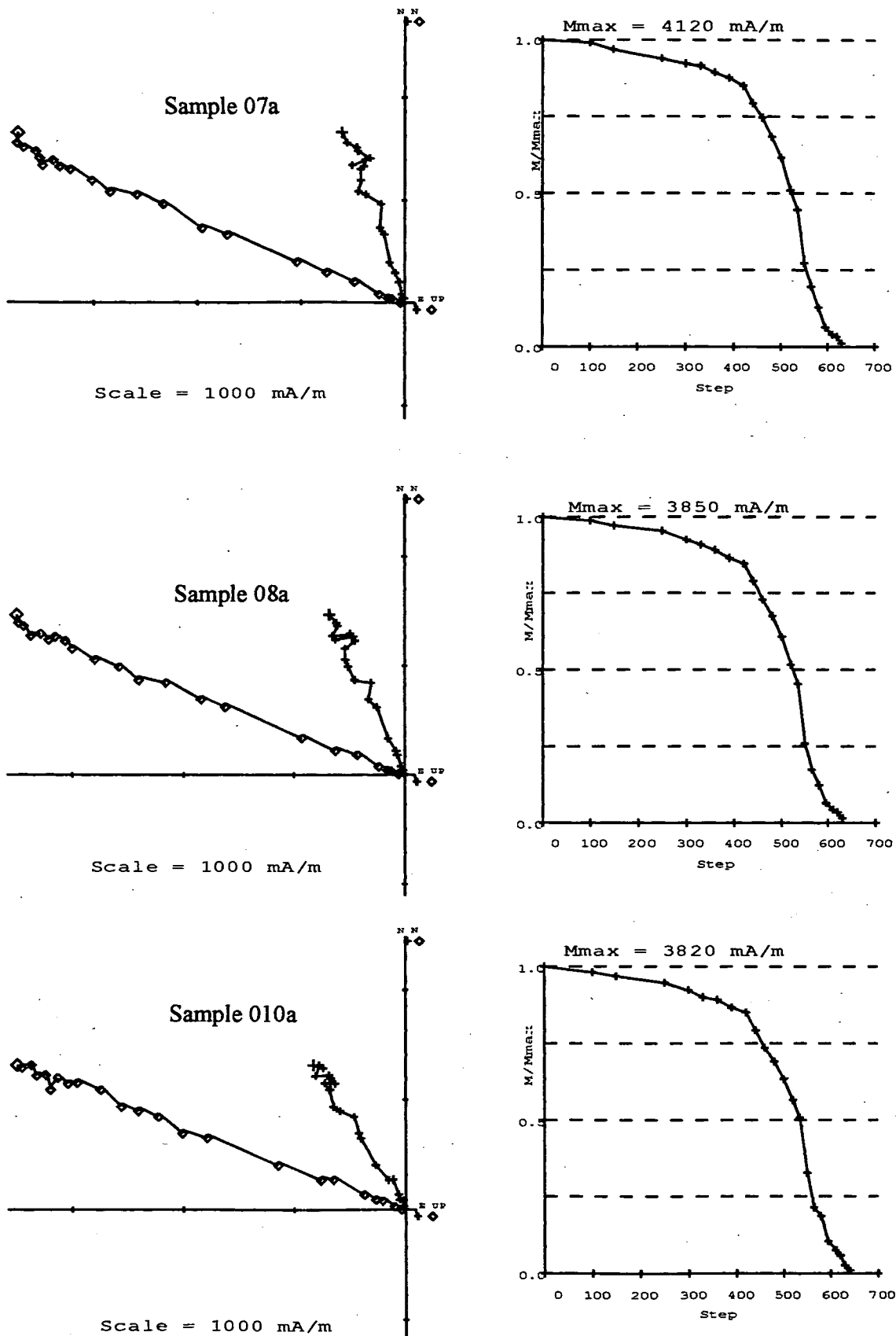
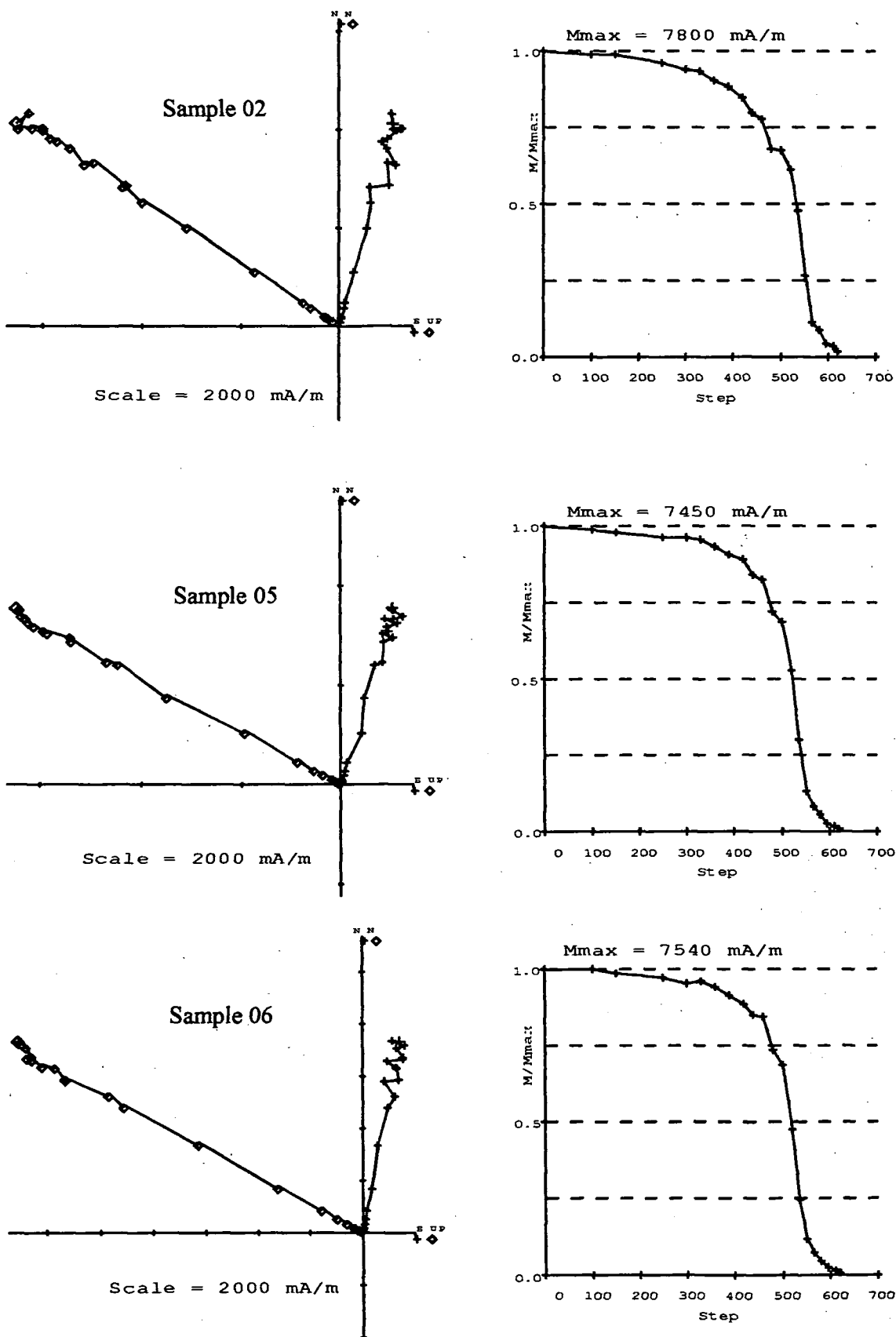**Fig. 5.31** - Site V40: Zijderveld diagrams and Intensity plots.
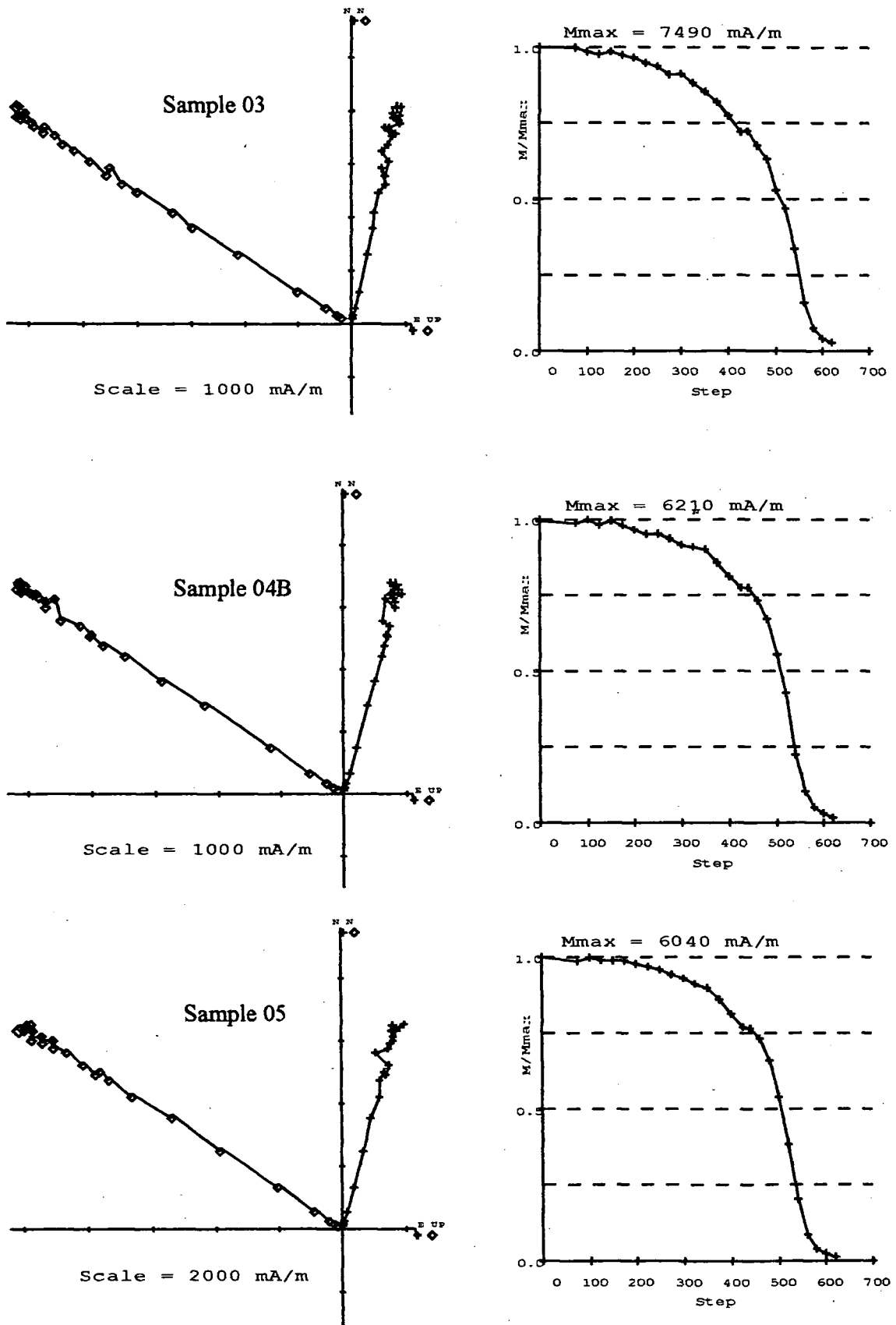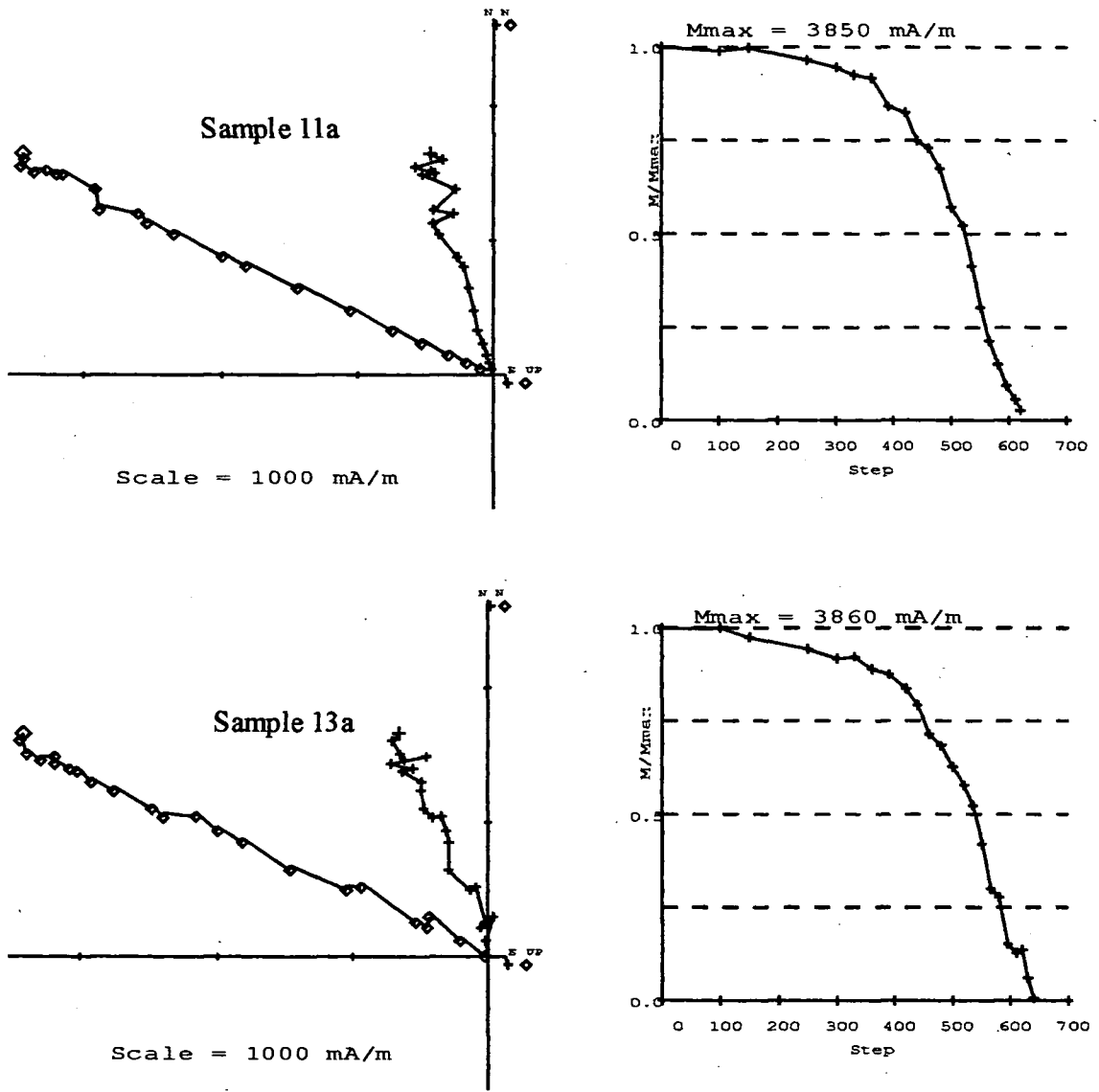
Fig. 5.32 - Site V40: Zijderveld diagrams and Intensity plots.

AD 1754 site V40

Sample 01			
Steps	Dec	Inc	MAD
"D" 565/630	343.6	63.7	2.3
"O" 565/630	342.4	65.4	2
"D" 420/550 (*)	335.9	62.5	2
"D" 565/610	344.8	63.9	2.6
"D" 565/620	343.4	63.7	2.6

(*) erasing step 500°C   (a)

Sample 05			
Steps	Dec	Inc	MAD
"D" 520/620	340.9	65.1	1.8
"D" 500/620	342.9	64.7	1.8

(b)

Sample 06			
Steps	Dec	Inc	MAD
"D" 535/620	342.4	62.7	1.9
"O" 535/620	342.9	63	1.1
"D" 535/620 (*)	342.5	62.7	1.1
"O" 535/620 (*)	342.4	63	0.7
"D" 390/500	328.5	69.7	9.1
"D" 390/500 (**)	326.7	69	5.5

(*) erasing step 580°C   (c)
(**) erasing step 440°C

Sample 07			
Steps	Dec	Inc	MAD
"D" 520/620	342.2	68.2	1.1
"O" 520/620	342.5	68.2	0.7

(d)

Sample 08			
Steps	Dec	Inc	MAD
"D" 520/620	342.2	68.2	1.1
"O" 520/620	342.5	68.2	0.7

(e)

Sample 10			
Steps	Dec	Inc	MAD
"D" 580/630	337.1	64.7	2.8
"O" 580/630	336.7	66.4	1.8

(f)

Sample 11			
Steps	Dec	Inc	MAD
"D" 520/620	345	65.4	0.7
"O" 520/620	344.2	65.1	0.5

(g)

Sample 13			
Steps	Dec	Inc	MAD
"D" 580/630	351.3	61.9	2

(h)

Tab. 5.14 - Site V40: Directional results calculated using principal component analysis (Kirschvink, 1980).

Sample 02a

Scale = 1000 mA/m

Mmax = 6610 mA/m

Sample 02b

Scale = 1000 mA/m

Mmax = 7050 mA/m

Sample 06a

Scale = 1000 mA/m

Mmax = 5970 mA/m

Fig. 5.33 - Site V41: Zijderveld diagrams and Intensity plots.

Sample 07a

Scale = 1000 mA/m

Mmax = 7100 mA/m

Sample 08b

Scale = 1000 mA/m

Mmax = 7150 mA/m

Sample 09b

Scale = 1000 mA/m

Mmax = 7250 mA/m
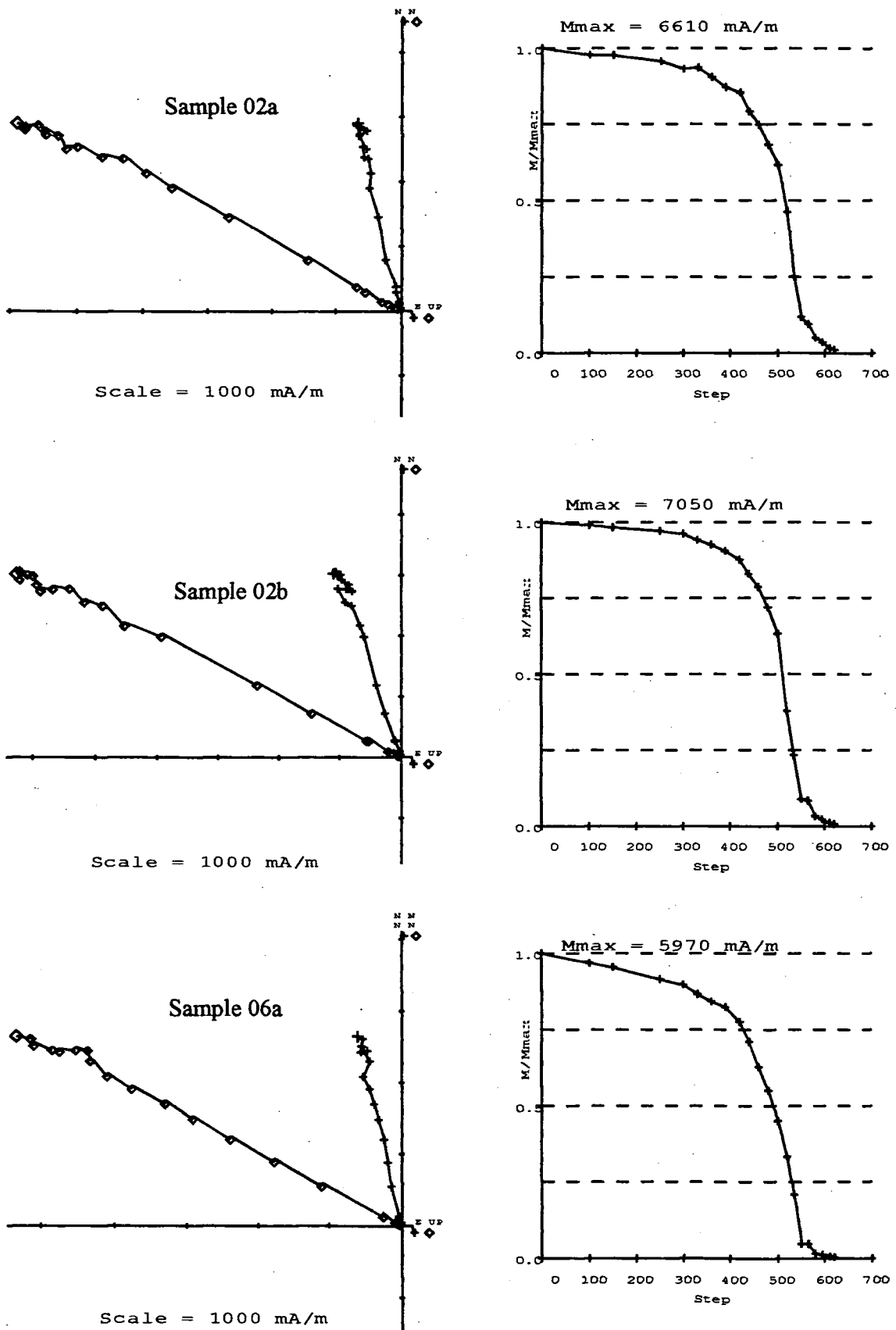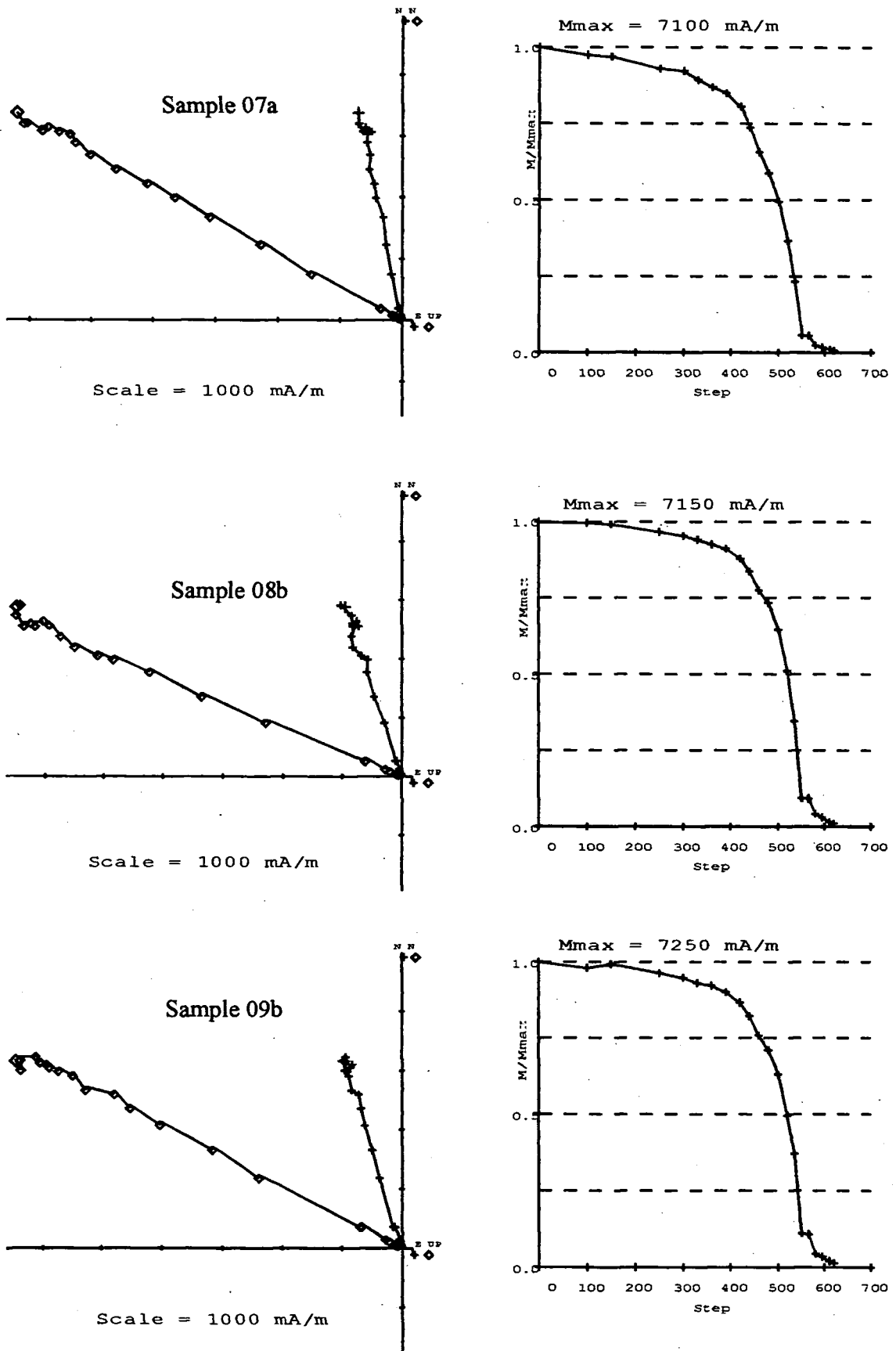
Fig. 5.34 - Site V41: Zijderveld diagrams and Intensity plots.

Sample 11a

Mmax = 6440 mA/m

Scale = 1000 mA/m

Sample 12a

Mmax = 6820 mA/m

Scale = 1000 mA/m
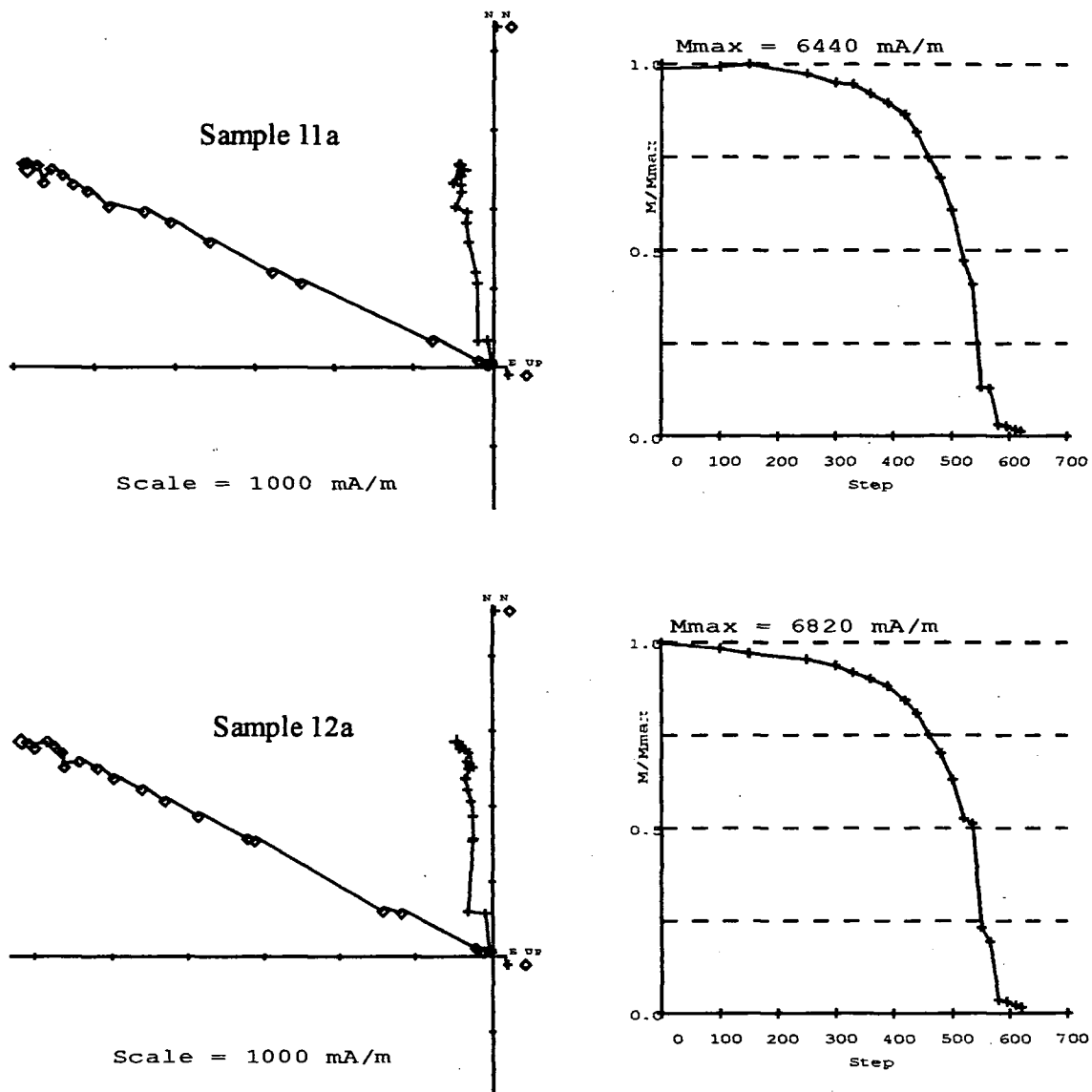
Fig. 5.35 - Site V41: Zijderveld diagrams and Intensity plots.

Sample 02			
Steps	Dec	Inc	MAD
"D" 565/620	343.8	61.3	1.8
"O" 565/620	343.4	61.5	1.1
"D" 500/620	345.9	60.8	0.7
"O" 500/620	345.6	60.8	0.6
"D" 500/620	342.8	62.1	0.6
"O" 500/620	342.3	62.1	0.5

(a)

Sample 08			
Steps	Dec	Inc	MAD
"D" 500/620	341.6	66.6	0.7
"O" 500/620	341.5	66.6	0.5

(d)

Sample 09			
Steps	Dec	Inc	MAD
"D" 460/620	344.1	61.3	0.9
"O" 460/620	343.7	61.4	0.7

(e)

Sample 06			
Steps	Dec	Inc	MAD
"D" 440/620	347.6	62.4	0.5
"O" 440/620	347.5	62.5	0.4

(b)

Sample 11			
Steps	Dec	Inc	MAD
"D" 480/620	349.6	65.7	0.5
"O" 480/620	349.2	65.7	0.4

(f)

Sample 07			
Steps	Dec	Inc	MAD
"D" 460/620	348.7	61	0.7
"O" 460/620	348.4	61.1	0.5

(c)

Sample 12			
Steps	Dec	Inc	MAD
"D" 520/620	351.3	63.7	0.5
"O" 520/620 (*)	350.7	63.7	0.5

(*) erasing step 550   (g)

Tab. 5.15 - Site V41: Directional results calculated using principal component analysis (Kirschvink, 1980).

Sample 01

Scale = 1000 mA/m

Mmax = 4120 mA/m

Sample 03

Scale = 1000 mA/m

Mmax = 4380 mA/m

Sample 06

Scale = 1000 mA/m

Mmax = 6530 mA/m

Fig. 5.36 - Site V32: Zijderveld diagrams and Intensity plots.

Sample 07

Scale = 1000 mA/m

Mmax = 7560 mA/m

Sample 11

Mmax = 6340 mA/m

Sample 12

Scale = 1000 mA/m

Mmax = 6760 mA/m
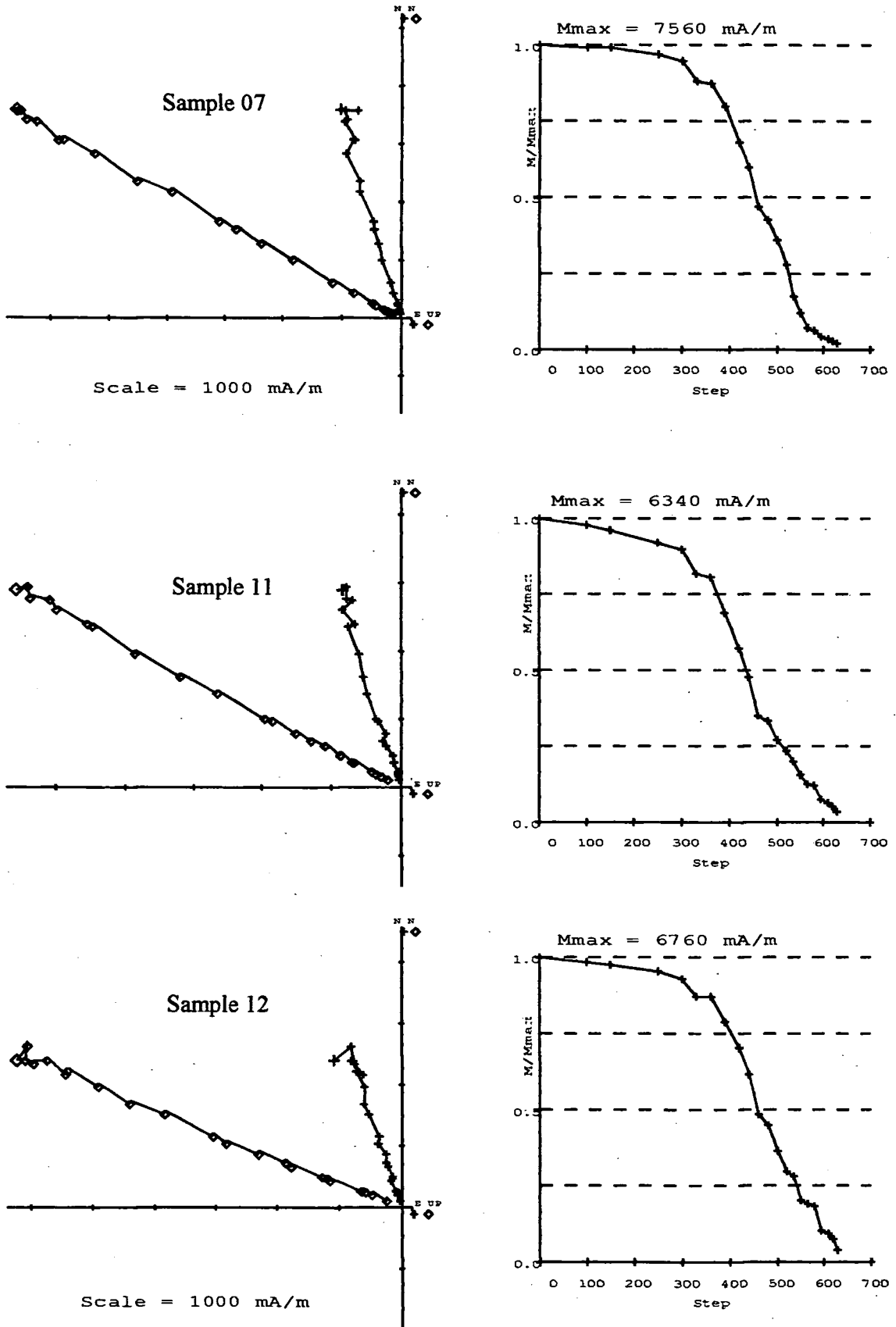
Fig. 5.37 - Site V32: Zijderveld diagrams and Intensity plots.

AD 1760 site V32

Sample 01			
Steps	Dec	Inc	MAD
"D" 550/630	345	65.3	1.3
"O" 550/630	344.1	65.5	0.5

(a)

Sample 07			
Steps	Dec	Inc	MAD
"D" 460/630	343.5	60.4	0.8
"O" 460/630	343.7	60.6	0.6

(d)

Sample 03			
Steps	Dec	Inc	MAD
"D" 565/630	343.6	62.9	1.4

(b)

Sample 11			
Steps	Dec	Inc	MAD
"D" 550/630	343.9	61.4	1.7
"O" 550/630	345	61.1	0.7

(e)

Sample 06			
Steps	Dec	Inc	MAD
"D" 480/595	336.2	64.8	1.2

c)

Sample 12			
Steps	Dec	Inc	MAD
"D" 535/630 (*)	341.5	68.8	1.2
"O" 535/630 (*)	342.1	67.9	0.8

(*) erasing step 580°C   (f)

Tab. 5.16 - Site V32: Directional results calculated using principal component analysis (Kirschvink, 1980).

Sample 01

Scale = 500 mA/m

Mmax = 3460 mA/m

Sample 02

Scale = 500 mA/m

Mmax = 3370 mA/m

Sample 03

Scale = 1000 mA/m

Mmax = 3740 mA/m

Fig. 5.38 - Site V34: Zijderveld diagrams and Intensity plots.

Sample 04

Scale = 500 mA/m

Mmax = 3420 mA/m

Sample 06

Scale = 500 mA/m

Mmax = 2990 mA/m

Sample 11

Scale = 500 mA/m

Mmax = 2570 mA/m
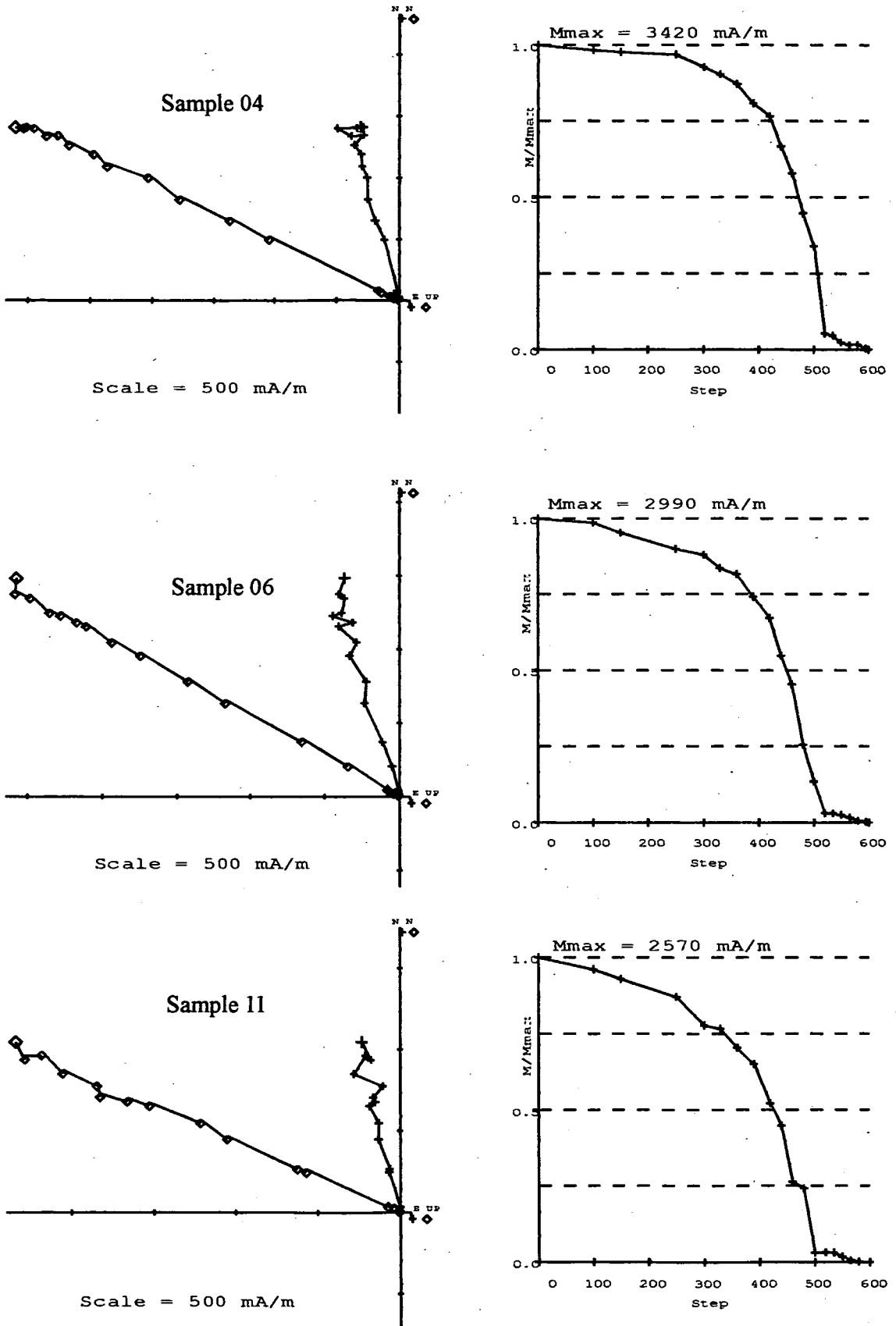
Fig. 5.39 - Site V34: Zijderveld diagrams and Intensity plots.

AD 1760 site V34

Sample 01			
Steps	Dec	Inc	MAD
"D" 520/595	347.5	63.3	0.9
"O" 520/595	347.2	63.6	0.7

(a)

Sample 04			
Steps	Dec	Inc	MAD
"D" 500/595	346.6	64	0.4
"O" 500/595	346.7	64	0.4

(d)

Sample 02			
Steps	Dec	Inc	MAD
"D" 520/595	344.7	60.1	0.4
"O" 520/595	344.7	60.2	0.3

(b)

Sample 06			
Steps	Dec	Inc	MAD
"D" 480/565	343.1	59	1.1
"O" 480/565	344	59.1	0.9

(e)

Sample 03			
Steps	Dec	Inc	MAD
"D" 520/595	346.2	64.5	0.9
"O" 520/595	346.2	64.5	0.6

c)

Sample 11			
Steps	Dec	Inc	MAD
"D" 390/535 (*)	343.4	66.1	0.4
"O" 390/535 (*)	344.4	66.1	0.4

(*) erasing step 420°C   (f)

Tab. 5.17 - Site V34: Directional results calculated using principal component analysis (Kirschvink, 1980).

Sample 03

Scale = 500 mA/m

Mmax = 3560 mA/m

Sample 04

Scale = 500 mA/m

Mmax = 3690 mA/m

Sample 05

Scale = 500 mA/m

Mmax = 3510 mA/m

Fig. 5.40 - Site V35: Zijderveld diagrams and Intensity plots.

Sample 06b

Scale = 500 mA/m

Mmax = 3850 mA/m

Sample 07b

Scale = 500 mA/m

Mmax = 3320 mA/m

Sample 08

Scale = 500 mA/m

Mmax = 3530 mA/m

Fig. 5.41 - Site V35: Zijderveld diagrams and Intensity plots.

123

Sample 10a

Scale = 500 mA/m

Mmax = 3430 mA/m

Sample 10b

Scale = 500 mA/m

Mmax = 3730 mA/m

Sample 11a

Mmax = 3690 mA/m

Fig. 5.42 - Site V35: Zijderveld diagrams and Intensity plots.

Sample 12

Scale = 500 mA/m

Mmax = 3690 mA/m

Sample 13

Scale = 1000 mA/m

Mmax = 3720 mA/m
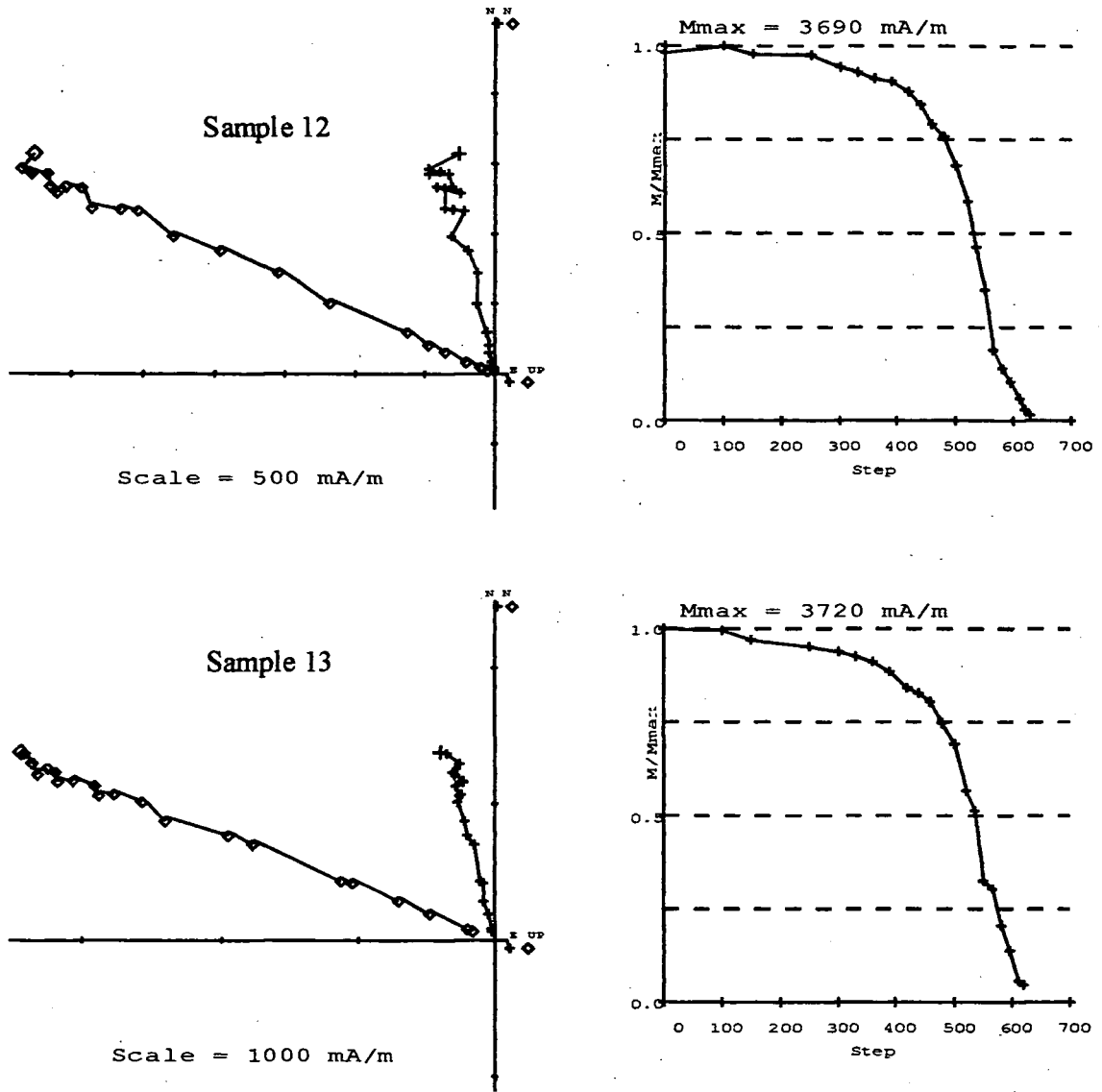
Fig. 5.43 - Site V35: Zijderveld diagrams and Intensity plots.

AD 1760 site V35

Sample 03

Steps	Dec	Inc	MAD
"D" 535/620	345.6	59.9	1.6
"O" 535/620	345.3	59.7	0.9

(a)

Sample 04

Steps	Dec	Inc	MAD
"D" 550/630	351.3	65.4	1.5
"O" 550/630	351.9	65.2	1

(b)

Sample 05

Steps	Dec	Inc	MAD
"D" 500/620	350.6	63.9	0.8
"O" 500/620	349.9	63.9	0.6

(c)

Sample 06B

Steps	Dec	Inc	MAD
"D" 550/630	341.7	59.7	1
"O" 550/630	341.5	59.9	0.7

(d)

Sample 07B

Steps	Dec	Inc	MAD
"D" 520/620	347.9	62	0.8
"O" 520/620	347.5	61.8	0.6

(e)

Sample 08

Steps	Dec	Inc	MAD
"D" 500/620	343.2	59.3	0.6
"O" 500/620	343.1	59.2	0.4

(f)

Sample 10A

Steps	Dec	Inc	MAD
"D" 520/620	337.2	59	0.6
"O" 520/620	337.6	58.7	0.5

(g)

Sample 10B

Steps	Dec	Inc	MAD
"D" 595/630	342.2	59.7	1.6
"O" 595/630	342	59.5	0.8
"D" 550/595	336.8	59	1.5

(h)

Sample 11A

Steps	Dec	Inc	MAD
"D" 595/630	344	63.1	1.3
"O" 595/630	344	63.2	0.7
"D" 480/630 (*)	347.7	62.4	0.8

(*) erasing step 520°C   (i)

Sample 12

Steps	Dec	Inc	MAD
"D" 595/630	345.1	65.9	1.1
"O" 595/630	346.2	65.9	0.7
"D" 520/630	348.5	65.2	1.4
"O" 520/630	348.4	65.3	0.9

(l)

Sample 13

Steps	Dec	Inc	MAD
"D" 535/620	348.8	68.2	1
"O" 535/620	347.6	67.9	0.7

(m)

Tab. 5.18 - Site V35: Directional results calculated using principal component analysis (Kirschvink, 1980).

5.7 - AD 1806

5.7.1 - Site V24

a) - Intensity Behaviour

These 6 samples showed two different sets of behaviour (Figs. 5.44, 5.45). Samples 04, 06 and 07 had an highest initial NRM (around 3700 mA/m) and, by 565°C, had been completely demagnetized, generally with a very small tail above 535°C. This first group of samples showed a little decreasing in intensity until 250-300°C (except 04 which had a significant linear decrease between 20-150°C) and showed an accelerating decrease in intensity terminating around 580°C. A significant deflection occurred around 460°C (except in 04), while minor irregularities occurred at different steps of temperatures.

The second group (samples 09, 10 and 12) had a lowest initial NRM around 2000 mA/m. These samples showed an almost linear decrease in intensity until 535°, where a little final tail took place. By 565°C they were completely demagnetized. Three clear breaks in the rate of decrease occurred: at 150, 360 and 480°C.

b) - Directional Behaviour

The two differences in intensity behaviour were also evident in the directional analyses. Sample 04, 06 and 07 showed a well defined high temperature component between 480 and 565°C. The vertical vector, in all the spectra, showed a linear trend while the horizontal one always had a zigzag behaviour especially at low and medium temperatures.

Samples 09, 10 and 12 showed a poorly defined component at low and medium temperatures. Starting from 460°C these samples had both the declination and inclination values moving away from the main value.

Although there was a clear difference in behaviour, the component analyses showed a unique group of declination and inclination values with a quite low MAD in all the samples (Tab. 5.19).

5.7.2 - Site V25

a) - Intensity Behaviour

All these 6 samples had an initial NRM around 2500 mA/m and, by 580°C, had been completely demagnetized (Figs. 5.46, 5.47). They showed an almost linear decay terminating with a little tail at 550°C. Only samples 07, 08 and 09 showed a clear break at 250°C followed by a quite concave curve. Some minor irregularities occurred at different steps of temperature.

b) – Directional Behaviour

In almost all the samples the horizontal vector showed an uncertain trend until 420°C, while the vertical vector was almost linear over all the temperature steps. Visual analyses showed a poorly defined component especially at low and medium temperatures with declination and declination values very similar for all the samples (Tab. 5.20).

At the highest temperature (above 500°C) all samples had both the declination and inclination values moving away from the main value.

5.8 - AD 1839

5.8.1 - Site V42

a) - Intensity Behaviour

All 8 samples showed a very similar behaviour (Figs. 5.48, 5.49, 5.50). The initial NRM was about 4500 mA/m and, by 620°C, was almost completely demagnetized (< 1%). All curves, starting from 390°C, showed an accelerating decrease in intensity with increasing temperature terminating with a small tail at 550°C. A very little irregularity occurred at about 560°C for samples 08A, 10A and 12A.

b) – Directional Behaviour

All the samples showed a well defined high temperature component usually between 440/500 and 595/620°C. Both vertical and horizontal vectors showed a linear trend for all samples, at medium and high temperatures, and a zigzag behaviour at low temperatures.

Although some steps needed to be erased because of their poor definition, all samples showed a unique direction with a very low value of MAD In fact both declination and inclination values were really consistent for all the samples (Tab. 5.21).

At the highest temperature (610 to 620°C) samples 01A, 06A, 08A and 13A) had both the declination and inclination values moving slightly away from the main value.

5.8.2 - Site V43

a) - Intensity Behaviour

These 8 samples showed mainly a similar behaviour (Figs. 5.51, 5.52, 5.53): an initial NRM around 5000 mA/m, an accelerating decrease in intensity starting around 330°C and, around 550°C, a little tail with a concave trend (sometimes linear).

Minor irregularities occurred in all the samples around 560°C.

b) – Directional Behaviour

All the samples showed a well defined high temperature component usually between 440/500 and 595/620°C. Both vertical and horizontal vector showed a linear trend for all the samples, above 500°C, and an uncertain behaviour at low temperatures.

Both declination and inclination values were very consistent for all the samples (Tab. 5.22), but in some samples few steps needed to be erased because of their poor definition.

At the highest temperature (610 to 620°C) sample 08A had both the declination and inclination values moving slightly away from the main value.

5.8.3 - Site V44

a) - Intensity Behaviour

These 8 samples had an initial NRM around 3000 mA/m, and by 565°C, had been completely demagnetized, but they showed an anomalous behaviour (Figs. 5.54, 5.55, 5.56). Samples 03A, 04B, 07A, 09A and 11A showed an almost linear decrease in intensity with a clear break (420°C) in the rate of decrease. A significant deflection also occurred at 500°C

Samples 08a and 12A showed an increase in intensity until 150°C followed by an accelerating decrease until 500°C where a little convex tail took place. They showed the same irregularities as the previous samples.

Sample 01A showed a linear decay until 250°C, a very zigzag behaviour until 440°C and again a linear trend until the end.

b) – Directional Behaviour

The differences in intensity behaviour were still evident in the directional analyses. In samples 01A, 03A, 04B, 07A, 09A and 11A, a vertical vector, in all spectra, showed a linear trend while the horizontal one always had a zigzag behaviour, especially at low and medium temperatures. Samples 08A and 12A showed a curving trend from the initial NRM to 360-390°C followed by an almost linear trend until 565°C

Although there were clear differences in behaviour and some steps needed to be erased because of their poor definition, the component analyses showed similarity in declination and inclination values with an acceptable MAD for all the samples (Tab. 5.23).

Sample 04

Scale = 500 mA/m

Mmax = 3590 mA/m

Sample 06

Scale = 1000 mA/m

Mmax = 4050 mA/m

Sample 07

Scale = 500 mA/m

Mmax = 3700 mA/m

Fig. 5.44 - Site V24: Zijderveld diagrams and Intensity plots.

Mmax = 2170 mA/m

Sample 09

Scale = 500 mA/m

Mmax = 2450 mA/m

Sample 10

Scale = 500 mA/m

Mmax = 2230 mA/m

Sample 12

Scale = 500 mA/m
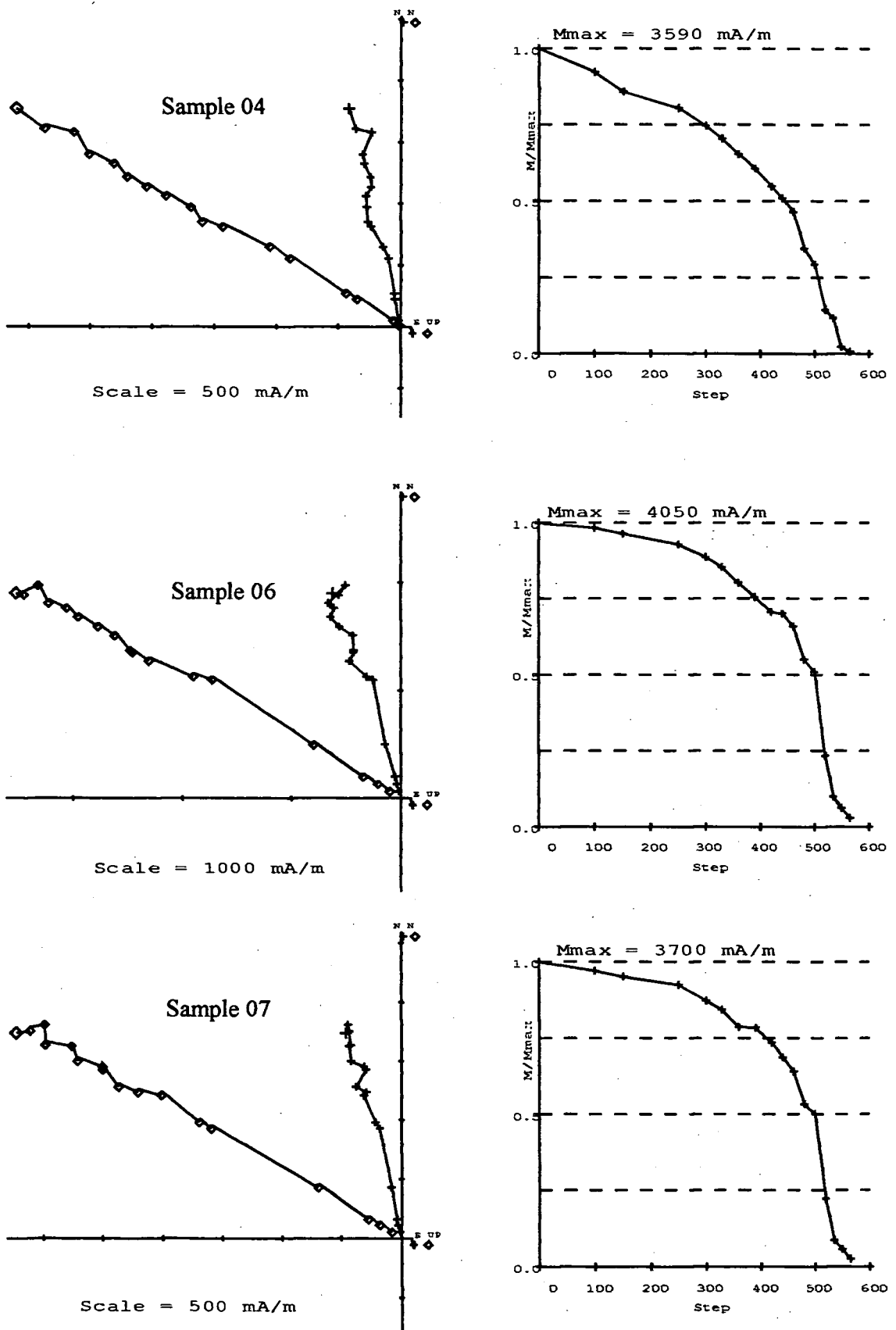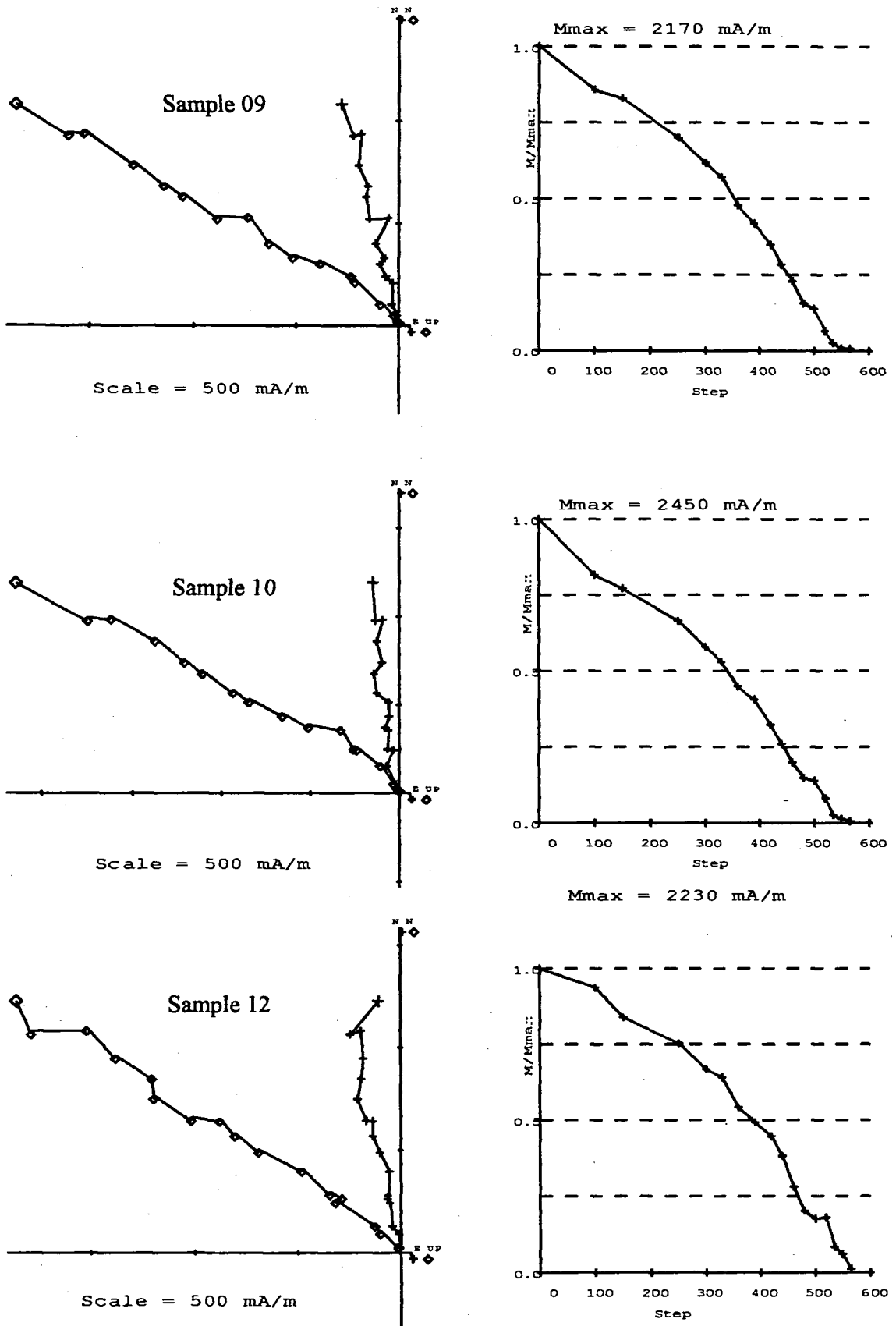
Fig. 5.45 - Site V24: Zijderveld diagrams and Intensity plots.

AD 1806 site V24

Sample 04

Steps	Dec	Inc	MAD
"D" 500/ 565	350.2	58.2	0.8
"O" 500/ 565	349.5	57.5	0.9
"D" 480/ 535	348.4	58.2	1.4
"O" 480/ 535	348.6	57.7	0.6

(a)

Sample 09

Steps	Dec	Inc	MAD
"D" 20/565	346.7	60	2.9
"O" 20/565	346.8	58.1	2.4
"D" 150/360	353.4	56.9	2.6
"D" 20/440	347.1	59.6	2.4
"D" 20/440 (*)	346	59.9	1.6
"O" 20/440 (*)	346	58.6	0.7

(*) erasing steps 150,390°C   (d)

Sample 06

Steps	Dec	Inc	MAD
"D" 500/ 565	347.2	56.7	0.8
"O" 500/ 565	346.5	56.9	0.7

(b)

Sample 10

Steps	Dec	Inc	MAD
"D" 150/ 440	356	60.1	4.4
"D" 150/ 500 (*)	354.7	61.6	3.6
"O" 150/ 440	351.8	58.1	1.7
"O" 150/ 420	352	58.2	1.4

(*) erasing step 460°C   (e)

Sample 07

Steps	Dec	Inc	MAD
"D" 500/ 565	349.4	59.4	0.8
"O" 500/ 565	348.9	59	0.7
"O" 480/ 565 (*)	347.6	59	0.7
"D" 480/ 565 (*)	347.8	59.4	0.8

(*) erasing step 500°C   (c)

Sample 12

Steps	Dec	Inc	MAD
"D" 150/ 550	348.2	56.5	3.5
"D" 390/ 550 (*)	347.6	55.5	2
"D" 390/ 535 (*)	348.3	56	1.9

(*) erasing steps 460,500°C   (f)

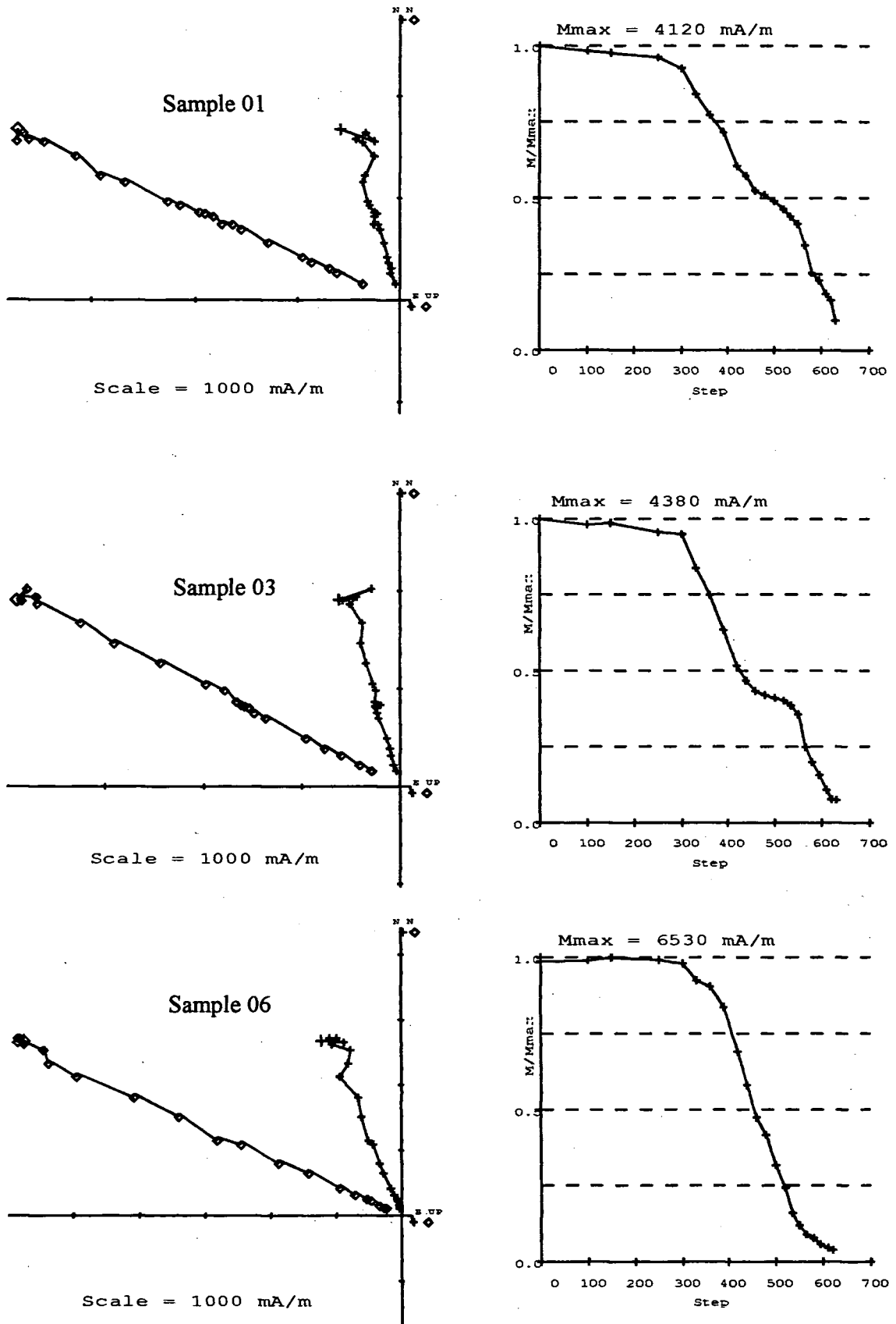Tab. 5.19 - Site V24: Directional results calculated using principal component analysis (Kirschvink, 1980).

Sample 03

Scale = 500 mA/m

Mmax = 2610 mA/m

Sample 05

Scale = 500 mA/m

Mmax = 2480 mA/m

Sample 07

Scale = 500 mA/m

Mmax = 2900 mA/m

Fig. 5.46 - Site V25: Zijderveld diagrams and Intensity plots.

Sample 08

Scale = 500 mA/m

Mmax = 2970 mA/m

Sample 09

Scale = 500 mA/m

Mmax = 2880 mA/m

Sample 11

Scale = 500 mA/m

Mmax = 2570 mA/m
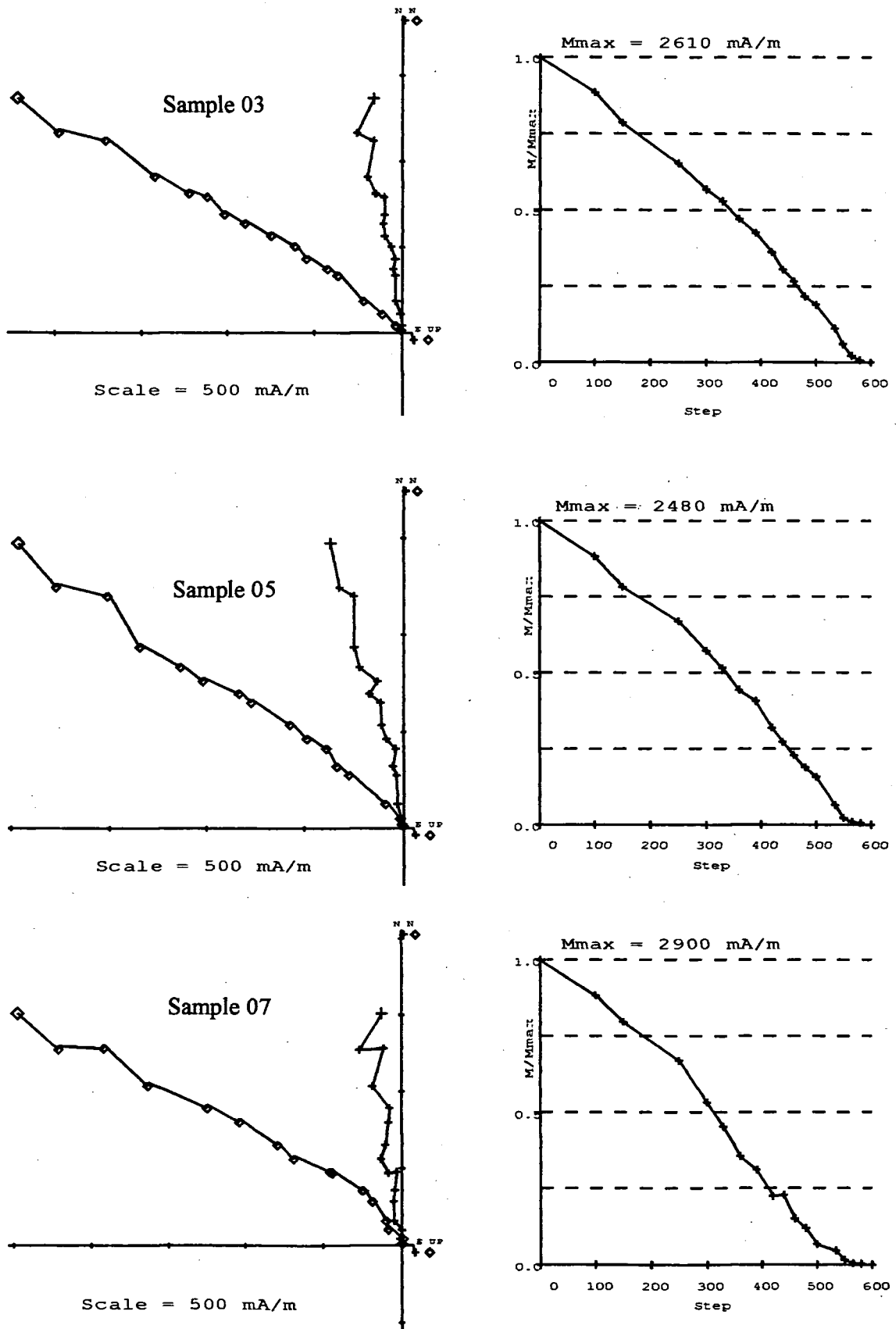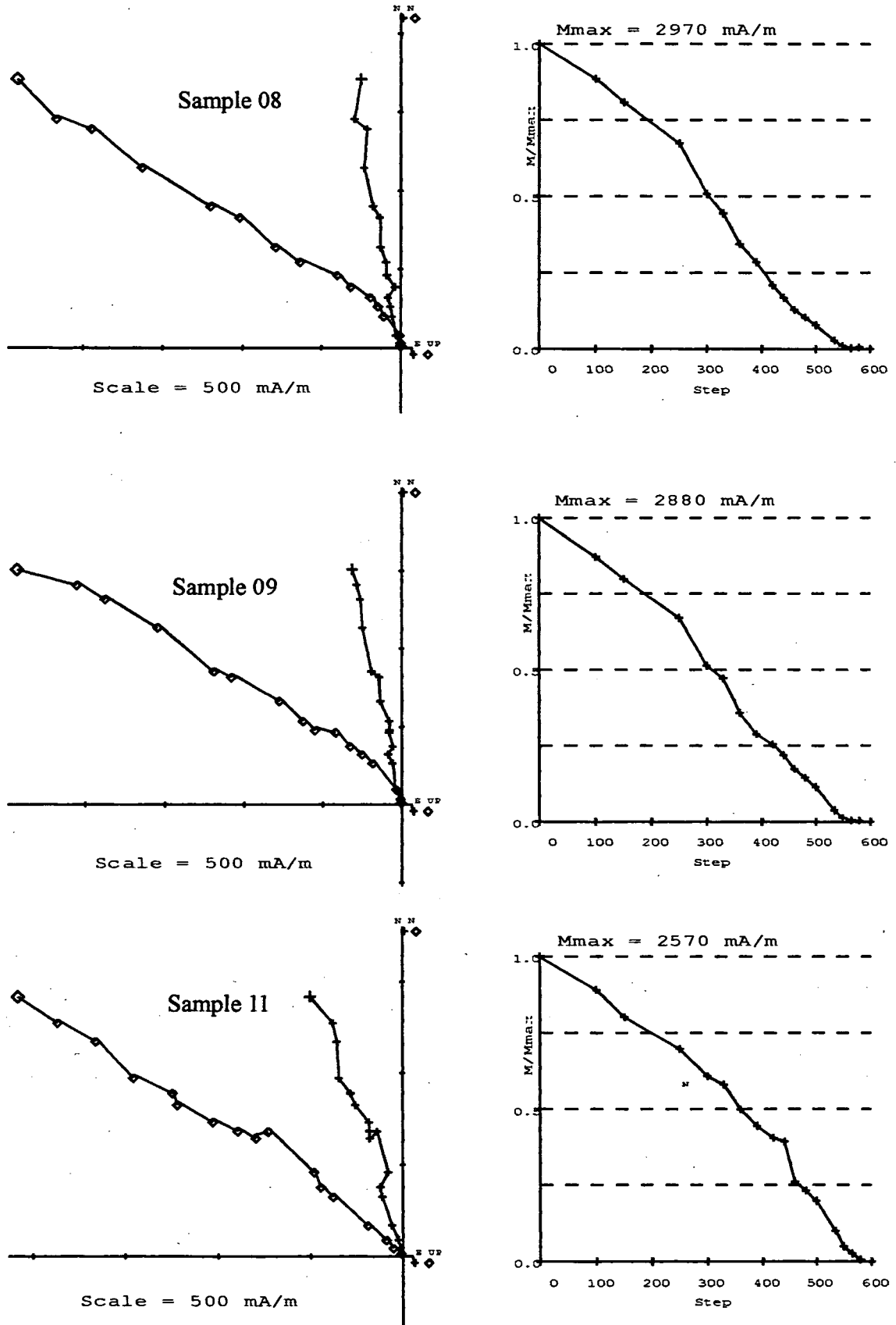
Fig. 5.47 - Site V25: Zijderveld diagrams and Intensity plots.

AD 1806 site V25

Sample 03			
Steps	Dec	Inc	MAD
"D" 330/ 500	350.2	59.6	3.4

(a)

Sample 08			
Steps	Dec	Inc	MAD
"D" 250/ 420	348.3	59.3	2.9

(d)

Sample 05			
Steps	Dec	Inc	MAD
"D" 20/500	344.2	55.3	3.6

(b)

Sample 09			
Steps	Dec	Inc	MAD
"D" 20/500	347.3	59.6	2.7

(e)

Sample 07			
Steps	Dec	Inc	MAD
"D" 250/ 420	348.3	59.3	2.9

c)

Sample 11			
Steps	Dec	Inc	MAD
"D" 360/ 565 (*)	345.9	53.2	3.1

(*) erasing step 440°C   (f)

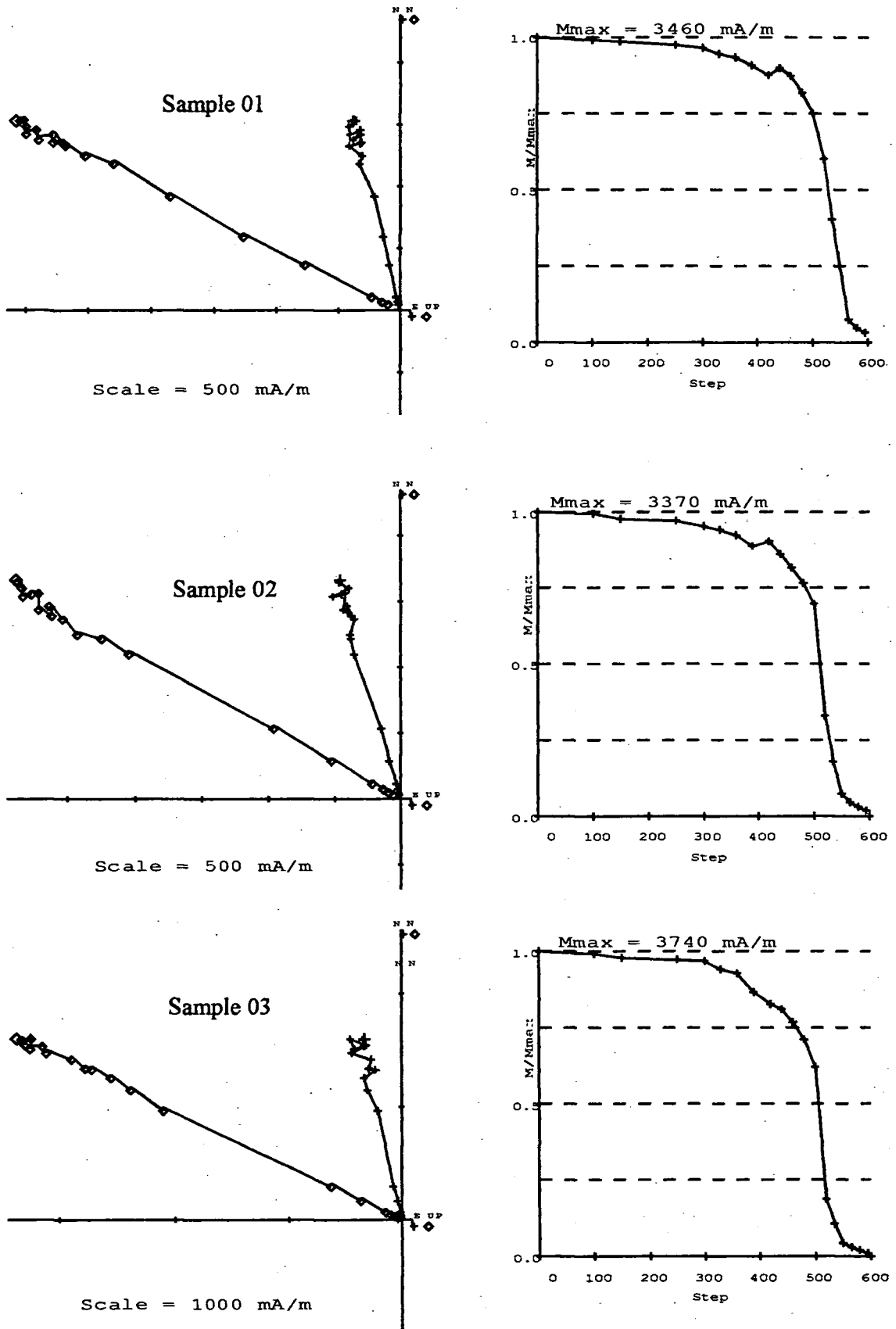**Tab. 5.20** - Site V25: Directional results calculated using principal component analysis (Kirschvink, 1980).

Sample 01a

Scale = 1000 mA/m

Mmax = 4620 mA/m

Sample 02a

Scale = 1000 mA/m

Mmax = 4550 mA/m

Sample 04a

Scale = 1000 mA/m

Mmax = 4420 mA/m
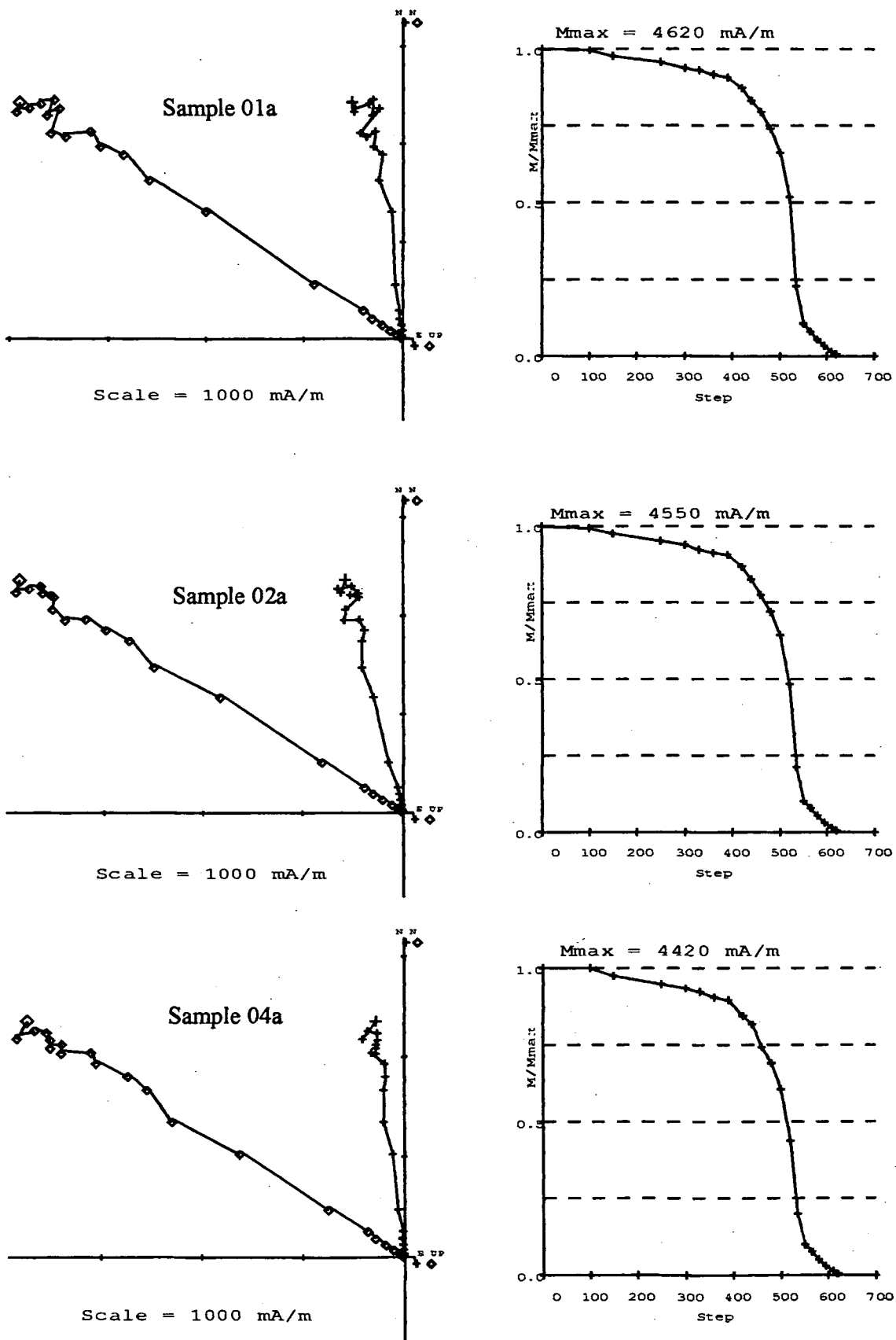
Fig. 5.48 - Site V42: Zijderveld diagrams and Intensity plots.

137
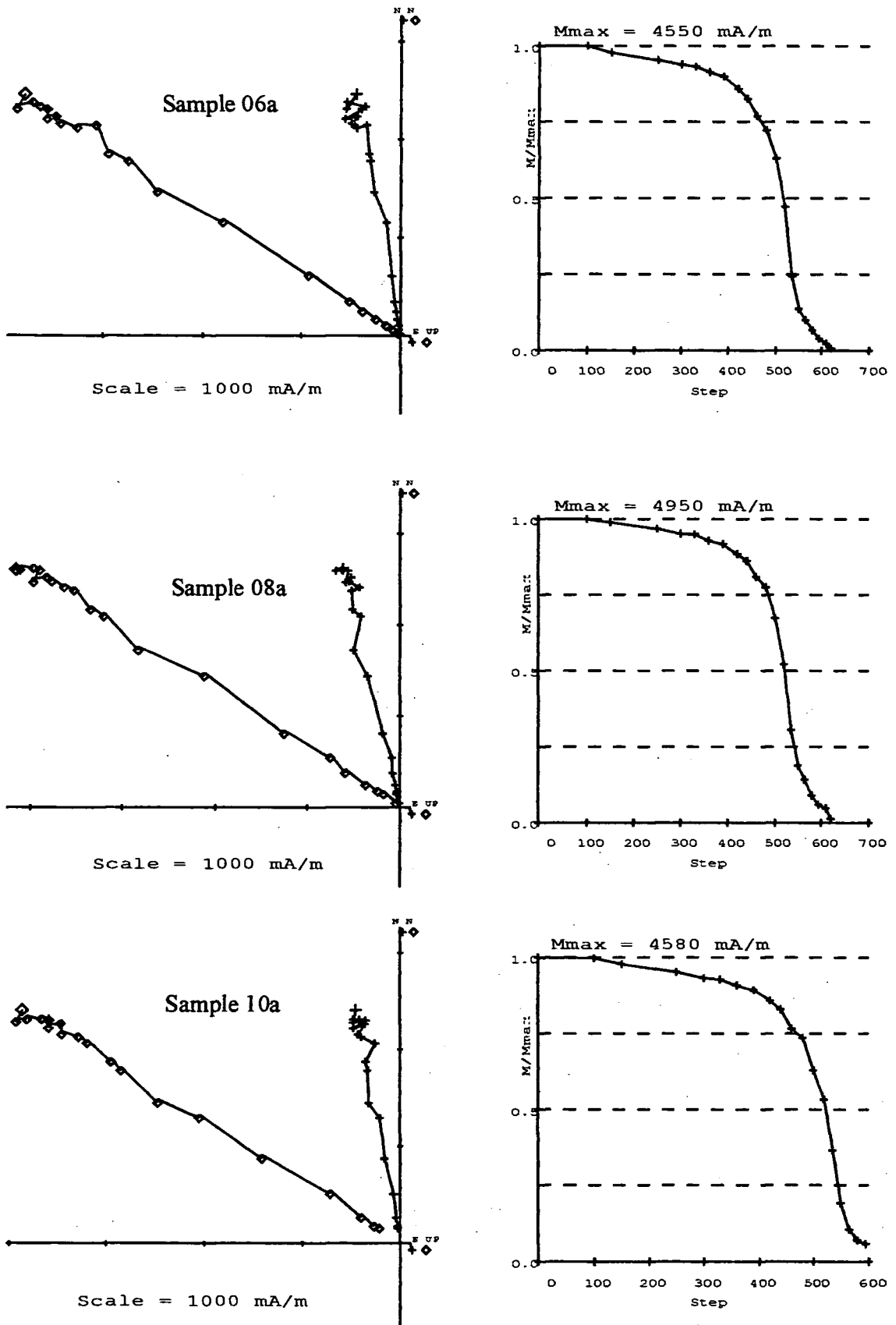
Fig. 5.49 - Site V42: Zijderveld diagrams and Intensity plots.

Sample 12a

Scale = 1000 mA/m

Mmax = 5080 mA/m

Sample 13a

Scale = 1000 mA/m

Mmax = 4310 mA/m
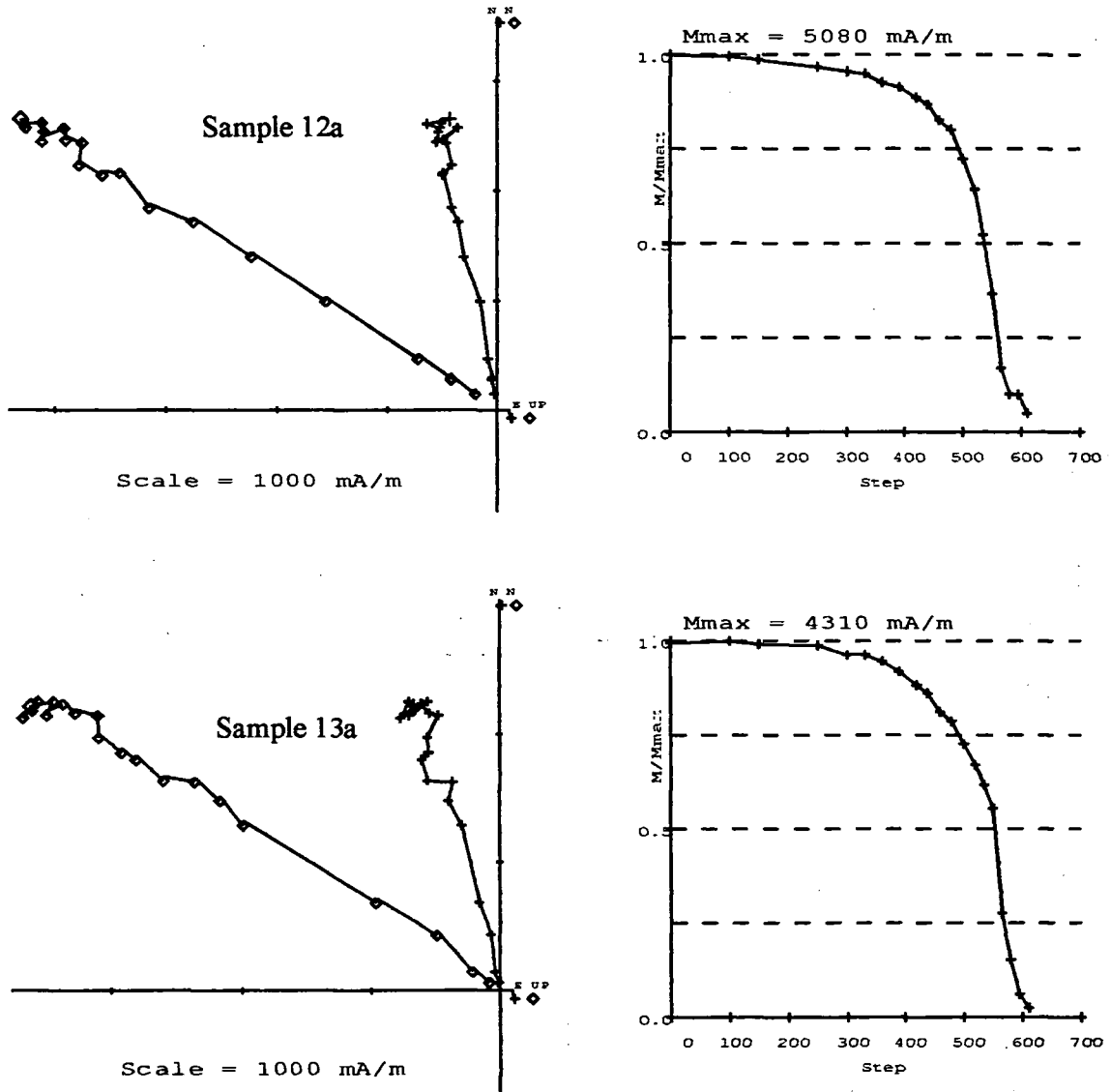
Fig. 5.50 - Site V42: Zijderveld diagrams and Intensity plots.

AD 1839 site V42

Sample 01A

Steps	Dec	Inc	MAD
"D" 580/ 620	357.3	55.5	0.4
"D" 520/ 620	355	57	1.2
"O" 520/ 620	354.5	56.7	1

(*) erasing steps 480°C   (a)

Sample 02A

Steps	Dec	Inc	MAD
"D" 550/ 620	349.3	56.3	1.2
"O" 550/ 620	349.2	55.9	0.8
"D" 500/ 580	344.5	58.3	1.6
"D" 500/ 620	344.7	58.1	1.4
"O" 500/ 620	345.2	57.7	1.2

(*) erasing step 500°C   (b)

Sample 04A

Steps	Dec	Inc	MAD
"D" 565/ 620	354.2	56.9	0.9
"O" 565/ 620	353.3	56.2	0.8
"D" 520/ 620	353.5	57.6	0.9
"O" 520/ 620	353.5	57.2	0.8
"D" 440/ 620 (*)	353.9	57.1	0.8
"O" 440/ 620 (*)	353.9	57	0.6

(*) erasing step 500°C   (c)

Sample 06A

Steps	Dec	Inc	MAD
"D" 520/ 620	353.2	57.2	0.7
"O" 520/ 620	352.4	56.9	0.8

(e)

Sample 08A

Steps	Dec	Inc	MAD
"D" 550/ 620	350.2	55.7	3.3
"O" 550/ 620	350	54.6	1.9
"D" 500/ 550	341.4	58.2	2.8
"D" 520/ 620 (*)	346	55.7	1.2
"O" 520/ 620 (*)	346.7	55.5	1

(*) erasing step 550°C   (e)

Sample 10A

Steps	Dec	Inc	MAD
"D" 520/ 595	350.2	58.1	1.4
"O" 520/ 595	350.6	57.3	1.1
"D" 460/ 595 (*)	349.2	57.7	0.9
"O" 460/ 595 (*)	349.7	57.3	0.7

(*) erasing step 500°C   (f)

Sample 12A

Steps	Dec	Inc	MAD
"D" 550/ 610	351.3	57.9	0.7
"O" 550/ 610	351.1	57	0.7
"D" 480/ 550	344	58	3.4
"D" 480/ 610 (*)	346.9	58.1	1.4
"O" 480/ 610 (*)	347.6	57.7	0.9

(*) erasing step 550°C   (g)

Sample 13A

Steps	Dec	Inc	MAD
"D" 580/ 610	351.8	46.5	2.9
"O" 580/ 610	350.5	49.2	2.5
"D" 535/ 580	343.7	57.5	2.4
"D" 535/ 610	345.3	56	2.4
"O" 535/ 610	346.1	55.1	1.7
"D" 550/ 610 (*)	347.1	56.3	1.4
"O" 550/ 610 (*)	347	55.8	1

(*) erasing step 580°C   (h)

Tab. 5.21 - Site V42: Directional results calculated using principal component analysis (Kirschvink, 1980).
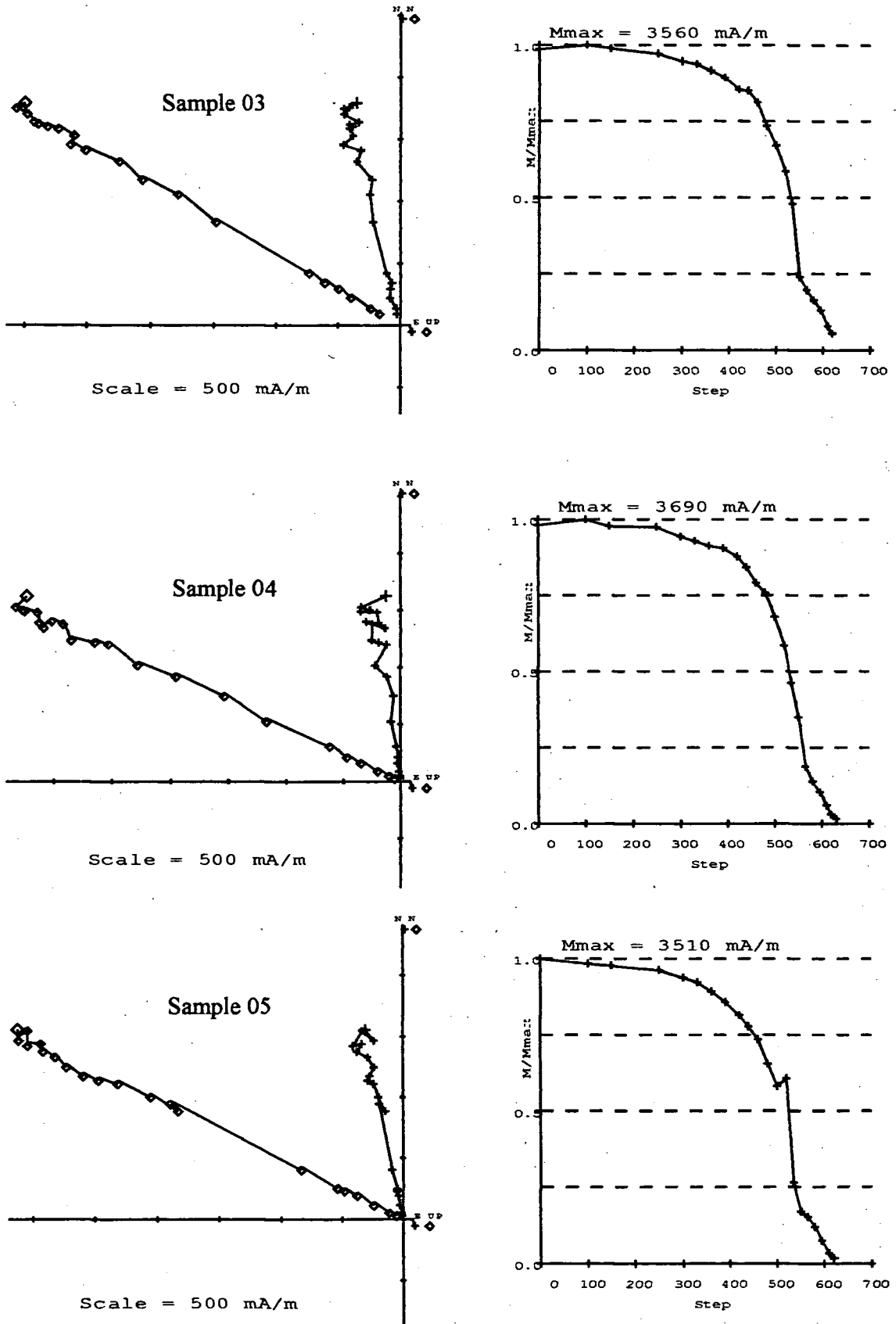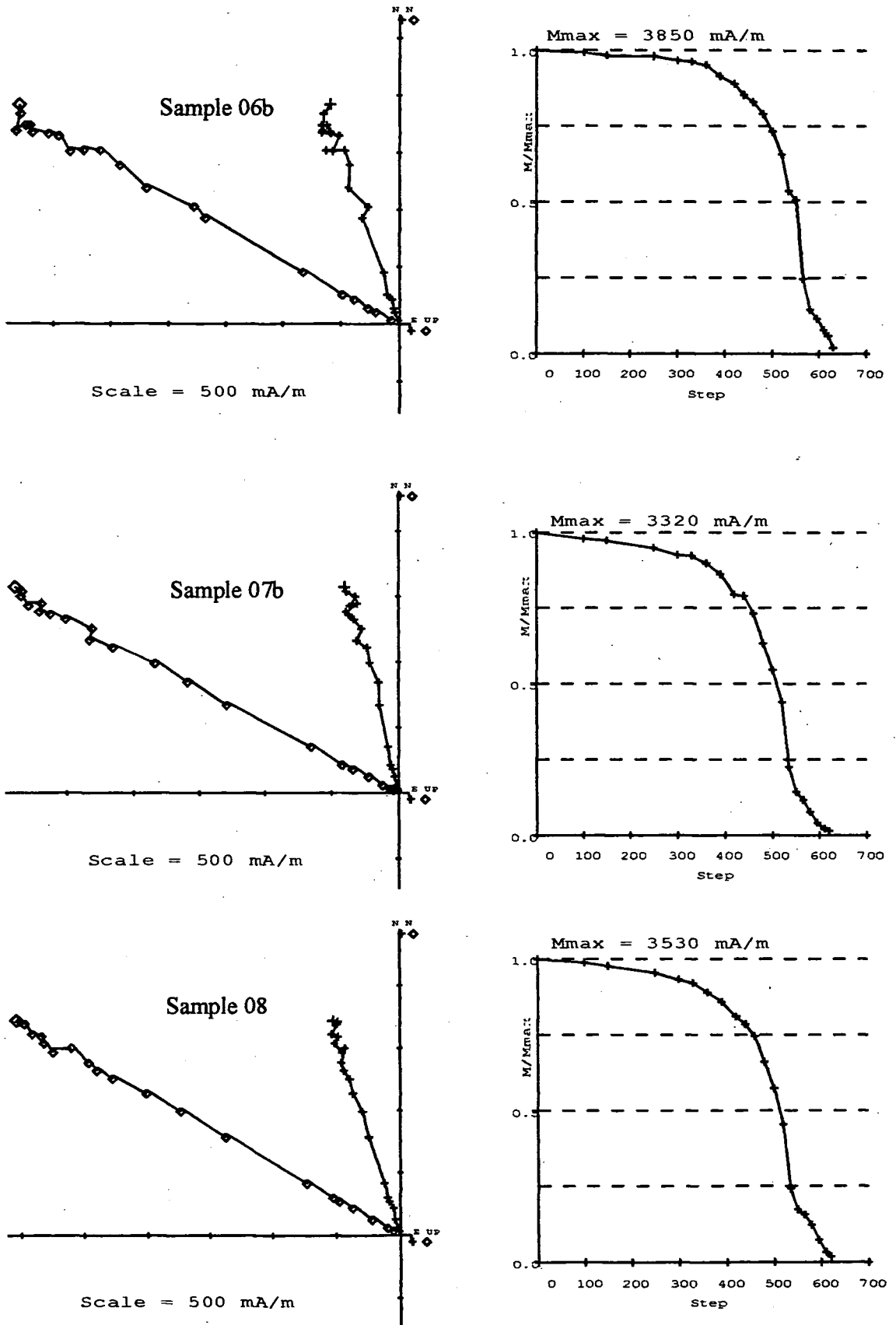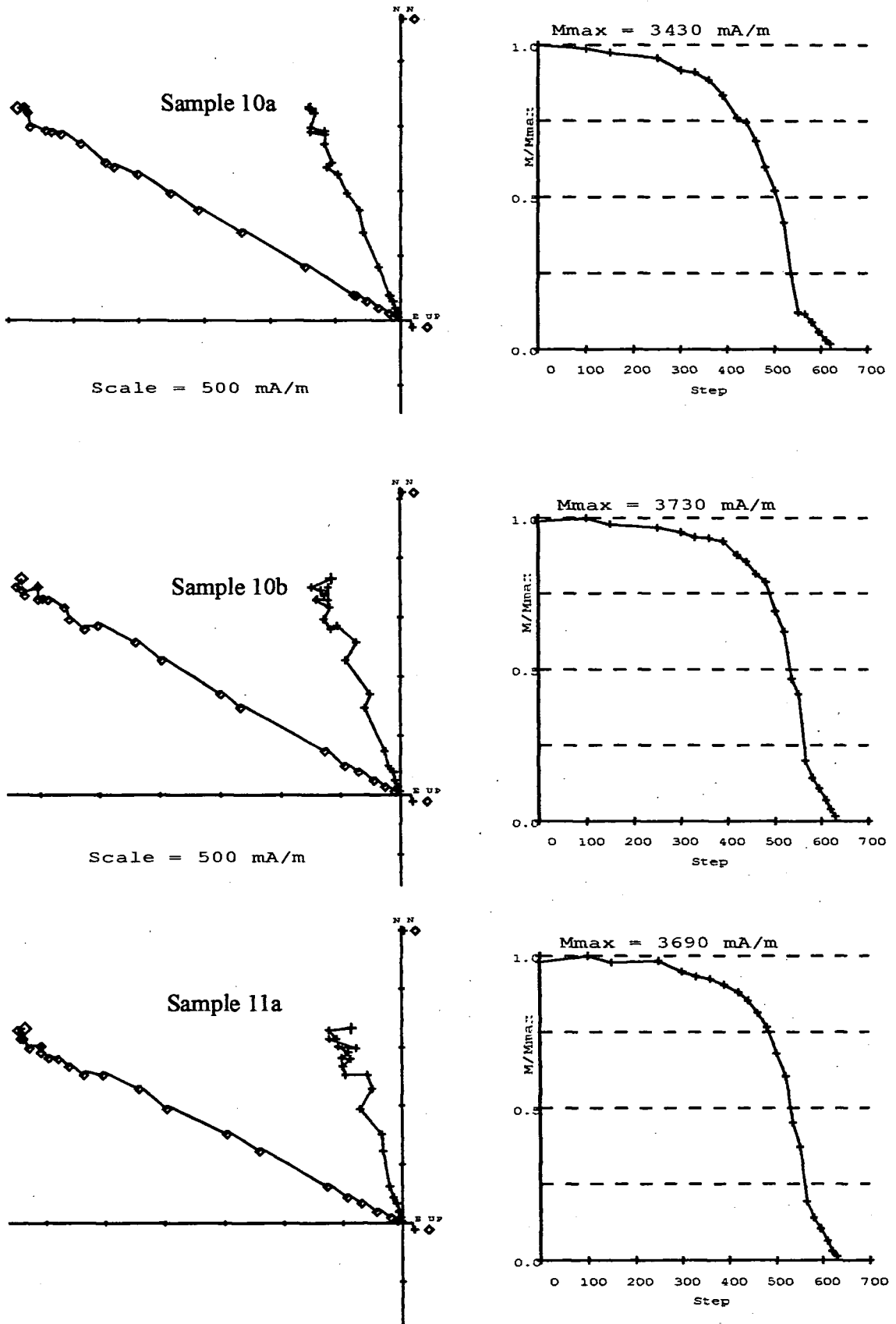
Sample 01b

Scale = 1000 mA/m

Mmax = 4950 mA/m

Sample 03a

Scale = 1000 mA/m

Mmax = 4940 mA/m

Sample 04a

Scale = 1000 mA/m

Mmax = 5370 mA/m
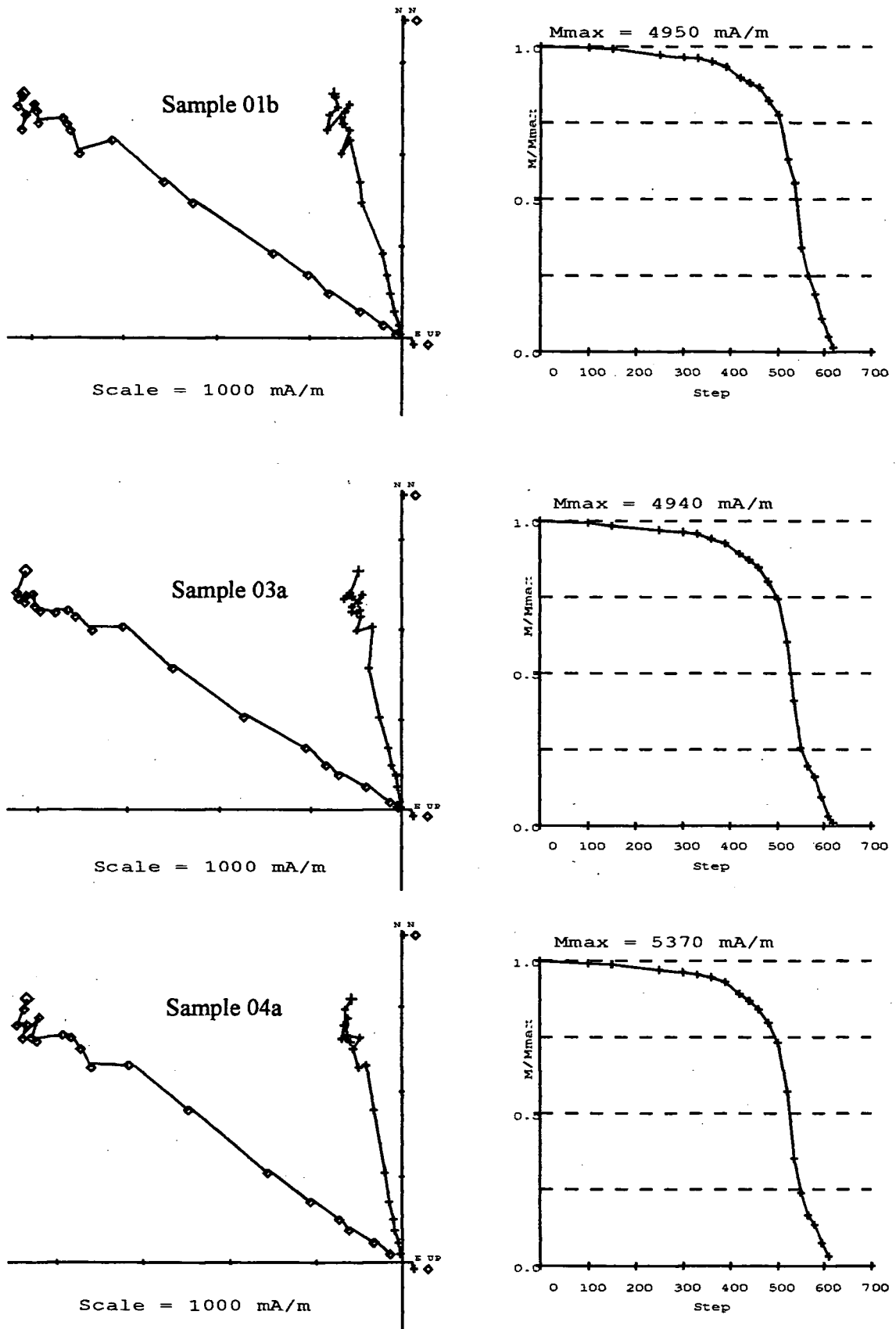
Fig. 5.51 - Site V43: Zijderveld diagrams and Intensity plots.
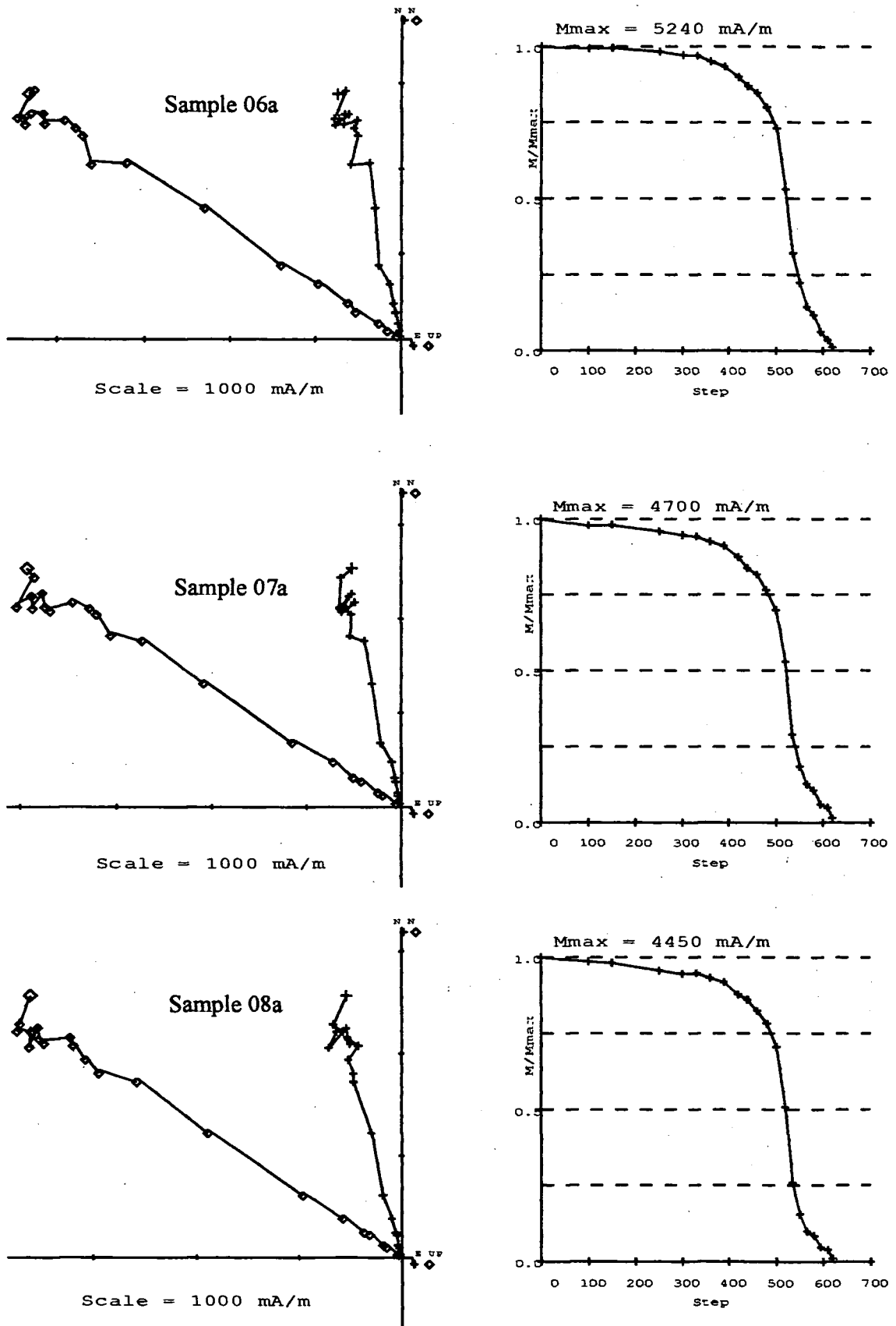
Fig. 5.52 - Site V43: Zijderveld diagrams and Intensity plots.

Sample 09b

Scale = 1000 mA/m

Mmax = 5290 mA/m

Sample 12a

Scale = 1000 mA/m

Mmax = 4940 mA/m
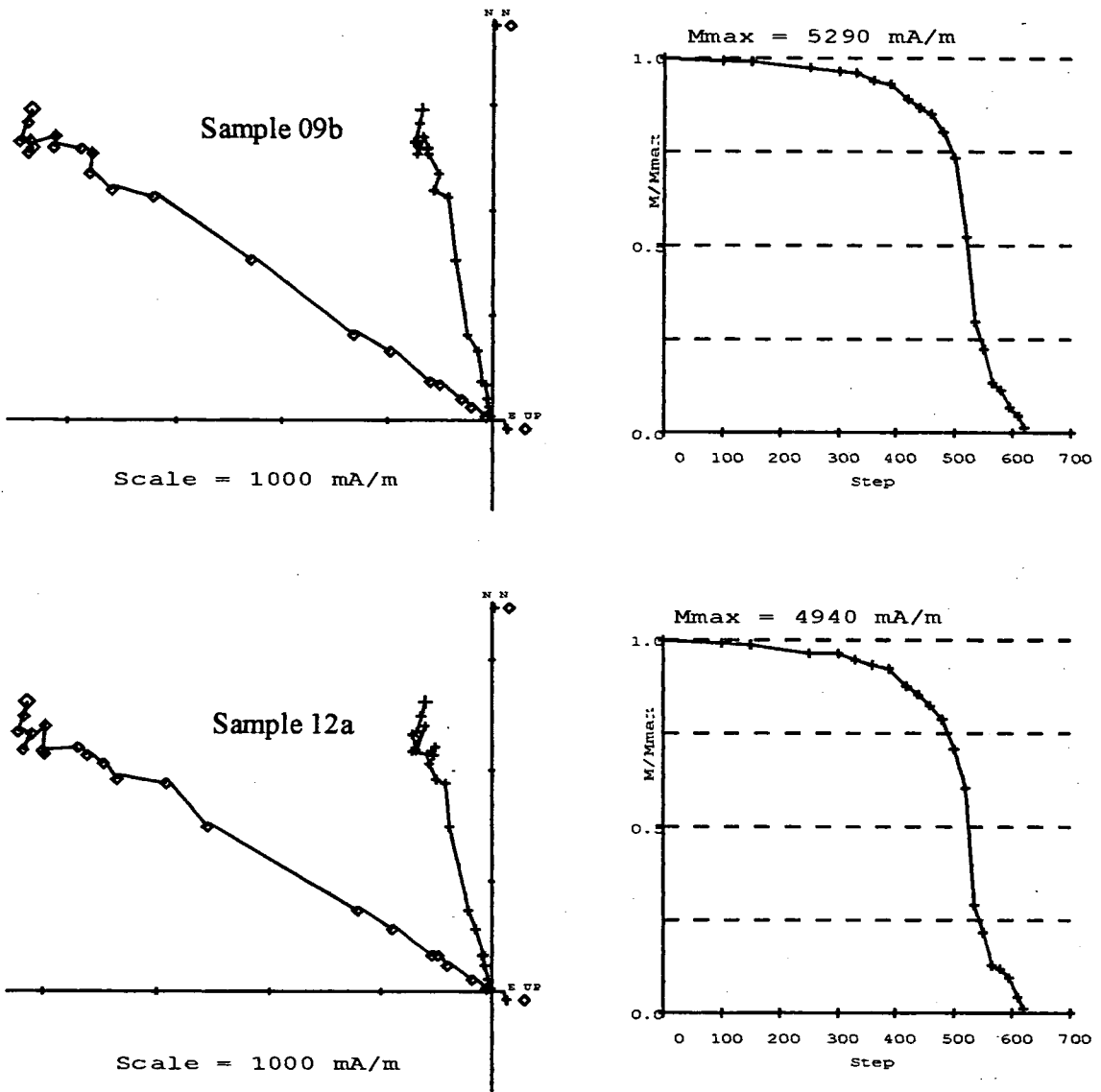
Fig. 5.53 - Site V43: Zijderveld diagrams and Intensity plots.

AD 1839 site V43

Sample 01B			
Steps	Dec	Inc	MAD
"D" 550/ 620	347.3	56.1	1.5
"O" 550/ 620	346.6	56.2	0.9
"D" 500/ 550	344	53.5	2.5
"D" 500/ 620	344.8	54.9	1.4
"O" 500/ 620	345.1	55.3	0.9

(a)

Sample 07A			
Steps	Dec	Inc	MAD
"D" 550/ 620	349	56.1	1.8
"O" 550/ 620	347.6	56.6	1.1
"D" 500/ 620 (*)	347.5	56.8	0.6
"O" 500/ 620 (*)	347.3	56.9	0.5

(*) erasing step 535°C   (e)

Sample 03A			
Steps	Dec	Inc	MAD
"D" 580/ 620	351.5	60.6	2.4
"O" 580/ 620	350.6	59.4	1.9
"D" 520/ 580	346.1	56.8	1.9
"D" 520/ 620 (*)	346.9	57.7	1.3
"O" 520/ 620 (*)	347.2	57.6	0.8

(*) erasing step 580°C   (b)

Sample 08A			
Steps	Dec	Inc	MAD
"D" 580/ 620	349.6	54.5	2.1
"O" 580/ 620	347.5	54.3	1.3
"D" 500/ 620	345.3	55.9	1.1
"O" 500/ 620	345.4	55.8	0.8

(f)

Sample 04A			
Steps	Dec	Inc	MAD
"D" 500/ 610	349.9	53.2	1.3
"O" 500/ 610	349.5	54	1.1
"D" 550/ 610	348	56	2.1
"O" 550/ 610	348.2	55.9	1

(c)

Sample 09B			
Steps	Dec	Inc	MAD
"D" 580/ 620	350.4	54.7	1.3
"O" 580/ 620	348.2	55	1
"D" 500/ 620 (*)	348.4	55.9	0.7
"O" 500/ 620 (*)	348.2	55.8	0.5

(*) erasing steps 535,575°C   (g)

Sample 06A			
Steps	Dec	Inc	MAD
"D" 550/ 620	348.6	55.8	2.2
"O" 550/ 620	348.5	56	1.3
"D" 500/ 620 (*)	349.7	56.5	1
"O" 500/ 620 (*)	349.4	56.4	0.7

(*) erasing step 535°C   (d)

Sample 12A			
Steps	Dec	Inc	MAD
"D" 520/ 620	345.6	58.9	1
"O" 520/ 620	345.5	58.5	0.8

(*) erasing step 580°C   (h)

Tab. 5.22 - Site V43: Directional results calculated using principal component analysis (Kirschvink, 1980).

Sample 01a

Scale = 500 mA/m

Mmax = 2930 mA/m

Sample 03a

Scale = 500 mA/m

Mmax = 3210 mA/m

Sample 04b

Scale = 500 mA/m

Mmax = 3470 mA/m

Fig. 5.54 - Site V44: Zijderveld diagrams and Intensity plots.

Sample 07a

Scale = 500 mA/m

Mmax = 3090 mA/m

Sample 08a

Scale = 500 mA/m

Mmax = 1950 mA/m

Sample 09a

Scale = 500 mA/m

Mmax = 3580 mA/m
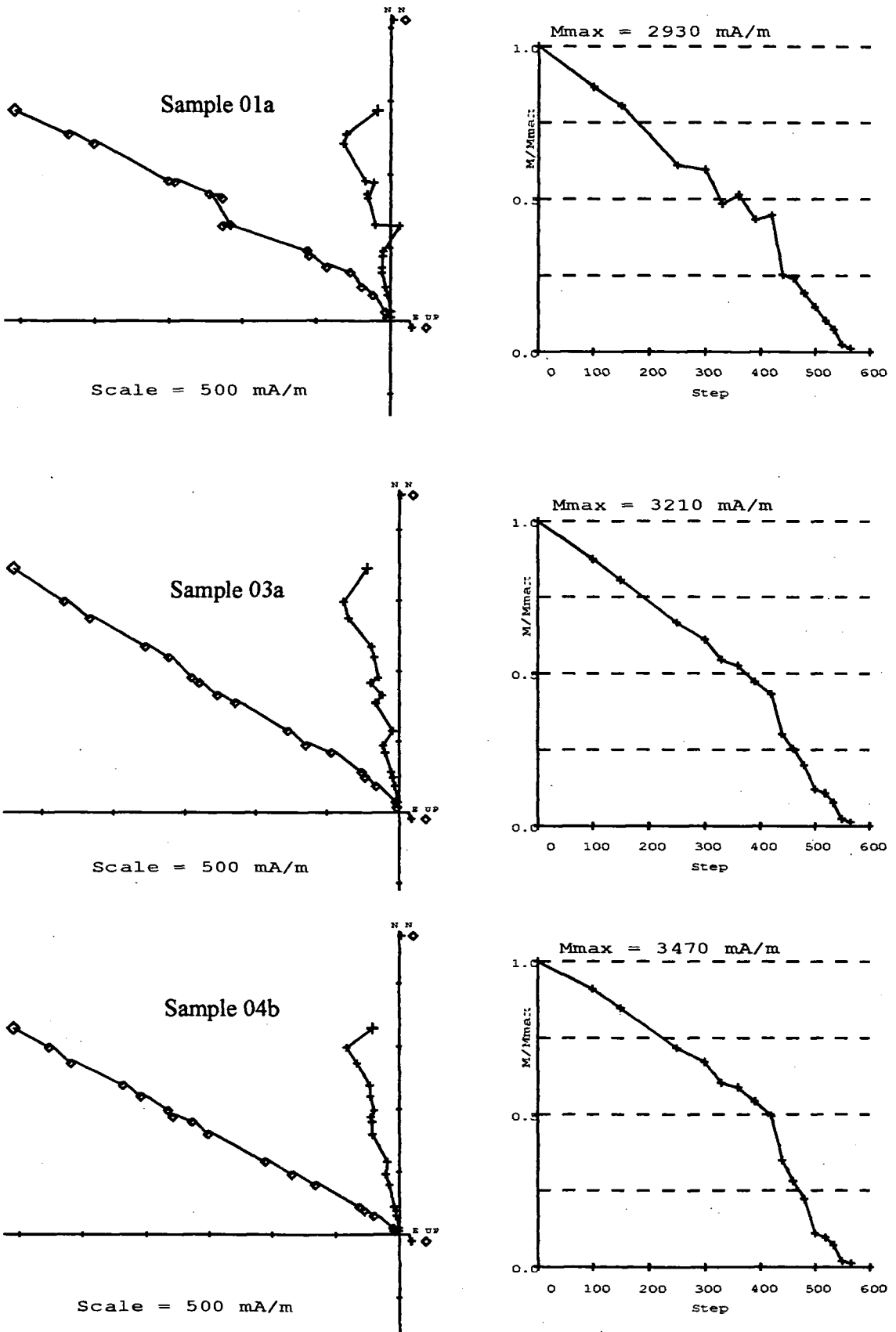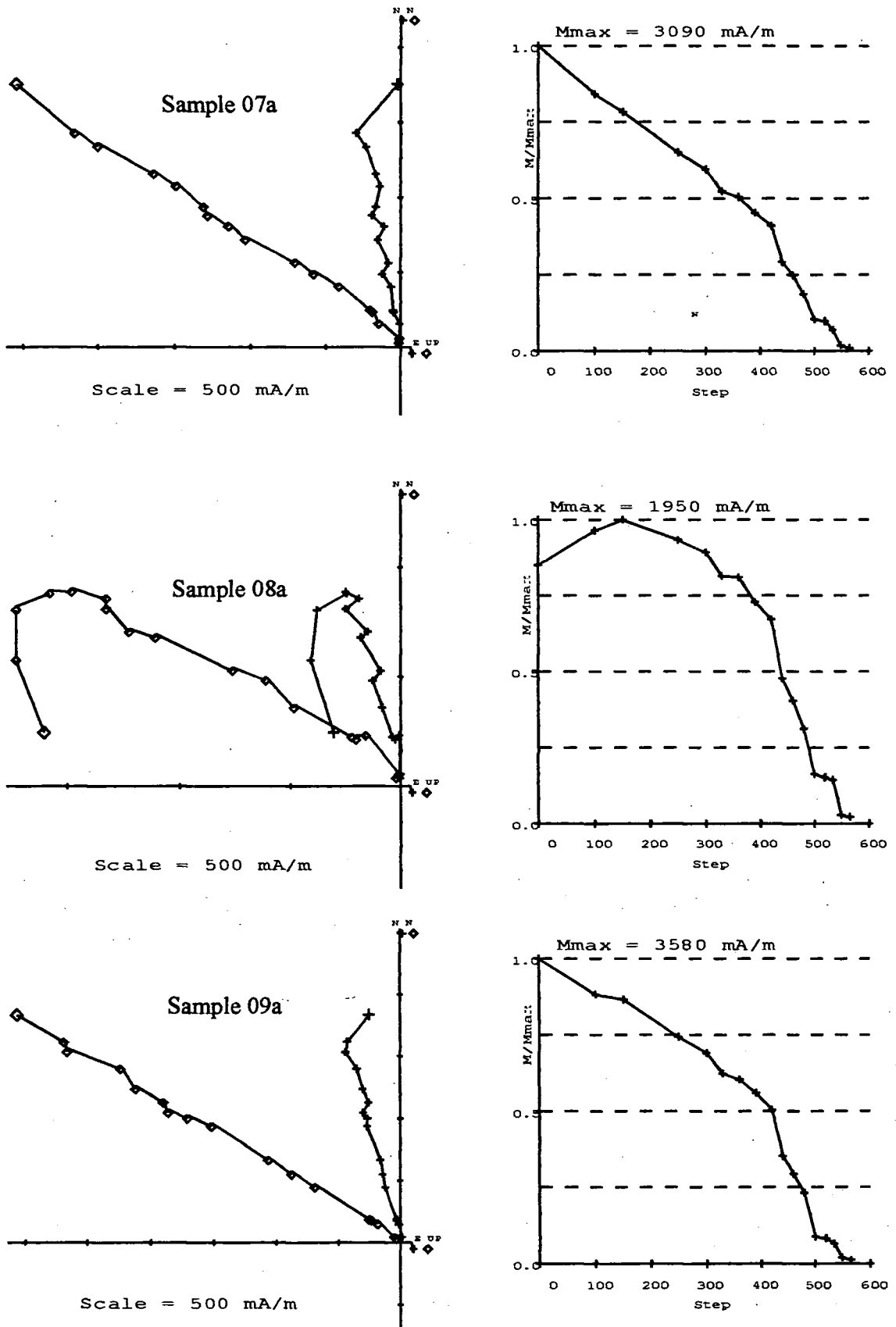
Fig. 5.55 - Site V44: Zijderveld diagrams and Intensity plots.
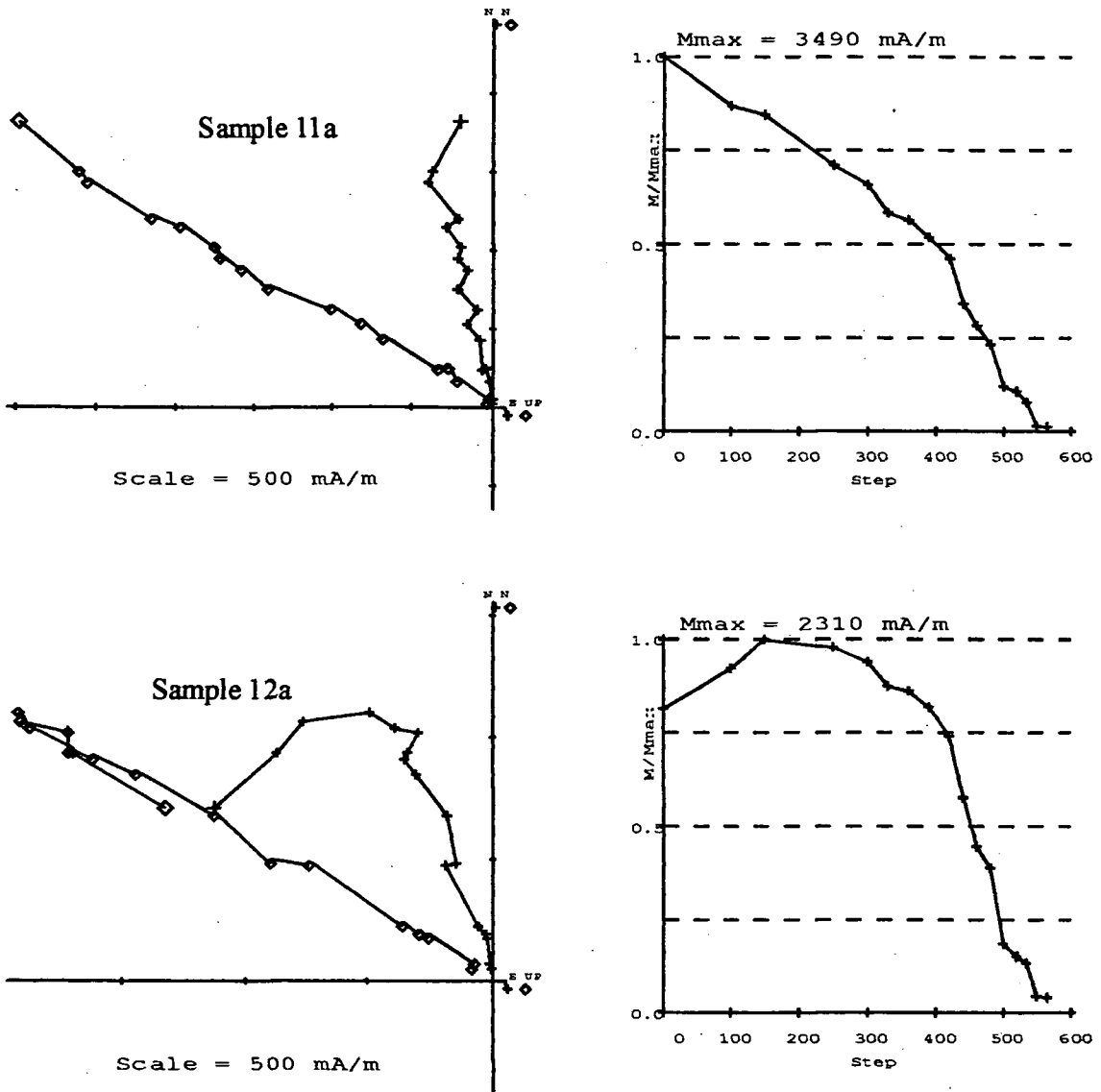
Fig. 5.56 - Site V44: Zijderveld diagrams and Intensity plots.

Sample 01A			
Steps	Dec	Inc	MAD
"D" 500/ 565	348.7	39.7	3.5
"D" 150/ 480	344.8	61.1	4.4
"D" 250/ 480 (*)	348.6	61.8	3.1

(*) erasing steps 300,330,360°C   (a)

(*) erasing steps ,420,440°C

Sample 08A			
Steps	Dec	Inc	MAD
"D" 460/ 520	340.1	56.1	4
"D" 360/ 520 (*)	340.7	60.9	2.6

(*) erasing steps 390,440°C   (e)

Sample 03A			
Steps	Dec	Inc	MAD
"D" 480/ 565	346.3	49.3	3.4
"D" 20/ 460	348.4	58.4	4.8
"D" 250/ 440 (*)	346.3	57.9	2.6

(*) erasing steps 360,420°C   (b)

Sample 09A			
Steps	Dec	Inc	MAD
"D" 420/ 565	343.4	57.8	1.2
"D" 390/ 520 (*)	344.2	59.6	1.1

(*) erasing step 420°C   (f)

Sample 04B			
Steps	Dec	Inc	MAD
"D" 480/ 565	347.9	59.4	2.5
"D" 480/ 550	347.5	60.3	2.1
"D" 250/ 480	347.9	62.1	2.5
"D" 420/ 550	344.5	62.4	1.3

(c)

Sample 11A			
Steps	Dec	Inc	MAD
"D" 520/620	351.3	63.7	0.5
"O" 520/620 (*)	350.7	63.7	0.5

(g)

Sample 07A			
Steps	Dec	Inc	MAD
"D" 100/ 520	350.2	58.3	2.7

(d)

Sample 12A			
Steps	Dec	Inc	MAD
"O" 440/ 565 (*)	345.1	58.7	1.9

(*) erasing step 480, 550°C   (h)

Tab. 5.23 - Site V44: Directional results calculated using principal component analysis (Kirschvink, 1980).

Chapter VI

THELLIER PALAEOINTENSITY PROPERTIES

6.1 - Introduction

In this chapter all the results obtained from the MTT experiment (section 3.4a) will be analysed and described using Zijderveld diagrams, Intensity plots and stereographic projections.

Intensity - A complete description of its general behaviour throughout the experiments will be given together with the initial and final NRM values. Anomalies and significant T_{ub} will also be pointed out.

Directions - Both vertical and horizontal components will be peculiarly analysed, pointing out break points and anomalies.

Palaeointensity results – As described in section 3.4, tests for magnetic alteration during experiments are normally carried out in Thellier-type methods and pTRM checks are used to identify the temperature at which alteration starts. Furthermore comparisons between the intensity and direction obtained from the first thermal demagnetization at Tj and those obtained from the second, again at Tj, can be useful to check for MD remanence or CRM growth. For this study (see the stringent experimental procedure adopted described in section 3.4a) pTRM checks have been performed for each temperature steps used. Because of the large number of information obtained from steps C and D of the MTT experiment (respectively demag2 and pTRMck) and because of the difficulty of display all of them in a conventional NRM/TRM plot, a different way to use and display the pTRM checks will be adopted. Steps C and D will be used to get another estimate of the palaeofield while, taken singularly, they will still give information about the onset of the alteration and on the presence of MD or CRM remanence. In other words the pTRM checks data will be also used to calculate a "backup" field intensity. The palaeofield value obtained from the first two steps of the MTT experiment (A-demag1 and B-pTrm) will be considered as principal value. It will be used as a guide when detecting the palaeofield from the other two steps (C-demag1 and D-pTRmck),

especially when more then one slope is present. However all the possible slopes will be reported in a table with the relative temperature ranges and statistical parameters. Any anomalous point on the NRM/TRM plots will be excluded from the computation of the palaeointensity, provided that they also appear to be clearly irregular on the NRM demagnetization and TRM acquisition curves. The first two steps of the MTT experiment will be referred to as MTT (A-B) while the other two will be MTT (C-D).

6.2 - AD 79 - AD 1631

6.2.1 - Site V30

A-Demag1

Intensity Behaviour - Sample 8 had an initial NRM of 2660 mA/m but, by 595 °C, was not completely demagnetized (Fig. 6.1). It showed a smooth decrease in intensity all over the spectra, with no tail at the end, and some 10% of the original remanence still remained. Some small irregularities occurred around 500 and 565°C.

Directional Behaviour - Both vertical and horizontal components moved towards the origin (although they did not reach it), with a very linear trend especially above 360°C. Minor anomalies occurred around 300°C (Fig. 6.1).

B-pTRM

Intensity Behaviour - The sample showed a linear decrease from 2600 to 1780 mA/m (500°C), with a small deflection at 300°C. From 500 to 595°C it showed a zigzag behaviour without any significant increase or decrease in intensity. At the end of the process the intensity was 1750 mA/m (Fig. 6.1).

Directional Behaviour- The vertical component moved gradually downwards from the NRM direction starting from the first steps. The horizontal component showed an unclear linear trend towards the origin. The stereo plot showed an unmistakable gradual movement of the Inc toward 90° as a consequence of gradually removing the NRM and progressively applying a TRM along the z-axis (Fig. 6.1).

150

Palaeointensity results from A-B - The NRM/TRM plot showed a unique slope (Fig.6.2a) therefore one possible value of the palaeofield was determined (Tab. 6.1). Both NRM demagnetization and TRM acquisition curves (Figs 6.2b,c) did not show any particular irregularities.

C-Demag2

Intensity Behaviour - In this second demagnetization the sample behaved almost exactly the same as in Demag1. It showed an initial NRM of 2660 mA/m and by 595°C it was not completely demagnetized; a smooth decrease in intensity all over the spectra, with no tail at the end; some 10% of the original remanence still remained. A small but clear irregularity occurred at 565°C (Fig. 6.3a).

Directional Behaviour - Both vertical and horizontal components behaved as in Demag1. Only the vertical component showed a significant deflection downward at 565°C. The stereo plot underlined the same irregularity with a clear movement of Inc toward 90° (Fig. 6.3a).

D-pTRMck

Intensity Behaviour - The initial intensity was 2560 mA/m at 100°C. There was a steep decrease from this temperature to 150° followed by a very shallow one until 300°. From this point, to 500°C, the behaviour was the same as in the pTRM. A clear increase occurred between 520 and 550° followed by a decrease until 580°C. The final intensity was 1650 mA/m (Fig. 6.3b).

Directional Behaviour - Vertical and horizontal components showed an unclear trend until 520°C when a significant deflection, towards the North, occurred. This was followed by a random behaviour. In general both components moved downward and westward, respectively. The stereo plot showed, as expected, a gradual movement of Inc toward 90° but also a clear deflection of Dec at 520°C (Fig. 6.3b).

Palaeointensity results from C-D - The NRM/TRM plot showed a slightly concave curve (Fig. 6.4a). Two different slopes were considered (Tab. 6.2) plus another one excluding two points which appeared anomalous on both NRM and TRM curves (Fig. 6.4b,c).

A-Demag1

B-pTRM

Scale 500 mA/m

Scale 500 mA/m

Mmax = 2660 mA/m

Mmax = 2690 mA/m

☐ Lower
▲ Upper

Core
Coordinates
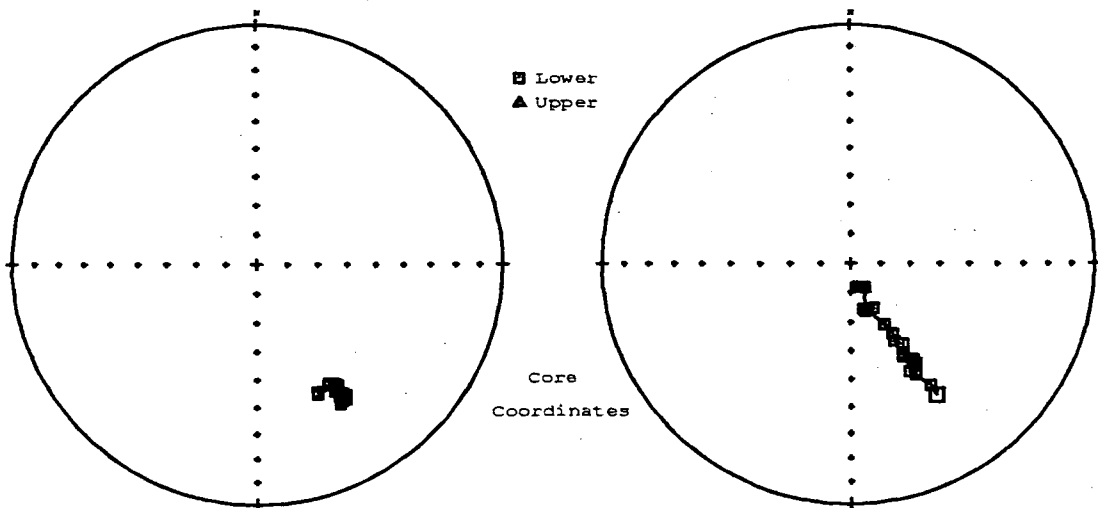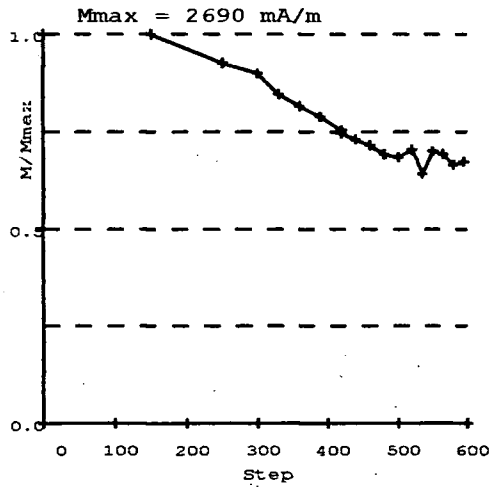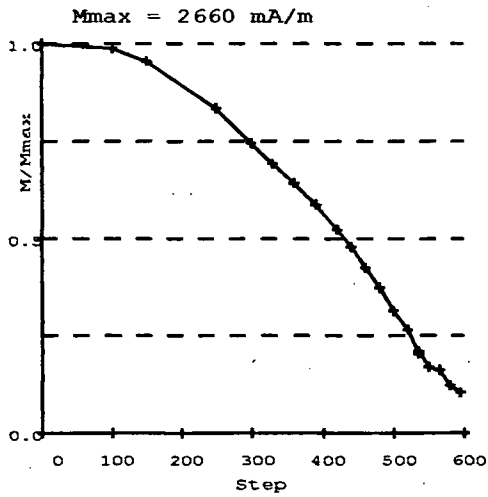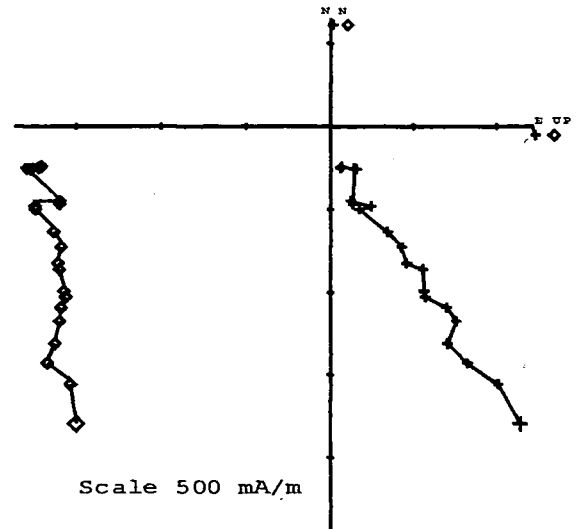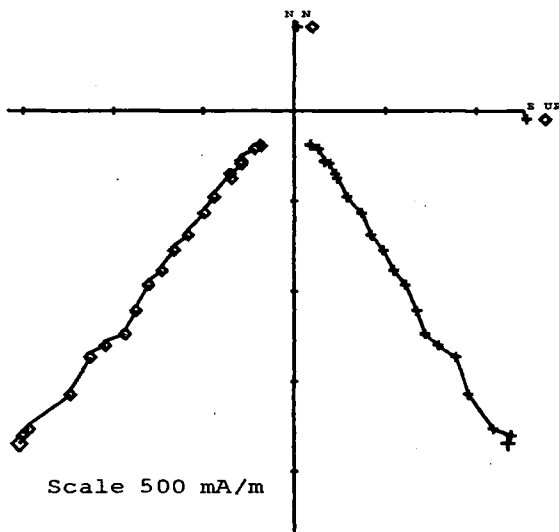
Fig. 6.1 - Site V30: Zijderveld diagrams, Intensity and stereo plots.

V30.8 steps	NRM (A/m)	TRM (A/m)
20	2.662	0.000
100	2.628	0.000
150	2.538	0.071
250	2.217	0.305
300	1.978	0.553
330	1.844	0.588
360	1.708	0.668
390	1.563	0.716
420	1.395	0.769
440	1.270	0.870
460	1.127	0.949
480	0.994	1.009
500	0.836	1.144
520	0.708	1.307
535	0.557	1.264
550	0.453	1.512
565	0.432	1.486
580	0.327	1.496
595	0.278	1.549

a)

MTT (A-B) - AD 79 -1631 - Sample V30.8
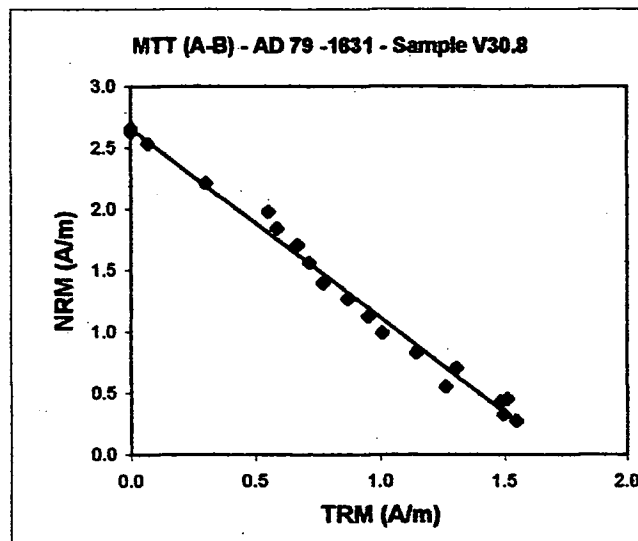
sample	Temp (°C)	N	f	g	q	b	R^2	Fpalaeo (μT)	σ_b
V30.8	150 - 595	17	0.849	0.924	24.607	-1.574	0.959	78.718	0.050

NRM - sample V30.8

TRM - Sample V30.8
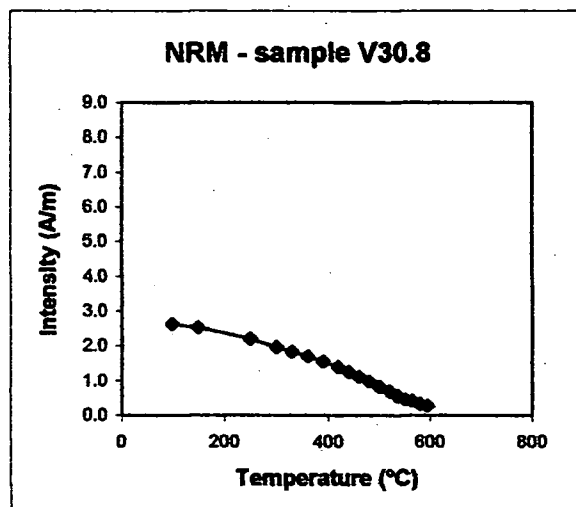
b)
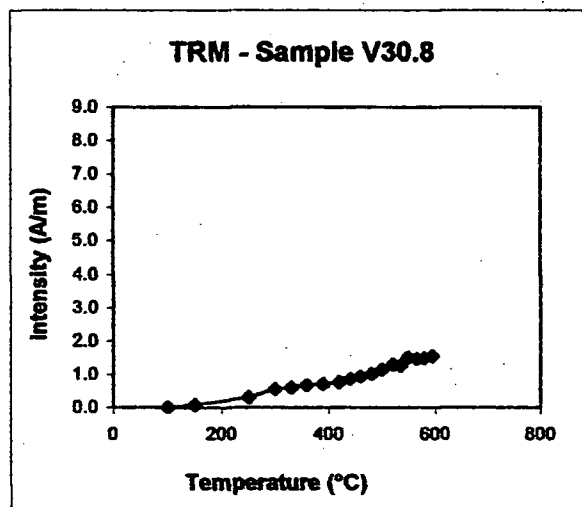
c)

Fig. 6.2 - Site V30: a)NRM/TRM plot and respective values, b)NRM demagnetization and c)TRM acquisition curves.

Tab. 6.1 - Site V30: Palaeofields estimated and statistical parameters

C-Demag2

D-pTRMck

Scale 500 mA/m

Scale 500 mA/m

Mmax = 2550 mA/m

Mmax = 2560 mA/m

☐ Lower
▲ Upper

Core
Coordinates
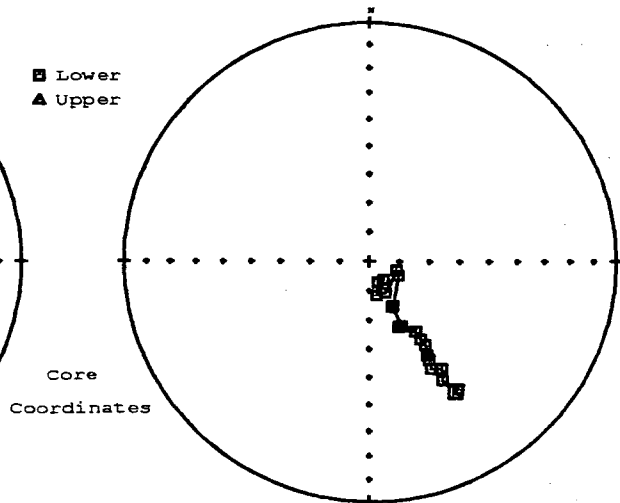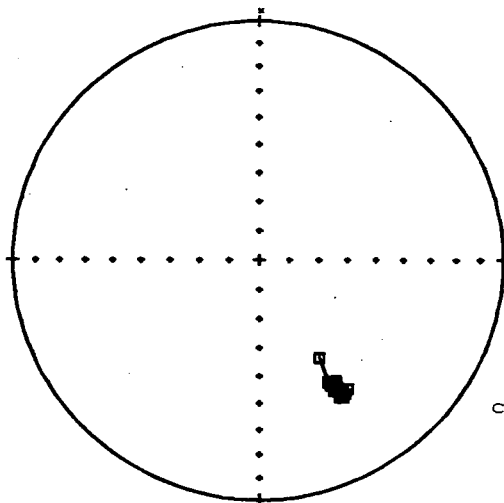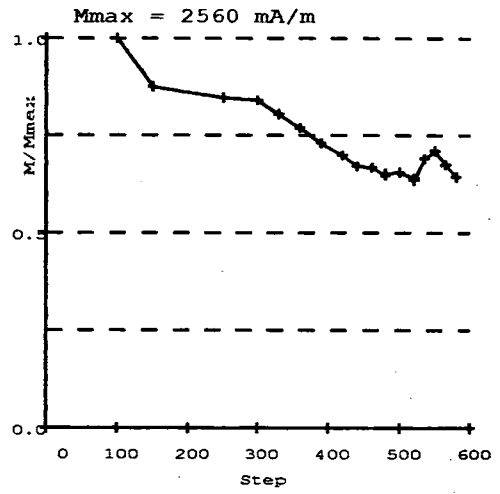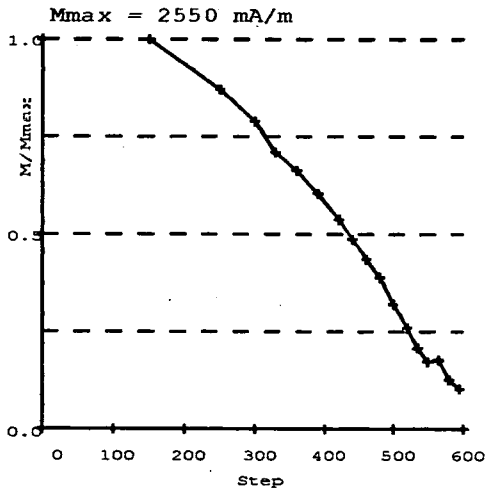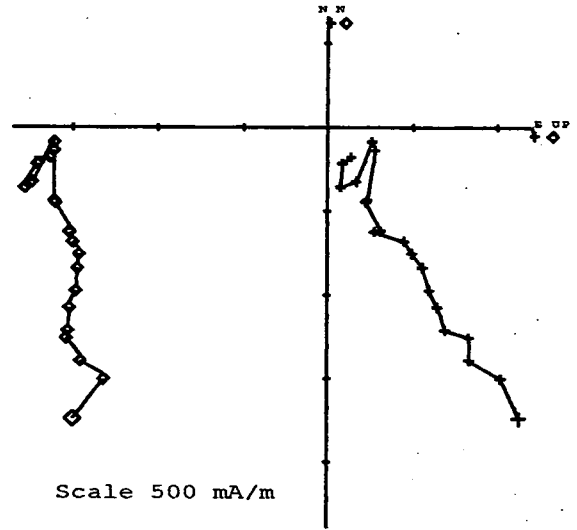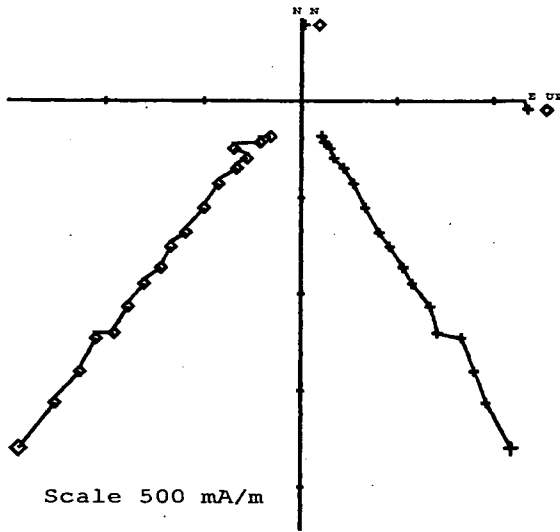
Fig. 6.3 - Site V30: Zijderveld diagrams, Intensity and stereo plots.

MTT (C-D)		
V30.8 steps	NRM (A/m)	TRM (A/m)
20	0.000	0.000
100	0.000	0.000
150	2.550	0.331
250	2.220	0.295
300	2.010	0.440
330	1.810	0.505
360	1.690	0.582
390	1.540	0.610
420	1.370	0.678
440	1.240	0.753
460	1.110	0.835
480	0.990	0.931
500	0.815	1.109
520	0.660	1.232
535	0.528	1.404
550	0.439	1.505
565	0.451	1.362
580	0.321	1.425
595	0.000	0.000

a)

MTT (C-D) - AD 79 -1631 - Sample V30.8
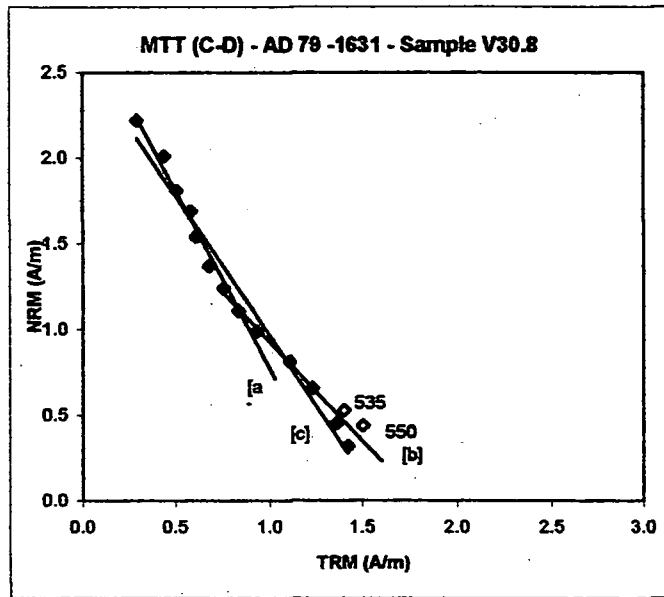
sample	Temp (°C)	N	f	g	q	b	R^2	Fpalaeo (μT)	σ_b
V30.8	[a] 250 - 480	9	0.482	0.869	8.670	-2.092	0.982	104.619	0.101
	[b] 440 - 580	9	0.360	0.848	4.192	-1.175	0.963	58.758	0.086
	*[c] 250 - 580	13	0.745	0.913	14.401	-1.646	0.976	82.319	0.078

*excluding 535,550 (empty diamonds)

NRM - sample V30-8

c)

TRM - Sample V30-8
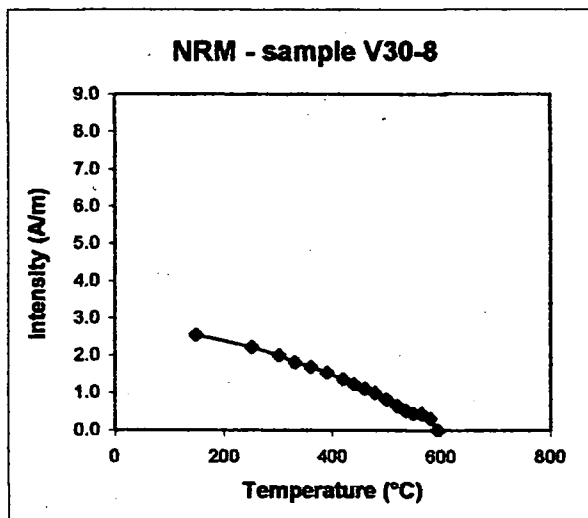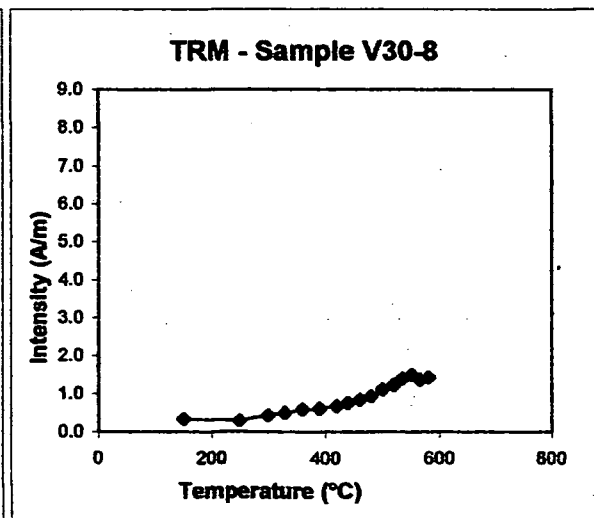
b)

Fig. 6.4 - Site V30: a)NRM/TRM plot and respective values, b)NRM demagnetization and c)TRM acquisition curves.

Tab. 6.2 - Site V30: Palaeofields estimated and statistical parameters

155

6.2.2 - Site V36

A-Demag1

Intensity Behaviour- Sample 17 had an initial NRM of 7080 mA/m and, by 595°C, was almost completely demagnetized (< 2%). The intensity decay had an accelerating decrease with increasing temperature terminating with a very small tail. An anomalous increase (about 1500 mA/m) occurred at 565°C (Fig. 6.5).

Directional Behaviour - The vertical component moved toward the origin with a very linear trend but showed a significant deflection downwards at 565°C. The same irregularity was clear in the stereo plot, which showed the Inc moving toward 90° at 565°C. The horizontal component showed a linear trend especially above 460°C, and moved clearly toward the origin (Fig. 6.5).

B-pTRM

Intensity Behaviour - The sample had a decrease trend, from 7020 to 2340 mA/m (535°C), very similar to that described in Demag1 except for a clear deflection at 390°C. From 535 to 595°C it showed a zigzag behaviour with very significant increases and decreases in intensity (about 2600 mA/m). At the end of the process the intensity was 4220 mA/m (Fig. 6.5).

Directional Behaviour - The horizontal component showed a moderately linear trend towards the origin but without reaching it. The vertical one moved almost linearly northwards until 520°C, except for an upward deflection at 390°C. Another upward deflection occurred at 535°C followed by a zigzag behaviour until the end of process. The stereo plot showed the usual movement of the Inc toward 90° but with a noticeable jump at 520°C (Fig. 6.5).

156

Palaeointensity results from A-B - The NRM curve showed an anomalous behaviour at 565°C (Fig. 6.6b) while the TRM one showed a zigzag trend above 520°C (Fig. 6.6c). Two distinct slopes were showed by the NRM/TRM plot (Fig. 6.6a) excluding two clearly irregular points (Tab. 6.3).

C-Demag2

Intensity & Directional Behaviour -In this second demagnetization, the sample behaved in exactly the same way as in Demag1 (Fig. 6.7).

D-pTRMck

Intensity Behaviour - The intensity decreased from 7030 to 2210 mA/m (500°C), similarly to Demag1, but with a small deflection at 300°C. From 500 to 550°C it showed a significant increase (about 2600 mA/m) followed by a small decrease until 580°C. The final intensity was 4030 mA/m (Fig. 6.7).

Directional Behaviour - The horizontal component showed a linear trend towards the origin but without reach it. The vertical one moved almost linearly northwards until 480°C when a significant upward deflection occurred. After this point it moved downward until 550°C. The stereo plot showed an irregular movement of the Inc toward 90° (Fig. 6.7).

Palaeointensity results from D-C - Some points above 520°C which appeared irregular in all the curves (Fig. 6.8a,b,c) were not considered. The NRM/TRM plot showed a very unreadable behaviour and several possibles slopes were considered (Tab. 6.4).

AD 79-1631 sample V36.17

A-Demag1

B-pTRM

Scale 1000 mA/m

Scale 1000 mA/m

Mmax = 7080 mA/m

Mmax = 7020 mA/m

Fig. 6.5 - Site V36: Zijderveld diagrams, Intensity and stereo plots.

□ Lower
▲ Upper
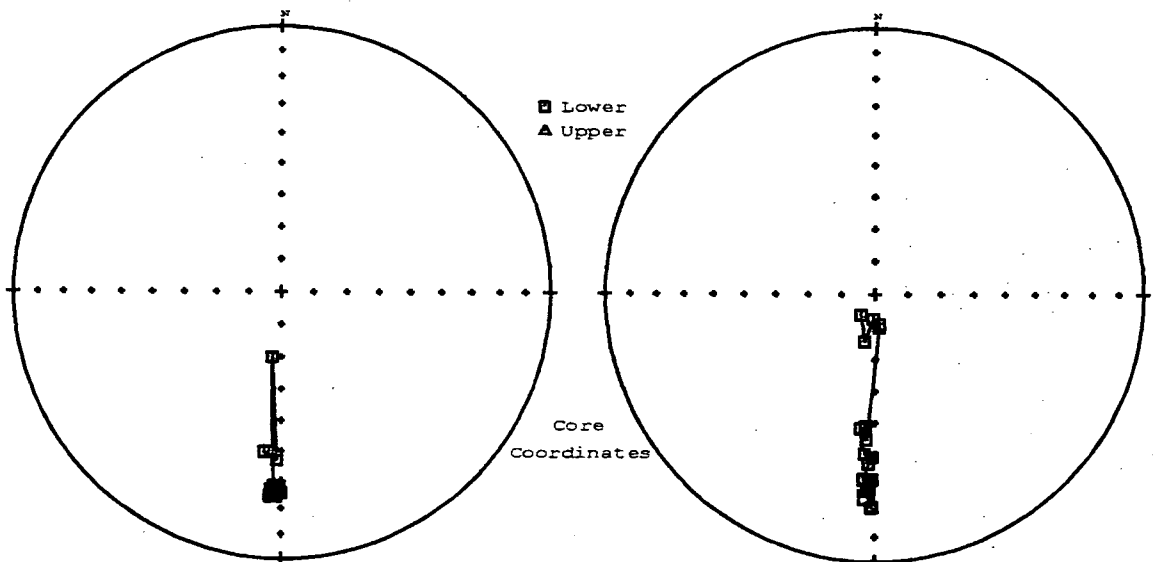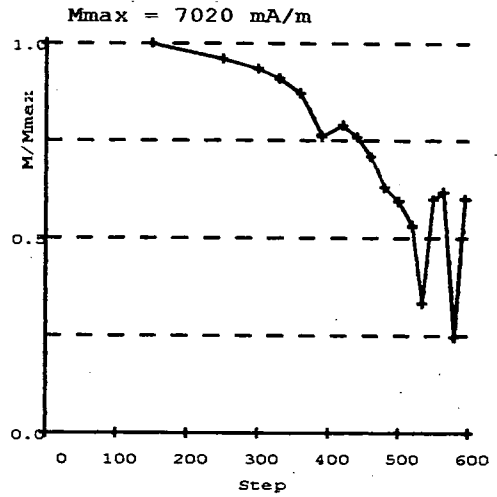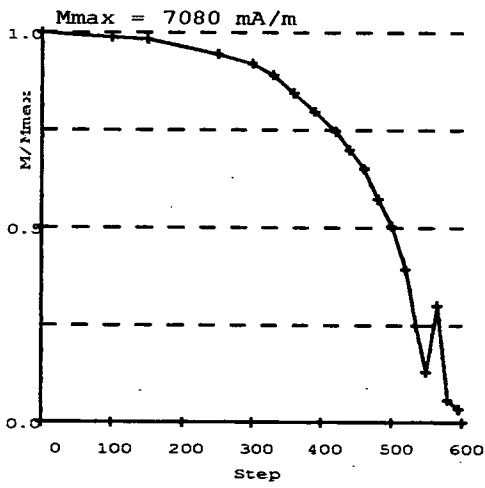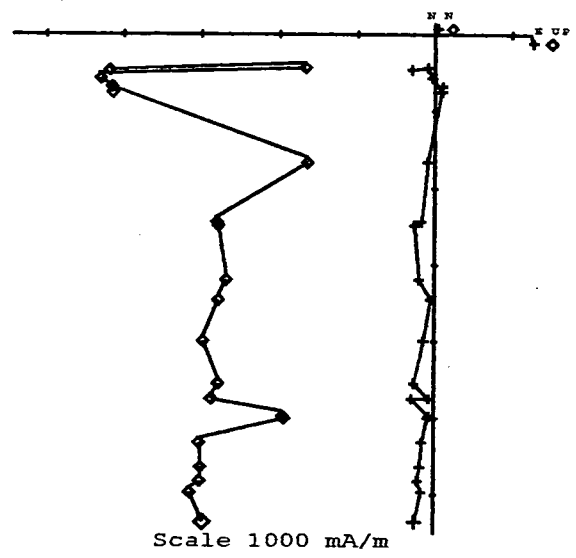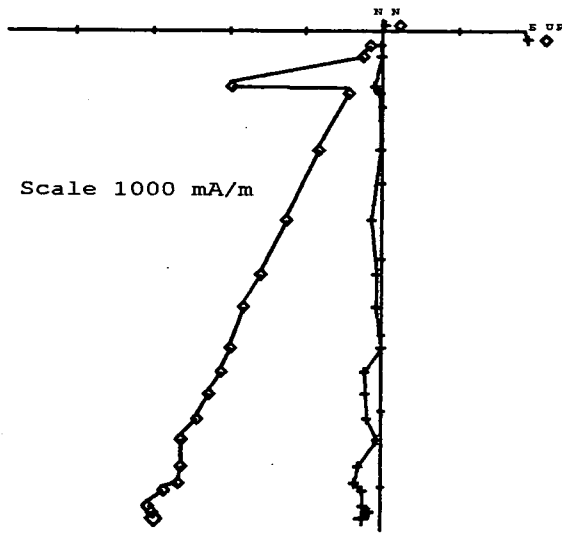
Core
Coordinates

MTT (A-B)		
V36.17	NRM	TRM
steps	(A/m)	(A/m)
20	7.080	0.000
100	7.000	0.000
150	6.970	0.130
250	6.690	0.311
300	6.520	0.388
330	6.310	0.399
360	5.980	0.409
390	5.650	0.500
420	5.290	0.615
440	4.950	0.687
460	4.610	1.017
480	4.060	0.988
500	3.570	1.110
520	2.780	1.556
535	1.760	0.831
550	0.923	3.725
565	2.120	2.325
580	0.416	1.429
595	0.243	4.047

a)
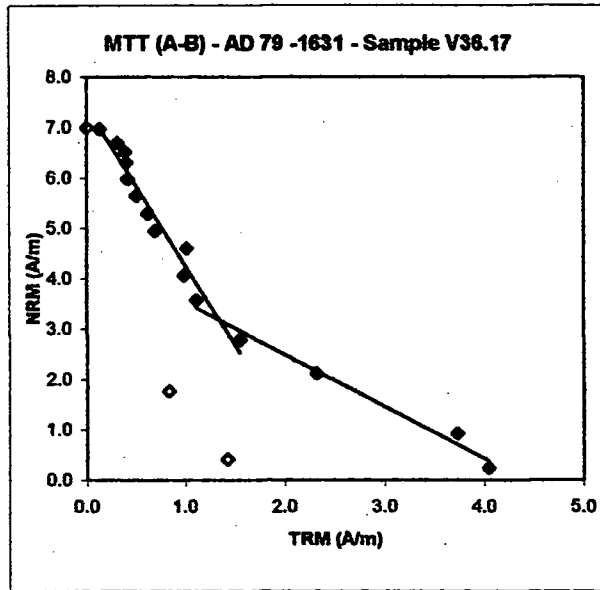
sample	T range (°)	N	f	g	q	b	R^2	Fpalaeo (μT)	σ_b
V36.17	150 - 520	12	0.945	0.958	14.076	-3.210	0.959	160.485	0.206
	*500 - 595	5	0.470	0.184	1.174	-1.042	0.984	52.090	0.077

*excluding 535,580 (empty diamonds)

b)

c)
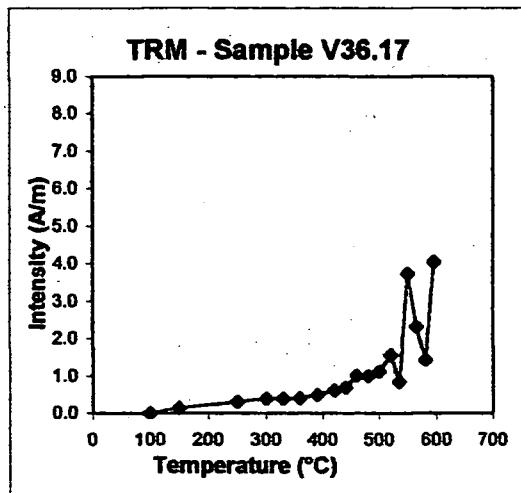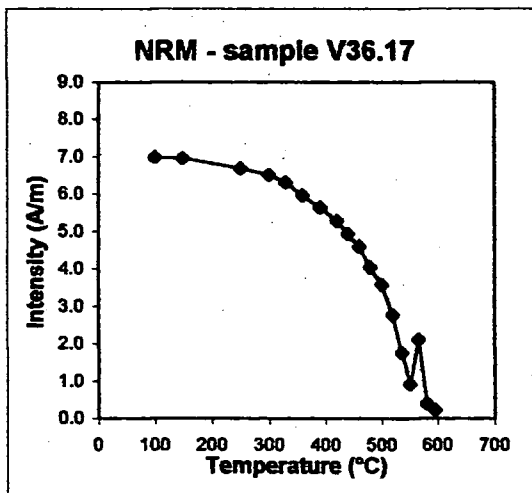
Fig. 6.6 - Site V36: a)NRM/TRM plot and respective values, b)NRM demagnetization and c)TRM acquisition curves.

Tab. 6.3 - Site V36: Palaeofields estimated and statistical parameters

159

AD 79-1631 sample V36.17

C-Demag2

Scale 1000 mA/m

Mmax = 7020 mA/m

D-pTRMck

Scale 1000 mA/m

Mmax = 7030 mA/m
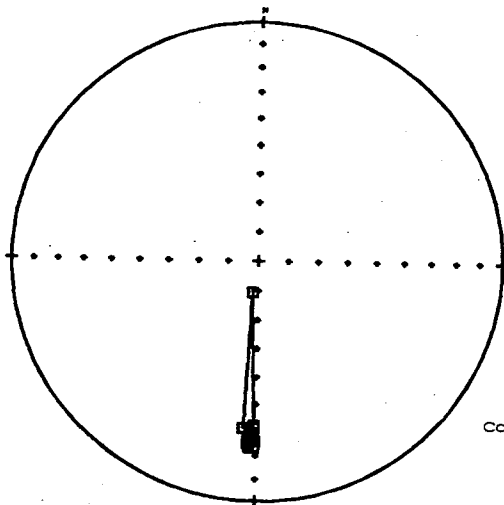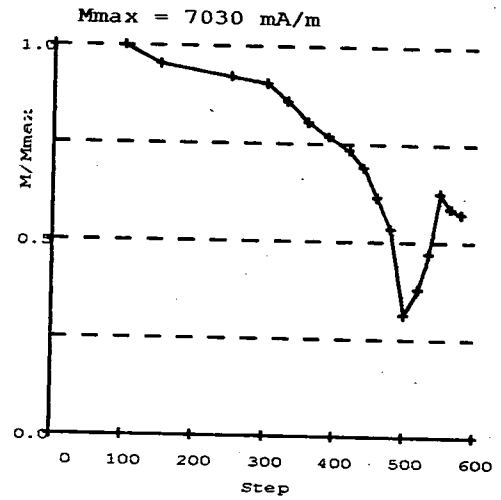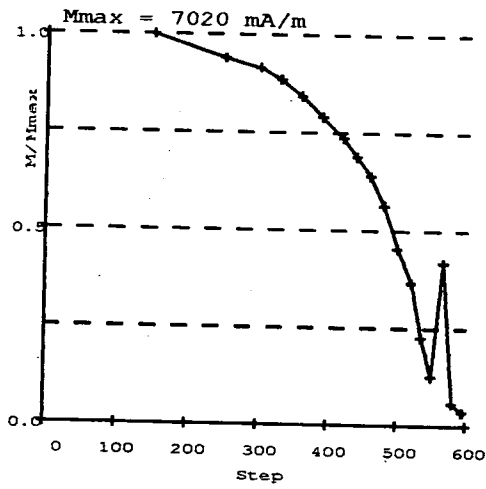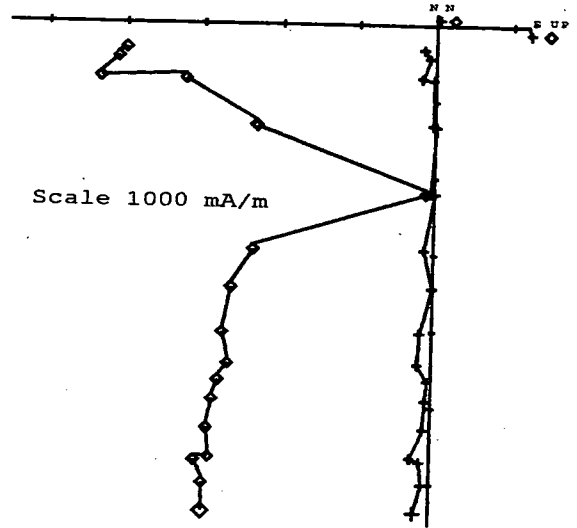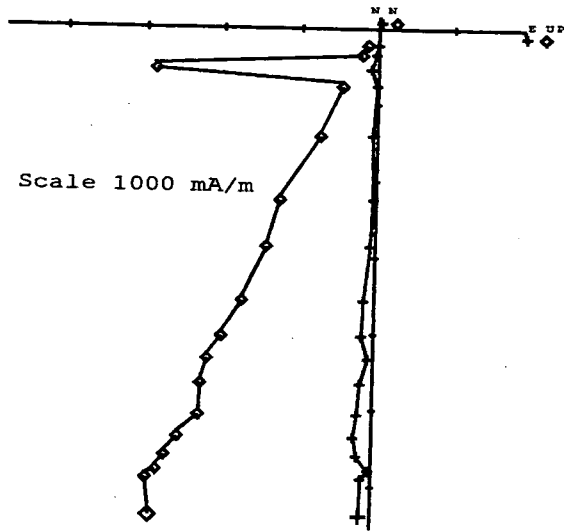
■ Lower
▲ Upper
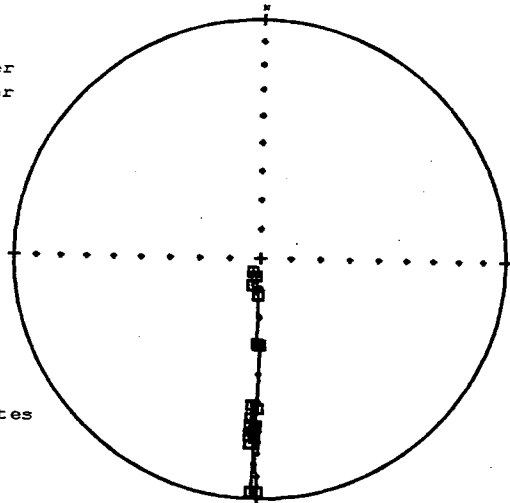
Core
Coordinates

Fig. 6.3 - Site V36: Zijderveld diagrams, Intensity and stereo plots.

MTT (D-C)		
V36.17	NRM	TRM
steps	(A/m)	(A/m)
20	0.000	0.000
100	0.000	0.000
150	7.020	0.389
250	6.590	0.229
300	6.430	0.266
330	6.220	0.384
360	5.920	0.566
390	5.570	0.661
420	5.170	0.456
440	4.840	0.638
460	4.490	0.880
480	3.960	0.881
500	3.190	1.458
520	2.570	1.424
535	1.590	2.595
550	0.884	3.885
565	2.930	1.231
580	0.407	3.804
595	0.000	0.000

a)

MTT (D-C) - AD 79 -1631 - Sample V36.17
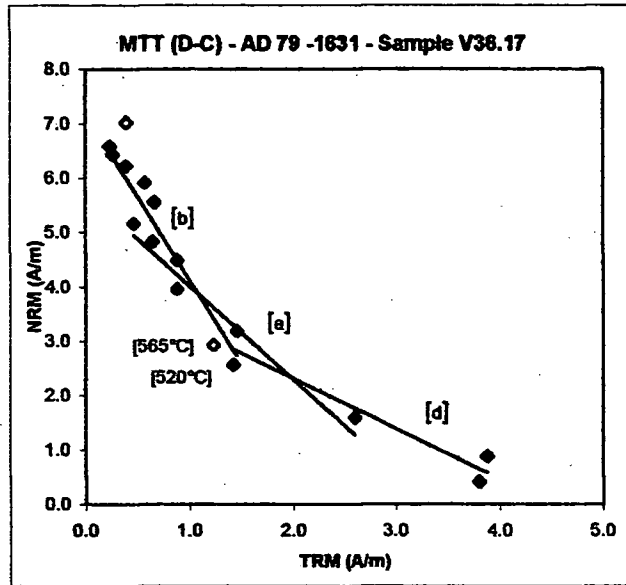
sample	Temp (°C)	N	f	g	q	b	R^2	Fpalaeo (μT)	σ_b
V36.17	**[a] 420 - 535	6	0.510	0.714	4.409	-1.682	0.982	84.088	0.139
	[b] 250 - 520	11	0.573	0.881	5.104	-3.185	0.975	159.227	0.315
	*[c] 250 - 580	14	0.881	0.905	8.154	-1.679	0.889	83.933	0.164
	*[d] 500 - 580	5	0.396	0.733	1.811	-0.959	0.924	47.970	0.154

*excluding 565
**excluding 520

NRM - sample V36.17

b)

TRM - Sample V36.17
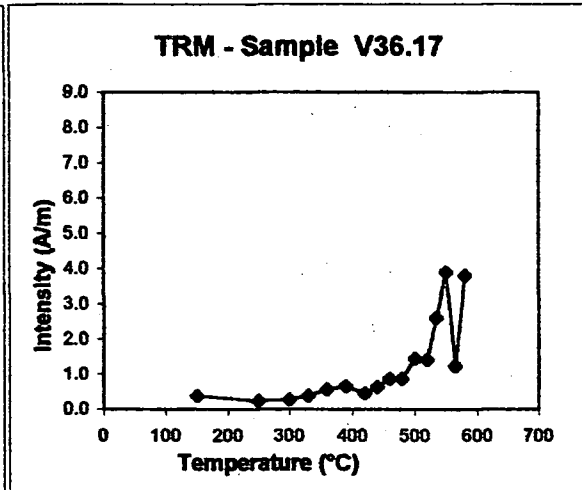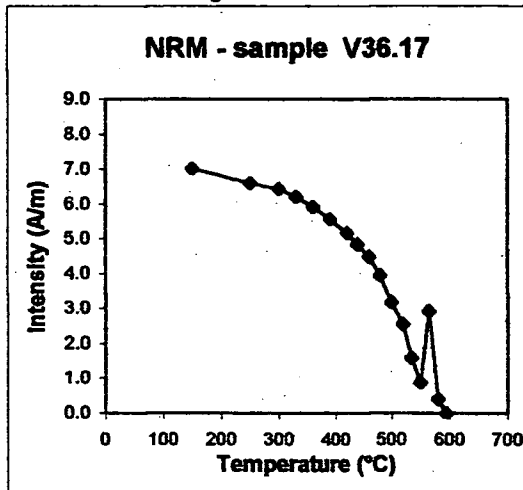
c)

Fig. 6.8 - Site V36: a)NRM/TRM plot and respective values, b)NRM demagnetization and c)TRM acquisition curves.

Tab. 6.4 - Site V36: Palaeofields estimated and statistical parameters

6.2.3 - Site V37

A-Demag1

Intensity Behaviour - Initial NRM for the sample 9B was 6330 mA/m and, by 595°C, had been demagnetized almost completely. It showed an accelerating decrease in intensity with increasing temperature starting from 150-250°C and terminating with a small tail (Fig. 6.9). A clear increase occurred at 565°C (about 1600 mA/m).

Directional Behaviour - Both vertical and horizontal components moved towards the origin with a very linear trend especially above 390°C. The vertical component showed a single downward marked excursion at 565°, followed the previous trend (Fig. 6.9).

B-pTRM

Intensity Behaviour - The decreasing trend, from 6330 to 1330 mA/m (535°C), was similar to Demag1, except for a more linear decay between 150 and 330°C. From 535 to 595°C the intensity showed alternated significant increases and decreases (about 2300 mA/m). When the process ended, the intensity was 2620 mA/m (Fig. 6.9).

Directional Behaviour - The horizontal component moved toward the origin with a linear trend, but at 565 and 580°C it showed a small deflection northward. The vertical component moved gradually away from the NRM direction until 565° when a marked spike occurred. The same anomaly was underlined by the stereo plot (Fig. 6.9).

Palaeointensity results from A-B - In the NRM/TRM plot some clear irregular points above 535°C, which also appeared in both NRM and TRM curves, were excluded (Fig. 6.10a,b,c). The different estimates of the palaeofield were considered (Tab. 6.5).

C-Demag2

Intensity & Directional Behaviour - This second demagnetization showed the same behaviour as in Demag1, but the spike at 565°C had a more significant North direction contribution (Fig. 6.11).

D-pTRMck

Intensity Behaviour - From 6300 to 2370 mA/m (500°C) the decreasing trend was similar to Demag1, except for a marked decrease at 460°C. From 500 to 550°C the intensity showed an increase followed by a small decrease until 595°C. At the end the intensity was 2760 mA/m (Fig. 6.11).

Directional Behaviour - The horizontal component moved toward the origin with a linear trend until 500°C. After this it started to move northwards with a small deflection at 550°C. The vertical component moved gradually away from the NRM direction until 460° when a marked upwards spike occurred (Fig. 6.11).

Palaeointensity results from D-C - As in MTT A-B, two slopes were defined (Fig. 6.12a), but some points, which were considered irregular on the TRM curve, were excluded (Tab. 6.6).

6.2.4 - Site V27

A-Demag1

Intensity Behaviour - Sample 11 had an initial NRM around 6220 mA/m and, by 595°C, had been demagnetized almost completely (< 5 remained), with a final steep decay above 535°C (Fig. 6.13). It showed a marked decrease at 100°C (about 1500 mA/m) followed by a smooth decrease until 535°C with two clear breaks at 400 and 480°C.

Directional Behaviour - Both vertical and horizontal components moved towards the origin with a very linear trend especially above 460°C (Fig. 6.13).

B-pTRM

Intensity Behaviour - This showed a curving decay from 100 (4790 mA/m) to 440°C with a little deflection at 250°. Two clear breaks occurred at 440 and 535 C° both followed by a small increase and then an accelerating decrease in intensity. When the process ended, the intensity was 2580 mA/m (Fig. 6.13).

Directional Behaviour - The vertical component moved gradually away from the NRM direction while the horizontal one moved toward the origin with a very linear trend. On the stereo plot the Dec was constant, while the Inc moved toward 90°, as expected (Fig. 6.13).

Palaeointensity results from A-B - The NRM/TRM plot showed a concave curve (Fig. 6.14a). Two different slopes were considered (Tab. 6.7) plus another one excluding points which appeared anomalous also on the TRM curves (Fig. 6.14c).

C-Demag2

Intensity Behaviour - It showed an accelerating decrease from 150°C (4670 mA/m) with a clear break in the trend at 480°C. At the end it showed a little concave tail and at 595° there was some 9% of NRM still remaining (Fig. 6.15).

Directional Behaviour - The sample behaved exactly in the same way as in Demag1 (Fig. 6.15).

D-pTRMck

Intensity Behaviour- It behaved similarly as in B-pTRM showing a curving decay from 100° (4730 mA/m) to 500°C with the same deflection at 250°, but with two smaller deflections at 390 and 440°C (Fig. 6.15). From 500 to 595°C the intensity was almost constant (2500 mA/m).

Directional Behaviour - Both the horizontal and the vertical components behaved as in B-pTRM (Fig. 6.15).

Palaeointensity results from C-D - The NRM/TRM plot showed a more linear behaviour curve then in MTT A-B (Fig. 6.16a). However two different slopes were considered (Tab. 6.8) plus another one considering the entire range of temperature.

6.2.5 - Site V33

A-Demag1

Intensity Behaviour - Sample 9 had an initial NRM of 1630 mA/m and, by 595°C, was demagnetized almost completely. It showed a quite linear decrease in intensity all over the spectra but there were two clear deflections at 300° and 460°C. A significant increase (about 250 mA/m) occurred at 565°C (Fig. 6.17).

Directional Behaviour - The horizontal component showed a marked zigzag trend with clear breaks at 250, 360 and 460°C, but in general it moved toward the origin. The vertical component showed an almost linear trend throughout the entire spectra of temperatures with a small irregularity at 460°. A significant irregularity occurred at 565°C when the total vector moved toward a downward direction (Fig. 6.17).

B-pTRM

Intensity Behaviour- It showed a hyperbolic increase all over the spectra starting from 1450mA/m (150°C) to 5880 mA/m (595°C). A small peak occurred at 300°C (Fig. 6.17).

Directional Behaviour - The horizontal component moved toward the origin with a similar trend as in Demag1, while the vertical one moved rapidly away from the NRM direction, toward a clear downward direction. The stereo plot showed the usual behaviour (Fig. 6.17).

Palaeointensity results from A-B - The NRM/TRM plot showed two very distinct slopes (Fig. 6.18a). Two points (Tab. 6.9) which appeared anomalous on both NRM and TRM curves (Fig. 6.18b,c) were excluded.

C-Demag2

Intensity Behaviour - The initial NRM (150°C) was 1360 mA/m and, by 595°C, was demagnetized completely. It showed a quite linear decrease, as in demag1, but with a deflection at 480°C. A marked increase (about 600 mA/m) occurred at 565°C (Fig. 6.19).

Directional Behaviour - Both the horizontal and vertical components behaved as in Demag1. The same irregularity occurred at 565°C, when the vertical vector moved toward a downward direction, but was much more marked (Fig. 6.19).

D-pTRMck - *Intensity & Directional Behaviours*

They were exactly the same as in pTRM (Fig. 6.19). The initial NRM was 1390 mA/m (100°C) and, at the end (580°C), it was 6140 mA/m.

Palaeointensity results from C-D - As in MTT A-B value at 565°C were not considered and in the same way two slopes were defined (Fig. 6.20, Tab. 6.10).

6.2.6 - Site V26

A-Demag1

Intensity Behaviour - Sample 11A had an initial NRM of 2570 mA/m and, by 550°C, was demagnetized almost completely. It showed a quite linear decrease in intensity until 460°C with a small convex deflection between 250 and 400°C. At 480° a significant increase in intensity occurred, followed by a steep linear decay, until 550° terminating with a small tail at 595° (Fig. 6.21).

Directional Behaviour - The horizontal component showed an almost linear trend throughout the entire spectra of temperatures with just two small irregularities at 390 and

480°C. The vertical component showed at least three different directions; between 100 and 330°C, 360 and 460°C and 480 and 595°C. A significant irregularity occurred at 480°C when the total vector moved toward a downward direction (Fig. 6.21).

B-pTRM

Intensity Behaviour – The sample showed a linear decrease from 2045 to 1180 mA/m (420°C), from which it increased until 500°C. This was followed by a rapid increase to the end of the process (595°C) when it was 8180 mA/m (Fig. 6.21).

Directional Behaviour - The vertical and horizontal components moved downward and westward especially from 420°C. This behaviour was particularly clear for the vertical component. The stereo plot showed the usual gradual movement of the Inc toward 90° (Fig. 6.21).

Palaeointensity results from A-B - The NRM/TRM plot showed a clear concave curve (Fig. 6.22a) and two slopes were defined up to 535°C. Points above this temperature, which showed anomalous high values on the TRM plot (Fig. 6.22c), were not considered (Tab. 6.11).

C-Demag2 -

Intensity Behaviour - In this second demagnetization, started at 150°C, the NRM was 1840 mA/m and, by 550°C, was demagnetized almost completely. The intensity decay showed a slightly convex curve between 300 and 440°C. A significant increase occurred at 480°, followed by a steep linear decay, until 550°, terminating with a small tail at 595° (Fig. 6.23). At 250-300°C the two steps showed the same value of intensity; probably due to an experimental error.

Directional Behaviour - The horizontal component showed an almost linear trend throughout the entire spectra. The vertical component showed an unclear trend until 390°C followed by three different directions. The first one was between 390 and 440°C,

the second one was between 440 and 480°C and moved clearly toward a downward direction. The third one was between 480 and 595°C, and moved toward the origin. The stereo plot showed a good consistency in Dec until 535°C while the Inc had a gradual movement toward 90° especially starting from 420°C (Fig. 6.23)

D-pTRMck

Intensity Behaviour - There was a shallow linear decrease from 1790 to 1140 mA/m (360°C), from which it increased slowly until 500°C. This was followed by a rapid increase to the end of the process (595°C) where it was 8350 mA/m. A small convex deflection occurred between 440 and 500° (Fig.6.23).

Directional Behaviour - The vertical component moved clearly towards the downward direction especially starting from 500°C. The horizontal one moved toward the origin but above 535°C, it showed a small movement towards the West. The stereo plot showed, as expected, a gradual movement of the Inclination toward 90° (Fig. 6.23).

Palaeointensity results from C-D - The NRM/TRM plot showed two distinct slopes (Fig. 6.24a). Although the TRM curve behaved as in MTT A-B (Fig. 6.24c) the anomalous high values were considered, but the palaeofield estimate obtained was unacceptable (Tab. 6.12).

6.2.7 - Site V31

A-Demag1

Intensity Behaviour - Initial NRM for sample 2 was 5980 mA/m (Fig. 6.25) and, at 595°C, there was some 5% still remaining. It showed an accelerating decrease in intensity with increasing temperature starting from 150-250°C and terminating with a small

concave tail. A marked spike occurred at 565°C when the intensity increased of about 600 mA/m.

Directional Behaviour - Both vertical and horizontal components moved towards the origin with a very linear trend. The vertical component showed a single downward marked excursion at 565°. The stereo plot showed a slight movement of Inc toward 90° above 550°C (Fig. 6.25).

B-pTRM

Intensity Behaviour - The decreasing trend, from 6190 to 2330 mA/m (535°C), was quite similar to Demag1, except for a very small increase at 500°C. Between 535 and 565°C the intensity showed a significant increase (about 3200 mA/m). This was followed by a minor linear decrease and, at the end of the process the, intensity was 4450 mA/m (Fig. 6.25).

Directional Behaviour - The horizontal component moved toward the origin with a linear trend, but without reaching it. The vertical component moved gradually away from the NRM direction until 535°, when a marked downward spike occurred. The same behaviour was underlined by the stereo plot (Fig. 6.25).

Palaeointensity results from A-B - The NRM/TRM plot showed a very linear trend until 520°C when points started to behave almost randomly (Fig. 6.26a). A second slope were considered (Tab. 6.13) excluding two points which appeared anomalous on both NRM and TRM curves (Fig. 6.26b,c).

C-Demag2

Intensity & Directional Behaviour - In this second demagnetization the behaviours were exactly the same as in Demag1 (Fig. 6.27).

D-pTRMck

Intensity Behaviour - The initial intensity was 6200 mA/m (100°C) and decreased with a shallow linear trend until 300°C. Between 300 and 520°C it showed a steeper linear decrease with a small break at 390°C. From 520 to 550°C the intensity showed a marked increase (about 1500 mA/m) followed by a decrease until 595°C. The final intensity was 4620 mA/m (Fig. 6.27).

Directional Behaviour - It was very similar to that one showed in pTRM (Fig. 6.27).

Palaeointensity results from D-C - Both NRM and TRM behaved as in MTT A-B (Fig. 6.28b,c). Two possible values of the palaeofield were estimated (Tab. 6.14).

AD 79-1631 sample V37.9B

A-Demag1

Scale 1000 mA/m

Mmax = 6330 mA/m

B-pTRM

Scale 1000 mA/m

Mmax = 6330 mA/m

☐ Lower
▲ Upper

Core
Coordinates
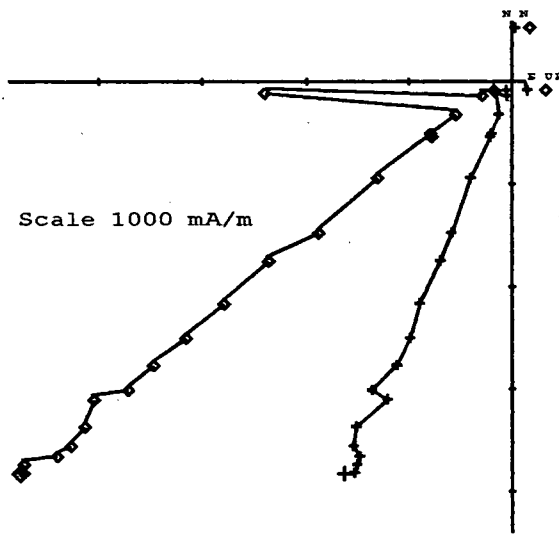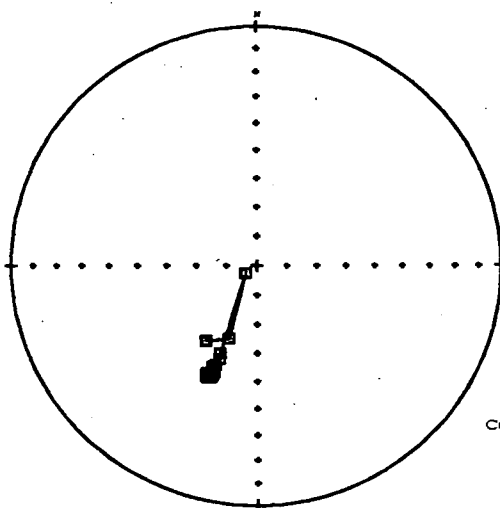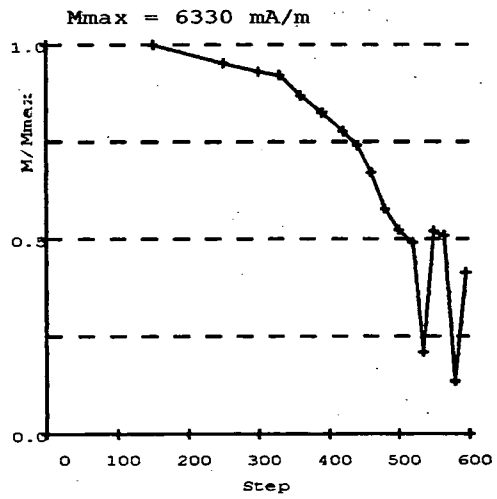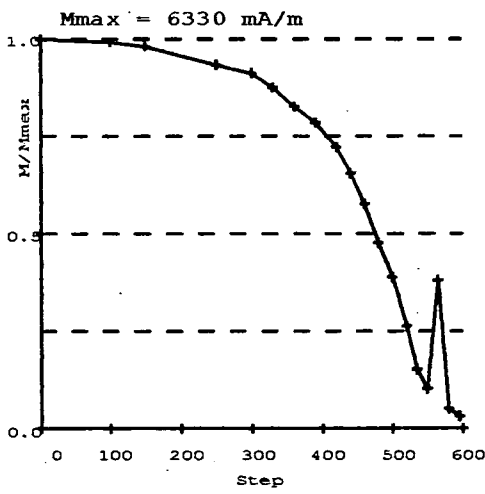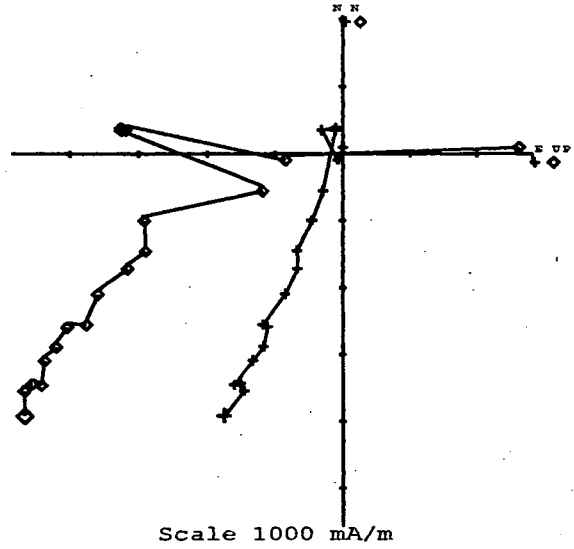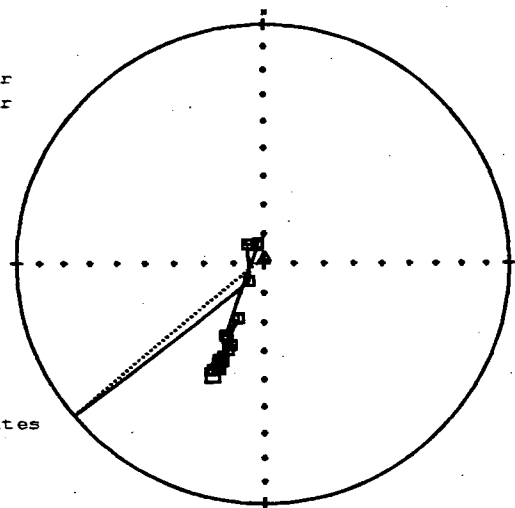
Fig. 6.9 - Site V37: Zijderveld diagrams, Intensity and stereo plots.

MTT (A-B)		
V37.9b	NRM	TRM
steps	(A/m)	(A/m)
20	6.330	0.000
100	6.280	0.000
150	6.210	0.309
250	5.910	0.274
300	5.770	0.303
330	5.540	0.299
360	5.230	0.340
390	4.970	0.544
420	4.570	0.601
440	4.150	0.640
460	3.650	0.814
480	3.020	0.801
500	2.460	1.023
520	1.660	1.611
535	0.965	0.416
550	0.645	2.811
565	2.410	0.931
580	0.326	0.554
595	0.204	2.801

a)

MTT (A-B) - AD 79 -1631 - Sample V37.9b
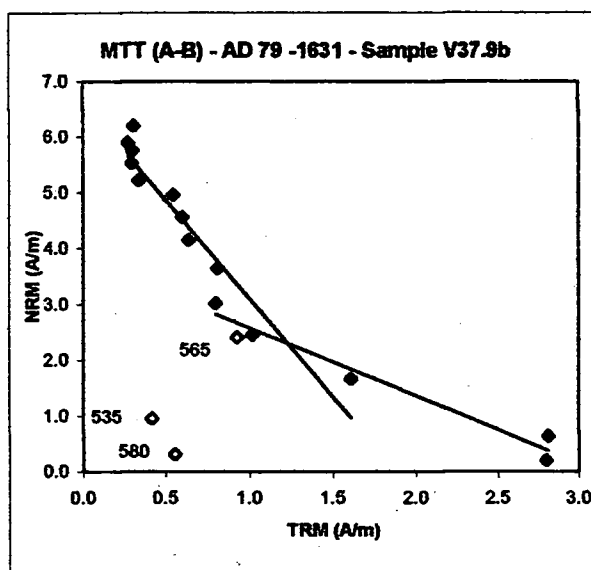
sample	T range (°)	N	f	g	q	b	R^2	Fpalaeo (μT)	σ_b
V37.9b	150 - 520	12	0.719	0.891	6.609	-3.703	0.359	185.168	0.359
	*480 - 595	5	0.445	0.725	3.063	-1.239	0.967	61.956	0.131

*excluding 535,565,580

NRM - sample V37.9b

b)
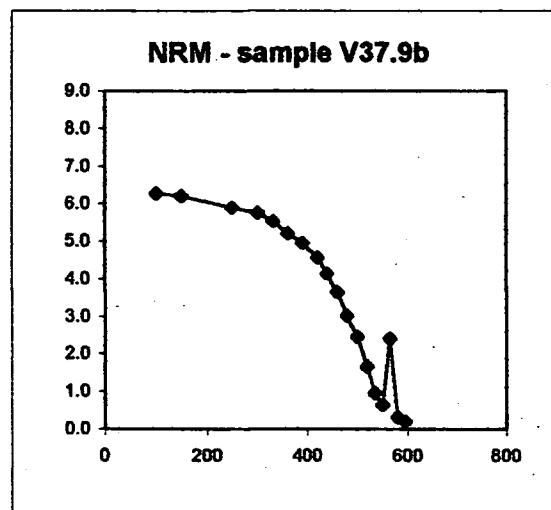
TRM - Sample V37.9b
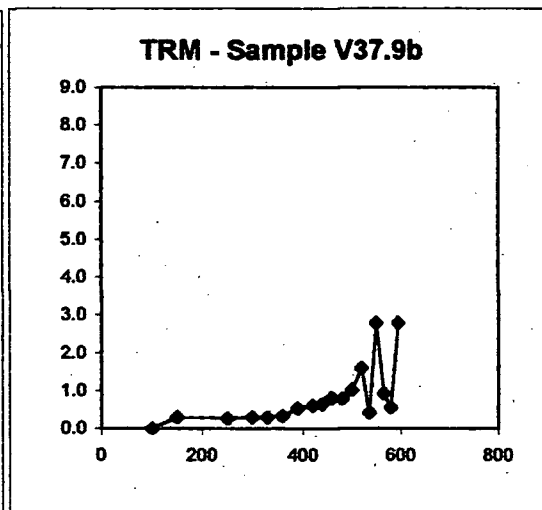
c)

Fig. 6.10 - Site V37: a)NRM/TRM plot and respective values, b)NRM demagnetization and c)TRM acquisition curves.

Tab. 6.5 - Site V37: Palaeofields estimated and statistical parameters

AD 79-1631 sample V37.9b

C-Demag2

D-pTRMck

Scale 1000 mA/m

Scale 1000 mA/m

Mmax = 6310 mA/m

Mmax = 6300 mA/m

☒ Lower
▲ Upper

Core
Coordinates
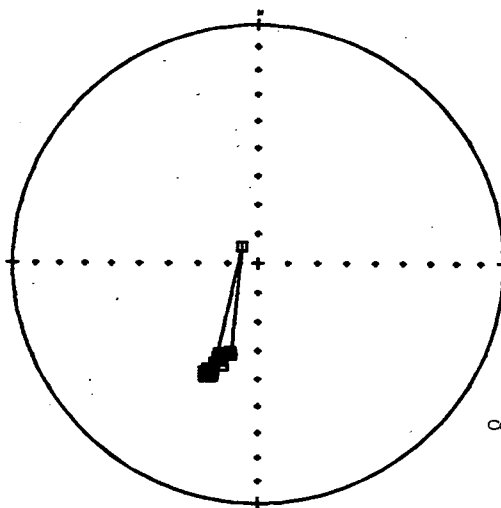
Fig. 6.11 - Site V37: Zijderveld diagrams, Intensity and stereo plots.

MTT (C-D)		
V37.9b	NRM	TRM
steps	(A/m)	(A/m)
20	0.000	0.000
100	0.000	0.000
150	6.310	0.464
250	5.810	0.133
300	5.690	0.176
330	5.510	0.166
360	5.220	0.506
390	4.910	0.563
420	4.480	0.338
440	4.040	0.457
460	3.530	1.272
480	2.980	0.632
500	2.480	0.903
520	1.480	1.315
535	0.841	2.380
550	0.657	2.750
565	2.530	0.491
580	0.282	2.560
595	0.000	0.000

a)

MTT (C-D) - AD 79 -1631 - Sample V37.9b
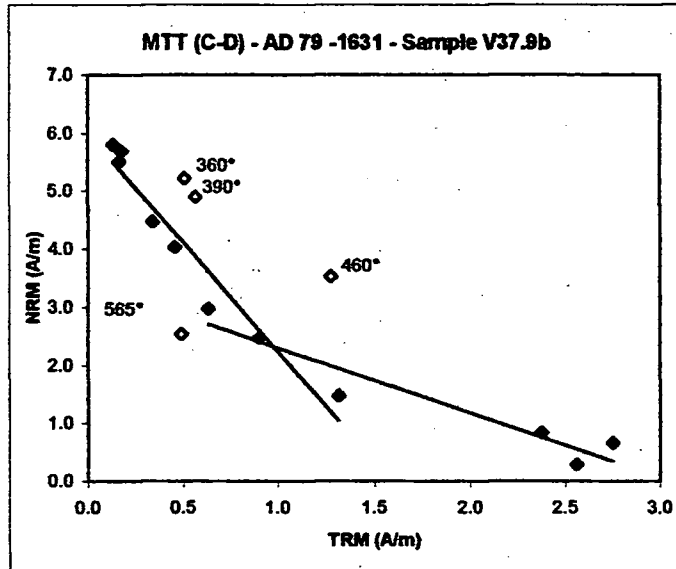
sample	Temp (°C)	N	f	g	q	b	R^2	Fpalaeo (μT)	σ_b
V37.9b	*250 - 520	8	0.686	0.804	5.837	-3.871	0.947	193.545	0.366
	**480 - 580	6	0.428	0.748	2.203	-1.171	0.917	58.528	0.170

*excluding 360,390,460
**excluding 565

NRM - sample V37.9b

b)
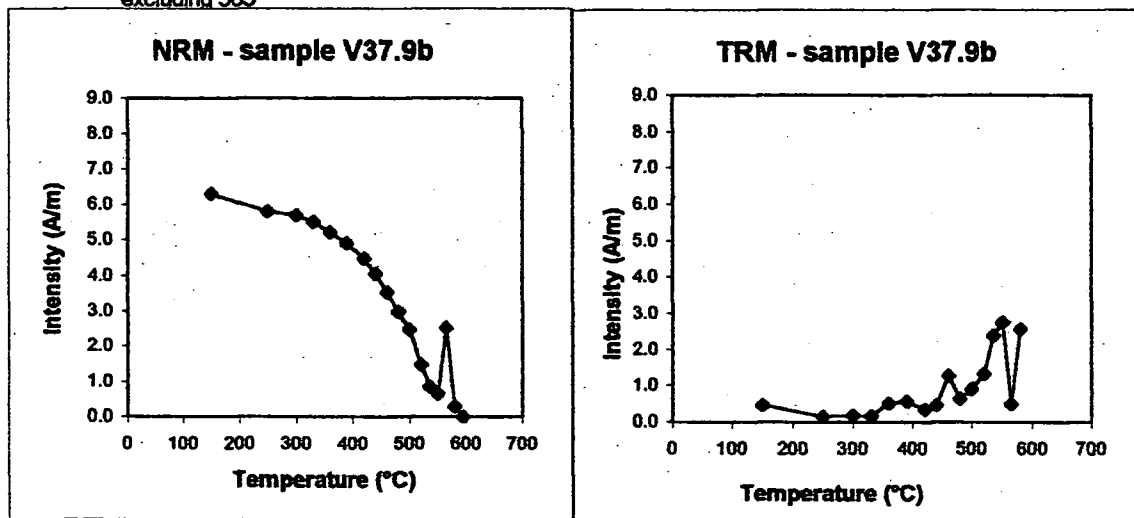
TRM - sample V37.9b

c)

Fig. 6.12 - Site V37: a)NRM/TRM plot and respective values, b)NRM demagnetization and
c)TRM acquisition curves.

Tab. 6.6 - Site V37: Palaeofields estimated and statistical parameters

AD 79-1631 sample V27.11a

A-Demag1

B-pTRM

Scale 1000 mA/m

Scale 1000 mA/m

Mmax = 6220 mA/m

Mmax = 4790 mA/m
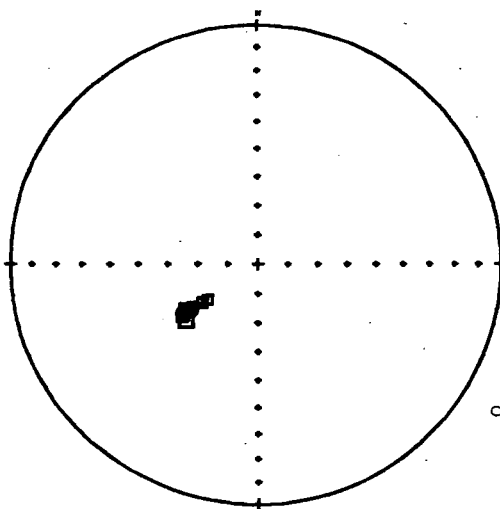
Step

Step

☐ Lower
▲ Upper

Core
Coordinates

Fig. 6.13 - Site V27: Zijderveld diagrams, Intensity and stereo plots.

MTT (A-B)		
V27.11a	NRM	TRM
steps	(A/m)	(A/m)
20	6.220	0.000
100	4.770	0.050
150	4.730	0.146
250	4.370	0.211
300	4.250	0.315
330	4.180	0.278
360	4.050	0.319
390	3.800	0.339
420	3.490	0.454
440	3.190	0.498
460	2.980	0.845
480	2.960	0.792
500	2.280	1.103
520	1.580	1.438
535	1.090	1.741
550	0.893	2.018
565	0.704	2.136
580	0.523	2.264
595	0.318	2.284

a)

MTT (A-B) - AD 79 -1631 - Sample V27.11a
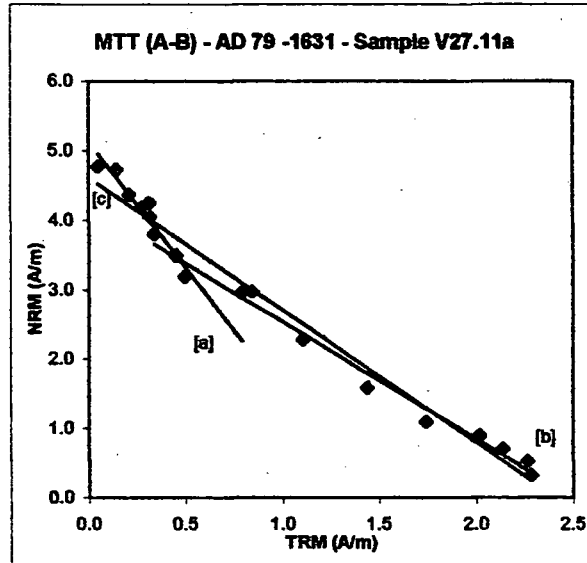
sample	T range (°)	N	f	g	q	b	R^2	Fpalaeo (µT)	σ_b
V27.11	[c] 100 - 595	17	0.400	0.708	4.698	-1.941	0.978	97.048	0.117
	[a] 100 - 440	9	0.254	0.833	2.123	-3.753	0.932	187.634	0.374
	[b] 390 - 595	12	0.560	0.870	13.796	-1.706	0.988	85.277	0.060

NRM - sample V27.11

b)

TRM - Sample V27.11
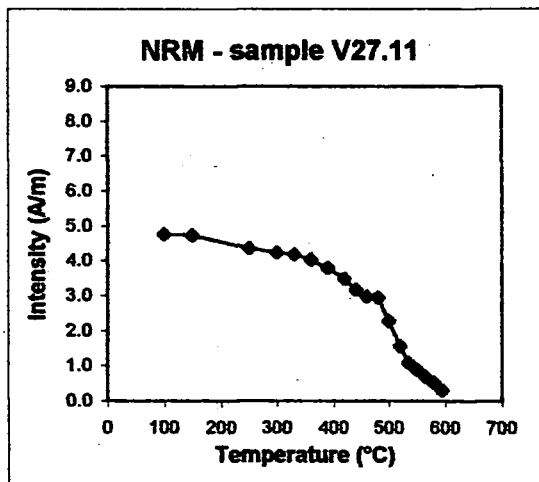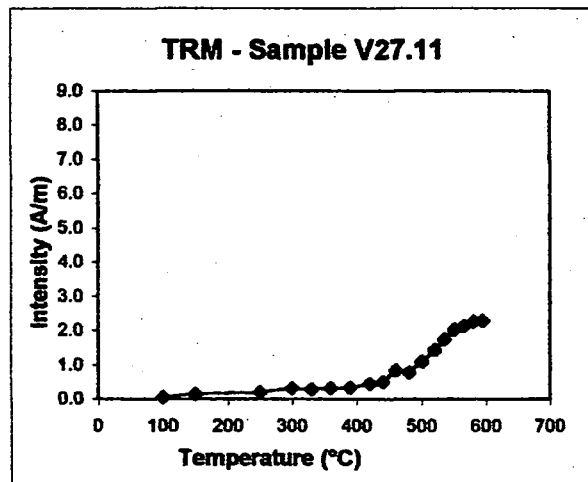
c)

Fig. 6.14 - Site V27: a)NRM/TRM plot and respective values, b)NRM demagnetization and c)TRM acquisition curves.

Tab. 6.7 - Site V27: Palaeofields estimated and statistical parameters

C-Demag2   D-pTRMck

Scale 1000 mA/m   Scale 1000 mA/m

4670

Mmax = 4670 mA/m   Mmax = 4730 mA/m

Core
Coordinates

□ Lower
▲ Upper
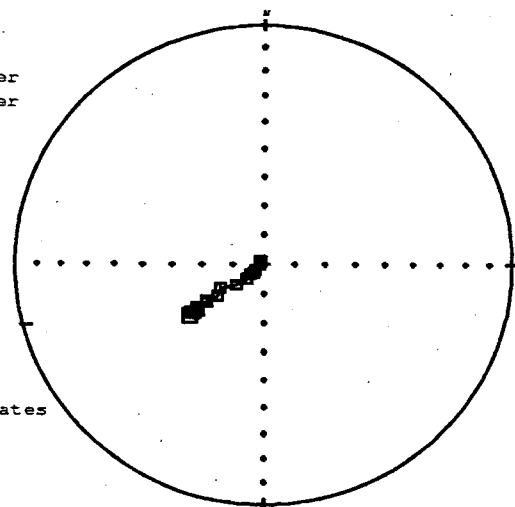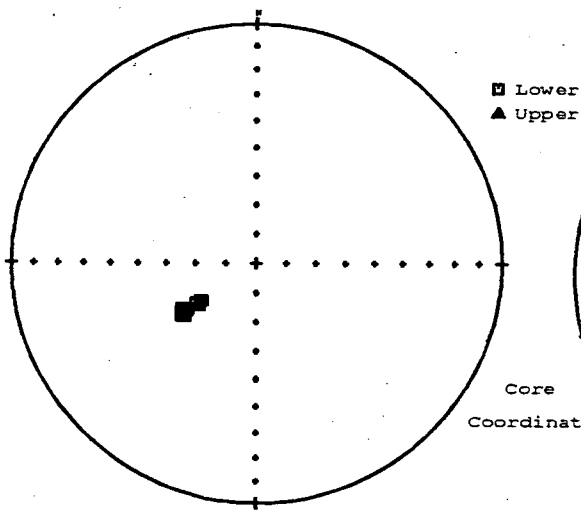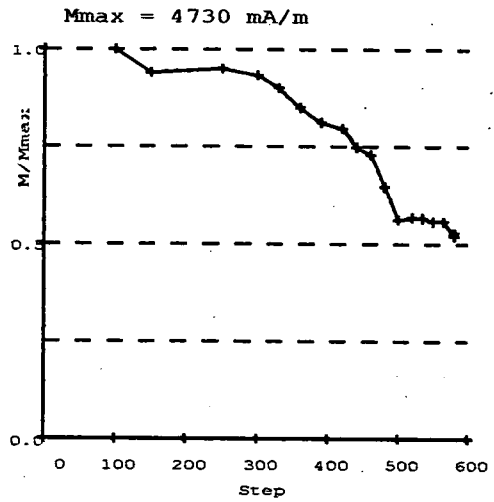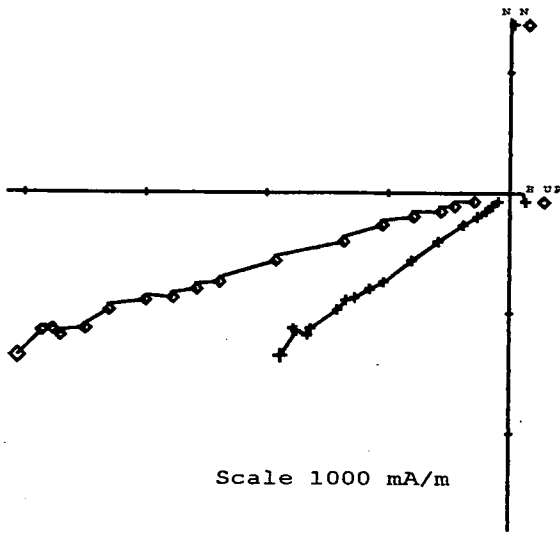
Fig. 6.15 - Site V27: Zijderveld diagrams, Intensity and stereo plots.

MTT (C-D)		
V27.11	NRM	TRM
steps	(A/m)	(A/m)
20	0.000	0.000
100	0.000	0.000
150	4.670	0.248
250	4.380	0.119
300	4.310	0.221
330	4.220	0.053
360	4.010	0.250
390	3.720	0.163
420	3.400	0.391
440	3.180	0.548
460	2.930	0.623
480	2.700	0.613
500	2.150	0.695
520	1.540	1.287
535	1.140	1.614
550	0.857	1.838
565	0.620	2.069
580	0.491	1.998
595	0.000	0.000

a
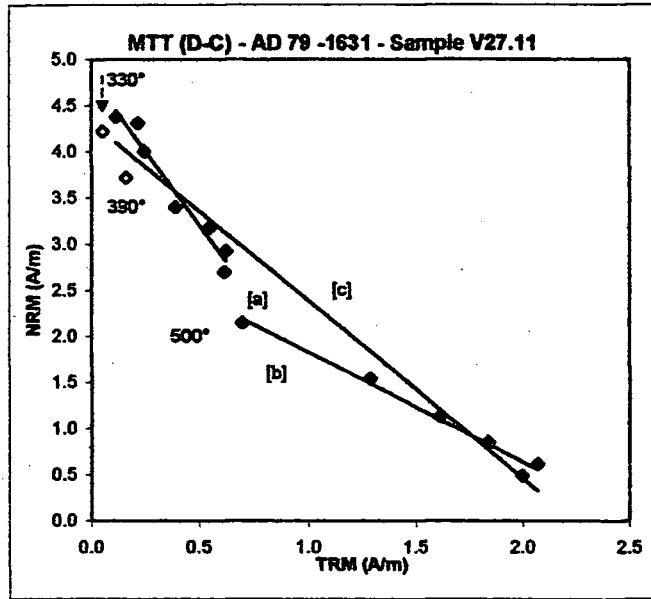
sample	Temp (°C)	N	f	g	q	b	R^2	Fpalaeo (μT)	σ_b
V27.11	[b] 500-580	6	0.355	0.751	4.074	-1.202	0.983	60.099	0.079
	*[a] 250-480	7	0.360	0.777	2.977	-3.308	0.957	165.388	0.310
	**[c] 250-580	12	0.833	0.849	12.649	-1.967	0.969	98.375	0.110

* excluding 330,390
** excluding 330,390,500
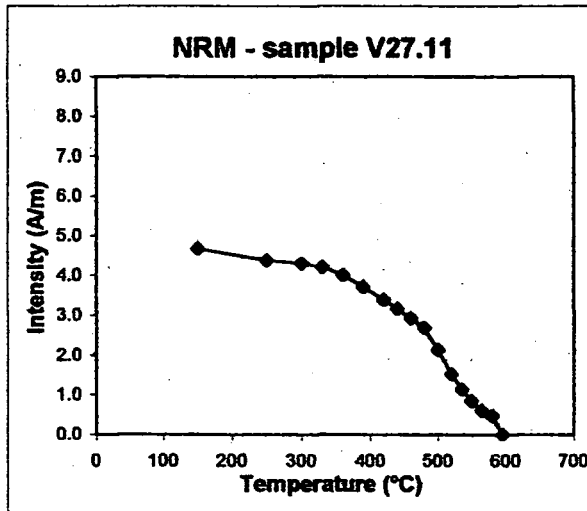
b)
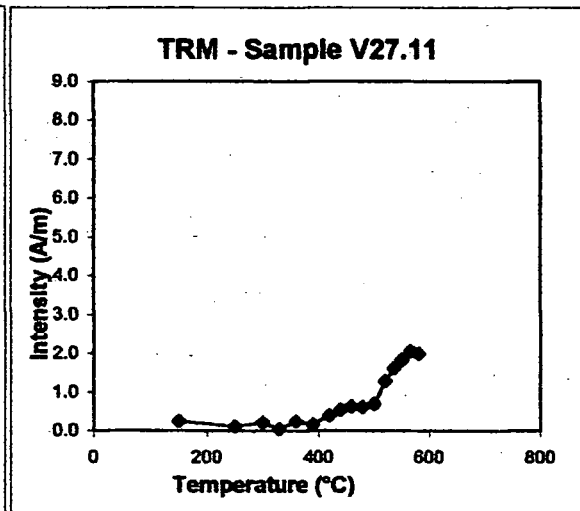
c)

Fig. 6.16 - Site V27: a)NRM/TRM plot and respective values, b)NRM demagnetization and c)TRM acquisition curves.

Tab. 6.8 - Site V27: Palaeofields estimated and statistical parameters

178

AD 79-1631 sample V33.9

A-Demag1

Scale 200 mA/m

B-pTRM

Scale 1000 mA/m

Mmax = 1630 mA/m

Mmax = 5880 mA/m

☐ Lower
▲ Upper

Core
Coordinates
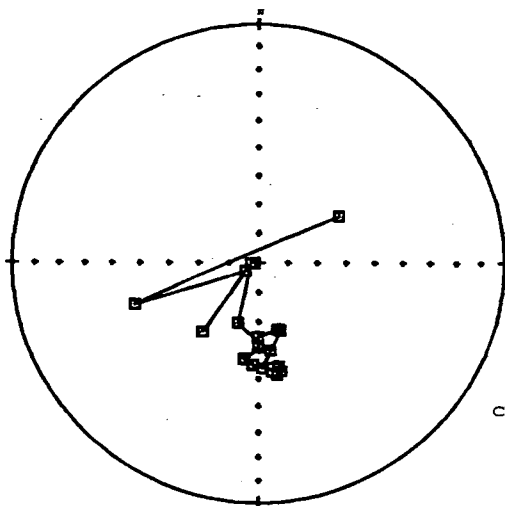
Fig. 6.17 - Site V33: Zijderveld diagrams, Intensity and stereo plots.

MTT (A-B)		
V33.9	NRM	TRM
steps	(A/m)	(A/m)
NRM	1.630	0.000
100	1.440	0.000
150	1.330	0.271
250	0.939	0.747
300	0.800	1.313
330	0.759	0.895
360	0.686	1.019
390	0.599	1.102
420	0.444	1.227
440	0.382	1.513
460	0.342	1.734
480	0.340	1.746
500	0.280	2.041
520	0.224	2.583
535	0.135	2.656
550	0.084	3.787
565	0.331	3.998
580	0.035	4.405
595	0.021	5.857

a
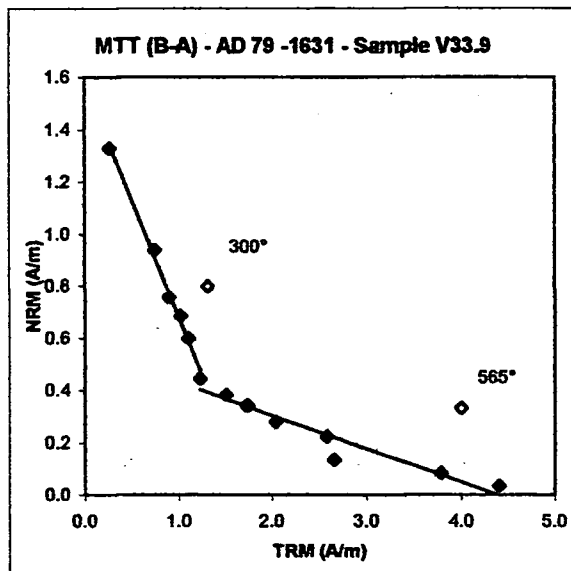
sample	T range (°)	N	f	g	q	b	R^2	Fpalaeo (µT)	σ_b
V33.9	*150-420	6	0.544	0.717	10.167	-0.913	0.994	45.661	0.035
	** 420-580	9	0.251	0.850	2.126	-0.132	0.931	6.600	0.013

*excluding 300°
**excluding 565°
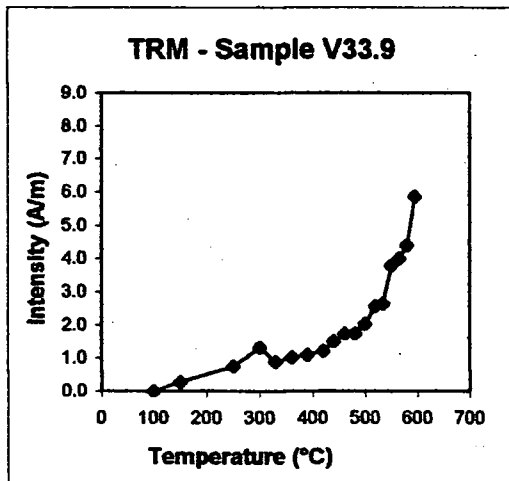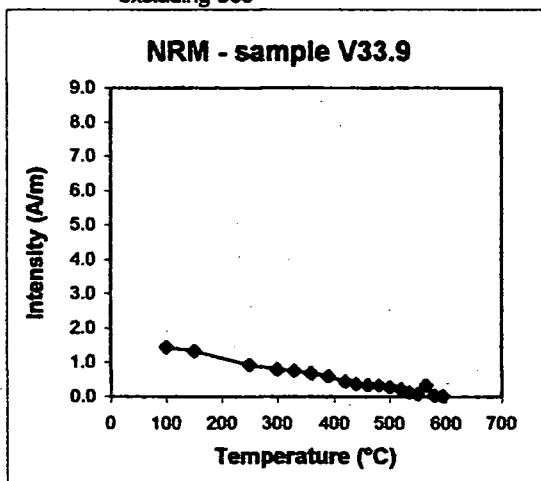
b

c)

Fig. 6.18 - Site V33: a)NRM/TRM plot and respective values, b)NRM demagnetization and c)TRM acquisition curves.

Tab. 6.9 - Site V33: Palaeofields estimated and statistical parameters

180

AD 79-1631 sample V33.9

C-Demag2

D-pTRMck

Scale 200 mA/m

Scale 1000 mA/m

Mmax = 1360 mA/m

Mmax = 6140 mA/m

☐ Lower
▲ Upper

Core
Coordinates
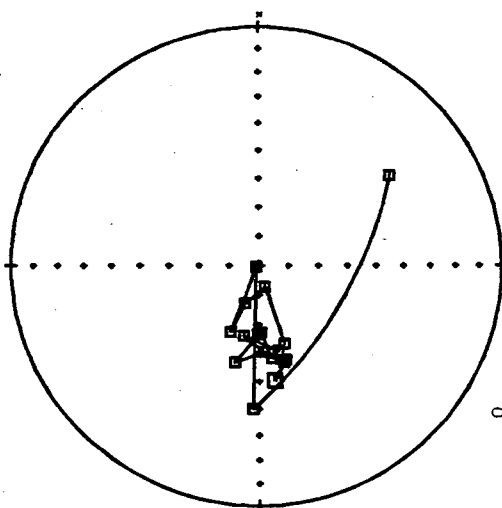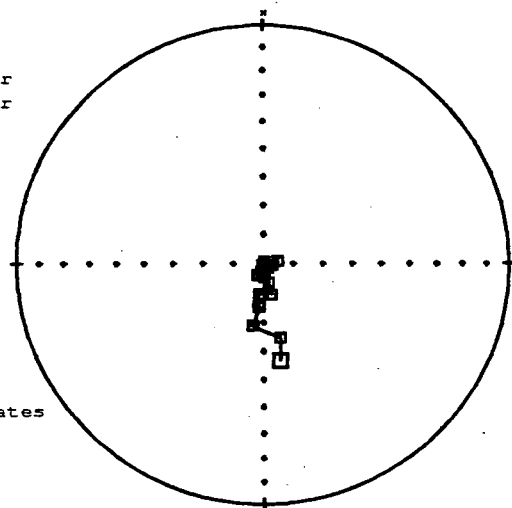
Fig. 6.19 - Site V33: Zijderveld diagrams, Intensity and stereo plots.

V33.9	NRM	TRM
steps	(A/m)	(A/m)
20	0.000	0.000
100	0.000	0.000
150	1.360	0.394
250	0.978	0.597
300	0.944	0.775
330	0.787	0.899
360	0.725	1.007
390	0.580	1.007
420	0.480	1.045
440	0.468	1.273
460	0.374	1.699
480	0.429	1.750
500	0.348	2.355
520	0.248	2.821
535	0.140	3.657
550	0.116	4.395
565	0.659	4.641
580	0.035	6.110
595	0.000	0.000

a

MTT (D-C) - AD 79 -1631 - Sample V33.9
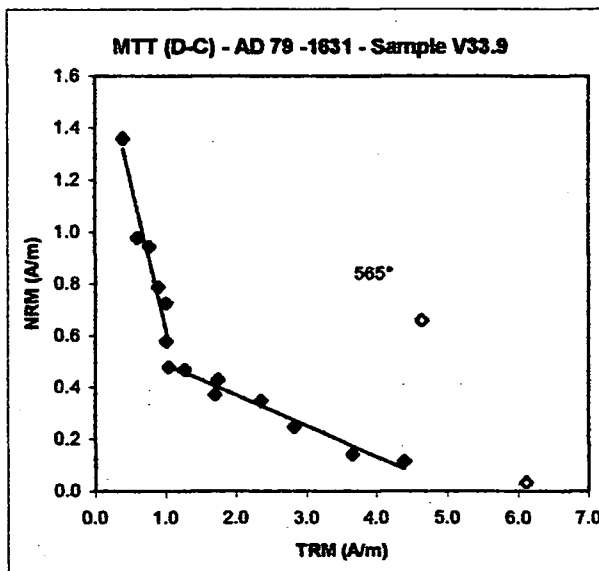
sample	Temp (°C)	N	f	g	q	b	R²	Fpalaeo (μT)	σ_b
V33.9	150-420	7	0.647	0.733	3.717	-1.193	0.920	59.660	0.152
	420-550	8	0.268	0.692	2.397	-0.121	0.965	6.034	0.009

NRM - sample V33.9

TRM - Sample V33.9

b

c
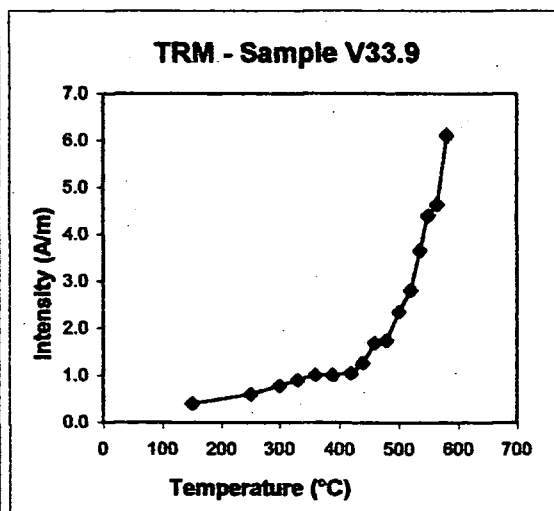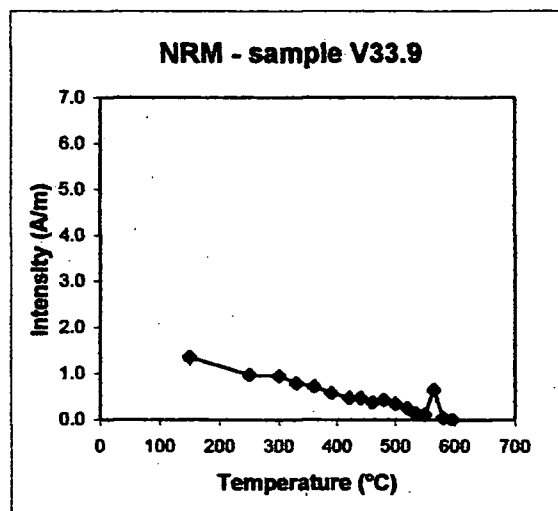
Fig. 6.20 - Site V33: a)NRM/TRM plot and respective values, b)NRM demagnetization and c)TRM acquisition curves.

Tab. 6.10 - Site V33: Palaeofields estimated and statistical parameters

182

A-Demag1

B-pTRM

Scale 500 mA/m

Scale 2000 mA/m

Mmax = 2570 mA/m

Mmax = 8180 mA/m

⊟ Lower
▲ Upper

Core
Coordinates
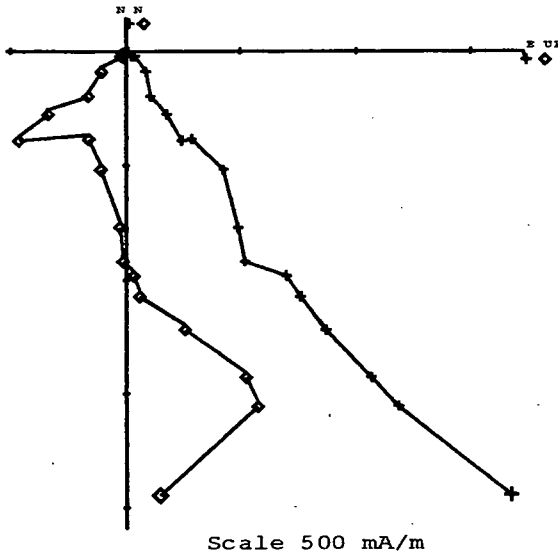
Fig. 6.21 - Site V26: Zijderveld diagrams, Intensity and stereo plots.

MTT (A-B)		
V26.11a	NRM	TRM
steps	(A/m)	(A/m)
20	2.570	0.000
100	2.040	0.000
150	1.850	0.145
250	1.520	0.303
300	1.420	0.310
330	1.310	0.439
360	1.210	0.509
390	1.060	0.614
420	0.913	0.668
440	0.677	0.705
460	0.506	0.910
480	0.654	1.198
500	0.471	1.809
520	0.277	2.166
535	0.163	2.899
550	0.044	4.432
565	0.038	5.982
580	0.014	7.313
595	0.011	8.180

a) MTT (A-B) - AD 79 -1631 - Sample V26.11a
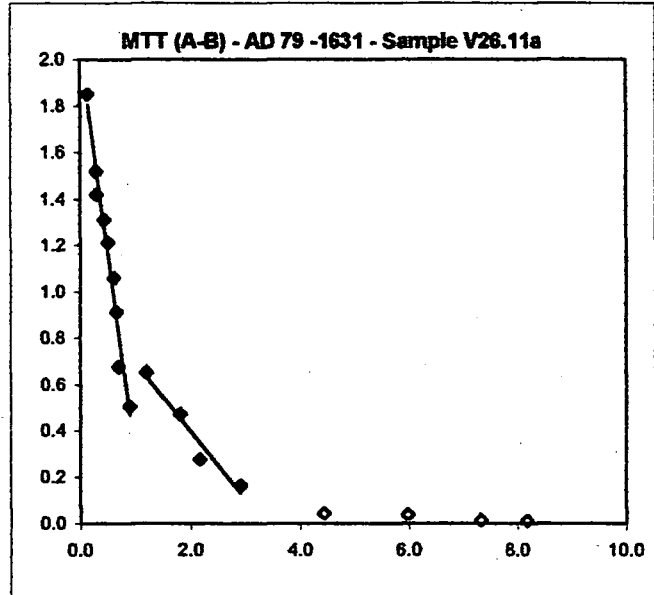
sample	Temp. (°C)	N	f	g	q	b	R²	Fpalaeo (µT)	σ_b
V26.11a	150 - 460	9	0.523	0.851	6.727	-1.774	0.970	88.697	0.117
	480 - 535	4	0.191	0.651	0.799	-0.305	0.952	15.233	0.047

b) NRM - sample V26.11a

c) TRM - Sample V26.11a
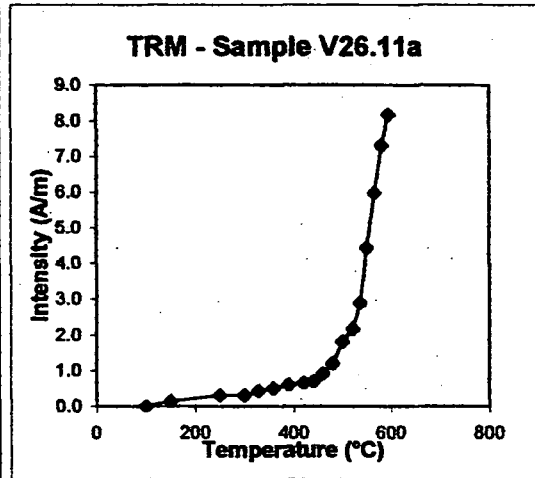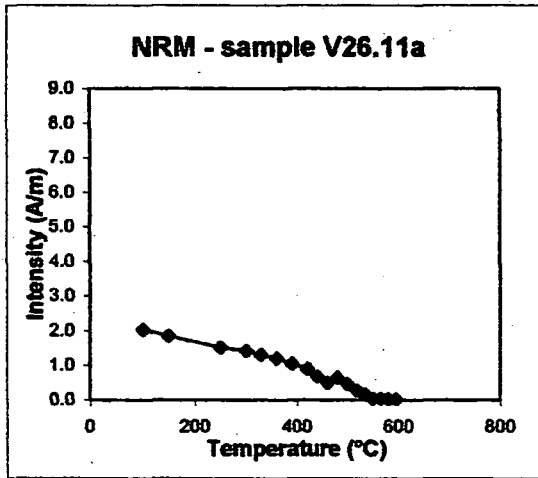
Fig. 6.22 - Site V26: a)NRM/TRM plot and respective values, b)NRM demagnetization and c)TRM acquisition curves.

Tab. 6.11 - Site V26: Palaeofields estimated and statistical parameters

184
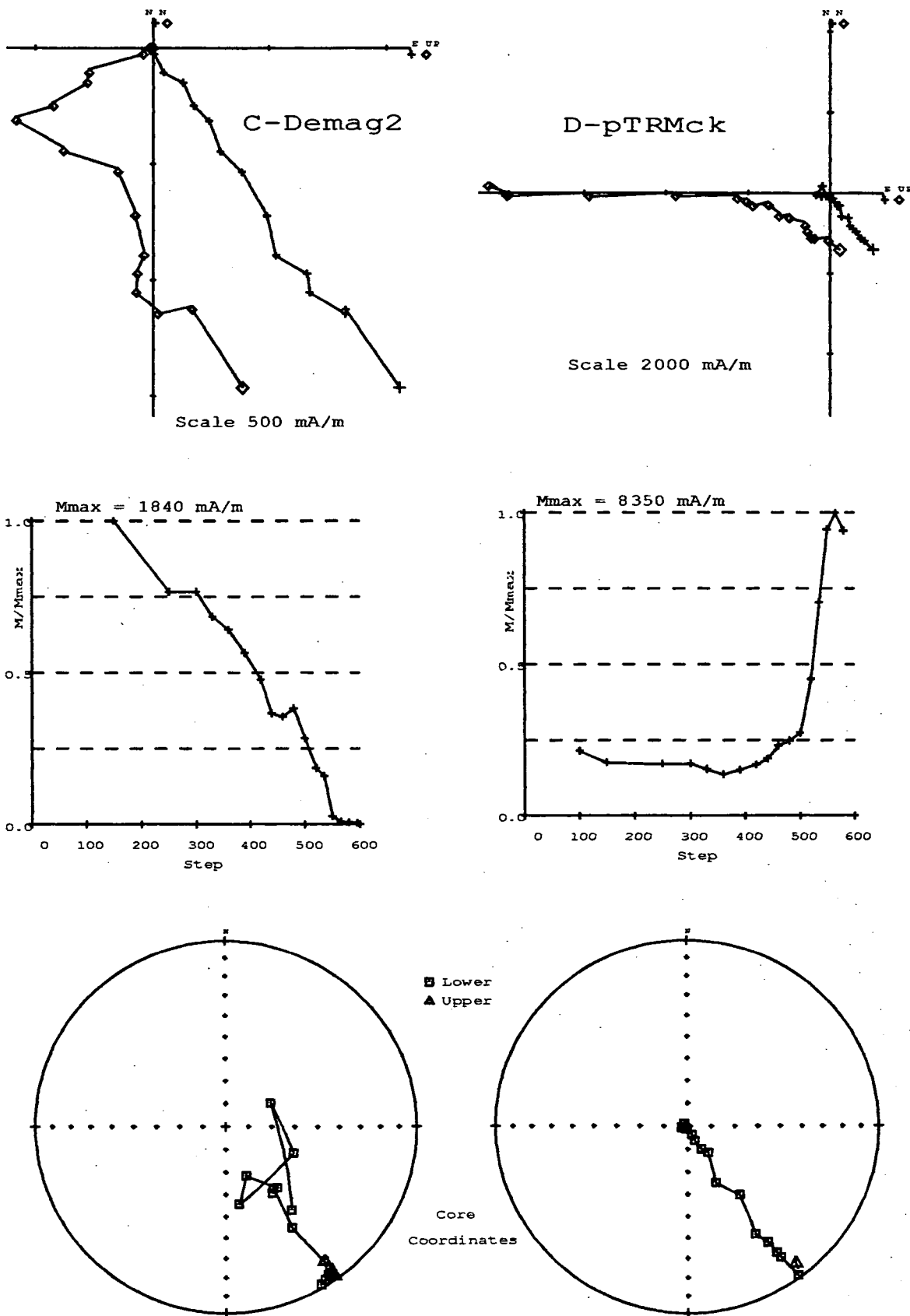
Fig. 6.23 - Site V26: Zijderveld diagrams, Intensity and stereo plots.

MTT (C-D)		
V26.11a	NRM	TRM
steps	(A/m)	(A/m)
20	0.000	0.000
100	0.000	0.000
150	1.840	0.542
250	1.410	0.551
300	1.410	0.493
330	1.260	0.505
360	1.180	0.596
390	1.040	1.001
420	0.878	1.206
440	0.673	1.397
460	0.653	1.527
480	0.703	1.483
500	0.523	1.854
520	0.342	3.489
535	0.294	5.618
550	0.049	7.851
565	0.016	8.336
580	0.012	7.842
595	0.000	0.000

a)

MTT(C-D) - AD 79 -1631 - Sample V26.11a
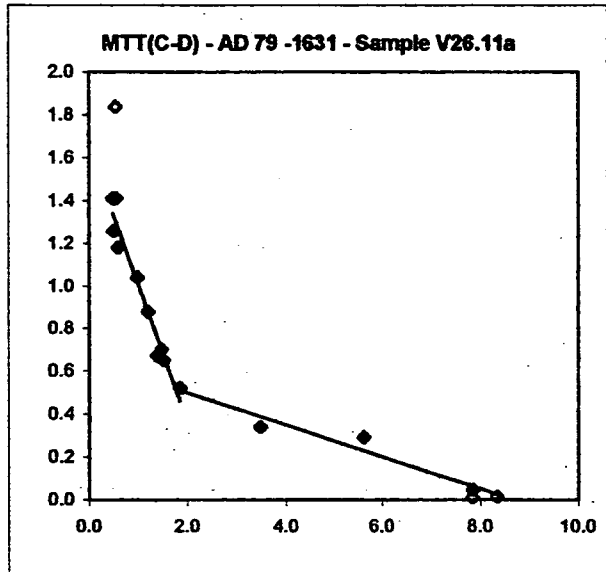
sample	Temp (°C)	N	f	g	q	b	R²	Fpalaeo (µT)	σb
V26.11a	250-500	10	0.482	0.807	5.279	-0.660	0.957	32.994	0.049
	500-565	5	0.275	0.626	1.533	-0.076	0.961	3.815	0.009

NRM - Sample V26.11a

b)

TRM - Sample V26.11a
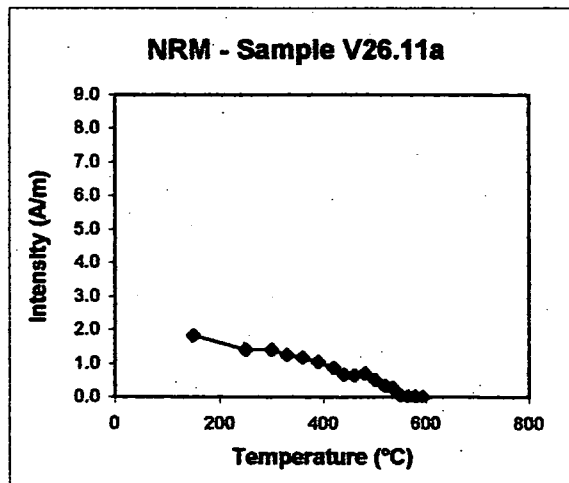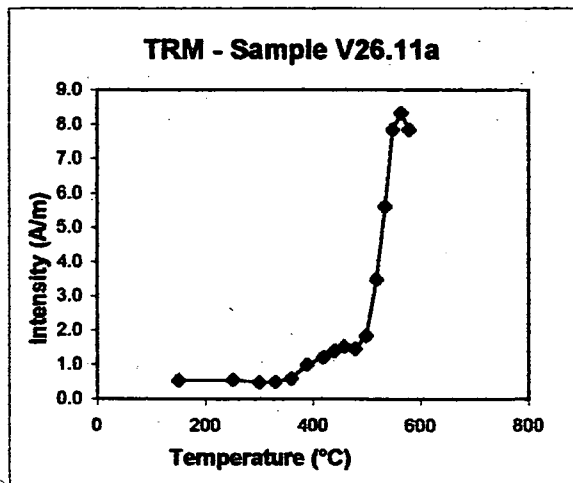
c)

Fig. 6.24 - Site V26: a)NRM/TRM plot and respective values, b)NRM demagnetization and c)TRM acquisition curves.

Tab. 6.12 - Site V26: Palaeofields estimated and statistical parameters

186

A-Demag1

B-pTRM

Scale 1000 mA/m

Scale 1000 mA/m

Mmax = 6040 mA/m

Mmax = 6190 mA/m
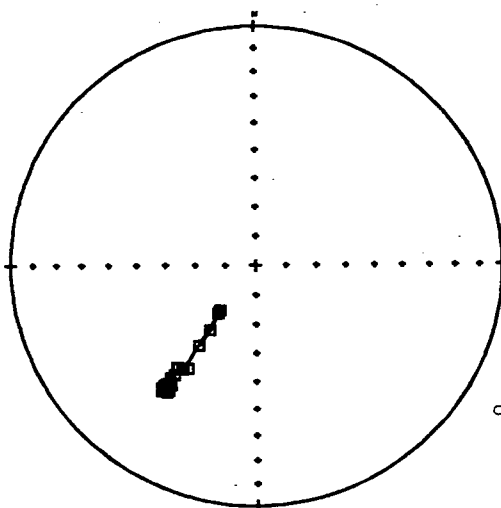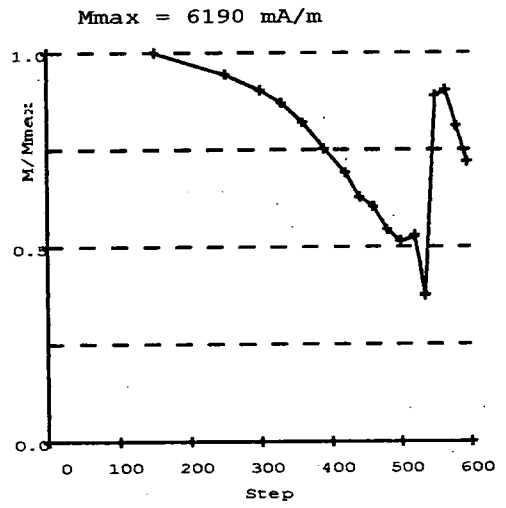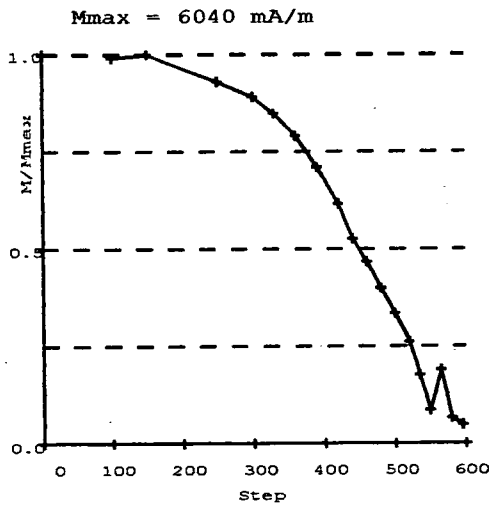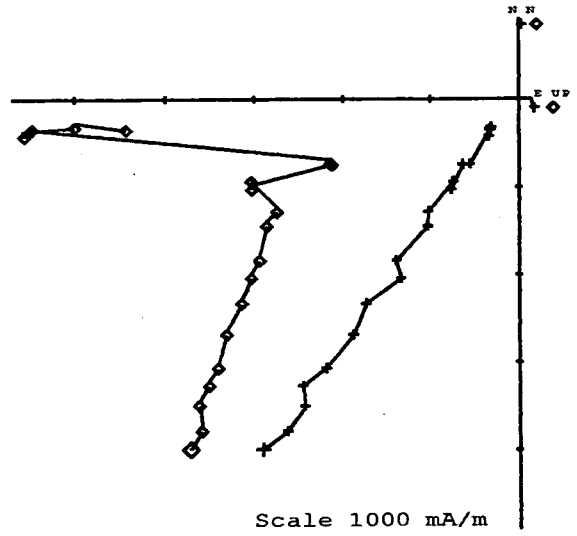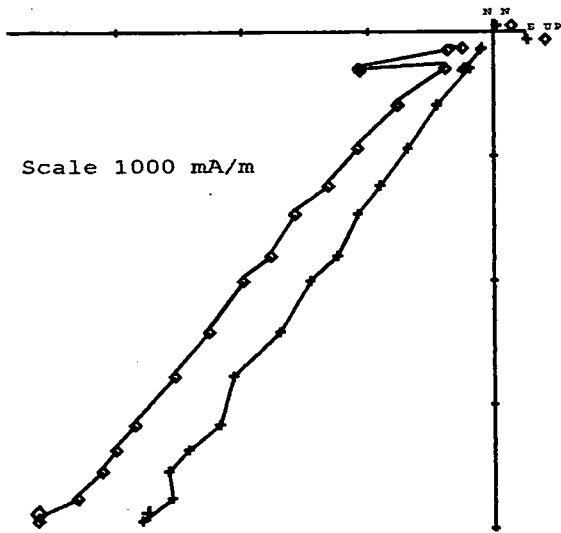
B Lower
▲ Upper
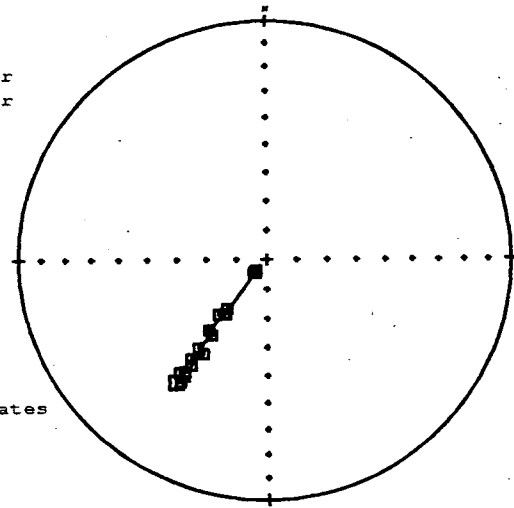
Core
Coordinates

Fig. 6.25 - Site V31: Zijderveld diagrams, Intensity and stereo plots.

MTT (A-B)		
V31.2	NRM	TRM
steps	(A/m)	(A/m)
20	0.000	0.000
100	5.980	0.000
150	6.040	0.156
250	5.620	0.293
300	5.380	0.533
330	5.120	0.518
360	4.780	0.562
390	4.290	0.807
420	3.720	0.887
440	3.180	1.053
460	2.820	1.183
480	2.410	1.283
500	2.020	1.433
520	1.580	1.949
535	1.060	1.395
550	0.522	5.096
565	1.140	4.494
580	0.401	4.650
595	0.293	4.194

a)

MTT (A-B) - AD 79 -1631 - Sample V31.2
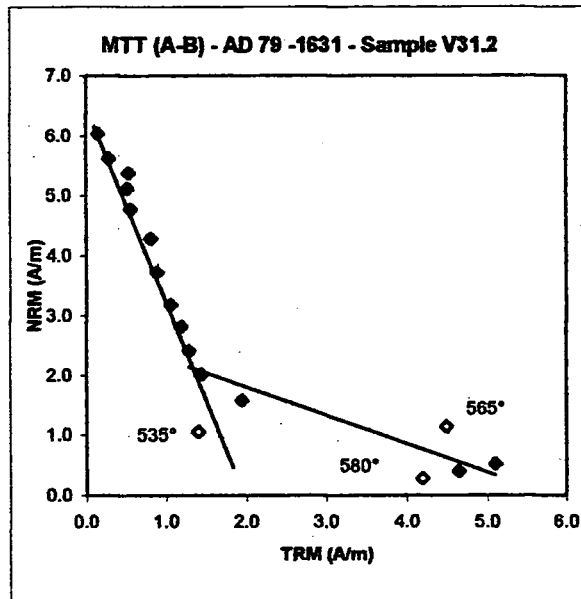
sample	T range (°)	N	f	g	q	b	R^2	Fpalaeo (μT)	σ_b
V31.2	150-500	11	0.666	0.893	14.006	-3.318	0.934	165.910	0.141
	*480-580	5	0.333	0.633	1.483	-0.486	0.904	24.314	0.069

*excluding 535,565°

NRM - Sample V31.2

b)
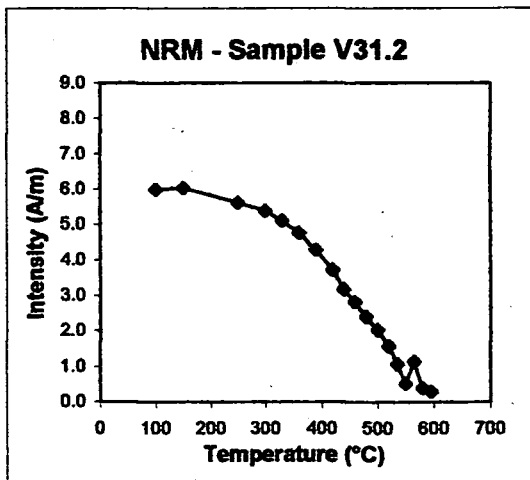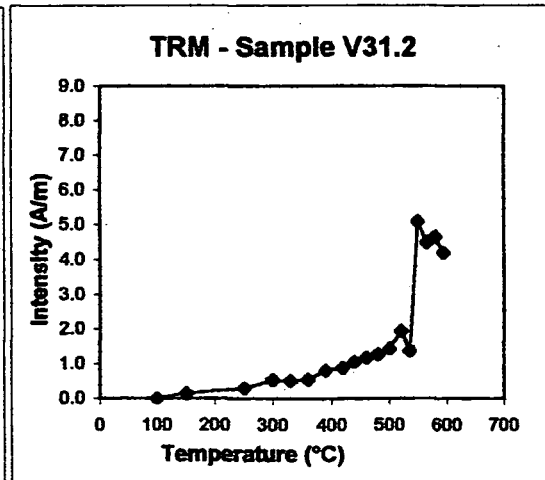
TRM - Sample V31.2

c)

Fig. 6.26 - Site V31: a)NRM/TRM plot and respective values, b)NRM demagnetization and c)TRM acquisition curves.
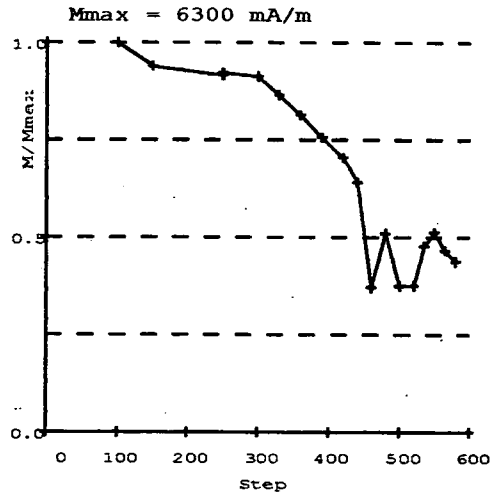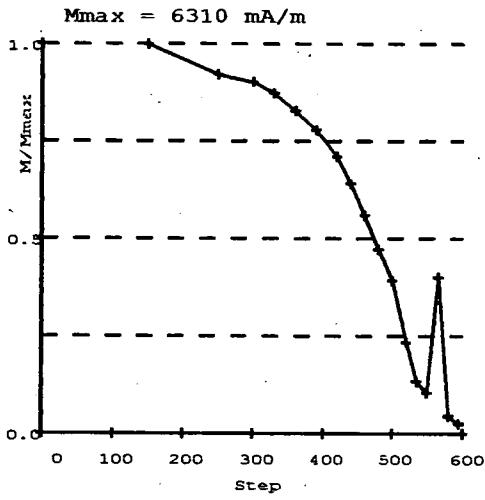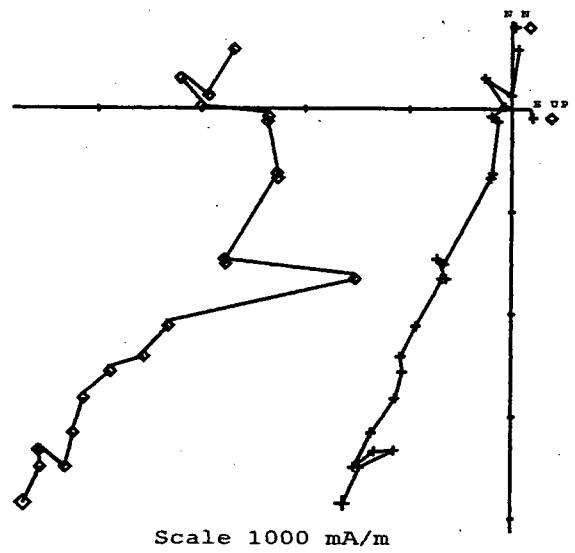
Tab. 6.13 - Site V31: Palaeofields estimated and statistical parameters

188

AD 79-1631 sample V31.2

C-Demag2

Scale 1000 mA/m

Mmax = 6120 mA/m

B-pTRMck

Mmax = 6200 mA/m
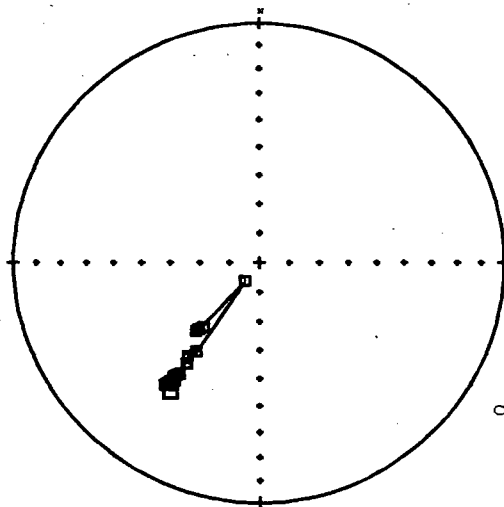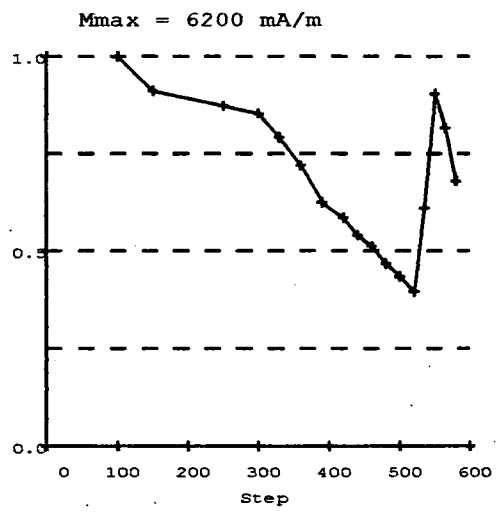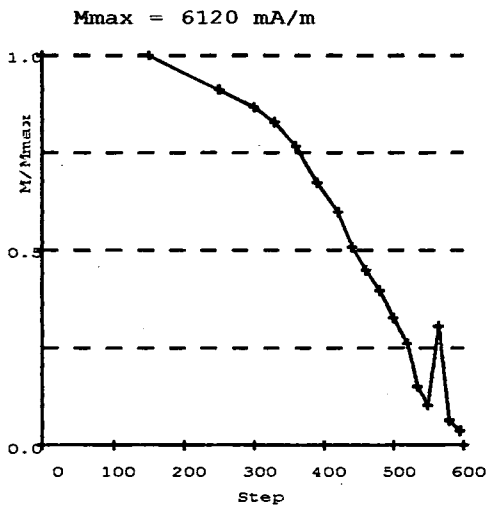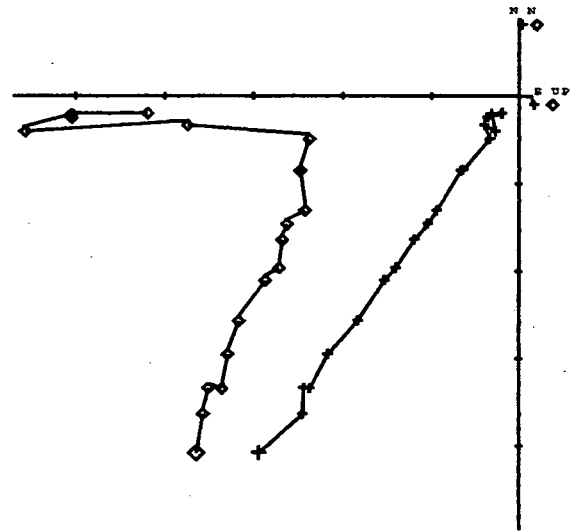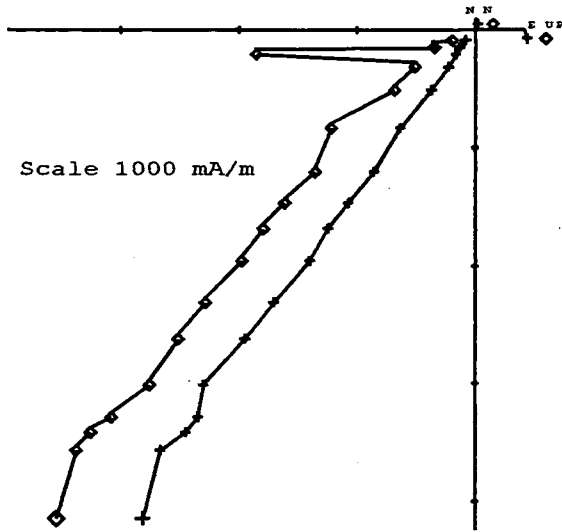
■ Lower
▲ Upper
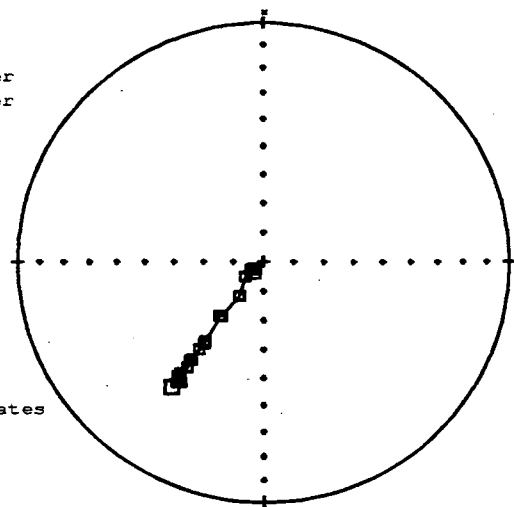
Core
Coordinates

Fig. 6.27 - Site V31: Zijderveld diagrams, Intensity and stereo plots.

MTT (C-D)		
V31.2 steps	NRM (A/m)	TRM (A/m)
20	0.000	0.000
100	0.000	0.000
150	6.120	0.635
250	5.580	0.359
300	5.310	0.155
330	5.070	0.440
360	4.690	0.768
390	4.120	0.754
420	3.660	0.631
440	3.110	0.797
460	2.750	0.883
480	2.430	0.837
500	2.000	1.194
520	1.600	1.239
535	0.920	3.076
550	0.627	5.075
565	1.870	3.198
580	0.388	3.862
595	0.000	0.000

a)

MTT (C-D) - AD 79 -1631 - Sample V31.2
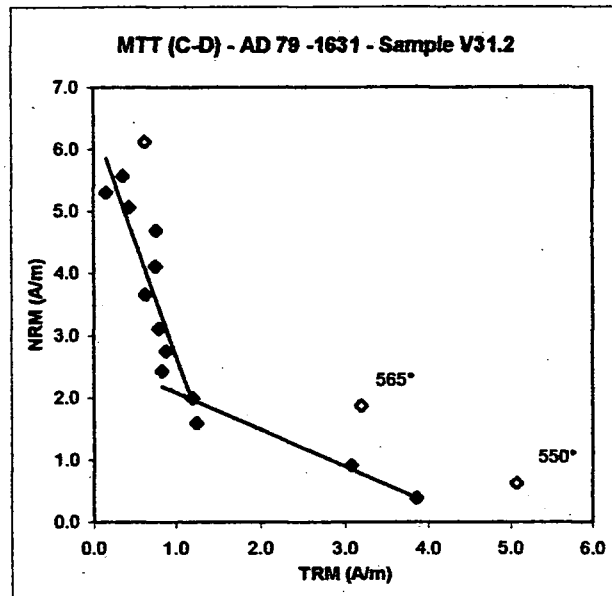
sample	Temp (°C)	N	f	g	q	b	R^2	Fpalaeo (μT)	σ_b
V31.2	150-420	11	0.650	0.893	4.080	-4.233	0.826	211.625	0.603
	*480-580	5	0.334	0.739	1.615	-0.612	0.931	30.579	0.093

* excluding 550,565

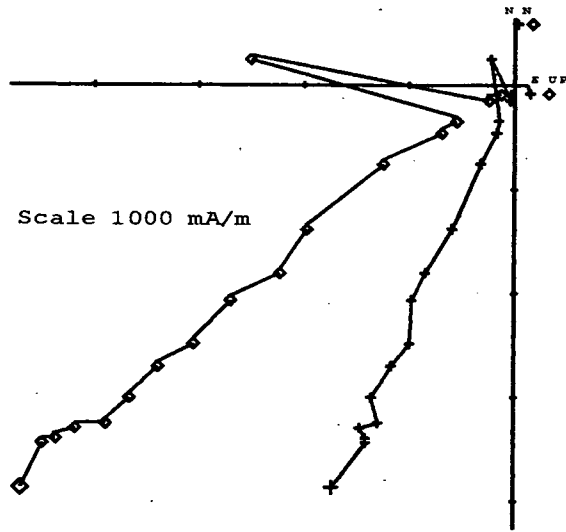NRM - sample V31.2

TRM - Sample V31.2
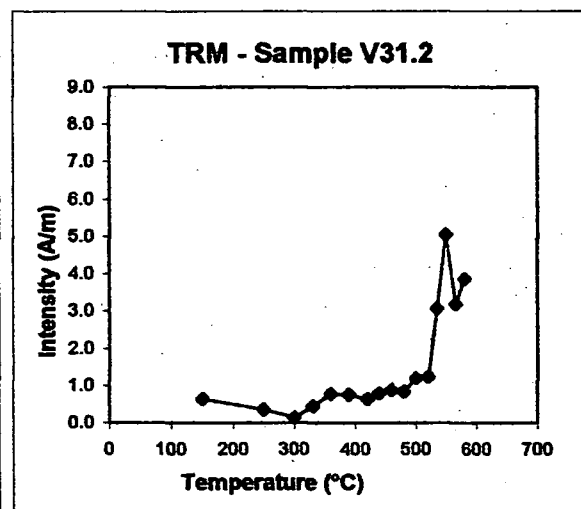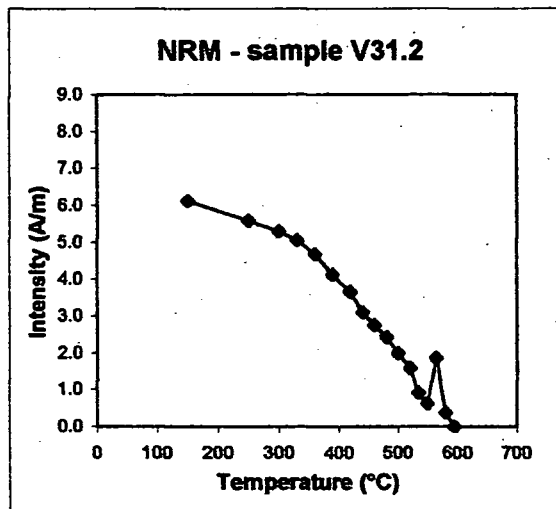
b)   c)

Fig. 6.28 - Site V31: a)NRM/TRM plot and respective values, b)NRM demagnetization and c)TRM acquisition curves.

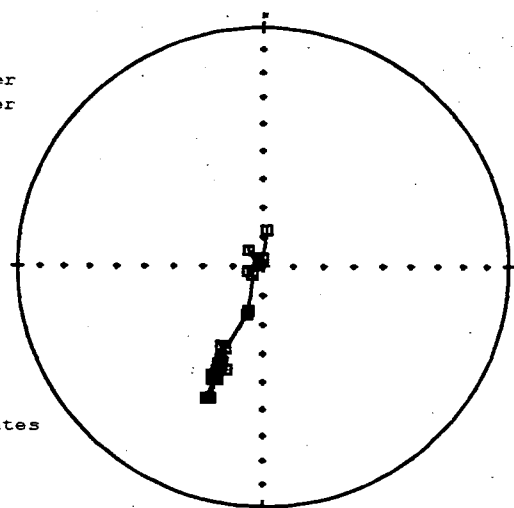Tab. 6.14 - Site V31: Palaeofields estimated and statistical parameters

190

6.3 - AD 1697

6.3.1 - Site V28

A-Demag1

Intensity Behaviour - Initial NRM for sample 3 was very high (10700) mA/m (Fig. 6.29) and, by 595°C, there was some 3% still remaining. It showed a marked decrease (about 1700 mA/m) at 100°C followed by a more usual accelerating decrease with increasing temperature, which terminated with a small concave tail (Fig. 6.29).

Directional Behaviour - Both vertical and horizontal components moved towards the origin with a very linear trend (Fig. 6.29).

B-pTRM

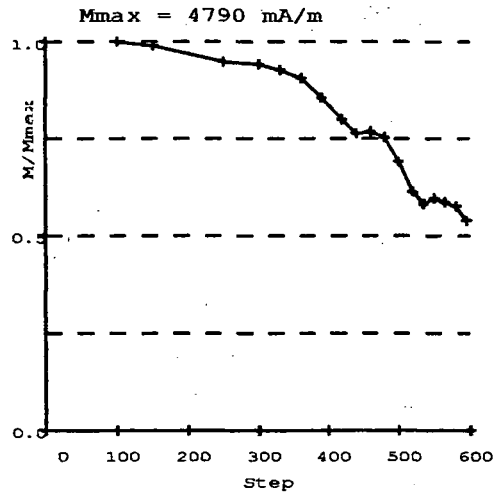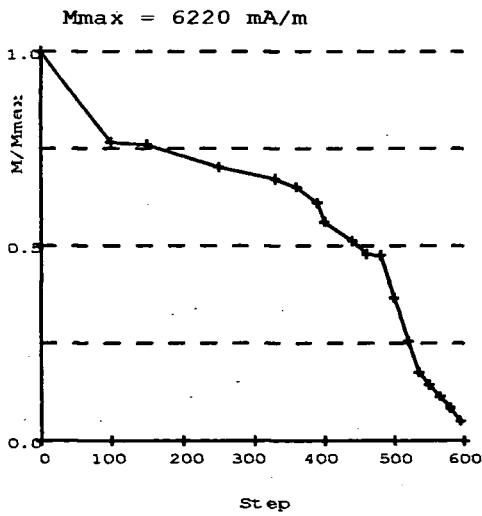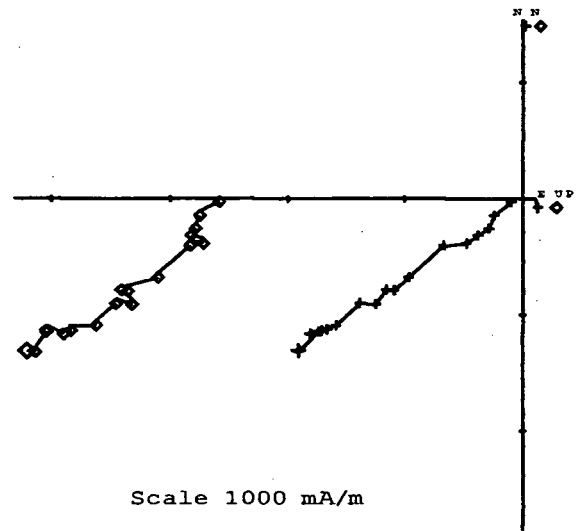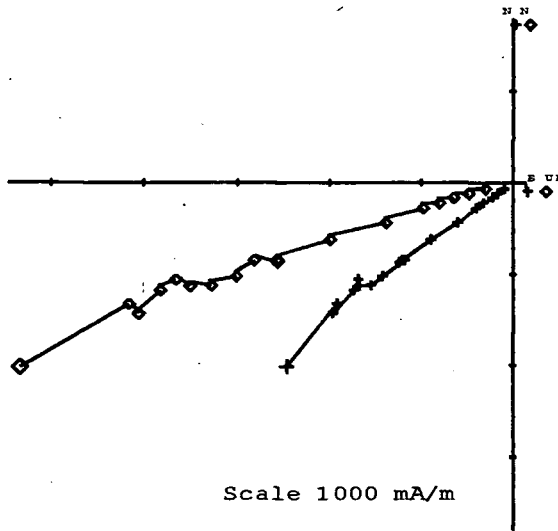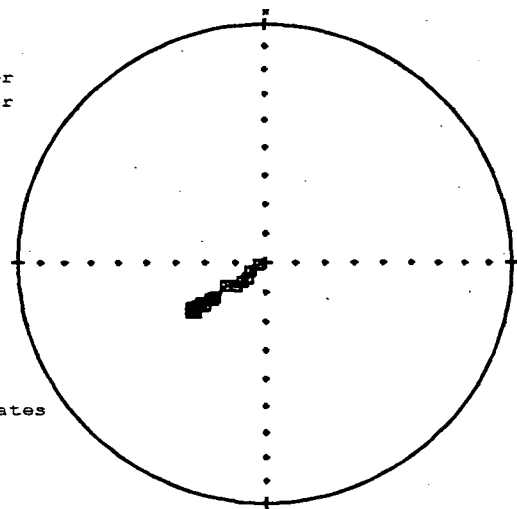*Intensity Behaviour* - The decreasing trend, from 8370 to 4300 mA/m (535°C), was identical to that one in Demag1. Between 535 and 595°C the intensity showed a very small increase and, at the end of the process the, intensity was 4470 mA/m (Fig. 6.29).

Directional Behaviour - The horizontal component moved toward the origin with a linear trend while the vertical one moved northwards, gradually away from the NRM direction. The Inc behaved as usual, as shown by the stereo plot (Fig. 6.29).

Palaeointensity results from A-B - The NRM/TRM plot showed two slopes (Fig. 6.30a) therefore two different value of the palaeofield were determined (Tab. 6.15). Both NRM demagnetization and TRM acquisition curves (Figs 6.30b,c) did not show any particular irregularities.

C-Demag2

Intensity & Directional Behaviour - In this second demagnetization the behaviours were exactly the same as in Demag1. The only difference was the NRM at 20°, which was 8210 mA/m. This value was much more consistent with the general trend showed during

the first steps of demagnetization. This suggested that the high initial NRM showed in Demag1 was probably due to instrumental or experimental error (Fig. 6.31).

D-pTRMck

Intensity & Directional Behaviours - The initial intensity was 8230 mA/m (100°C) and, at the end of the process, was 4740 mA/m. The two behaviours were exactly the same to those ones showed in pTRM (Fig. 6.31).

Palaeointensity results from C-D - The NRM/TRM plot showed two distinct slopes (Fig. 63.2a). Two value of the palaeofield were determined (Tab. 6.16) although all points below 390°C, which appeared anomalous, (Fig. 6.32b,c) were excluded.

6.3.2 - Site V29

A-Demag1

Intensity Behaviour - Initial NRM for the sample 6 was 6770 mA/m (Fig. 6.33) and, with an accelerating decrease in intensity, by 595°C had been demagnetized almost completely. It showed a very small deflection at 565°C.

Directional Behaviour - Both vertical and horizontal components moved towards the origin with a very linear trend especially above 360°C (Fig. 6.33).

B-pTRM

Intensity Behaviour - From 6380 (150°) to 2940 mA/m (535°C), it was similar to Demag1, but the values were in general slightly higher. From this point the intensity showed a small increase and at the ended it was 3680 mA/m (Fig. 6.33)

Directional Behaviour - The horizontal component moved toward the origin, with a linear trend, until 520°C then it moved slightly northwards. The vertical component

moved gradually away from the NRM but above 520°C it behaved as the horizontal one. The stereo plot showed this anomaly (Fig. 6.33).

Palaeointensity results from A-B - The NRM/TRM plot showed a slightly concave curve (Fig. 6.34a) and two different slopes were considered (Tab. 6.17). The NRM curve did not show any particular irregularities while a small one were present at 520/535° in the TRM curve (Fig. 6.34b,c).

C-Demag2

Intensity & Directional Behaviour - They were both similar as in Demag1, but there was a small spike at 565°C showed clearly by the intensity, the vertical vector and the Inc behaviours (Fig. 6.35).

D-pTRMck

Intensity Behaviour - From 100 (6760 mA/m) to 300°C it showed a shallow linear decrease, then it was similar to Demag1 until 480°C. Between 500 and 550°C the intensity had a small increase (about 500 mA/m). Above 550°C the intensity was constant and at the end it was 3540 mA/m (Fig. 6.35).

Directional Behaviour - It was very similar to pTRM (Fig. 6.35).

Palaeointensity results from C-D - As in MTT A-B two different slopes were taken in account (Fig. 6.36a, Tab. 6.18). Both the NRM and TRM curves showed irregularities (Fig. 6.36b,c) which were not considered.

AD 1697 sample V28.3

A-Demag1

B-pTRM

Scale 2000 mA/m

Scale 1000 mA/m

Mmax = 10700 mA/m

Mmax = 8370 mA/m
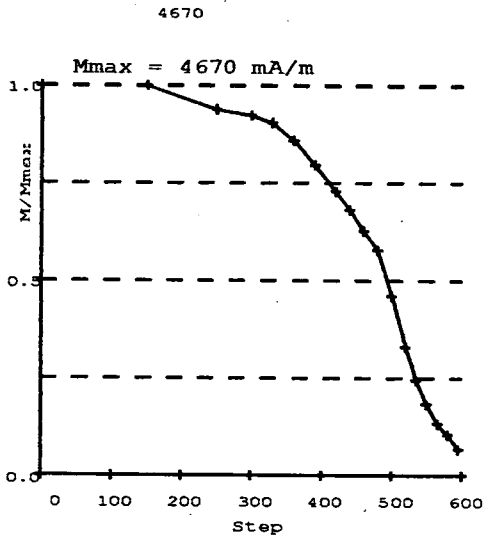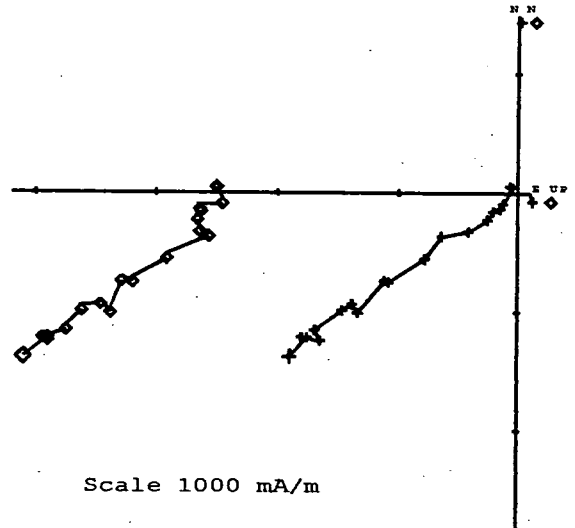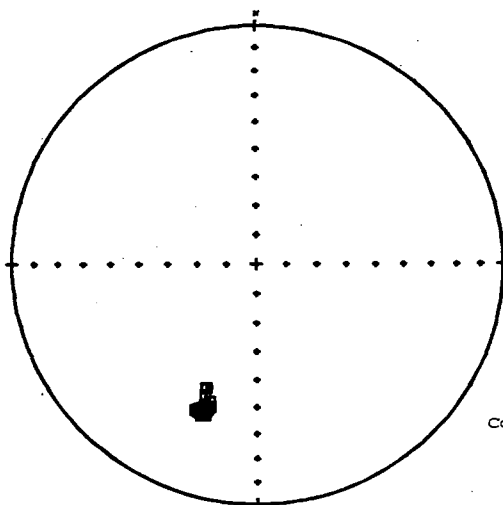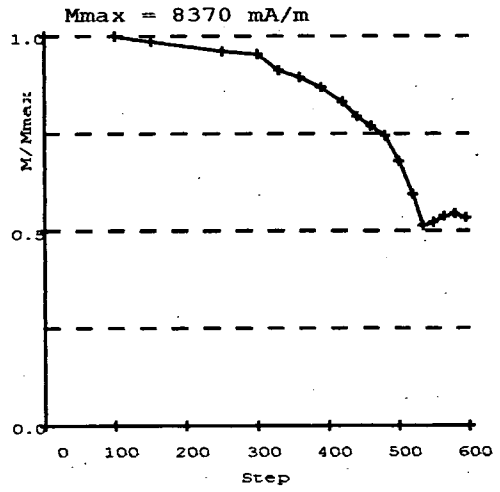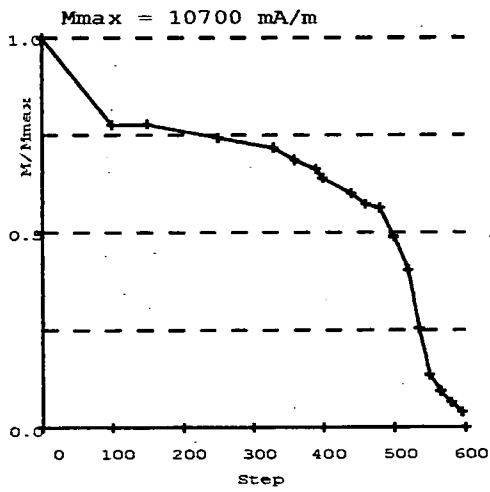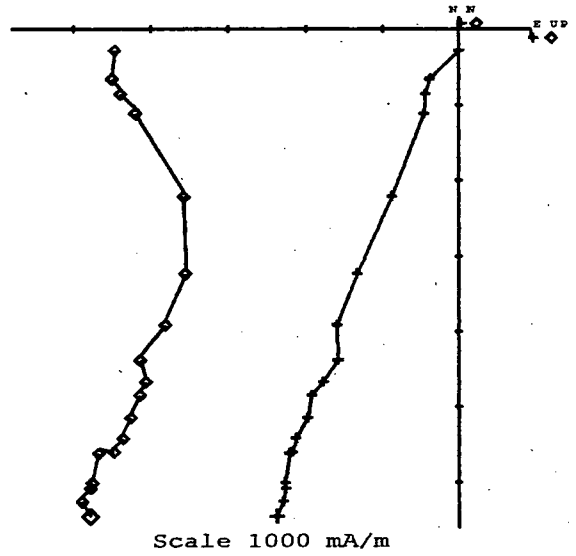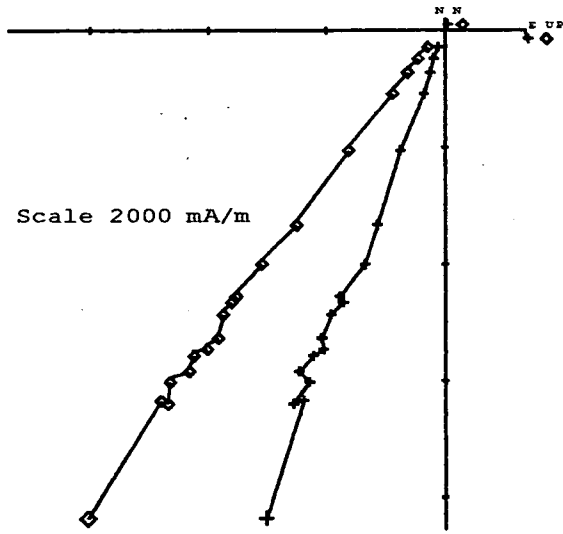
☐ Lower
▲ Upper
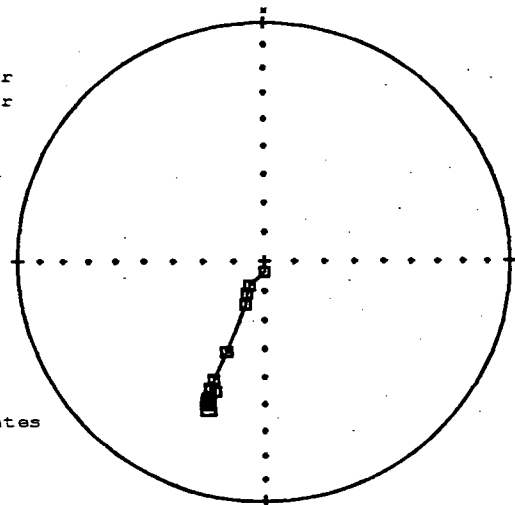
Core
Coordinates

**Fig. 6.29** - Site V28: Zijderveld diagrams, Intensity and stereo plots.

MTT (A-B)		
V28.3 steps	NRM (A/m)	TRM (A/m)
20	10.700	0.000
100	8.310	0.112
150	8.330	0.355
250	7.950	0.131
300	7.840	0.238
330	7.680	0.476
360	7.350	0.231
390	7.090	0.351
420	6.840	0.455
440	6.430	0.392
460	6.130	0.469
480	6.030	0.664
500	5.230	0.776
520	4.320	1.078
535	2.720	1.975
550	1.440	3.328
565	0.987	3.774
580	0.683	4.061
595	0.421	4.175

a)
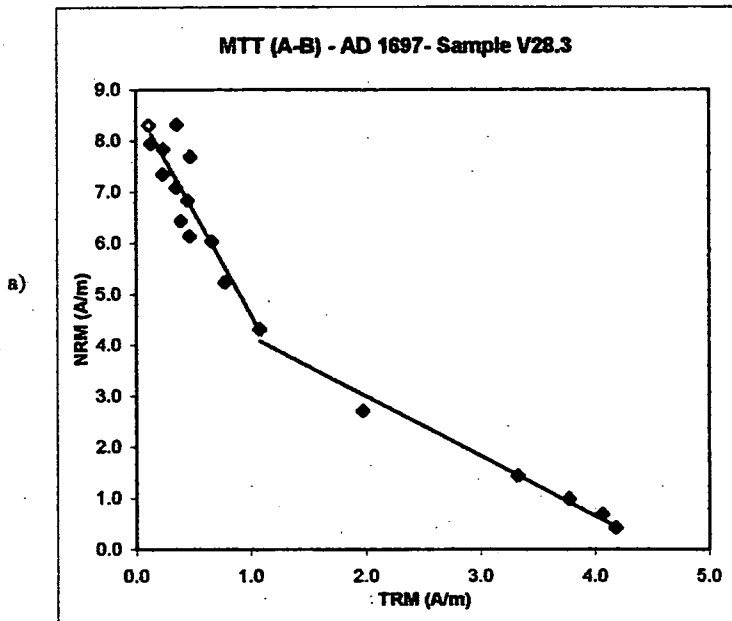
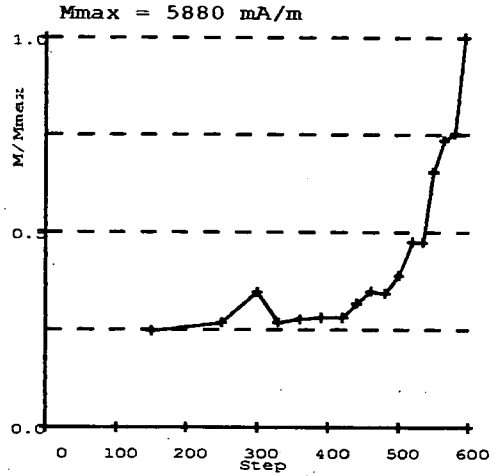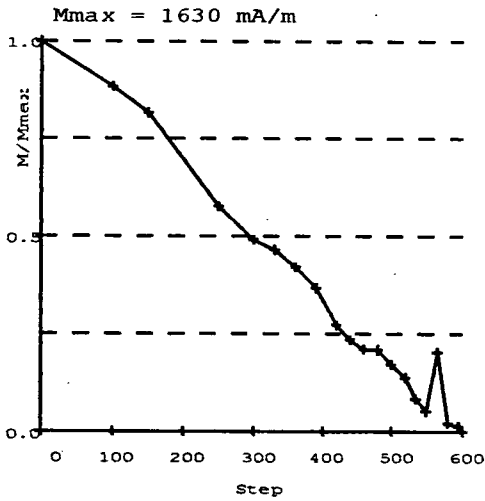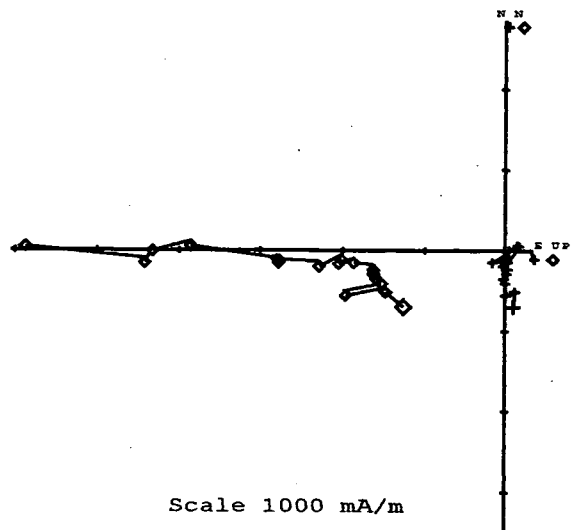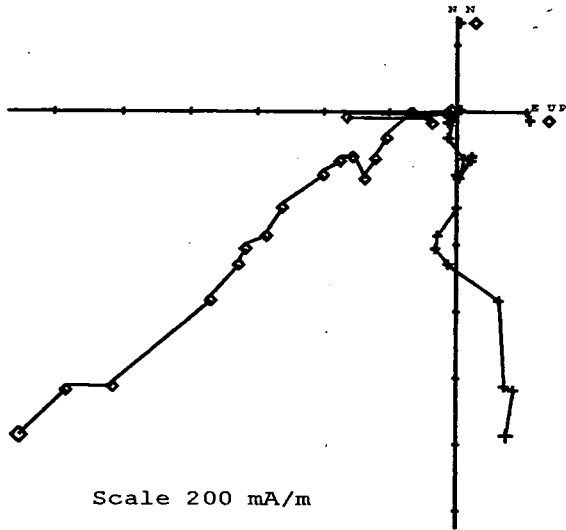| sample	Temp (°C)	N	f	g	q	b	R^2	Fpalaeo (μT)	σ_b
V28.3	150-520	13	0.480	0.864	3.154	-4.517	0.819	225.825	0.594
	520-595	6	0.579	0.767	6.491	-1.314	0.977	65.676	0.090
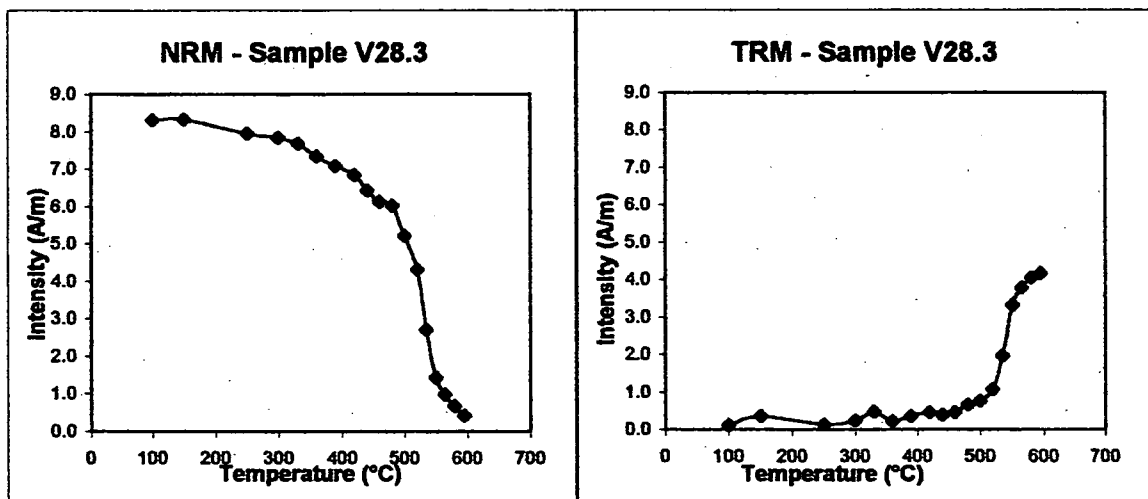
b)

c)

Fig. 6.30 - Site V28: a)NRM/TRM plot and respective values, b)NRM demagnetization and c)TRM acquisition curves.

Tab. 6.15 - Site V28: Palaeofields estimated and statistical parameters

195

AD 1697 sample V28.3

C-Demag2

Scale 1000 mA/m

Mmax = 8210 mA/m

D-pTRMck

Scale 1000 mA/m

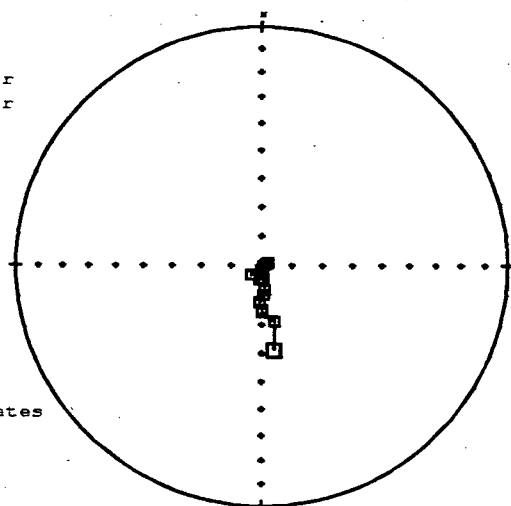Mmax = 8230 mA/m

◘ Lower
▲ Upper

Core
Coordinates

Fig. 6.31 - Site V28: Zijderveld diagrams, Intensity and stereo plots.

MTT (C-D)		
V28.3	NRM	TRM
steps	(A/m)	(A/m)
20	0.000	0.000
100	0.000	0.000
150	8.210	0.281
250	7.960	0.356
300	7.870	0.213
330	7.590	0.222
360	7.290	0.326
390	6.950	0.193
420	6.630	0.150
440	6.330	0.440
460	5.960	0.386
480	5.730	0.535
500	5.040	0.711
520	4.130	1.257
535	2.650	1.807
550	1.360	3.285
565	0.888	3.758
580	0.610	3.807
595	0.398	0.000

MTT (C-D) - AD 1697 - Sample V28.3
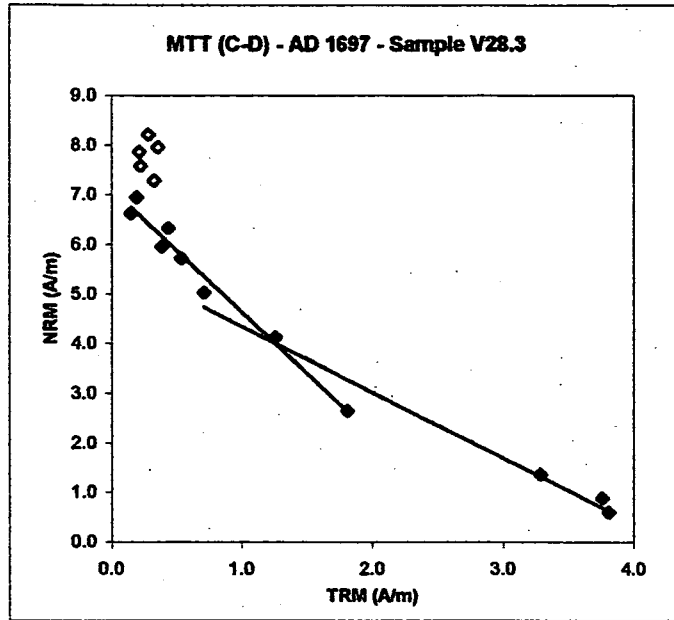
sample	Temp (°C)	N	f	g	q	b	R^2	Fpalaeo (μT)	σ_b
V28.3	[a] 390-535	8	0.524	0.790	6.410	-2.518	0.975	125.905	0.163
	[b] 500-580	6	0.540	0.552	10.731	-1.384	0.998	69.204	0.038

NRM - sample V28.3

TRM - Sample V28.3

b)   c)
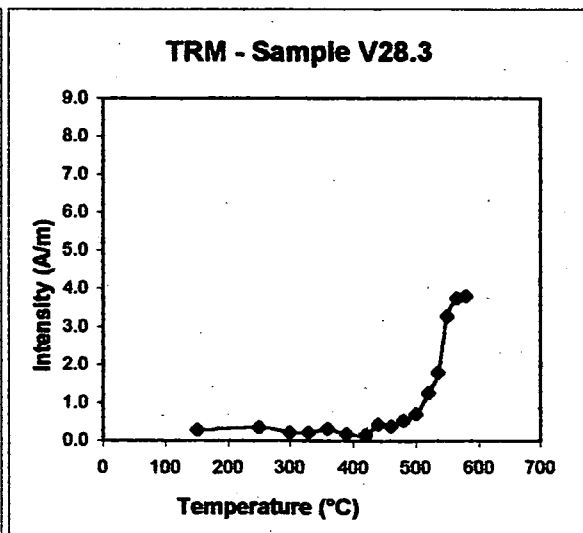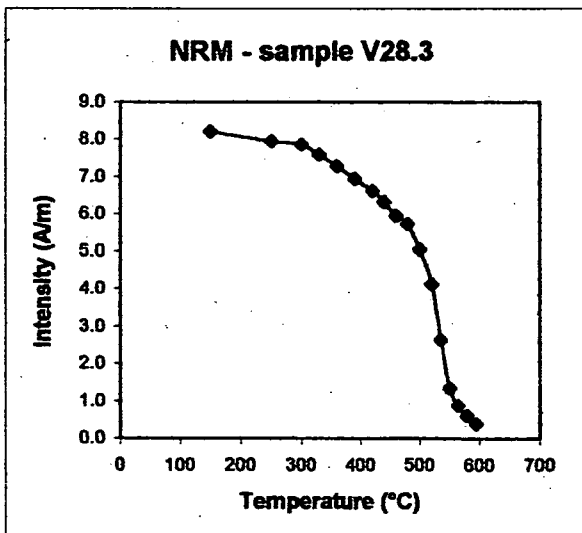
Fig. 6.32 - Site V28: a)NRM/TRM plot and respective values, b)NRM demagnetization and
c)TRM acquisition curves.
Tab. 6.16 - Site V28: Palaeofields estimated and statistical parameters

AD 1697 sample V29.6

A-Demag1

B-pTRM

Scale 1000 mA/m

Scale 1000 mA/m

Mmax = 6770 mA/m

Mmax = 6680 mA/m

■ Lower
▲ Upper

Core
Coordinates
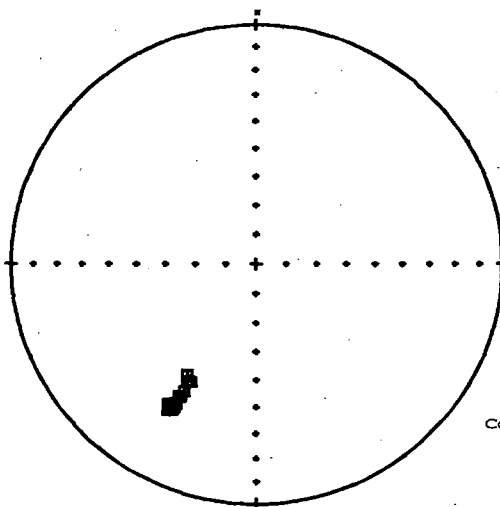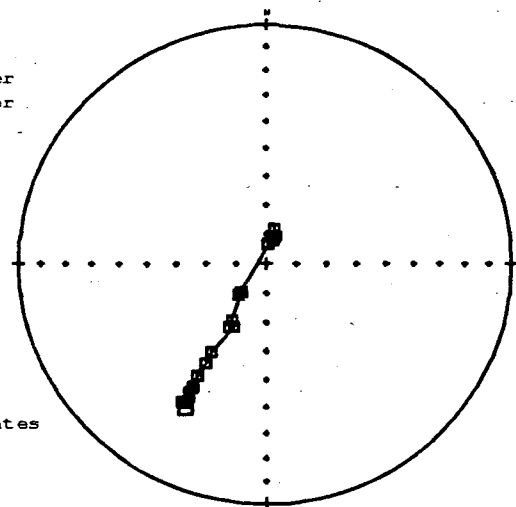
Fig. 6.33 - Site V29: Zijderveld diagrams, Intensity and stereo plots.

MTT (A-B)		
V29.6	NRM	TRM
steps	(A/m)	(A/m)
20	0.000	0.000
100	6.770	0.000
150	6.710	0.103
250	6.350	0.334
300	6.110	0.366
330	5.820	0.400
360	5.380	0.502
390	4.960	0.674
420	4.520	0.783
440	4.090	0.896
460	3.540	1.021
480	3.050	1.209
500	2.420	1.539
520	1.830	2.243
535	1.150	2.178
550	0.634	3.045
565	0.533	3.201
580	0.251	3.161
595	0.199	3.254

a)

MTT (A-B) - AD 1697- Sample V29.6
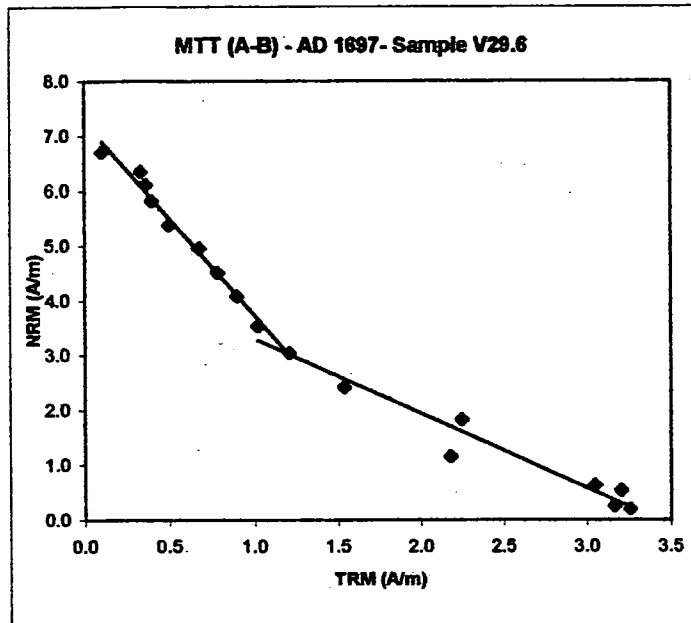
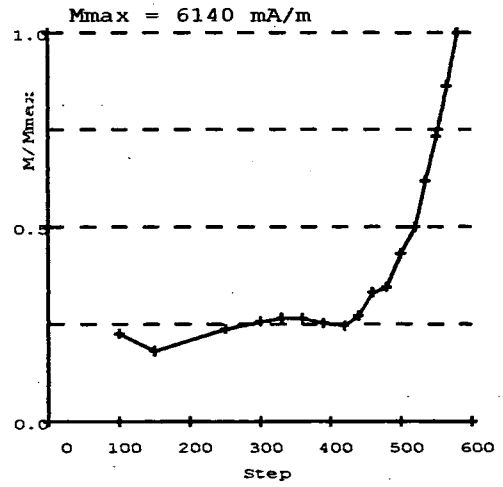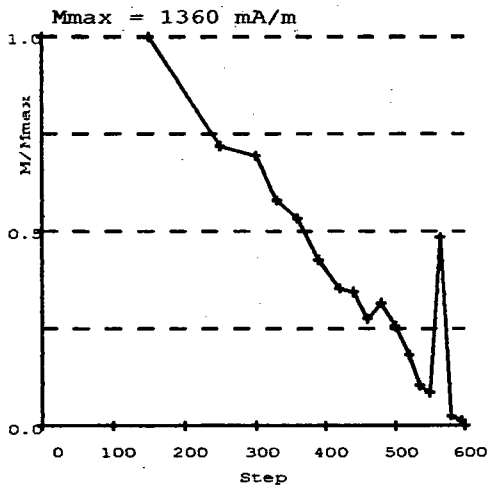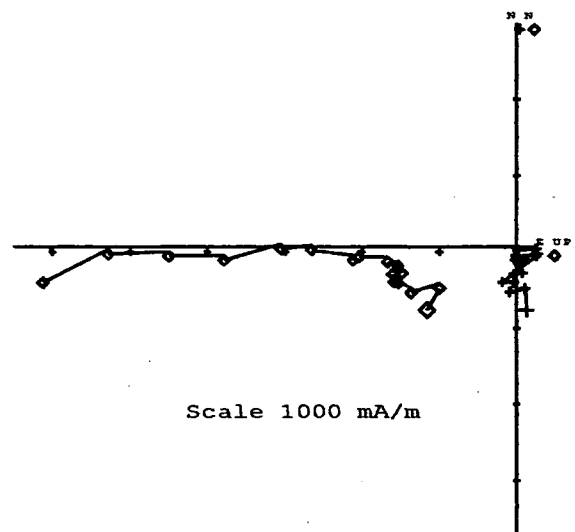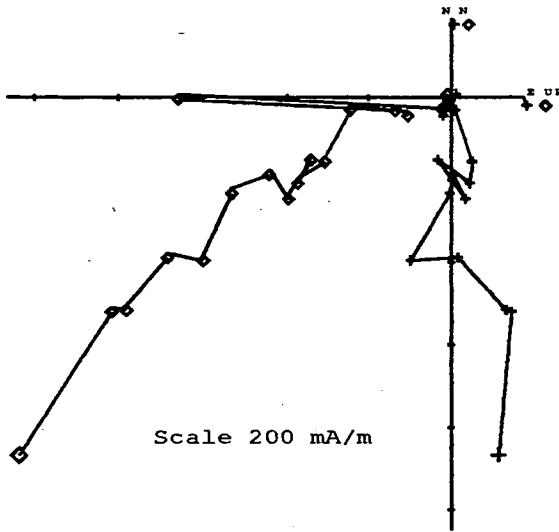| sample	Temp (°)	N	f	g	q	b	R^2	Fpalaeo (μT)	σ_b
V29.6	150-480	11	0.634	0.894	12.918	-3.300	0.983	165.015	0.145
	460-595	9	0.494	0.838	5.354	-1.398	0.959	69.895	0.108

NRM - Sample V29.6

TRM - Sample V29.6

b)
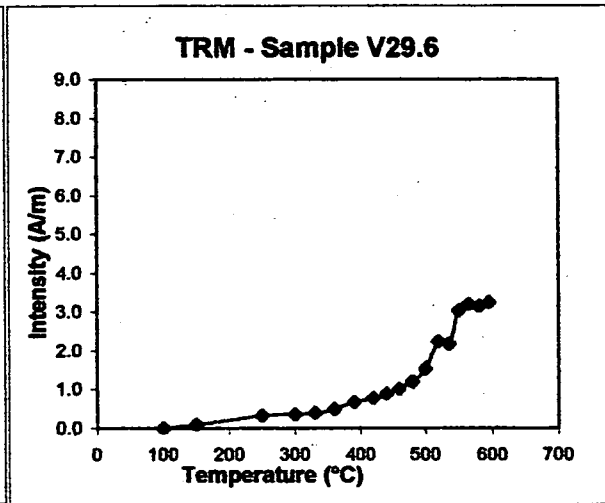
c)

Fig. 6.34 - Site V29: a)NRM/TRM plot and respective values, b)NRM demagnetization and c)TRM acquisition curves.

Tab. 6.17 - Site V29: Palaeofields estimated and statistical parameters

199

AD 1697 sample V29.6

## C—Demag2

D—pTRMck

Scale 1000 mA/m

Scale 1000 mA/m

Mmax = 6680 mA/m

Mmax = 6760 mA/m
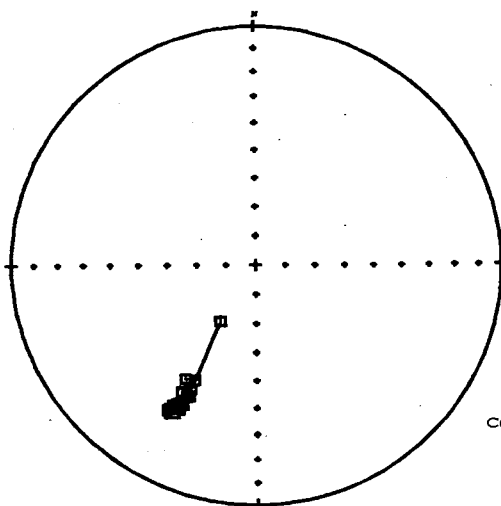
Lower
Upper
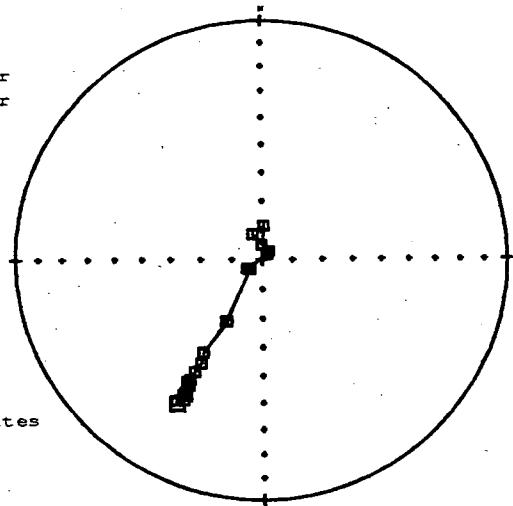
Core
Coordinates

Fig. 6.35 - Site V29: Zijderveld diagrams, Intensity and stereo plots.

MTT (C-D)		
V29.6	NRM	TRM
steps	(A/m)	(A/m)
20	0.000	0.000
100	0.000	0.000
150	6.680	0.568
250	6.210	0.353
300	5.920	0.213
330	5.710	0.510
360	5.390	0.903
390	4.860	0.734
420	4.400	0.770
440	3.930	0.879
460	3.420	0.994
480	3.000	1.078
500	2.280	1.516
520	1.560	2.072
535	0.989	2.469
550	0.529	3.166
565	0.627	2.813
580	0.238	3.157
595	0.169	0.000

a)
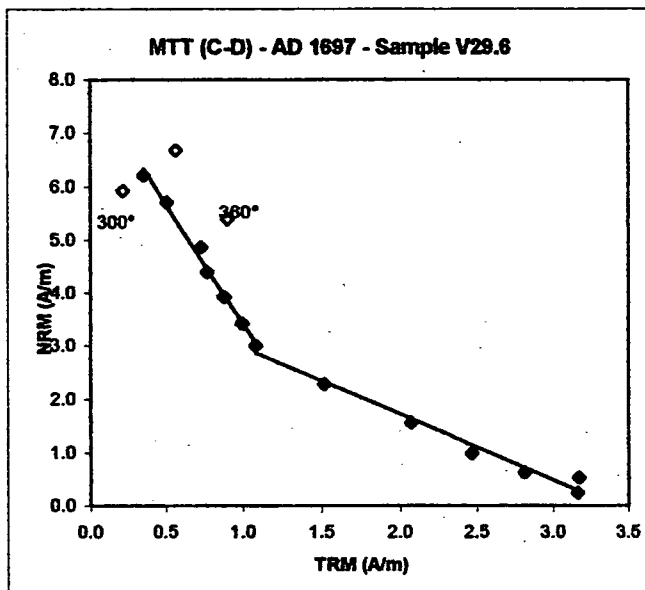
| sample	Temp (°C)	N	f	g	q	b	R²	Fpalaeo (μT)	σ_b
V29.6	*250-480	7	0.481	0.821	8.408	-4.555	0.989	227.736	0.214
	480-580	7	0.413	0.773	5.078	-1.254	0.980	62.721	0.079

* excluding 300,360
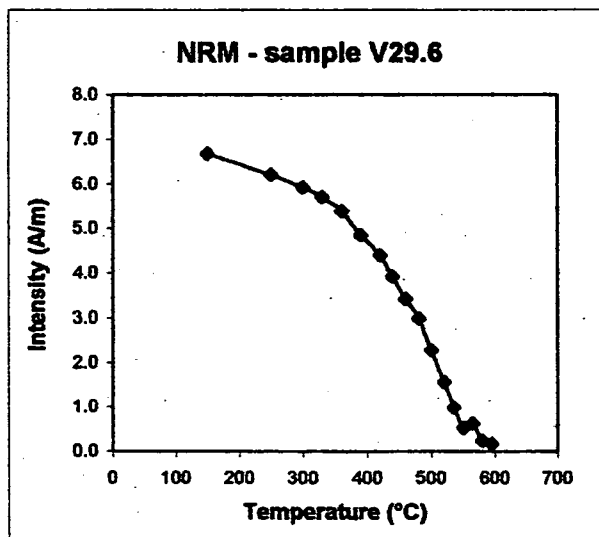
b)
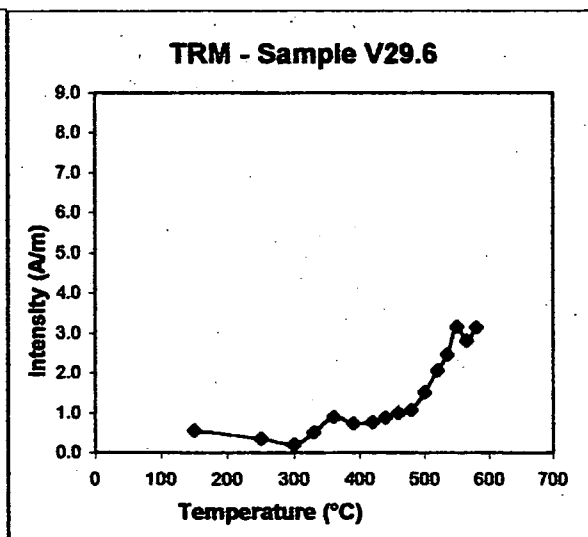
c)

Fig. 6.36 - Site V29: a)NRM/TRM plot and respective values, b)NRM demagnetization and c)TRM acquisition curves.

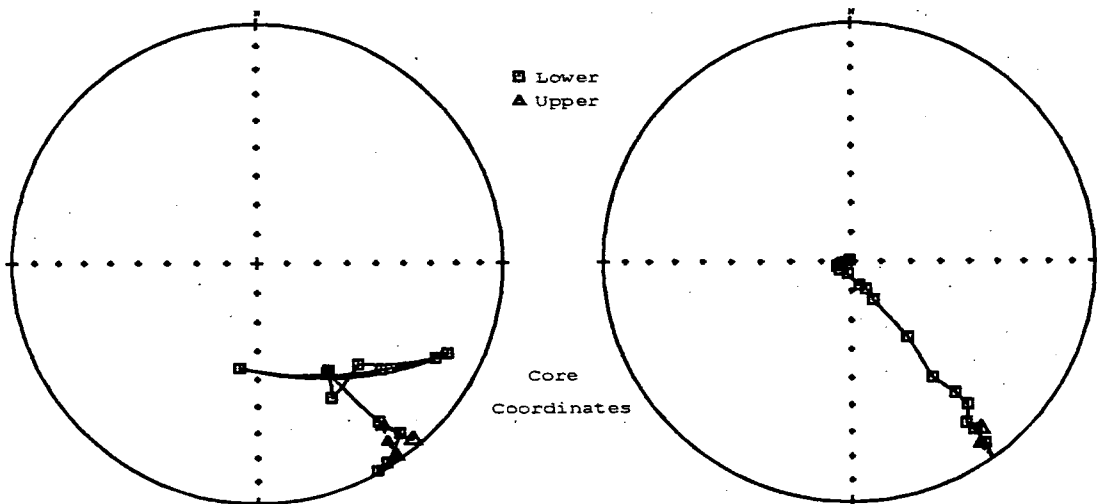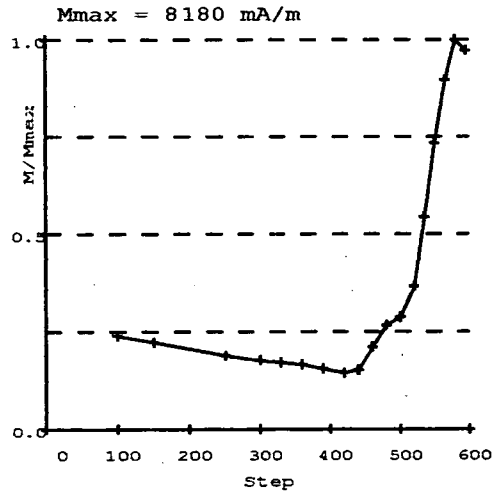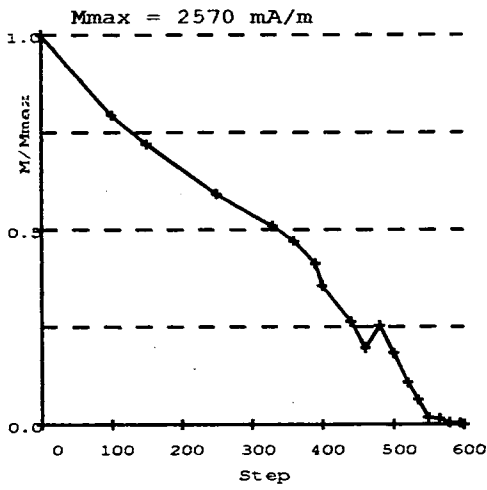Tab. 6.18 - Site V29: Palaeofields estimated and statistical parameters

6.4 - AD 1714/(1906?)
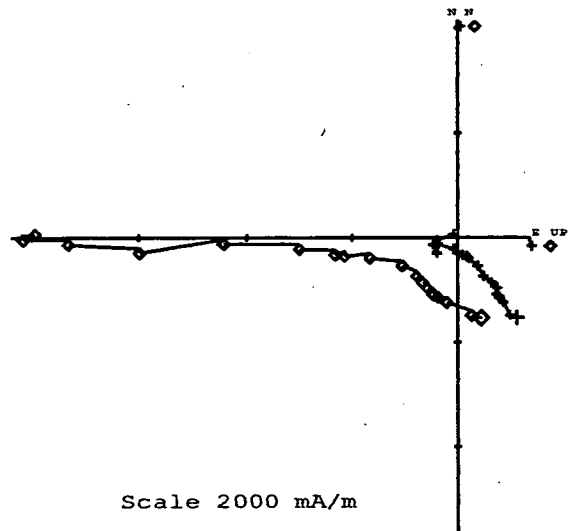
6.4.1 - Site V38

A-Demag1

Intensity Behaviour- Initial NRM for sample 3B was 5640 mA/m (Fig. 6.37) but at 100° it was about 1300 mA/m lower. After this marked decrease it showed the usual accelerating decrease with increasing temperature, which terminated with a small concave tail. At 595° there was some 5% of initial NRM still remaining.

Directional Behaviour - Both vertical and horizontal components moved towards the origin with a very linear trend (Fig. 6.37).

B-pTRM

Intensity Behaviour - From 100°C (4340 mA/m) it showed a smooth decrease until 535°C (2820 mA/m) with a clear break between 440 and 480°C when the intensity was constant. Starting from 535°C the intensity showed a marked increase (about 1000 mA/m) and, at the end of the process (595°C) it was 3900 mA/m (Fig. 6.37).

Directional Behaviour - The horizontal component moved toward the origin with a quite linear trend but, at 535°C it showed a clear deflection towards the west. The vertical one moved northwards, gradually away from the NRM direction until 535°, then it moved downward. The Inc behaved as usual, as shown by the stereo plot (Fig. 6.37).

Palaeointensity results from A-B - Two very distinct slopes were considered (Fig. 6.38a, Tab. 6.19). Both NRM demagnetization and TRM acquisition curves (Fig. 6.38b,c) did not show any particular irregularities.

C-Demag2

Intensity & Directional Behaviour - In this second demagnetization the behaviours were exactly the same as in Demag1 (Fig. 6.39), but because the process started at 150°C

(4230 mA/m), the marked difference between the initial NRM (20°) and that one at 100°C, observed in Demag1, could not be repeated.

D-pTRMck

Intensity & Directional Behaviours - The two behaviours were exactly the same to those shown in pTRM. The initial intensity was 4220 mA/m (100°C) and, at the end of the process, was 3700 mA/m (Fig. 6.39).

Palaeointensity results from C-D - As in MTT A-B, two slopes were defined (Fig. 6.40a) and, as no clear anomalies were present in both NRM and TRM curves (Fig. 6.40b,c), all the points were considered (Tab. 6.20).

6.5 - AD 1754

6.5.1 - Site V39

A-Demag1

Intensity Behaviour - Sample 7A showed an initial NRM, at 20°C much higher then at 100°C. In fact the intensity was 6190 mA/m and, the next step of temperature, it dropped down of about 1550 mA/m. Starting from 250°C it showed an accelerating decrease (Fig. 6.41) terminating with a small concave tail. At 595°C, there was some 11% of initial NRM still remaining. A small irregularity occurred between 250-400°C.

Directional Behaviour - Both vertical and horizontal components moved towards the origin with a linear trend, especially above 460°C. Thy showed the same deflection between 250 and 400°C (Fig. 6.41).

B-pTRM

Intensity Behaviour - It showed a decreasing trend, from 4790 (100°C) to 2960 mA/m (535°C) that was quite similar to Demag1 especially until 360°C. In fact above this

temperature there were two small but clear anomalies between 360-440°C and between 460-500°C. Above 535°C the intensity showed a significant increase (about 2000 mA/m). (Fig. 6.41)

Directional Behaviour - The horizontal component moved toward the origin with an almost linear trend, but without reaching it. The vertical component moved gradually away from the NRM direction but it showed an anomalous trend between 360° and 460°C. At 535°C a marked downward spike occurred. The Inc moved towards 90° as shown by the stereo plot (Fig. 6.41).

Palaeointensity results from A-B - The NRM/TRM plot showed two distinct slopes (Fig. 6.42a) and to very different value of the palaeofield were defined (Tab. 6.21). No clear anomalous points appeared on both NRM and TRM curves (Fig. 6.42b,c).

C-Demag2

Intensity & Directional Behaviour - The initial NRM (150°C) was 4590 mA/m. Above this the two behaviours were very similar to Demag1 (Fig. 6.43).

D-pTRMck

Intensity Behaviour - The initial intensity was 4680 mA/m (100°C) and behaved similarly to pTRM but without showing anomalies between 360° and 535°C. After the marked increase to 535°C the intensity was 4810 mA/m (Fig. 6.43).

Directional Behaviour - It was very similar to that one showed in pTRM (Fig. 6.43).

Palaeointensity results from C-D - The NRM and TRM showed almost the same behaviour as in MTT A-B (Fig. 6.44b,c), therefore two slopes were obtained (Fig. 6.44a, Tab. 6.22).

6.5.2 - Site V40

A-Demag1

Intensity Behaviour - The initial NRM (at 20°C), in sample 12A was 4930 mA/m, but at 100°C it dropped down about 1100 mA/m. From 250°C it showed the usual accelerating decrease (Fig. 6.45) terminating with a linear trend at 595°C and some 10% of initial NRM still remaining. Small irregularities were present at 400 and 480°C.

Directional Behaviour - Both vertical and horizontal components moved towards the origin with a linear trend (Fig. 6.45).

B-pTRM

Intensity Behaviour - The decreasing trend showed from 3820 (100°C) to 2300 mA/m (535°C) was very similar to Demag1 especially below 360°C, when it showed a slight deceleration in the decrease until 535°C. Above this temperature the intensity showed a significant increase (about 1500 mA/m).

Directional Behaviour - The vertical component moved gradually away from the NRM direction but at 535°C it showed a marked downward deflection (Fig. 6.45). The horizontal component moved toward the origin with an almost linear trend and, at 535°C showed a small spike westwards. The Inc moved clearly towards 90°.

Palaeointensity results from A-B - The NRM/TRM plot showed two slopes (Fig. 6.46a) therefore two different value of the palaeofield were determined (Tab. 6.23). Both NRM and TRM curves (Fig. 6..46b,c) behaved almost regularly.

C-Demag2

Intensity & Directional Behaviour - The two behaviours were very similar to Demag1. The initial NRM (150°C) was 3730 mA/m (Fig. 6.47).

D-pTRMck

Intensity Behaviour - The initial intensity was 3800 mA/m (100°C) and showed an initial decreasing trend that was similar to demag1 below 535°C, when the intensity was 2400 mA/m. After the marked increase occurred above 535°C, as in pTRM, the intensity was 4810 mA/m (Fig. 6.47).

Directional Behaviour - This was very similar to that showed by the pTRM (Fig. 6.47).

Palaeointensity results from C-D - The NRM/TRM plot showed two distinct slopes (Fig. 6.48a). Two value of the palaeofield were determined (Tab. 6.24) although few points below 330°C appeared slightly anomalous (Fig. 6.48b,c).

6.5.3 - Site V41

A-Demag1

Intensity Behaviour - Sample 7B showed a very high initial NRM (9100 mA/m) at 20°C. At 100°C it dropped down of about 2200 mA/m and kept steady until 330° when it showed the usual accelerating decrease (Fig. 6.49). This terminated with a small concave tail and, by 595°C, had been demagnetized almost completely.

Directional Behaviour - Both components moved towards the origin with a very linear trend especially above 480°C (Fig. 6.49).

B-pTRM

Intensity Behaviour - This behaviour (Fig. 6.49) was exactly the same as in Demag1 from 7070 (100°C) to 3320 mA/m (535°C). Above this temperature the intensity increased significantly (about 2000 mA/m).

Directional Behaviour - The horizontal component moved toward the origin with an almost linear trend until 535°C. Above this it moved slightly westwards. The vertical

component moved gradually away from the NRM direction and, at 535°C, showed a marked downward deflection (Fig. 6.49). This behaviour was underlined in the stereo plot, where the Dec changed above 535°C. while the Inc moved towards 90°, as usual.

Palaeointensity results from A-B - Two different slopes were considered (Fig. 6.50a, Tab. 6.25). The NRM curve did not show any particular irregularities while the TRM one showed small anomalies at low temperatures (Fig. 6.50b,c)

C-Demag2

Intensity & Directional Behaviour - The two behaviours were similar to Demag1 but the vertical component moved slightly downwards, with a curving trend, between 420 and 500C°. The initial NRM (150°C) was 6980 mA/m (Fig. 6.51).

D-pTRMck

Intensity Behaviour - It was very similar to pTRM. The initial NRM was 6850 mA/m (100°C); at 535°C, when the intensity started to increase, it was 2820 mA/m; at the end of the process (595°) the intensity was 5440 mA/m (Fig. 6.51).

Directional Behaviour - It was very similar to that one showed in pTRM (Fig. 6.51).

Palaeointensity results from C-D - As in MTT A-B, two slopes were defined (Fig. 6.52a) and, as no clear anomalies were present in both NRM and TRM curves (Fig. 6.52b,c), all the points were considered (Tab. 6.26).

207

A-Demag1

Scale 1000 mA/m

B-pTRM

Scale 1000 mA/m

Mmax = 5640 mA/m

Mmax = 4340 mA/m
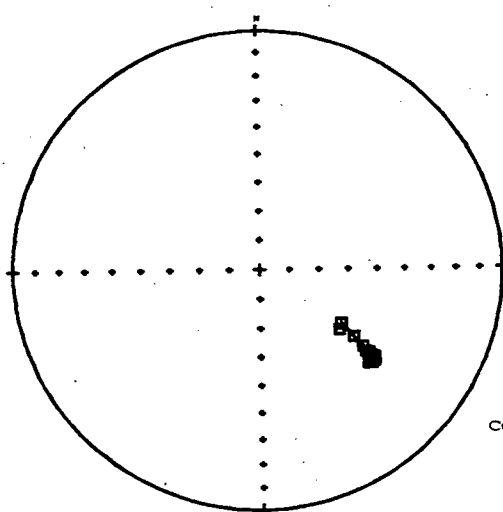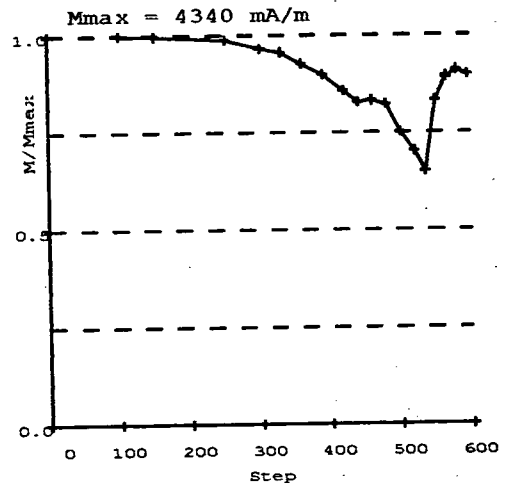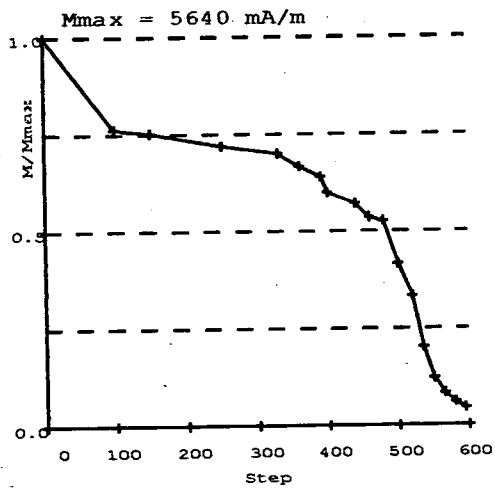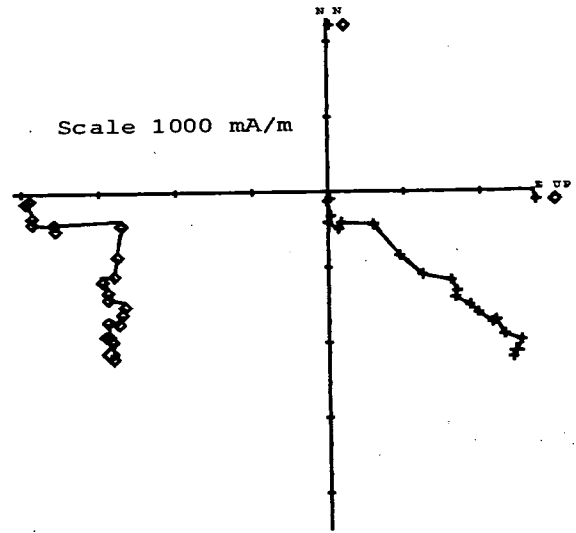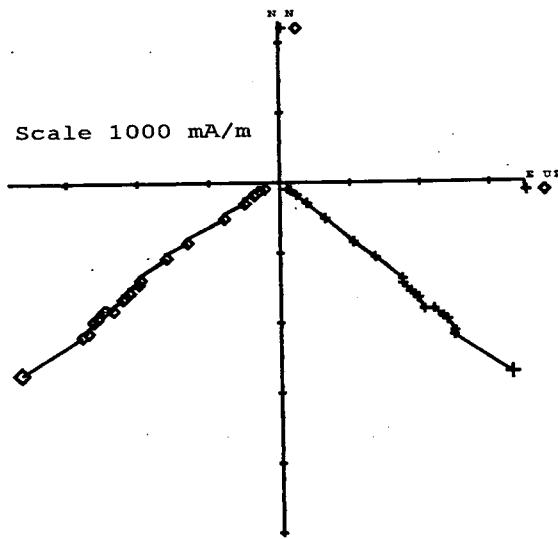
☐ Lower
▲ Upper
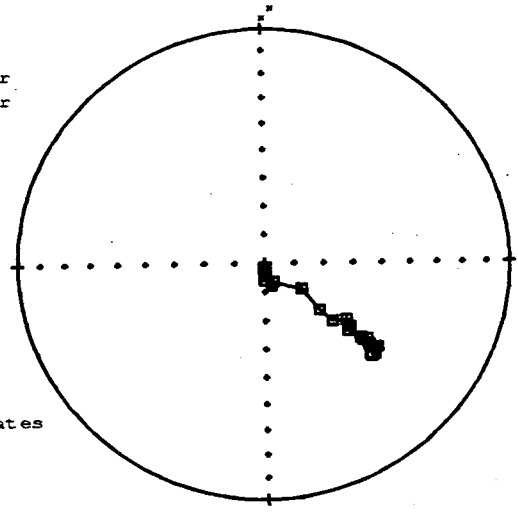
Core
Coordinates

Fig. 6.37 - Site V38: Zijderveld diagrams, Intensity and stereo plots.

MTT (A-B)		
V38.3b	NRM	TRM
steps	(A/m)	(A/m)
20	5.640	0.000
100	4.310	0.000
150	4.250	0.160
250	4.060	0.260
300	4.010	0.341
330	3.950	0.318
360	3.760	0.437
390	3.610	0.427
420	3.380	0.501
440	3.220	0.556
460	3.020	0.904
480	2.970	1.028
500	2.350	1.215
520	1.880	1.477
535	1.140	1.936
550	0.689	3.094
565	0.469	3.518
580	0.342	3.664
595	0.253	3.692

a)

MTT (A-B) - AD1714(1906)- Sample V38.3b
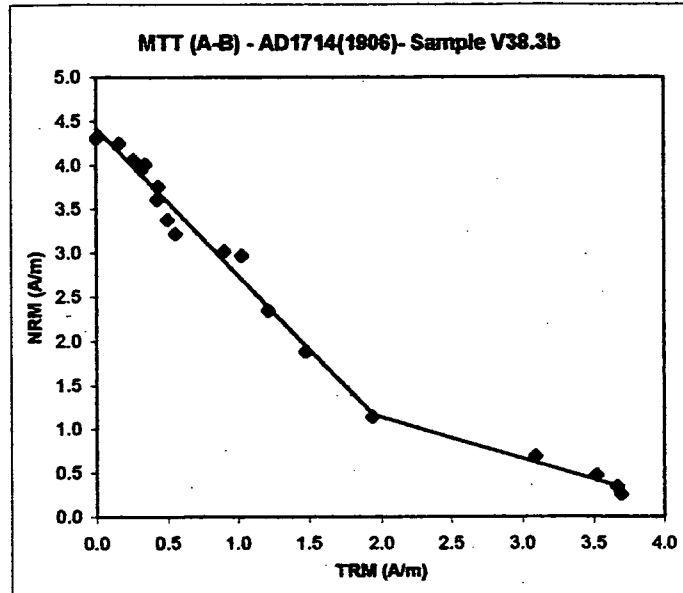
sample	Temp (°)	N	f	g	q	b	R^2	Fpalaeo (µT)	σ$_b$
V38.3b	100-535	14	0.562	0.863	10.798	-1.697	0.976	84.872	0.076
	535-595	5	0.157	0.649	1.015	-0.481	0.970	24.066	0.048
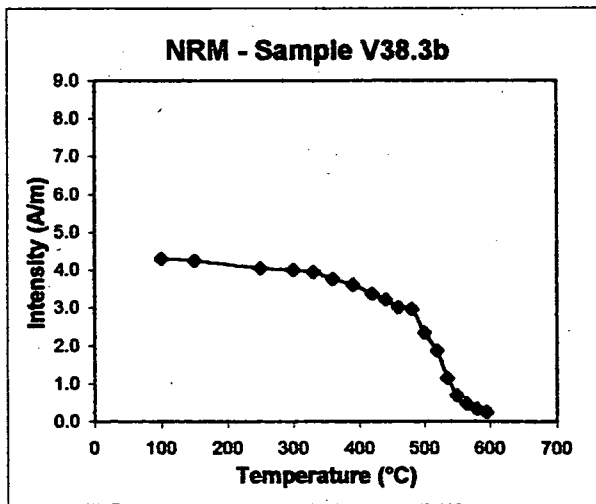
b)
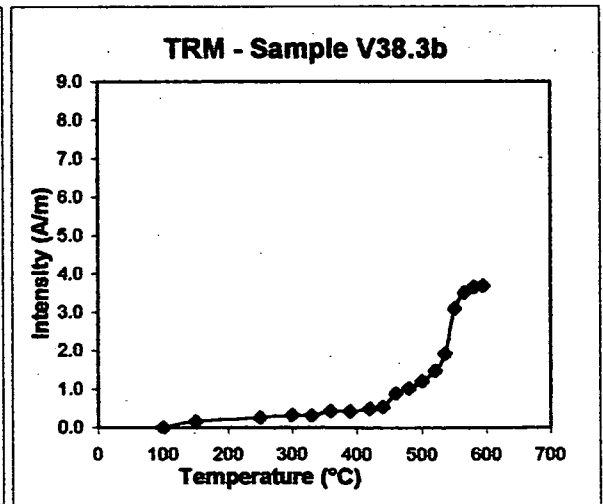
c)

Fig. 6.38 - Site V38: a)NRM/TRM plot and respective values, b)NRM demagnetization and c)TRM acquisition curves.

Tab. 6.19 - Site V38: Palaeofields estimated and statistical parameters

209

C-Demag2

Scale 1000 mA/m

Mmax = 2300 mA/m

D-pTRMck

Scale 1000 mA/m

Mmax = 4220 mA/m
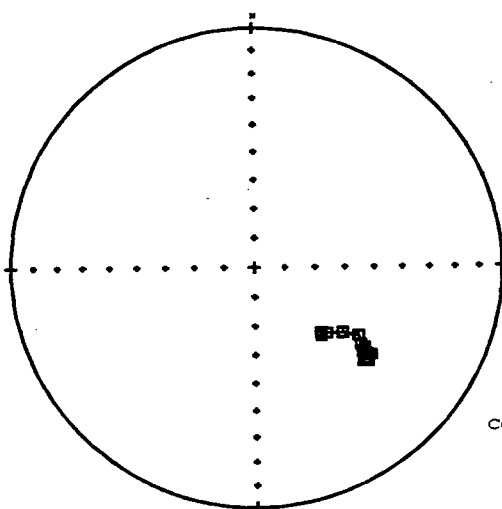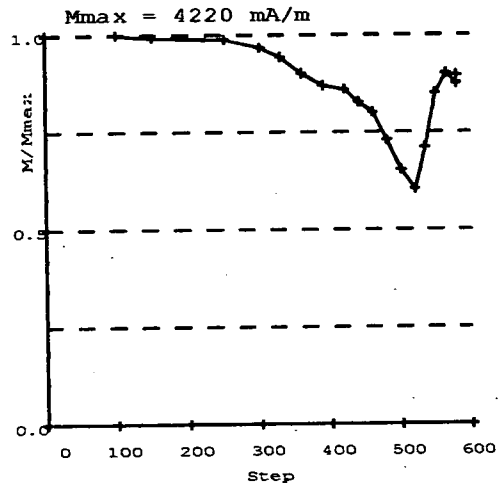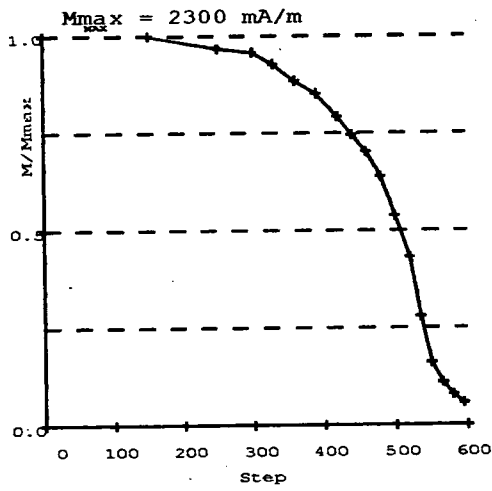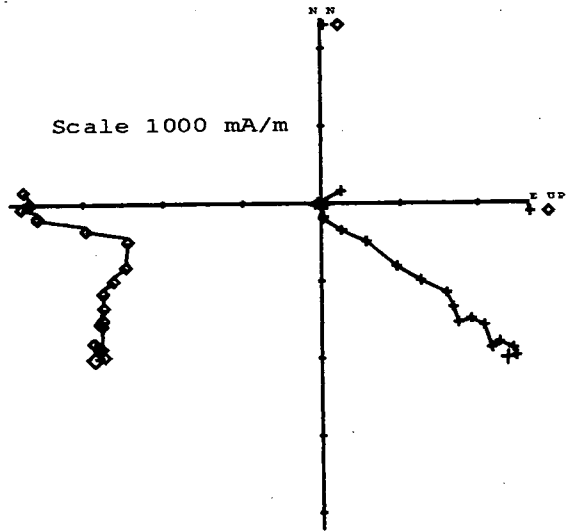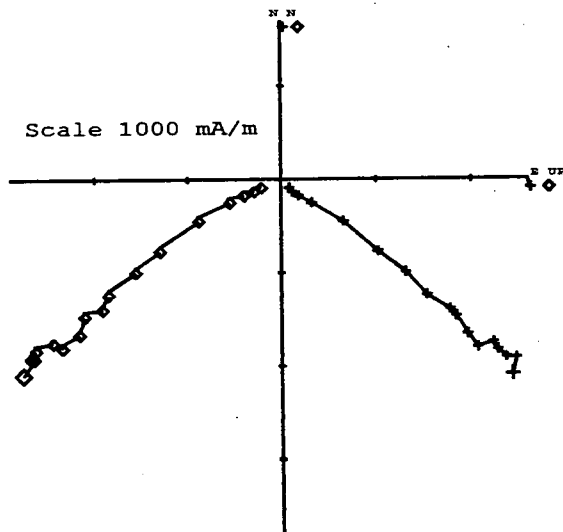
☐ Lower
▲ Upper

Core
Coordinates

Fig. 6.39 - Site V38: Zijderveld diagrams, Intensity and stereo plots.

MTT (C-D)		
V38.3b	**NRM**	**TRM**
steps	**(A/m)**	**(A/m)**
20	0.000	0.000
100	0.000	0.000
150	4.230	0.139
250	4.090	0.161
300	4.050	0.242
330	3.920	0.173
360	3.740	0.394
390	3.600	0.536
420	3.350	0.672
440	3.150	0.667
460	2.970	0.888
480	2.700	0.844
500	2.270	0.983
520	1.820	1.255
535	1.180	2.126
550	0.680	3.062
565	0.463	3.416
580	0.334	3.412
595	0.241	0.000

a)

MTT (C-D) - AD 1697 - Sample V38.3b
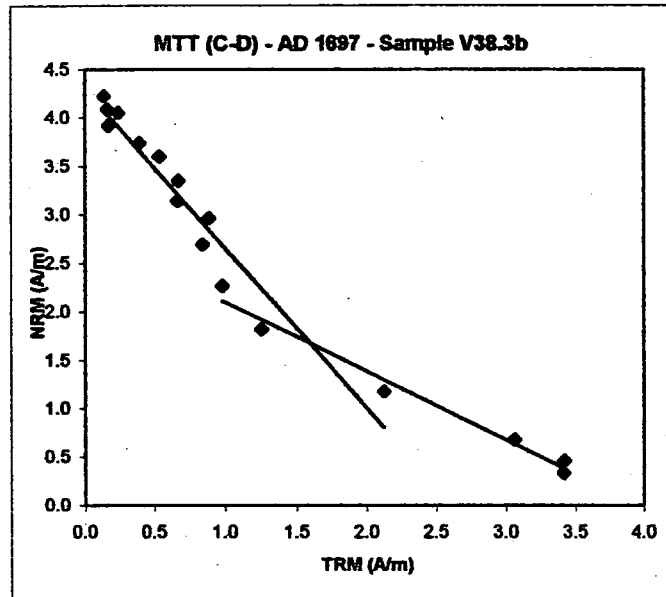
sample	Temp (°C)	N	f	g	q	b	R^2	Fpalaeo (μT)	σ_b
V38.3b	150-535	13	0.721	0.882	8.350	-1.703	0.937	85.136	0.130
	500-580	6	0.458	0.753	4.893	-0.721	0.980	36.050	0.051

NRM1 - sample V38.3b

TRM - Sample V38.3b

b)

c)
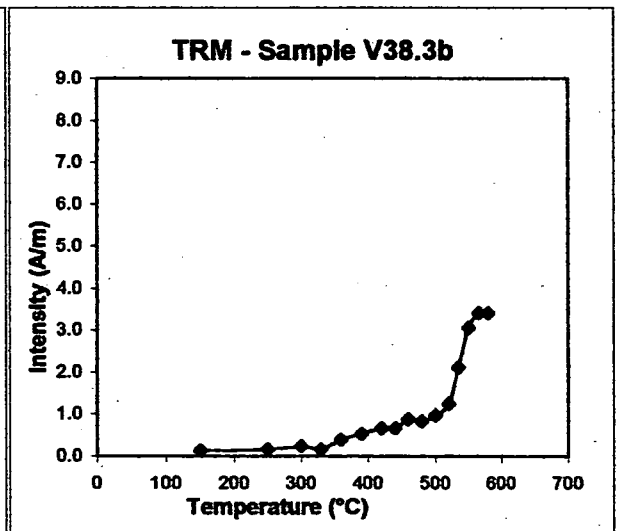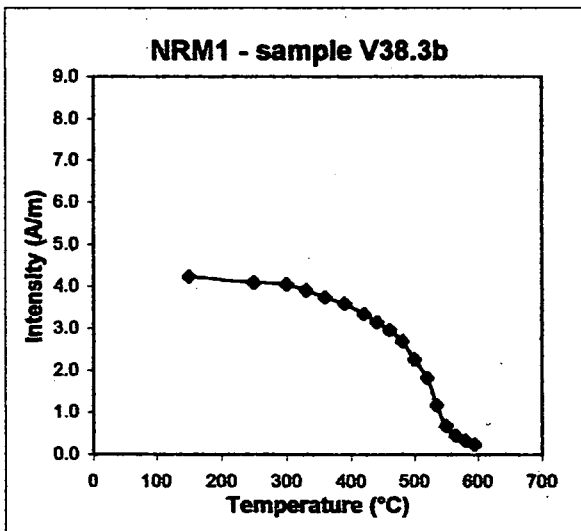
Fig. 6.40 - Site V38: a)NRM/TRM plot and respective values, b)NRM demagnetization and c)TRM acquisition curves.

Tab. 6.20 - Site V38: Palaeofields estimated and statistical parameters

A-Demag1

B-pTRM

Scale 1000 mA/m

Scale 1000 mA/m

Mmax = 6190 mA/m

Mmax = 5230 mA/m
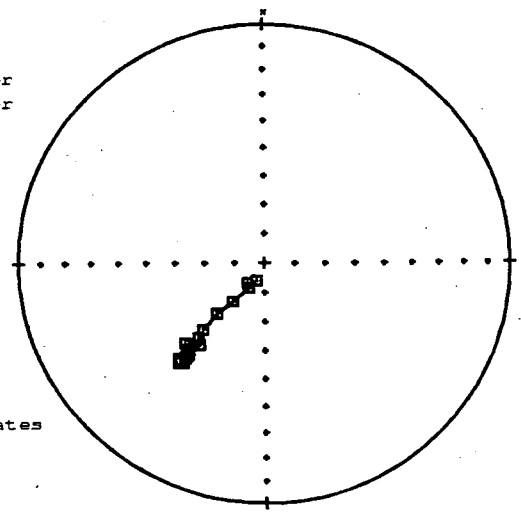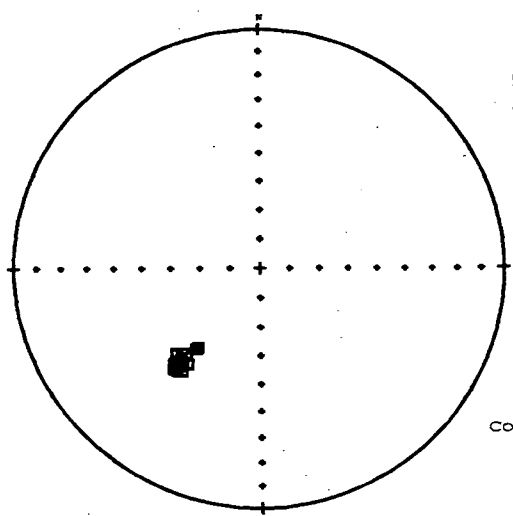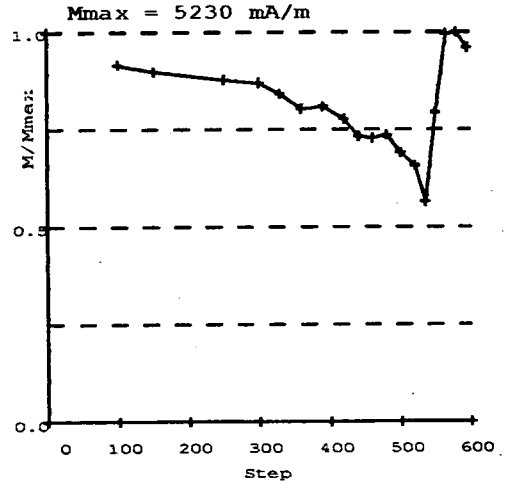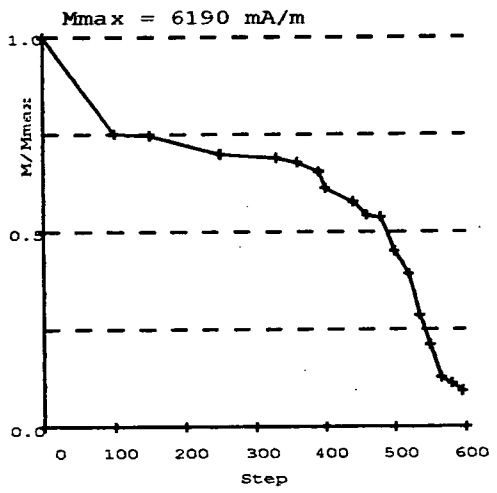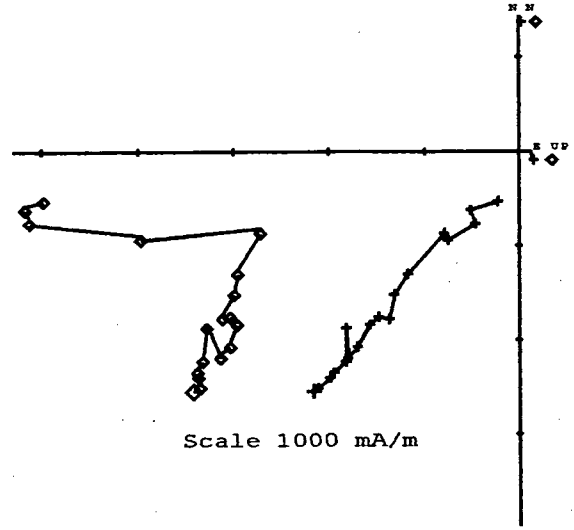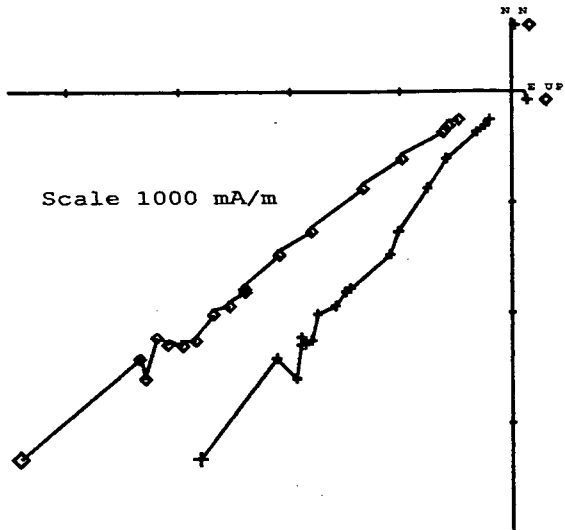
Fig. 6.41 - Site V39: Zijderveld diagrams, Intensity and stereo plots.

MTT (A-B)		
V39.7a steps	NRM (A/m)	TRM (A/m)
20	6.190	0.000
100	4.650	0.000
150	4.620	0.199
250	4.330	0.267
300	4.300	0.272
330	4.270	0.237
360	4.230	0.530
390	4.050	0.296
420	3.790	0.354
440	3.570	0.430
460	3.360	0.630
480	3.330	0.713
500	2.790	0.923
520	2.430	1.158
535	1.770	1.382
550	1.300	3.014
565	0.783	4.533
580	0.690	4.626
595	0.575	4.515

a)

MTT (B-A) - AD1754 - Sample V39.7a

sample	T range (°)	N	f	g	q	b	R^2	Fpalaeo (μT)	σ_b
V39.7a	*250-535	11	0.414	0.837	6.346	-2.106	0.973	105.310	0.115
	535-595	5	0.193	0.643	1.233	-0.354	0.970	17.687	0.036

* excluding 360

NRM - Sample V39.7a

TRM - Sample V39.7a
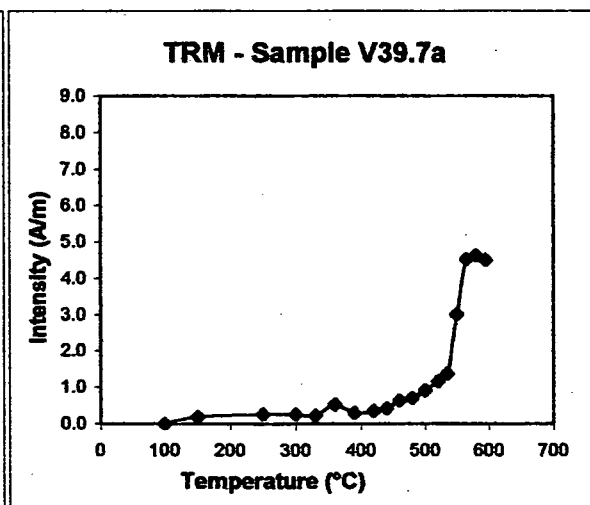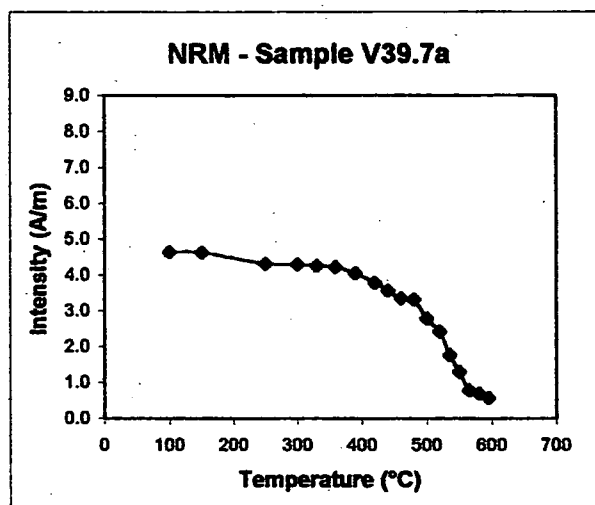
b)   c)

Fig. 6.42 - Site V39: a)NRM/TRM plot and respective values, b)NRM demagnetization and c)TRM acquisition curves.

Tab. 6.21 - Site V39: Palaeofields estimated and statistical parameters

AD 1754 sample V39.7a

C-Demag2

Scale 500 mA/m

D-pTRMck

Scale 1000 mA/m

Mmax = 4590 mA/m

Mmax = 5010 mA/m
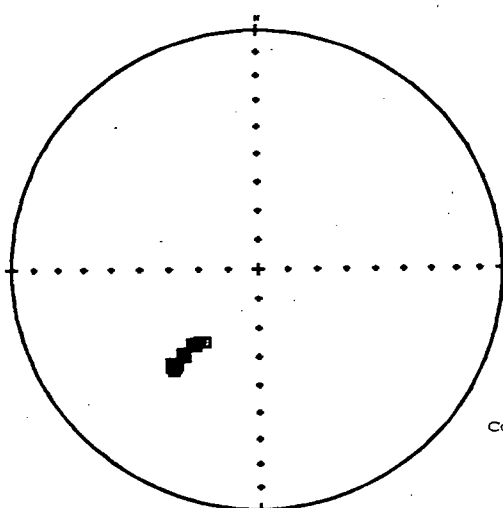
B Lower
▲ Upper

Core
Coordinates

Fig. 6.43 - Site V39: Zijderveld diagrams, Intensity and stereo plots.

MTT (C-D)		
V39.7a	NRM	TRM
steps	(A/m)	(A/m)
20	0.000	0.000
100	0.000	0.000
150	4.590	0.173
250	4.460	0.111
300	4.430	0.215
330	4.410	0.176
360	4.160	0.232
390	3.960	0.241
420	3.760	0.281
440	3.550	0.530
460	3.320	0.511
480	3.150	0.633
500	2.800	0.475
520	2.400	0.806
535	1.980	1.257
550	1.400	3.102
565	0.847	4.264
580	0.669	4.107
595	0.554	0.000

a)

MTT (C-D) - AD 1754 - Sample V39.7a
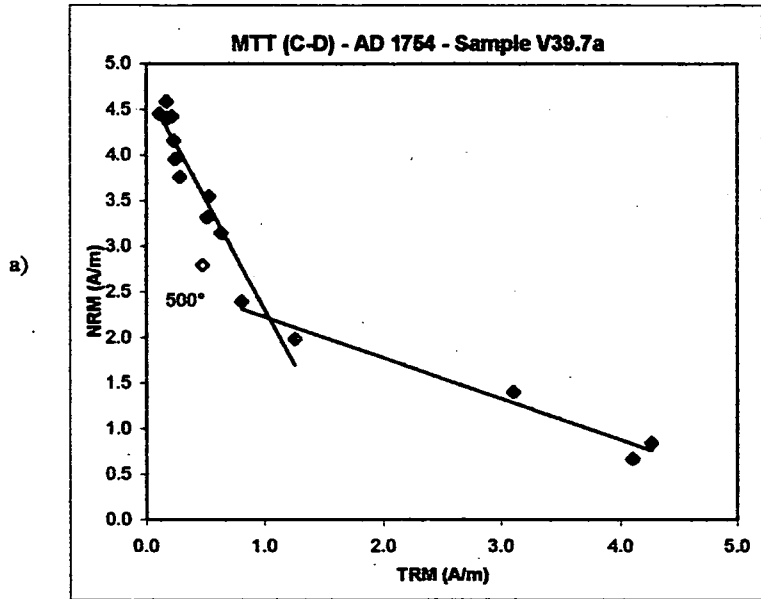
sample	Temp (°C)	N	f	g	q	b	R²	Fpalaeo (µT)	σ_b
V39.7a	*150-535	12	0.617	0.875	6.356	-2.923	0.932	146.139	0.248
	520-580	5	0.409	0.716	2.765	-0.459	0.967	22.939	0.049

* excluding 500

NRM - sample V39.7a

b)

TRM - Sample V39.7a
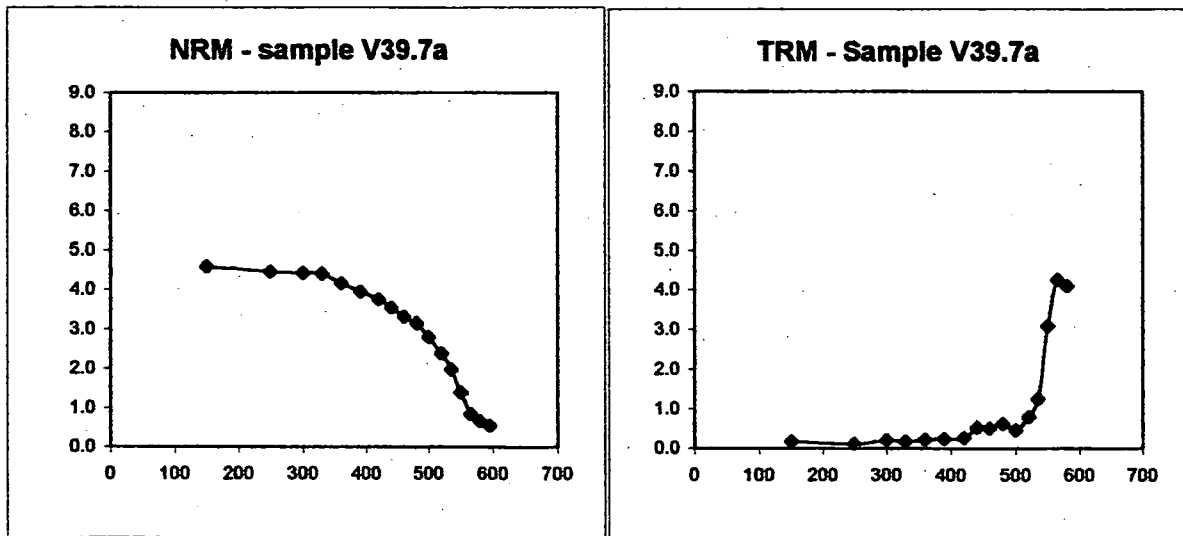
c)

Fig. 6.44 - Site V39: a)NRM/TRM plot and respective values, b)NRM demagnetization and c)TRM acquisition curves.

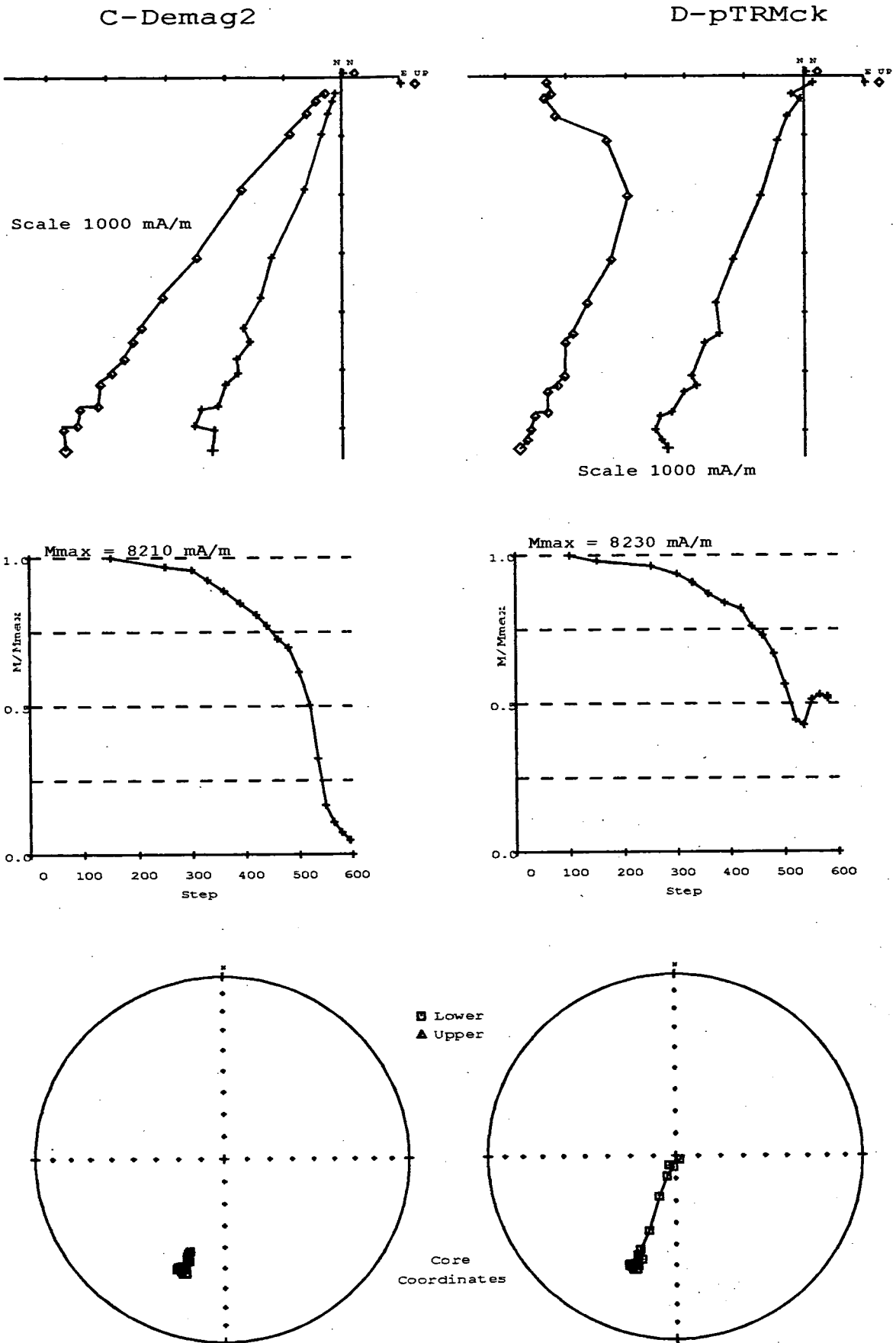**Tab. 6.22** - Site V39: Palaeofields estimated and statistical parameters

AD 1754 sample V40.12a

A-Demag1

Scale 500 mA/m

B-pTRM

Scale 1000 mA/m

Mmax = 4930 mA/m

Mmax = 3820 mA/m
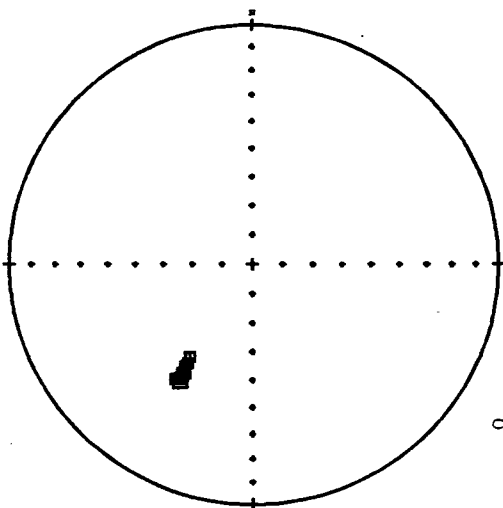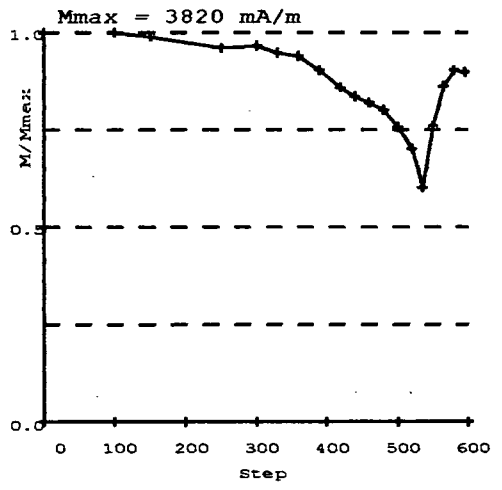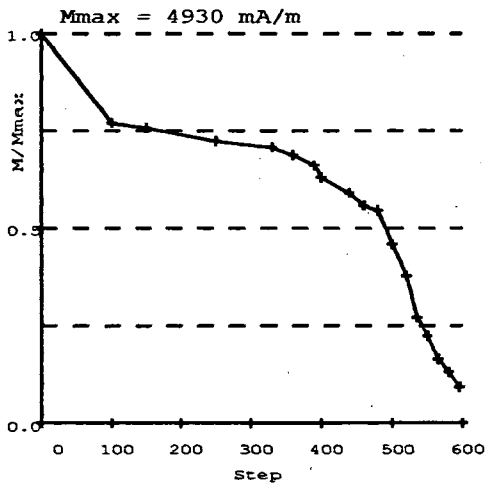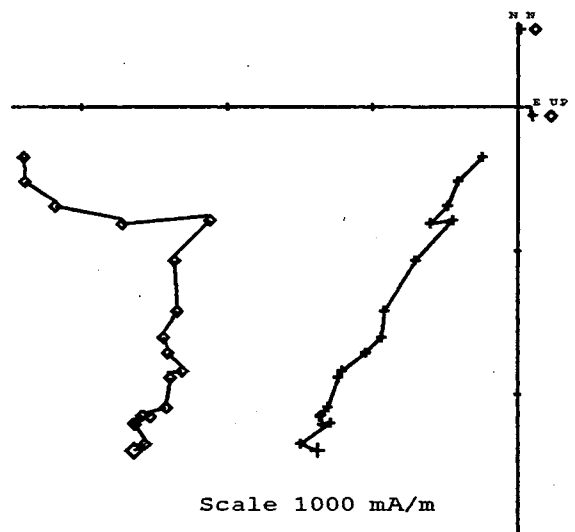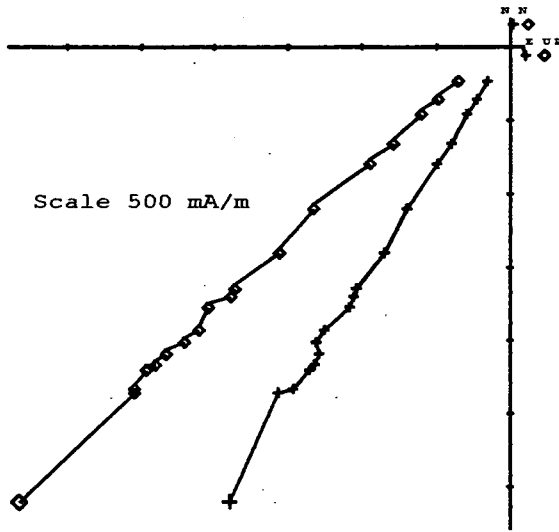
☐ Lower
▲ Upper

Core
Coordinates
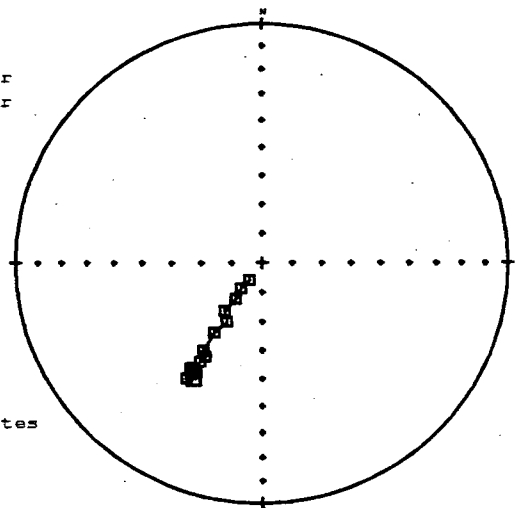
Fig. 6.45 - Site V40: Zijderveld diagrams, Intensity and stereo plots.

MTT (A-B)		
V40.12a	NRM	TRM
steps	(A/m)	(A/m)
20	4.930	0.000
100	3.800	0.000
150	3.740	0.045
250	3.570	0.184
300	3.530	0.193
330	3.490	0.186
360	3.390	0.222
390	3.260	0.233
420	3.110	0.295
440	2.910	0.308
460	2.750	0.527
480	2.690	0.592
500	2.260	0.794
520	1.860	1.037
535	1.330	1.174
550	1.100	1.946
565	0.812	2.596
580	0.645	2.912
595	0.452	3.049

a)

MTT (A-B) - AD 1754 - Sample V40.12a
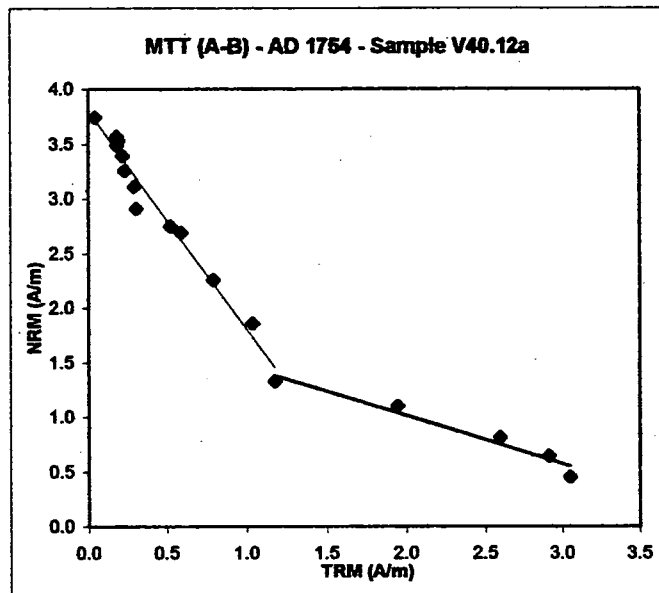
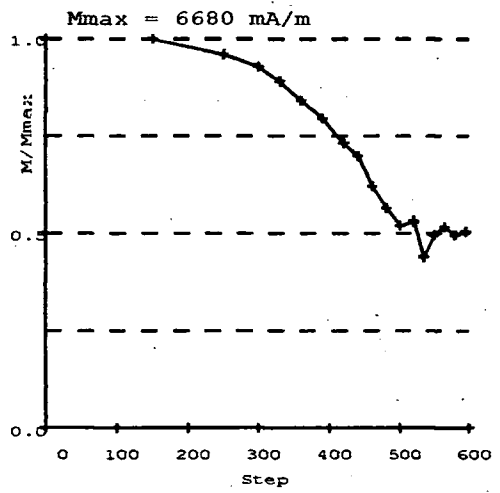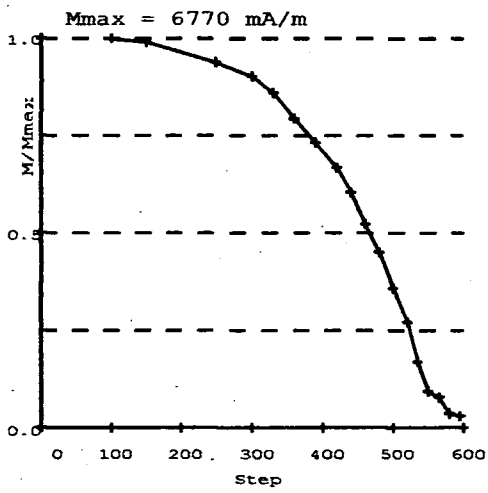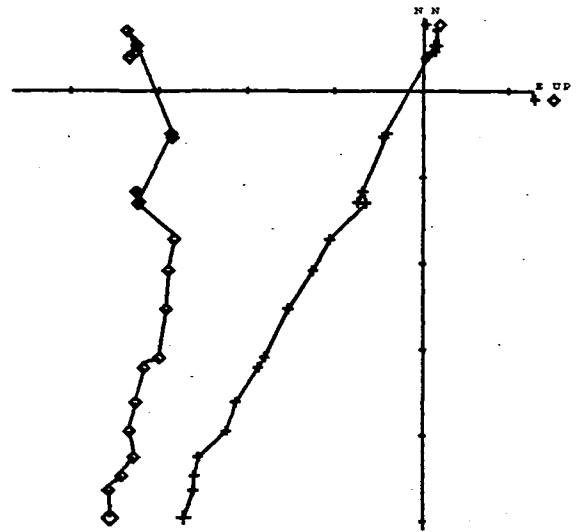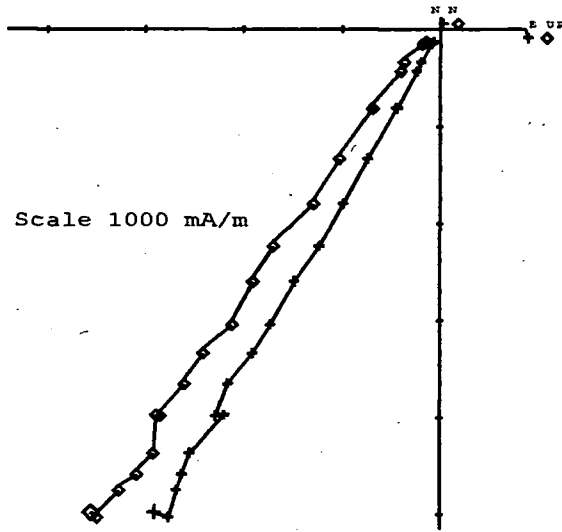| sample	Temp (°C)	N	f	g	q	b	R^2	Fpalaeo (μT)	σ_b
V40.12a	150-535	13	0.489	0.866	8.546	-2.037	0.973	101.838	0.101
	535-595	5	0.178	0.739	1.102	-0.452	0.958	22.614	0.054

NRM - Sample V40.12a

b)

TRM - Sample V40.12a
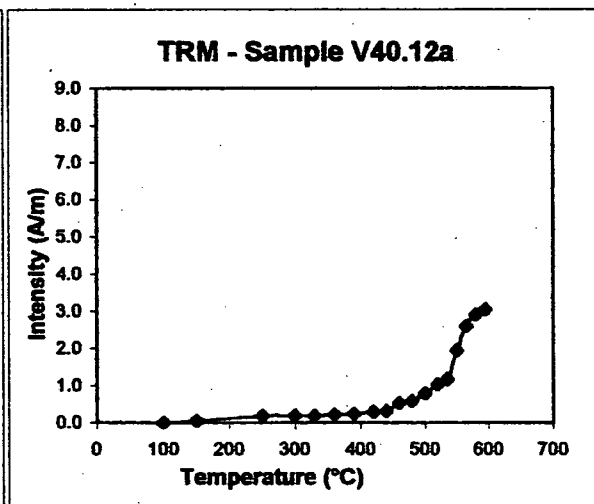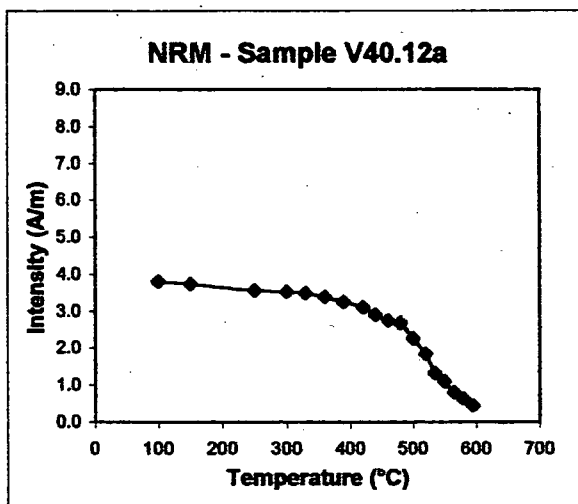
c)

Fig. 6.46- Site V40 a)NRM/TRM plot and respective values, b)NRM demagnetization and c)TRM acquisition curves.

Tab. 6.23 - Site V40: Palaeofields estimated and statistical parameters

217

AD 1754 sample V40.12a

C-Demag2

Scale 500 mA/m

D-pTRMck

Scale 500 mA/m

Mmax = 3730 mA/m

Mmax = 3800 mA/m
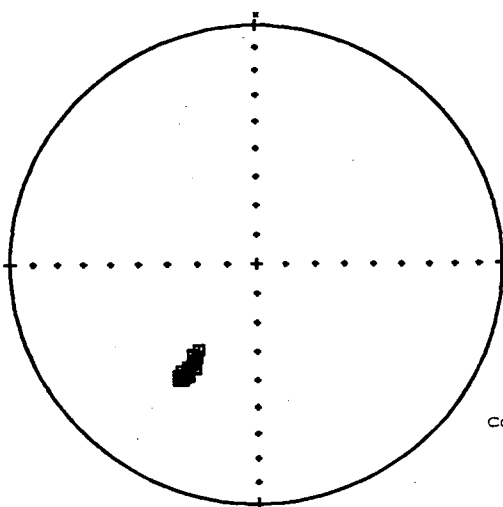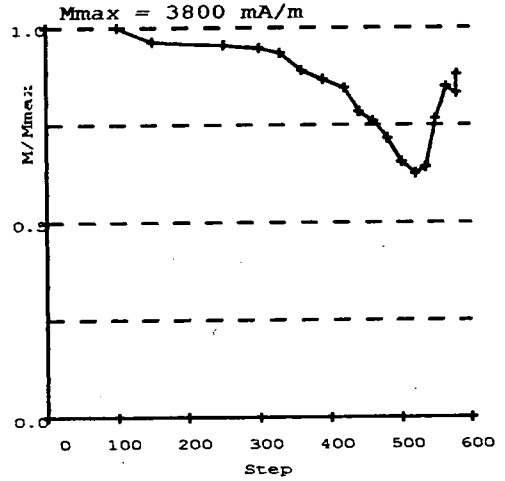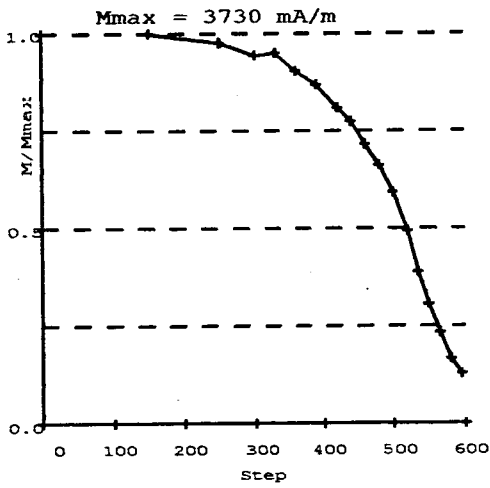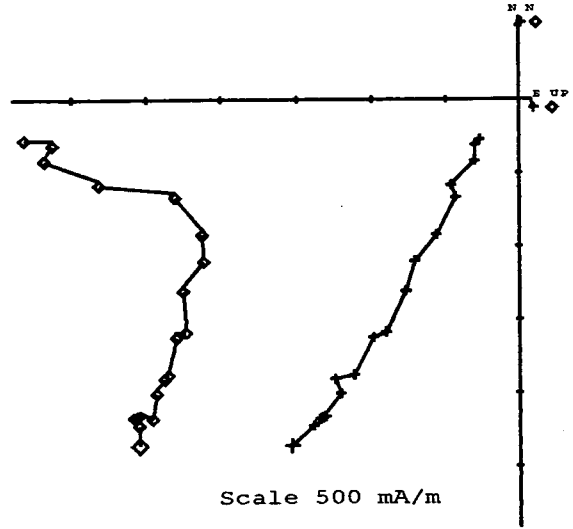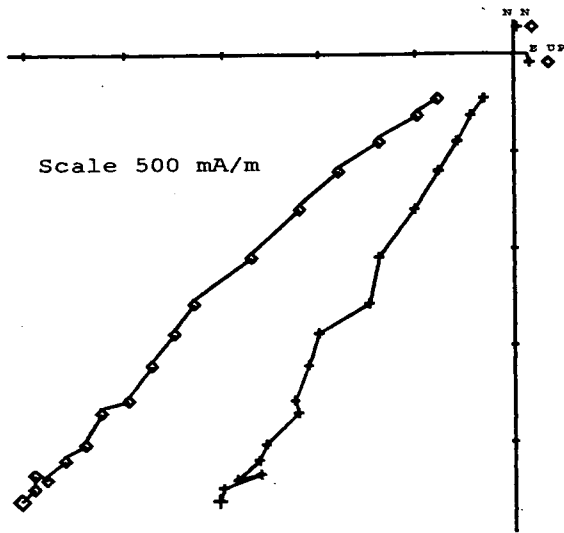
🔳 Lower
▲ Upper
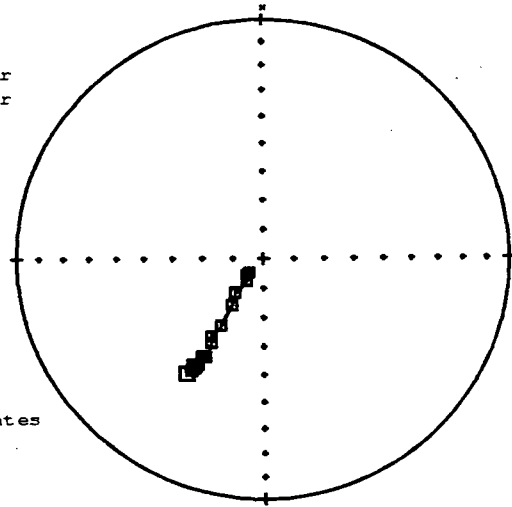
Core
Coordinates

Fig. 6.47 - Site V40: Zijderveld diagrams, Intensity and stereo plots.

MTT (C-D)		
V40.12a	NRM	TRM
steps	(A/m)	(A/m)
20	0.000	0.000
100	0.000	0.000
150	3.730	0.156
250	3.640	0.232
300	3.520	0.109
330	3.540	0.111
360	3.370	0.197
390	3.240	0.215
420	3.020	0.238
440	2.890	0.383
460	2.670	0.402
480	2.470	0.573
500	2.210	0.507
520	1.840	0.793
535	1.450	1.218
550	1.140	1.924
565	0.869	2.497
580	0.622	2.831
595	0.475	0.000

a)
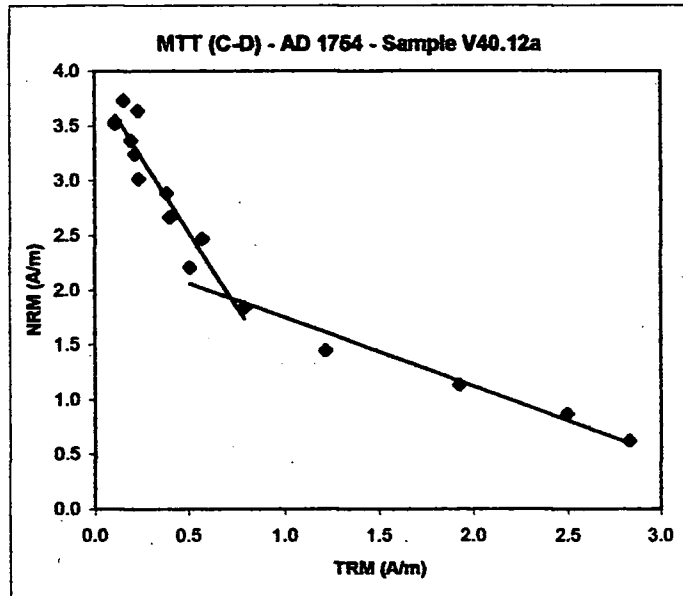
sample	Temp (°C)	N	f	g	q	b	R²	Fpalaeo (µT)	σ_b
V40.12a	150-520	12	0.507	0.880	4.371	-2.888	0.898	144.402	0.295
	500-580	6	0.426	0.794	3.827	-0.638	0.969	31.897	0.056
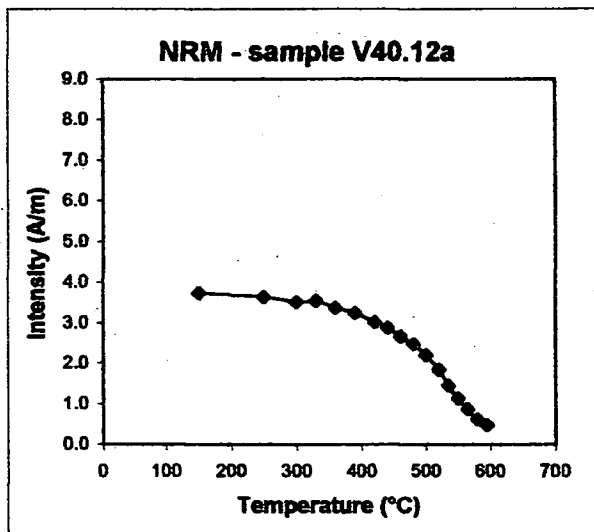
b)
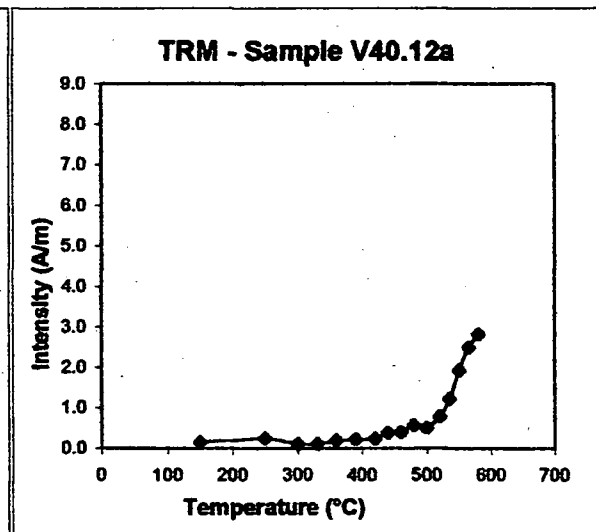
c)

Fig. 6.48 - Site V40: a)NRM/TRM plot and respective values, b)NRM demagnetization and c)TRM acquisition curves.

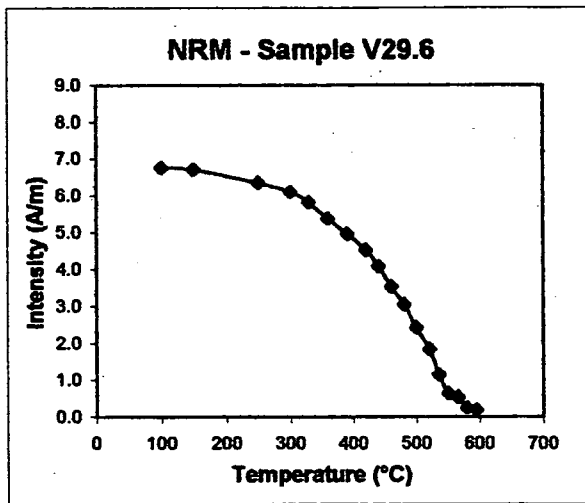Tab. 6.24 - Site V40: Palaeofields estimated and statistical parameters

219

AD 1754 sample V41.7b

A-Demag1

Scale 2000 mA/m

Mmax = 9100 mA/m

B-pTRM

Scale 2000 mA/m

Mmax = 7070 mA/m
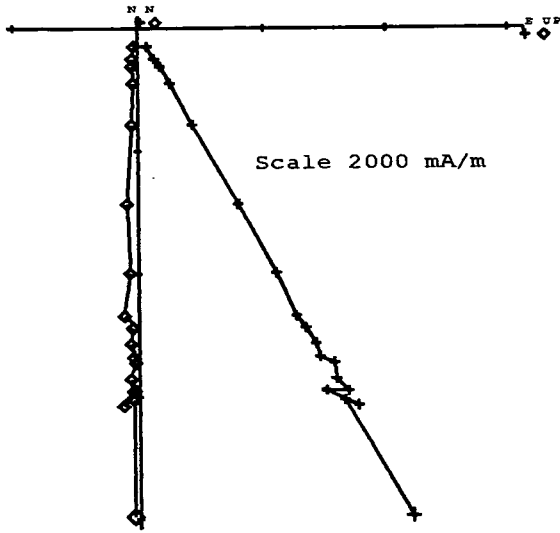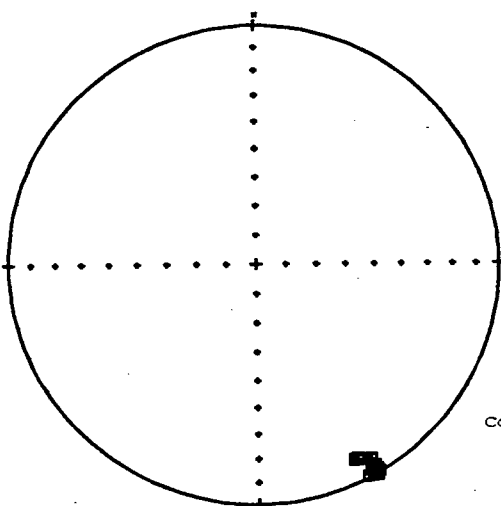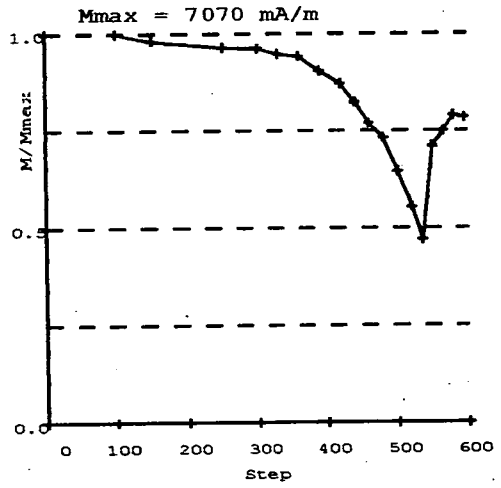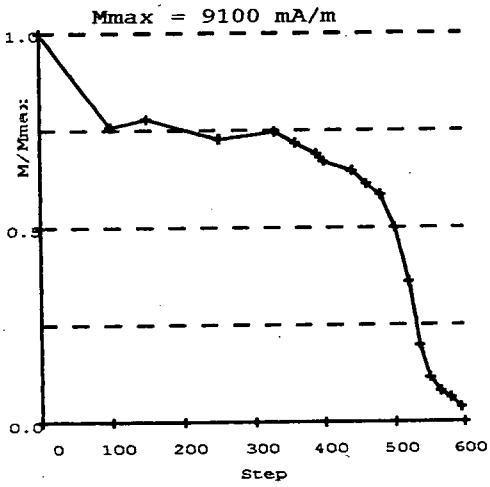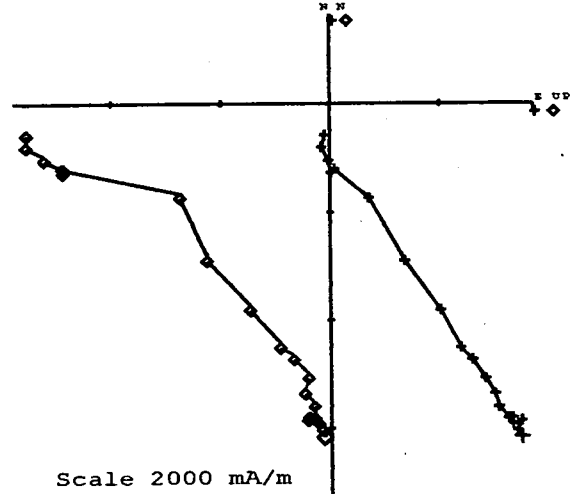
☒ Lower
▲ Upper
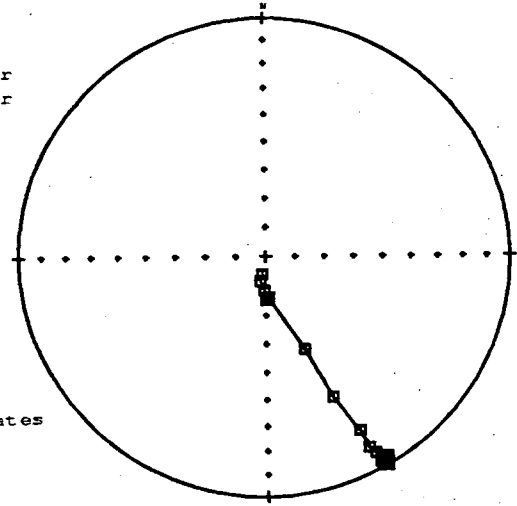
Core
Coordinates

Fig. 6.49 - Site V41: Zijderveld diagrams, Intensity and stereo plots.

MTT (A-B)		
V41.7b	NRM	TRM
steps	(A/m)	(A/m)
20	9.100	0.000
100	7.090	0.000
150	6.900	0.131
250	6.800	0.365
300	6.620	0.367
330	6.590	0.417
360	6.530	0.221
390	6.280	0.316
420	6.100	0.410
440	5.880	0.309
460	5.570	0.624
480	5.320	0.756
500	4.550	1.379
520	3.280	2.098
535	1.800	2.655
550	1.040	4.831
565	0.720	5.141
580	0.571	5.460
595	0.342	5.462

a)
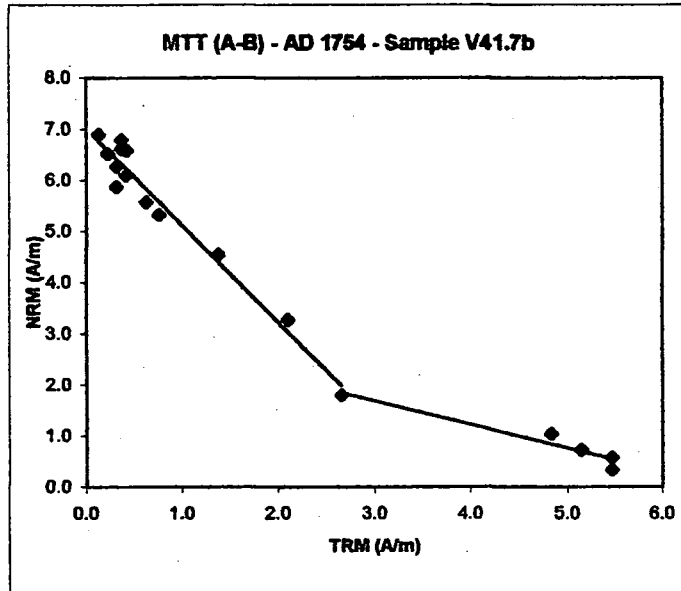
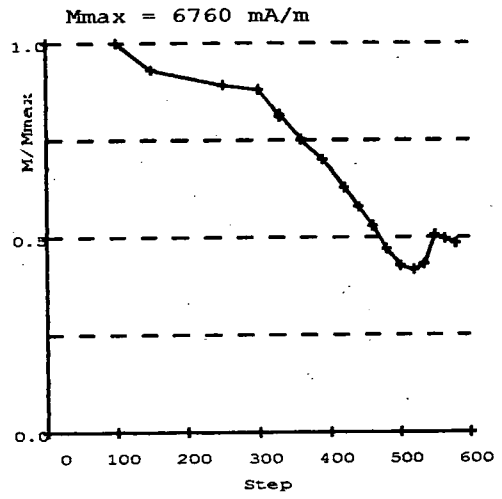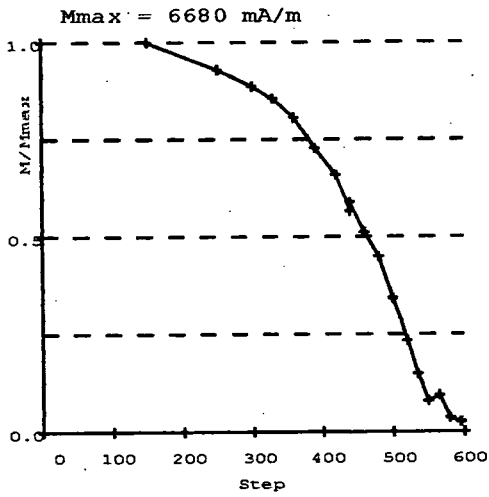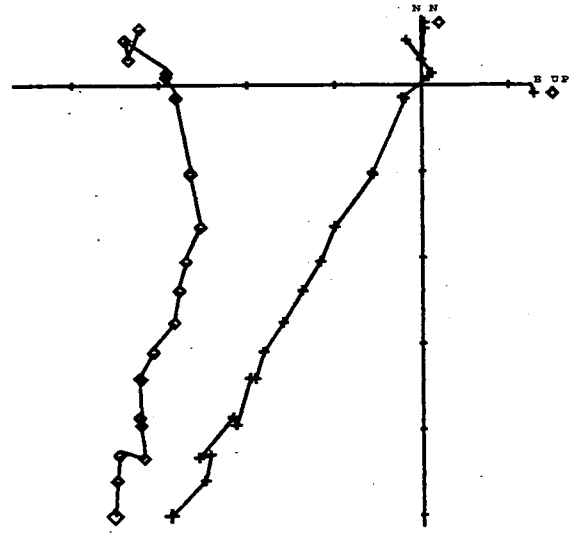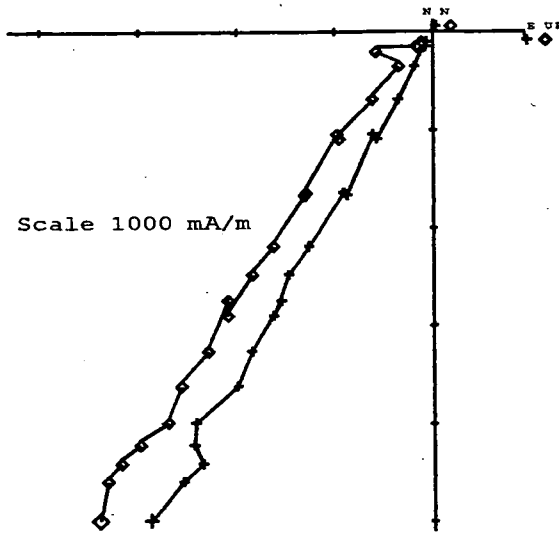| sample	Temp (°C)	N	f	g	q	b	R^2	Fpalaeo (μT)	σ_b
V41.7b	150-535	13	0.560	0.818	7.731	-1.935	0.962	96.761	0.115
	535-595	5	0.160	0.645	0.686	-0.480	0.933	24.024	0.072

b)

c)
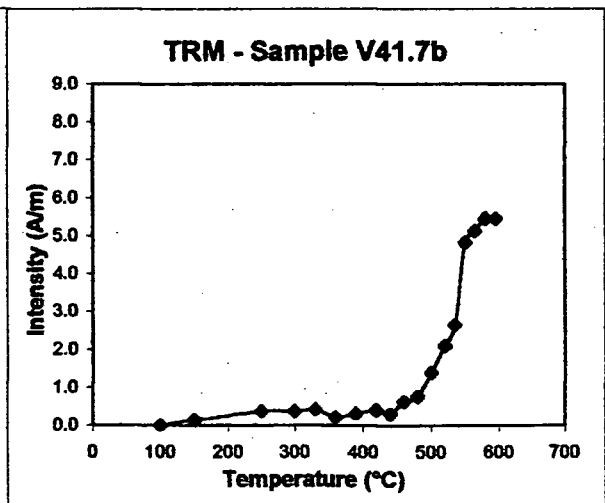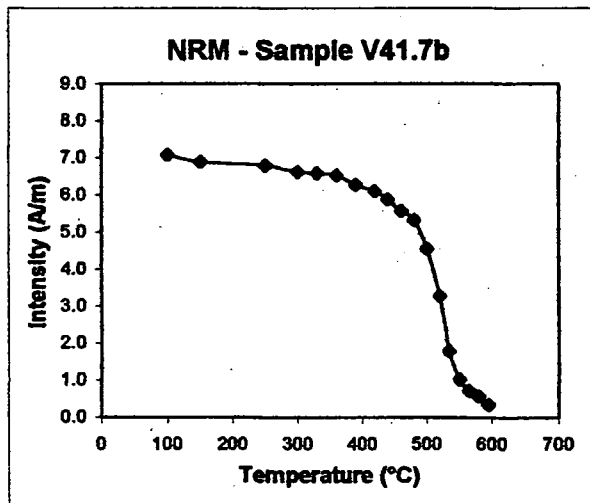
Fig. 6.50 - Site V41: a)NRM/TRM plot and respective values, b)NRM demagnetization and c)TRM acquisition curves.

**Tab. 6.25** - Site V41: Palaeofields estimated and statistical parameters

221

AD 1754 sample V41.7b

C-Demag2

Scale 1000 mA/m

D-pTRMck

Scale 2000 mA/m

Mmax = 6980 mA/m

Mmax = 6850 mA/m
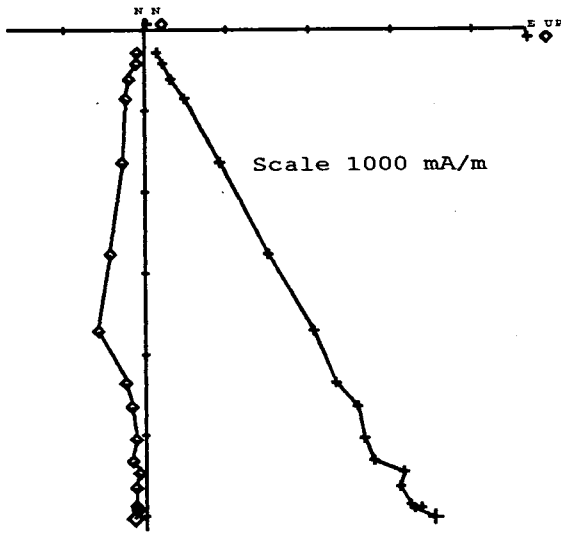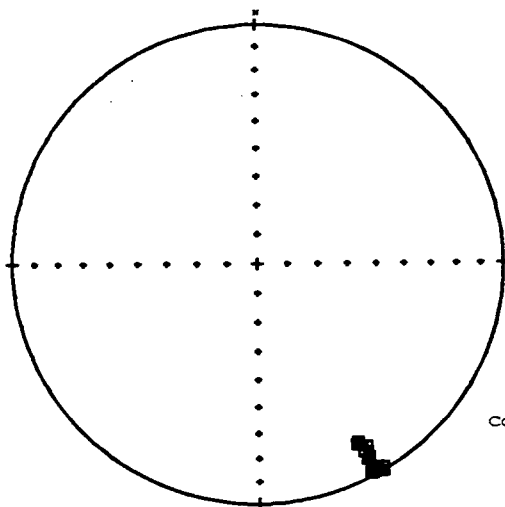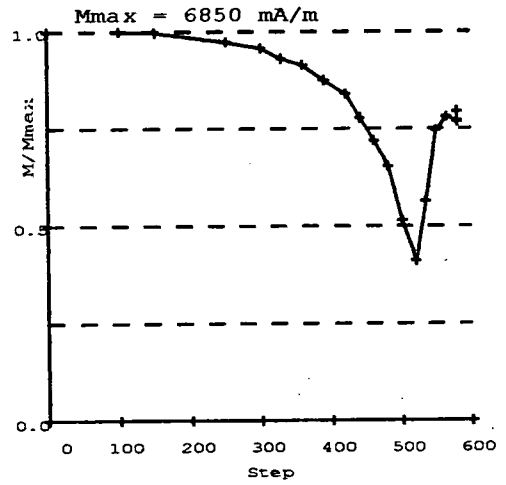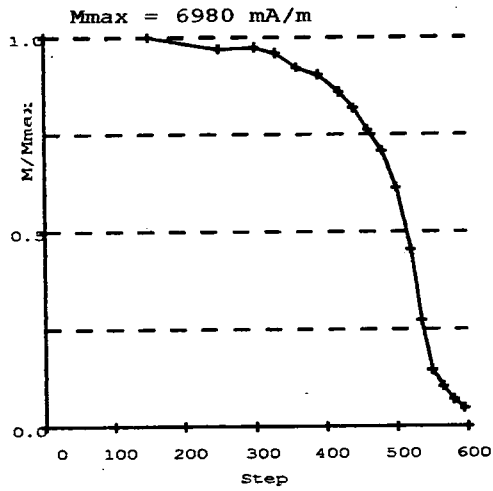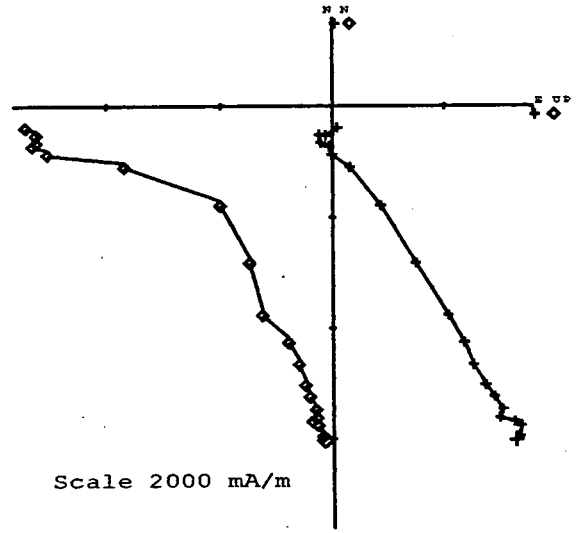
☐ Lower
▲ Upper
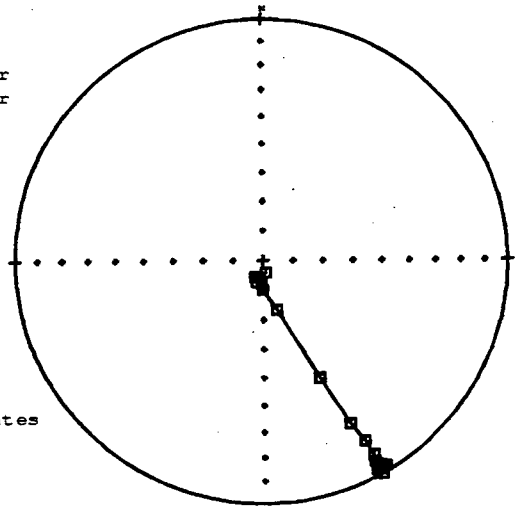
Core
Coordinates

Fig. 6.51 - Site V41: Zijderveld diagrams, Intensity and stereo plots.

MTT (C-D)		
V41.7b	NRM	TRM
steps	(A/m)	(A/m)
20	0.000	0.000
100	0.000	0.000
150	6.980	0.208
250	6.770	0.255
300	6.800	0.360
330	6.700	0.383
360	6.440	0.268
390	6.310	0.476
420	6.000	0.445
440	5.710	0.643
460	5.320	0.772
480	4.940	1.208
500	4.280	1.402
520	3.170	1.972
535	1.900	3.510
550	1.010	4.833
565	0.718	5.121
580	0.483	5.331
595	0.327	0.000

a)
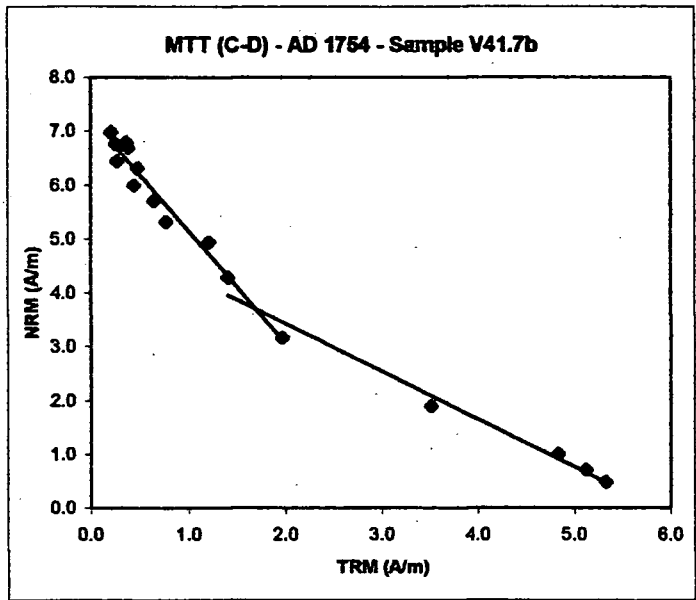
sample	Temp (°C)	N	f	g	q	b	R^2	Fpalaeo (μT)	σ_b
V41.7b	150-520	12	0.546	0.843	7.648	-2.125	0.964	106.242	0.128
	500-580	6	0.544	0.738	5.635	-0.897	0.980	44.830	0.064
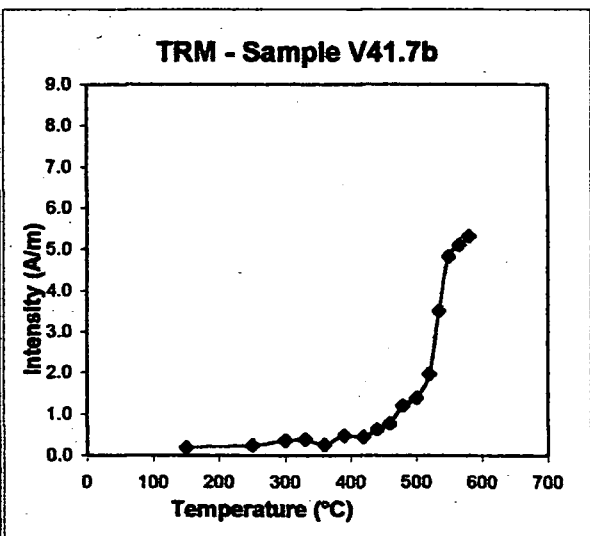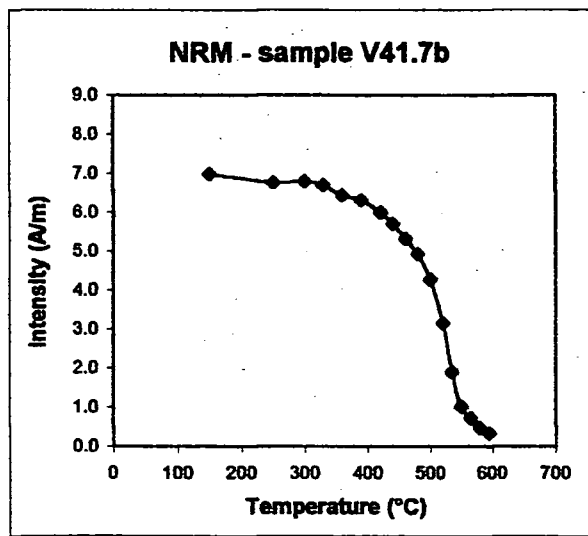
b)

c)

Fig. 6.52 - Site V41: a)NRM/TRM plot and respective values, b)NRM demagnetization and c)TRM acquisition curves.

Tab. 6.26 - Site V41: Palaeofields estimated and statistical parameters

6.6 - AD 1760

6.6.1 - Site V32

A-Demag1

Intensity Behaviour - Initial NRM of sample 9B was 4080 mA/m (Fig. 6.53) and, by 595°C, had been demagnetized almost completely. It showed an accelerating decrease in intensity with increasing temperature starting from 330°C. A small increase occurred at 565°C (about 200 mA/m).

Directional Behaviour - Both vertical and horizontal components moved towards the origin with a very linear trend especially above 390°C. The vertical component showed a single downward marked excursion at 565°, followed by the previous trend. The Inc moved toward 90° above 565°C (Fig. 6.53).

B-pTRM

Intensity Behaviour - This showed a smooth decreasing trend from 3990 (20°) to 2080 mA/m (535°C) that was quite similar to Demag1. From 535 to 595°C the intensity showed alternating significant increases (about 1000 mA/m between 535 and 565°C) and decreases. Finally the intensity was 3170 mA/m (Fig. 6.53).

Directional Behaviour - The horizontal component moved toward the origin with a linear trend, but it showed an unclear direction above 565°C. The vertical component moved northwards, gradually away from the NRM direction, until 565° when it started to move toward down. The Inc behaved as usual (Fig. 6.53).

Palaeointensity results from A-B - The NRM/TRM plot showed a linear trend until 520°C when points started to behave almost randomly (Fig. 6.54a). One value of the palaeofield were estimated (Tab. 6.27) and all the anomalous points above 520°C were not considered (Fig. 54b,c).

C-Demag2

Intensity & Directional Behaviours - This second demagnetization showed the same behaviours as in Demag1, but the spike at 565°C had a more significant downward direction, as shown by the vertical component and the Inc on the stereo plot (Fig. 6.55).

D-pTRMck

Intensity Behaviour - From 3930 (20°) to 2200 mA/m (520°C) the decreasing trend was very similar to Demag1. From 520 to 550°C the intensity showed an increase (about 1000 mA/m) followed by a small decrease until 595°C. At the end the intensity was 3000 mA/m (Fig. 6.55).

Directional Behaviour- The horizontal component moved toward the origin with a linear trend, while the vertical one moved, as usual, gradually away from the NRM direction, until 520°. After this, it moved clearly downwards until 550°C and then northwards again until the end (Fig. 6.55).

Palaeointensity results from C-D - The NRM/TRM plot showed a concave curve (Fig. 6.56a) and two slopes were defined (Tab. 6.28).

6.6.2 - Site V34

A-Demag1

Intensity Behaviour - Sample 12A had an initial NRM of 2210 mA/m and, by 595°C, was demagnetized almost completely. The intensity decreased almost linearly but showing three different slopes; between 20 and 330°C, 360 and 440°C, and from 460 to 520°C. At 565° a significant increase in intensity occurred (Fig. 6.57).

Directional Behaviour - Both the horizontal and vertical components showed an almost linear trend until 330°C followed by a curving trend until 520°C. A significant

irregularity occurred at 565°C when the vertical vector moved toward a downward direction (Fig. 6.57).

B-pTRM

Intensity Behaviour - It showed a constant intensity (about 2000mA/m) between 150 and 420°C followed by an hyperbolic increase until the end (595°C) when the intensity was 5090 mA/m. Two small but clear decreases were present at 535 and 580°C (Fig. 6.57).

Directional Behaviour - The horizontal component moved clearly toward the origin especially below 520°C. After, it showed a very unclear trend. The vertical component moved rapidly away from the NRM direction toward down. The stereo plot showed the usual gradual movement of the Inc toward 90° (Fig. 6.57).

Palaeointensity results from A-B - Some points above 520°C which appeared irregular in all the curves (Fig. 6.58a,b,c) were not considered. Two different value of the palaeofield were obtained (Tab. 6.29).

C-Demag2

Intensity Behaviour - At 150°C, the NRM was 1940 mA/m and, by 595°C, was demagnetized completely. The intensity decay was similar to Demag1 with the same small breaks at 360 and 440°C. A significant increase at 565° was also present (Fig. 6.59).

Directional Behaviour - This showed the same behaviour as in Demag1 although it was much more indistinct. The stereo plot showed the usual behaviour of both Inc and Dec below 535°C, but above this temperature they behaved randomly (Fig. 6.59).

D-pTRMck

Intensity & Directional Behaviours - The initial NRM (100°C) was 2000 mA/m and, at the end of the process, it was 5260 mA/m. Both behaviours were very similar to pTRM (Fig. 6.59).

Palaeointensity results from C-D - As in MTT A-B two slopes were showed by the NRM/TRM plot (Fig. 6.60a) excluding the irregular point at 550°C (Tab. 6.30).

6.6.3 - Site V35

A-Demag1

Intensity Behaviour - Initial NRM for sample 7A was 3610 mA/m (Fig. 6.61). It showed the usual accelerating decrease in intensity starting from 150°C and terminated at 595°C, with some 11% still remaining. A marked spike occurred at 565°C when the intensity increased by about 400 mA/m.

Directional Behaviour - Both vertical and horizontal components moved towards the origin with a very linear trend. The vertical one showed a single downward marked excursion at 565° as, also underlined by the Inc behaviour on the stereo plot (Fig. 6.61).

B-pTRM

Intensity Behaviour - The decreasing trend, from 3530 to 1970 mA/m (535°C), was almost similar to Demag1, except for a minor difference in deceleration rate. Between 535 and 595°C the intensity showed alternated significant increases (about 1500 mA/m) and decreases. Finally it was 3660 mA/m (Fig. 6.61).

Directional Behaviour - The horizontal component moved toward the origin with a linear trend below 550°C, but above 580°C it moved clearly northwards. The vertical component moved gradually away from the NRM direction until 520°. After it showed a

227

zigzag behaviour with marked downward spikes. The same behaviour was underlined by the stereo plot (Fig. 6.61).

Palaeointensity results from A-B - In the NRM/TRM plot some clear irregular points above 500°C, which also appeared in both NRM and TRM curves, were excluded (Fig. 6.62a,b,c). Two different estimates of the palaeofield were considered (Tab. 6.31).

C-Demag2

Intensity & Directional Behaviour - In this second demagnetization the behaviours were exactly the same as in Demag1, but the increase in intensity and the spike showed by the vertical component, at 535°C, were very marked (Fig. 6.63).

D-pTRMck

Intensity Behaviour - The initial intensity was 3540 mA/m (100°C) and decreased as in pTRM until 520°C. From 520 to 550°C the intensity showed a marked increase (about 2000 mA/m) followed by a small decrease until 595°C. The final intensity was 3600 mA/m (Fig. 6.63).

Directional Behaviour - The horizontal component was very similar to that one showed in pTRM. The vertical one showed a downward deflection between 520 and 550°C followed by a northward movement at 565°C (Fig. 6.63).

Palaeointensity results from C-D - As in MTT A-B, two slopes were defined (Fig. 6.64a), but the value at 565° , which was clearly irregular on both the NRM and TRM curves, was excluded (Tab. 6.32).

AD 1760 sample V32.10

A-Demag1

Scale 500 mA/m

B-pTRM

Scale 500 mA/m

Mmax = 4080 mA/m

Mmax = 3990 mA/m
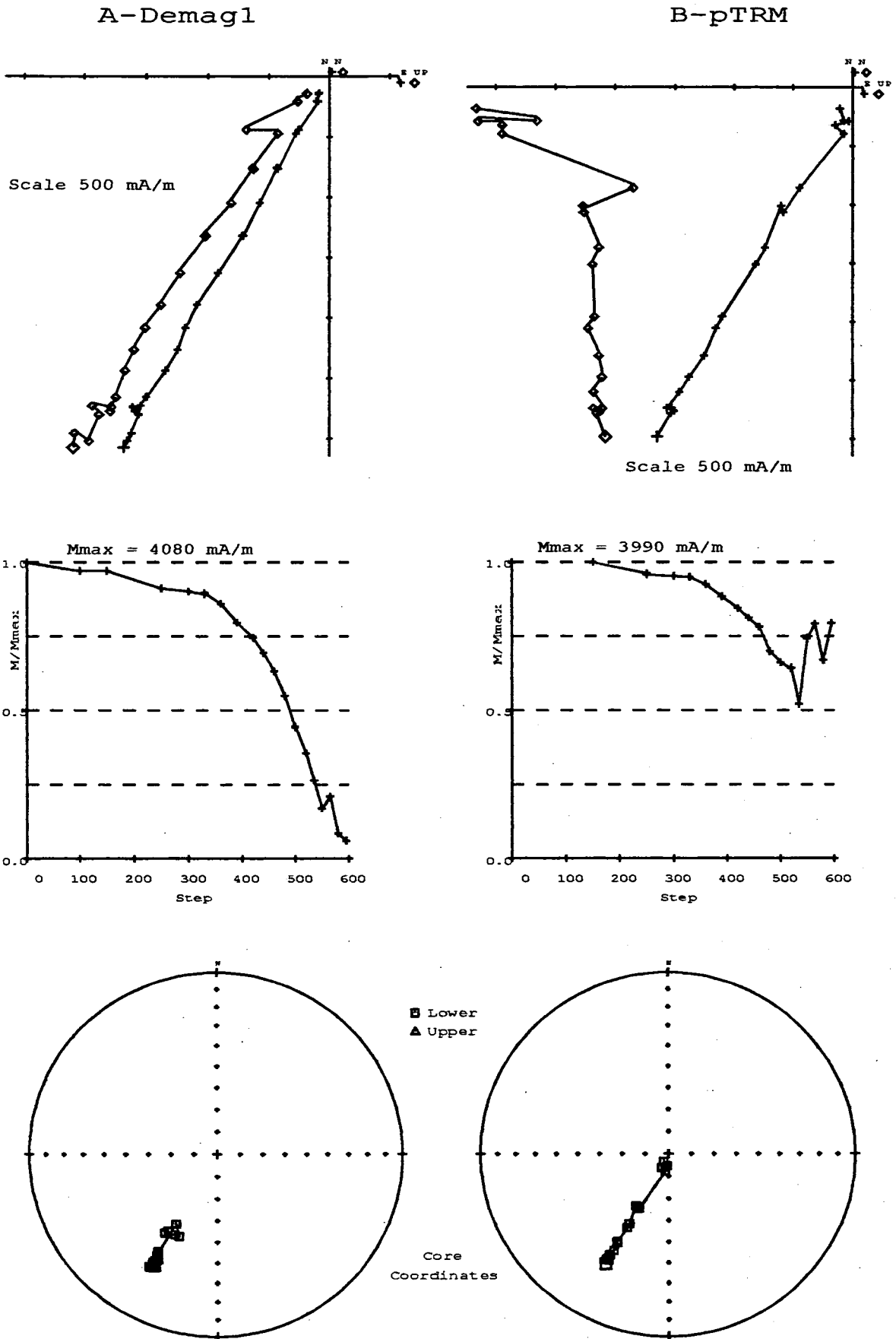
Fig. 6.53 - Site V32: Zijderveld diagrams, Intensity and stereo plots.

B Lower
A Upper

Core
Coordinates

MTT (A-B)		
V32.10	NRM	TRM
steps	(A/m)	(A/m)
20	4.080	0.000
100	3.970	0.000
150	3.960	0.124
250	3.720	0.275
300	3.680	0.198
330	3.660	0.321
360	3.510	0.441
390	3.250	0.439
420	3.040	0.537
440	2.830	0.719
460	2.580	0.794
480	2.240	0.976
500	1.810	1.119
520	1.450	1.451
535	1.080	1.215
550	0.694	2.526
565	0.854	2.474
580	0.348	2.393
595	0.246	2.979

a)

MTT (A-B) - AD1760 - Sample V32.10
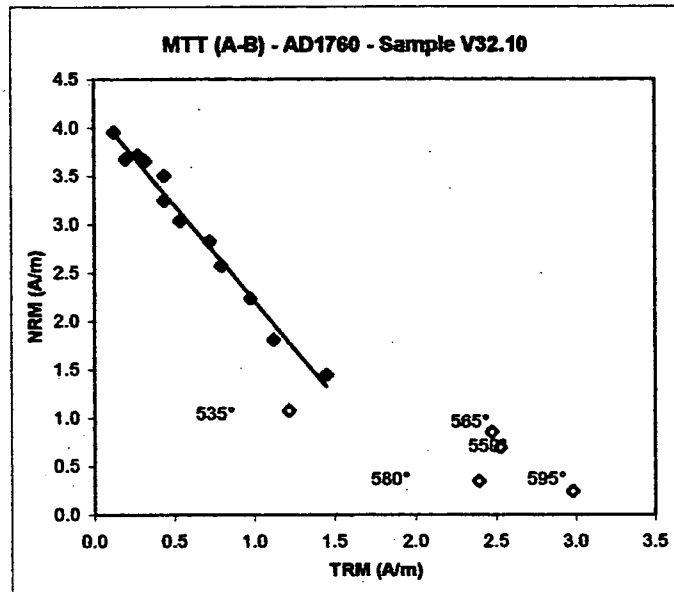
sample	T range (°)	N	f	g	q	b	R^2	Fpalaeo (μT)	σ_b
V32.10	150-520	12	0.615	0.884	12.786	-2.002	0.982	100.106	0.085

NRM - Sample V32.10

b)

TRM - Sample V32.10
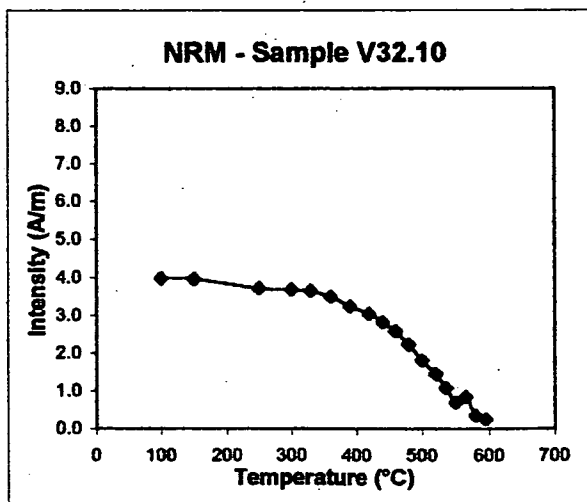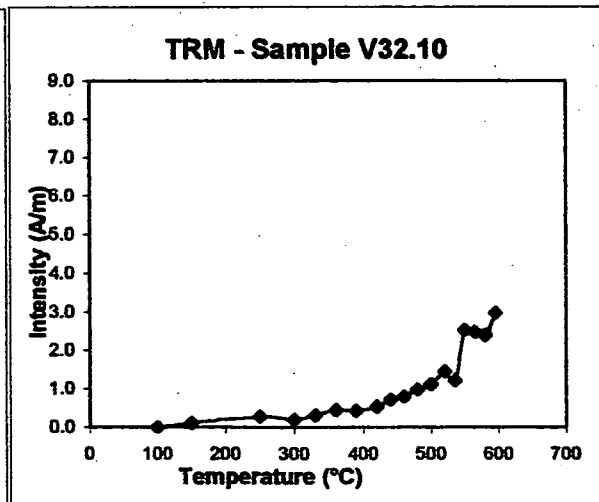
c)

Fig. 6.54 - Site V32: a)NRM/TRM plot and respective values, b)NRM demagnetization and c)TRM acquisition curves.

Tab. 6.27- Site V32: Palaeofields estimated and statistical parameters

230

C-Demag2

D-pTRMck

Scale 500 mA/m

Scale 500 mA/m

Mmax = 3920 mA/m

Mmax = 3930 mA/m
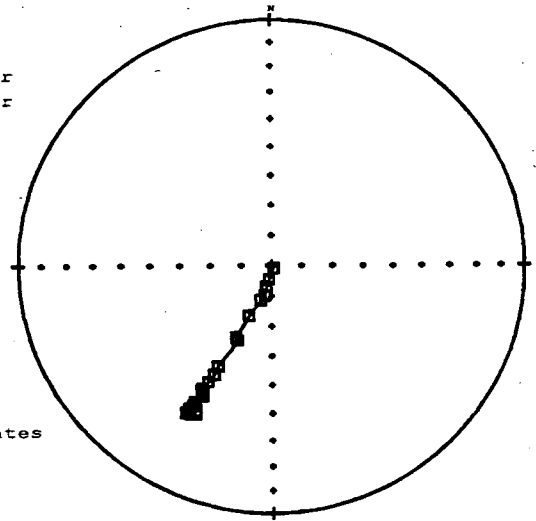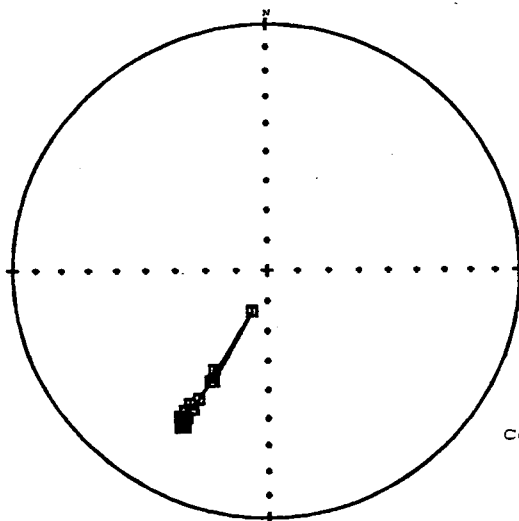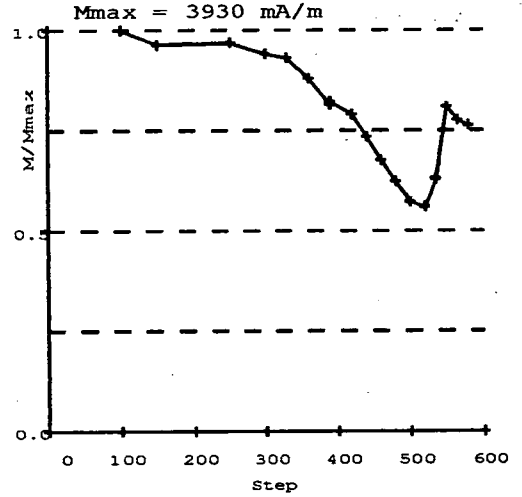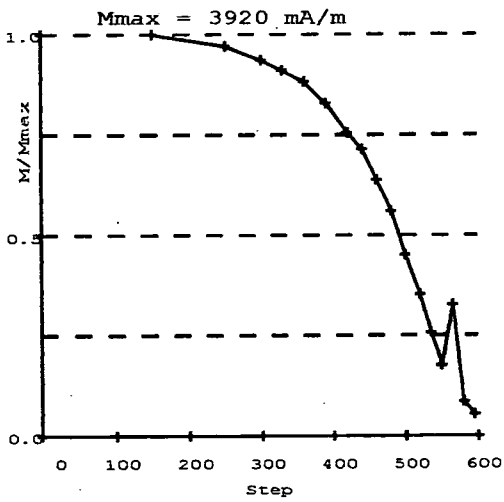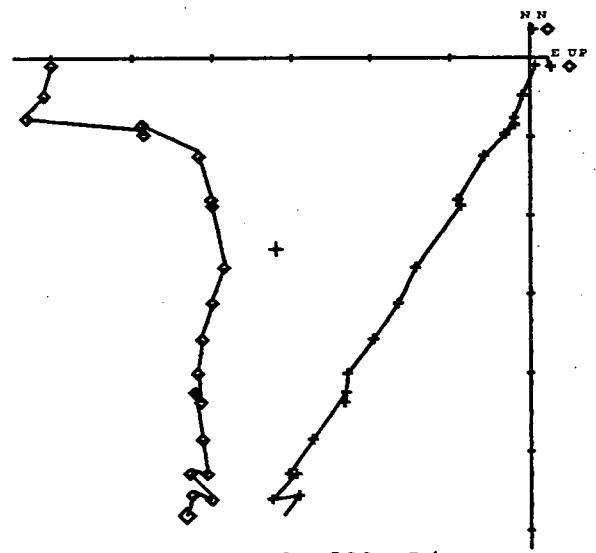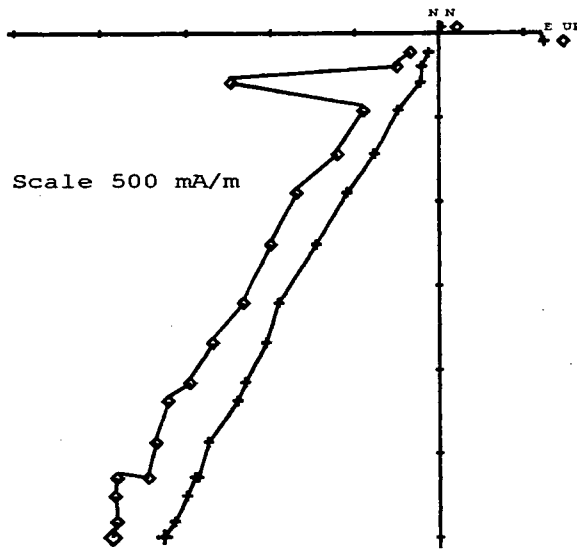
■ Lower
▲ Upper

Core
Coordinates

Fig. 6.55 - Site V32: Zijderveld diagrams, Intensity and stereo plots.

MTT (C-D)		
V32.10	NRM	TRM
steps	(A/m)	(A/m)
20	0.000	0.000
100	0.000	0.000
150	3.920	0.342
250	3.810	0.152
300	3.670	0.254
330	3.570	0.142
360	3.460	0.407
390	3.250	0.571
420	2.960	0.518
440	2.800	0.673
460	2.500	0.741
480	2.200	0.845
500	1.770	1.091
520	1.380	1.305
535	1.010	1.879
550	0.688	2.709
565	1.280	1.811
580	0.336	2.757
595	0.214	0.000

a)
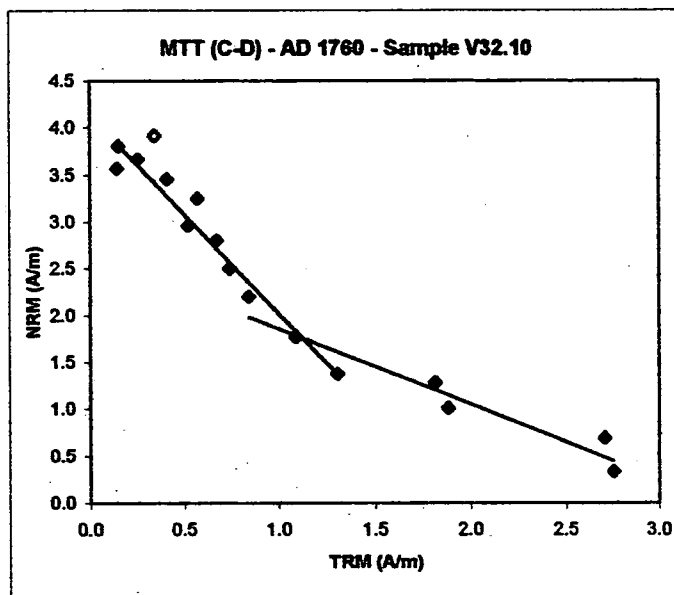
sample	Temp (°C)	N	f	g	q	b	R^2	Fpalaeo (μT)	σ_b
V32.10	250-535	12	0.714	0.892	8.152	-1.831	0.940	91.531	0.143
	480-580	7	0.476	0.476	1.829	-0.840	0.925	41.983	0.104

b)

c)
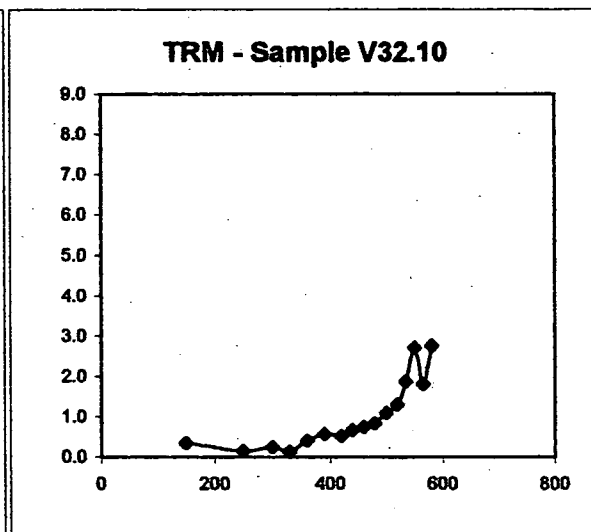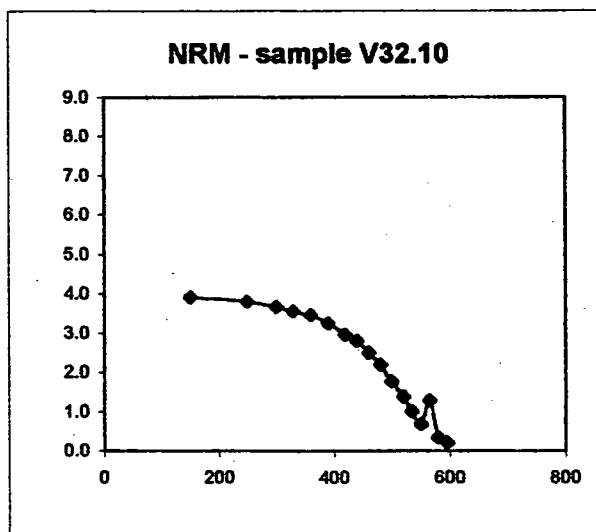
Fig. 6.56 - Site V32: a)NRM/TRM plot and respective values, b)NRM demagnetization and c)TRM acquisition curves.

Tab. 6.28 - Site V32: Palaeofields estimated and statistical parameters

AD 1760 sample V34.12a

A-Demag1

Scale 500 mA/m

B-pTRM

Scale 1000 mA/m

Mmax = 2210 mA/m

Mmax = 5090 mA/m
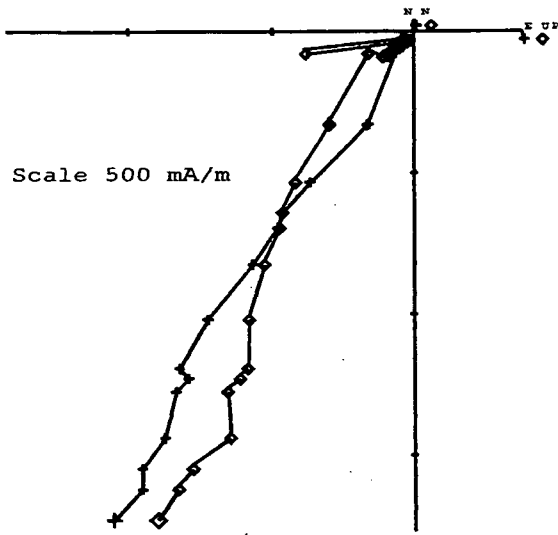
■ Lower
▲ Upper

Core
Coordinates

Fig. 6.57 - Site V34: Zijderveld diagrams, Intensity and stereo plots.

MTT (A-B)		
V34.12a steps	NRM (A/m)	TRM (A/m)
20	2.210	0.000
100	2.050	0.000
150	1.980	0.160
250	1.810	0.460
300	1.660	0.527
330	1.580	0.527
360	1.570	0.707
390	1.380	0.809
420	1.130	1.020
440	0.971	1.353
460	0.918	1.548
480	0.773	1.871
500	0.477	2.480
520	0.191	3.184
535	0.165	2.819
550	0.093	3.880
565	0.403	3.841
580	0.059	4.083
595	0.041	5.073

a)
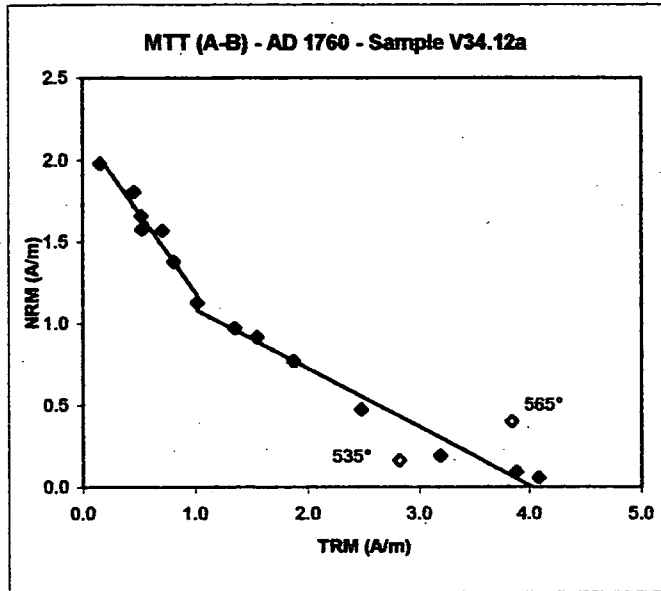
| sample	Temp (°C)	N	f	g	q	b	R^2	Fpalaeo (μT)	σ_b
V34.12a	150-420	7	0.385	0.783	2.890	-1.007	0.946	50.334	0.105
	*420-580	5	0.160	0.645	0.686	-0.480	0.977	24.024	0.933

*excluding 535,565
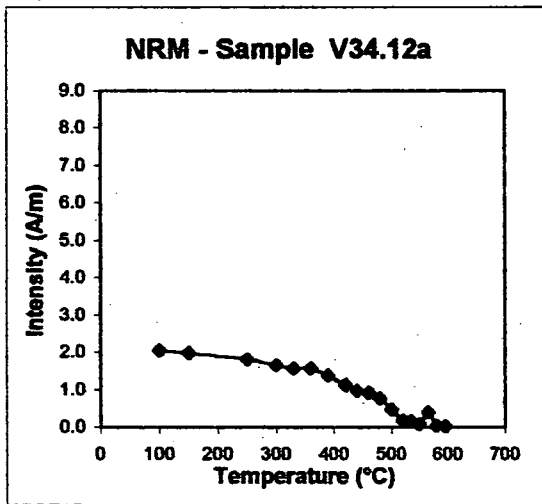
b)
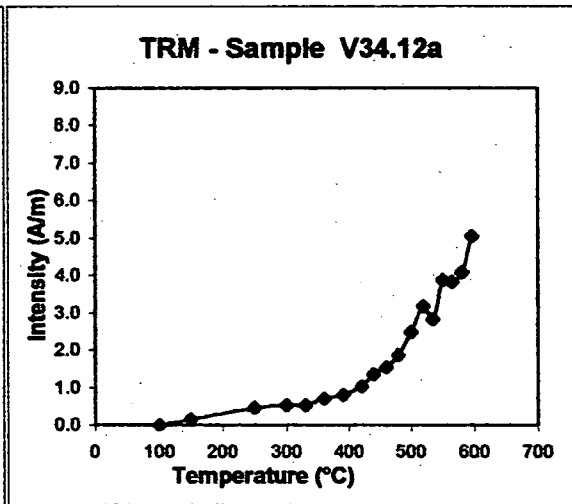
c)

Fig. 6.58 - Site V34: a)NRM/TRM plot and respective values, b)NRM demagnetization and c)TRM acquisition curves.

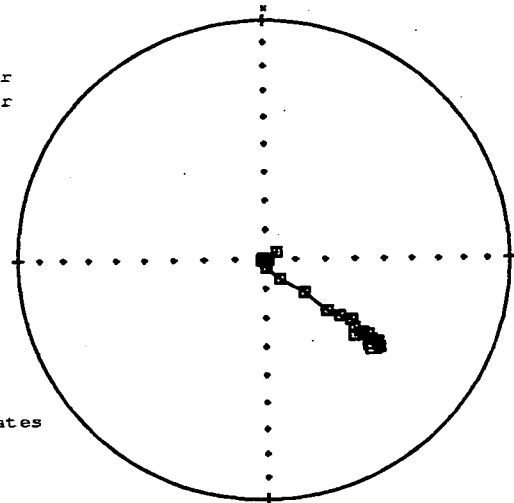Tab. 6.29 - Site V34: Palaeofields estimated and statistical parameters

234

C-Demag2

D-pTRMck

Scale 500 mA/m

Scale 1000 mA/m

Mmax = 1940 mA/m

Mmax = 5260 mA/m
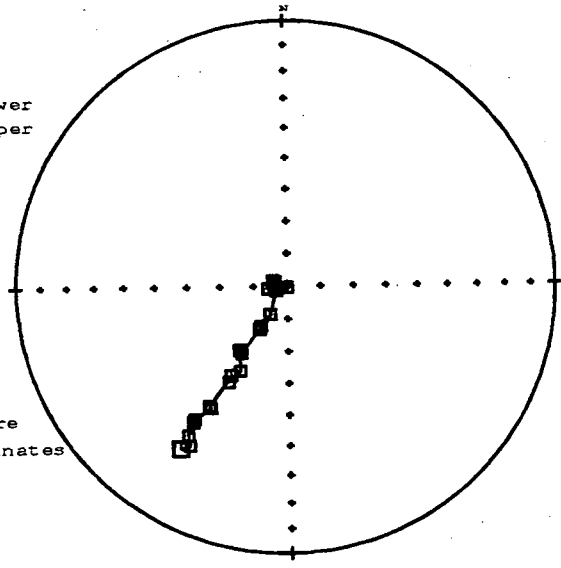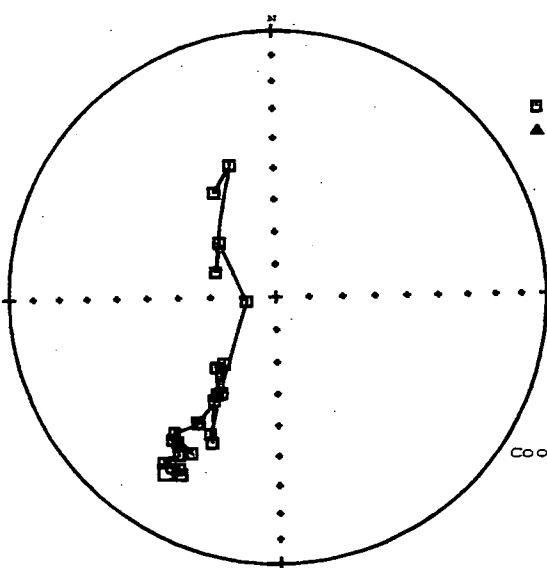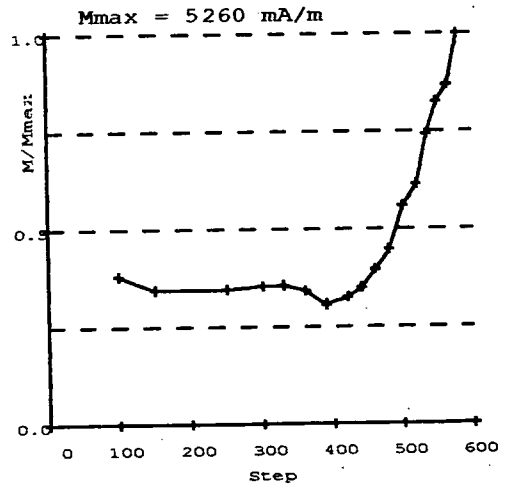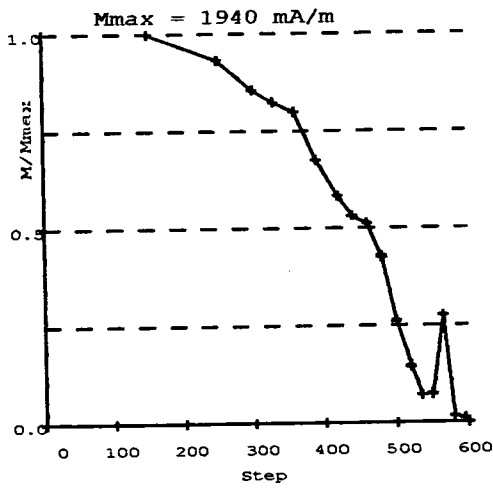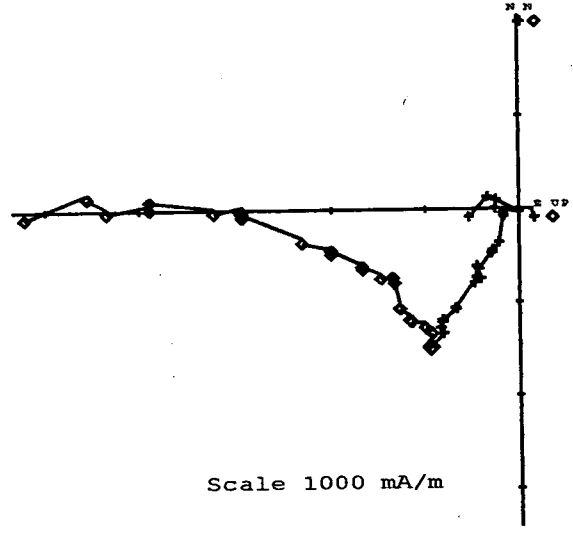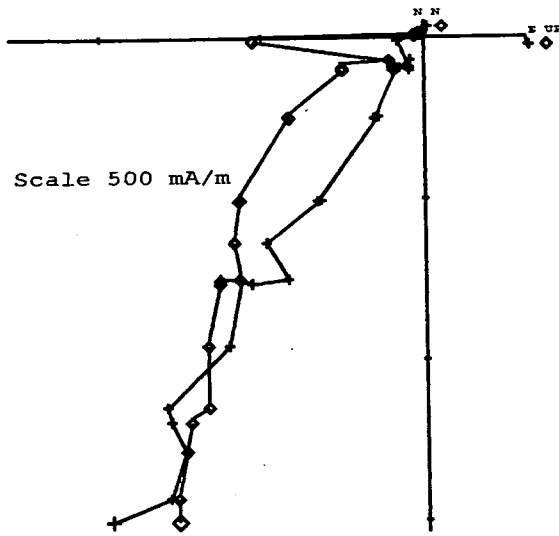
☐ Lower
▲ Upper

Core
Coordinates

Fig. 6.59 - Site V34: Zijderveld diagrams, Intensity and stereo plots.

MTT (C-D)		
V34.12a	NRM	TRM
steps	(A/m)	(A/m)
20	0.000	0.000
100	0.000	0.000
150	1.940	0.288
250	1.810	0.295
300	1.660	0.427
330	1.600	0.456
360	1.550	0.628
390	1.310	0.737
420	1.130	0.858
440	0.993	1.087
460	0.832	1.439
480	0.508	1.899
500	0.279	2.688
520	0.136	2.830
535	0.139	3.135
550	0.533	3.369
565	0.033	4.315
580	0.021	4.552
595	0.000	0.000

a)

MTT (C-D) - AD 1760 - Sample V34.12a
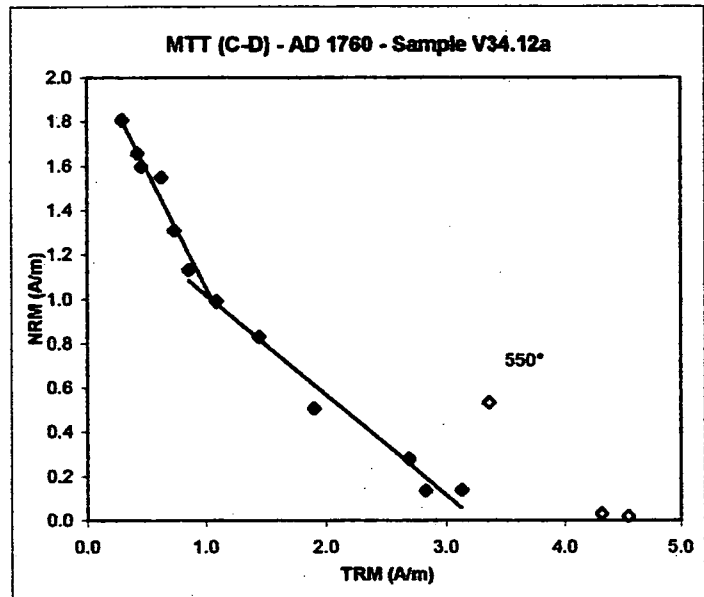
sample	Temp (°C)	N	f	g	q	b	R^2	Fpalaeo (μT)	σ_b
V34.12a	250-440	7	0.421	0.794	4.015	-1.085	0.966	54.253	0.090
	420-535	7	0.511	0.773	5.725	-0.457	0.976	22.827	0.032

NRM - sample V34.12a

TRM - Sample V34.12a
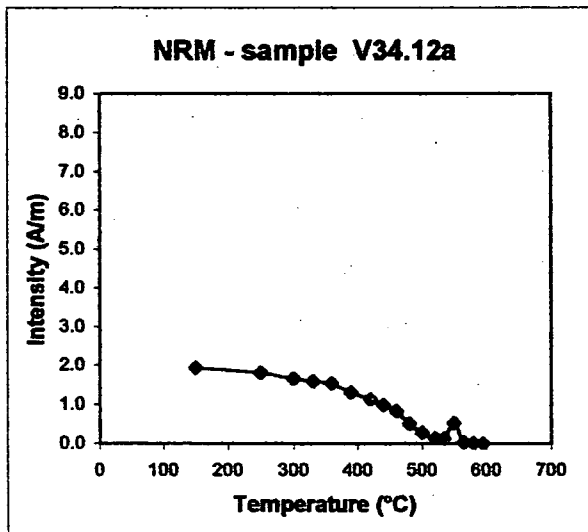
b)
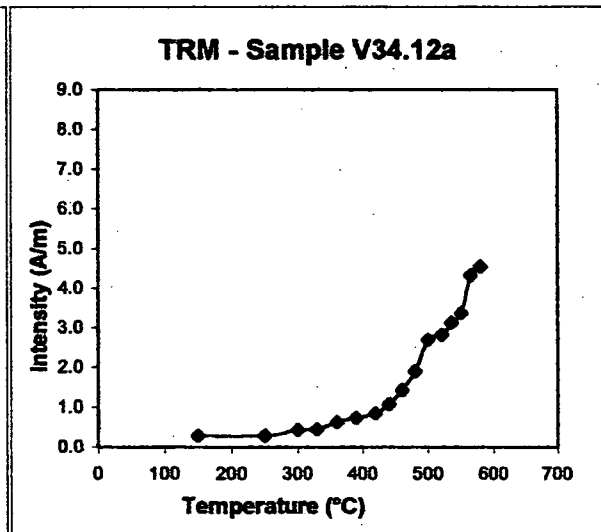
c)

Fig. 6.60 - Site V34: a)NRM/TRM plot and respective values, b)NRM demagnetization and c)TRM acquisition curves.

Tab. 6.30 - Site V34: Palaeofields estimated and statistical parameters

236

AD 1760 sample V35.7a

A-Demag1

Scale 500 mA/m

B-pTRM

Scale 1000 mA/m

Mmax = 3610 mA/m

Mmax = 3880 mA/m

M/Mmax

Step

M/Mmax
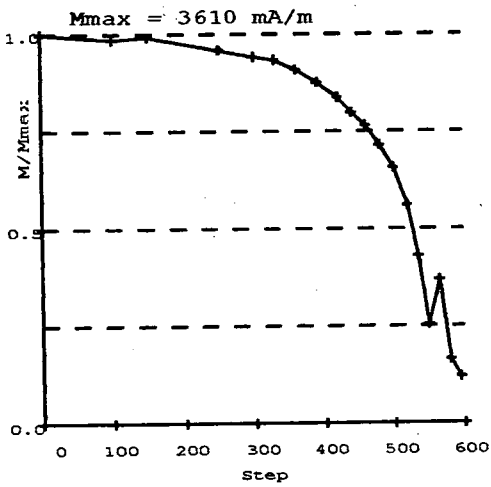
Step

☐ Lower
▲ Upper

Core
Coordinates

Fig. 6.61 - Site V35: Zijderveld diagrams, Intensity and stereo plots.

MTT (A-B)		
V35.7a	NRM	TRM
steps	(A/m)	(A/m)
20	3.610	0.000
100	3.560	0.000
150	3.500	0.174
250	3.460	0.157
300	3.400	0.139
330	3.370	0.200
360	3.280	0.313
390	3.160	0.362
420	3.020	0.277
440	2.880	0.420
460	2.760	0.456
480	2.580	0.564
500	2.370	0.658
520	2.020	0.973
535	1.550	0.607
550	0.914	2.943
565	1.330	2.664
580	0.592	1.486
595	0.431	3.469

a)
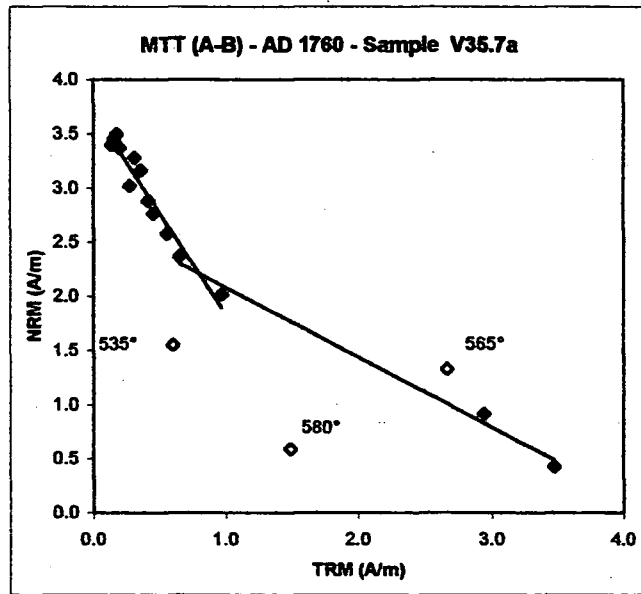
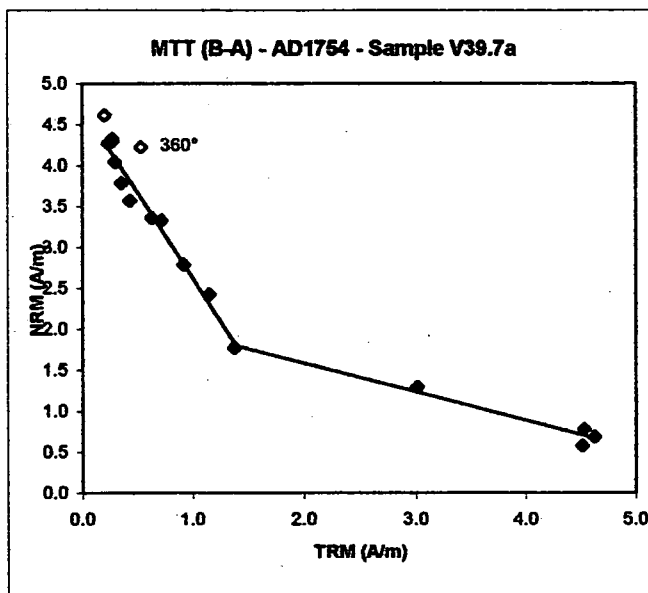| sample	Temp (°C)	N	f	g	q	b	R^2	Fpalaeo (μT)	σ_b
V35.7a	150-520	12	0.410	0.872	4.812	-1.923	0.143	96.159	19.984
	*500-595	4	0.537	0.580	4.744	-0.650	0.043	32.511	6.853

*excluding 535,565,580
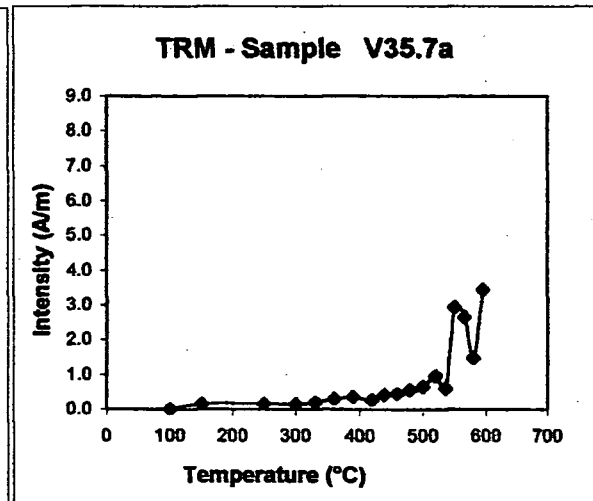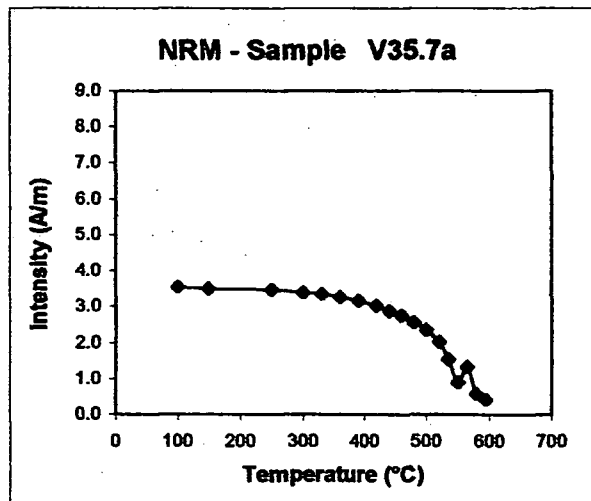
b)

c)

Fig. 6.62 - Site V35: a)NRM/TRM plot and respective values, b)NRM demagnetization and c)TRM acquisition curves.

Tab. 6.31 - Site V35: Palaeofields estimated and statistical parameters

238

C-Demag2

D-pTRMck

Scale 500 mA/m

Scale 1000 mA/m

Mmax = 3500 mA/m

Mmax = 3910 mA/m
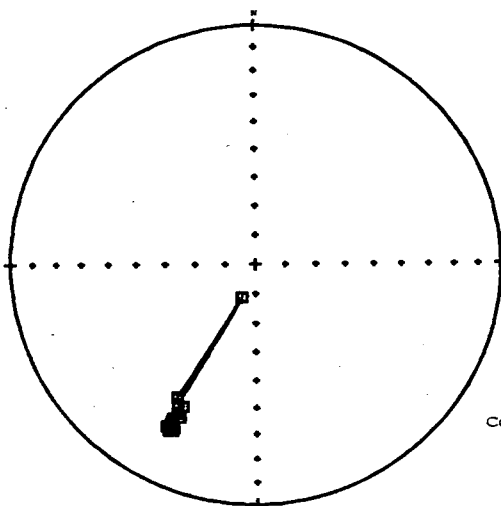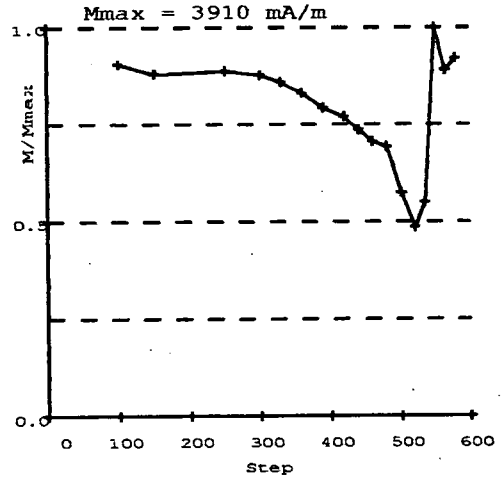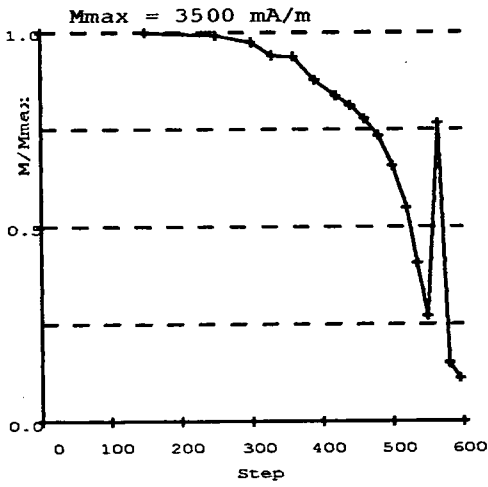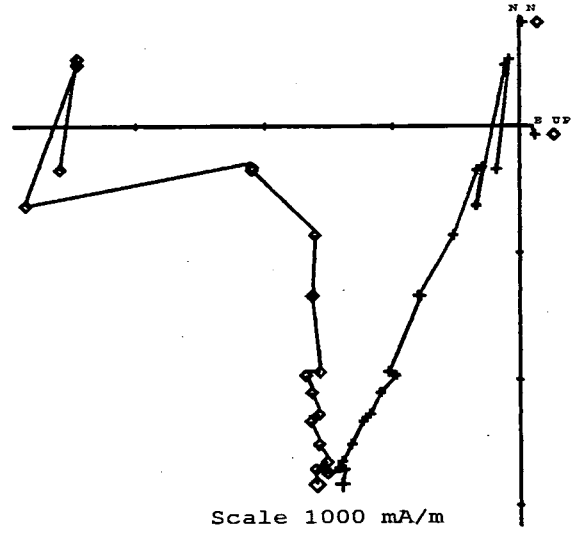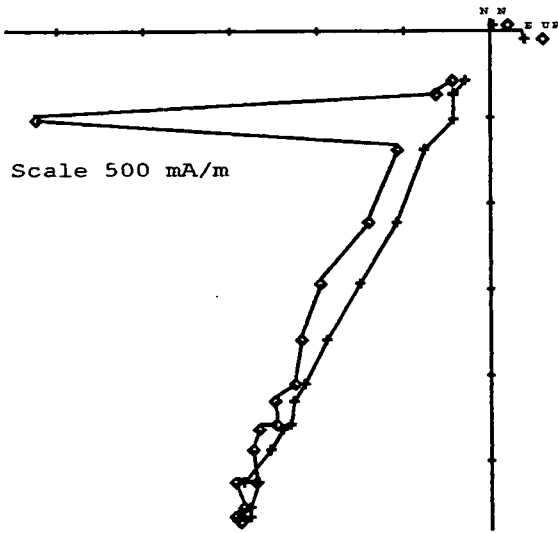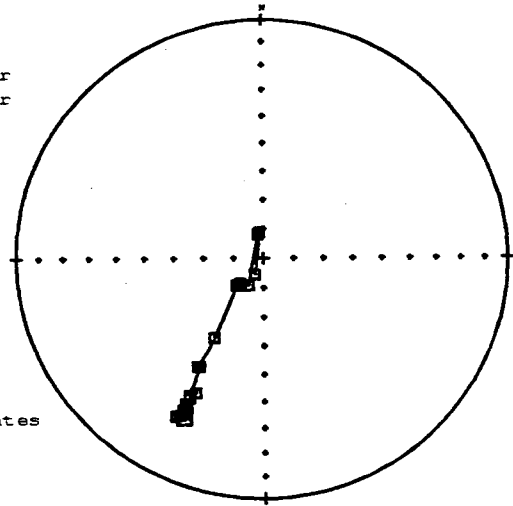
Fig. 6.63 - Site V35: Zijderveld diagrams, Intensity and stereo plots.

MTT (C-D)		
V35.7a	**NRM**	**TRM**
steps	**(A/m)**	**(A/m)**
20	0.000	0.000
100	0.000	0.000
150	3.500	0.220
250	3.470	0.144
300	3.410	0.147
330	3.290	0.076
360	3.280	0.271
390	3.070	0.293
420	2.930	0.249
440	2.840	0.443
460	2.720	0.497
480	2.570	0.460
500	2.300	0.717
520	1.920	0.902
535	1.420	1.620
550	0.950	3.311
565	2.680	1.335
580	0.527	3.273
595	0.388	0.000

a)
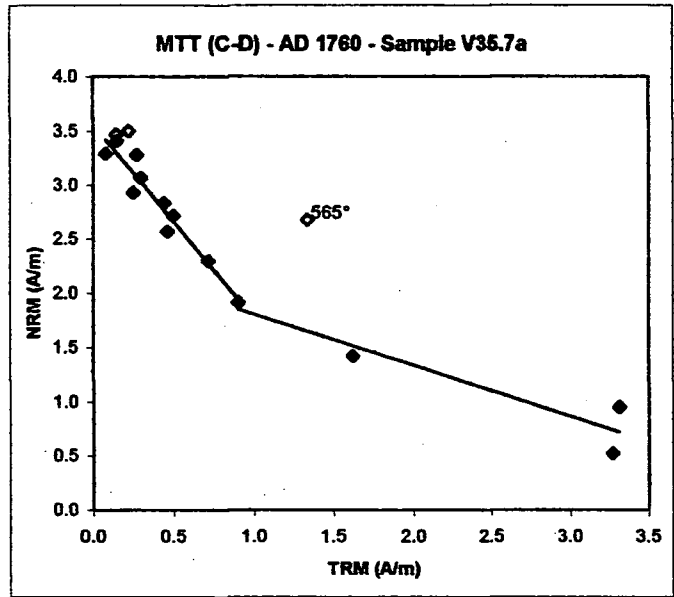
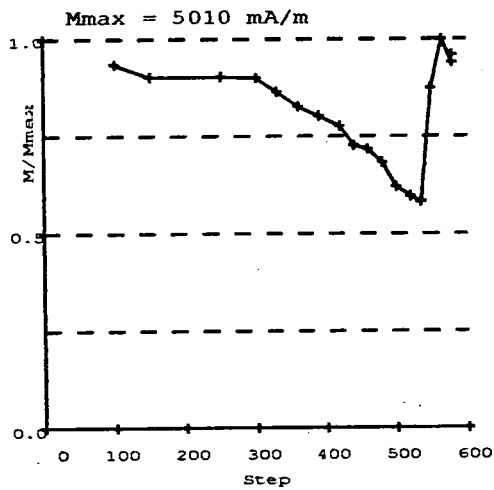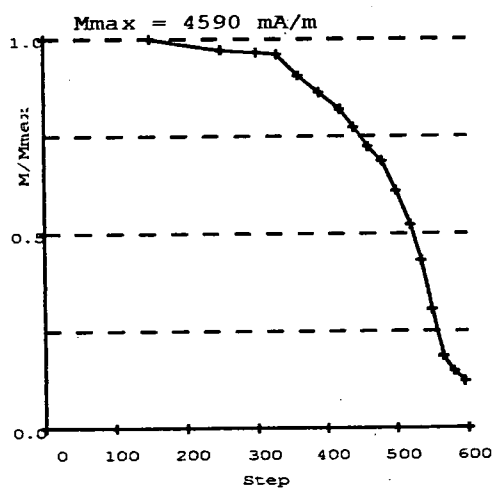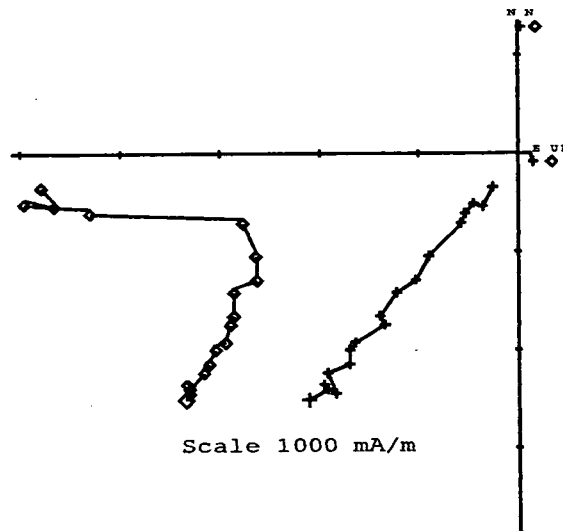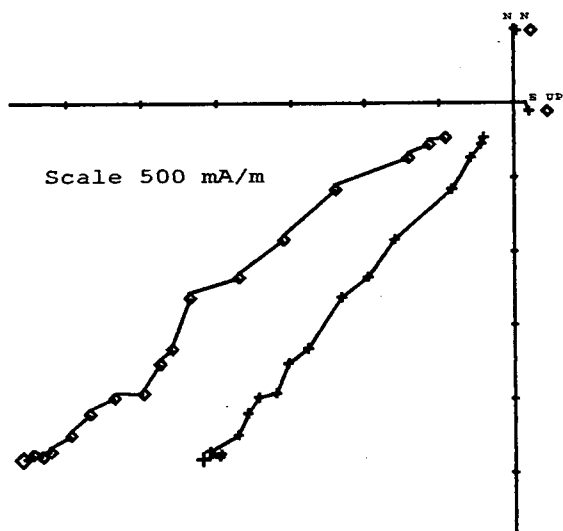| sample	Temp (°C)	N	f	g	q	b	R^2	Fpalaeo (μT)	σ_b
V35.7a	300-520	10	0.426	0.847	3.761	-1.848	0.923	92.404	0.177
	*520-580	4	0.398	0.665	1.154	-0.497	0.898	24.848	0.114

* excluding 565
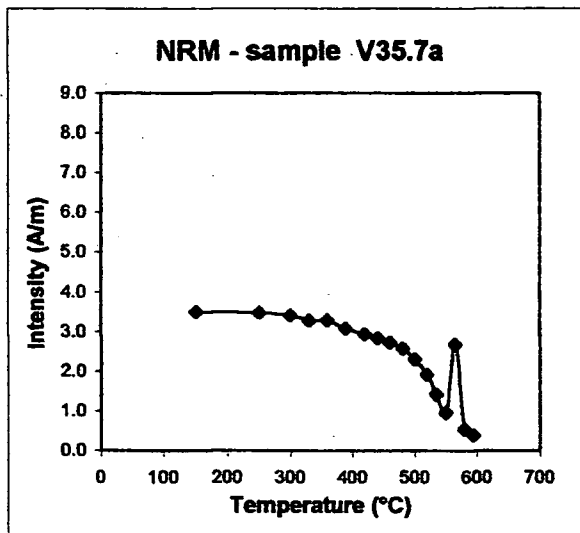
b)
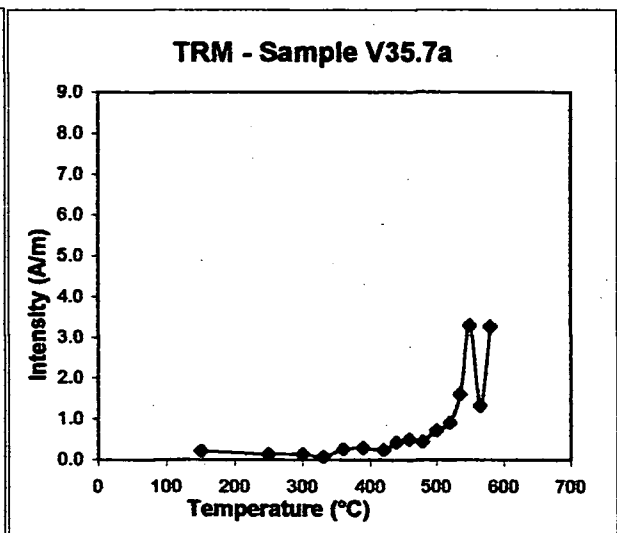
c)

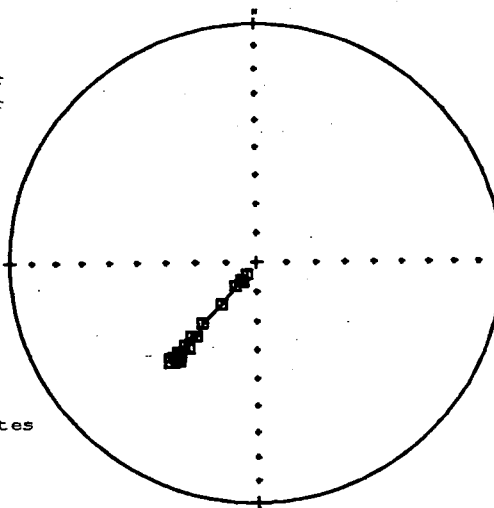Fig. 6.64 - Site V35: a)NRM/TRM plot and respective values, b)NRM demagnetization and c)TRM acquisition curves.

Tab. 6.32 - Site V35: Palaeofields estimated and statistical parameters

240

6.7 - AD 1806

6.7.1 - Site 24

A-Demag1

Intensity Behaviour - Initial NRM (20°C) of sample 5A was 5370 mA/m, but at 100°C it was 4110 mA/m. After it showed a smooth decrease until 520°C followed by a small linear tail until 595°C, when the intensity had been completely demagnetized. There were two small deflections at 400 and 480°C (Fig. 6.65).

Directional Behaviour - Both vertical and horizontal components moved towards the origin with a very linear trend. The Inc as shown by the stereo plot, moved slightly toward 90° above 500°C (Fig. 6.656).

B-pTRM

Intensity Behaviour - It showed a constant intensity (about 4000mA/m) between 100 and 300°C followed by a linear decrease until 460°C when the intensity was 2990 mA/m. After it showed a significant increase (4520 mA/m) until 535°C followed by another linear decrease until the end (595°C) (Fig. 6.65).

Directional Behaviour - The horizontal component moved toward the origin especially below 520°C. After this, its trend was very unclear. The vertical component moved toward the origin until 460°C then, it moved away from the NRM direction toward down. From 535°C it moved upwards (Fig. 6.65).

Palaeointensity results from A-B - All the points above 535°C behaved irregularly as shown by the NRM/TRM plot and by both the demagnetization and acquisition curves (Fig. 6.66a,b,c). Two different slopes up to that temperature were defined (Tab. 6.33).

C-Demag2

Intensity Behaviour - At 150°C, the NRM was 4090 mA/m and, by 595°C, was demagnetized completely. The intensity decay was similar to Demag1 with a break at 480°C (Fig. 6.67).

Directional Behaviour - It showed the same behaviour as in Demag1 but the vertical component showed a clear deflection at 480°C (Fig. 6.67).

D-pTRMck - *Intensity & Directional Behaviours*

The initial NRM behaved almost similarly as in pTRM. At 100°C it was 4150 mA/m and, at the end of the process, it was 3670 mA/m. The vertical component moved slightly away from the NRM until 480°C. Between 480 and 520°C it showed a clear movement downward followed by an upwards one until 580°C (Fig. 6.67).

Palaeointensity results from C-D - The behaviour was similar to A-B and, up to 520°C, two slopes were considered (Tab. 6.34). All the point above that temperature were excluded as also the value at 480° which was clearly anomalous on all the curves (Fig. 6.68a,b,c).

6.7.2 - Site 25

A-Demag1

Intensity Behaviour - Sample 1 had a low initial NRM (1970 mA/m) and showed a very unusual trend. In fact it showed: a linear decay until 150°C; a marked convex trend until 400°C; again linear until 460°C; a significant increase (about 200 mA/m) at 480°C followed by a very steep linear decay until 535°C; a small tail between 535 and 595°C when the intensity had been completely demagnetized (Fig. 6.69).

Directional Behaviour - Both horizontal and vertical components showed an almost linear trend toward the origin, below 500°C. After they behaved quite randomly, as also

shown by the stereo plot (Fig. 6.69). The vertical component showed a significant irregularity at 480°C when the total vector moved toward a downward direction.

B-pTRM

Intensity Behaviour - It showed a constant intensity (about 2000mA/m) between 150 and 440°C followed by a hyperbolic increase until 580°C when the intensity was 9030 mA/m (Fig. 6.69). The process ended (595°C) whit a small decrease.

Directional Behaviour- The horizontal component moved clearly toward the origin especially below 520°C, but after it showed an unclear trend. The vertical component moved rapidly away from the NRM direction toward down. The stereo plot showed the usual gradual movement of the Inc toward 90° (Fig. 6.69).

Palaeointensity results from A-B - The TRM curve showed a very steep increase in intensity above 535°C (Fig. 6.70c). A suspicious behaviour was also noticed on the NRM/TRM above the same temperature (Fig. 6.70a). Two different value of the palaeofield were considered (Tab. 6.35) excluding all the anomalous points mentioned above and also the value at 480°C.

C-Demag2

Intensity Behaviour - In this second demagnetization, started at 150°C, the NRM was 1620 mA/m and, by 550°C, was demagnetized completely. The intensity decay showed a shallow linear decay between 150 and 330°C, followed by a much more steeper linear decay until 440°C. A significant increase occurred between 440 and 480°C, followed by a steep linear decay, until 520°, terminating with a small tail at 595° (Fig. 6.71).

Directional Behaviour - The horizontal component showed an almost linear trend especially below 520°C. The vertical component moved northwards between 150 and

330°C then toward the origin until 440°C when a spike downward occurred. From 480°C it moved again toward the origin (Fig. 6.71).

The stereo plot showed a good consistency in Dec until 535°C while the Inc had a gradual, but not clear movement toward 90°.

D-pTRMck

Intensity & Directional Behaviours - Both were similar to those showed by pTRM (Fig. 6.71).

Palaeointensity results from C-D -Two different value of the palaeofield were considered (Tab. 6.36) excluding points which showed irregular behaviour on the NRM/TRM plot above 565°C (Fig. 6.72a) and also some points which appeared clearly irregular on the NRM curve (Fig. 6.72b).

6.8 - AD 1839

6.8.1 - Site 42

A-Demag1

Intensity Behaviour - The initial NRM in sample 6B was 6590 mA/m but at 100°C it dropped down to 4930 mA/m. It stayed constant until 330° when it showed the usual accelerating decrease (Fig. 6.73). This terminated with a linear tail and, by 595°C it had been demagnetized almost completely (some 5% of initial NRM still remaining). A small irregularity was present at 520°C.

Directional Behaviour - Both components moved towards the origin with a very linear trend especially above 480°C (Fig. 6.73).

B-pTRM

Intensity Behaviour - It was the same as in Demag1 from 5000 (100°C) to 3850 mA/m (520°C), except for a significant deflection occurred between 440 and 500°C. Above 535°C the intensity increased significantly (about 1500 mA/m) and, at the end, it was 5310 mA/m (Fig. 6.73).

Directional Behaviour - The horizontal component moved toward the origin with an almost linear trend until 535°C. Above this it showed a small-curved westward deflection but terminating at 595°C toward the origin. The vertical component moved gradually away from the NRM direction but, at 535°C it showed a marked downward spike (Fig. 6.73). This behaviour was also underlined by the stereo plot, where the Dec slightly changed above 535°C. while the Inc moved towards 90°.

Palaeointensity results from A-B - The NRM/TRM plot showed three different slopes (Fig. 6.74a) therefore three value of the palaeofield were determined. Both NRM and TRM curves (Fig. 6.74b,c) behaved almost regularly, although some points (Tab. 6.37) were considered irregular when the slope, referred to as [c], was defined.

C-Demag2

Intensity & Directional Behaviour - The two behaviours were similar to Demag1, except for a small irregularity at 330°C. The initial NRM (150°C) was 4990 mA/m (Fig. 6.75).

D-pTRMck

Intensity & Directional Behaviour - It was very similar to pTRM. The initial NRM was 5040 mA/m (100°C); the intensity started to increase at 520°C, when it was 2820 mA/m; finally (595°) the intensity was 5240 mA/m (Fig. 6.75).

Palaeointensity results from C-D - Three different value of the palaeofield were determined (Fig. 6.76a). As in MTT A-B, NRM and TRM curves (Fig. 6.76b,c) behaved

almost regularly, but two points (Tab. 6.38) were considered irregular when defining the slope referred to as [c].

6.8.2 - Site 43

A-Demag1

Intensity Behaviour - Sample 13B showed an initial NRM, at 20°C higher then at 100°C. In fact the intensity was 6300 mA/m and, the next step, it dropped down of about 1400 mA/m. Starting from 330°C it showed an accelerating decrease (Fig. 6.77) terminating with a small convex tail. At 595°C, there was some 3% of initial NRM still remaining. A small irregularity occurred at 480°C.

Directional Behaviour - Both vertical and horizontal components moved towards the origin with a linear trend above 480°C, but they showed small irregularities below this temperature (Fig. 6.77).

B-pTRM

Intensity Behaviour - It showed a general shallow decreasing trend, from 4940 (100°C) to 4200 mA/m (520°C). A small convex deflection between 250 and 440°C and a small spike at 480°C, were present. Above 520°C the intensity showed a significant increase (about 1400 mA/m). From 550°C it stayed mostly constant and, at the end (595°C) was 5790 mA/m (Fig. 6.77).

Directional Behaviour - The horizontal component moved linearly toward the origin between 330 and 535°C but from 440°C it moved slightly westwards. At 565°C a marked westwards spike occurred followed by a linear trend toward the origin, but without reaching it. The vertical component moved gradually away from the NRM direction but it showed a zigzag trend between 360° and 500°C. At 535°C a marked downward spike

occurred followed by an almost linear trend toward north. The Inc moved towards 90° rapidly from 500°C (Fig. 6.77).

Palaeointensity results from A-B - Two different values of the palaeofield were considered excluding all the points below 390°C, which appeared anomalous on the NRM/TRM. Some other values were excluded when interpreting the second slope (Tab. 6.39) although they did not appear clearly irregular on both NRM and TRM curves (Fig. 6.78b,c).

C-Demag2

Intensity & Directional Behaviour - The initial NRM (150°C) was 4770 mA/m. Above this the two behaviours were very similar to Demag1, except for a little irregularity at 330°C and for the tail that was less convex (Fig. 6.79).

D-pTRMck

Intensity Behaviour - The initial intensity was 4860 mA/m (100°C) and behaved similarly to pTRM but between 460 and 500°C it showed a more significant decrease (as in Demag1). After the marked increase to 535°C the intensity was 5440 mA/m (Fig. 6.79).

Directional Behaviour - It was almost similar to that one showed in pTRM but between 460 and 500°C the vertical vector, moved clearly upward (Fig. 6.79).

Palaeointensity results from C-D - Two different values of the palaeofield were considered (Fig. 6.80a,Tab. 6.40). Both NRM and TRM curves did not show any particular irregularity (Fig. 6.80b,c).

6.8.3 - Site 44

A-Demag1

Intensity Behaviour - Sample 6A had an initial NRM of 2350 mA/m but, by 100°C it dropped down to 1690 mA/m.. It stayed steady below 330°C then it started to decay almost linearly until 535°C when it showed a small concave tail and, by 595°C had been demagnetized completely. A marked spike occurred at 480°C when the intensity increased of about 1200 mA/m (Fig. 6.81).

Directional Behaviour - The horizontal component moved toward a southeast direction below 250°C then it moved toward the origin but with a very unclear trend (Fig. 6.81). The vertical component moved downward, clearly away from the origin, below 250°C then it changed drastically direction moving toward the origin. A marked downward spike occurred at 480°C but after this it moved again toward the origin although with a random trend. The general unclear trend was clearly shown by the stereo plot.

B-pTRM

Intensity Behaviour - At 100°C the intensity was 1660 mA/m and showed a shallow increase below 360°C.. After it decreased until 440°C when it was 888 mA/m. Above this point there was a very steep increase until the end of the process (595°C) where the intensity was 9300 mA/m. All the increases and decreases occurred were almost linear (Fig. 6.81).

Directional Behaviour - The horizontal component showed several different trends. In fact it moved; toward a southeast direction below 360°C; toward the origin until 440°C; toward west until 500°C; again toward the origin until 535°C. Above this temperature it behaved randomly. The vertical component moved downward until 360°C, then toward the origin until 440°C. After it moved clearly downward. The stereo plot showed a gradually movement of Inc toward 90° although unclear (Fig. 6.81).

Palaeointensity results from A-B - Some points in the medium range of temperature, which appeared irregular in all the curves, (Fig. 6.82a,b,c) were not considered as also values above 550 °C. The NRM/TRM plot showed a quite anomalous behaviour and two possible slopes were considered (Tab. 6.41).

C-Demag2

Intensity Behaviour - The initial NRM (at 150°) was 1670 mA/m and stayed almost constant until 300°C when it decayed linearly until 440°C. A small increase occurred at 460°C followed by another linear trend terminating with a small tail (Fig. 6.83).

Directional Behaviour- Both the horizontal and vertical components moved toward the origin with a very unclear trend. The stereo plot showed a random behaviour of Dec and Inc above 520°C (Fig. 6.83).

D-pTRMck

Intensity Behaviour- It was exactly the same as in pTRM. The initial intensity was 1740 mA/m and, at 595°C it was 9640 mA/m (Fig. 6.83).

Directional Behaviour- The horizontal showed a general unclear trend toward the origin below 460°C. After it showed two marked northward spike at 480 and 550°C. The vertical component moved away from the NRM direction with a zigzag trend below 460°C then it moved clearly downward. At 595°C, a marked upward spike occurred, as also shown by the Inc behaviour (Fig. 6.83).

Palaeointensity results from C-D - The NRM/TRM plot showed two different slopes (Fig. 6.84a). No points were excluded (Tab. 6.42) although both NRM and TRM curves (Fig. 6.84b,c) did not show clear behaviours.

AD 1806 sample V24.5

A-Demag1

B-pTRM

Scale 1000 mA/m

Scale = mA/m 1000

Mmax = 5370 mA/m

Mmax = 4520 mA/m
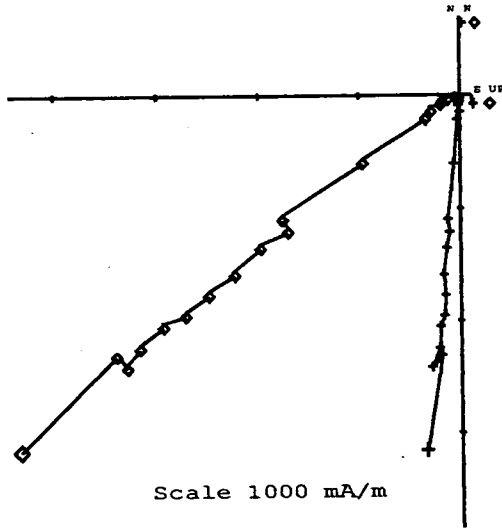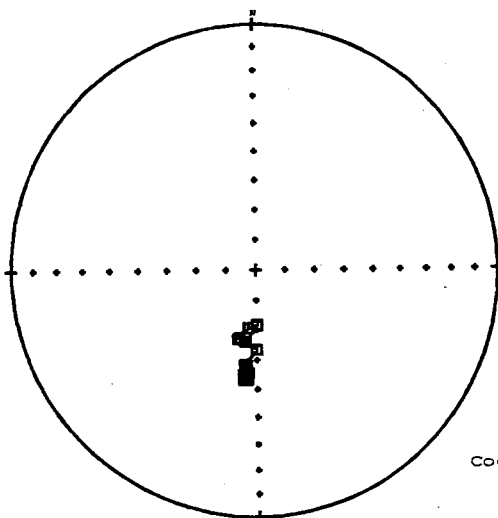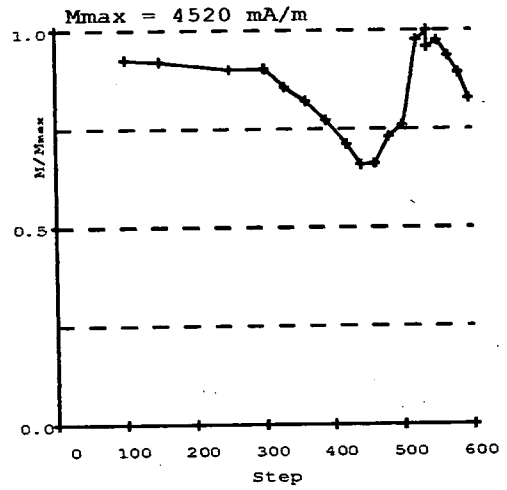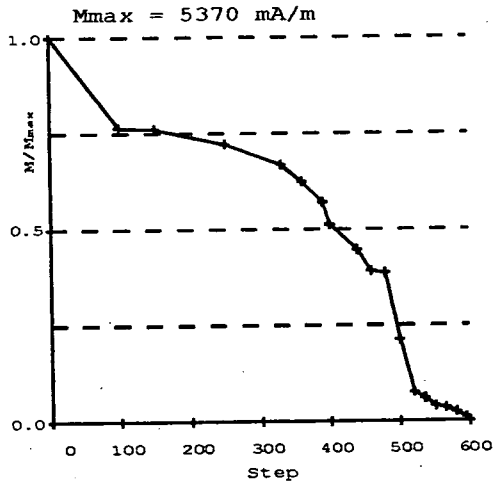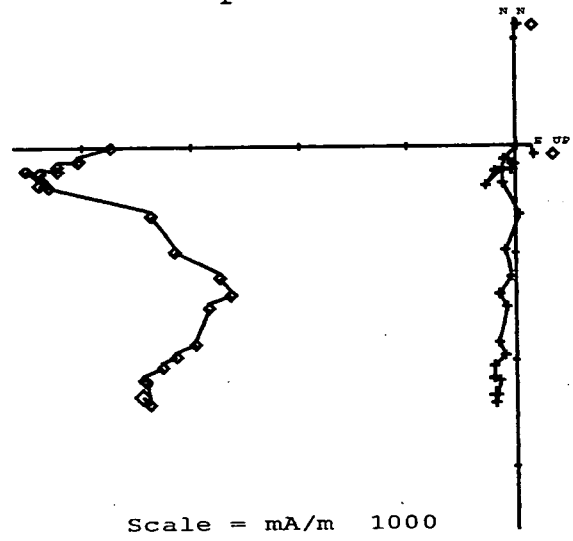
Lower
Upper
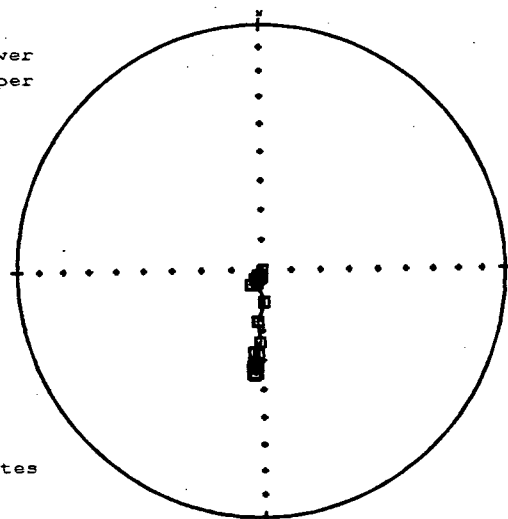
Core
Coordinates

Fig. 6.65 - Site V24: Zijderveld diagrams, Intensity and stereo plots.

MTT (C-D)		
V24.5	NRM	TRM
steps	(A/m)	(A/m)
20	0.000	0.000
100	0.000	0.000
150	4.090	0.137
250	3.920	0.108
300	3.790	0.217
330	3.600	0.152
360	3.300	0.293
390	2.990	0.347
420	2.660	0.468
440	2.340	0.684
460	2.120	1.087
480	2.050	0.583
500	1.070	2.620
520	0.425	4.117
535	0.330	4.036
550	0.211	4.052
565	0.140	3.971
580	0.098	3.577
595	0.000	0.000

a)

MTT (C-D) - AD 1806 - Sample V24.5
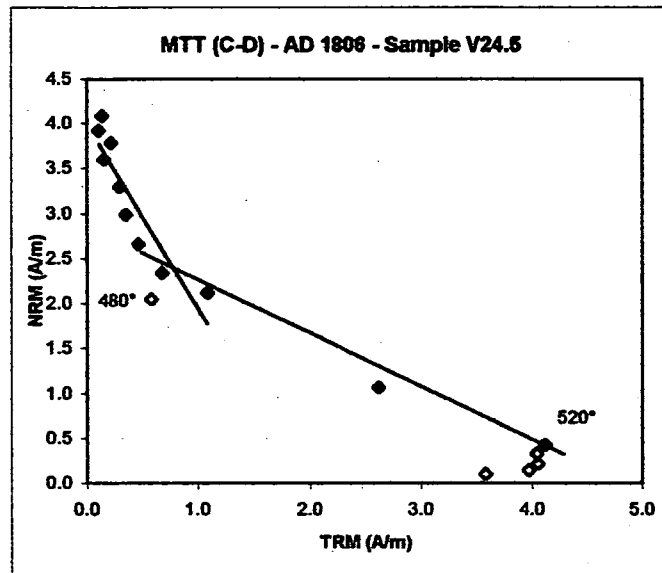
sample	Temp (°C)	N	f	g	q	b	R^2	Fpalaeo (μT)	σ_b
V24.5	300-520	8	0.428	0.843	2.935	-3.194	0.911	159.697	0.393
	*420-520	5	0.546	0.666	4.952	-0.607	0.984	30.358	0.045

* excluding 480

NRM - sample V24.5
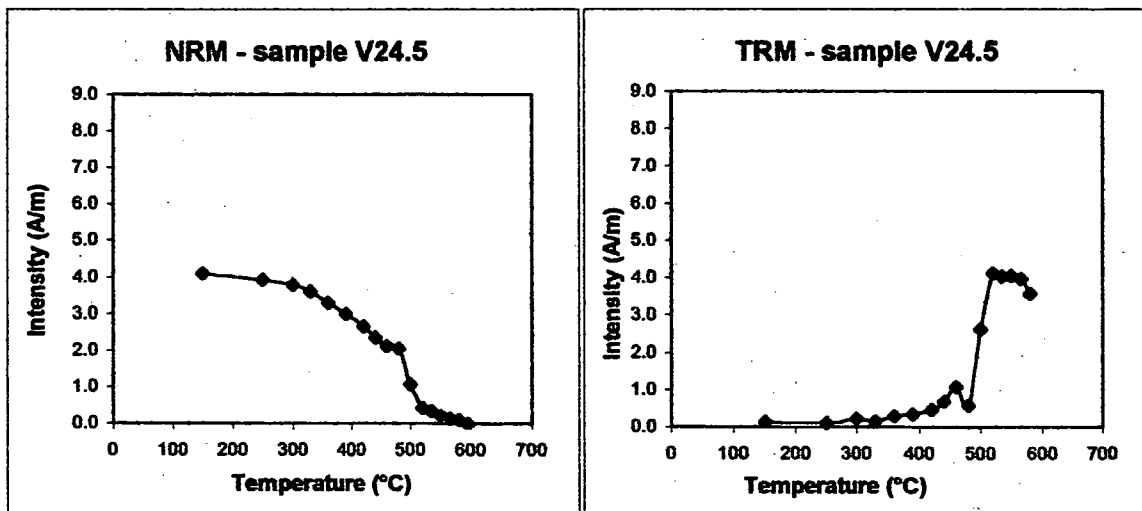
TRM - sample V24.5

b)

c)

Fig. 6.68 - Site V24: a)NRM/TRM plot and respective values, b)NRM demagnetization and c)TRM acquisition curves.

Tab. 6.34 - Site V24: Palaeofields estimated and statistical parameters

251

AD 1806 sample V24.5

C-Demag2

Scale = 500 mA/m

D-pTRMck

Scale = 1000 mA/m

Mmax = 4090 mA/m

Mmax = 4500 mA/m

□ Lower
▲ Upper

Core
Coordinates
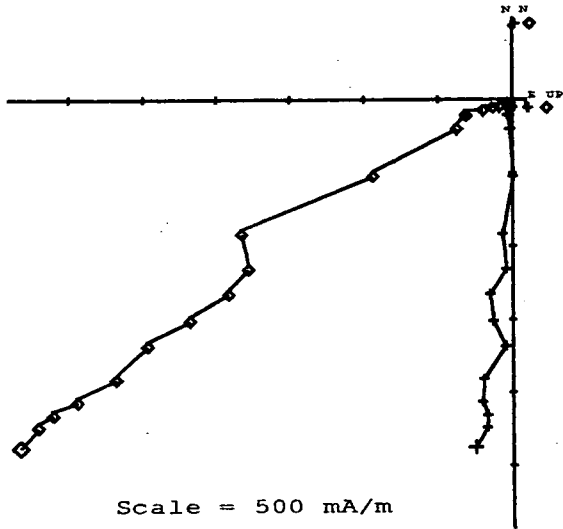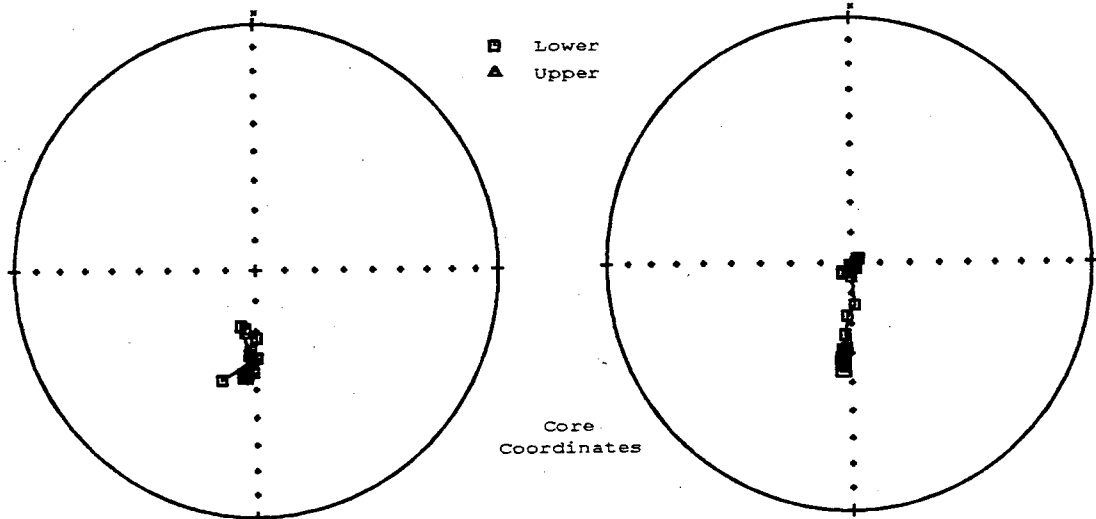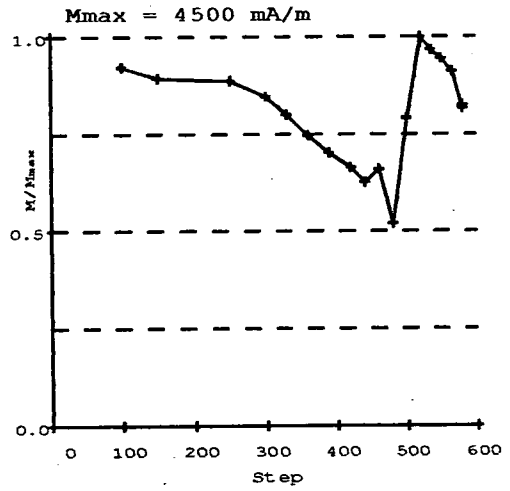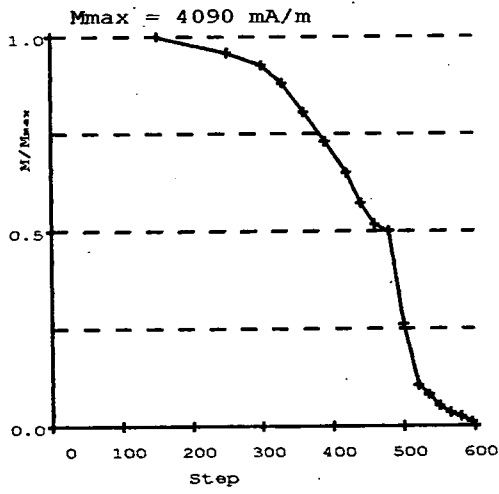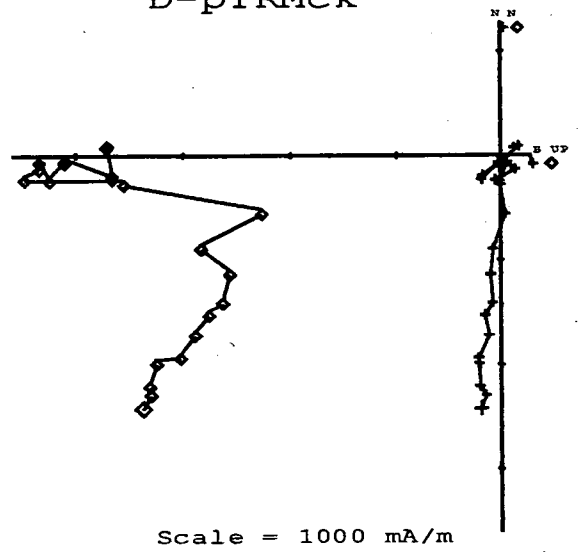
Fig. 6.67 - Site V24: Zijderveld diagrams, Intensity and stereo plots.

MTT (A-B)		
V24.5	**NRM**	**TRM**
steps	**(A/m)**	**(A/m)**
20	5.370	0.000
100	4.110	0.000
150	4.090	0.146
250	3.880	0.278
300	3.590	0.523
330	3.590	0.336
360	3.350	0.432
390	3.060	0.477
420	2.750	0.613
440	2.400	0.655
460	2.100	1.030
480	2.080	1.397
500	1.140	2.411
520	0.408	4.057
535	0.325	4.229
550	0.214	4.202
565	0.188	4.052
580	0.129	3.916
595	0.053	3.688

a)

MTT (A-B) - AD1806 - Sample V24.5
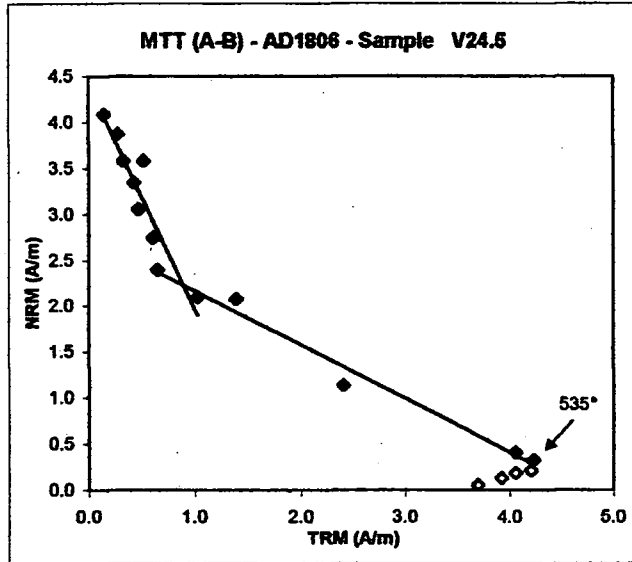
sample	Temp (°C)	N	f	g	q	b	R^2	Fpalaeo (μT)	σ_b
V24.5	150-460	9	0.371	0.854	2.220	-2.639	0.863	131.932	0.376
	440-535	6	0.386	0.648	3.903	-0.590	0.987	29.491	0.038

NRM - Sample V24.5
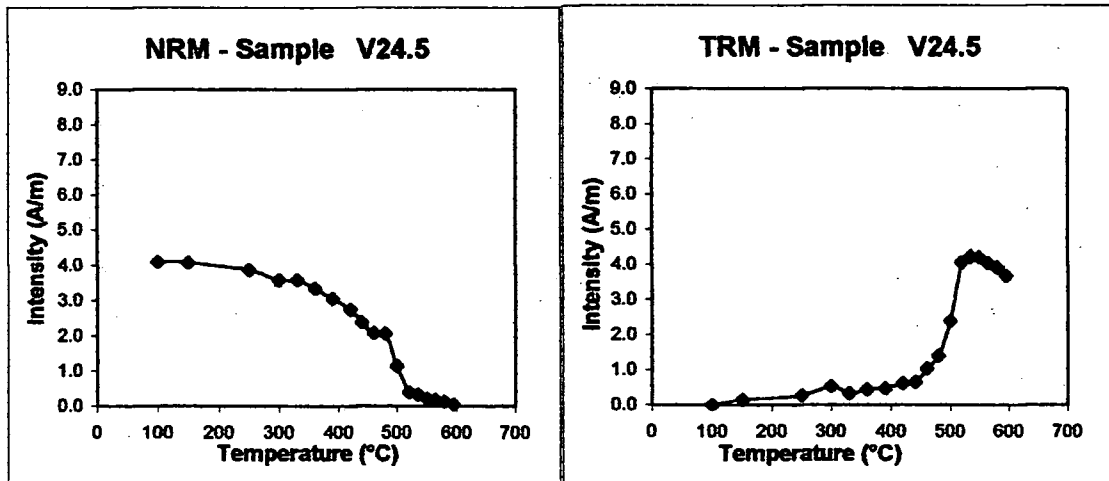
TRM - Sample V24.5

b)   c)

Fig. 6.66 - Site V24: a)NRM/TRM plot and respective values, b)NRM demagnetization and c)TRM acquisition curves.

Tab. 6.33 - Site V24: Palaeofields estimated and statistical parameters

AD 1806 sample V25.1

A-Demag1

B-pTRM

Scale 500 mA/m

Scale 2000 mA/m

Mmax = 1970 mA/m

Mmax = 9030 mA/m

Lower
Upper

Core
Coordinates
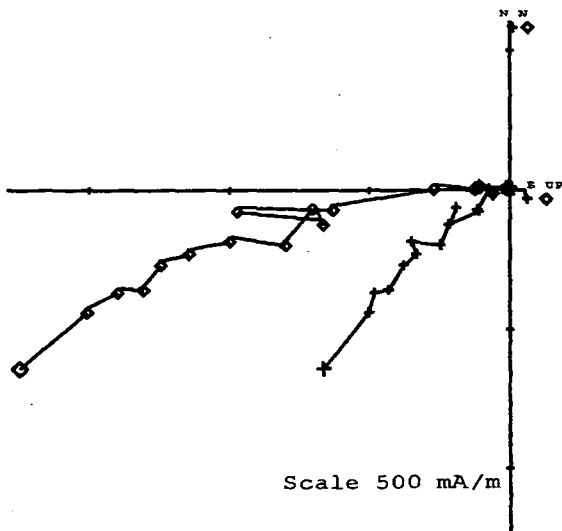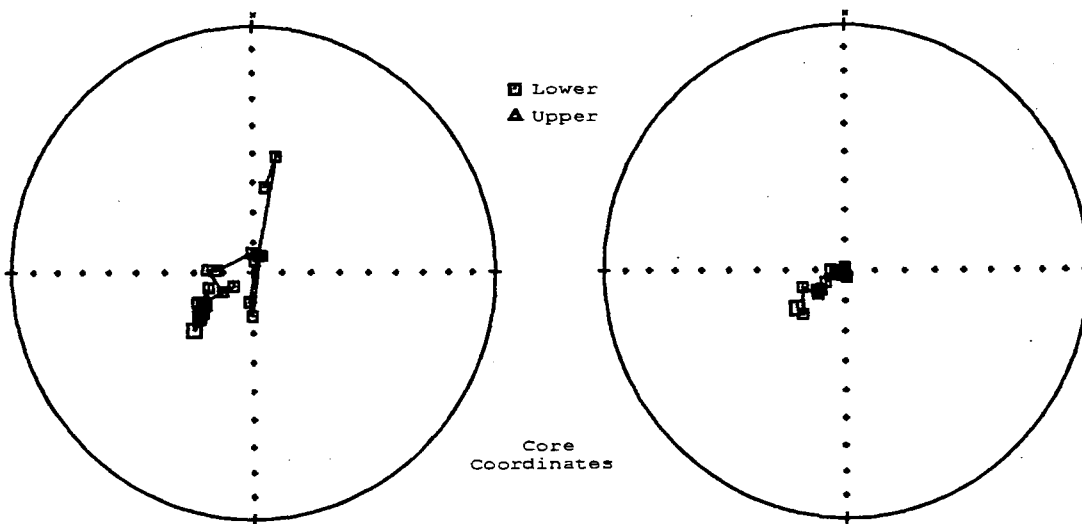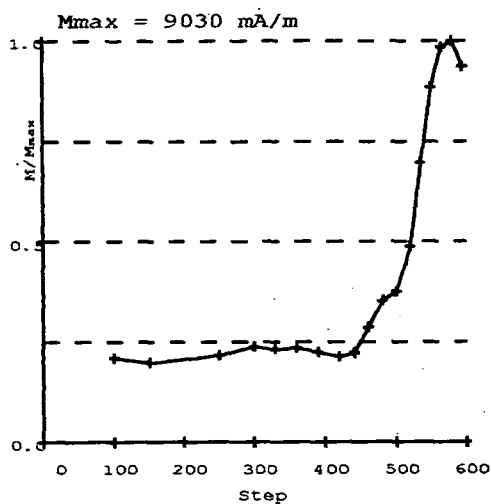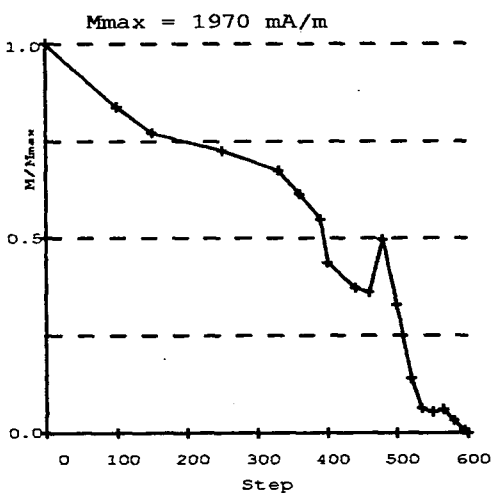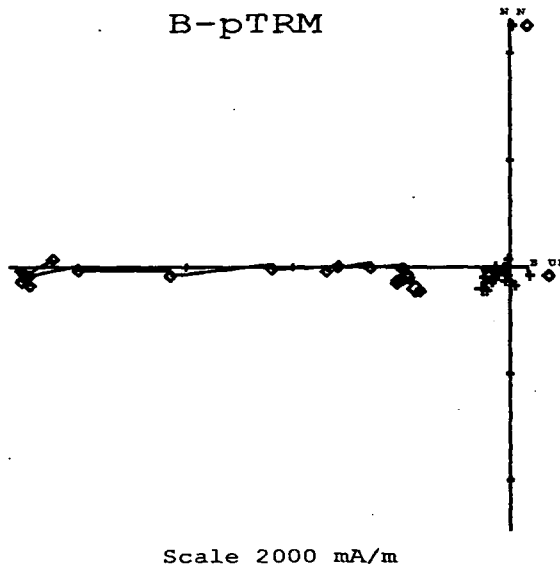
Fig. 6.69 - Site V25: Zijderveld diagrams, Intensity and stereo plots.

MTT (A-B)		
V25.1	NRM	TRM
steps	(A/m)	(A/m)
20	1.970	0.000
100	1.650	0.267
150	1.520	0.297
250	1.430	0.607
300	1.393	0.822
330	1.330	0.801
360	1.210	0.946
390	1.080	1.003
420	0.862	1.109
440	0.733	1.297
460	0.711	1.921
480	0.982	2.207
500	0.647	2.749
520	0.277	4.128
535	0.126	6.174
550	0.106	7.889
565	0.118	8.766
580	0.063	8.971
595	0.015	8.444

a)

MTT (A-B) - AD1806 - Sample V25.1
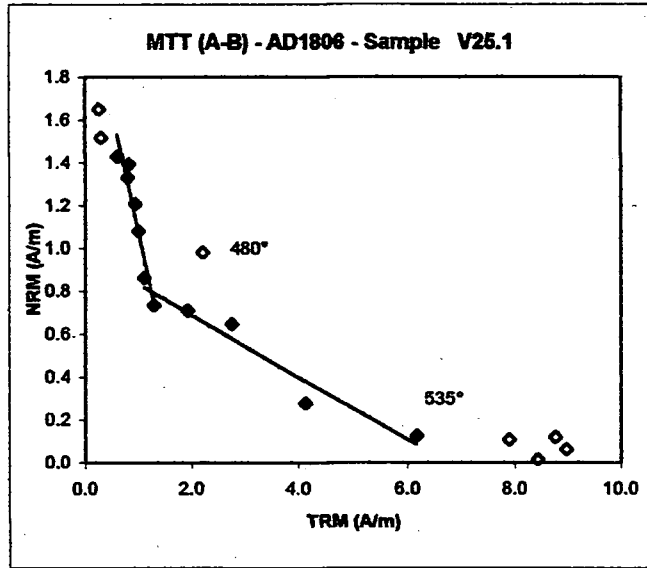
sample	Temp (°C)	N	f	g	q	b	R^2	Fpalaeo (μT)	σ_b
V25.1	250-440	7	0.354	0.793	2.160	-1.195	0.918	59.751	0.155
	*420-535	6	0.374	0.666	2.146	-0.149	0.947	7.436	0.017

*excluding 480

NRM - Sample V25.1

TRM - Sample V25.1

b)   c)
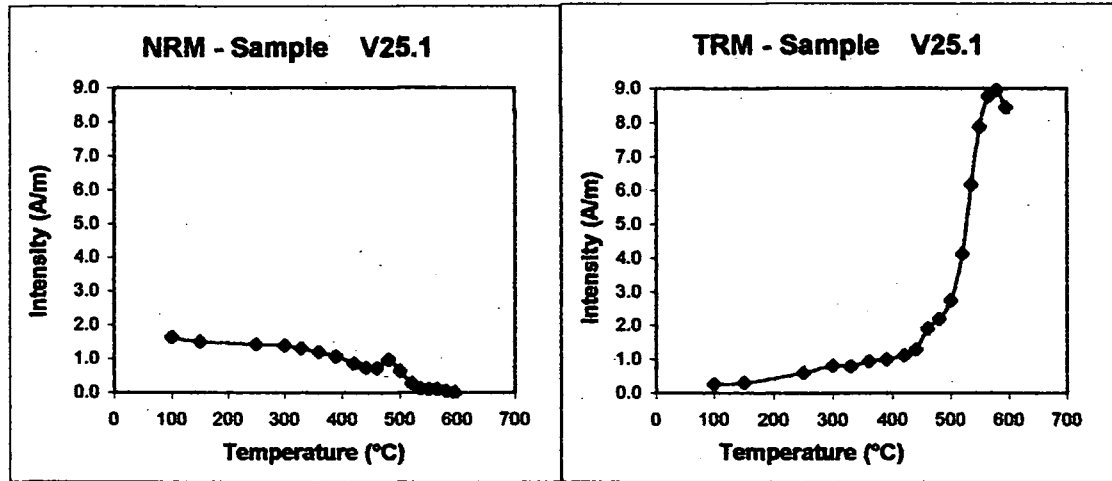
Fig. 6.70 - Site V25: a)NRM/TRM plot and respective values, b)NRM demagnetization and c)TRM acquisition curves.

Tab. 6.35 - Site V25: Palaeofields estimated and statistical parameters

AD 1806 sample V25.1

C-Demag2

D-pTRMck

Scale 200 mA/m

Scale 2000 mA/m

Mmax = 1620 mA/m

Mmax = 9190 mA/m

■ Lower
▲ Upper

Core
Coordinates
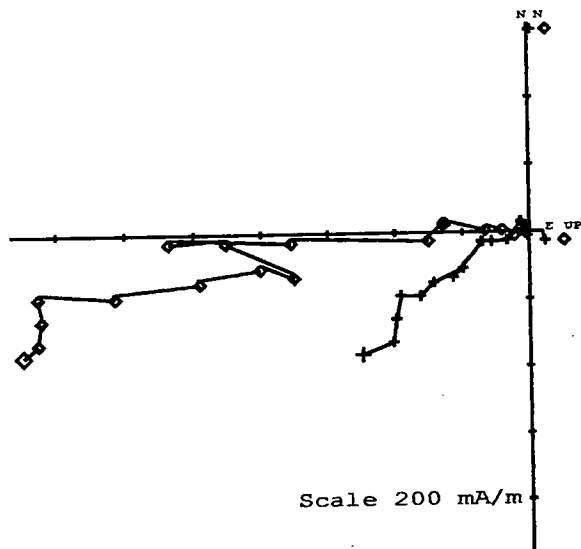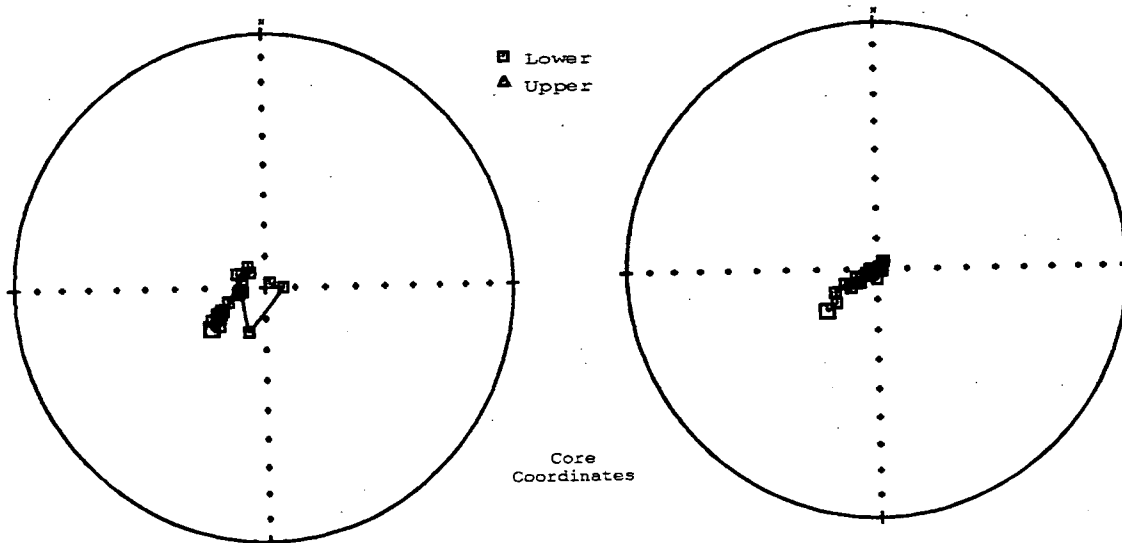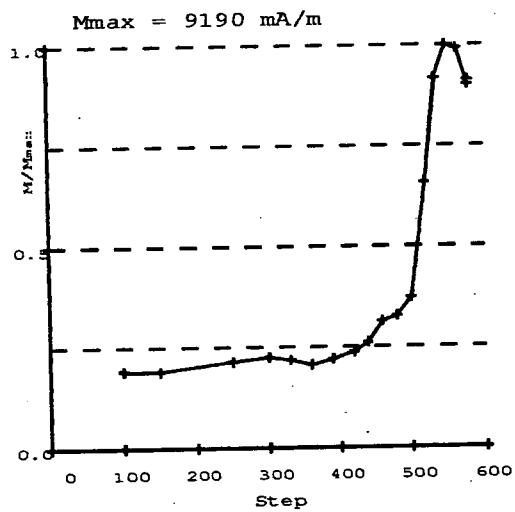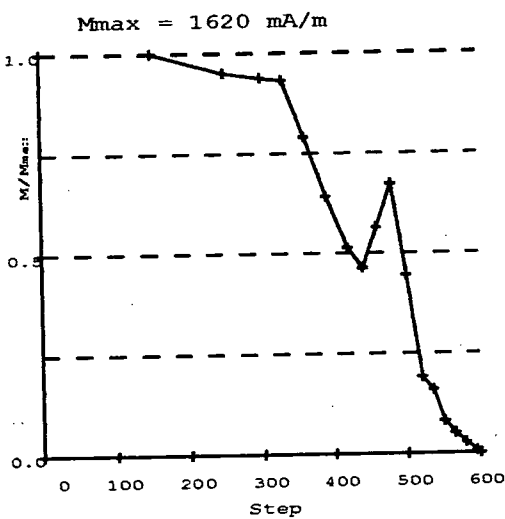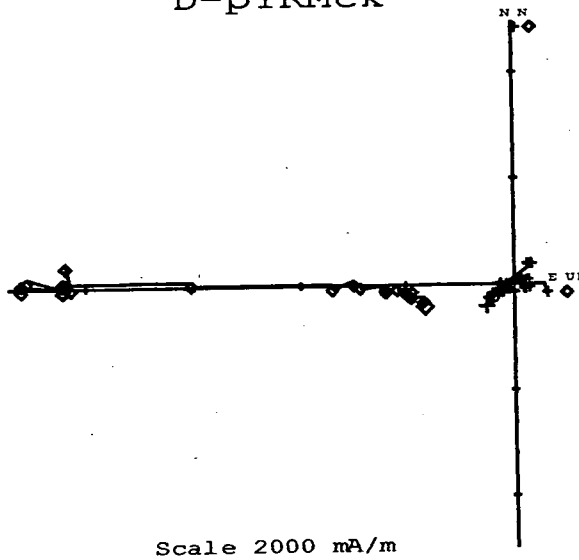
Fig. 6.71 - Site V25: Zijderveld diagrams, Intensity and stereo plots.

MTT (C-D)		
V25.1 steps	**NRM (A/m)**	**TRM (A/m)**
20	0.000	0.000
100	0.000	0.000
150	1.620	0.198
250	1.540	0.456
300	1.520	0.570
330	1.510	0.525
360	1.280	0.671
390	1.040	1.021
420	0.832	1.373
440	0.750	1.695
460	0.914	1.981
480	1.090	1.928
500	0.721	2.699
520	0.308	5.748
535	0.258	8.175
550	0.132	9.057
565	0.084	9.010
580	0.045	8.345
595	0.000	0.000

a)
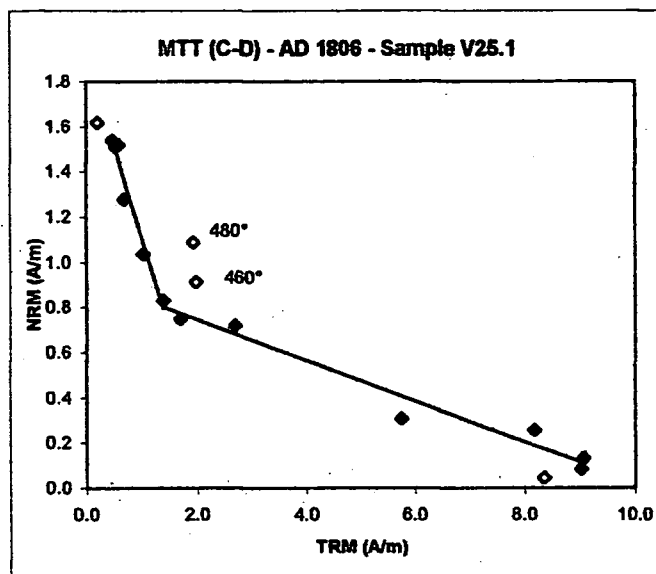
sample	Temp (°C)	N	f	g	q	b	R^2	Fpalaeo (μT)	σ_b
V25.1	250-420	6	0.437	0.692	3.114	-0.829	0.950	41.434	0.081
	*420-565	9	0.462	0.300	1.140	-0.111	0.968	5.549	0.013

* excluding 460,480
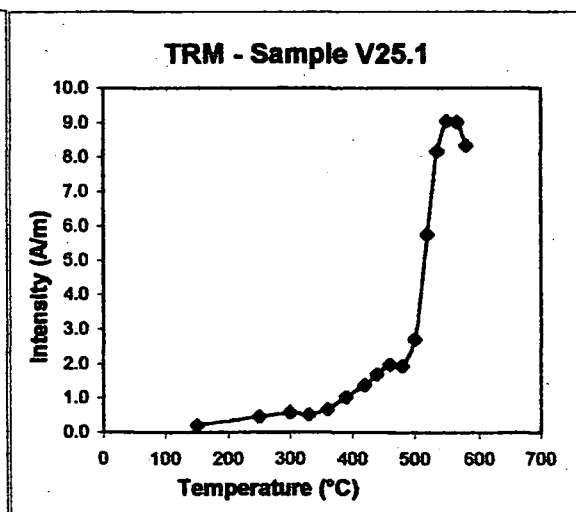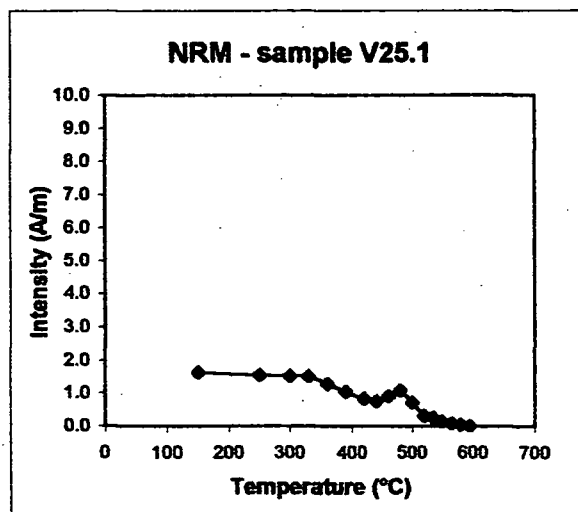
b)

c)

Fig. 6.72 - Site V25: a)NRM/TRM plot and respective values, b)NRM demagnetization and c)TRM acquisition curves.

Tab. 6.36 - Site V25: Palaeofields estimated and statistical parameters

AD 1839 sample V42.6b

A-Demag1

Scale 1000 mA/m

Mmax = 6590 mA/m

B-pTRM

Scale 1000 mA/m

Mmax = 5400 mA/m

☐ Lower
▲ Upper

Core
Coordinates
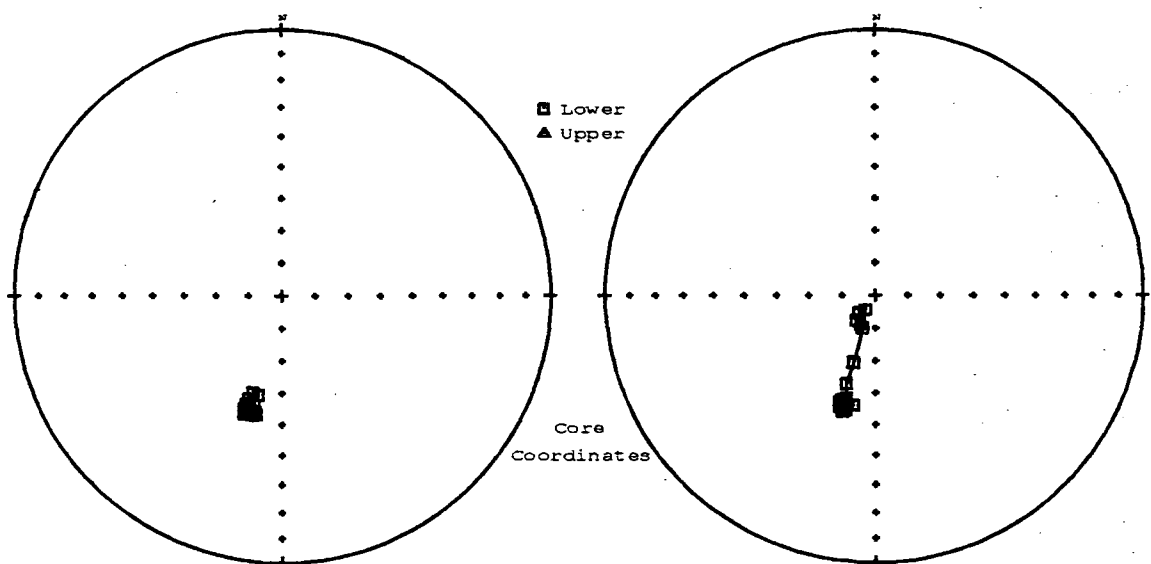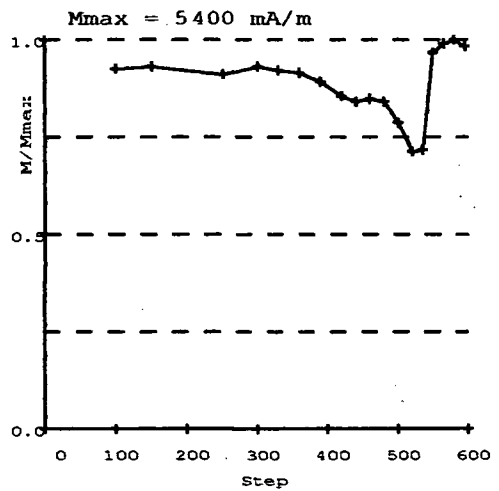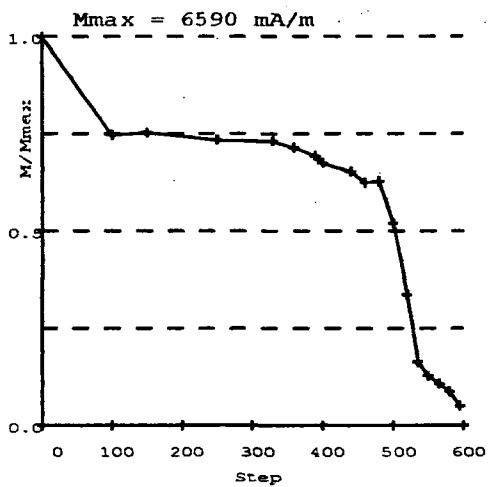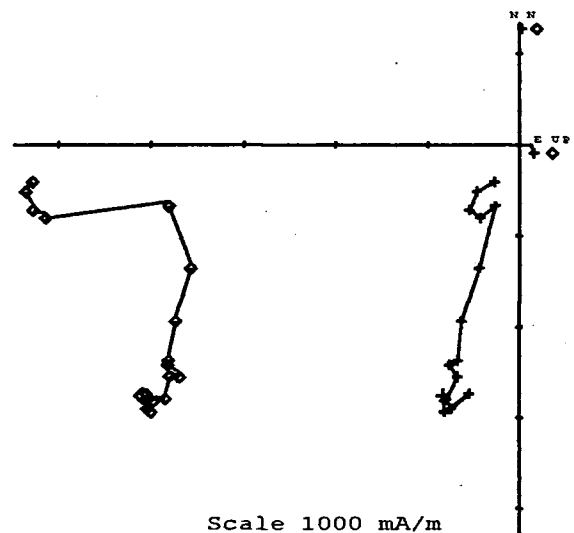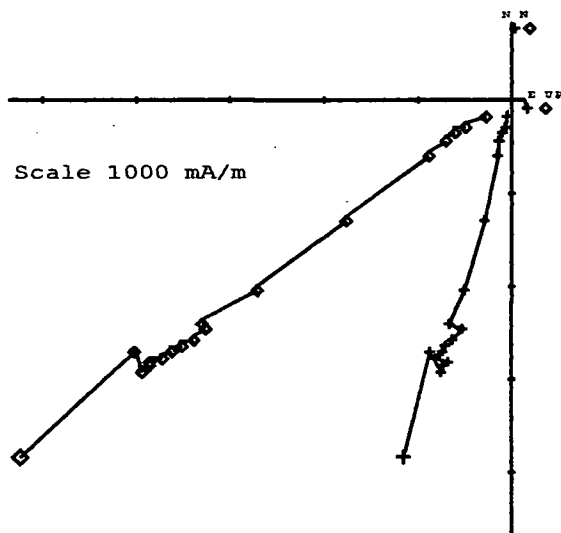
Fig. 6.73 - Site V42: Zijderveld diagrams, Intensity and stereo plots.

MTT (A-B)		
V42.6b	NRM	TRM
steps	(A/m)	(A/m)
20	6.590	0.000
100	4.960	0.238
150	4.920	0.243
250	4.840	0.285
300	4.830	0.207
330	4.820	0.224
360	4.710	0.259
390	4.570	0.251
420	4.450	0.307
440	4.300	0.312
460	4.110	0.610
480	4.130	0.519
500	3.420	1.048
520	2.210	1.816
535	1.080	2.929
550	0.841	4.457
565	0.709	4.699
580	0.576	4.884
595	0.329	5.021

a)
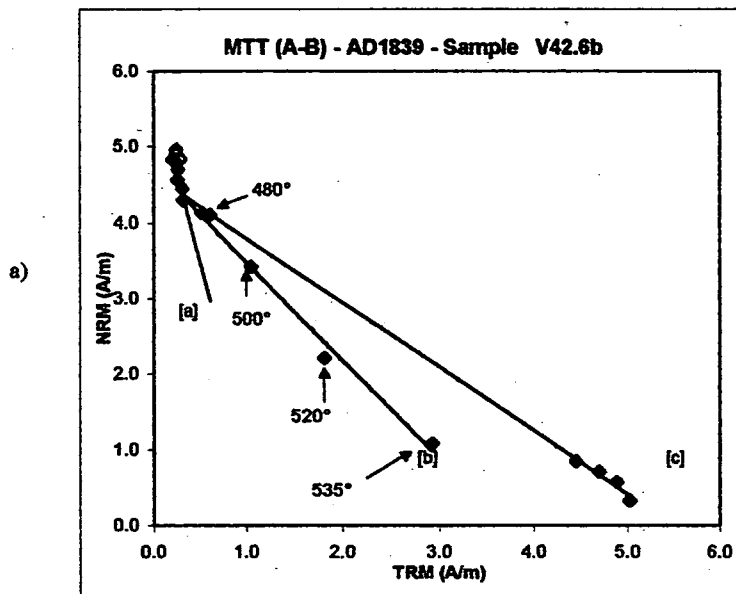
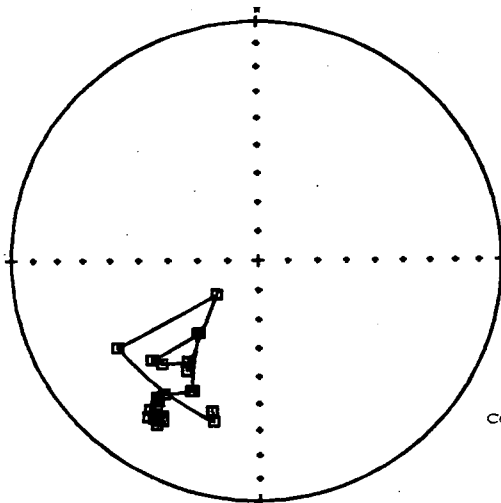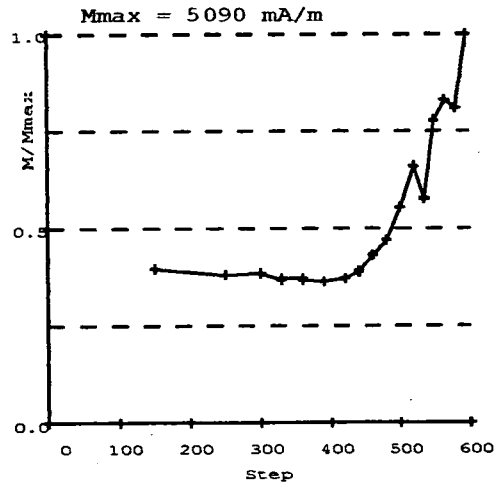| sample	Temp (°C)	N	f	g	q	b	R²	Fpalaeo (μT)	σ_b
V42.6b	[a] 300-440	6	0.080	0.755	0.356	-4.973	0.887	248.658	0.848
	[b] 440-535	6	0.489	0.683	7.027	-1.299	0.991	64.964	0.062
	[c] *420-595	7	0.625	0.362	16.448	-0.844	0.999	42.191	0.012

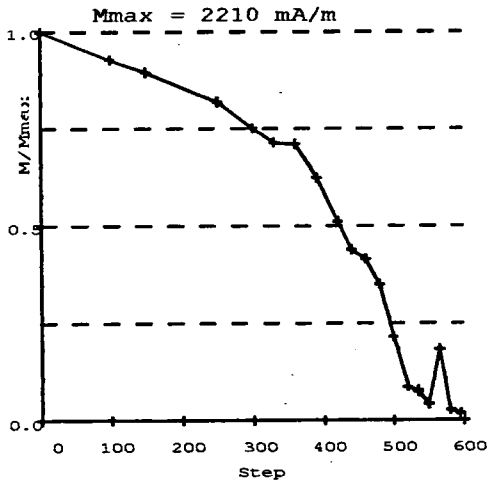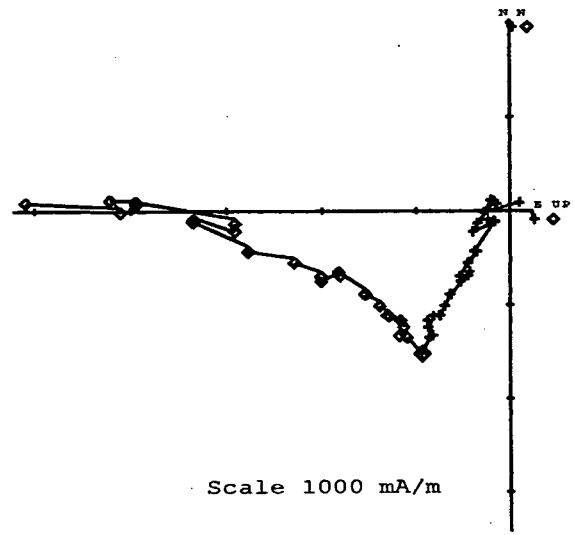*excluding 480,500,520,535

b)

c)
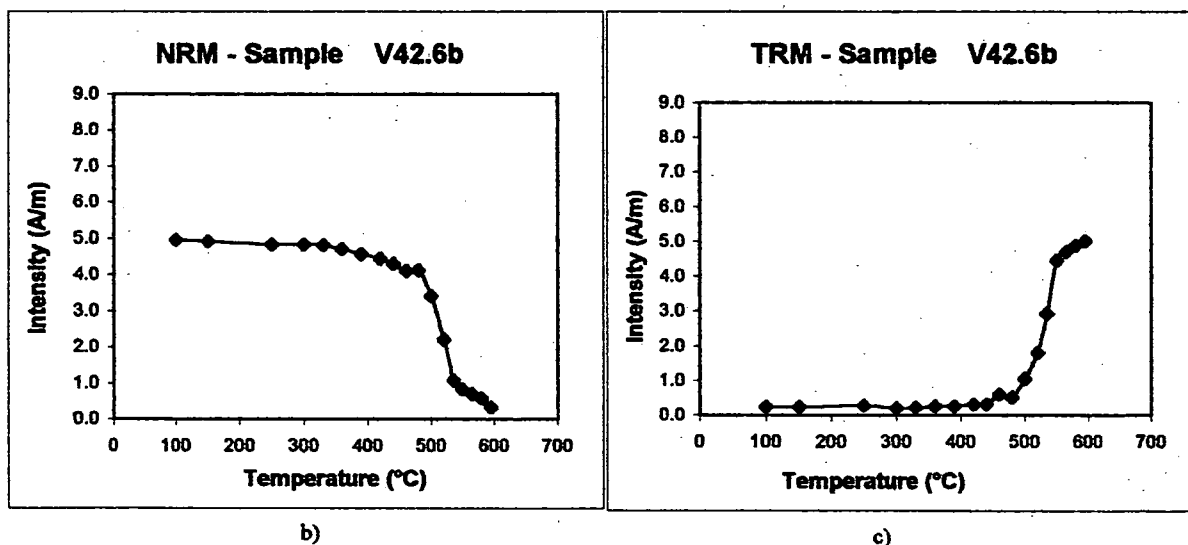
Fig. 6.74 - Site V42: a)NRM/TRM plot and respective values, b)NRM demagnetization and c)TRM acquisition curves.

Tab. 6.37 - Site V42: Palaeofields estimated and statistical parameters
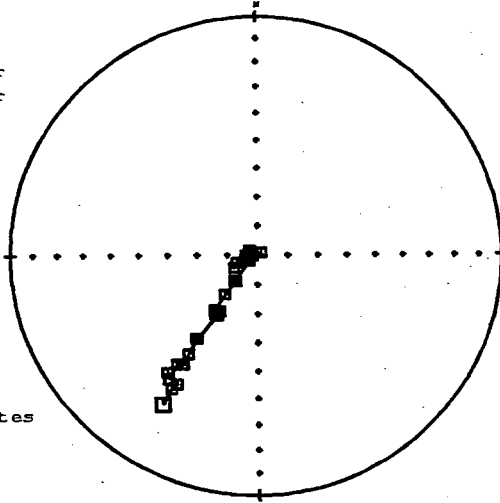
AD 1839 sample V42.6b

C-Demag2

Scale 1000 mA/m

Mmax = 4990 mA/m

D-pTRM

Scale 1000 mA/m

Mmax = 5320 mA/m

□ Lower
▲ Upper

Core
Coordinates
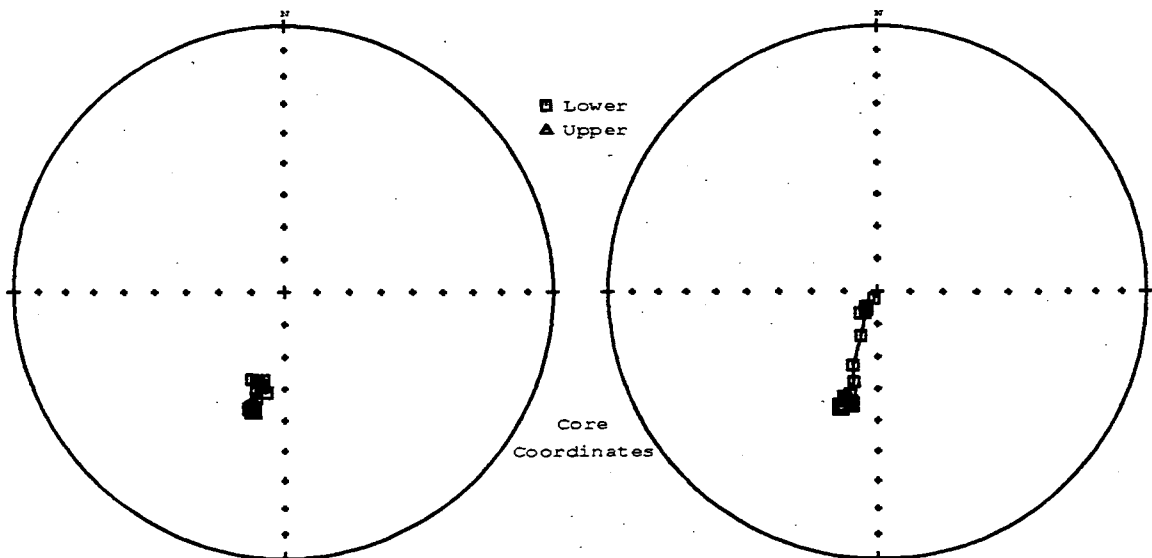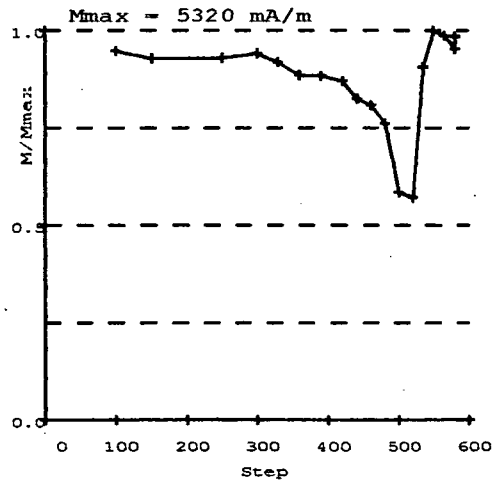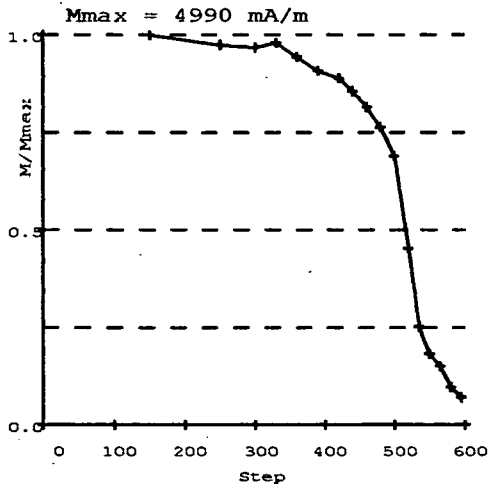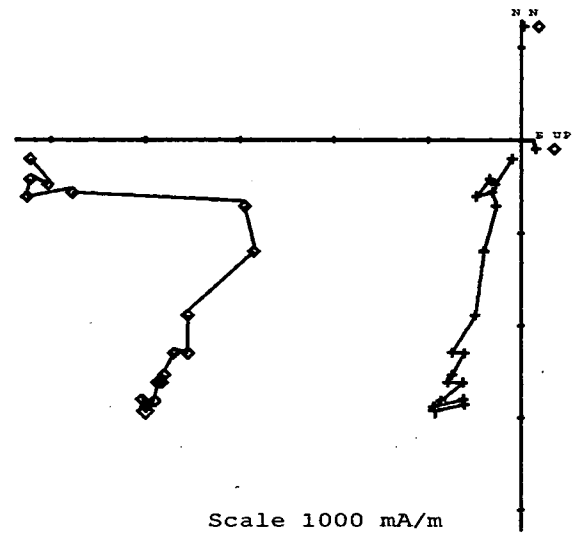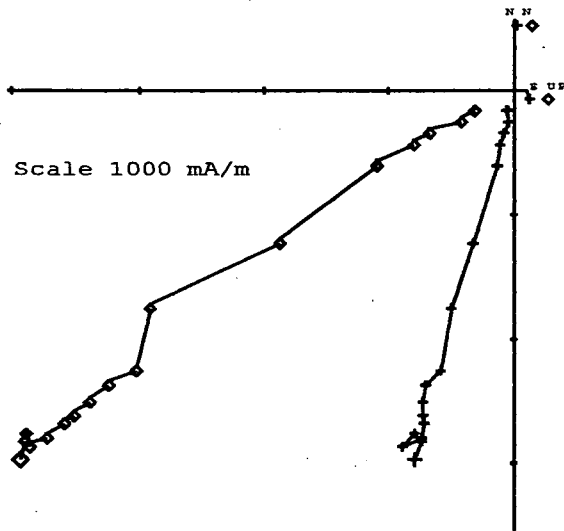
Fig. 6.75 - Site V42: Zijderveld diagrams, Intensity and stereo plots.

MTT (C-D)		
V42.6b	NRM	TRM
steps	(A/m)	(A/m)
20	0.000	0.000
100	0.000	0.000
150	4.990	0.222
250	4.860	0.186
300	4.830	0.220
330	4.890	0.078
360	4.710	0.261
390	4.530	0.265
420	4.440	0.303
440	4.270	0.396
460	4.070	0.329
480	3.810	0.654
500	3.440	0.567
520	2.260	1.191
535	1.260	3.686
550	0.909	4.492
565	0.751	4.570
580	0.486	4.814
595	0.000	0.000

a)
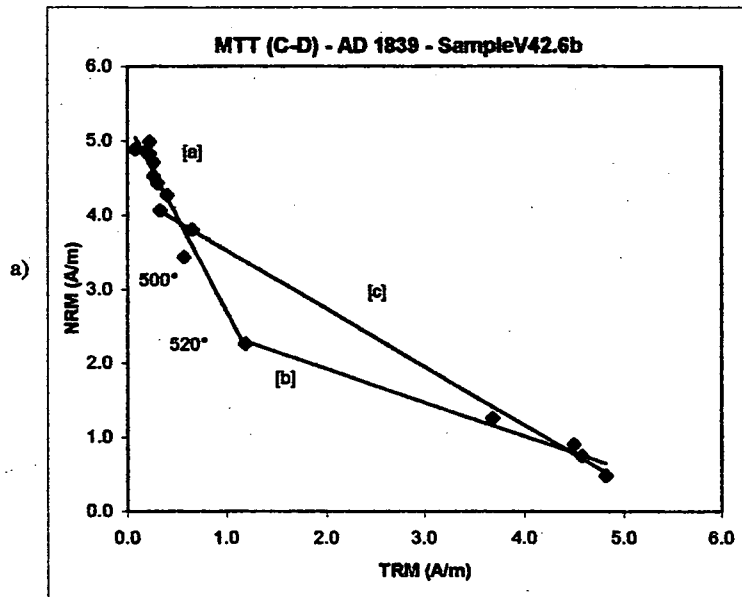
sample	Temp (°C)	N	f	g	q	b	R^2	Fpalaeo (μT)	σ_b
V42.6b	[a] 150-520	12	1.685	0.764	15.373	-2.637	0.931	131.861	0.221
	[b] 520-580	5	1.095	0.613	7.108	-0.462	0.973	23.097	0.044
	*[c] 460-580	6	2.212	0.472	36.186	-0.788	0.997	39.396	0.023

* excluding 500,520

b)

c)
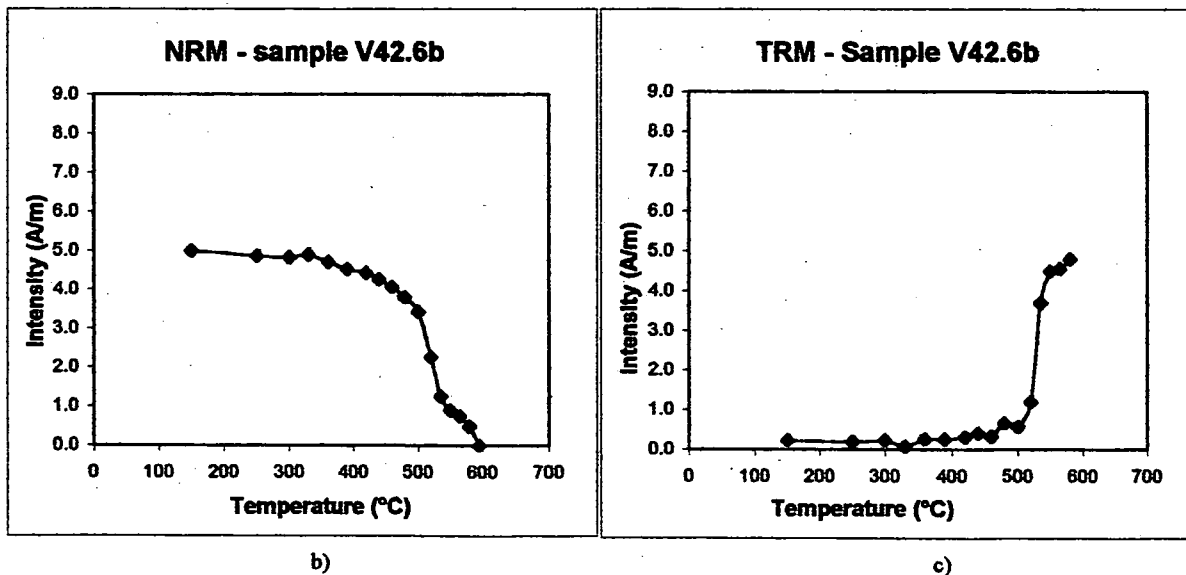
Fig. 6.76 - Site V42: a)NRM/TRM plot and respective values, b)NRM demagnetization and c)TRM acquisition curves.

Tab. 6.38 - Site V42: Palaeofields estimated and statistical parameters

261

AD 1839 sample V43.13b

A-Demag1

B-pTRM

Scale 1000 mA/m

Scale 1000 mA/m

Mmax = 6300 mA/m

Mmax = 5790 mA/m

▣ Lower
▲ Upper

Core
Coordinates
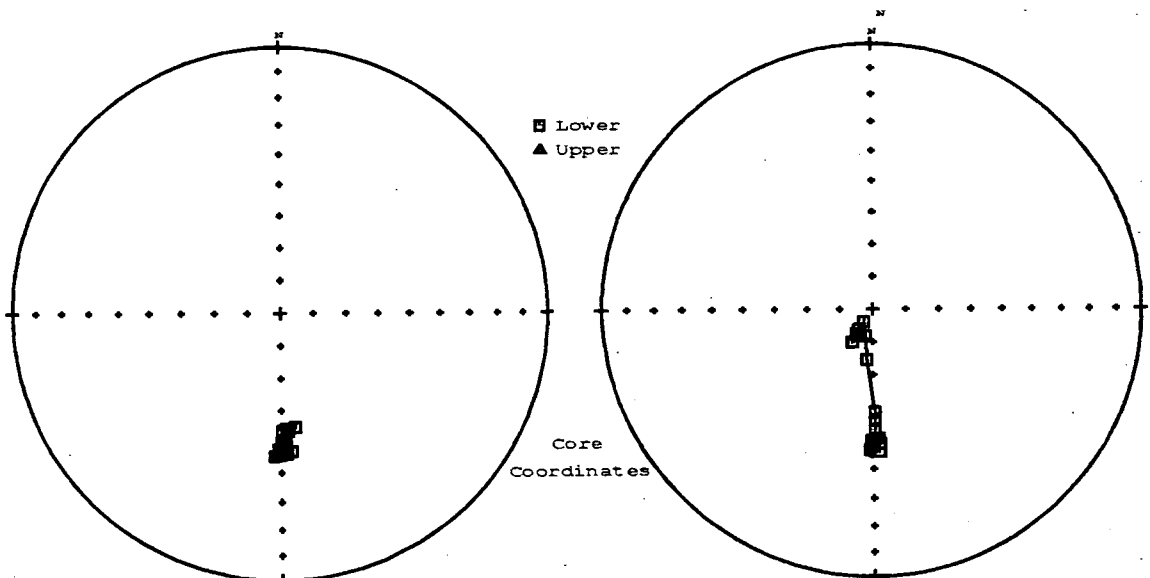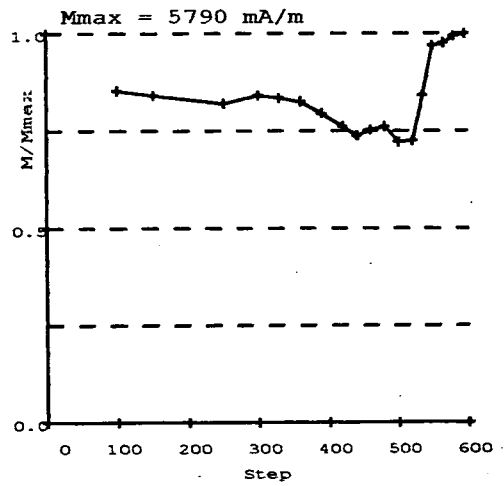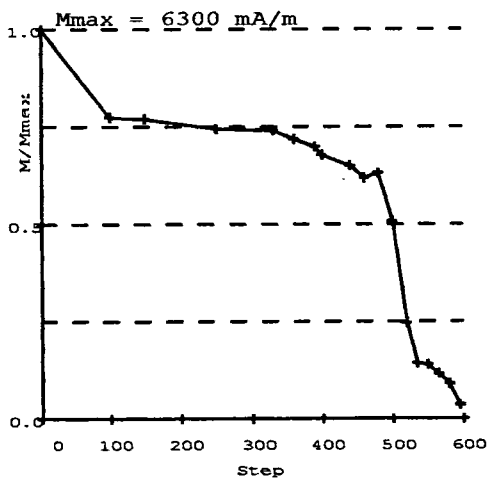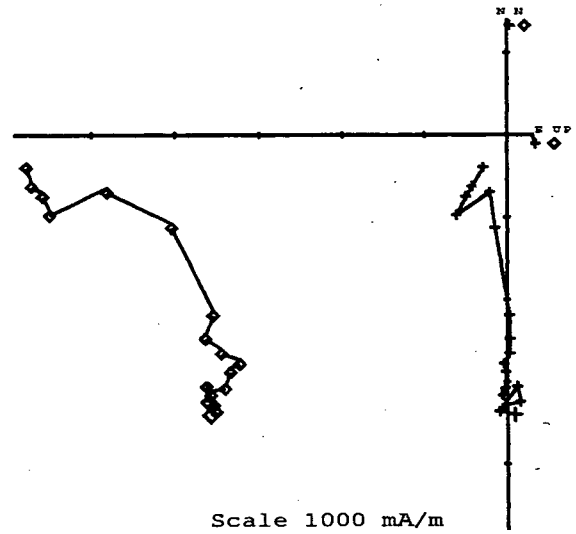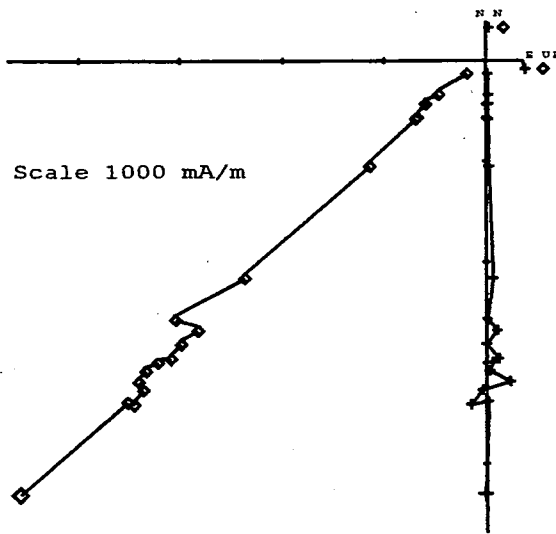
Fig. 6.77 - Site V43: Zijderveld diagrams, Intensity and stereo plots.

MTT (A-B)		
V43.13b	NRM	TRM
steps	(A/m)	(A/m)
20	6.300	0.000
100	4.880	0.097
150	4.850	0.098
250	4.690	0.378
300	4.680	0.307
330	4.670	0.299
360	4.530	0.277
390	4.400	0.228
420	4.270	0.296
440	4.100	0.250
460	3.900	0.632
480	3.980	0.607
500	3.200	1.183
520	1.550	2.906
535	0.899	4.138
550	0.876	4.876
565	0.730	5.019
580	0.573	5.264
595	0.224	5.595

a)

MTT (A-B) - AD1839 - Sample V43.13b
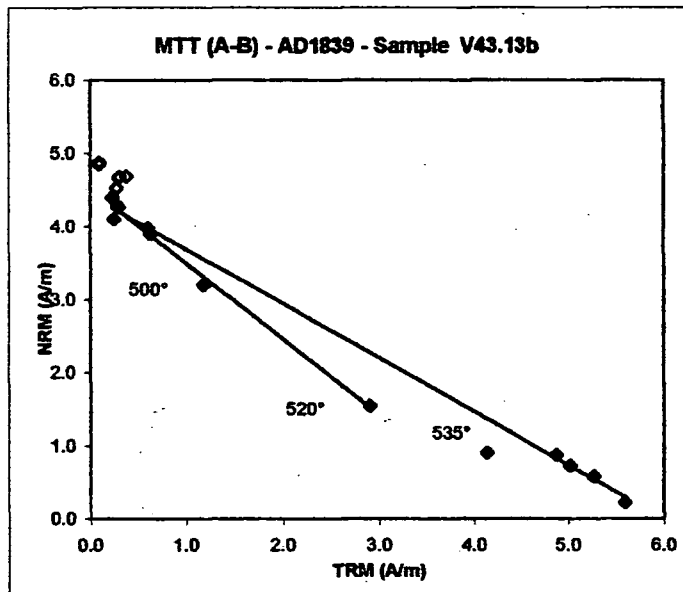
sample	Temp (°C)	N	f	g	q	b	R^2	Fpalaeo (μT)	σ_b
V43.13b	390-520	7	0.452	0.579	5.743	-1.039	0.990	51.940	0.047
	*390-595	9	0.663	0.433	16.932	-0.739	0.998	36.972	0.013

*excluding 500,520,535

NRM - Sample V43.13b

b)
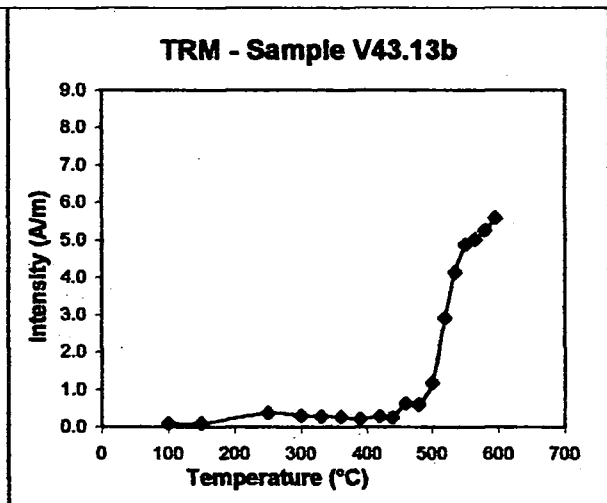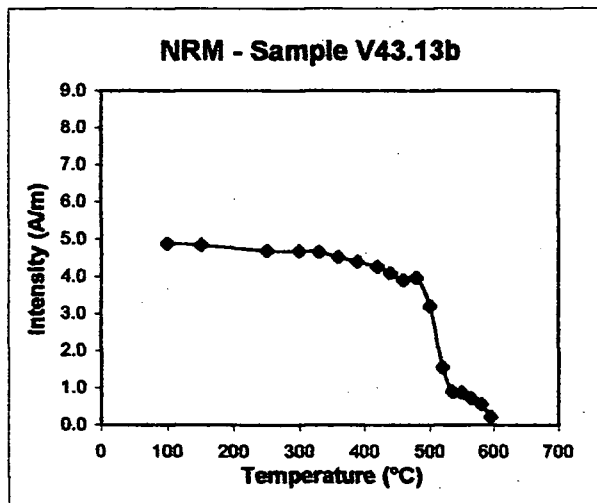

TRM - Sample V43.13b

c)

Fig. 6.78 - Site V43: a)NRM/TRM plot and respective values, b)NRM demagnetization and c)TRM acquisition curves.

**Tab. 6.39** - Site V43: Palaeofields estimated and statistical parameters

AD 1839 sample V43.13b

C-Demag2

Scale 1000 mA/m

D-pTRMck

Scale 1000 mA/m

Mmax = 4770 mA/m

Mmax = 5760 mA/m

🞑 Lower
▲ Upper

Core
Coordinates
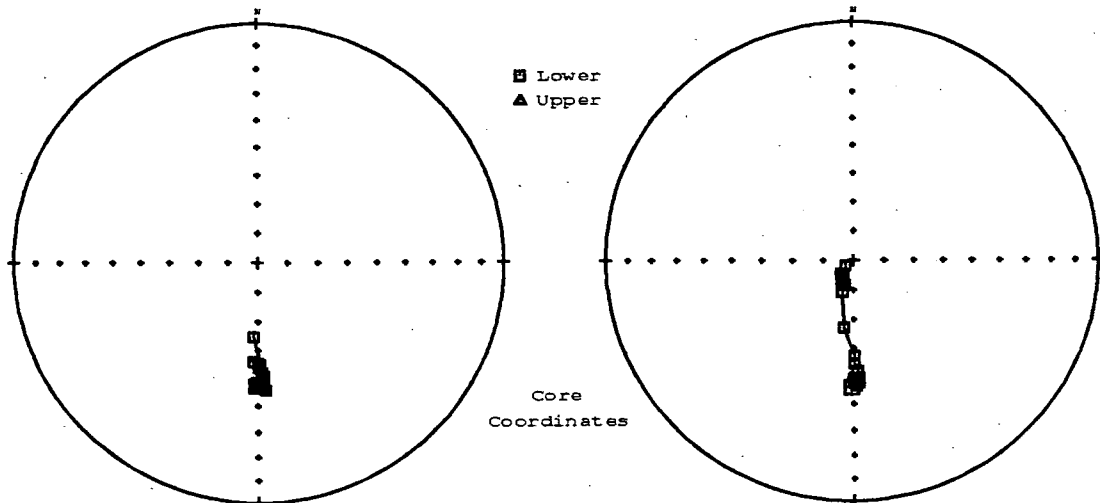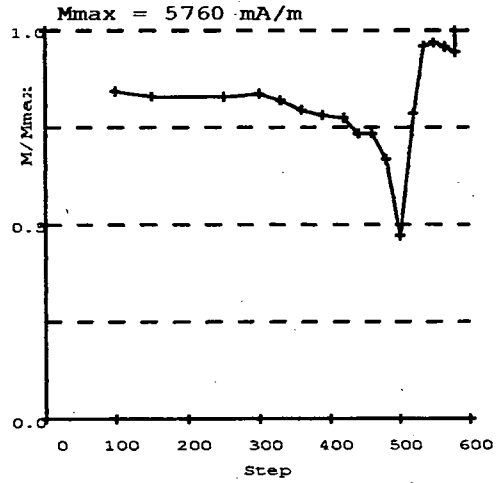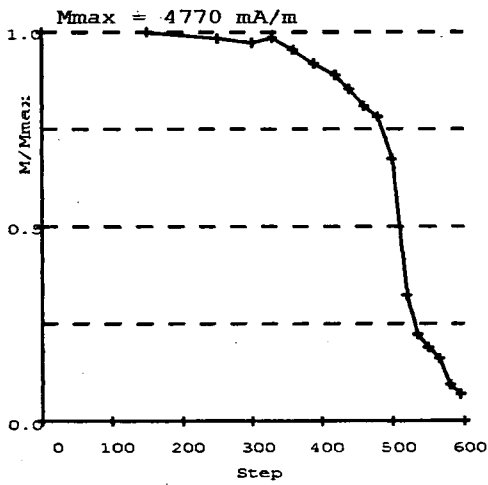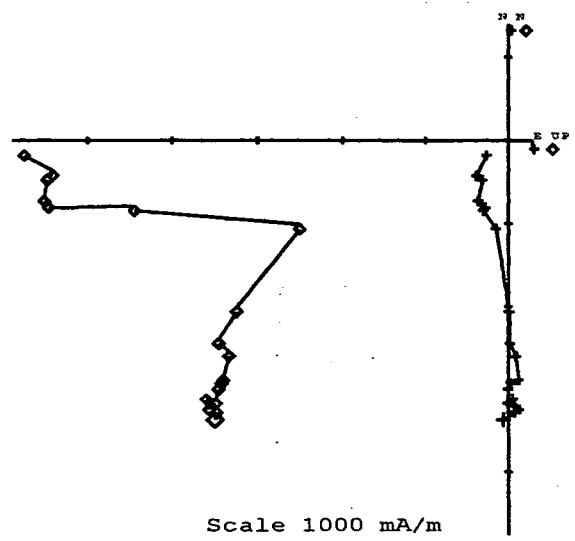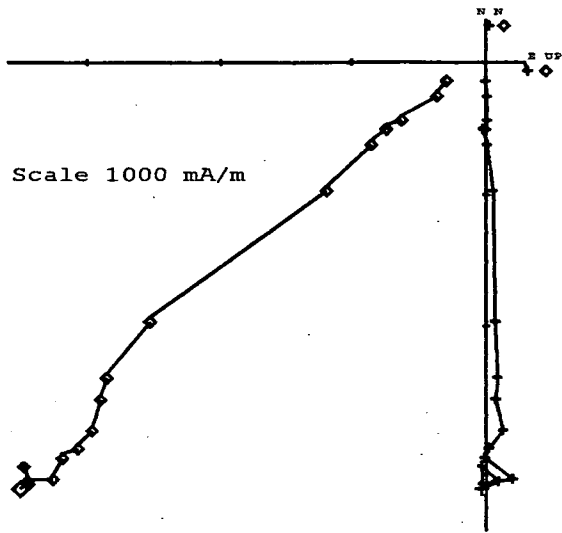
Fig. 6.79 - Site V43: Zijderveld diagrams, Intensity and stereo plots.

MTT (C-D)		
V43.13b	**NRM**	**TRM**
steps	(A/m)	(A/m)
20	0.000	0.000
100	0.000	0.000
150	4.770	0.112
250	4.690	0.164
300	4.640	0.257
330	4.700	0.056
360	4.550	0.323
390	4.380	0.251
420	4.240	0.345
440	4.070	0.421
460	3.860	0.568
480	3.730	0.515
500	3.210	0.927
520	1.540	3.266
535	1.060	4.621
550	0.901	4.795
565	0.768	4.863
580	0.446	5.396
595	0.000	0.000

a)

MTT (C-D) - AD 1839 - Sample V43.13b
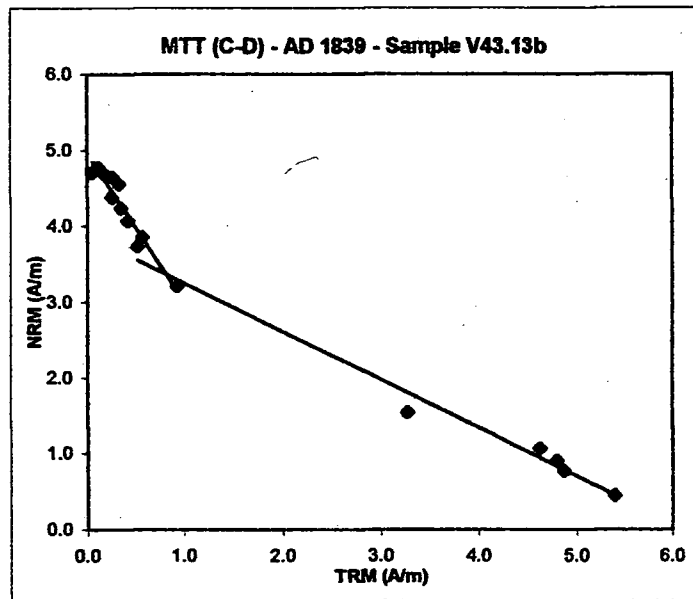
sample	Temp (°C)	N	f	g	q	b	R^2	Fpalaeo (μT)	σ_b
V43.13b	150-500	11	0.327	0.818	2.971	-2.012	0.996	100.580	0.181
	480-580	7	0.688	0.681	9.272	-0.643	0.984	32.144	0.033

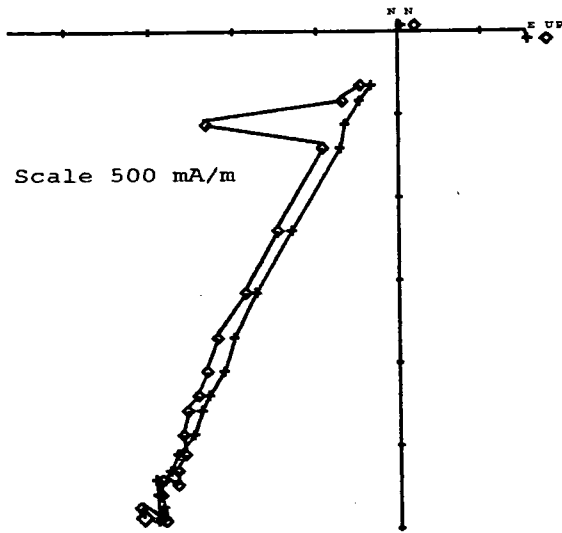NRM - sample V43.13b

TRM - Sample V43.13b
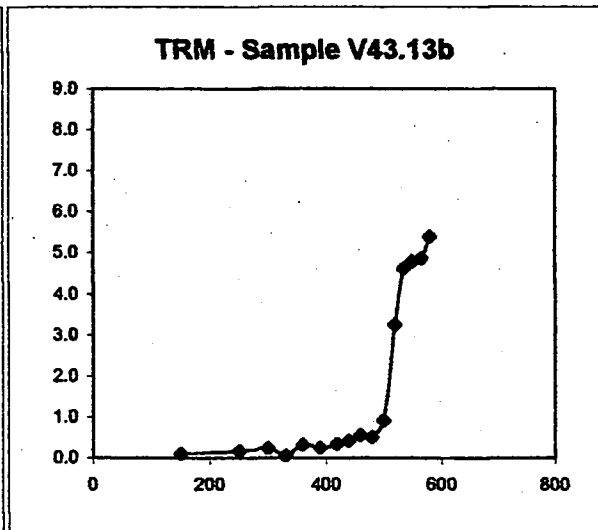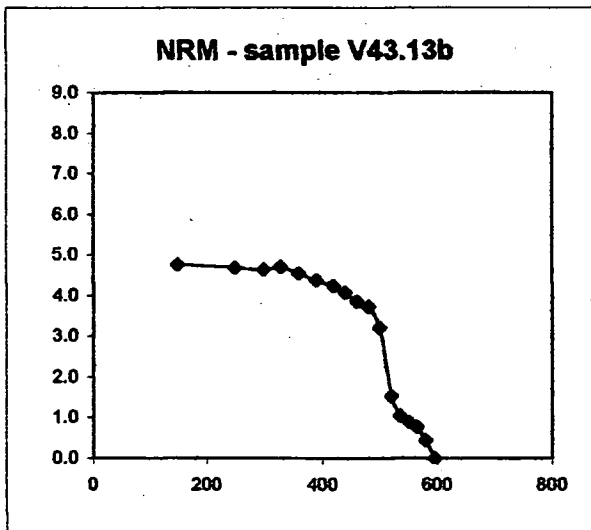
b)   c)

Fig. 6.80 - Site V43: a)NRM/TRM plot and respective values, b)NRM demagnetization and c)TRM acquisition curves.

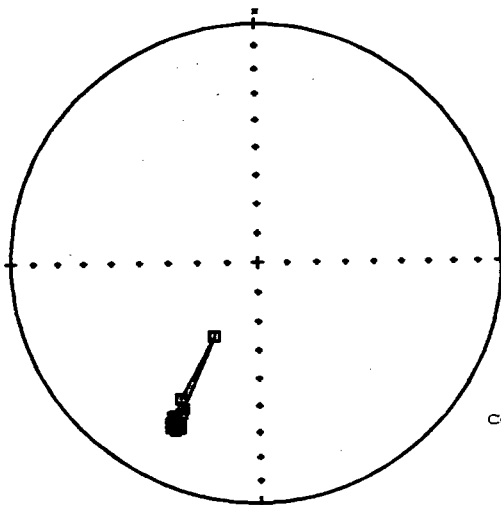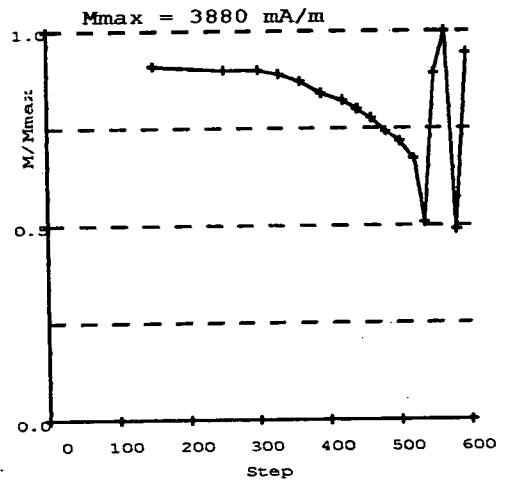**Tab. 6.40** - Site V43: Palaeofields estimated and statistical parameters

265

AD 1839 sample V44.6a

A-Demag1

B-pTRM

Scale 500 mA/m

N N

E UP

Scale 2000 mA/m

E UP

Mmax = 2350 mA/m

Mmax = 9300 mA/m

M/Mmax

M/Mmax

Step

Step

■ Lower
▲ Upper

Core
Coordinates
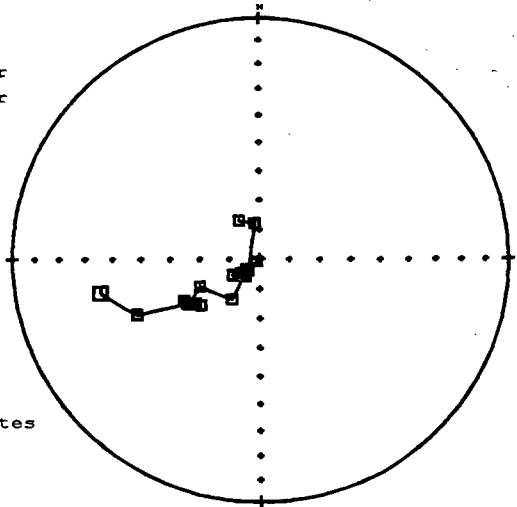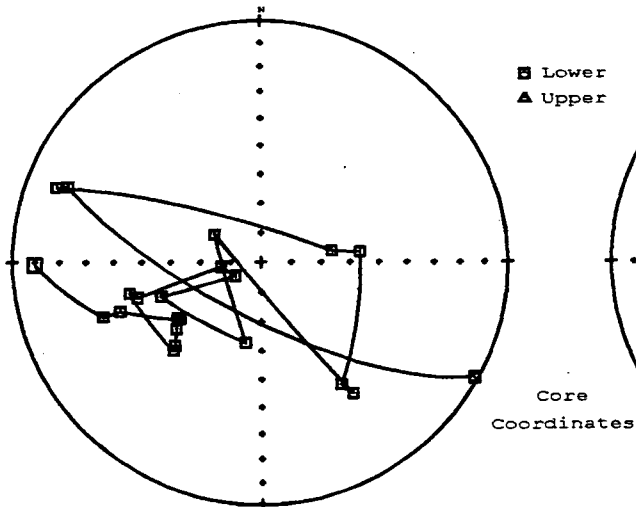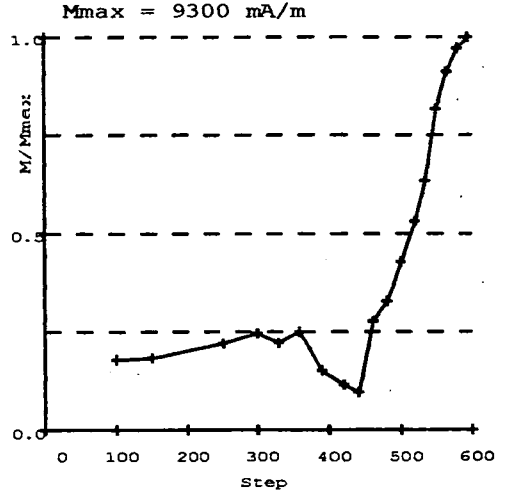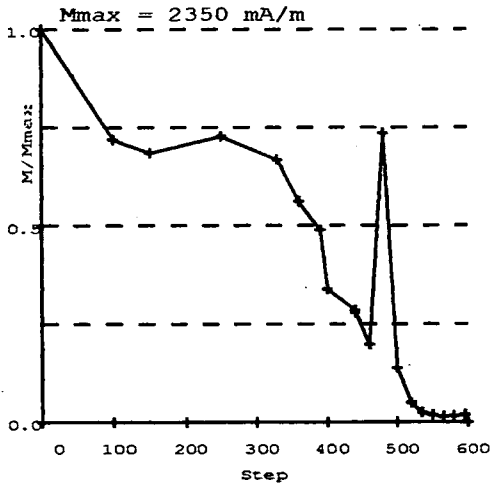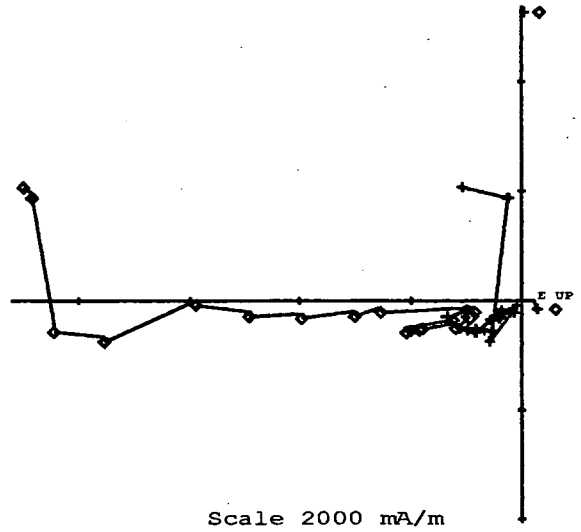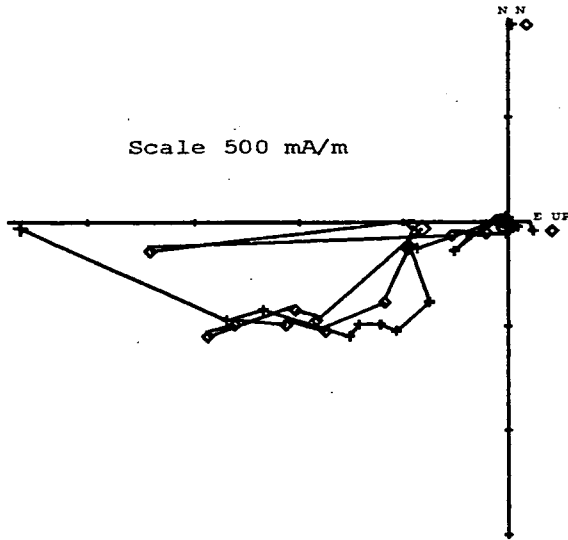
Fig. 6.81 - Site V44: Zijderveld diagrams, Intensity and stereo plots.

MTT (A-B)		
V44.6a	NRM	TRM
steps	(A/m)	(A/m)
20	2.350	0.000
100	1.690	0.179
150	1.610	0.204
250	1.710	0.372
300	1.640	0.751
330	1.570	0.558
360	1.320	1.055
390	1.150	0.398
420	0.795	0.457
440	0.654	0.483
460	0.464	2.106
480	1.730	1.317
500	0.325	3.705
520	0.117	4.834
535	0.058	5.837
550	0.042	7.568
565	0.032	8.453
580	0.035	9.022
595	0.042	9.306

a)

MTT (A-B) - AD1839 - Sample V44.6a
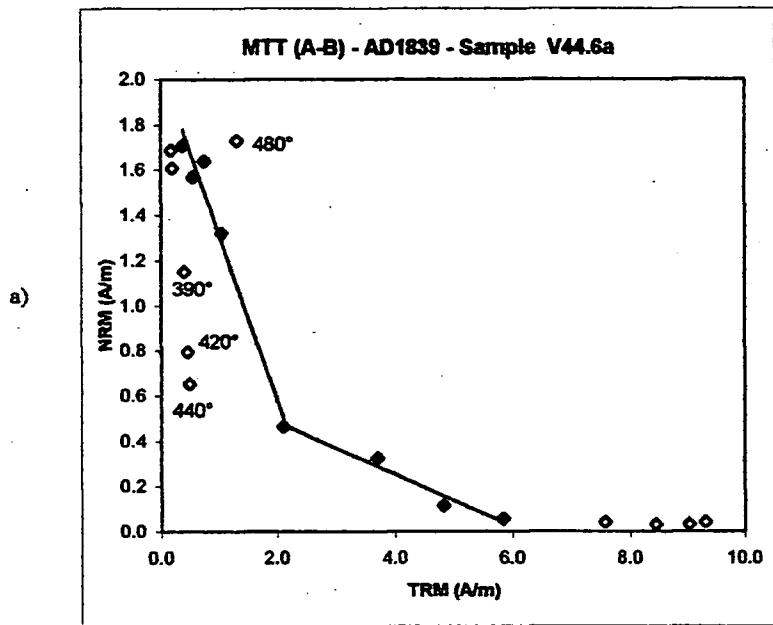
sample	Temp (°C)	N	f	g	q	b	R^2	Fpalaeo (μT)	σ_b
V44.6a	*250-460	5	0.530	0.481	2.483	-0.748	0.970	37.385	0.077
	**460-535	4	0.173	0.599	0.820	-0.117	0.968	5.864	0.015

*excluding 390,420,440
**excluding 480

NRM - Sample V44.6a
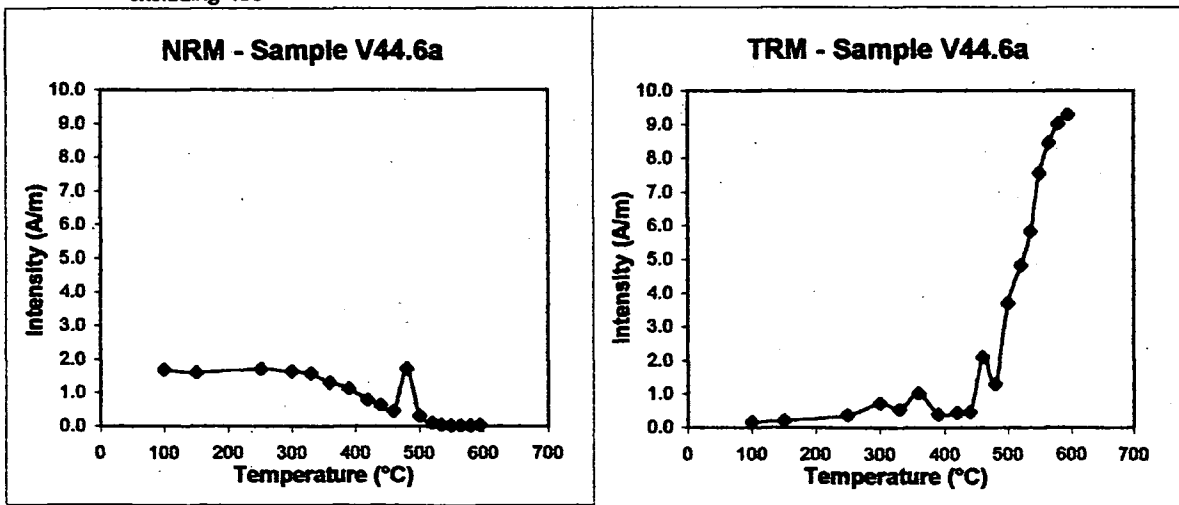
TRM - Sample V44.6a

b)

c)

Fig. 6.82 - Site V44: a)NRM/TRM plot and respective values, b)NRM demagnetization and c)TRM acquisition curves.

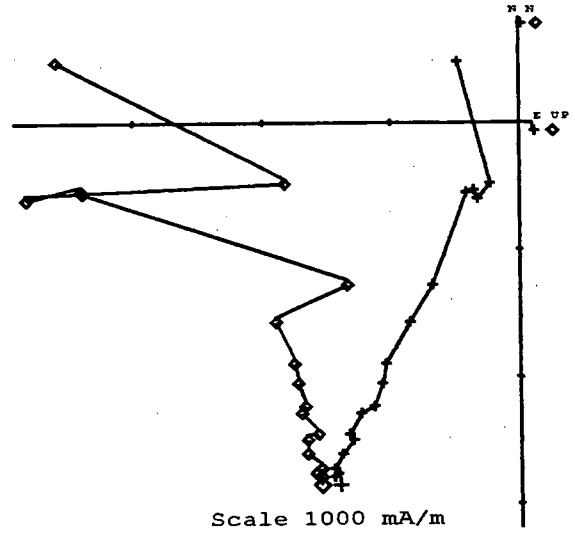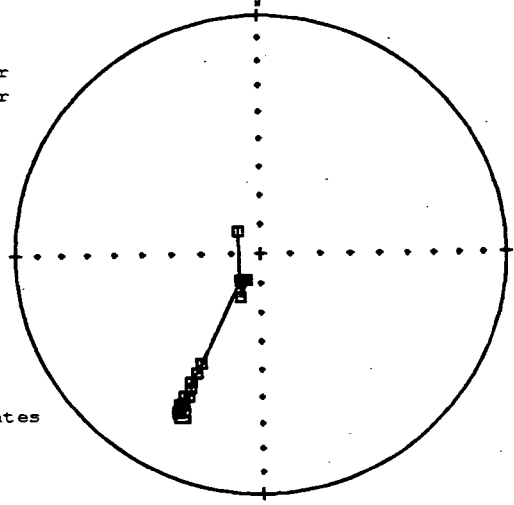Tab. 6.41 - Site V44: Palaeofields estimated and statistical parameters

267

C-Demag2   D-pTRMck

Scale 200 mA/m

Scale 5000 mA/m

Mmax = 1740 mA/m   Mmax = 9650 mA/m
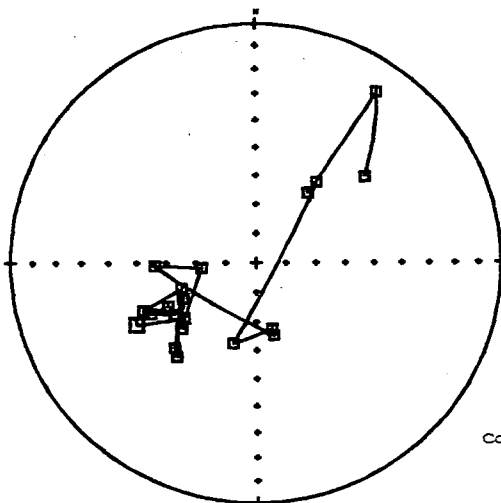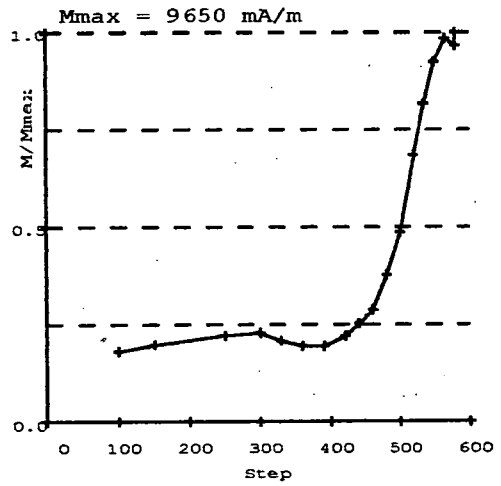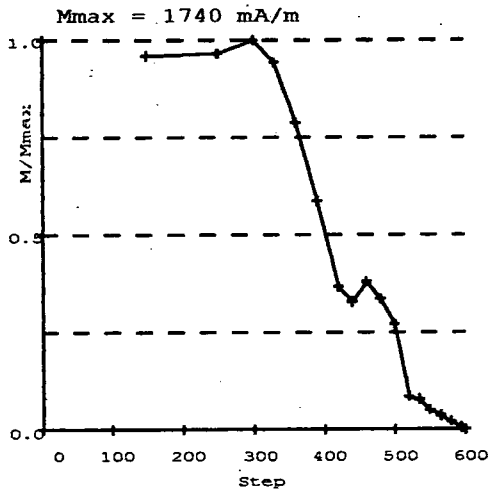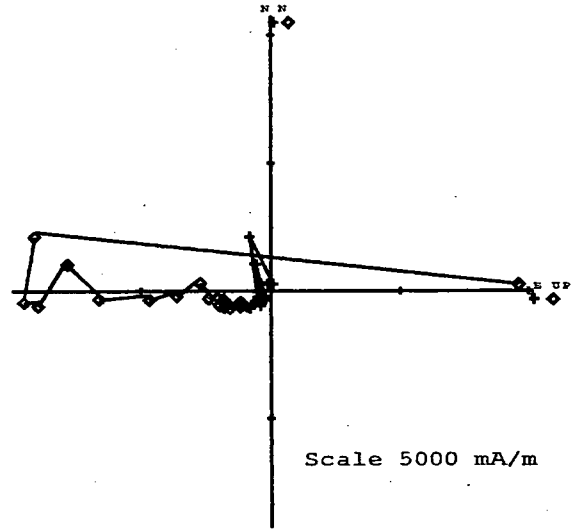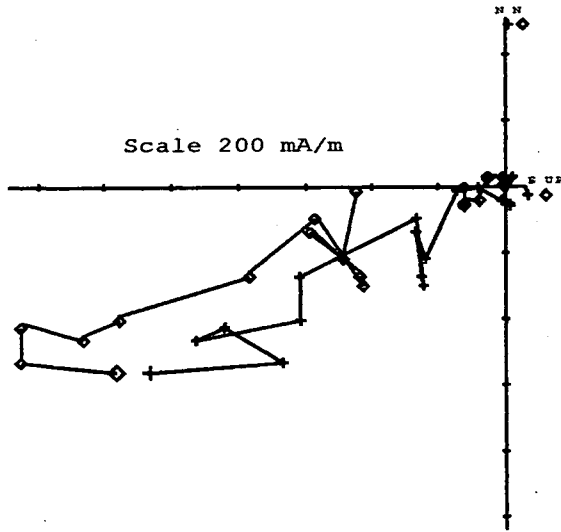
☐ Lower
▲ Upper
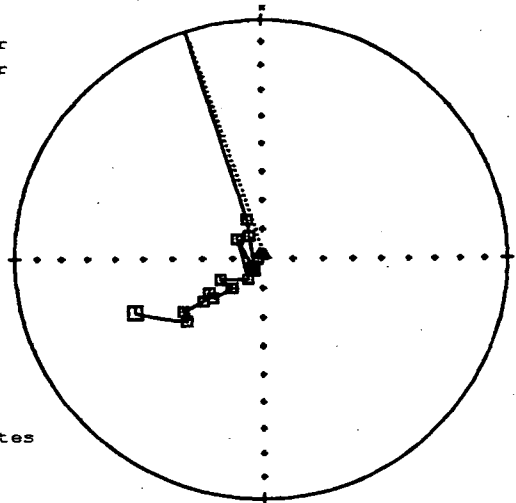
Core
Coordinates

Fig. 6.83 - Site V44: Zijderveld diagrams, Intensity and stereo plots.

MTT (C-D)		
V44.6a	NRM	TRM
steps	(A/m)	(A/m)
20	0.000	0.000
100	0.000	0.000
150	1.670	0.524
250	1.680	0.453
300	1.740	0.568
330	1.640	0.683
360	1.370	0.607
390	1.020	1.090
420	0.638	1.493
440	0.571	1.964
460	0.661	2.190
480	0.584	3.140
500	0.470	4.248
520	0.147	6.480
535	0.134	7.765
550	0.088	8.848
565	0.061	9.428
580	0.036	9.649
595	0.000	0.000

a)

MTT (C-D) - AD 1839 - Sample V44.6a
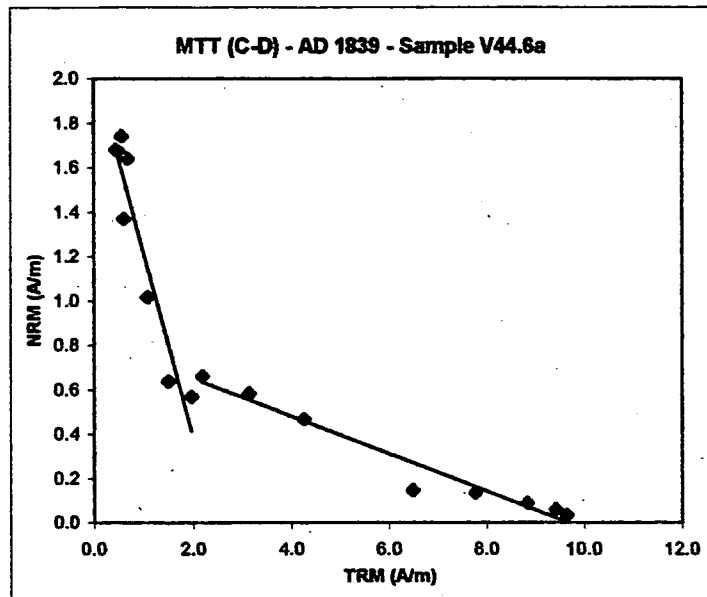
| sample	Temp (°C)	N	f	g	q	b	R^2	Fpalaeo (μT)	σ_b
V44.6a	150-440	8	0.658	0.702	3.670	-0.884	0.907	44.210	0.111
	480-580	8	0.375	0.676	2.884	-0.087	0.954	4.343	0.008

NRM - sample V44.6a

b)

TRM - Sample V44.6a
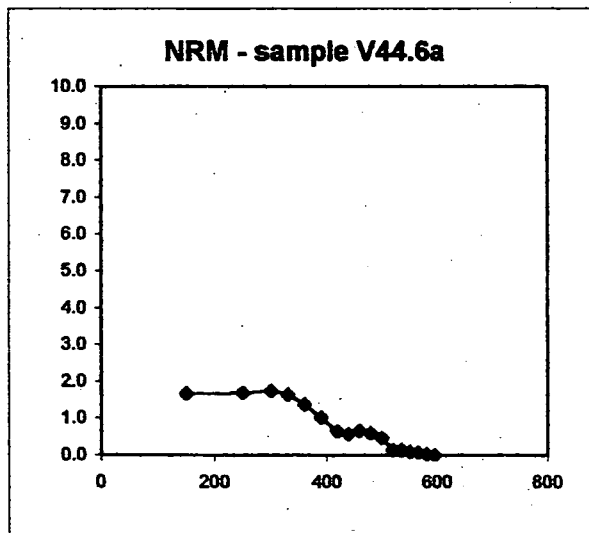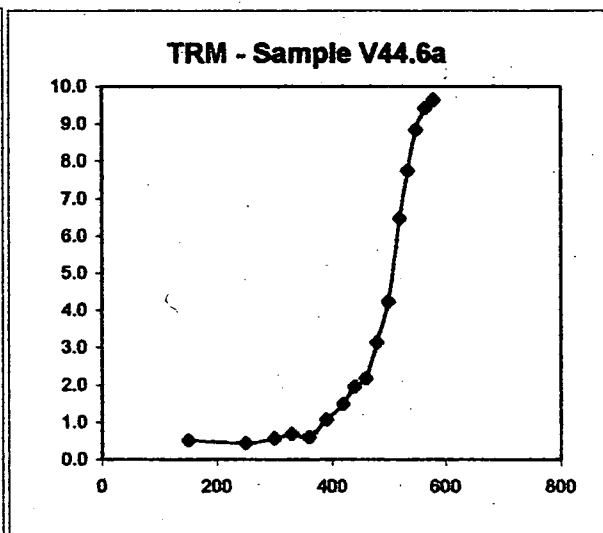
c)

Fig. 6.84 - Site V44: a)NRM/TRM plot and respective values, b)NRM demagnetization and c)TRM acquisition curves.

Tab. 6.42- Site V44: Palaeofields estimated and statistical parameters

Chapter VII

## Microwave Palaeointensity Properties

7.1 Introduction

In this chapter, the palaeointensity properties of samples submitted to microwave experiment will be discussed. As described in section 3.4b, the NRM direction is that obtained after few demagnetising step at low power, and in "the perpendicular field palaeointensity method" (Hill, 2000, Kono & Ueno, 1978; Hill & Shaw, 1999), the TRM was applied perpendicularly to the NRM vector. Consequently the total vector should swing completely through 90° from the direction of the NRM to the direction of the TRM. If the NRM direction does not change throughout the experiment, all the vector end points should define a single great circle which should go through the constant applied TRM direction (Dec=*"NRM Dec"*+ 90°; Inc=0°). The actual behaviour will be described, using stereo plots, and evaluated, using the angular difference Theta (θ) between NRM and TRM components. These parameters are evaluated using an Excel spreadsheet, lavadata.xls (Hill, 2000), where the total vector of magnetisation is decomposed into its NRM and TRM components using two different methods. All possible slopes, and therefore all the possible palaeofields, will be considered on the conventional NRM/TRM plots. Data points will be accepted if (1) they fell on a straight line, (2) θ = 90° and (3) the two vector decomposition methods give comparable values. Throughout, Coe's statistical parameters (Coe, 1978) will be given for each palaeofield estimate.

7.2 – AD 79 – AD 1631

7.2.1 – Site V30

The vector end points of sample V30.1–1 did not all lie on a great circle. The Dec at maximum power (188 W) was some 50° away from the initial value while the Inc had stayed almost constant (Fig.7.10a). NRM and TRM components, obtained after decomposing the total magnetization vector, and the angular difference (θ) between them are shown in Tab. 7.1. As suggested by the stereo plot θ was only constant during the first six steps which were used to estimate the palaeofield. (Fig. 7.1, Tab. 7.2). Theta increased progressively from M7 (105W) although its value was very close to 90° until the last two steps. One possible slope has been considered [a] but the fraction of total NRM used was very small. However, all the points excluded because, of $\theta > 90$ or because they did not fell on the great circle, still seemed to fell on the same straight line [b].

7.2.2 – Site V36

In sample V36.13-1 the final vector had its Dec value about 90° away from the NRM direction, but did not equate to the TRM direction nor did it lie on the same great circle defined by almost all the other vectors (Fig. 7.10b). Theta (Tab. 7.3) showed a constant value until the last two steps. The NRM/TRM plots showed one possible slope, excluding the last points (Fig. 7.2, Tab. 7.4).

7.2.3 – Site V37

In sample V37p8a-1 the Dec showed small changes until the last step when it jumped by about 90° from the initial NRM value. Although the total vector did not change much it still defined a great circle (Fig. 7.10b) and θ (Tab. 7.5) stayed constant until the last step when the NRM dropped drastically. The NRM/TRM plots showed one possible slope, even including the last point although it showed $\theta= 91.69°$ (Fig. 7.3, Tab. 7.6). [This because in the perpendicular field method used to analyse the microwave palaeointensity a larger error in θ seem to be admissible when the NRM component is small.]

7.2.4 – Site V27

Sample V27.10-1

Only five vectors defined a great circle (Fig. 7.10a) while the last three points, did not fell on it, as also showed by the θ value (Tab. 7.7). However the NRM/TRM plots showed one possible slope, even including the last points. Although the first point, D(NRM), seemed to be on the same straight line, including it to estimate the palaeofield (slope [b]), gave a quite different value (Fig. 7.4, Tab. 7.8).

Sample V27.10-2

The vectors defined two different great circles (Fig. 7.10a). At 75 W (step M6) the direction changed and the total vector moved away from the previous direction defining a different great circle. Theta (Tab. 7.9) was, in fact stable until 75 W, then it started to increase gradually (except the last point). The NRM/TRM plots showed one possible slope (a), excluding the points where θ was > 90°. The slope [b], which included also the D(NRM) showed a value comparable with [a] (Fig. 7.5,Tab. 7.10).

7.2.5 – Site V33

In sample V33.12-1 the vector did not define a unique great circle (Fig. 7.10b). At 27 W (point n°9) the total vector moved to define a different great circle. Theta (Tab. 7.11) was, in fact stable until that point, after which it started to change gradually (except the last two points). The NRM/TRM plots showed one possible slope, excluding the points where θ was > 90° (Fig. 7.6, Tab. 7.12).

7.2.6 – Site V26

On the stereo projection, the vector end point of the total magnetization of sample V26.6b-1 defined a perfect great circle. It swung from the direction of the NRM through 90° to the direction of the TRM (Fig. 7.10a). The angular difference between the two directions stayed

272

very constant throughout the experiments (Tab. 7.13). Although a stable NRM direction can be hypothesised, something occurred at about 42/46W as the NRM/TRM plots showed a break on the straight line and two slopes were identified. Therefore two different values of the estimated palaeofield were considered (Fig. 7.7, Tab. 7.14).

7.2.7 – Site V31

Sample V31.5-1 & V31.5-2

For both samples the vectors defined a great circle (Fig. 7.10a) except for the last five points. The θ values also stayed almost constant for the first 5/7 steps then increased progressively until the last 2 steps (Tabs. 7.15,17). The NRM/TRM plots showed one possible slope excluding the last points (even excluding some which had θ slightly $> 90°$) (Figs 7.8,9, Tabs. 7.16,18). In sample V31.5-2 the first point D(NRM) was also considered because it fell on the same straight line defined by the other points.

Sample V30.1-1		Arbitrary Units						
Steps	Power (W)	x	y	z	Moment	Nrm 10³	Trm 10³	theta (°)
D (NRM)	50	-42650	-50010	-90460	111816.97	117.61	0.00	
M1	58	-41960	-50710	-89950	111459.18	111.45	1.05	90.04
M2	65	-41480	-50700	-90030	111339.49	111.33	1.34	90.01
M3	75	-38170	-51360	-87840	108676.88	108.59	4.28	90.01
M4	82	-32420	-51970	-85820	105437.23	105.05	9.17	90.07
M5	88	-31110	-51050	-84150	103223.82	102.79	9.61	90.09
M6	95	-29450	-50760	-82240	101031.17	100.48	10.66	90.08
M7	105	-29030	-50380	-82470	100906.82	100.35	10.83	90.14
M8	118	-20430	-48350	-75180	91690.46	90.31	16.26	90.28
M9	128	-19110	-46220	-74010	89325.03	87.98	16.25	90.53
M10	140	-16920	-45290	-72240	86925.76	85.35	17.47	90.65
M11	150	-14120	-43570	-69950	83610.54	81.76	18.84	90.92
M12	160	-11960	-42310	-67690	80716.25	78.62	19.82	91.07
M13	170	-9430	-40600	-65850	77932.71	75.56	21.09	91.46
M14	188	6430	-33550	-53500	63475.96	57.72	30.25	93.57

Tab. 7.1 - V30.1-1:Values of NRM lost and TRM gained and their angular difference θ.
In light grey the data used to calculate the palaeointensity.

Microwave - AD 79 - 1631- Sample V30.1-1

[a] $R^2 = 0.954$

[b]

Fig. 7.1 - Conventional NRM/
TRM plot for sample V30.1-1
Statistical parameters relative to the
slope and palaeofield estimate are
shown in Tab.7.2. Empty diamond
indicate points excluded from the
palaeofield calculation.

Power	Sample V30.1-1							
range (W)	N	f	g	q	b	σb	Fpalaeo (µT)	Uncertainty
[a] 58 - 95	6	0.093	0.747	0.646	-1.054	0.114	52.681	81.569

Tab. 7.2 - V30.1-1 palaeointensity values and statistical parameters.

Fpalaeo calculated within a range of power applied with the following statistical parameters.
N = number of points used.   f = fraction of the total NRM used.
g = gap value e.g. uniformity along x-axis.
q = index of quality of palaeointensity values. uncertainty of palaeointensity values
b = slope. R^2 = correlation coefficient.   σb = standard error of the slope.
For a complete description, see section 3.4b

Sample V36.13-1		Arbitrary Units						
Steps	Power (W)	x	y	z	Moment	Nrm 10³	Trm 10³	theta (°)
D (NRM)	42	-54590	145140	55870	164824.59	175.21	0.00	
M1	50	-63580	134360	52400	157609.60	157.14	12.24	90.02
M2	58	-64250	134180	52440	157741.21	157.21	12.93	90.02
M3	72	-65530	116020	49150	142023.04	140.54	20.55	90.03
M4	85	-70950	82720	40010	116091.78	109.94	37.40	90.07
M5	95	-74030	21970	27100	81838.45	53.93	62.32	90.82
M6	98	-37950	-16580	22510	47135.96	24.36	50.42	111.85

Tab. 7.3 - V36.1-1:Values of NRM lost and TRM gained and their angular difference θ.
In light grey the data used to calculate the palaeointensity.

Fig. 7.2 - Conventional
NRM/ TRM plot for sample
V36.13-1
Statistical parameters
relative to the slope and
palaeofield estimate are
shown in Tab.7.4. Empty
diamond indicate points
excluded from the
palaeofield calculation.

Power	Sample V36.13-1							
range (W)	N	f	g	q	b	σ_b	Fpalaeo (μT)	Uncertainty
50 - 85	4	0.269	0.455	4.156	-1.903	0.056	95.157	22.899

Tab. 7.4 - V36.13-1 palaeointensity values and statistical parameters.

| Sample V37.8a-1 | | Arbitrary Units | | | | | | |
Steps	Power (W)	x	y	z	Moment	Nrm 10³	Trm 10³	theta (°)
D (NRM)	33	-149210	35460	-1E+05	185280.10	196.35	0.00	
M1	37	-148630	28600	-1E+05	183614.92	183.50	6.65	90.04
M2	42	-146750	27370	-1E+05	181582.22	181.44	7.55	90.08
M3	50	-141150	20910	-97840	173012.19	172.57	12.35	90.03
M4	60	-135910	16470	-94880	166568.31	165.85	15.56	90.06
M5	72	-124130	1520	-84580	150214.33	147.73	27.30	90.04
M6	85	-113930	-7450	-78510	138561.78	134.43	33.80	90.10
M7	98	-107640	-8130	-74060	130909.70	126.73	32.99	90.10
M8	108	-29210	-84120	-18080	90864.10	20.19	89.19	91.69

Tab. 7.5 - V37.8a-1:Values of NRM lost and TRM gained and their angular difference θ.
In light grey the data used to calculate the palaeointensity.

Microwave - AD 79 - 1631- Sample V37.8a-1

$R^2 = 0.997$

NRM x 10³ (Arbitrary Units)

TRM x 10³ (Arbitrary Units)
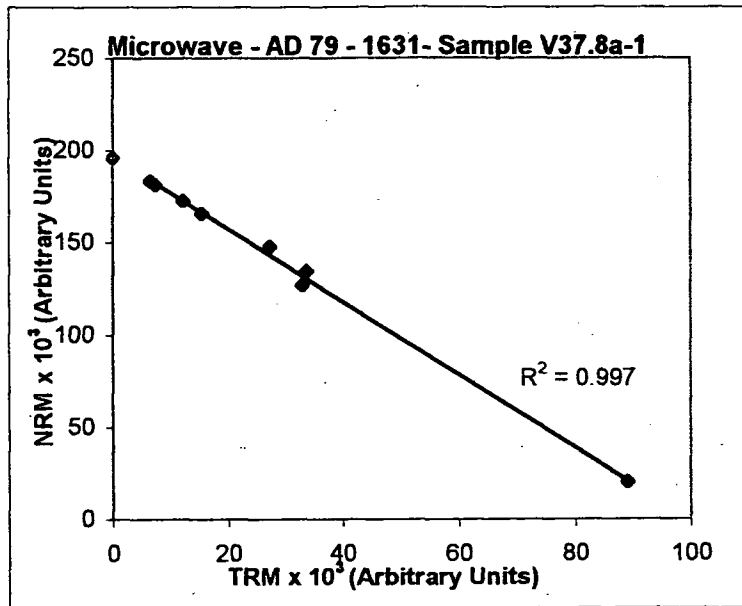
Fig. 7.3 - Conventional NRM/TRM plot for sample V37.8a-1 Statistical parameters relative to the slope and palaeofield estimate are shown in Tab.7.6. Empty diamond indicate points excluded from the palaeofield calculation.

Power range (W)	N	f	g	q	b	σ_b	Fpalaeo (μT)	Uncertainty
							Sample V37.8a-1	
33 - 98	8	0.832	0.548	19.429	-1.982	0.047	99.094	5.100

Tab. 7.6 - V37.8-1 palaeointensity values and statistical parameters.

Sample V27.10-1		Arbitrary Units						
Steps	Power (W)	x	y	z	Moment	Nrm 10³	Trm 10³	theta (°)
D (NRM)	62	-19650	73840	175180	191119.07	210.20	0.00	
M1	70	-32330	66960	169870	185431.09	184.90	14.06	90.02
M2	75	-30370	64000	168600	182877.82	182.42	13.37	90.16
M3	82	-34820	59560	165080	178916.83	177.98	19.01	90.23
M4	90	-36020	53390	160840	173255.41	171.98	22.74	90.56
M5	100	-44370	33850	143020	153522.77	149.72	38.06	91.50
M6	105	-43620	-2540	121870	129466.03	123.34	59.62	97.84
M7	108	-11740	-8600	121220	122090.44	129.46	58.69	110.41

Tab. 7.7 - V27.10-1:Values of NRM lost and TRM gained and their angular difference θ.
In light grey the data used to calculate the palaeointensity.
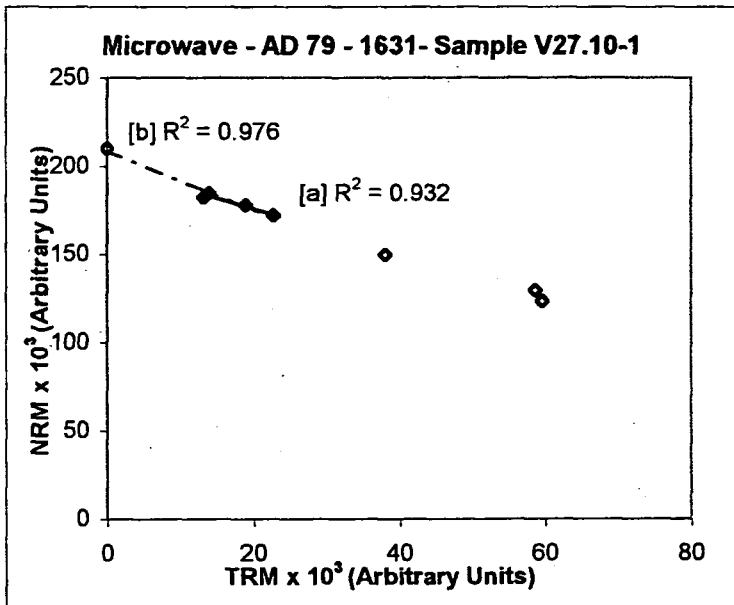
Fig. 7.4 - Conventional NRM/TRM plot for sample V27.10-1 Statistical parameters relative to the slope and palaeofield estimate are shown in Tab.7.8. Empty diamond indicate points excluded from the palaeofield calculation.

Power range (W)	N	f	g	q	b	σ_b	Fpalaeo (μT)	Uncertainty
[b] 62 - 90*	5	0.182	0.520	1.058	-1.699	0.152	84.945	80.315
[a] 70 - 90	4	0.061	0.629	0.209	-1.285	0.238	64.255	307.869

*including D(NRM)

Tab. 7.8 - V27.10-1 palaeointensity values and statistical parameters.

Sample V27.10-2		Arbitrary Units						
Steps	Power (W)	x	y	z	Moment	Nrm 10^3	Trm 10^3	theta (°)
D (NRM)	42	-41940	-44300	-118540	133316.11	141.99	0.00	
M1	50	-32390	-49580	-116020	130261.00	129.83	10.64	90.04
M2	52	-31100	-48420	-115770	129284.18	128.84	11.04	90.16
M3	58	-26620	-48160	-112670	125389.55	124.63	14.40	90.29
M4	62	-21440	-47460	-107750	119675.34	118.46	17.94	90.43
M5	70	-10580	-45530	-99720	110131.72	107.59	25.56	91.04
M6	75	1250	-38900	-91350	99295.49	95.50	32.74	93.06
M7	78	2060	-30610	-89180	94309.53	92.05	31.87	95.83
M8	80	4670	-26660	-86660	90788.33	88.95	33.64	97.71
M9	82	4130	-24270	-87510	90907.04	89.86	33.75	99.01
M10	88	36210	-7850	-63890	73856.07	73.04	61.43	114.04

Tab. 7.9 - V27.10-2:Values of NRM lost and TRM gained and their angular difference θ. In light grey the data used to calculate the palaeointensity.
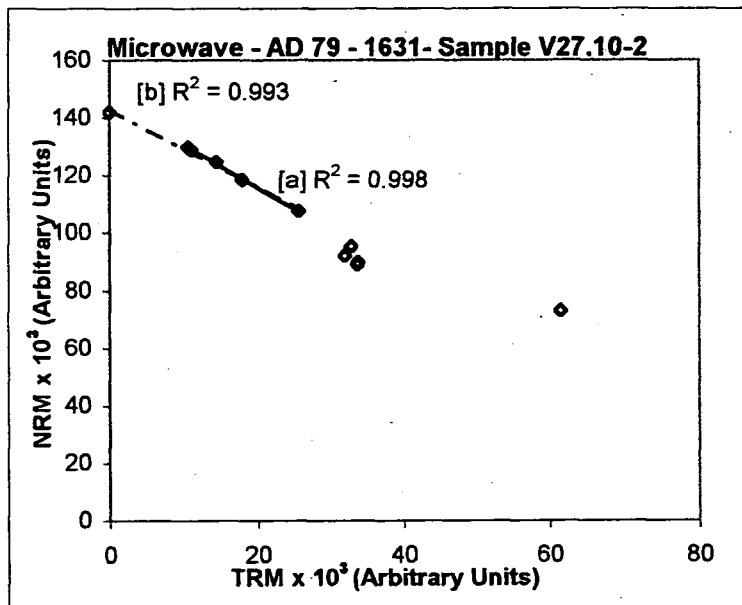
Fig. 7.5 - Conventional NRM/TRM plot for sample V27.10-2 Statistical parameters relative to the slope and palaeofield estimate are shown in Tab.7.5. Empty diamonds indicate points excluded from the palaeofield calculation.

Power range (W)	N	f	g	q	b	σ$_b$	Fpalaeo (μT)	Uncertainty
[b] 42 - 70*	6	0.242	0.727	4.104	-1.363	0.059	68.147	16.604
[a] 50 - 70	5	0.157	0.646	4.465	-1.490	0.034	74.495	16.684

*including D(NRM)

Tab. 7.10 - V27.10-2 palaeointensity values and statistical parameters.

Sample V33.12-1		Arbitrary Units						
Steps	Power (W)	x	y	z	Moment	Nrm 10³	Trm 10³	theta (°)
D (NRM)	12	-36710	-24830	-30720	53924.68	59.35	0.00	
M1	15	-30840	-30390	-30170	52772.02	52.18	7.91	90.03
M2	16	-28540	-30290	-29830	51203.95	50.39	9.20	90.13
M3	17	-27430	-30080	-29540	50297.34	49.38	9.70	90.19
M4	18	-25780	-30260	-28980	49194.68	48.03	10.81	90.23
M5	20	-22000	-30830	-27570	46846.49	44.95	13.43	90.29
M6	22	-20920	-30310	-27640	46046.85	44.06	13.76	90.49
M7	24	-19700	-30090	-27290	45146.90	42.96	14.33	90.60
M8	27	-14680	-30020	-26000	42340.32	38.94	17.34	91.03
M9	30	-11810	-28050	-25410	39647.78	36.02	17.80	91.89
M10	33	-6070	-27690	-23790	37007.37	31.47	21.08	92.82
M11	36	-3620	-24010	-24080	34196.94	29.31	20.78	95.73
M12	38	460	-20200	-22690	30382.36	25.56	21.36	99.85
M13	40	1250	-16310	-22070	27471.14	24.27	20.25	104.42
M14	42	2410	-13140	-21660	25448.44	23.76	20.40	110.11
M15	45	4450	-9010	-21160	23424.95	24.64	22.51	120.64
M16	47	3460	-920	-20170	20485.28	35.06	31.29	144.62

Tab. 7.11 - V33.12-1:Values of NRM lost and TRM gained and their angular difference θ.
In light grey the data used to calculate the palaeointensity.

Fig. 7.6 - Conventional NRM/ TRM plot for sample V33.12-1 Statistical parameters relative to the slope and palaeofield estimate are shown in Tab.7.12. Empty diamond indicate points excluded from the palaeofield calculation.

Power	Sample V33.12-1							
range (W)	N	f	g	q	b	σ_b	Fpalaeo (μT)	Uncertainty
15 - 24	7	0.155	0.793	3.848	-1.378	0.044	68.915	17.910

Tab. 7.12 - V33.12-1 palaeointensity values and statistical parameters.

Sample V26.6b-1			Arbitrary Units					
Steps	Power (W)	x	y	z	Moment	Nrm 10³	Trm 10³	theta (°)
D (NRM)	35	-39730	91130	-28320	103369.11	103.37	0.00	
M1	37	-64150	57020	-23930	89101.90	81.50	36.06	90.03
M2	38	-65540	54330	-23970	88440.95	79.69	38.43	90.05
M3	40	-67650	49240	-20100	86052.95	74.92	42.34	90.01
M4	42	-67120	50050	-23260	86897.21	76.33	41.60	90.06
M5	46	-66600	46910	-21860	84344.34	72.97	42.35	90.04
M6	55	-66020	42030	-20950	81018.91	68.21	43.79	90.06
M7	65	-65450	37320	-17690	77391.35	62.91	45.08	90.01
M8	78	-69000	33970	-17680	78914.79	61.32	49.68	90.01
M9	92	-68110	26860	-17700	75324.11	54.78	51.78	90.09
M10	108	-70380	22260	-16340	75603.22	51.21	55.67	90.07
M11	122	-92250	-7510	-10150	93110.07	31.65	87.58	90.03
M12	128	-92930	-10700	-9510	94026.14	28.94	89.48	90.04
M13	135	-107200	-30860	-7980	111838.54	16.60	110.66	90.22
M14	140	-111200	-33070	-6270	116182.52	15.45	115.17	90.08
M15	148	-126300	-54660	-950	137623.79	1.02	137.62	90.17

Tab. 7.13- V26.6b-1:Values of NRM lost and TRM gained and their angular difference θ.
In light grey the data used to calculate the palaeointensity.
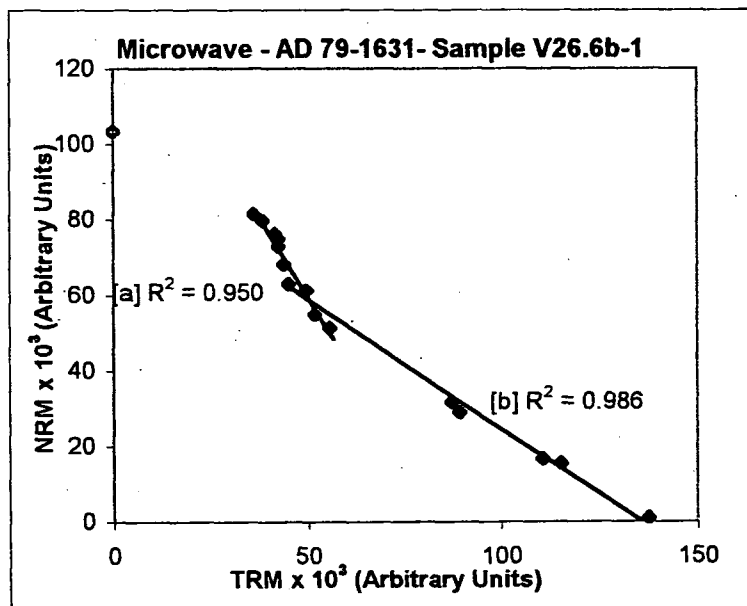
Fig. 7.7 - Conventional NRM/ TRM plot for sample V26.6b-1 Statistical parameters relative to the slope and palaeofield estimate are shown in Tab.7.14. Empty diamond indicate points excluded from the palaeofield calculation.

Power range (W)	N	f	g	q	b	σ_b	Fpalaeo (μT)	uncertainty
				Sample V26.6b-1				
[b] 55-148	10	0.650	0.814	12.509	-0.689	0.029	34.473	2.756
[a] 37-108	10	0.293	0.839	3.081	-1.726	0.138	86.320	28.013

Tab. 7.14 -V26.6b-1 palaeointensity values and statistical parameters.

Sample V31.5-1		Arbitrary Units						
Steps	Power (W)	x	y	z	Moment	Nrm 10³	Trm 10³	theta (°)
D (NRM)	29	61210	-86010	-49450	116574.81	134.80	0.00	
M1	31	60730	-84620	-49410	115282.37	115.28	0.70	90.15
M2	34	61010	-82500	-47450	113048.54	113.03	1.95	90.05
M3	42	61290	-71950	-44780	104587.36	104.26	8.24	90.02
M4	50	61120	-60620	-41500	95565.10	94.44	14.74	90.06
M5	58	59810	-47720	-38630	85712.96	83.09	21.40	90.24
M6	65	57410	-38580	-36240	78087.53	74.18	24.99	90.46
M7	72	55240	-34480	-34770	73819.24	69.46	25.72	90.59
M8	80	53800	-13670	-29530	62875.51	51.63	36.97	91.19
M9	82	45310	-10540	-29410	55036.68	45.66	33.04	92.82
M10	88	36730	15590	-24980	47075.91	26.93	44.17	101.16
M11	90	12450	12300	-24400	30027.53	31.97	37.74	129.81

Tab. 7.15 - V31.5-1:Values of NRM lost and TRM gained and their angular difference θ. In light grey the data used to calculate the palaeointensity.

Fig. 7.8 - Conventional NRM/ TRM plot for sample V31.5-1 Statistical parameters relative to the slope and palaeofield estimate are shown in Tab.7.16. Empty diamond indicate points excluded from the palaeofield calculation.

Power	Sample V31.5-1							
range (W)	N	f	g	q	b	σ_b	Fpalaeo (μT)	Uncertainty
31 - 58	5	0.239	0.703	7.663	-1.535	0.034	76.734	10.013

Tab. 7.16 - V31.5-1 palaeointensity values and statistical parameters.

Sample V31.5-2		Arbitrary Units						
Steps	Power (W)	x	y	z	Moment	Nrm 10^3	Trm 10^3	theta (°)
D (NRM)	28	-43890	-66790	37060	88094.72	99.03	0.00	
M1	30	-36810	-69780	37150	87202.91	86.87	7.59	90.03
M2	31	-36210	-69460	36710	86507.11	86.15	7.90	90.02
M3	32	-34460	-68440	36270	84776.40	84.32	8.83	90.04
M4	34	-32730	-68330	35930	83852.29	83.23	10.22	90.04
M5	37	-30990	-67860	35620	82668.88	81.88	11.44	90.06
M6	42	-26880	-66150	34430	79270.31	78.05	13.98	90.09
M7	50	-20110	-62830	32390	73492.40	71.33	17.90	90.17
M8	55	-19180	-61170	32130	71707.59	69.52	17.86	90.25
M9	62	-12050	-57760	29920	66156.08	62.51	22.03	90.35
M10	68	-11910	-55490	29790	64097.05	60.73	21.07	90.52
M11	75	550	-49730	26600	56399.78	49.10	28.59	90.96
M12	78	1860	-44710	26360	51935.47	44.92	27.51	91.79
M13	82	2740	-42650	25570	49803.16	42.68	27.20	92.01
M14	88	7540	-38000	24120	45635.80	36.72	29.08	92.99
M15	90	13300	-29910	22820	39903.01	29.05	30.76	96.36

Tab. 7.17 - V31.5-2:Values of NRM lost and TRM gained and their angular difference θ.
In light grey the data used to calculate the palaeointensity.

Fig. 7.9 - Conventional NRM/
TRM plot for sample V31.5-2
Statistical parameters relative to
the slope and palaeofield estimate
are shown in Tab.7.18. Empty
diamond indicate points excluded
from the palaeofield calculation.

Power	Sample V31.5-2							
range (W)	N	f	g	q	b	σ_b	Fpalaeo (μT)	Uncertainty
28 - 62	10	0.369	0.800	9.806	-1.629	0.049	81.464	8.308

Tab. 7.18- V31.5-2 palaeointensity values and statistical parameters.

AD 79 - 1631 lava flows specimens
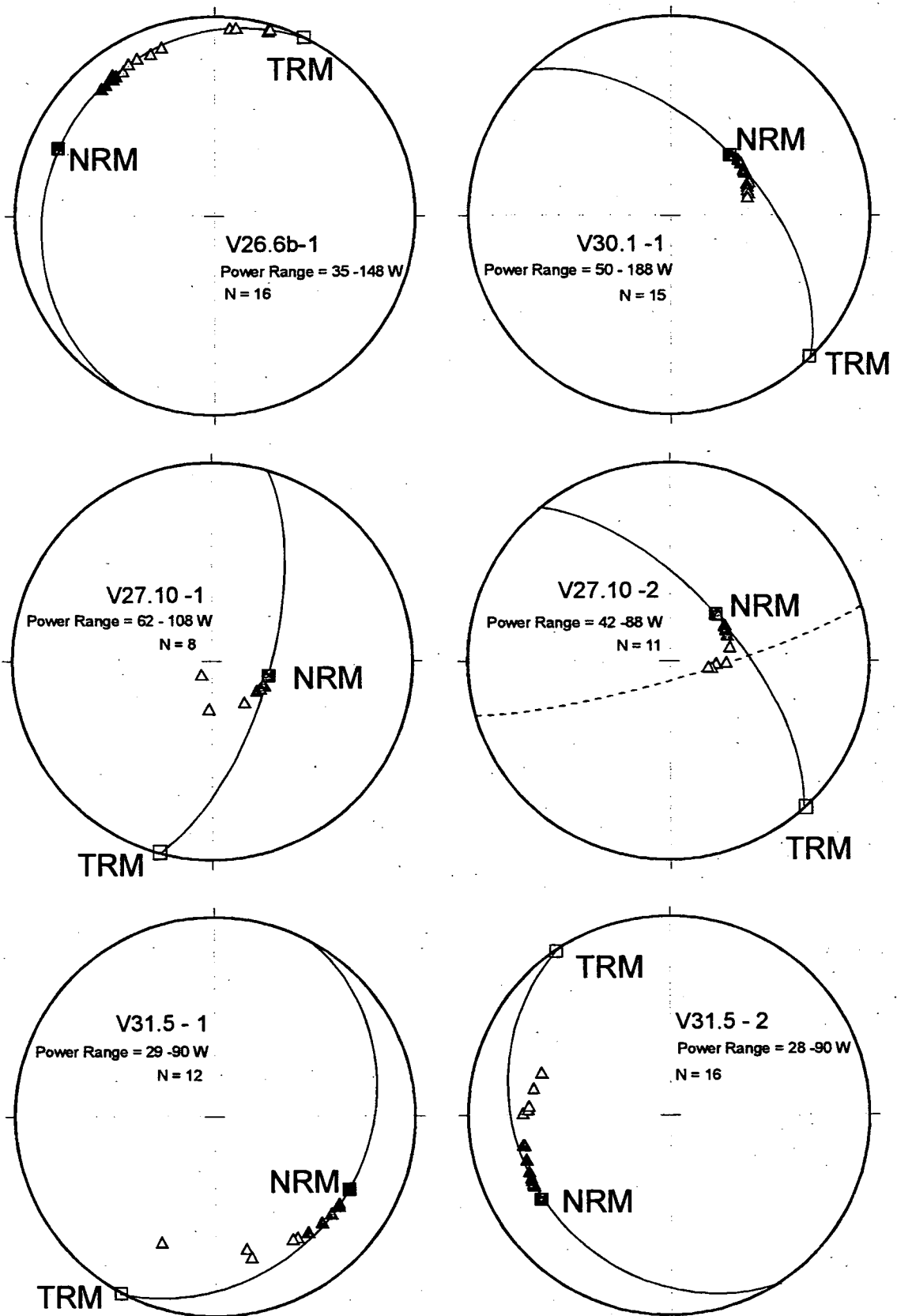
Fig. 7.10a. Stereo plots showing total vectors moving from the measured NRM(■) towards the applied TRM direction (□) along great circles.
Dashed great circles show secondary direction. Dark triangles indicate points used to calculate the palaeointensity.

AD 79 - 1631 lava flows specimens

V36.13 - 1
Power Range = 42 -98 W
N =7

NRM

TRM

V33.12 - 1
Power Range = 12 -47 W
N = 17

NRM

TRM

NRM

TRM

V37.8a - 1
Power Range = 33 -108 W
N = 9
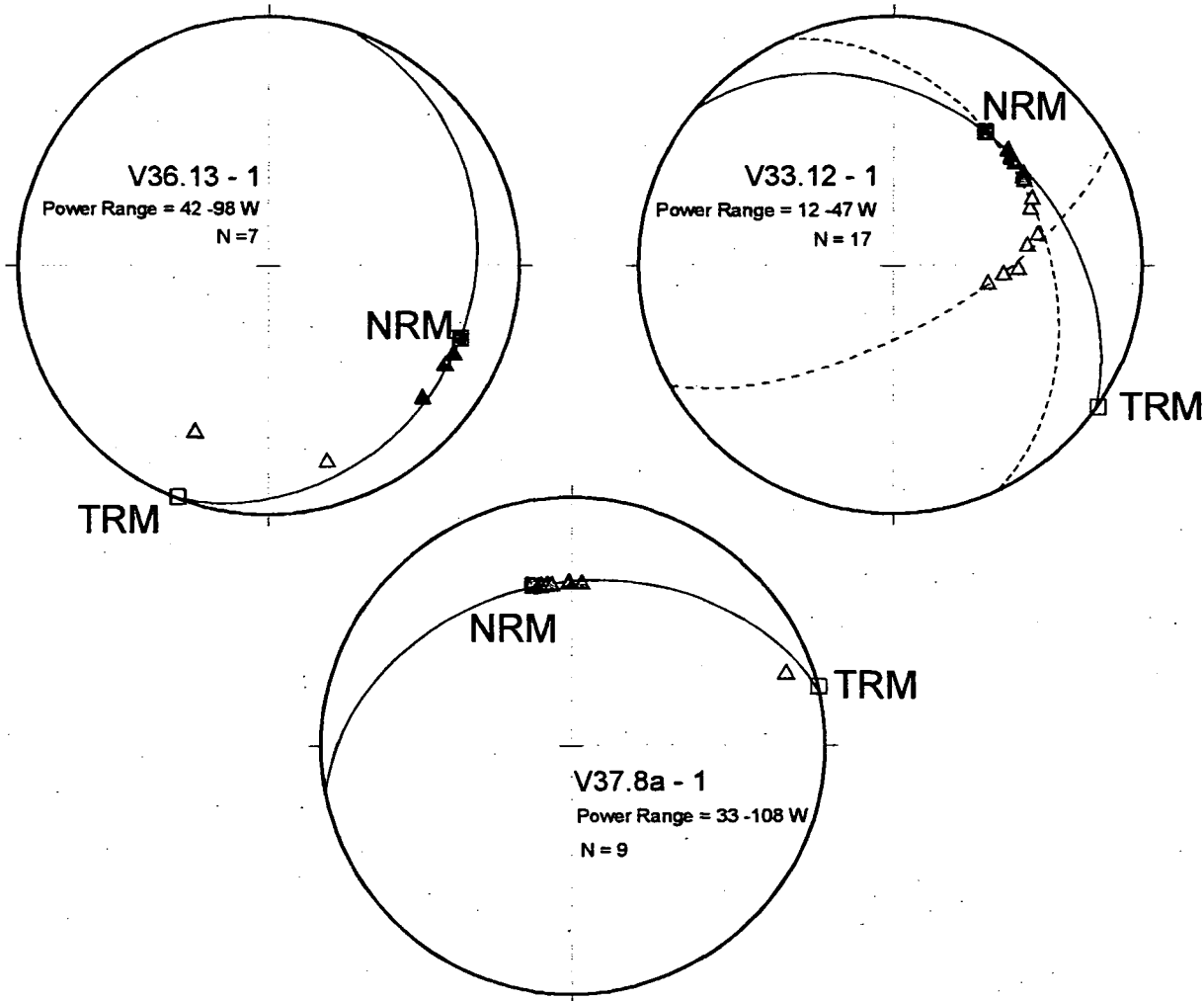
Fig. 7.10b. Stereo plots showing total vectors moving from the measured NRM(◼) towards the applied TRM direction (□) along great circles.
Dashed great circles show secondary direction. Dark triangles indicate points used to calculate the palaeointensity.

7.3 – AD 1697

7.3.1 – Site V28

In sample V28.1-2 only the first four data points were considered. All the other vectors moved gradually away from the great circle (Fig. 7.15) and the θ value did not change drastically until the last point (Tab. 7.19). The NRM/TRM plots showed one possible slope including the first point D(NRM) which fell on the same straight line defined by the following three points (Fig. 7.11, Tab. 7.20).

7.3.2 – Site V29

Sample V29.7-1 All the vectors defined a great circle (Fig. 7.15) but at 175 W the Dec was only some 50° away from the initial value. The NRM direction was very stable as shown by the θ value (Tab. 7.21). The NRM/TRM plots showed one possible slope using all the data points (Fig. 7.12, Tab. 7.22).

Sample V29.7-2 The vectors defined two different great circles (Fig. 7.15). At 92 W (step M4) the total vector moved away to define a different great circle. Theta value (Tab. 7.23) was stable until that point, then it started to increase gradually. The points where θ was > 90° were then excluded (Fig. 7.13, Tab. 7.24) and the NRM/TRM plots showed one possible slope [a]. A second one has been considered [b] included D(NRM), and showed a slightly different result.

7.4 – AD 1714 (1906)

7.4.1 – Site V38

In sample V38.p6a-1 the Dec moved some 50° away from the initial NRM direction. Only the first five points defined a great circle. At the last step the vector jumped away by about 60° (Fig. 7.15). Theta (Tab. 7.25), although <90°, increased slightly until the 5th step when it started to change more clearly while at the last step, it changed drastically. The

NRM/TRM plots showed one possible slope although another one could has been considered including also the point with 90°< θ < 93° (Fig. 7.14, Tab. 7.26).

7.5 – AD 1754

7.5.1 – Site V39

Sample V39.10b-1 & V39.10b-2

Both samples behaved similarly. Almost all the data points fell on a straight line on the NRM/TRM plots but only the first 6/7 points were on the great circle towards TRM (Fig.7.21). The θ values also stayed almost constant for the first few steps then it increased slightly until the last steps where changes were more evident (Tabs. 7.27,29). The NRM/TRM plots showed one possible slope, excluding all the points with θ < 90° and not falling on the great circle (Figs. 7.16,17; Tabs. 7.28,30).

7.5.2 – Site V40

Only the first six points defined a great circle towards the TRM (Fig. 7.21). At about 80 W the total vector moved away from the previous direction. Theta angle (Tab. 7.31) showed, little change until that point, after which it started to gradually increase. Above 95 W the changes were more drastic. NRM/TRM plot showed one possible slope even including the first point D(NRM) (Fig. 7.18, Tab. 7.32).

7.5.1 – Site V41

Sample V41.4a-1 & V41.4a-2

For both samples only the first six vectors lay on the great circle (Fig. 7.21) while the last points moved away from it, accompanied by a clear change in the θ values (Tabs. 7.33,35). The NRM/TRM plots showed one possible slope, excluding the last two points and also including the first point D(NRM) which fell on the same straight line (Fig. 7.19,20 Tabs. 7.34,36).

Sample V28.1-2		Arbitrary Units						
Steps	Power (W)	x	y	z	Moment	Nrm 10^3	Trm 10^3	theta (°)
D (NRM)	50	180000	134800	-1E+05	248482.45	262.66	0.00	
M1	60	159200	140800	-1E+05	235051.99	234.42	17.29	90.01
M2	65	141800	138500	-95200	219892.09	218.37	25.99	90.04
M3	70	92900	134800	-78600	181602.34	173.94	52.46	90.09
M4	72	66900	120700	-71100	155239.52	144.59	57.53	90.41
M5	75	63700	119100	-70700	152449.96	141.34	58.38	90.51
M6	80	25500	107500	-58600	125061.82	103.14	72.77	91.13
M7	82	20800	92100	-58600	111126.10	92.81	65.30	92.51
M8	88	-55400	57700	-34200	86994.77	37.93	92.59	110.37

Tab. 7.19 - V28.1-2:Values of NRM lost and TRM gained and their angular difference θ. In light grey the data used to calculate the palaeointensity.

Fig. 7.11 - Conventional NRM/TRM plot for sample V28.1-2 Statistical parameters relative to the slope and palaeofield estimate are shown in Tab.7.20. Empty diamond indicate points excluded from the palaeofield calculation.

Power range (W)	Sample V28.1-2							
	N	f	g	q	b	σ_b	Fpalaeo (μT)	Uncertainty
50 - 70*	4	0.338	0.615	19.262	-1.697	0.018	84.828	4.404
60 - 70	3	0.230	0.390	4.644	-1.710	0.033	85.506	18.412

*including D(NRM)

Tab. 7.20 - V28.1-2palaeointensity values and statistical parameters.

Sample V29.7-1		Arbitrary Units						
Steps	Power (W)	x	y	z	Moment	Nrm 10³	Trm 10³	theta (°)
D (NRM)	100	-68200	-242200	-144500	290159.15	310.23	0.00	
M1	108	-54300	-238900	-139900	282123.57	281.85	12.50	90.01
M2	115	-52400	-237600	-140900	281162.46	280.82	14.01	90.02
M3	125	-51900	-235000	-140600	278723.82	278.39	13.92	90.04
M4	138	-40000	-228100	-133600	267354.76	266.34	23.35	90.01
M5	148	-32200	-217700	-127700	254435.49	252.89	28.09	90.02
M6	158	-15500	-197500	-118100	230638.48	227.38	39.02	90.11
M7	162	-11700	-193300	-118600	227085.31	223.33	42.02	90.24
M8	175	42200	-143900	-89500	174637.62	155.43	80.91	90.48

Tab. 7.21 -V29.7-1:Values of NRM lost and TRM gained and their angular difference θ.
In light grey the data used to calculate the palaeointensity.

Fig. 7.12 - Conventional NRM/
TRM plot for sample V29.7-1
Statistical parameters relative to
the slope and palaeofield estimate
are shown in Tab.7.22. Empty
diamond indicate points excluded
from the palaeofield calculation.

Power	Sample V29.7-1							
range (W)	N	f	g	q	b	σ_b	Fpalaeo (μT)	Uncertainty
100 - 175	9	0.499	0.732	14.154	-1.918	0.050	95.891	6.775

Tab. 7.22 - V29.7-1 palaeointensity values and statistical parameters.

Sample V29.7-2		Arbitrary Units						
Steps	Power (W)	x	y	z	Moment	Nrm 10³	Trm 10³	theta (°)
D (NRM)	50	54940	-2E+05	-79940	190065.01	207.07	0.00	
M1	60	60340	-2E+05	-76630	180357.97	180.14	8.91	90.02
M2	75	63890	-1E+05	-67610	159138.36	157.95	19.46	90.02
M3	90	80230	-37620	-39000	96814.86	72.59	64.79	90.58
M4	92	46380	-6320	-36090	59106.13	42.24	49.03	99.65
M5	95	28980	540	-35130	45543.92	39.25	42.82	112.76
M6	98	12210	20360	-29570	37920.95	75.76	86.09	153.90

Tab. 7.23 - V29.7-2:Values of NRM lost and TRM gained and their angular difference θ. In light grey the data used to calculate the palaeointensity.
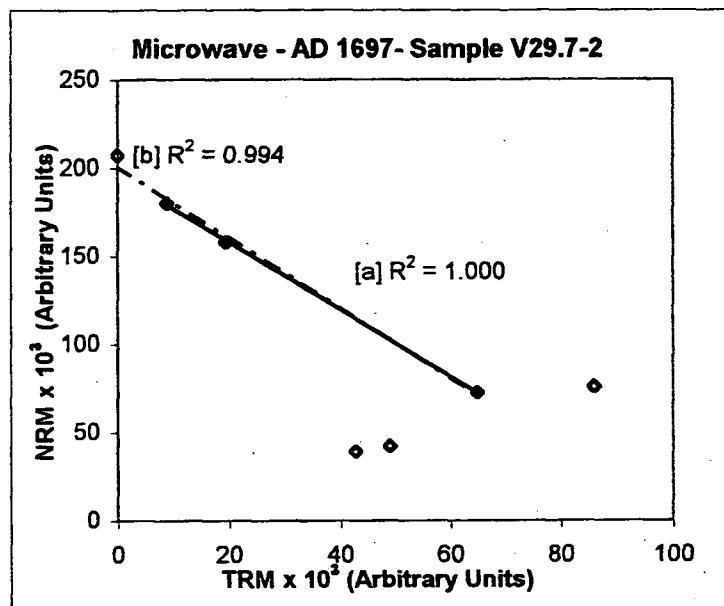
Fig. 7.13 - Conventional NRM/ TRM plot for sample V29.7-2 Statistical parameters relative to the slope and palaeofield estimate are shown in Tab.7.24. Empty diamond indicate points excluded from the palaeofield calculation.

Power	Sample V29.7-2							
range (W)	N	f	g	q	b	σ_b	Fpalaeo (μT)	Uncertainty
[b]50 - 90*	4	0.649	0.530	6.121	-2.020	0.114	100.996	16.501
[a] 60 - 90	3	0.519	0.328	9.475	-1.913	0.034	95.637	10.094

* including D(NRM)

Tab. 7.24 - V29.7-2 palaeointensity values and statistical parameters.

Sample V38.6a-1		Arbitrary Units						
Steps	Power (W)	x	y	z	Moment	Nrm 10³	Trm 10³	theta (°)
D (NRM)	42	48040	-69350	131055	88094.72	146.97	0.00	
M1	45	64090	-66590	124972	87202.91	123.12	21.53	90.04
M2	48	63070	-66300	121606	86507.11	119.55	22.57	90.15
M3	52	64690	-64420	117488	84776.40	114.48	26.79	90.20
M4	58	67160	-61310	110050	83852.29	104.73	34.53	90.41
M5	60	64730	-59770	104043	82668.88	98.18	35.76	90.76
M6	65	64120	-53780	92211	79270.31	82.57	42.97	91.30
M7	68	60720	-53890	87822	73492.40	78.09	43.34	92.24
M8	70	59340	-52660	83690	71707.59	72.49	45.93	93.11
M9	72	56360	-52380	80843	66156.08	70.35	44.80	93.83
M10	78	62220	-34160	110027	64097.05	84.64	152.44	135.17

Tab. 7.25 - V38.6a-1:Values of NRM lost and TRM gained and their angular difference θ. In light grey the data used to calculate the palaeointensity.

Fig. 7.14 - Conventional NRM/TRM plot for sample V38.6a-1 Statistical parameters relative to the slope and palaeofield estimate are shown in Tab.7.26. Empty diamond indicate points excluded from the palaeofield calculation.

Power range (W)	N	f	g	q	b	σ_b	Fpalaeo (μT)	Uncertainty
45 - 60	5	0.170	0.716	1.209	-1.567	0.158	78.341	64.789

Tab. 7.26 - V38.6a-1 palaeointensity values and statistical parameters.

AD 1697 lava flow specimens

V29.7 -1
Power Range = 100 -175 W
N = 9

NRM

TRM

V29.7 -2
Power Range = 50 -98 W
N = 7

NRM

TRM

TRM

V28.1- 2
Power Range = 50 -88 W
N = 9

NRM

AD 1714 lava flow specimen

TRM

V38.6a - 1
Power Range = 42 -78 W
N = 11

NRM

Fig. 7.15. Stereo plots showing total vectors moving from the measured NRM(◼) towards the applied TRM direction (☐) along great circles.
Dashed great circles show secondary direction. Dark triangles indicate points used to calculate the palaeointensity.

Sample V39.10b-1		Arbitrary Units						
Steps	Power (W)	x	y	z	Moment	Nrm 10³	Trm 10³	theta (°)
D (NRM)	37	42590	42750	-70230	92594.40	96.55	0.00	
M1	42	36350	45480	-69050	90319.74	90.10	6.44	90.07
M2	45	36490	44980	-69510	90478.51	90.29	6.11	90.14
M3	50	34260	44990	-68030	88464.28	88.15	7.70	90.15
M4	55	31700	44890	-66620	86361.02	85.87	9.51	90.20
M5	60	31500	44970	-67150	86739.11	86.23	9.81	90.27
M6	65	28750	44740	-64930	83929.35	83.18	11.57	90.26
M7	70	25690	44620	-63060	81409.36	80.32	13.71	90.31
M8	75	20260	43980	-60020	77117.50	75.29	17.32	90.49
M9	78	18700	42480	-59570	75517.05	73.65	17.77	90.82
M10	82	17690	41490	-58950	74225.73	72.32	18.03	91.02
M11	90	7980	40780	-53660	67868.14	63.83	24.75	91.46
M12	95	6990	36170	-53530	64981.46	61.72	23.70	92.91
M13	102	-1390	32580	-49200	59025.66	54.13	28.55	94.85
M14	108	-8600	22810	-46130	52175.02	48.28	32.25	102.03
M15	110	-14730	5470	-40290	43245.55	48.79	41.03	123.23

Tab. 7.27 - V39.10b-1:Values of NRM lost and TRM gained and their angular difference θ.
In light grey the data used to calculate the palaeointensity.
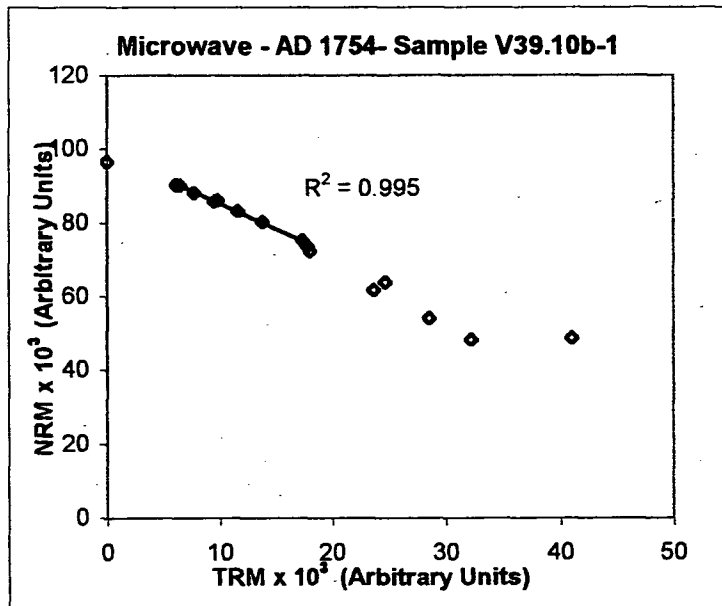
Fig. 7.16 - Conventional NRM/
TRM plot for sample V39.10b-1
Statistical parameters relative to the
slope and palaeofield estimate are
shown in Tab.7.28. Empty diamond
indicate points excluded from the
palaeofield calculation.

Power	Sample V39.10b-1							
range (W)	N	f	g	q	b	σ_b	Fpalaeo (μT)	Uncertainty
42 - 78	9	0.170	0.795	5.079	-1.399	0.037	69.935	13.770

Tab. 7.28 - V39.10b-1 palaeointensity values and statistical parameters.

Sample V39.10b-2		Arbitrary Units						
Steps	Power (W)	x	y	z	Moment	Nrm 10³	Trm 10³	theta (°)
D (NRM)	17	-47660	27170	-65000	85056.95	86.67	0.00	
M1	33	-49340	19790	-62220	81837.69	81.52	7.24	90.01
M2	37	-48450	19490	-60950	80263.10	79.95	7.07	90.01
M3	45	-47470	14050	-58060	76300.50	75.46	11.32	90.02
M4	50	-45680	12000	-56370	73540.73	72.52	12.29	90.08
M5	55	-43830	7020	-53620	69609.29	67.84	15.86	90.22
M6	58	-41770	4890	-52370	67165.93	65.13	16.97	90.47
M7	60	-40580	2870	-51710	65794.36	63.40	18.39	90.72
M8	62	-39300	2190	-51050	64462.30	62.03	18.56	90.93
M9	65	-37670	-550	-49480	62190.05	59.19	20.42	91.25
M10	68	-36090	-360	-49370	61155.66	58.41	19.88	91.67
M11	70	-34980	-3150	-47820	59331.91	55.87	21.92	91.92
M12	72	-31230	-5050	-45990	55820.21	52.25	22.65	93.08
M13	75	-20650	-17100	-39220	47508.32	40.82	31.27	98.72
M14	78	1120	-15180	-36210	39279.14	46.47	40.49	126.84

Tab. 7.29 - V39.10b-2:Values of NRM lost and TRM gained and their angular difference θ.
In light grey the data used to calculate the palaeointensity.
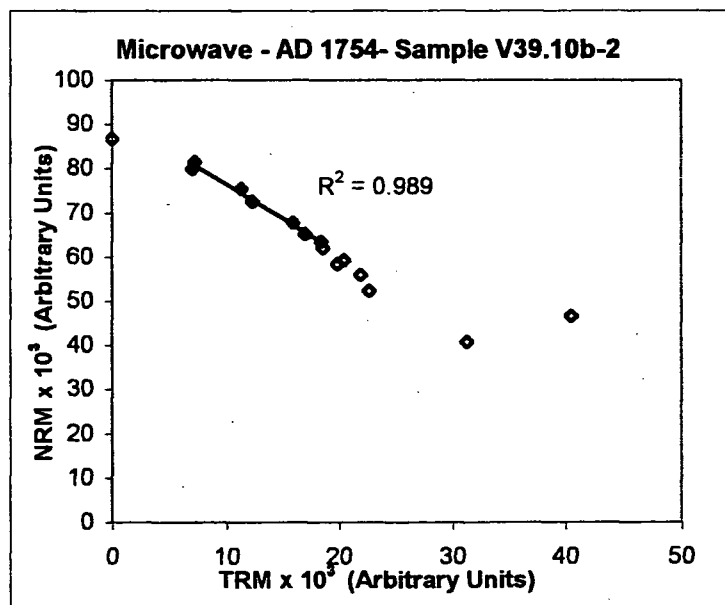
Fig. 7.17 - Conventional NRM/
TRM plot for sample V39.10b-2
Statistical parameters relative to the
slope and palaeofield estimate are
shown in Tab.7.30. Empty diamond
indicate points excluded from the
palaeofield calculation.

Power	Sample V39.10b-2							
range (W)	N	f	g	q	b	σ_b	Fpalaeo (μT)	Uncertainty
33 - 60	7	0.209	0.806	3.526	-1.565	0.075	78.244	22.193

Tab. 7.30 - V39.10b-2 palaeointensity values and statistical parameters.

Sample V40.7b-1		Arbitrary Units						
Steps	Power (W)	x	y	z	Moment	Nrm 10^3	Trm 10^3	theta (°)
D (NRM)	46	-28220	49200	76080	94895.60	101.91	0.00	
M1	50	-33600	42760	74810	92487.37	92.15	8.03	90.10
M2	55	-33880	40890	73040	90303.31	89.85	9.20	90.11
M3	62	-34450	36190	69460	85564.07	84.74	12.16	90.20
M4	68	-33740	34750	68700	84057.36	83.20	12.46	90.34
M5	75	-35680	28680	66210	80494.53	78.75	17.53	90.63
M6	80	-34140	23840	63350	75809.68	73.72	19.34	91.24
M7	82	-33530	20440	61450	72925.70	70.46	21.02	91.72
M8	85	-31710	16580	58180	68303.24	65.59	22.00	92.40
M9	88	-30130	10610	55710	64218.32	60.89	25.13	94.03
M10	90	-28090	9300	55850	63204.12	60.30	25.34	95.33
M11	95	-26350	-6450	48440	55518.99	49.89	35.33	100.71
M12	98	-9790	-6490	48330	49736.84	53.79	35.32	116.03

Tab. 7.31 - V40.7b-1:Values of NRM lost and TRM gained and their angular difference θ. In light grey the data used to calculate the palaeointensity.

Fig. 7.18 - Conventional NRM/ TRM plot for sample V40.7b-1 Statistical parameters relative to the slope and palaeofield estimate are shown in Tab.7.32. Empty diamond indicate points excluded from the palaeofield calculation.

Power range (W)	N	f	g	q	b	σ_b	Fpalaeo (μT)	Uncertainty
Sample V40.7b-1								
46 - 75*	6	0.227	0.723	2.554	-1.390	0.089	69.500	27.216
50 - 75	5	0.131	0.702	0.733	-1.450	0.182	72.486	98.856

*including D(NRM)

Tab. 7.32 - V40.7b-1palaeointensity values and statistical parameters.

Sample V41.4a-1		Arbitrary Units						
Steps	Power (W)	x	y	z	Moment	Nrm 10³	Trm 10³	theta (°)
D (NRM)	46	-82440	-187460	-66560	215331.93	223.04	0.00	
M1	50	-72190	-186800	-65000	210548.42	210.35	9.12	90.01
M2	58	-63910	-182620	-62810	203419.88	202.87	15.01	90.01
M3	65	-52460	-175000	-60600	192482.24	191.17	22.48	90.02
M4	72	-42010	-168010	-57660	182529.11	180.18	29.25	90.03
M5	80	67610	-133780	-39450	154998.40	103.09	116.03	90.16
M6	82	50640	-68990	-38830	93977.65	57.89	78.00	93.84
M7	85	40620	-30360	-36090	62243.09	39.53	60.79	106.74
M8	88	25090	17880	-33640	45616.36	1847.07	1862.34	178.69

Tab. 7.33 - V41.4a-1:Values of NRM lost and TRM gained and their angular difference θ. In light grey the data used to calculate the palaeointensity.
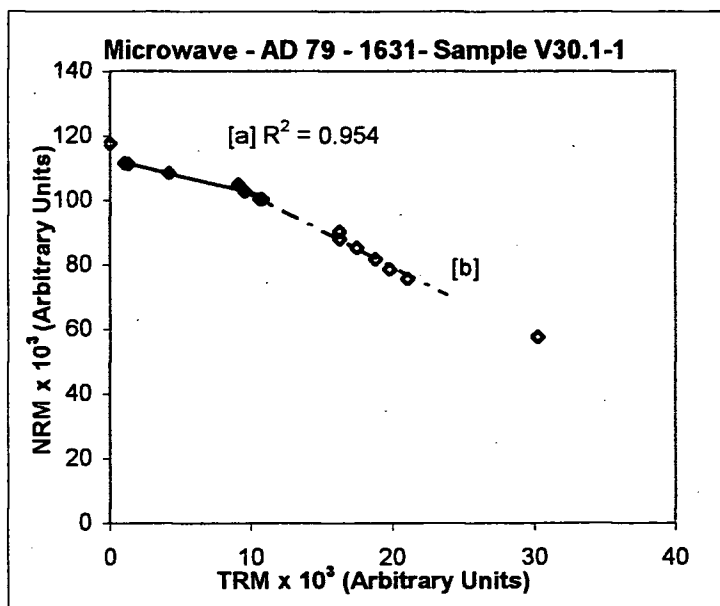

Fig. 7.19 - Conventional NRM/ TRM plot for sample V41.4a-1 Statistical parameters relative to the slope and palaeofield estimate are shown in Tab.7.34. Empty diamond indicate points excluded from the palaeofield calculation.

Power range (W)		Sample V41.4a-1						
	N	f	g	q	b	σ_b	Fpalaeo (μT)	Uncertainty
46 - 72*	5	0.192	0.742	5.347	-1.460	0.039	72.996	13.652
50 - 72	4	0.135	0.656	2.514	-1.510	0.053	75.519	30.038

*including D(NRM)

Tab. 7.34 - V41.4a-1 palaeointensity values and statistical parameters.

Sample V41.4a-2		Arbitrary Units						
Steps	Power (W)	x	y	z	Moment	Nrm 10³	Trm 10³	theta (°)
D (NRM)	50	140700	45620	40620	153387.28	162.27	0.00	
M1	55	132870	53690	40630	148955.87	148.61	10.18	90.04
M2	60	122190	57750	39750	140874.13	139.81	17.48	90.10
M3	62	113050	62440	37110	134373.39	132.12	24.63	90.05
M4	65	97100	70730	35960	125396.43	119.71	37.60	90.13
M5	68	61380	80680	31120	106043.49	88.90	58.36	90.36
M6	70	28160	71610	27810	81819.15	56.26	61.06	91.66
M7	72	4780	54300	26750	60719.86	34.46	54.51	97.22
M8	75	-40460	21630	21260	50565.36	198.32	227.65	168.89

Tab. 7.35 - V41.4a-2:Values of NRM lost and TRM gained and their angular difference θ. In light grey the data used to calculate the palaeointensity.
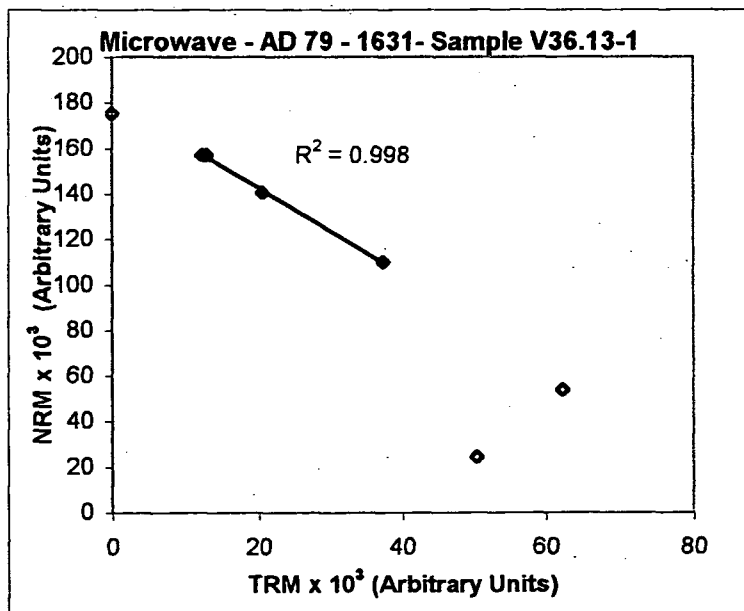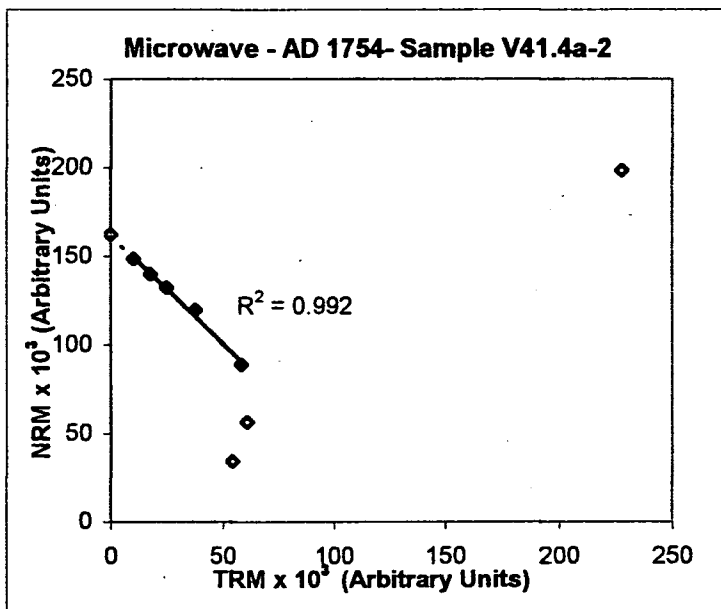

Fig. 7.20- Conventional NRM/ TRM plot for sample V41.4a-2. Statistical parameters relative to the slope and palaeofield estimate are shown in Tab.7.36. Empty diamond indicate points excluded from the palaeofield calculation.

Power range (W)		Sample V41.4a-2						
	N	f	g	q	b	σ_b	Fpalaeo (μT)	Uncertainty
50 - 68*	6	0.452	0.735	8.899	-1.225	0.046	61.269	6.885
55 - 68	5	0.368	0.652	4.530	-1.223	0.065	61.174	13.504

*including D(NRM)

Tab. 7.36 - V41.4a-2 palaeointensity values and statistical parameters.

AD 1754 lava flow specimens
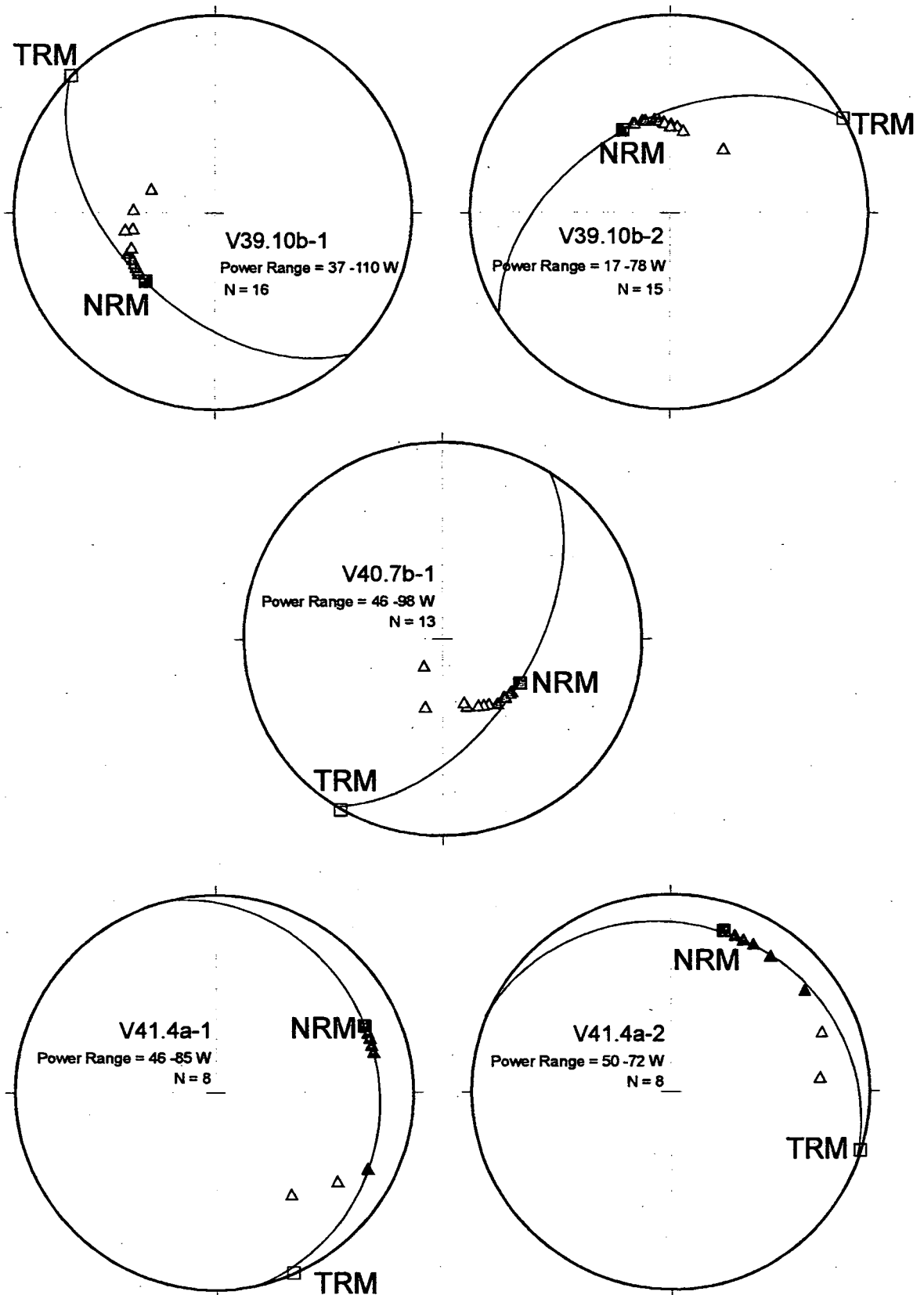
Fig. 7.21. Stereo plots showing total vectors moving from the measured NRM(▧) towards the applied TRM direction (□) along great circles.
Dashed great circles show secondary direction. Dark triangles indicate points used to calculate the palaeointensity.

7.6 – AD 1760

7.6.1 – Site V32

Samples V32.13-1 & V32.13-2 In sample 13-1 almost all the vectors moved away from the defined NRM/TRM great circle (Fig. 7.28) except for the first 4/5 points, as also shown by the θ values (Tab. 7.37). Theta, in fact, started to change gradually starting from 60W until it reached 78W where it changed more drastically. The NRM/TRM plots showed one possible slope and even the excluded points that showed θ >90° seem to fell on the same straight line (except for the last one). Including the first point D(NRM) did not change the palaeointensity estimate (Fig. 7.22, Tab. 7.38). A demagnetisation experiment using microwave has been also carried out on a sister sample, 13-2, to check the stability of the NRM. As shown in Tab. 7.39 both Dec and Inc were very stable until the end of the experiment but at the maximum power applied, which is also the maximum available, the moment was not demagnetised completely and there was some 30% left (Fig. 7.23).

7.6.2 – Site V35

Samples V35.9b-1 & V35.9b-2 All the vectors defined a unique great circle (Fig. 7.28) but at 182 W the Dec was only some 40° away from the initial value. The NRM direction was very stable as shown by the θ value (Tab. 7.40) but the NRM/TRM plots showed two possible slopes, [a] at low power (58-125W) and [b] at high power (125-175W), excluding the last two points (Fig. 7.24, Tab. 7.41). Another paleointensity estimate has been calculated, [c], considering the entire spectra of power. The demagnetisation of the sister sample 9b-2 showed a quite stable NRM, especially in declination, up to 165W where there was some 20% of the moment still remaining (Fig. 7.25, Tab. 7.42).

7.6.3 – Site V34

Sample V34.8-1 & V34.8-2 For both samples the vectors defined a great circle (Fig. 7.28) but the Dec did not swing gradually towards the TRM direction. The total vector jumped of about 50° at the last point but did not lie on the great circle. This behaviour was also clearly

shown by the θ values (Tabs 7.43,45). The NRM/TRM plots showed one possible slope, for both samples, considering only the first 6/7 two points (Figs. 7.26,27, Tabs. 7.44,46).

7.7 –AD 1806

7.7.1 – Site V25

Sample V25.2-1 The vector end point of the total magnetization defined an almost perfect great circle and it swung from the direction of the NRM through 90° to the direction of the TRM (Fig. 7.33). The angular difference between the two directions had stayed very constant throughout the experiments (Tab. 7.47) and a stable NRM direction can be hypothesised until at least 75W. The NRM/TRM plots showed a concave shape and the last four points can not be considered because they were slightly away from the great circle although θ was still about 90°, except the last point (Fig. 7.29, Tab. 7.48).

Sample V25.2-2 Almost all the points did not lie on the great circle defined by the NRM/TRM directions but they seemed to define a secondary direction (Fig. 7.33). The θ angles showed unacceptable behaviour; in fact it was always bigger then 90° (Tab. 7.49). Therefore, no acceptable palaeofield were estimated from this sample (Fig. 7.30).

7.7.2 – Site V24

Sample V24.3-1 & V24.3-2 In sample 3-2, only the vectors within the range 17 - 27 W lay on the NRM/TRM great circle while the other vectors seemed to follow a secondary direction (Fig. 7.33). The angular difference θ, increased slightly until step M7 after which the increases were more significant (Tab. 7.50). Only the points which showed θ <90° were considered and from the NRM/TRM plots one slope and one value of the palaeofield were estimated although its statistical parameters were not well defined (Fig. 7.31, Tab. 7.51). The demagnetisation of the sister sample 3-1 showed a quite stable Inclination while the Declination increased progressively to about 5°, up to 152W where there was some 10% of the original moment still remaining (Fig. 7.32, Tab. 7.52).

Sample V32.13-1		Arbitrary Units						
Steps	Power (W)	x	y	z	Moment	Nrm 10³	Trm 10³	theta (°)
D (NRM)	33	-49950	26620	93810	109562.51	117.19	0.00	
M1	40	-52140	18550	94590	109589.92	109.29	8.39	90.13
M2	45	-51010	15950	92500	106830.11	106.37	10.31	90.22
M3	52	-50250	10600	88760	102546.38	101.55	14.73	90.26
M4	60	-46790	2450	86050	97979.13	95.96	21.44	90.96
M5	65	-43150	-2030	82590	93204.89	90.59	24.63	91.62
M6	68	-39910	-1690	82980	92094.22	89.93	24.31	92.59
M7	72	-38080	-4750	80980	89612.55	86.97	26.73	93.06
M8	78	-31730	-14140	74120	81856.62	77.42	34.06	94.94
M9	80	-13660	-21420	67420	72047.68	69.76	43.13	104.80
M10	82	19480	-8950	59800	63526.47	103.04	79.87	141.95

Tab. 7.37 - V32.13-1:Values of NRM lost and TRM gained and their angular difference θ.
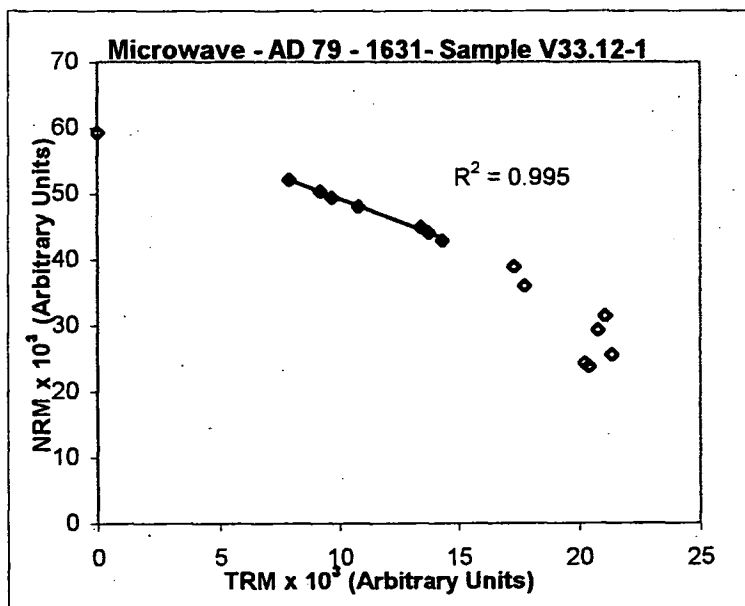In light grey the data used to calculate the palaeointensity.
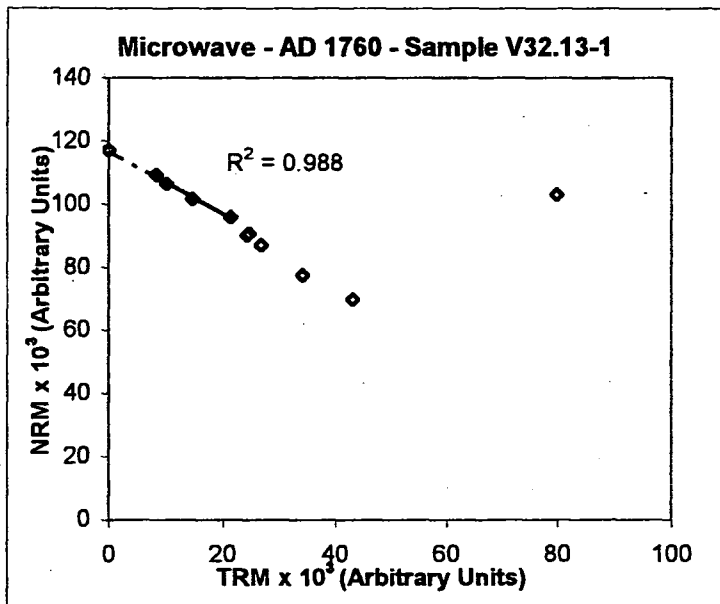
Fig. 7.22 - Conventional NRM/
TRM plot for sample V32.13-1
Statistical parameters relative to the
slope and palaeofield estimate are
shown in Tab.7.38. Empty diamond
indicate points excluded from the
palaeofield calculation.

Power		Sample V32.13-1						
range (W)	N	f	g	q	b	σ_b	Fpalaeo (μT)	Uncertainty
33 - 60*	5	0.181	0.722	3.234	-1.011	0.041	50.548	15.632
40 - 60	4	0.114	0.645	0.937	-1.008	0.079	50.378	53.751

*including D(NRM)

Tab. 7.38 - V32.13-1 palaeointensity values and statistical parameters.

Sample V32.13-2   Arbitray Units

Steps Demag	Power (watts)	Moment 10^3	Dec	Inc
NRM	0	84.3	172.2	69.3
1	17	82.5	171.2	68.7
2	33	79.2	170.8	68.4
3	40	78.6	170.3	68.5
4	45	77.6	170.8	67.5
5	52	76.9	170.2	68.0
6	62	71.9	170.3	68.2
7	75	67.2	169.2	68.2
8	88	46.7	171.5	67.1
9	100	42.2	170.8	67.7
10	112	30.2	170.6	68.2
11	125	26.7	174.2	67.5
12	138	26.0	173.1	68.3
13	150	25.2	171.6	67.5
14	162	29.2	166.7	72.3
15	175	25.8	174.2	68.3

Tab. 7.39 - Directional and Intensity values of sample V32.13-2.
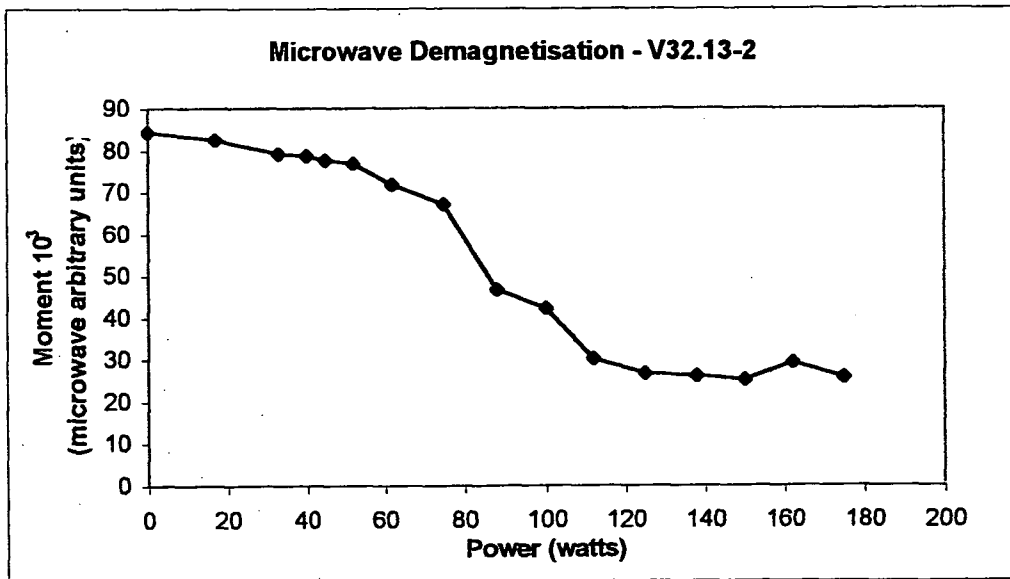
Fig. 7.23 - NRM demagnetisation of sample V32.13-2, using microwave, to check the behaviour of the NRM and in particular the stability of Dec and Inc throughout the experiment.

Sample V35.9b-1		Arbitrary Units						
Steps	Power (W)	x	y	z	Moment	Nrm 10³	Trm 10³	theta (°)
D (NRM)	50	-79950	-31530	-39140	94435.60	97.82	0.00	
M1	58	80510	-32660	-40090	95685.65	95.68	0.97	90.08
M2	68	-77280	-34280	-39100	93145.73	93.08	3.58	90.04
M3	80	-76060	-35460	-38870	92484.66	92.34	5.13	90.03
M4	95	-74150	-36790	-38210	91168.69	90.90	7.05	90.02
M5	108	-73580	-36470	-38210	90576.38	90.31	6.99	90.04
M6	125	-69820	-38130	-37130	87791.61	87.24	9.91	90.04
M7	138	-62850	-39530	-35010	82088.02	80.93	13.81	90.07
M8	142	-59740	-39550	-33980	79295.08	77.89	14.99	90.09
M9	148	-59350	-39550	-33800	78924.43	77.48	15.13	90.09
M10	155	-58540	-39560	-33650	78257.57	76.74	15.46	90.11
M11	165	-54790	-40520	-32400	75455.78	73.38	17.73	90.11
M12	172	-45360	-42140	-29940	68772.91	64.97	22.81	90.23
M13	175	-26280	-45050	-25710	58147.61	48.38	32.90	90.76
M14	178	-22430	-39320	-25280	51848.30	43.43	29.57	91.62
M15	182	-21660	-38650	-24990	50867.26	42.48	29.29	91.73

Tab. 7.40 - V35.9b-1:Values of NRM lost and TRM gained and their angular difference θ.
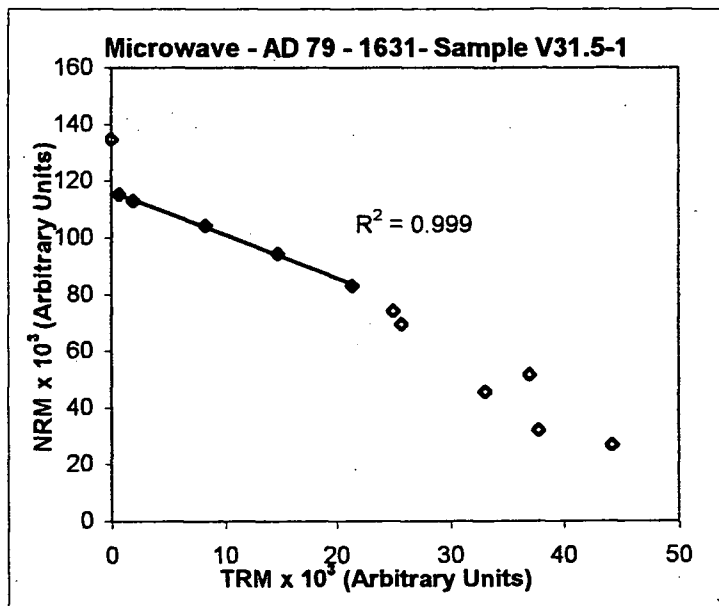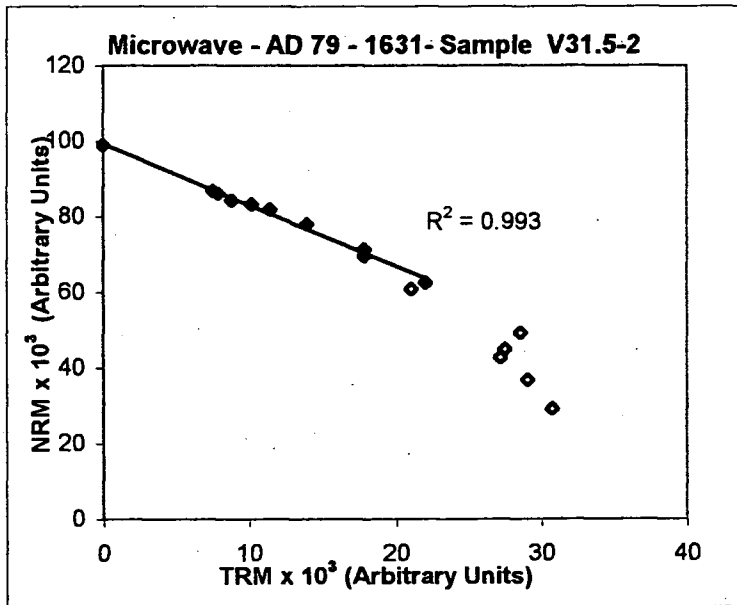In light and dark grey the data used to calculate the palaeointensity.
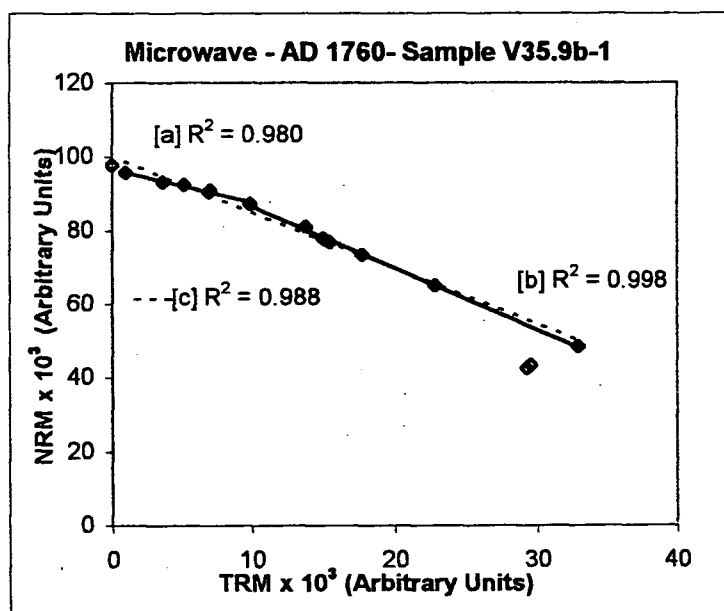
Fig. 7.24 - Conventional NRM/ TRM plot for sample V35.9b-1 Statistical parameters relative to the slope and palaeofield estimate are shown in Tab.7.41. Empty diamond indicate points excluded from the palaeofield calculation.

Power range (W)	Sample V35.9b-1							
	N	f	g	q	b	σ_b	Fpalaeo (μT)	Uncertainty
50- 125*	7	0.108	0.788	1.321	-0.991	0.064	49.526	37.500
[a] 58- 125	6	0.086	0.731	0.891	-0.916	0.065	45.821	51.412
[b] 125-175	8	0.397	0.730	17.090	-1.681	0.029	84.034	4.917
50- 175*	14	0.505	0.824	12.772	-1.507	0.049	75.362	5.900
[c] 58-175	13	0.484	0.810	11.765	-1.534	0.051	76.709	6.520

Tab. 7.41 - V35.9b-1palaeointensity values and statistical parameters.

Sample V35.9b-2   Arbitray Units

Steps Demag	Power (watts)	Moment 10³	Dec	Inc
NRM	0	107.8	165.5	-26.8
1	17	107.2	165.6	-25.8
2	37	105.7	165.0	-25.7
3	50	104.9	164.9	-25.6
4	62	101.3	165.0	-25.5
5	75	97.1	165.1	-25.4
6	80	94.8	165.2	-25.4
7	88	81.7	165.0	-25.1
8	100	44.2	164.3	-24.0
9	120	21.4	165.1	-23.5
10	128	21.8	164.2	-23.0
11	138	21.4	165.6	-23.2
12	140	20.1	167.2	-17.8
13	142	18.8	163.4	-22.4
14	155	18.2	165.8	-24.1
15	165	18.2	163.2	-22.0

Tab. 7.42 - Directional and Intensity values of sample V35.9b-2.
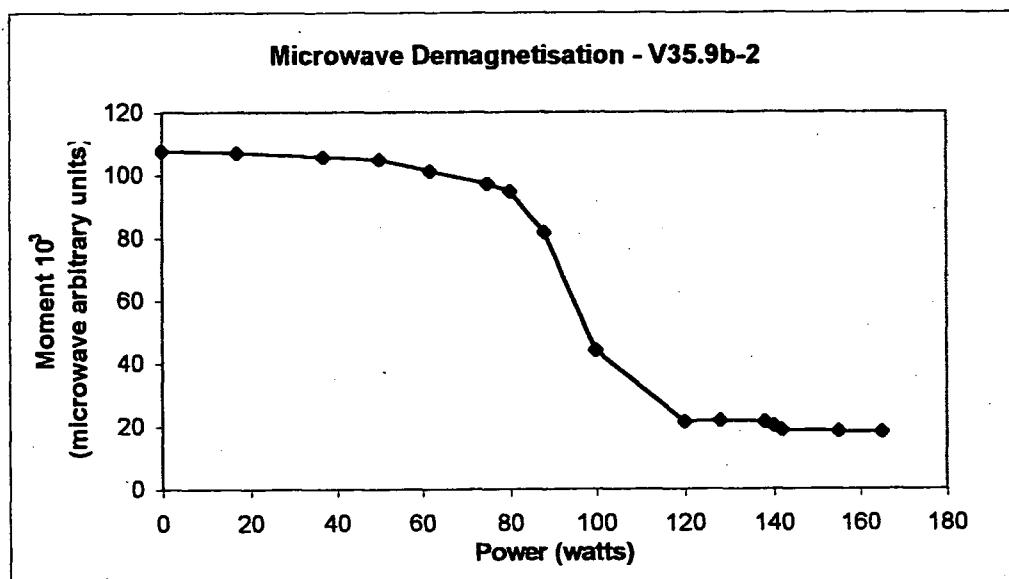
Fig. 7.25 - NRM demagnetisation of sample V35.9b-2, using microwave, to check the behaviour of the NRM and in particular the stability of Dec and Inc throughout the experiment.

Sample V34.8-1		Arbitrary Units						
Steps	Power (W)	x	y	z	Moment	Nrm 10³	Trm 10³	theta (°)
D (NRM)	37	-102120	31850	-49960	118063.20	123.11	0.00	
M1	42	-103170	25250	-49720	117276.13	117.09	6.62	90.01
M2	45	-101430	22450	-48970	114848.20	114.51	8.79	90.02
M3	50	-101640	21960	-49240	115054.37	114.68	9.33	90.02
M4	60	-101620	21860	-49200	115000.54	114.62	9.42	90.02
M5	72	-90970	5830	-43220	100883.59	98.56	21.59	90.04
M6	82	-80930	-8040	-40590	90894.74	85.16	32.18	90.28
M7	90	-70020	-17520	-37640	81403.44	72.22	38.42	90.68
M8	95	-14370	-90550	-27310	95664.18	32.05	101.03	108.77

Tab. 7.43 - V34.8-1:Values of NRM lost and TRM gained and their angular difference θ.
In light grey the data used to calculate the palaeointensity.
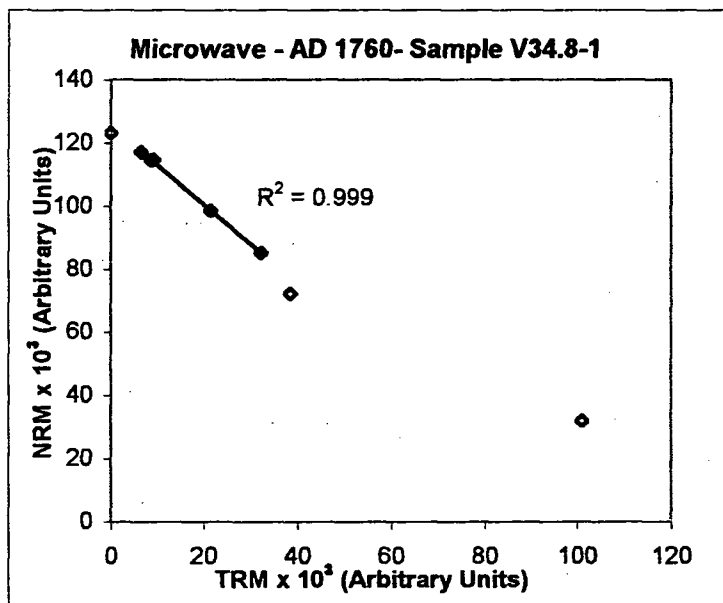
Fig. 7.26 - Conventional NRM/
TRM plot for sample V34.8-1
Statistical parameters relative to the
slope and palaeofield estimate are
shown in Tab.7.38. Empty diamond
indicate points excluded from the
palaeofield calculation.

Power range (W)	Sample V34.8-1							
	N	f	g	q	b	σb	Fpalaeo (μT)	Uncertainty
37 - 72	6	0.259	0.564	8.519	-1.270	0.022	63.490	7.452

Tab. 7.44 - V34.8-1 palaeointensity values and statistical parameters.

Sample V34.8-2		Arbitrary Units						
Steps	Power (W)	x	y	z	Moment	Nrm 10³	Trm 10³	theta (°)
D (NRM)	37	123980	-43700	-53760	142024.18	147.46	0.00	
M1	42	124740	-33600	-52810	139563.33	139.22	9.78	90.01
M2	45	119880	-27070	-52340	133579.47	132.81	14.50	90.08
M3	48	115270	-21040	-49500	127201.04	125.85	18.59	90.06
M4	50	116160	-19400	-49890	127900.42	126.28	20.44	90.06
M5	52	113120	-16890	-50220	124913.79	123.02	22.04	90.17
M6	55	108140	-7610	-45640	117623.05	114.05	28.90	90.07
M7	58	103570	-650	-45130	112977.36	107.80	34.14	90.18
M8	60	97930	3420	-43560	107235.51	101.09	36.25	90.27
M9	62	94890	4890	-43260	104400.44	97.94	36.79	90.38
M10	68	90970	71620	-33220	120451.37	70.33	98.06	90.23
M11	70	26440	52710	-33660	67900.02	35.48	66.92	103.73

Tab. 7.45 - V34.8-2:Values of NRM lost and TRM gained and their angular difference θ. In light grey the data used to calculate the palaeointensity.
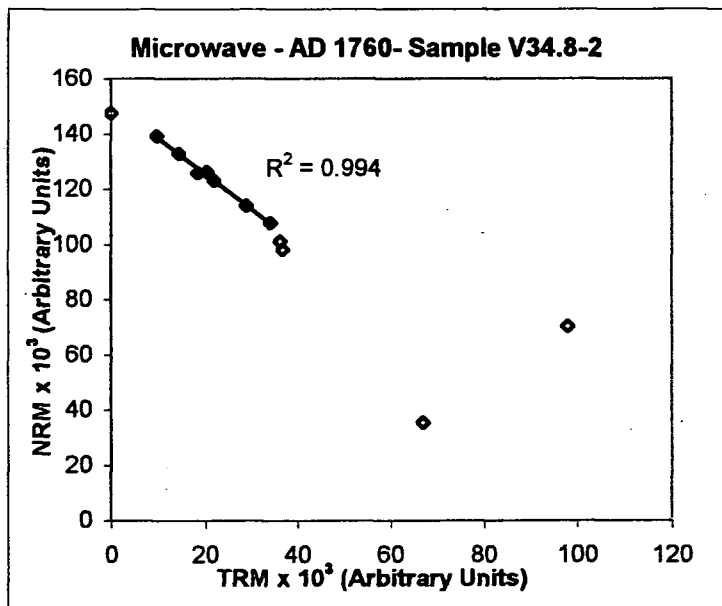
Fig. 7.27 - Conventional NRM/ TRM plot for sample V34.8-2 Statistical parameters relative to the slope and palaeofield estimate are shown in Tab.7.42. Empty diamond indicate points excluded from the palaeofield calculation.

Power	Sample V34.8-2							
range (W)	N	f	g	q	b	σb	Fpalaeo (μT)	Uncertainty
42 - 58	7	0.213	0.777	4.620	-1.288	0.046	64.380	13.934

Tab. 7.46 - V34.8-2 palaeointensity values and statistical parameters.

AD 1760 lava flow specimens
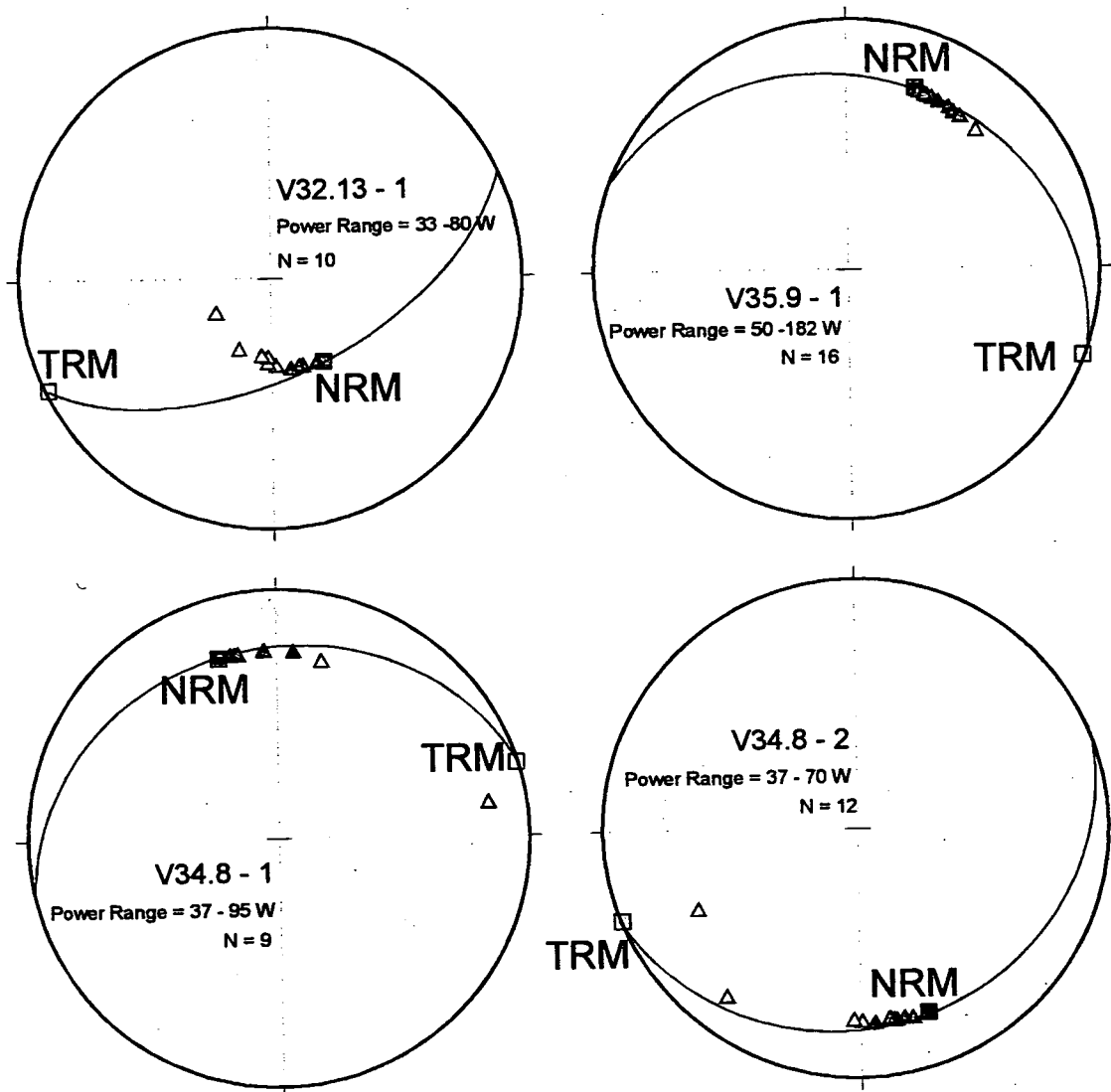
Fig. 7.28. Stereo plots showing total vectors moving from the measured NRM(▩) towards the applied TRM direction (□) along great circles.
Dark triangles indicate points used to calculate the palaeointensity.

| Sample V25.2-1 | | Arbitrary Units | | | | | | |
Steps	Power (W)	x	y	z	Moment	Nrm 10³	Trm 10³	theta (°)
D (NRM)	25	-32050	-33360	-185460	191142.63	228.44	0.00	
M1	26	-9340	-48320	-167720	174791.47	172.73	26.75	90.01
M2	27	-4890	-50390	-166460	173988.49	171.13	31.43	90.02
M3	28	-2310	-49910	-160590	168182.91	164.93	33.00	90.04
M4	30	-2260	-51880	-161590	169729.11	166.22	34.34	90.01
M5	32	870	-54530	-153440	162843.83	158.25	38.41	90.01
M6	36	6710	-55400	-141980	152553.28	146.30	43.22	90.01
M7	38	9780	-57580	-143190	154643.08	147.35	46.95	90.01
M8	42	12940	-58490	-137670	150138.44	141.62	49.87	90.01
M9	46	18710	-61500	-130910	145841.50	134.62	56.11	90.01
M10	50	29400	-66040	-118430	138749.08	121.53	66.99	90.02
M11	55	34280	-68790	-115840	139018.30	118.69	72.44	90.04
M12	62	38770	-69970	-110180	136156.33	112.68	76.53	90.05
M13	68	43990	-72060	-105970	135489.50	108.13	81.79	90.08
M14	75	47720	-76630	-100010	134726.97	102.44	87.54	90.03
M15	88	56980	-81900	-95840	138346.07	97.82	97.92	90.06
M16	105	82130	-96160	-83510	151545.38	84.43	126.11	90.19
M17	120	110020	-1E+05	-72220	174436.49	72.50	159.06	90.33
M18	135	188330	-2E+05	-39410	251532.46	41.72	249.19	91.57

Tab. 7.47 - V25.2-1:Values of NRM lost and TRM gained and their angular difference θ. In light grey the data used to calculate the palaeointensity.

Microwave - AD 1806 - Sample V25.2-1

$R^2 = 0.987$

NRM x 10³ (Arbitrary Units) vs TRM x 10³ (Arbitrary Units)
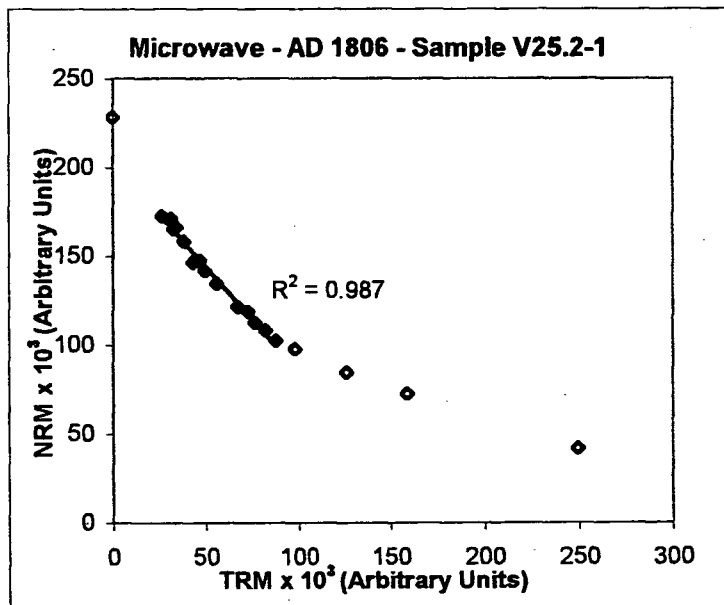
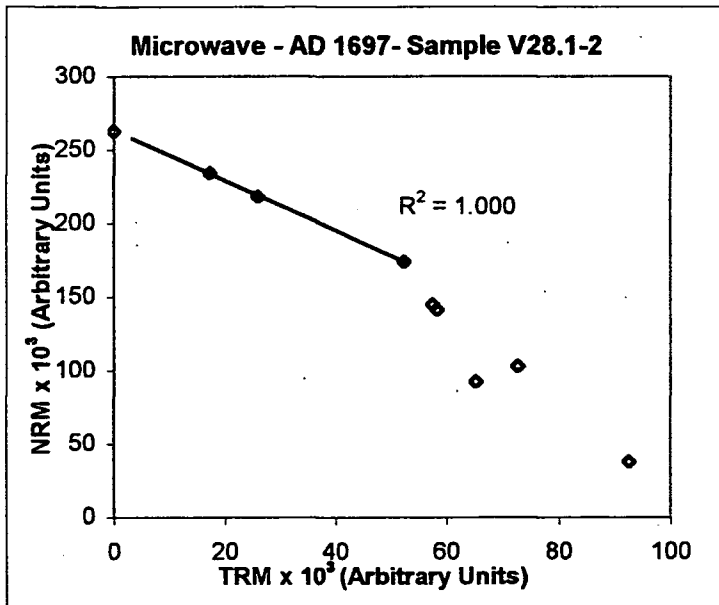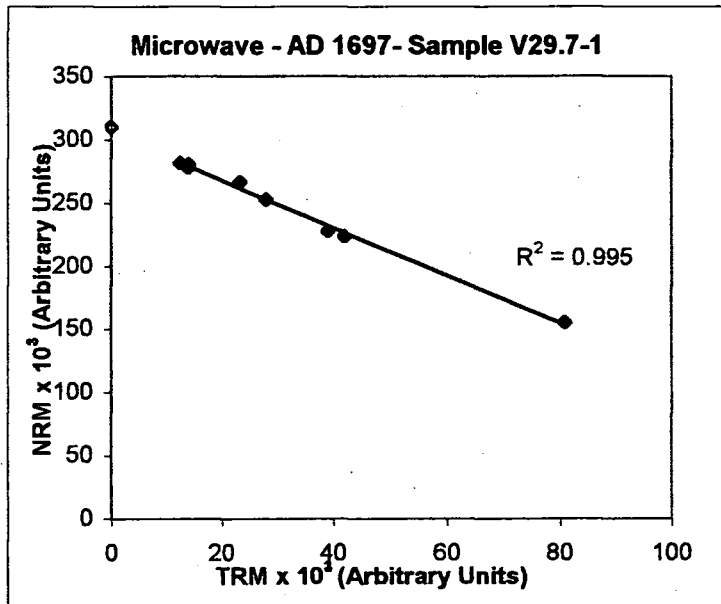Fig. 7.29 - Conventional NRM/TRM plot for sample V25.2-1 Statistical parameters relative to the slope and palaeofield estimate are shown in Tab.7.46. Empty diamond indicate points excluded from the palaeofield calculation.

Power	Sample V25.2-1							
range (W)	N	f	g	q	b	σ_b	Fpalaeo (μT)	Uncertainty
26 - 75	14	0.308	0.878	8.105	-1.198	0.040	59.904	7.391

Tab. 7.48 - V25.2-1 palaeointensity values and statistical parameters.

Sample V25.2-2		Arbitrary Units						
Steps	Power (W)	x	y	z	Moment	Nrm 10³	Trm 10³	theta (°)
D (NRM)	26	-34560	-13790	-48010	60741.40	66.57	0.00	
M1	28	-21590	-30810	-48110	61073.37	57.49	21.12	90.51
M2	29	-12300	-25450	-48300	55963.22	52.77	23.22	94.50
M3	30	-9290	-22920	-48270	54236.73	51.61	24.17	97.05
M4	31	-8230	-21680	-48470	53731.71	51.49	24.58	98.37
M5	32	-6210	-20050	-47470	51903.44	50.06	25.18	100.20
M6	33	-2910	-18120	-47840	51239.32	50.21	27.75	103.83
M7	35	-340	-14530	-47690	49855.52	50.72	29.67	108.75
M8	36	2720	-10420	-47230	48442.21	52.26	33.02	115.31
M9	37	2390	-3510	-46650	46842.87	56.35	35.74	124.11

Tab. 7.49 - V25.2-2:Values of NRM lost and TRM gained and their angular difference θ.

Microwave - AD 1806- Sample V25.2-2
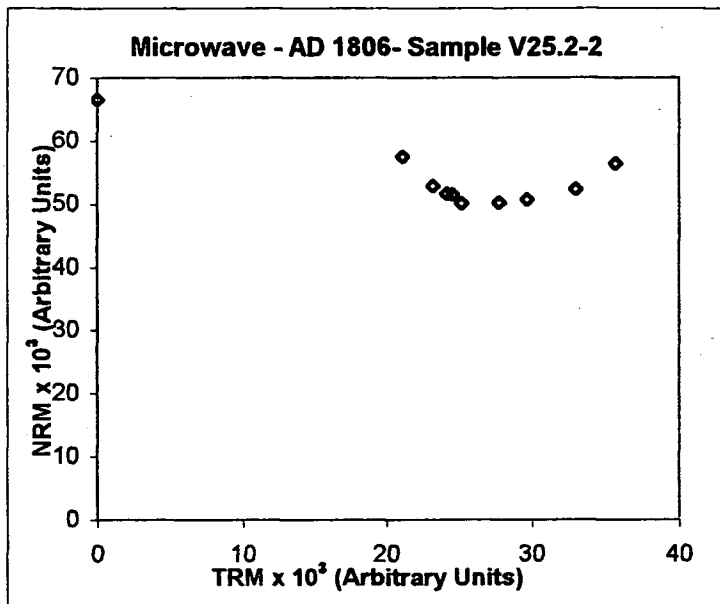
Fig. 7.30 - Conventional NRM/
TRM plot for sample V25.2-2

Sample V24.3-2		Arbitrary Units						
Steps	Power (W)	x	y	z	Moment	Nrm 10^4	Trm 10^4	theta (°)
D (NRM)	17	-34550	-56100	73830	98953.43	120.50	0.00	
M1	20	-31540	-56630	73800	98225.09	98.18	2.96	90.07
M2	21	-19470	-57510	69290	92128.09	91.12	13.72	90.10
M3	23	-15030	-53540	66480	86671.93	85.32	15.89	90.42
M4	27	-11770	-50620	63990	82435.66	80.77	17.53	90.72
M5	31	-6160	-46790	60950	77085.36	74.65	21.07	91.37
M6	35	-1920	-43400	58510	72874.32	69.79	23.67	92.09
M7	42	3100	-37430	55370	66906.29	63.24	26.52	93.87
M8	52	12970	-27610	50170	58715.94	53.46	33.37	98.45
M9	58	12080	-13300	47780	51046.50	51.28	35.19	110.48
M10	60	7280	-4220	46930	47678.42	55.86	38.71	122.86

Tab. 7.50 - V24.3-2:Values of NRM lost and TRM gained and their angular difference θ. In light grey the data used to calculate the palaeointensity.
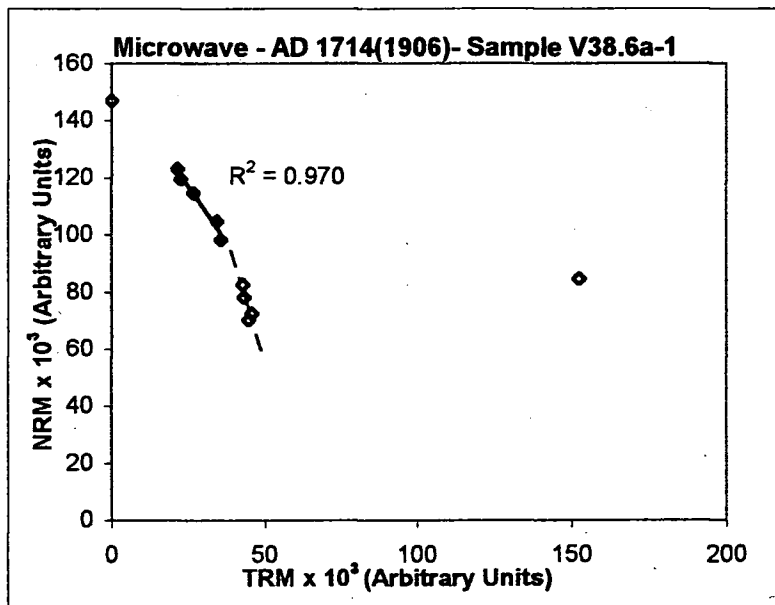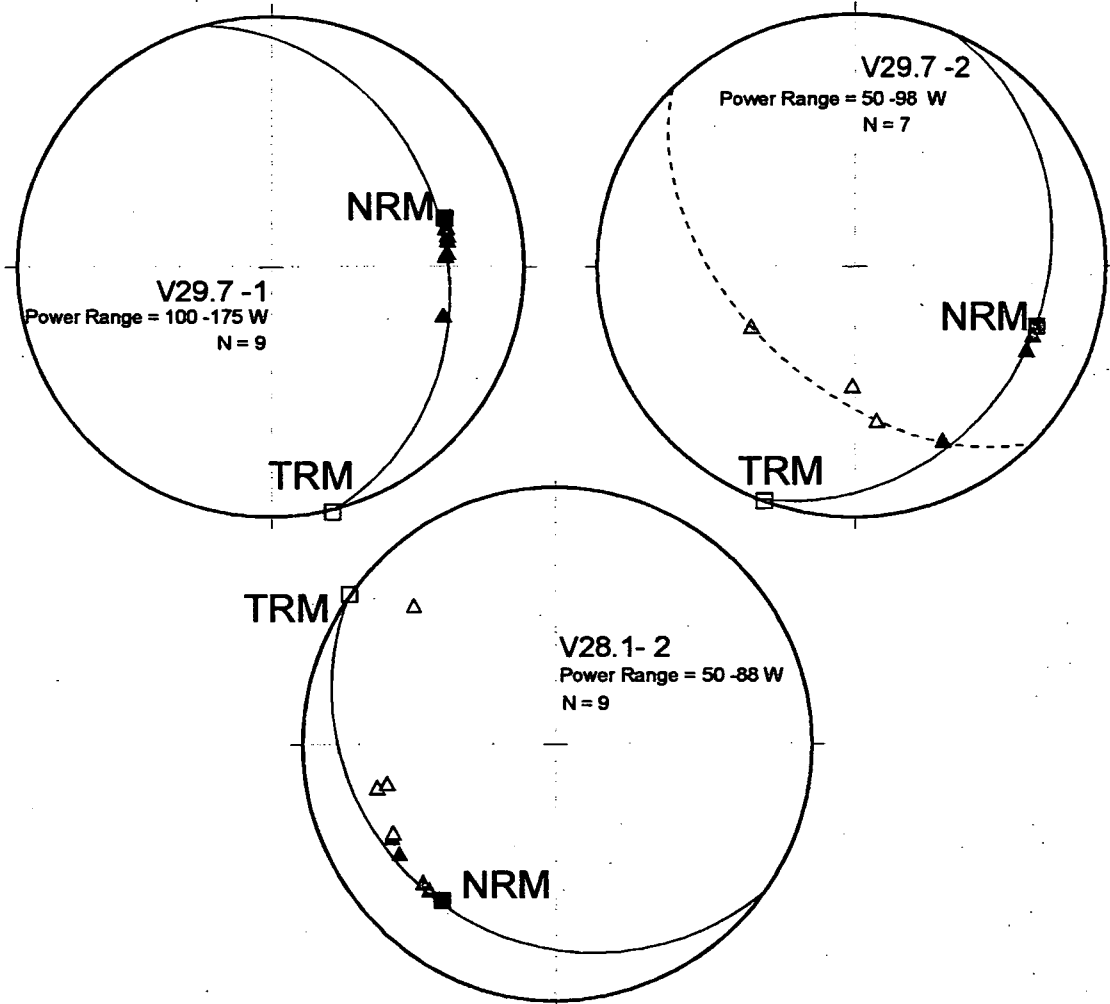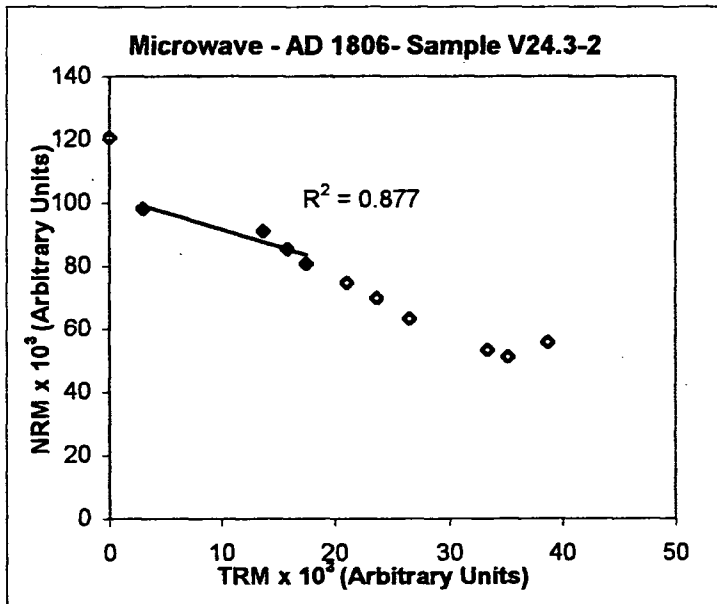

Fig. 7.31 - Conventional NRM/ TRM plot for sample V24.3-2 Statistical parameters relative to the slope and palaeofield estimate are shown in Tab.7.49. Empty diamond indicate points excluded from the palaeofield calculation.

Power range (W)	Sample V24.3-2							
	N	f	g	q	b	σ_b	Fpalaeo (μT)	Uncertainty
20 - 27	4	0.145	0.656	0.376	-1.147	0.289	57.337	152.294

Tab. 7.51 - V24.3-2 palaeointensity values and statistical parameters.

Sample V24.3-1　　Arbitray Units

Steps Demag	Power (watts)	Moment 10³	Dec	Inc
NRM	0	129.3	50.7	-32.4
1	8	128.0	50.8	-33.2
2	12	125.4	51.3	-33.5
3	17	122.1	51.5	-33.6
4	25	115.1	51.8	-33.9
5	29	110.9	52.8	-34.6
6	33	110.6	52.6	-34.1
7	42	102.3	52.8	-34.2
8	50	93.8	53.2	-34.6
9	58	91.8	52.7	-34.6
10	65	88.2	53.4	-35.5
11	70	85.2	53	-35.2
12	75	82.9	53.7	-35.6
13	80	82.1	52.9	-35.3
14	85	80.5	53.1	-35.1
15	95	75.9	53.4	-34.6
16	105	69.6	53.2	-35.2
17	112	67.8	53.5	-34.9
18	122	51.5	54.4	-36.5
19	132	43.7	54	-36.3
20	142	30.2	56.3	-34.3
21	152	13.1	55.3	-27.3

Tab. 7.52 - Directional and Intensity values of sample V24.3-1.
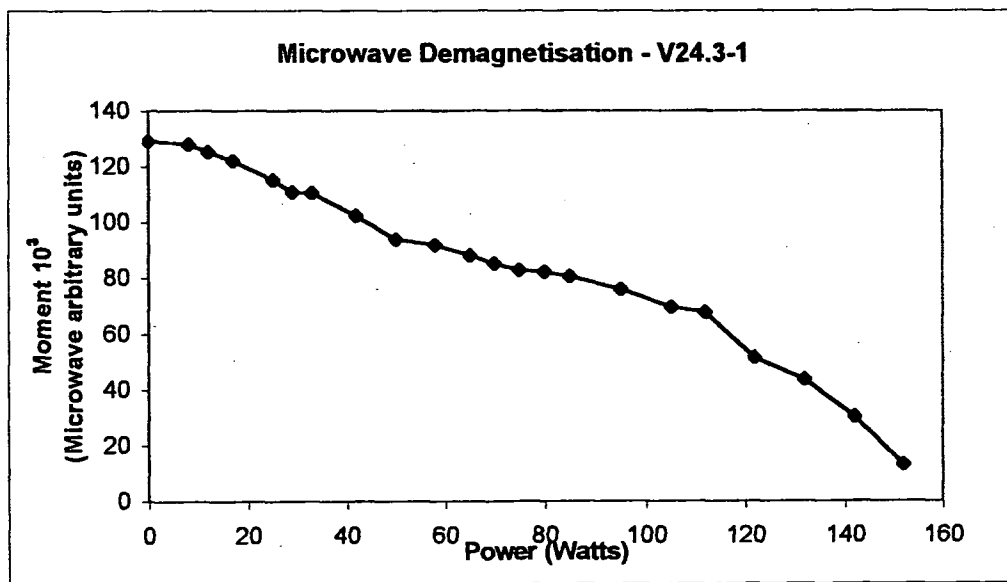
Fig. 7.32 - NRM demagnetisation of sample V24.3-1, using microwave, to check the behaviour of the NRM and in particular the stability of Dec and Inc throughout the experiment.
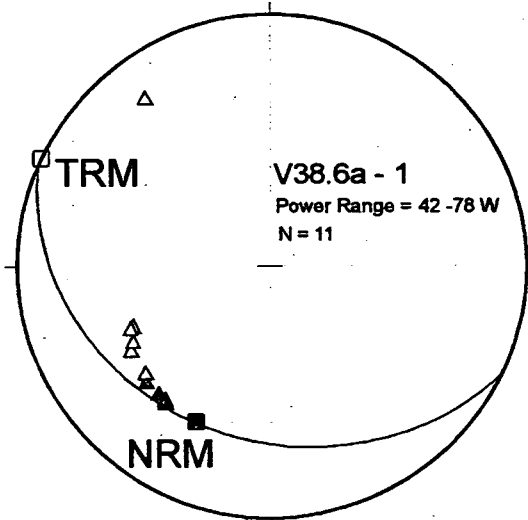
310

AD 1806 lava flow specimens
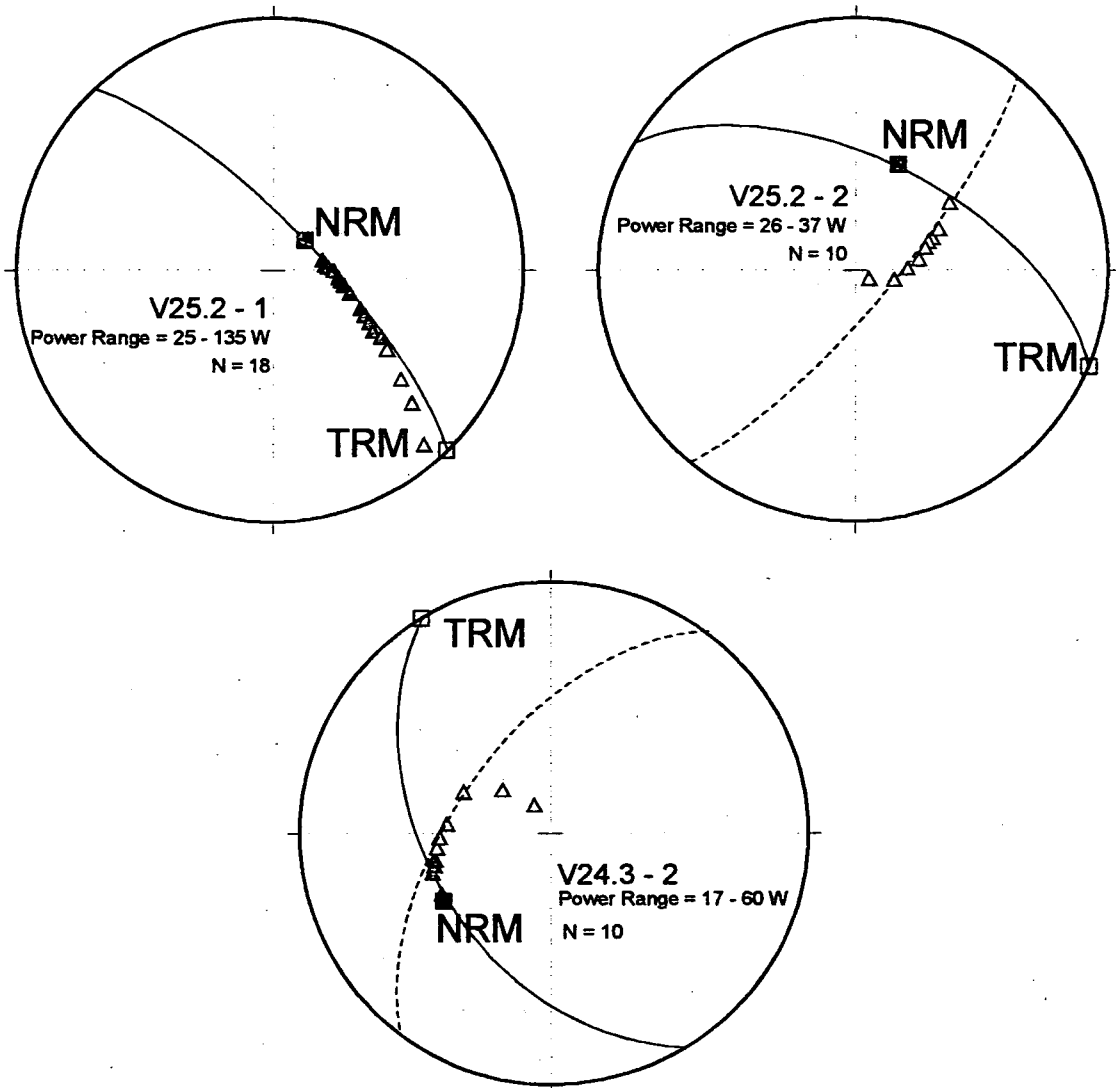
Fig. 7.33. Stereo plots showing total vectors moving from the measured NRM(▓) towards the applied TRM direction (□) along great circles.
Dashed great circles show secondary direction. Dark triangles indicate points used to calculate the palaeointensity.

7.7.1 – Site V42

For sample 13b-1 only the first four vectors defined a great circle (Fig. 7.39). Starting from 65W all subsequent vectors moved away it. The θ values showed significant changes (>90°) starting from step M3 (Tab. 7.53). The NRM/TRM plots showed one possible slope, considering only four points, D(NRM) included, and excluding the others although they fell on the same straight line (Fig. 7.34, Tab. 7.54).

7.7.2 – Site V43

Sample V43.9c-1 & V43.9c-2 For sample 9c-2 almost all the vectors defined a great circle (Fig. 7.39) except the last three. At step M9 the Dec of the total vector was only some 40° away from the NRM direction. The θ values showed an almost constant value until M10 (Tab. 7.55) when it started to increase. The NRM/TRM plots showed one possible slope, excluding the last four points. Considering or not the first point D(NRM) did not change the palaeofield estimation (Fig. 7.35, Tab. 7.56). The microwave demagnetisation of the sister sample 9c-1 showed high stability of NRM, especially in Inclination, starting from 55 up to 122W (Fig. 7.36, Tab. 7.57)

7.7.3 – Site V44

Sample V44.3b-1 It showed very anomalous behaviour (Fig. 7.39). Theta angle stayed constant until M8 when it slightly increased until M11 when it kept an almost constant value (~92.50°). After this point it increased again until the end of the experiment (Tab. 7.58). It was possible to determinate one slope (Fig. 7.37, Tab. 7.59) but this was very poorly defined.

Sample V44.3b-2 None of the vectors lied on the NRM/TRM great circle and they seemed to follow a secondary direction (Fig. 7.39). The angle θ was >90 starting from step M2 where it increased gradually until step M8, when changes were more significant (Tab. 7.60). Although almost all the points were on the same straight line (Fig. 7.38), none of these points fulfilled any of the three requirements needed to be accepted.

Sample V42.13b-1		Arbitrary Units						
Steps	Power (W)	x	y	z	Moment	Nrm 10³	Trm 10³	theta (°)
D (NRM)	50	-50600	-50320	-131600	149703.11	161.46	0.00	
M1	58	-38260	-59650	-130360	148376.82	147.58	15.37	90.03
M2	62	-28560	-58090	-125980	141637.15	140.07	21.96	90.38
M3	65	-20500	-55420	-119740	133526.38	131.21	26.76	90.85
M4	68	-17230	-52910	-119410	131738.72	129.32	28.69	91.48
M5	70	-12880	-51010	-116470	127801.31	124.97	31.41	91.99
M6	72	-11850	-49480	-115940	126612.70	123.86	31.82	92.36
M7	75	-3600	-48180	-111560	121572.64	117.56	38.06	93.14
M8	78	400	-41350	-110620	118096.43	114.84	40.48	95.44
M9	80	-180	-39660	-109830	116771.47	113.95	39.56	95.83
M10	85	25960	-29400	-96820	104462.40	99.15	60.38	102.37
M11	88	10000	4440	-93950	94584.97	111.91	63.84	122.39

Tab. 7.53 - V42.13b-1:Values of NRM lost and TRM gained and their angular difference θ. In light grey the data used to calculate the palaeointensity.

Microwave - AD 1839 - Sample V42.13b-1

$R^2 = 0.977$

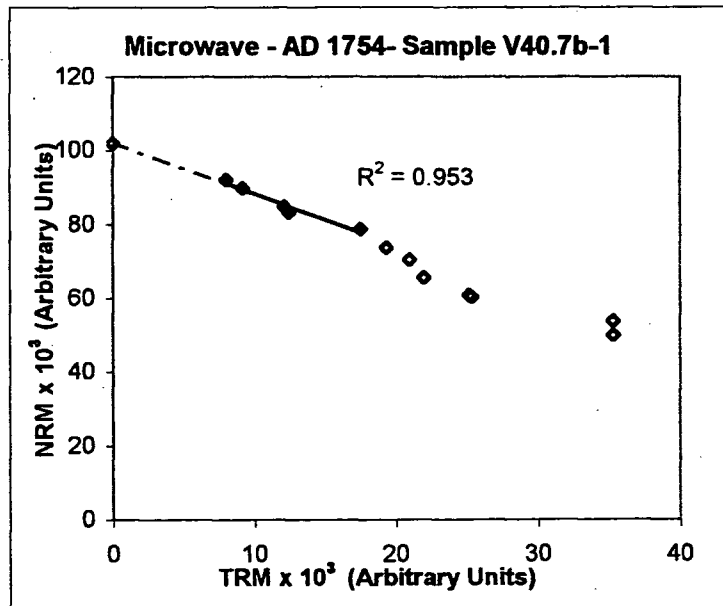NRM x 10³ (Arbitrary Units) vs TRM x 10³ (Arbitrary Units)
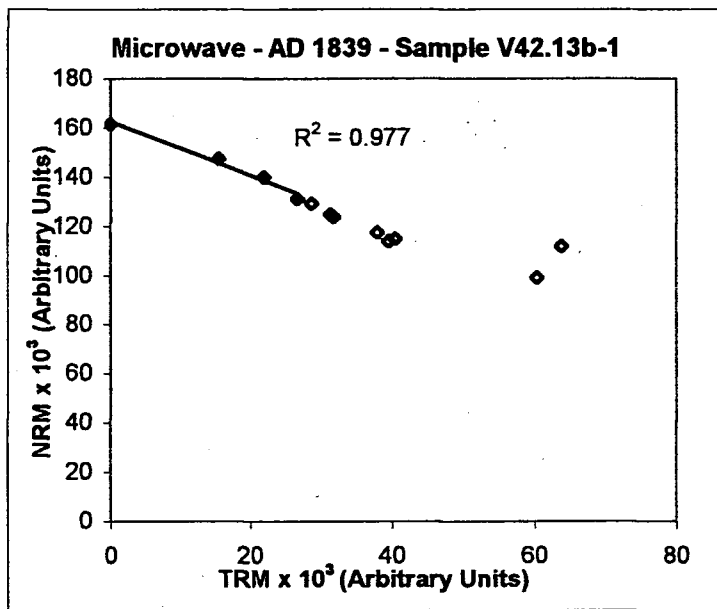
Fig. 7.34 - Conventional NRM/TRM plot for sample V42.13b-1 Statistical parameters relative to the slope and palaeofield estimate are shown in Tab.7.51. Empty diamond indicate points excluded from the palaeofield calculation.

Power range (W)		Sample V42.13b-1						
	N	f	g	q	b	σ_b	Fpalaeo (μT)	Uncertainty
50-65	4	0.187	0.642	1.124	-1.099	0.118	54.931	48.869

Tab. 7.54 - V42.13b-1 palaeointensity values and statistical parameters.

Sample V43.9c-2		Arbitrary Units						
Steps	Power (W)	x	y	z	Moment	Nrm 10³	Trm 10³	theta (°)
D (NRM)	42	-36780	-16100	59630	71886.82	75.68	0.00	
M1	45	-36050	-19000	59380	72017.96	71.96	3.00	90.05
M2	50	-34620	-19320	59790	71740.16	71.64	3.87	90.05
M3	55	-33970	-20060	59020	70991.02	70.83	4.78	90.03
M4	60	-32440	-20580	58620	70087.05	69.84	5.98	90.11
M5	65	-31210	-21230	57530	68807.54	68.46	7.06	90.12
M6	70	-28850	-22460	56100	66962.56	66.35	9.21	90.18
M7	75	-26910	-22710	55030	65331.41	64.56	10.38	90.33
M8	80	-25330	-23120	54140	64088.09	63.13	11.51	90.45
M9	88	-17160	-25670	50180	58918.99	56.53	17.84	91.23
M10	90	-1530	-26500	43840	51249.75	45.65	27.87	95.30
M11	92	1130	-16780	43380	46526.01	44.87	25.76	102.80
M12	95	5880	-8120	41000	42207.92	45.50	29.41	115.55

Tab. 7.55 - V43.9c-2:Values of NRM lost and TRM gained and their angular difference θ.
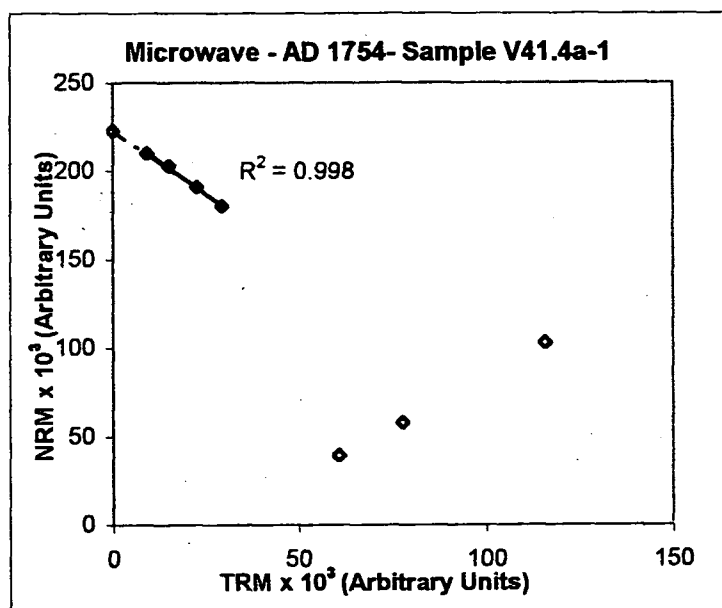In light grey the data used to calculate the palaeointensity.
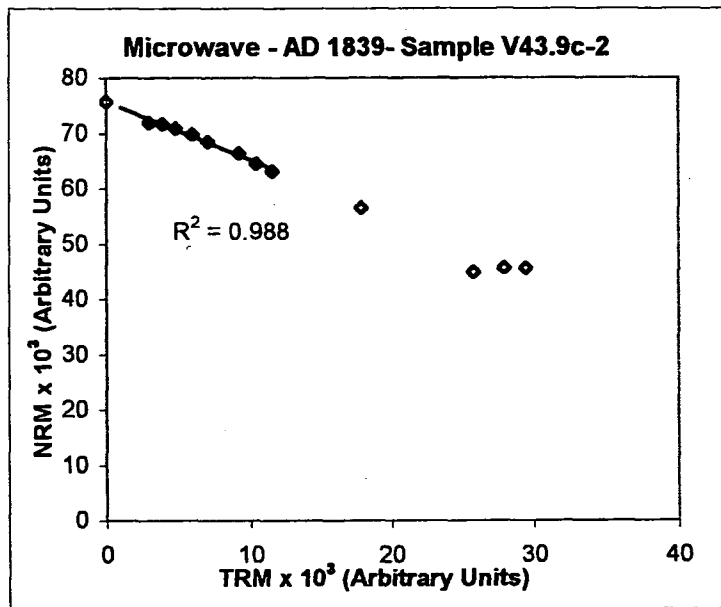
Fig. 7.35 - Conventional NRM/ TRM plot for sample V43.9c-2 Statistical parameters relative to the slope and palaeofield estimate are shown in Tab.7.53. Empty diamond indicate points excluded from the palaeofield calculation.

Power range (W)	N	f	g	q	b	σ_b	Fpalaeo (μT)	Uncertainty
42 - 80*	9	0.166	0.827	4.135	-1.061	0.035	53.031	12.826
45 - 80	8	0.117	0.829	2.124	-1.066	0.049	53.321	25.109

*including D(NRM)

Tab. 7.56 - V43.9c-2 palaeointensity values and statistical parameters.

314

Sample V43.9c-1   Arbitray Units

Steps Demag	Power (watts)	Moment 10^3	Dec	Inc
NRM	0	150.7	160.3	-61.0
1	17	148.7	159.9	-60.8
2	37	143.1	160.3	-60.4
3	50	143.5	159.9	-60.7
4	55	134.3	149.0	-58.6
5	58	133.8	148.9	-58.6
6	60	131.8	148.5	-58.5
7	65	128.1	148.5	-58.7
8	70	125.2	148.4	-58.7
9	78	111.4	148.0	-58.4
10	82	89.8	147.9	-58.5
11	88	73.4	146.3	-58.5
12	98	48.9	144.6	-58.3
13	122	46.9	146.3	-58.2

Tab. 7.57 - Directional and Intensity values of sample V43.9c-1.
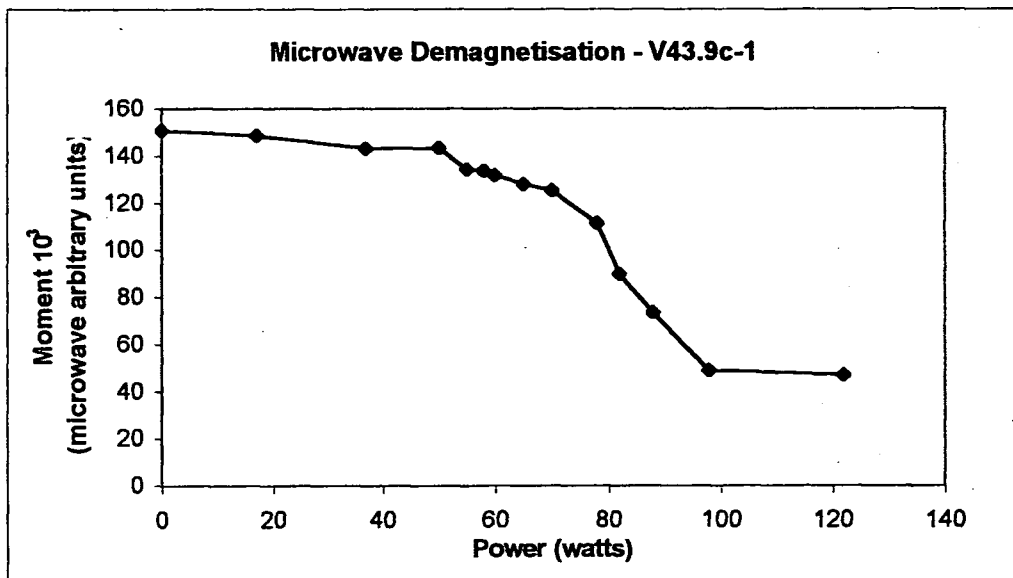
Fig. 7.36 - NRM demagnetisation of sample V43.9c-1, using microwave, to check the behaviour of the NRM and in particular the stability of Dec and Inc throughout the experiment.

Sample V44.3b-1		Arbitrary Units						
Steps	Power (W)	x	y	z	Moment	Nrm 10³	Trm 10³	theta (°)
D (NRM)	26	-18500	-42750	-49780	68175.22	78.14	0.00	
M1	29	-17820	-42110	-49680	67519.68	67.52	0.67	90.26
M2	33	-17140	-41010	-48080	65477.37	65.48	0.69	90.12
M3	40	-15310	-40260	-44570	61981.84	61.95	2.17	90.22
M4	42	-14910	-38850	-42900	59766.55	59.74	2.04	90.28
M5	50	-12190	-36960	-40110	55887.83	55.78	3.60	90.12
M6	60	-10920	-34400	-35900	50905.96	50.78	4.01	90.43
M7	72	-8810	-31320	-32170	45754.42	45.55	4.63	90.35
M8	82	-3870	-22760	-18730	29728.90	29.24	6.55	92.10
M9	90	1450	-17080	-8870	19300.41	17.57	9.54	94.68
M10	92	3440	-16270	-9330	19068.18	16.48	10.25	92.22
M11	95	2590	-14190	-7950	16470.18	14.41	8.68	92.68
M12	100	5020	-12520	-3230	13870.25	10.10	10.76	96.69
M13	105	5130	-10340	570	11556.70	7.79	11.02	106.44
M14	108	5450	-9850	2510	11533.65	8.08	12.33	115.02
M15	110	6070	-8720	4880	11691.78	9.44	14.86	128.15
M16	112	6580	-7090	4440	10643.22	7.38	13.28	126.84
M17	115	7970	-6210	6840	12201.25	11.91	19.19	142.24
M18	118	8680	-3570	8030	12351.85	22.95	30.89	159.53

Tab. 7.58 - V44.3b-1:Values of NRM lost and TRM gained and their angular difference θ.
In light grey the data used to calculate the palaeointensity.

Microwave - AD 1839- Sample V44.3b-1

$R^2 = 0.933$

NRM x 10³ (Arbitrary Units)

TRM x 10³ (Arbitrary Units)
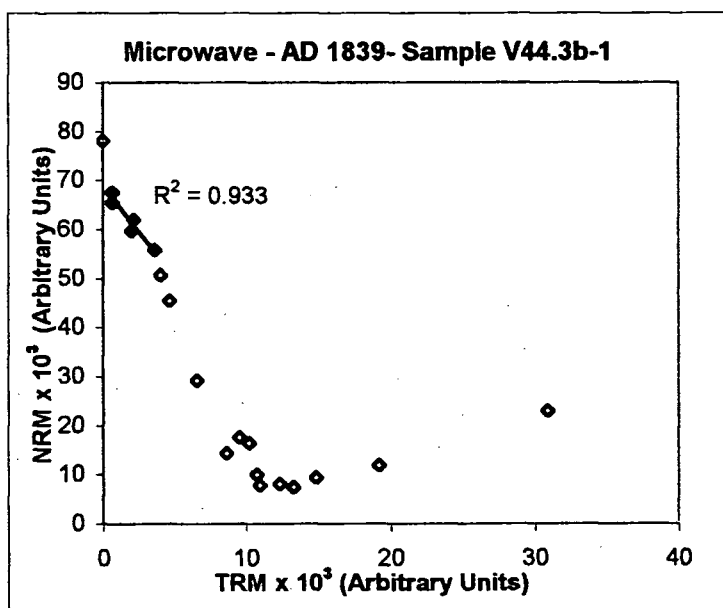
Fig. 7.37 - Conventional NRM/ TRM plot for sample V44.3b-1 Statistical parameters relative to the slope and palaeofield estimate are shown in Tab.7.55. Empty diamond indicate points excluded from the palaeofield calculation.

Power		Sample V44.3b-1						
range (W)	N	f	g	q	b	σ_b	Fpalaeo (μT)	Uncertainty
29 - 60	6	0.214	0.778	1.369	-4.409	0.537	220.455	161.011

Tab. 7.59 - V44.3b-1 palaeointensity values and statistical parameters.

316

Sample V44.3b-2		Arbitrary Units						
Steps	Power (W)	x	y	z	Moment	Nrm 10³	Trm 10³	theta (°)
D (NRM)	25	-17280	-41460	52210	68872.45	71.27	0.00	
M1	29	-570	-44190	51440	67817.07	65.79	16.66	90.17
M2	30	1570	-38730	51260	64265.58	62.17	17.71	91.26
M3	31	3320	-36560	50930	62781.53	60.43	19.18	91.95
M4	32	4520	-34700	50870	61743.64	59.27	20.30	92.70
M5	33	6080	-33140	50180	60442.19	57.68	21.60	93.23
M6	35	7690	-30180	49680	58635.07	55.75	23.16	94.59
M7	37	9190	-28600	49020	57492.40	54.32	24.47	95.28
M8	42	12910	-23320	47620	54572.47	50.94	28.20	98.26
M9	45	15650	-12710	45290	49574.70	47.71	33.20	106.91
M10	48	9730	-1950	45050	46130.01	53.38	38.30	122.36

Tab. 7.60 - V44.3b-2:Values of NRM lost and TRM gained and their angular difference θ.
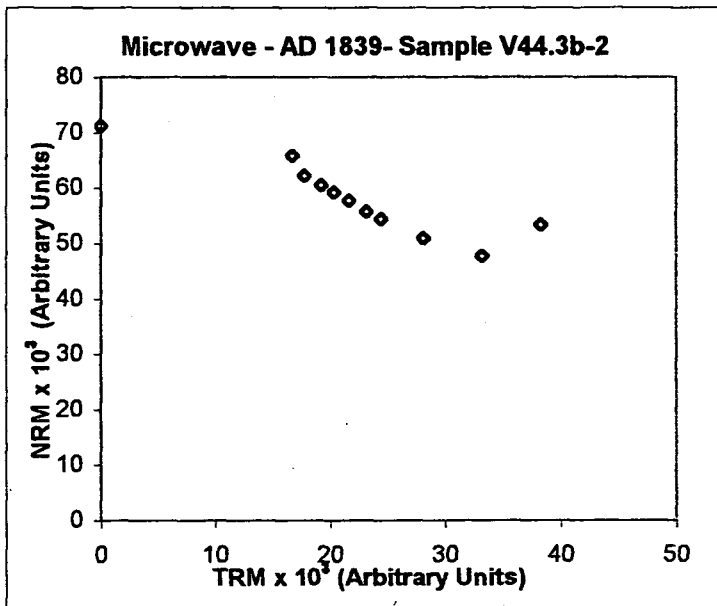
Fig. 7.38 - Conventional NRM/ TRM plot for sample V44.3b-2

AD 1839 lava flow specimens
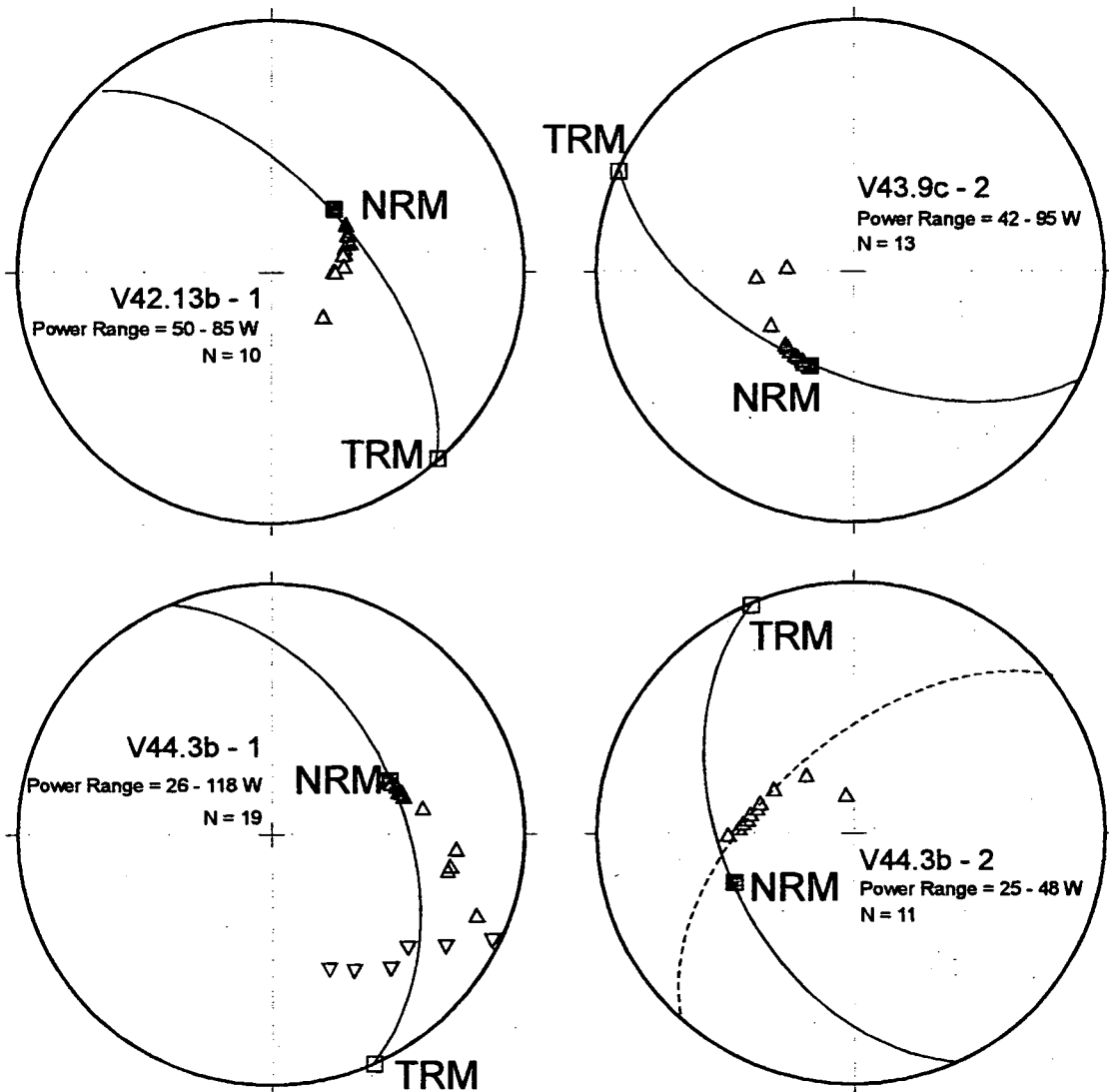
Fig. 7.39. Stereo plots showing total vectors moving from the measured NRM(■) towards the applied TRM direction (□) along great circles.
Dashed great circles show secondary directions, dark triangles indicate points used to calculate the palaeointensity and up-side down triangles indicate points in the upper hemisphere.

Chapter VIII -

Rock Magnetic Properties

8.1 Introduction

In this chapter the rock magnetic properties, investigated using the techniques described in chapter 3, are described. The results have been divided into three different types; A1, A2 and B plus the anomalous behaviour showed by one sample, which will be referred to as Ex (for exception). The first order discrimination for these groups was based on the IRMs 3 component and the low field susceptibility (K) behaviour. A second order discrimination was based on the coercivity of remanence (H_{CR}) and the K_{ARM}/K ratio. Representative examples for each case will be illustrated.

8.2 Description of Type A1 samples

a) First order discriminators

3 axes IRM - All the samples in this group showed a dominance of the medium coercivity fractions that were mainly removed at 580°C following a convex demagnetization curve (Fig. 8.1). The initial intensities of the soft fractions were no more than 30% of the maximum initial intensity of the medium component and it was removed at about 560-580°C. The initial intensities of the hard fractions were mostly negligible, being only about 15 % of the intermediate fraction initial intensity in a few cases, and all were completely removed at 560-580°C.

Low field susceptibility - All the samples showed an initial value of K, at room temperature, within the range 15-25 x 10^{-3} SI. They had a linear trend throughout the heating experiment, with a slight decrease (not always present) starting from 500° (Figs. 8.1, 8.9).
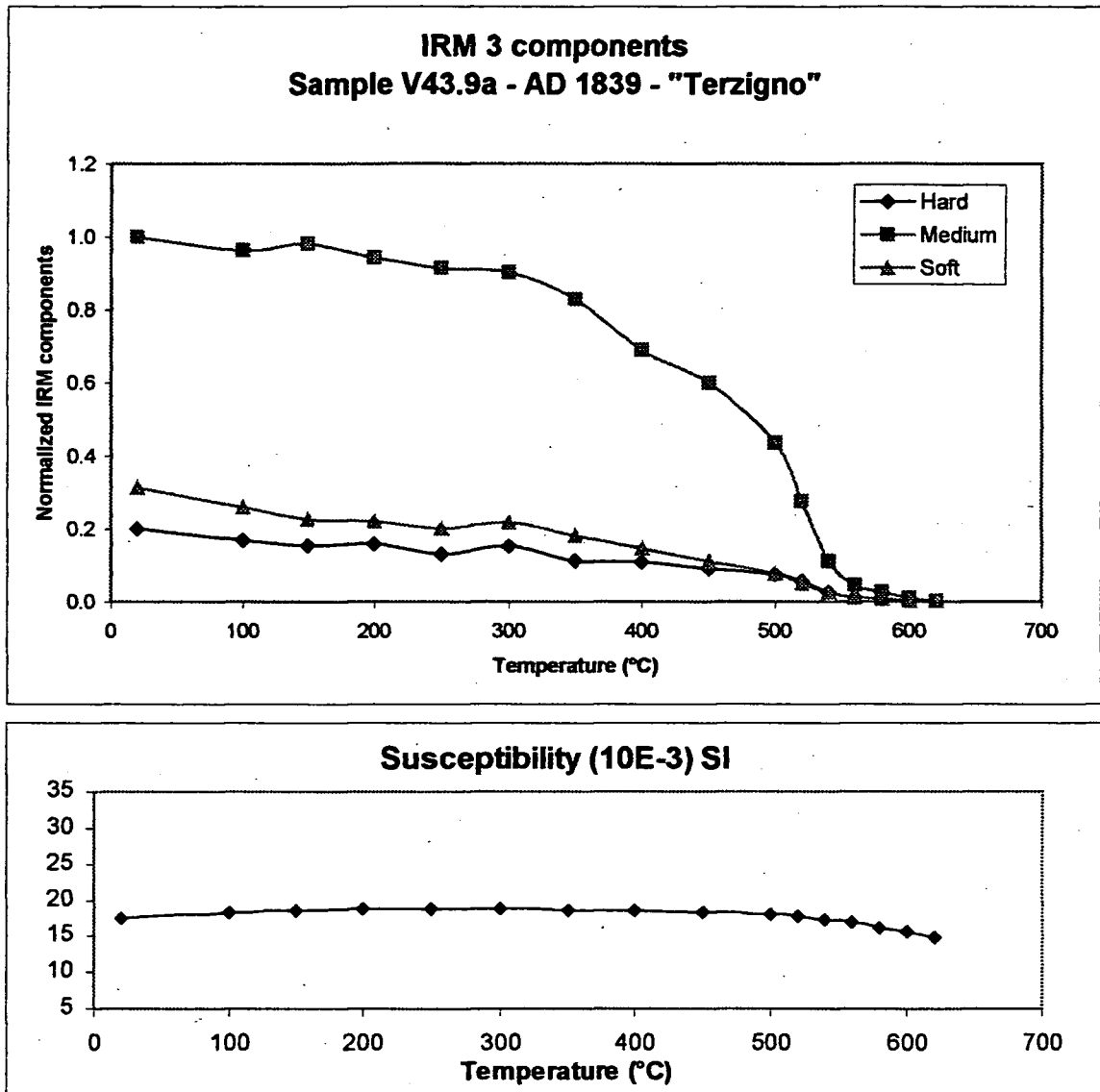
Fig. 8.1 - IRMs 3 components and susceptibility behaviours for sample V43.9a

b) Second order discriminators

Coercivity of remanence - Most of the samples showed the higher values of H_{CR} (~70 mT) and all were in the range 50-70 mT (Fig. 8.2, Tab.8.1). Part of this experiment was used to analyse the IRM acquisition along the z-axis. This showed that the majority of samples saturated in a field of about 200 mT.

320
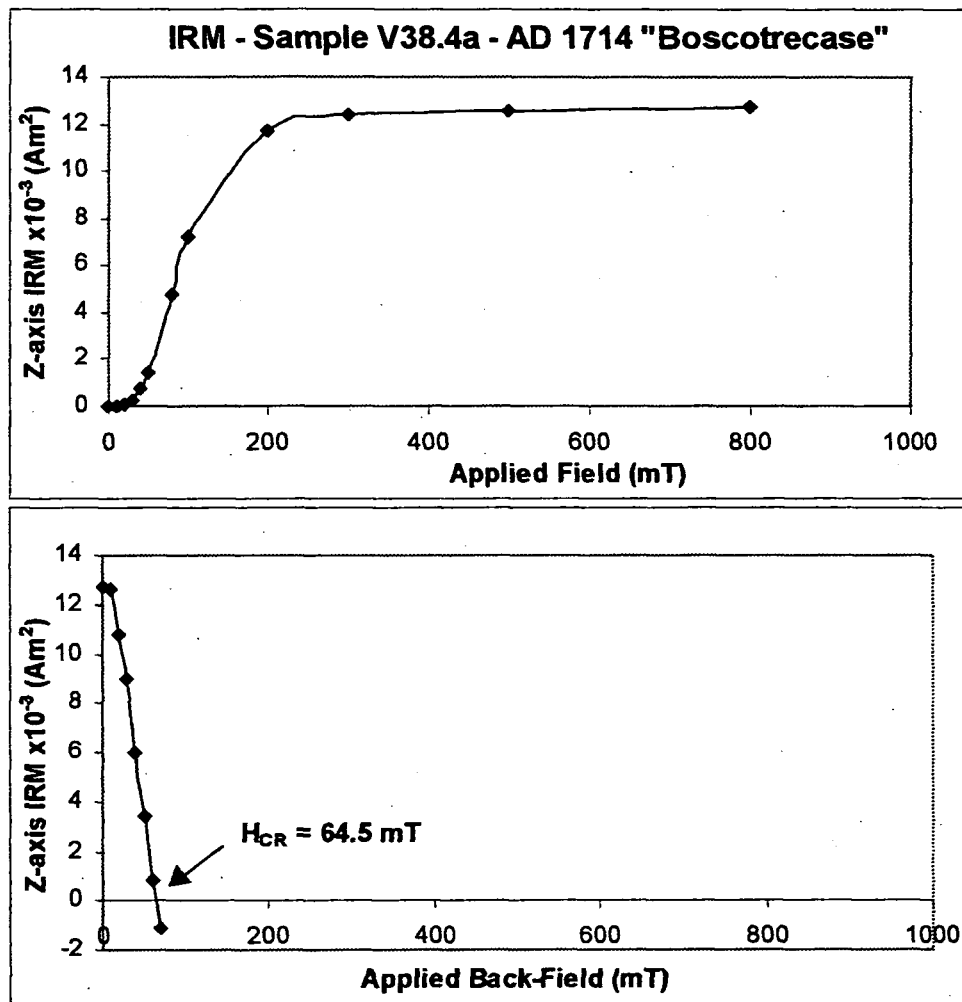
Fig. 8.2 - IRM acquisition along z and -z for sample V38.4a.

c) K_{ARM}/K ratio

The mean value obtained from this experiment was 2.43 (Tab. 8.1). Samples V34.5, V41.0b and V43.9a showed a relatively higher values (~3).

8.3 Description of Type A2 samples

a) First order discriminators

3 axes IRM - The medium coercivity fractions were dominant (as in Type A1), but the soft fractions had initial intensities not less than 60% of the maximum initial intensity of the

medium component and behaved similarly to the medium fraction. The initial intensity of the hard fractions was about 10-15%. Although they decayed mainly around 540-580°C, they were not completely demagnetized at 620°C. The only exception was sample V29.8 in which all the coercivity fractions were completely removed at ~580°C.

In all the samples the medium coercivity decayed with an approximately convex curve with increasing temperature of demagnetization (Fig. 8.3).
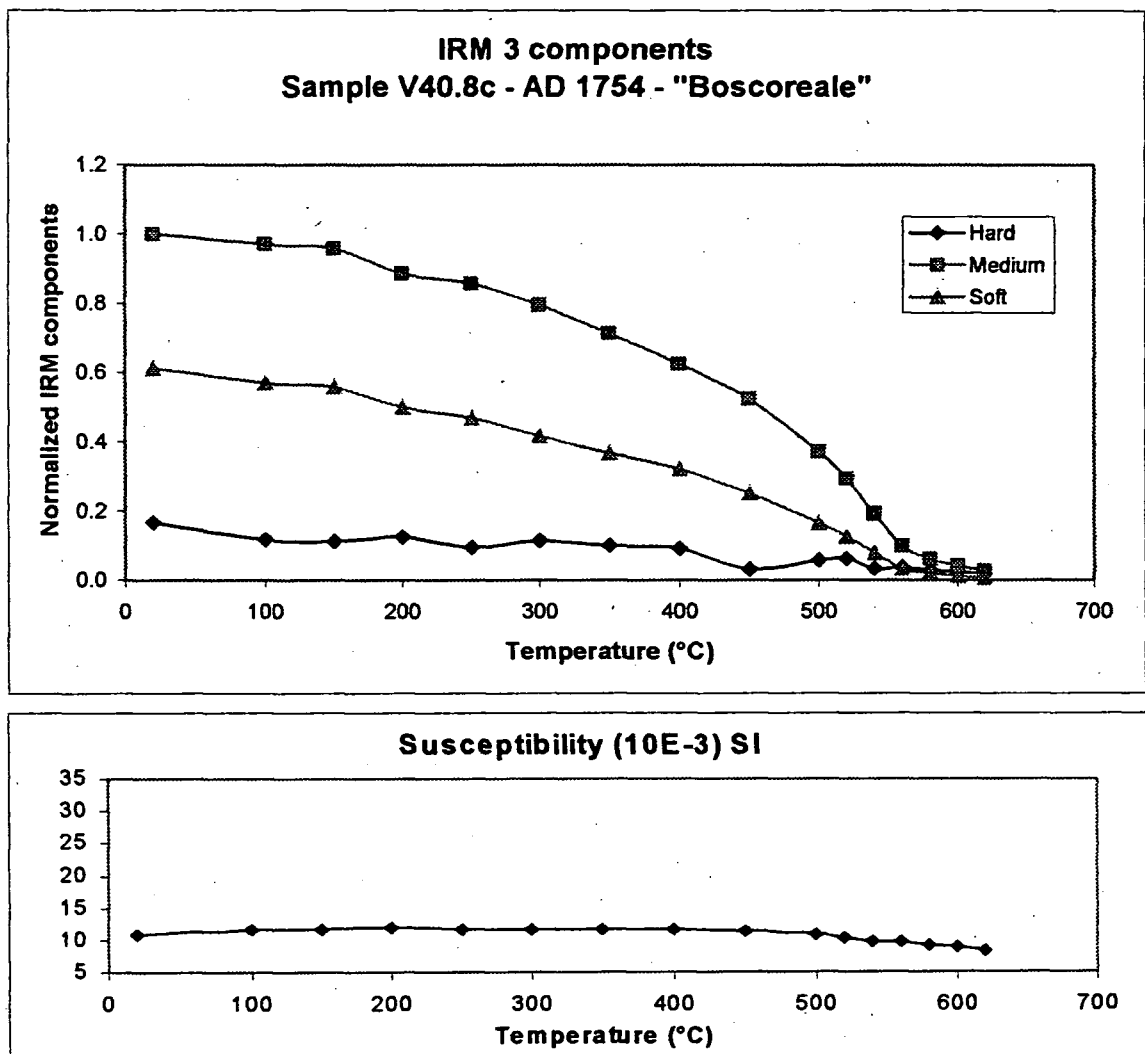
Fig. 8.3 - IRMs 3 components and Susceptibility behaviours for sample V40.8c

Low field susceptibility - All samples behaved as in Type A1 (Fig. 8.3, 8.9), but their K values were within a lower range ($5\text{-}15 \times 10^{-3}$).

b) Second order discriminators

Coercivity of remanence - As in A1 Type, samples had values in the range 50-70 mT. The IRM analyses showed that all samples were not completely saturated at 800 mT, although from 200 mT the demagnetisation curve showed a very low gradient (Fig. 8.4, Tab.1).
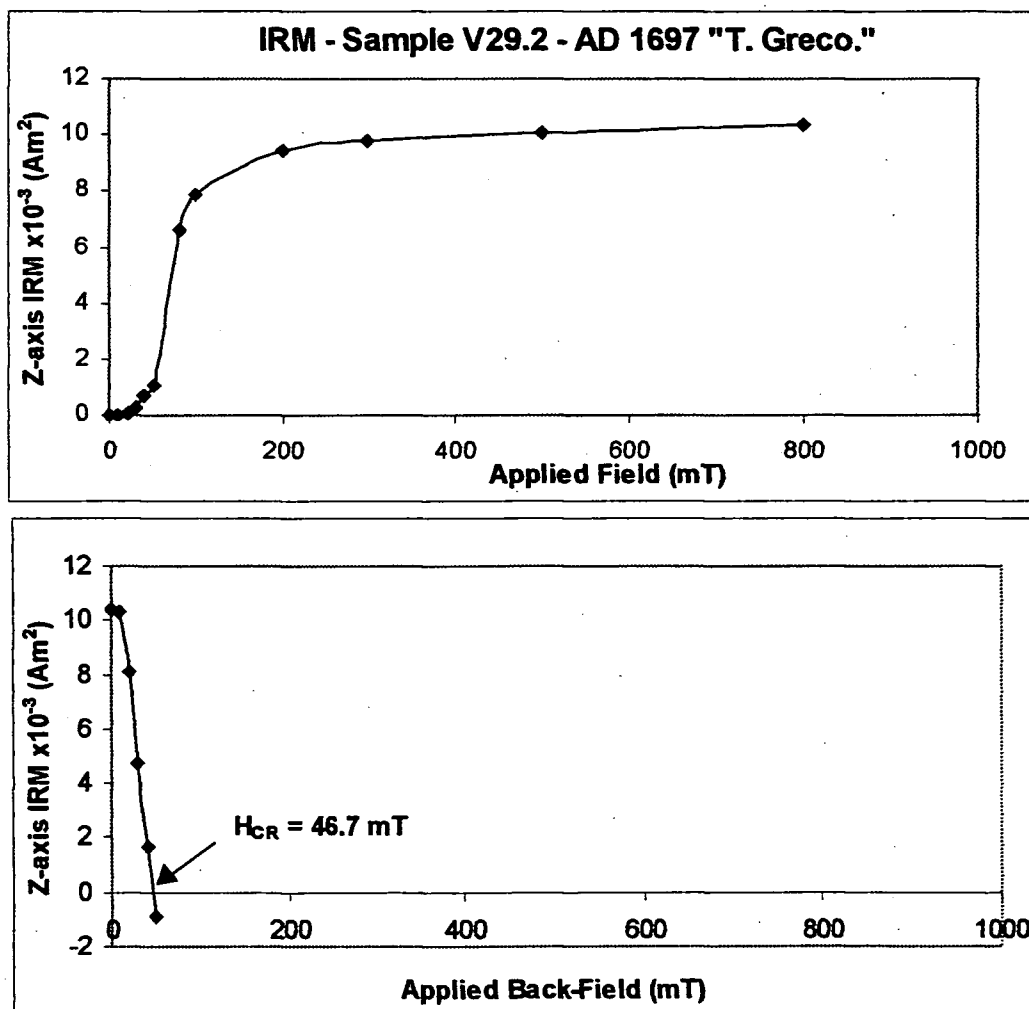
Fig. 8.4 - IRM acquisition along z and -z for sample V29.2.

K$_{ARM}$/K ratio - These values, compared to those for Type A1, were relatively higher (~2.6). For sample V32.5 it was 3.081 (Tab. 8.1).

8.4 Description of Type B samples

a) First order discriminators

3 axes IRM - In these samples the hard coercivity fraction was always negligible and the soft one was in many cases dominant (Fig. 8.5). All the fractions were completely removed at 520-560°C showing a quite linear trend (sometime concave) on demagnetization.

Low field susceptibility - Samples in this group showed initial higher values ($35-40 \times 10^{-3}$) compared with the other groups. They remained constant during the experiment until 450°C where a steep decay occurred. In some samples, at high temperatures (560-580°C), there was a slight increase (Fig. 8.5, 8.9).

b) Second order discriminators

Coercivity of remanence - These had the lowest values, within the range 20-30 mT (Fig. 8.6, Tab. 8.1), except for the sample V24.2 which was 53.1 mT. The IRM analyses showed an almost complete saturation mostly around 100 mT, except for V24.2 and V33.11b, which saturated at 200 mT. Sample V24.2 also showed an anomalous behaviour at 60 mT as occurred in sample V30.2 (Fig. 8.8).

K_{ARM}/K ratio - All the ratios were below 2 (~1.5) except for V33.11b that was 2.102 (Tab. 8.1).
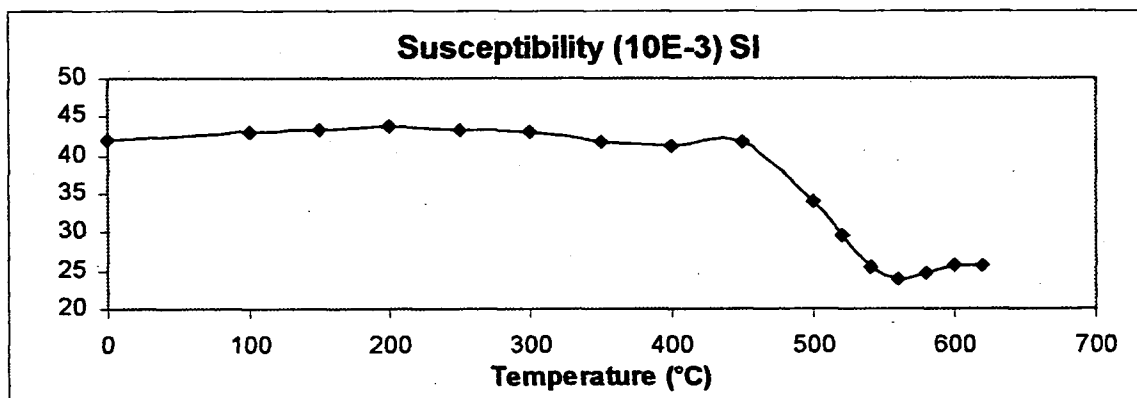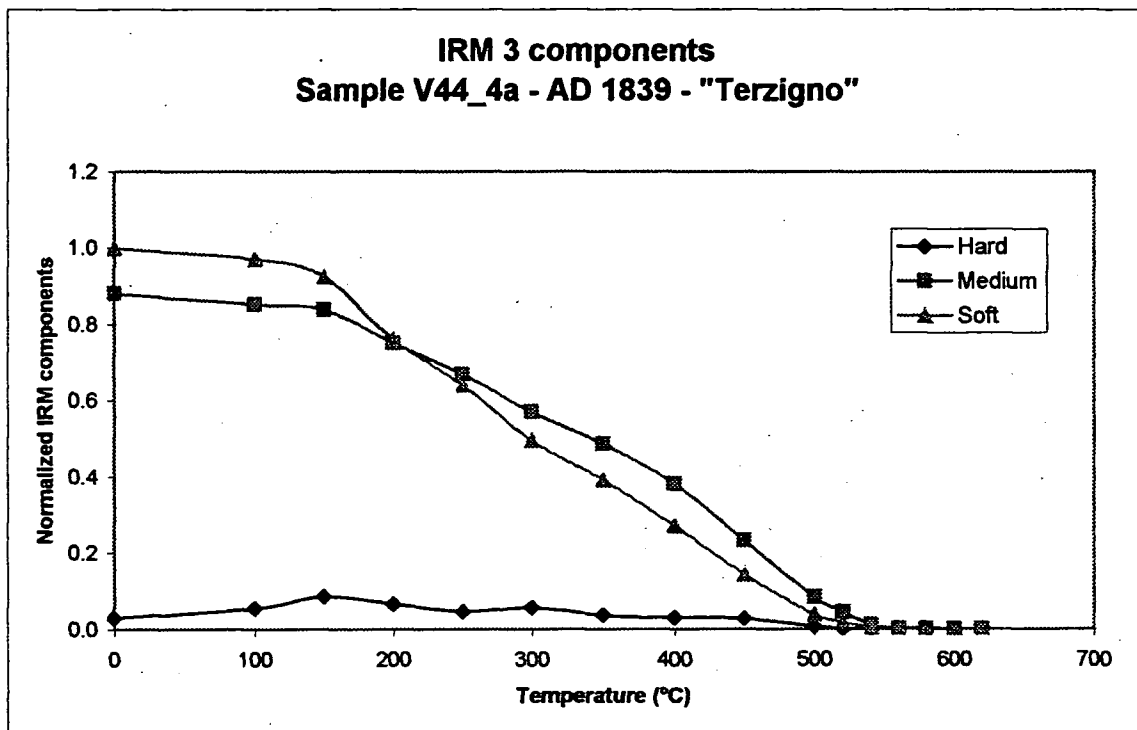
Fig. 8.5 - IRMs 3 components and Susceptibility behaviours for sample V44.4a

325

IRM - Sample V26.5b - AD 79-1631 "T.Annunziata"
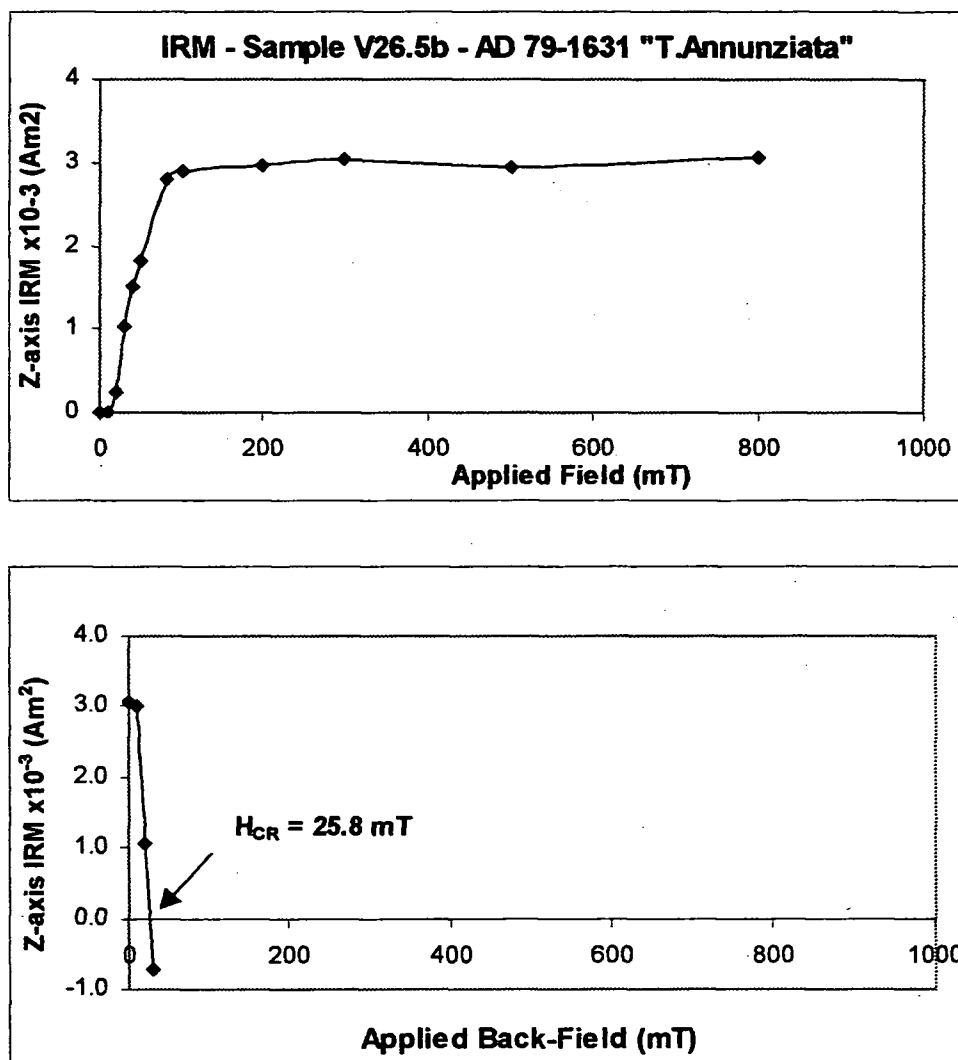
Fig. 8.6 - IRM acquisition along z and -z for sample V26.5b.

8.5 Description of Type Ex sample (V30.2)

a) First order discriminators

3 axes IRM - The hard coercivity fraction was the dominant. It decayed slowly until 500° then it showed a significant increase until 560°C (Fig. 8.7). From this temperature it dropped rapidly down until 620°C where there was some 15% of the initial intensity left. The soft fraction had the same initial intensity as the hard fraction, but a linear steep decay

until 400°C, followed by another linear trend but with a very low gradient. At 620°C it was almost completely demagnetized.
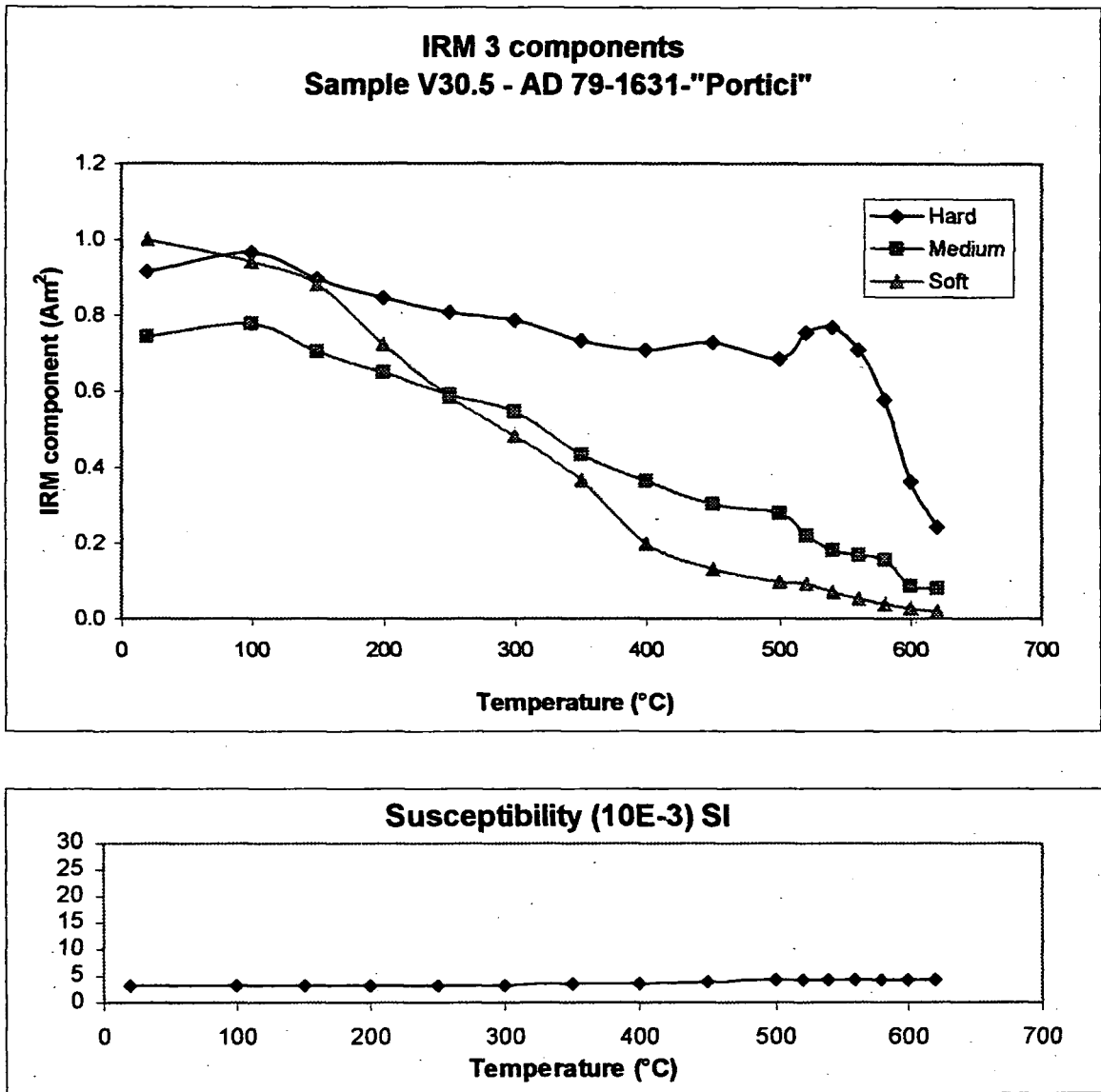
Fig. 8.7 - IRMs 3 components and Susceptibility behaviours for sample V30.5

Low field susceptibility - This sample showed the lowest value, ~5×10^{-3} SI. It was constant until 400°C then it increased slightly (Fig. 8.7).

b) Second order discriminators

Coercivity of remanence - The value was 40 mT (Tab. 8.1). The IRM showed the same anomalous behaviour as sample V33.11b (Type B) but below 80 mT. At 800 mT it was not fully saturated (Fig. 8.8).

K_{ARM}/K *ratio* - It showed a high value, 2.9 (Tab. 8.1).
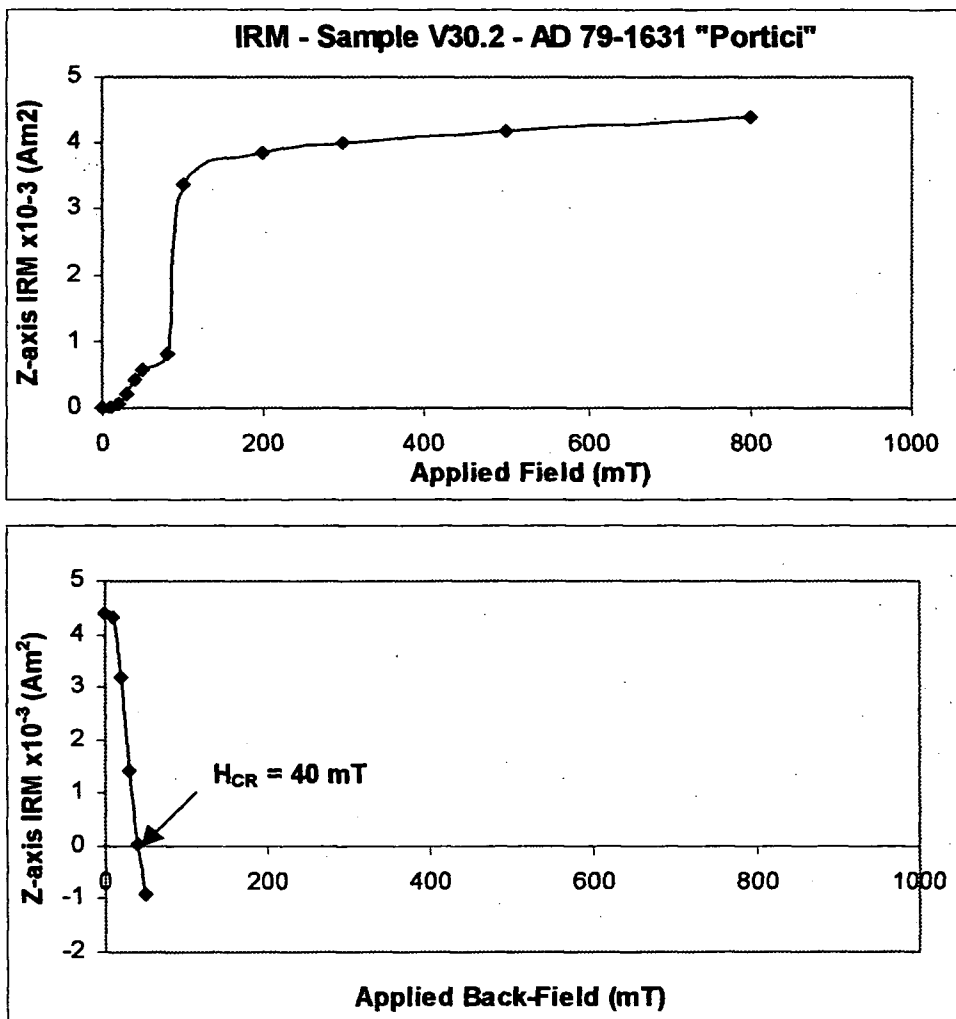
Fig. 8.8 - IRM acquisition along z and -z axes for sample V30.2.
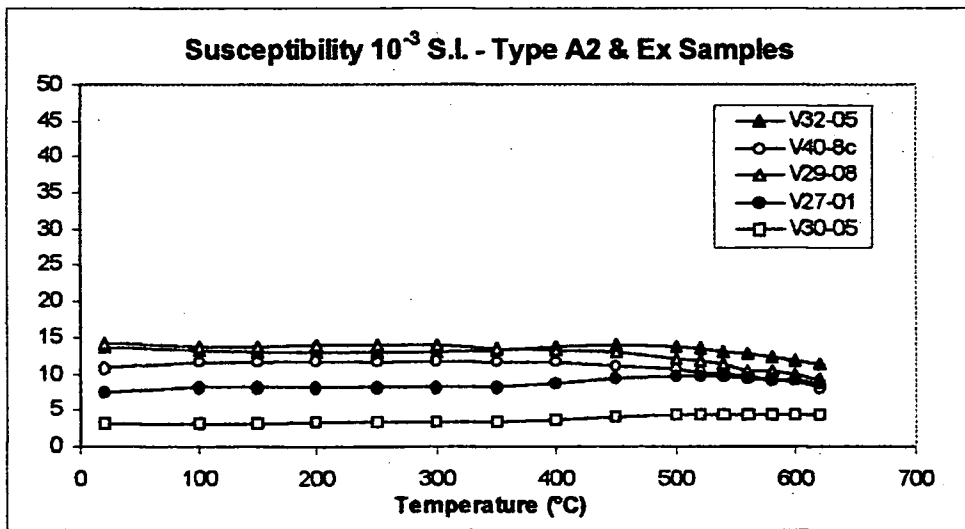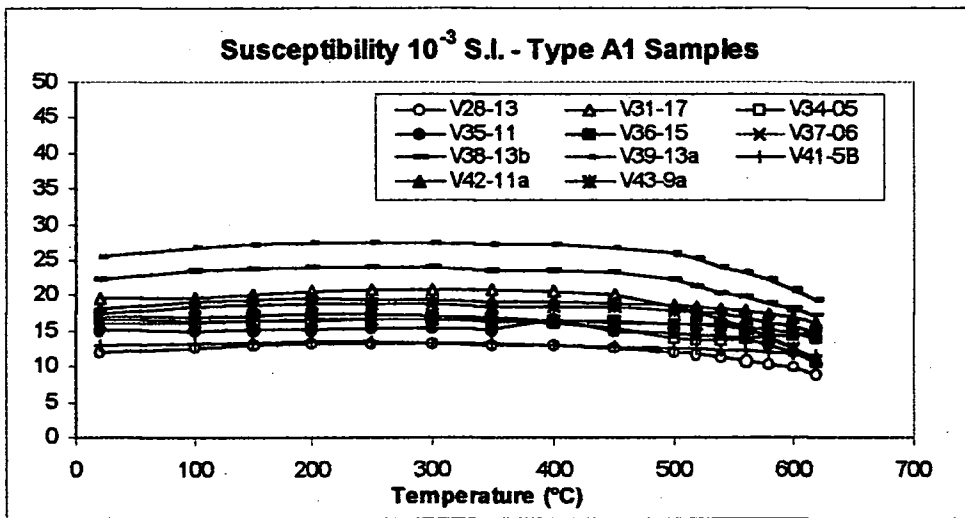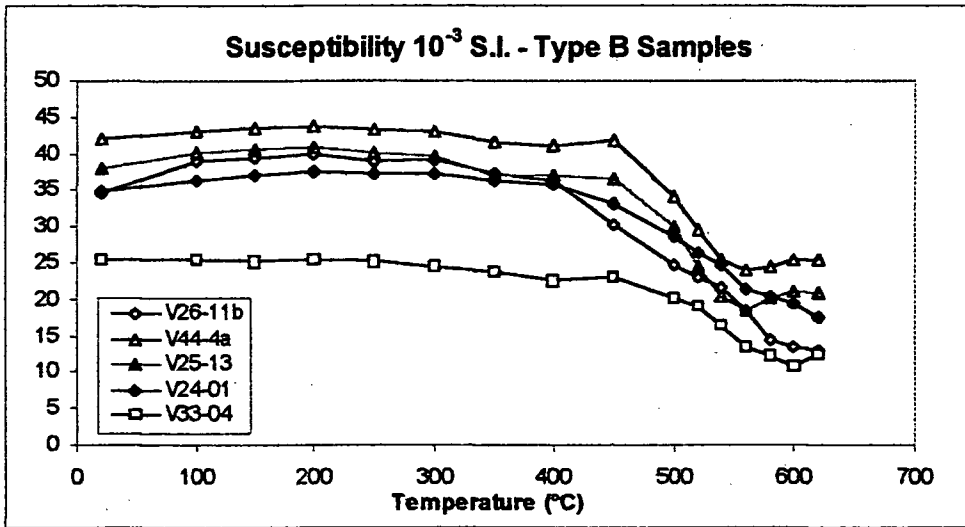
Fig. 8.9 - Different K behaviours for Type B, Ex and Types A1, A2
Different types discriminated as described in sect. 8.2

a) - Type A1

Samples	K (10^{-3})	K$_{ARM}$ (10^{-3})	K$_{ARM}$/K	H$_{CR}$ (mT)
V28-4	14.66	29.92	2.04	71.60
V31-7	25.69	67.30	2.62	63.00
V34-9	16.52	48.87	2.96	62.00
V35-9A	13.38	26.02	1.95	69.00
V36-12	16.76	36.05	2.15	70.00
V37-9A	14.97	31.35	2.09	66.10
V38.4A	33.48	65.19	1.95	64.50
V39-8A	20.87	52.61	2.52	68.00
V41-5A	12.91	41.88	3.24	60.10
V42-9B	18.77	40.19	2.14	74.40
V43-10B	12.44	37.86	3.04	51.20
Mean			**2.43**	**65.45**

c) - Type B

Samples	K (10^{-3})	K$_{ARM}$ (10^{-3})	K$_{ARM}$/K	H$_{CR}$ (mT)
V24-2	39.15	64.37	1.64	53.10
V25-4	40.02	57.56	1.44	27.90
V26-5B	30.92	45.52	1.47	25.80
V33-11B	20.16	42.38	2.10	24.20
V44-2B	44.82	77.89	1.74	24.20
Mean			**1.68**	**31.04**

b) - Type A2

Samples	K (10^{-3})	K$_{ARM}$ (10^{-3})	K$_{ARM}$/K	H$_{CR}$ (mT)
V27-9	10.73	26.55	2.47	71.40
V29-2	13.40	35.77	2.67	56.00
V32-8	12.90	39.74	3.08	46.70
V40-9A	13.50	29.62	2.19	70.00
Mean			**2.60**	**61.03**

d) - Type Ex

Samples	K (10^{-3})	K$_{ARM}$ (10^{-3})	K$_{ARM}$/K	H$_{CR}$ (mT)
V30-2	6.48	18.94	2.92	40.00

Tab. 8.1 - Summary of all the magnetic properties investigated. Values of low field susceptibility at room temperature, anhysteretic susceptibility, their ratio & coercivity of remanence for samples of types A1, A2, B and Ex.

8.6 Discussion

a) Type A1

In all samples the three different coercivity fractions had a Tub of about 560°C and, in few cases, a very small tail above that temperature. This suggests that the magnetic carrier could be a very Ti-poor titanomagnetite (x<0.1). A decrease in H$_C$ and H$_{RC}$ with increasing grain-size (from 0.1 to 150 μm) for titanomagnetite with the same composition has been reported (Day, 1977). This can probably explain the behaviours of the medium and soft coercivities. The behaviour of the coercivity fraction with 50<H$_C$<300 mT (which is the dominant one) could be due to smaller grains compared to that associated with the lower coercivity (<50 mT). In the hard fraction there is little or no sign of haematite and

330

probably, in few cases, some small amount of a Ti-poor titanomagnetite with H_C slightly greater than 300mT. It is important to emphasise that the coercivity fractions higher than 800 mT (haematite, goethite) could still have an influence along the y (medium) and z (soft) axes, as well as in the z (hard) axis since the Pulse magnetizer has a maximum field of 800 mT. Furthermore the absence of high coercivity behaviour does not exclude haematite, as only low coercivity grains of this mineral may be present. Such grains could be possible explanations for the few cases where the medium fraction showed a little tail above 560°C. The H_{RC} and K_{ARM}/K results also confirm the dominance of high coercivity Ti-poor titanomagnetite. In fact, their mean values (Tab. 8.1) suggest the predominance of single/pseudo-single domains (Day, 1977; King, 1982).

In general, alteration during heating experiments can be considered negligible, as suggested by the consistent low field susceptibility behaviour during thermal demagnetisation.

b) Type A2

In this group the magnetic properties were quite similar to A1 except for a relatively higher content of titanium (0.1<x<0.2), as suggested by a lower Tub for all three coercivity fractions. The dominance of the high coercivity titanomagnetite was not as strong as in Type A and there was a relatively greater contribution by the soft coercivity component.

H_{RC} and K_{ARM}/K values were almost the same as type A1 (Tab. 8.1). In general the magnetic carrier is still a Ti-poor titanomagnetite in the form of SD/PSD grains. In two cases (V27-1 and V32-5) the low field susceptibility showed a slight increase above 450°C, suggesting that some alteration occurred during the heating. In these two samples the hard coercivity fraction showed a greater contribution. It is reasonable to think that some haematite may have been created during the heating experiment.

c) Type B

331

The major thing that makes this group different from the others is the low field susceptibility behaviour. Some samples also showed a dominance of the soft coercivity fraction over the medium one while the hard one was almost non existent. All the fractions were almost completely demagnetized at about 500-520° but in few cases there was a small tail until 540-560°C. In sample V33.04 almost 50% of the soft coercivity fraction was removed at 250°C. This behaviour could be due to titanomagnetites with a relatively higher content of Ti (x $\cong$ 0.2) and in some samples at least (V26.11b, V44.4a) this coexist with Ti-poor titanomagnetites (x<0.2). The soft fraction behaviour in sample V33.04 could also be due to the presence of a richer in Ti titanomagnetite (x $\cong$ 0.5). In general the amount of low coercivity titanomagnetite, which could be due to larger grains, seems to be equal or even larger than the high coercivity titanomagnetite amount. This could explain the initial higher value of the low field susceptibility.

The predominance of larger grain of titanomagnetite is also confirmed by the lower mean values of H_{RC} and K_{ARM}/K obtained (Tab. 8.1). In general they suggest behaviour predominantly within the PSD range.

d) Type Ex (Sample V30.2)

The magnetic carrier in these samples could be titano-haematite. This is suggested by the dominance of the hard coercivity fraction, and by the fact that both the medium and the hard fractions were not removed at 620°C. Furthermore the IRM acquisition along the z-axes showed no indication of saturation at 800 mT. The soft fraction behaviour could be due to a titanomagnetite (x=0.2) superimposed to a low coercivity titano-haematite. It appears that significant alteration could be occurring during heating as suggested by the slight increase in low field susceptibility above 450°C. This seems to be related to the increase in the hard coercivity fraction above 500°C. The formation of new titano-haematite seems to be a possible hypothesis to explain this behaviour. The relatively high

values (Tab 8.1) of H_{RC} and K_{ARM}/K, which suggested SD behaviour, probably have reflected the influences of titano-haematite as the low field susceptibility showed the lowest values.

8.7 Conclusions

A poor-Ti titanomagnetite ($x \leq 0.2$) seems to be the predominant magnetic carrier while the grain-size analyses seems to exclude the clear presence of significant MD behaviour. This is particularly true for samples of groups A1 and A2 although group B does not show a significant difference from the former groups.

In terms of relation between magnetic properties and individual lava flows (Tab. 8.2), there is a good consistency between them. In fact all the samples taken from the same lava flow show the same characteristics. They in general belong to the groups A1/A2 or the group B except for very large lava flows where there was considerable distance between the sampling areas

Lava flows	Magnetic Property Groups	Lava flows	Magnetic property groups
AD 79 – 1631		**AD 1754**	
V30*	EX	V39	A1
V36*	A1	V40	A2
V37*	A1	V41	A1
V27	A2	**AD 1760**	
V33	B	V32	A2
V26*	B	V34	A1
V31*	A1	V35	A1
AD 1697		**AD 1806**	
V28	A1	V24	B
V29	A2	V25	B
AD 1714		**AD 1839**	
V38	**A1**	V42*	A1
		V43*	A1
		V44*	B

Tab. 8.2 - Magnetic property and lava flows relationship.
With the asterisks sites sampled distantly within the same large lava flow

Chapter IX

Results

9.1 - Introduction

In this chapter all the site and sample results, both palaeodirections and palaeointensities, will be combined and discussed at a lava level. Palaeodirectional results, at site and lava flow level, will be presented in terms of mean values using the statistical parameters and criteria described in section 3.7. Palaeointensity values, both thermal and microwave, will be described using the following terminology to distinguish the components for different ranges of temperature or microwave power. For thermal studies, *low* is used for T< 390°C; *medium*, used for 390°C <T < 530°C; *high* for T >530°C. However, not all components lie within these temperature ranges; sometimes both low and medium, or both medium and high ranges, were involved. In the first case more weight is given to the lowest limit while in the second case the upper limit is considered more meaningful. For example, a component defined in the range 150 - 500 °C will be referred to as *low* component while one defined in the range 420 - 595 will be referred to as *high* component.

9.2 - AD 79 - AD 1631

9.2.1 - Palaeodirections

a - Sites mean values

Site V30 - As described in section 5.2.1., almost all samples had a single, very well defined high temperature component and therefore a unique value of the ChRM (Tabs. 9.1a,b).

Sample	N steps	Dec	Inc	MAD	T°C range
03	5	18.7	66.7	1.1	580/630
06	15	14.7	61.9	1.0	390/630
09	5	11.9	66.5	1.3	565/620
11	9	14.0	66.5	0.9	535/630
12	8	15.8	65.5	1.0	520/620
13	7	11.3	62.4	0.9	535/630

a)

Site	N samples	Dec	Inc	k	α_{95}
V30	6	14.3	64.9	1080	2.0

b)

Tabs. 9.1a,b - Site V30 directional results.
a) Sample best representative directions. b) Site mean value.
MAD = diagonal angle; **k** = estimate of the true precision parameter K; α_{95} = confidence limit on the mean direction. For a fuller description see section 3.7.

Site V36 - Two different, but both very well defined directions were found at higher temperature (Tabs. 9.2.a,b). The major difference was in declination; the inclination being almost identical. As these could not be combined, two different values of the ChRM were retained (Tab. 9.2.c).

Sample	N steps	Dec	Inc	MAD	T°C range
01B	7	16.2	64.5	0.5	550/620
14	13	15.5	60.9	0.5	420/620
16	7	14.8	65.3	0.8	550/620
17B	8	17.8	66.1	0.4	535/620

a)

Sample	N steps	Dec	Inc	MAD	T°C range
01B	6	24.1	63.6	2.3	460/550
03	8	23.5	66.3	0.5	520/620
05	4	25.1	63.1	0.3	580/620
06	5	24.0	62.3	0.7	580/620
08	8	27.7	64.0	0.3	520/620
11	13	28.1	67.4	0.6	390/620
14	4	22.7	63.7	2.6	420/480
17B	7	24.5	67.6	3.9	420/535

b)

Site	N samples	Dec	Inc	k	α_{95}
V36(i)	4	16.0	64.2	1180	2.7
V36(ii)	8	24.9	64.7	1287	1.5

c)

Tabs. 9.2a,b,c - Site V36 directional results.
a, b) Sample best representative directions grouped according to the site
discussions in section 9.2.1. c) Alternative site mean values.

Site V37 - Two different directions were found, both very well defined, especially between 520 and 635° (Tabs. 9.3.a, b). The inclination was almost the same for all samples. Two different values of the ChRM were obtained (Tab. 9.3.c).

Sample	N steps	Dec	Inc	MAD	T °C range
01	11	16.9	64.2	0.6	420/595
05	6	18.5	66.5	0.5	520/595
10A	8	11.4	60.4	1.6	535/635
10B	9	9.5	55.9	1.0	520/635
11	6	14.2	62.8	0.7	535/610
13	7	14.7	65.6	0.7	535/635
14	8	11	64.5	0.4	480/610

a)

Sample	N steps	Dec	Inc	MAD	T °C range
06	6	1.6	61.8	0.4	520/595
07A	7	357.5	59.4	0.4	500/595
07B	6	357.8	58.8	1.5	480/610

b)

Site	N samples	Dec	Inc	k	α_{95}
V37(i)	7	14.3	64.0	1033	2.1
V37(i*)	6	15.0	64.7	1906	1.8
V37(ii)	3	358.9	60.0	1734	3.0

c)

Tabs. 9.3a,b,c - Site V37 directional results
a, b) Sample best representative directions. c) Site mean values.
*mean value obtained erasing 10B

Site V27

A single very well defined component was revealed at high temperature and, therefore

a unique value of the ChRM was obtained (Tabs. 9.4a,b).

Samp	N steps	Dec	Inc	MAD	T °C
03	9	12.3	62.5	1.1	500/620
04	8	9.3	62.8	1.1	520/620
06	6	7.7	63.4	0.7	550/630
07	7	9.1	61.4	0.8	535/620
12	9	10.0	63.5	1.4	520/630
13	6	16.7	60.1	0.8	550/620

a)

Site	N	Dec	Inc	k	α_{95}
V27	6	10.9	62.3	1612	1.7

b)

Tabs. 9.4a,b - Site V27 directional results
a) Sample best representative directions. b) Site mean values.

Site V33 - All the samples behaved very irregularly (Section 5.2.5). However

similarity in directions were found at low-medium temperature (Tabs. 9.5a,b), although

these characterised by high MAD values (about 3.5).

.Sam	N steps	Dec	Inc	MAD	T °C
01	9	356.8	53.6	3.2	20/420
02	9	348.5	59.0	2.6	100/440
03	8	345.0	55.6	3.9	20/390
05	9	351.9	49.4	2.8	20/420
10	8	352.0	55.0	3.7	250/480
13	13	349.5	57.9	2.9	300/565

a)

337

Site	N	Dec	Inc	K	α_{95}
V33	6	350.7	55.1	370	3.5

b)

Site V26 - Two different groups of directions, with MAD values in the range 2-4°, were found which characterized respectively the low-medium and high temperature range (Tabs. 9.6.a,b). Two completely different values of the ChRM were obtained (Tab. 9.6.c).

Sample	N steps	Dec	Inc	MAD	T °C range
01	4	353.5	62	2.1	390/460
03	8	10.2	50.6	3.6	150/440
04	11	5.5	57.3	2.4	150/500
07A	8	9.9	55.2	3.3	150/440
09A	6	16.7	54.6	1.5	420/565
10A	7	11.3	58.6	2.0	460/565

a)

Sample	N steps	Dec	Inc	MAD	T °C range
01	6	19.8	29.9	3.3	460/565
03	5	27.8	27.5	2.5	500/565
04	5	24.2	36.8	3.4	500/565
07	5	25.9	43	2.4	500/565

b)

Site	N samples	Dec	Inc	k	α_{95}
V26(i)	6	8.3	56.6	203.6	4.7
V26(i*)	5	10.8	55.3	452.6	3.6
V26(ii)	4	24.4	34.3	114.4	8.6

c)

Site V31 - A single very well defined component was revealed at high temperatures and also including the medium range after erasing anomalous points (Section 5.2.7). A unique value of the ChRM was obtained (Tabs. 9.7a,b).

Sample	N steps	Dec	Inc	MAD	T °C range
01	16	15.3	65.2	1.0	300/620
06	14	14.2	60.7	0.7	360/620
08	15	9.8	64.1	0.6	330/620
11	4	10.5	66.0	0.8	580/620

a)

Site	N samples	Dec	Inc	k	α_{95}
V31	4	12.5	64	960.7	3.0

b)

Tabs. 9.7a,b. Site V31 directional results.
a) Sample best representative directions. b) Site mean values.

b - Lava flow mean value

As shown in the previous section, sites V027, V030 and V031 have distinct mean values while the others sites have two different values. However in all sites, a very similar and statistically well defined ChRM is present (Tab. 9.8a). To obtain the most representative lava flow mean value (Tab. 9.8b) sites V026 and V033 were excluded from the calculation because of their poor statistical definition and different mean directions.

Sample	N samples	Dec	Inc	k	α_{95}
V026	5	10.8	55.3	452.6	3.6
V027	6	10.9	62.3	1612.4	1.7
V030	6	14.3	64.9	1080.1	2.0
V031	4	12.5	64.0	960.7	3.0
V033	6	350.7	55.1	369.7	3.5
V036	4	16.0	64.3	1180.4	2.7
V037	5	15.0	64.7	1906.1	1.8

a)

Lava	N samples	Dec	Inc	k	α_{95}
79-1631	7	13.1	62.6	451.6	3.2
	*5	13.7	64.1	3488	1.3

b)

Tabs. 9.8a,b - AD 79 - 1631 lava flows directional results.
a) Sites best representative directions. b) Lava flow mean values.
* excluding site V026 and V033

339

9.2.2 - Palaeointensities

a - MTT

For each samples at least two completely different estimates of the palaeofield were obtained from both MTT A-B and C-D (Tabs.9.9a, b). A general trend of decreasing palaeofield values, with the increasing of temperature, was found in all the samples. In most cases, the low part of the temperature spectrum showed too high values of the palaeointensity (up to 211 μT), despite the statistical parameters being acceptable. Most values from the analysis of the high temperature' ranges were more acceptable in terms of reliability (except for sample V33.9) and statistic properties.

In general there was no clear relation between temperature ranges and the most representative value for each site. The values chosen to get the lava flow mean value (Tab.9.9c, d) covered the entire spectrum of temperature ranges.

b - Microwave

For each sample one estimate of the palaeofield were obtained (Tabs.9.10a,). Only sample V26.6b-1 showed two different slopes and in this case a decrease in the palaeofield estimate with the increasing power range was observed.

The low part of the power range spectrum showed the more acceptable values although in terms of statistical definition they didn't show very high quality results. The low power values were used to get the lava flow mean value (Tab.9.10b, c).

9.3 - AD 1697

9.3.1 - Palaeodirections

a - Sites mean values

V 79-1631

MTT A-B

Samples	low T (°C)	F (µT)	N	g	q	σ_b	medium T (°C)	F (µT)	N	g	q	σ_b	high T (°C)	F (µT)	N	g	q	σ_b	All T (°C)	F (µT)	N	g	q	σ_b
V26.11a	150-460	88.7	9	0.85	6.73	0.12	480-535	15.2	4	0.65	0.80	0.05												
V27.11	100-440	187.6	9	0.88	2.12	0.37							390-595	85.3	12	0.87	13.80	0.06	100-595	97.1	17	0.71	4.70	0.12
V30.8	150-595	78.7	17	0.92	24.61	0.05																		
V31.2	150-500	165.9	11	0.89	14.01	0.14							480-580	24.3	5	0.63	1.48	0.07						
V33.9	150-420	45.6	6	0.72	10.17	0.04							420-580	6.6	9	0.85	2.13	0.01						
V36.17	150-520	160.5	12	0.96	14.08	0.21							500-595	52.1	5	0.18	1.17	0.08						
V37.9b	150-520	185.2	12	0.89	6.61	0.36							480-595	61.9	5	0.73	3.06	0.13						

a)

MTT C-D

Samples	low T (°C)	F (µT)	N	g	q	σ_b	medium T (°C)	F (µT)	N	g	q	σ_b	high T (°C)	F (µT)	N	g	q	σ_b	all T (°C)	F (µT)	N	g	q	σ_b
V26.11a	250-500	32.9	10	0.81	5.28	0.05							500-565	3.8	5	0.63	1.53	0.01						
V27.11	250-480	165.4	7	0.78	2.98	0.31							500-580	60.1	6	0.75	4.07	0.08	250-580	98.3	12	0.85	12.65	0.11
V30.8	250-480	104.6	9	0.87	8.67	0.10							440-580	58.7	9	0.85	4.19	0.09	250-580	76.4	13	0.91	14.10	0.08
V31.2	150-420	211.6	11	0.89	4.08	0.60							480-580	30.6	5	0.74	1.62	0.09						
V33.9	150-420	59.7	7	0.73	3.72	0.15							420-550	6.0	8	0.69	2.40	0.01						
V36.17	250-520	159.2	11	0.88	5.10	0.32	420-535	84.1	7	0.81	3.16	0.23	500-580	48.0	5	0.73	1.81	0.15	250-580	83.9	14	0.91	8.15	0.16
V37.9b	250-520	193.5	8	0.80	5.84	0.37							480-580	58.5	6	0.75	2.20	0.17						

b)

V 79-1631

Samples	T (°C)	F (µT)	N	g	q	σ_b
V26.11a	150-460	88.7	9	0.85	6.73	0.12
V27.11	390-595	85.3	12	0.87	13.80	0.06
V30.8	150-520	78.7	17	0.92	24.61	0.05
V31.2						
V33.9	150-420	59.7	7	0.73	3.72	0.15
V36.17	250-580	83.9	14	0.91	8.15	0.16
V37.9b	480-595	61.9	5	0.73	3.06	0.13

c)

mean value

F (µT)	std
76.37	12.50

d)

Tabs 9.9a,b,c,d - AD 79-1631: MTT palaeointensity results.
a,b) Palaeofield estimate grouped for temperature range.
c) Best site's representative values
d) Lava flow mean value

341

V 1631   Palaeointensity results from Microwave experiment

sample	sub sample	Power range (W)	N	f	g	q	b	σ_b	Fpalaeo (μT)	Uncertainty
v30	1-1	[a] 58 - 95	6	0.093	0.747	0.646	-1.054	0.114	52.681	81.569
v36	13-1	50 - 85	4	0.269	0.455	4.156	-1.903	0.056	95.157	22.899
v37	8a-1	33 - 98	8	0.832	0.548	19.429	-1.982	0.047	99.094	5.100
v27	10-1	[b] 62 - 90*	5	0.182	0.520	1.058	-1.699	0.152	84.945	80.315
		[a] 70 - 90	4	0.061	0.629	0.209	-1.285	0.238	64.255	307.869
v27	10-2	[b] 42 - 70*	6	0.242	0.727	4.104	-1.363	0.059	68.147	16.604
		[a] 50 - 70	5	0.157	0.646	4.465	-1.490	0.034	74.495	16.684
v33	12-1	15 - 24	7	0.155	0.793	3.848	-1.378	0.044	68.915	17.910
v26	6b-1	[b] 55-148	10	0.650	0.814	12.509	-0.689	0.029	34.473	2.756
		[a] 37-108	10	0.293	0.839	3.081	-1.726	0.138	86.320	28.013
v31	5-1	31 - 58	5	0.239	0.703	7.663	-1.535	0.034	76.734	10.013
v31	5-2	28 - 62	10	0.369	0.800	9.806	-1.629	0.049	81.464	8.308

a)   (*) Including the first point D(NRM)

sample	sub sample	Fpalaeo (μT)
v36	13-1	95.157
v37	8a-1	99.094
v27	10-1	84.945
v27	10-2	68.147
v33	12-1	68.915
v26	6b-1	86.320
v31	5-1	76.734
v31	5-2	81.464

b)

mean value

Fpalaeo (μT)	std
82.60	11.22

c)

Tabs 9.10a,b,c - AD 79-1631: Microwave palaeointensity results.
a) All possible palaeofield estimate.
b) Best site's representative values
c) Lava flow mean value

Site V28 - Although two different groups of directions were considered (both very well defined especially at higher temperature), the inclinations values were almost identical while the declinations ones did not show clearly different grouping of value (Tabs. 9.11.a, b). Three values of the ChRM were presented (Tab. 9.11.c) considering all samples best representative values and also the two different groups identified. Note that the high values of α_{95} obtained from the latest two vectors justify their combination to get the overall mean value.

Sample	N steps	Dec	Inc	MAD	T °C range
02	7	15.6	56.4	0.3	535/620
05	4	18.9	61.6	0.5	580/620
06	4	12.0	61.9	0.8	580/620

a)

Sample	N steps	Dec	Inc	MAD	T °C range
08	5	356.0	60.2	0.7	500/565
11	5	6.8	60.0	0.6	565/620
12	4	356.6	63.6	0.2	580/620

b)

Site	N samples	Dec	Inc	K	α_{95}
V28(i)	6*	7.9	60.9	234.6	4.4
V28(ii)	3	15.5	60.0	530.4	5.4
V28(iii)	3	359.9	61.4	515	5.4

c)

Tabs. 9.11a,b,c - Site V28 directional results.
a, b) Sample best representative directions. c) Site mean values.
* considering all the sample values

Site V29 - All the samples (except 13) showed a similar very well defined component at high temperature, mostly above 480°C). Two values of the ChRM were obtained; one erasing sample 13 (Tabs. 9.12.a, b).

Sample	N steps	Dec	Inc	MAD	T °C range
03	56	12.8	58.2	0.3	540/620
04	12	15.3	56.7	0.3	400/620
05	7	14.5	56.2	0.4	500/620
09	7	19.2	57.8	0.5	480/620
13	7	8.22	53.5	0.5	500/620
14	8	15.0	59.2	0.4	480/620
15	4	18.3	59.2	0.8	520/580

a)

Site	N samples	Dec	Inc	k	α_{95}
V29(i)	7	14.6	57.2	866.1	2.1
V29(i*)	6	15.8	57.7	2298	1.4

b)

Tabs. 9.12a,b - Site V29 directional results.
a) Sample best representative directions. b) Site mean values.
* excluding sample 13

b - Lava flow mean value

Site V029 showed a unique very well defined mean value. Site V28 showed two different values, both poorly defined, but one of which was similar to V029 (Tab. 9.13a). The lava flow mean value is shown in Tab.913b.

Sample	N samples	Dec	Inc	k	α_{95}
V028	3	15.5	60.0	530.4	5.4
V029	6	15.8	57.7	2298	1.4

a)

Lava	N samples	Dec	Inc	k	α_{95}
1697	2	15.7	58.9	2471	5

b)

Tabs. 9.13a,b - AD 1697 lava flows directional results.
a) Sites best representative directions. b) Lava flow mean values.

9.3.2 - Palaeointensities

a - MTT

Two completely different estimate of the palaeofield were obtained from both MTT A-B and C-D (Tabs.9.15a,b). The low part of the temperature spectrum showed

unacceptable high values of the palaeointensity (up to 227 µT), although the statistical

parameters were still acceptable. The values obtained at high temperature' ranges were

acceptable in terms of reliability and statistically and therefore they were used to calculate

the lava flow mean value (Tab.9.15c).

b- Microwave

The three samples showed quite similar value of palaeofield (Tab.9.17a) but for sample

V29.7-1 it was defined in the high range of microwave power. A unique mean value for

the lava flow was obtained (Tab.9.17b,c).

9.4 - AD 1714 (1906)

9.4.1 - Palaeodirections

Site V38 - For each sample a single component was considered at high temperature

because of its better d.a (Tab. 9.14a), although a similar direction was revealed also

considering the entire spectra of temperature. A unique value of the ChRM was obtained

(Tab. 9.14b).

Sample	N steps	Dec	Inc	MAD	T °C range
01	9	356.6	50.6	0.8	480/630
03	11	358.7	50.6	0.9	480/630
05	11	359.7	52.1	0.9	480/630
07A	5	356.1	53	0.8	520/610
08	6	357.5	51.3	1.4	565/630
09A	11	352.5	52.1	0.5	565/620
11A	7	355.6	50.2	0.9	480/630
12B	4	354.7	54.8	0.6	520/630

a)

Site	N samples	Dec	Inc	k	α_{95}
V38	8	356.4	51.9	1528.7	1.4

b)

Tabs. 9.14a,b - Site V38 directional results.
a) Sample best representative directions. b) Site mean values.

V1697

MTT A-B

Samples	low						medium						high						All					
	T (°C)	F (µT)	N	g	q	σ_b	T (°C)	F (µT)	N	g	q	σ_b	T (°C)	F (µT)	N	g	q	σ_b	T (°C)	F (µT)	N	g	q	σ_b
V28.3	150-520	225.8	13	0.86	3.15	0.59							500-595	65.7	7	0.77	6.49	0.09						
V29.6	150-500	165.0	11	0.89	12.92	0.15							460-595	69.9	9	0.84	5.35	0.11						

a)

MTT C-D

Samples	low						medium						high						all					
	T (°C)	F (µT)	N	g	q	σ_b	T (°C)	F (µT)	N	g	q	σ_b	T (°C)	F (µT)	N	g	q	σ_b	T (°C)	F (µT)	N	g	q	σ_b
V28.3							390-535	125.9	8	0.79	6.41	0.16	500-580	69.2	6	0.55	10.73	0.04						
V29.6	250-480	227.7	7	0.82	8.41	0.21							480-580	62.7	7	0.77	5.08	0.08						

b)

V1697

Samples	T (°C)	F (µT)	N	g	q	σ_b
V28.3	500-580	69.2	5	0.55	10.73	0.04
V29.6	460-595	69.9	9	0.84	5.35	0.11

c)

mean value

F (µT)	std
69.5	0.49

d)

Tabs 9.15a,b,c,d - AD 1697: MTT palaeointensity results.
a,b) Palaeofield estimate grouped for temperature range.
c) Best site's representative values
d) Lava flow mean value

V1714(1906)

MTT A-B

Samples	low						medium						high						All					
	T (°C)	F (µT)	N	g	q	σ_b	T (°C)	F (µT)	N	g	q	σ_b	T (°C)	F (µT)	N	g	q	σ_b	T (°C)	F (µT)	N	g	q	σ_b
V38.b	100-535	84.9	14	0.86	10.80	0.08							535-595	24.1	5	0.65	1.02	0.05						

a)

MTT C-D

Samples	low						medium						high						all					
	T (°C)	F (µT)	N	g	q	σ_b	T (°C)	F (µT)	N	g	q	σ_b	T (°C)	F (µT)	N	g	q	σ_b	T (°C)	F (µT)	N	g	q	σ_b
V38.b	150-535	85.1	13	1.88	8.35	0.13							500-580	36.1	6	0.75	4.89	0.05						

b)

Tabs 9.16a,b - AD 1714 (1906): MTT palaeointensity results.
a,b) Palaeofield estimate grouped for temperature range.

V 1697   Palaeointensity results from Microwave experiment

sample	sub sample	Power range (W)	N	f	g	q	b	σ_b	Fpalaeo (μT)	Uncertainty
v28	1-2	50 - 70*	4	0.338	0.615	19.262	-1.697	0.018	84.828	4.404
		60 - 70	3	0.230	0.390	4.644	-1.710	0.033	85.506	18.412
v29	7-1	100 - 175	9	0.499	0.732	14.154	-1.918	0.050	95.891	6.775
v29	7-2	[b]50 - 90*	4	0.649	0.530	6.121	-2.020	0.114	100.996	16.501
		[a] 60 - 90	3	0.519	0.328	9.475	-1.913	0.034	95.637	10.094

a)   (*) Including the first point D(NRM)

sample	sub sample	Fpalaeo (μT)
V28	1.1	85.606
V29	7.1	95.891
V29	7.2	95.637

b)

mean value

Fpalaeo (μT)	std
92.34	5.92

c)

Tabs 9.17a,b,c - AD 1697: Microwave palaeointensity results.
a) All possible palaeofield estimate.
b) Best site's representative values
c) Lava flow mean value

V 1714(1906)   Palaeointensity results from Microwave experiment

sample	sub sample	Power range (W)	N	f	g	q	b	σ_b	Fpalaeo (μT)	Uncertainty
v38	6a-1	45 - 60	5	0.170	0.716	1.209	-1.567	0.158	78.341	64.789

a)

Tab. 9.18 - AD 1714 (1906): Microwave paleointensity results.

9.4.2 - Palaeointensities

a - MTT

Both MTT A-B and C-D experiments (Tabs.9.16a,b) showed almost the same value of the palaeofield and both, the low and high part of the temperature spectrum, showed acceptable estimates of the palaeointensity. However the value obtained at low temperature' ranges was more statistically acceptable and was therefore used as lava flow mean value as no other values were available to calculate an average.

b- Microwave

Sample V38.6a-1 (the only one available for this lava flow) showed a unique estimate of the palaeofield at low power range, and statistically it was poorly defined (Tab.9.18a)

9.5 - AD 1754

9.5.1 - Palaeodirections

a - Sites mean values

Site V39 - Two different groups of directions, with MAD in the range 1-3, were found which characterized respectively the medium and high temperature range (Tabs. 9.19.a,b). Two different values of the ChRM were obtained (Tab. 9.19.c).

Sample	N steps	Dec	Inc	MAD	T °C range
04	4	333.4	67.1	1.2	500/550
05	7	337.7	66.1	1.0	440/565
06A	4	336.1	65.5	3.1	500/550
06B	4	337.7	63.0	1.6	520/565
09	5	335.5	65.5	2.4	500/565
14	5	330.8	65.8	1.3	480/565

a)

Sample	N steps	Dec	Inc	MAD	T °C range
04	4	345.8	67.7	2.9	565/610
05	4	345.8	65.7	0.8	565/610
06A	4	350.4	61.6	2.7	565/610
06B	5	340.7	63.5	0.8	565/620
14	6	340.9	65.6	1.9	565/610

b)

Site	N samples	Dec	Inc	k	α_{95}
V39(i)	6	335.3	65.5	2126.1	1.5
V39(ii)	6	344.8	64.9	765.5	2.8

c)

Tabs. 9.19a,b,c - Site V39 directional results
a,b) Sample best representative directions. c) Site mean values.

Site V40 - Two slightly different groups of directions, with MAD in the range 0.5-3, were found mostly at high temperature range (Tabs. 9.20.a,b). Two values of the ChRM were presented; one erasing sample 13A (Tab. 9.20.c).

Sample	N steps	Dec	Inc	MAD	T °C range
01	6	342.4	65.4	2.0	565/630
05	9	342.9	64.7	1.8	500/620
06A	9	342.4	63.0	0.7	535/620
07	8	342.5	68.2	0.7	520/620
11A	8	344.2	65.1	0.5	520/620
13A	4	351.3	61.9	2.0	580/630

a)

Sample	N steps	Dec	Inc	MAD	T °C range
01	7	335.9	62.5	2.0	420/550
08	7	337.8	67.8	1.1	535/620
10A	5	336.7	66.4	1.8	580/630

b)

Site	N samples	Dec	Inc	k	α_{95}
V40(i*)	5	342.9	65.3	1809.1	1.8
V40(ii)	3	336.7	65.6	853	4.2

c)

Tabs. 9.20,a,b,c - Site V40 directional results
a,b) Sample best representative directions. c) Site mean values.
*mean value obtained erasing 13A

Site V41 - All the samples showed a similar very well defined component at high temperature (mostly above 480°C). A unique value of the ChRM was obtained (Tabs. 9.21.a,b).

Sample	N steps	Dec	Inc	MAD	T °C range
02A	5	343.4	61.5	1.1	565/620
02B	9	345.6	60.8	0.6	500/620
06	12	347.5	62.5	0.4	440/620
07	11	348.4	61.1	0.5	460/620
08	9	341.5	66.6	0.5	500/620
09	11	343.7	61.4	0.7	460/620
11A	9	349.2	65.7	0.4	480/620
12B	7	351.3	63.7	0.5	520/620

a)

Site	N samples	Dec	Inc	k	α_{95}
V41	8	346.2	63.0	923.3	1.85

b)

Tabs. 9.21a,b - Site V41 directional results
a) Sample best representative directions. b) Site mean values.

b - Lava flow mean value

Site V041 showed a unique well defined mean value, which was also found in sites V40 and V39 (Tab. 9.22a). These two sites also showed another direction that was different in declination and also statistically acceptable. Therefore two lava flow mean value were considered (Tab. 9.22b).

Sample	N samples	Dec	Inc	k	α_{95}
V039(i)	5	344.8	64.9	765.5	2.8
V040(i)	5	342.9	65.3	1809.1	1.8
V041(i)	8	346.2	63	923.3	1.8
V039(ii)	6	335.3	65.5	2126.1	1.5
V040(ii)	3	336.7	65.6	853	4.2

a)

350

Lava	N samples	Dec	Inc	k	α_{95}
1754(i)	3	344.7	64.4	3245.1	2.2
1754(ii)	2	336	65.6	38130	1.3

b)

Tabs. 9.22a,b - AD 1754 lava flow directional results.
a,b. a) Sites best representative directions. b) Lava flow mean values.

9.5.2 - Palaeointensities

a - MTT

Two different estimate of the palaeofield were obtained from both MTT A-B and C-D (Tabs.9.23a,b). The low part of the temperature spectrum showed high values of the palaeointensity (which were acceptable only from MTT A-B), with statistical parameters still acceptable. The values obtained at high temperature' ranges were also acceptable in terms of reliability and statistically. Two mean values were considered (Tab.9.23c).

b- Microwave

A similar estimate of the palaeofield was obtained (Tab.9.25a) and it was defined, in each sample, in the low part of the microwave power range. A unique mean value was, therefore considered (Tab.9.25b,c)

9.6 - AD 1760

9.6.1 - Palaeodirections

a - Sites mean values

Sites V32, V34 &V35 - In all the samples a single very well defined component was revealed especially at high temperature (Tabs. 9.27a; 9.28a; 9.29a). For each of this the three sites two values of the ChRM were considered: the second value usually obtained excluding few samples with slightly different declination or inclination (Tabs. 9.27b; 9.28b; 9.29b).

V1754

MTT A-B

Samples	low						medium						high						All					
	T (°C)	F (µT)	N	g	q	σ_b	T (°C)	F (µT)	N	g	q	σ_b	T (°C)	F (µT)	N	g	q	σ_b	T (°C)	F (µT)	N	g	q	σ_b
V39.7a	250-535	105.3	11	0.84	6.35	0.12							535-595	17.7	5	0.64	1.23	0.12						
V40.12a	150-535	101.8	13	0.87	8.55	0.10							535-595	22.6	5	0.74	1.10	0.05						
V41.7b	150-535	96.8	13	0.82	7.73	0.12							535-595	24.0	5	0.65	0.69	0.07						

a)

MTT C-D

Samples	low						medium						high						all					
	T (°C)	F (µT)	N	g	q	σ_b	T (°C)	F (µT)	N	g	q	σ_b	T (°C)	F (µT)	N	g	q	σ_b	T (°C)	F (µT)	N	g	q	σ_b
V39.7a	150-535	146.1	12	0.88	6.36	0.25							520-580	22.9	5	0.72	2.77	0.05						
V40.12a	150-520	144.4	12	0.88	4.37	0.30							500-580	31.9	6	0.79	3.83	0.06						
V41.7b	150-250	106.2	12	0.84	7.65	0.13							500-580	44.8	6	0.74	5.64	0.06						

b)

V1754

Samples	T (°C)	F (µT)	N	g	q	σ_b
V39.7a	250-535	105.3	11	0.84	6.35	0.12
V40.12a	150-535	101.8	13	0.87	8.55	0.10
V41.7b	150-535	96.8	13	0.82	7.73	0.12

c)

Samples	T (°C)	F (µT)	N	g	q	σ_b
V39.7a	520-580	22.9	5	0.72	2.77	0.05
V40.12a	500-580	31.9	6	0.79	3.83	0.06
V41.7b	500-580	44.8	6	0.74	5.64	0.06

mean value

F (µT)	std
101.3	4.3

d)

F (µT)	std
33.2	11.0

Tabs 9.23a,b,c,d - AD 1754: MTT palaeointensity results.
a,b) Palaeofield estimate grouped for temperature range.
c) Best site's representative values
d) Lava flow mean value

352

V1760

MTT A-B

Samples	low T (°C)	F (µT)	N	g	q	σb	medium T (°C)	F (µT)	N	g	q	σb	high T (°C)	F (µT)	N	g	q	σb	All T (°C)	F (µT)	N	g	q	σb
V32.10	150-520	100.1	12	0.88	12.79	0.09																		
V35.7a	150-520	96.2	12	0.87	4.81	0.14							500-595	32.5	4	0.58	4.74	0.04						
V34.12a	150-420	50.3	7	0.78	2.89	0.11							420-580	24.0	5	0.65	0.69	0.93						

a)

MTT C-D

Samples	low T (°C)	F (µT)	N	g	q	σb	medium T (°C)	F (µT)	N	g	q	σb	high T (°C)	F (µT)	N	g	q	σb	all T (°C)	F (µT)	N	g	q	σb
V32.10	250-535	91.5	12	0.89	8.15	0.14							480-580	42.0	7	0.48	1.83	0.10						
V35.7a	300-520	92.4	10	0.85	3.76	0.18							520-580	24.8	4	0.67	1.15	0.11						
V34.12a	250-440	54.3	7	0.79	4.02	0.09	420-535	22.8	7	0.77	5.73	0.03												

b)

V1760

Samples	T (°C)	F (µT)	N	g	q	σb
V32.10	150-520	100.1	12	0.88	12.79	0.09
V35.7a	150-520	96.2	12	0.87	4.81	0.14
V34.12a						

c)

Samples	T (°C)	F (µT)	N	g	q	σb
V32.10	480-580	42.0	7	0.48	1.83	0.10
V35.7a	500-595	32.5	4	0.58	4.74	0.04
V34.12a	420-535	22.8	7	0.77	5.73	0.03

mean value

F (µT)	std
98.1	2.79

d)

F (µT)	std
32.4	9.58

Tabs 9.24a,b,c,d - AD 1760: MTT palaeointensity results.
a,b) Palaeofield estimate grouped for temperature range.
c) Best site's representative values
d) Lava flow mean value

V 1754   Palaeointensity results from Microwave experiment

sample	sub sample	Power range (W)	N	f	g	q	b	σ_b	Fpalaeo (μT)	Uncertainty
V39	10b-1	42 - 78	9	0.170	0.795	5.079	-1.399	0.037	**69.935**	13.770
V39	10b-2	33 - 60	7	0.209	0.806	3.526	-1.565	0.075	**78.244**	22.193
v40	7b-1	46 - 75*	6	0.227	0.723	2.554	-1.390	0.089	**69.500**	27.216
		50 - 75	5	0.131	0.702	0.733	-1.450	0.182	**72.486**	98.856
v41	4a-1	46 - 72*	5	0.192	0.742	5.347	-1.460	0.039	**72.996**	13.652
		50 - 72	4	0.135	0.656	2.514	-1.510	0.053	**76.519**	30.038
v41	4a-2	50 - 68*	6	0.452	0.735	8.899	-1.225	0.046	**61.269**	6.685
		55 - 68	5	0.368	0.652	4.530	-1.223	0.065	**61.174**	13.504

a)

(*) Including the first point D(NRM)

sample	sub sample	Fpalaeo (μT)
V39	10b-1	**69.935**
V39	10b-2	**78.244**
V40	7b-1	**69.500**
V41	4a-1	**72.996**
V41	4a-2	**61.269**

b)

mean value

Fpalaeo (μT)	std
70.39	6.18

c)

Tabs 9.25a,b,c - AD 1754: Microwave palaeointensity results.
a) All possible palaeofield estimate.
b) Best site's representative values
c) Lava flow mean value

V 1760   Palaeointensity results from Microwave experiment

sample	sub sample	Power range (W)	N	f	g	q	b	σ_b	Fpalaeo (μT)	Uncertainty
V32	13-1	33 - 60*	5	0.181	0.722	3.234	-1.011	0.041	**60.548**	15.632
		40 - 60	4	0.114	0.645	0.937	-1.008	0.079	**60.378**	53.751
v35	9-1	50- 125*	7	0.108	0.788	1.321	-0.991	0.064	**49.526**	37.500
		[a] 58- 125	6	0.086	0.731	0.891	-0.916	0.065	**46.821**	51.412
		[b] 125-175	8	0.397	0.730	17.090	-1.681	0.029	**84.034**	4.917
		50- 175*	14	0.505	0.824	12.772	-1.507	0.049	**76.382**	5.900
		[c] 58-175	13	0.484	0.810	11.765	-1.534	0.051	**76.709**	6.520
v34	8-1	37 - 72	6	0.259	0.564	8.519	-1.270	0.022	**63.490**	7.452
v34	8-2	42 - 58	7	0.213	0.777	4.620	-1.288	0.046	**64.380**	13.934

a)

(*) Including the first point D(NRM)

sample	sub sample	Fpalaeo (μT)
V32	13-1	**60.548**
V35	9-1	**76.709**
V34	8-1	**63.490**
V34	8-2	**64.380**

b)

mean value

Fpalaeo (μT)	std
63.78	10.69

c)

Tabs 9.26a,b,c -AD 1760: Microwave palaeointensity results.
a) All possible palaeofield estimate.
b) Best site's representative values
c) Lava flow mean value

Sample	N steps	Dec	Inc	MAD	T °C range
01	7	344.1	65.5	0.5	550/630
03	6	343.6	62.9	1.4	565/630
06	6	342.5	64.4	1.2	550/620
07	12	343.7	60.6	0.6	460/630
11	7	345.0	61.1	0.7	550/630
12	7	342.1	67.9	0.8	535/630

a)

Site	N samples	Dec	Inc	k	α_{95}
V32(i)	6	343.6	63.7	832.6	2.3
V32(i*)	5	343.8	62.9	1442.1	2.0

Tabs. 9.27a,b - Site V32 directional results. b)
a) Sample best representative directions. b) Site mean values.
*mean value obtained erasing sample 12

Sample	N steps	Dec	Inc	MAD	T °C range
01	6	347.2	63.6	0.7	520/595
02	6	344.7	60.2	0.3	520/595
03	6	346.2	64.5	0.6	520/595
04	7	346.7	64.0	0.4	500/595
06	6	344.0	59.1	0.9	480/565
11	7	344.4	66.1	0.4	390/535

a)

Site	N samples	Dec	Inc	k	α_{95}
V34(i)	6	345.5	62.9	862.1	2.3
V34(i*)	5	345.8	63.7	1317.5	2.1

b)

Tabs. 9.28a,b - Site V34 directional results.
a) Sample best representative directions. b) Site mean values.
*mean value obtained erasing sample 06

Sample	N steps	Dec	Inc	MAD	T °C range
03	7	345.3	59.7	0.9	535/620
04	7	351.9	65.2	1.0	550/630
05	8	349.9	63.9	0.6	500/620
06B	7	341.5	59.9	0.7	550/630
07B	8	347.5	61.8	0.6	520/620
08	9	343.1	59.2	0.4	500/620
10A	8	337.6	58.7	0.5	520/620
10B	4	342.0	59.5	0.8	595/630
11A	10	347.7	62.4	0.8	480/630
12	4	346.2	65.9	0.7	595/630
13	7	3476	67.9	0.7	535/620

a)

Site	N samples	Dec	Inc	k	α_{95}
V35(i)	11	345.2	62.2	482.9	2.1
V35(i*)	8*	345.3	61.6	831.1	1.9

b)

Tabs. 9.29a,b - Site V35 directional results.
a) Sample best representative directions. b) Site mean values.
*mean value obtained excluding samples 04,10A,13

b - Lava flow mean value

All the sites showed very similar mean directions and also statistically well defined (Tab. 9.30a.). One lava flow mean value was therefore obtained (Tab.9.30b).

Sample	N samples	Dec	Inc	k	α_{95}
V032	5	343.8	62.9	1442.1	2.0
V034	5	345.9	63.7	1317.5	2.1
V035	8	345.3	61.6	831.1	1.9

a)

Lava	N samples	Dec	Inc	k	α_{95}
1760	3	345.0	62.7	4871.4	1.8

b)

Tabs. 9.30a,b - AD 1760 lava flow directional results.
a) Sites best representative directions. b) Lava flow mean values.

9.6.2 - Palaeointensities

a - MTT

In both MTT A-B and C-D (Tabs.9.24a,b) the low part of the temperature spectrum showed high values of the palaeointensity with statistical parameters still acceptable. The low values obtained at high temperature' ranges were also acceptable in terms of reliability and statistically. Two mean values were considered (Tab.9.24c).

b- Microwave

All samples showed quite similar estimate of the palaeofield (Tab.9.26a). Sample V35.9-1 showed different slopes and in this case an increase in the palaeofield estimate with the increasing power range was observed. A unique mean value for this lava flow was obtained (Tab.9.26b,c).

356

9.7- AD 1806

9.7.1 - Palaeodirections

a - Sites mean values

Sites V24 - All the samples showed a very similar component but defined within different range of temperature (Tab. 9.31a). A unique value of ChRM was, therefore obtained (Tab. 9.31b)

Sample	N steps	Dec	Inc	MAD	T °C range
04	4	348.6	57.7	0.6	480/535
06	5	346.5	56.9	0.7	500/565
07	5	347.6	59.0	0.7	480/565
09	8	346.0	58.6	0.7	200/440
10	8	351.8	58.1	1.7	150/440
12	6	348.3	56.0	1.9	390/535

a)

Site	N samples	Dec	Inc	k	α_{95}
V24	6	348.1	57.7	2697.6	1.3

b)

Tabs. 9.31a,b - Site V24 directional results.
a) Sample best representative directions. b) Site mean values.

Sites V25 - All the samples showed a very similar component with a medium MAD (~ 3). A unique value of ChRM was obtained (Tab. 9.32a,b)

Sample	N steps	Dec	Inc	MAD	T °C range
03	7	348.2	60.6	3.6	360/500
05	13	344.2	55.3	3.6	20/500
07	6	350.6	63.3	3.7	250/460
08	7	347.1	59.2	2.6	250/440
09	13	348.0	59.3	2.5	20/500
11	6	344.2	50.4	2.0	420/565

a)

Site	N samples	Dec	Inc	k	α_{95}
V25	6	346.8	58.0	294.2	3.9

b)

Tabs. 9.32a,b - Site V25 directional results.
a) Sample best representative directions. b) Site mean values.

b - Lava flow mean value

Both sites showed very similar mean directions but only site V24 was very well defined (Tab. 9.33a.). The average of these two values gives obviously a very high value of k (Tab.9.33b).

Sample	N samples	Dec	Inc	k	α_{95}
V024	6	348.1	57.7	2697.6	1.3
V025	6	346.8	58	294.2	3.9

a)

Lava	N samples	Dec	Inc	k	α_{95}
1806	2	347.5	57.9	23173	1.6

b)

Tabs. 9.33a,b - AD 1806 lava flow directional results.
a) Sites best representative directions. b) Lava flow mean values.

9.7.2 - Palaeointensities

a - MTT

Sample V24.5 showed unacceptable high value of the palaeointensity at low temperature in both MTT A-B and C-D. The values obtained at high temperature' ranges which were acceptable in terms of reliability and statistic properties, were quite similar to those obtained at low temperature in sample V25.1 (Tabs.9.34a,b). Those values were used to calculate the mean values (Tab.9.34c).

b- Microwave

The only value considered was that one obtained at low power range for sample V25.2-1 as the best statistically defined (Tab.9.40a). Sample V24.3-2 showed a very similar palaeointensity estimate but it was statistically very poorly defined.

V1806

MTT (A-B)

Samples	low**						medium						high						All					
	T (°C)	F (μT)	N	g	q	σ_b	T (°C)	F (μT)	N	g	q	σ_b	T (°C)	F (μT)	N	g	q	σ_b	T (°C)	F (μT)	N	g	q	σ_b
V24.5	150-460	131.9	9	0.85	2.22	0.38	440-535	29.5	6	0.65	3.90	0.04												
V25.1	250-440	59.8	7	0.79	2.16	0.55	420-535	7.4	6	0.67	2.15	0.02												

a)

MTT (C-D)

Samples	low						medium						high						all					
	T (°C)	F (μT)	N	g	q	σ_b	T (°C)	F (μT)	N	g	q	σ_b	T (°C)	F (μT)	N	g	q	σ_b	T (°C)	F (μT)	N	g	q	σ_b
V24.5	300-520	159.7	8	0.84	2.94	0.39	420-520	30.4	5	0.67	4.95	0.05												
V25.1	250-420	41.4	6	0.69	3.11	0.08							420-565	5.5	9	0.30	1.14	0.01						

b)

V1806

Samples	T (°C)	F (μT)	N	g	q	σ_b
V24.5	420-520	30.4	5	0.67	4.95	0.05
V25.1	250-420	41.4	6	0.69	3.11	0.08

c)

mean value

F (μT)	std
35.9	7.83

d)

Tabs 9.34a,b,c,d - AD 1806: MTT palaeointensity results.
a,b) Palaeofield estimate grouped for temperature range.
c) Best site's representative values
d) Lava flow mean value

9.8 - AD 1839

9.8.1 - Palaeodirections

a - Sites mean values

Sites V42, V43 - In all the samples a single very well defined component was revealed especially at high temperature (Tabs. 9.35a; 9.36a). For each sites a unique value of the ChRM was considered (Tabs. 9.35b; 9.36b).

Sites V44 - All the samples showed similar component but defined within different range of temperature and with MAD between 0.5 and 4 (Tab. 9.37a). Two values of ChRM were obtained; one excluding sample 08 (Tab. 9.37b)

Sample	N steps	Dec	Inc	MAD	T °C range
01A	8	354.5	56.7	1.0	520/620
02A	6	349.2	55.9	0.8	550/620
04A	11	353.9	57.0	0.6	440/620
06A	10	350.5	57.4	1.0	460/610
08A	5	346.7	55.5	0.8	520/595
10A	8	349.7	57.3	0.7	460/595
12A	6	348.3	57.4	0.6	520/610
13A	4	347.0	55.8	1.0	550/610

a)

Site	N samples	Dec	Inc	k	α_{95}
V42	8	349.9	56.7	2065	1.2

b)

Tabs. 9.35a,b - Site V42 directional results.
a) Sample best representative directions. b) Site mean values.

Sample	N steps	Dec	Inc	MAD	T °C range
01B	6	346.6	56.2	0.9	550/620
03A	7	347.2	57.6	0.8	520/620
04A	5	348.2	55.9	1.0	550/610
06A	6	348.5	56.0	1.3	550/620
07A	6	347.6	56.6	1.1	550/620
08A	9	345.4	55.8	0.8	500/620
09B	7	348.2	55.8	0.5	500/620
12A	7	345.5	58.5	0.8	520/620

a)

Site	N samples	Dec	Inc	k	α_{95}
V43	8	347.2	56.6	4594.7	0.8

b)

Tabs. 9.36a,b - Site V43 directional results.
a) Sample best representative directions. b) Site mean values.

Sample	N steps	Dec	Inc	MAD	T °C range
01A	4	348.6	61.8	3.1	250/480
03A	5	346.3	57.9	2.6	250/440
04B	5	347.5	60.3	2.1	480/550
07A	13	350.2	58.3	2.7	100/520
08A	6	340.7	60.9	2.6	360/520
09A	6	344.2	59.6	1.1	390/520
11A	4	348.6	56.2	2.1	480/565
12A	6	345.1	58.7	1.9	440/565

a)

Site	N samples	Dec	Inc	k	α_{95}
V44(i)	8	346.7	59.2	1170.1	1.6
V44(i*)	7	347.2	59.0	1472.4	1.6

b)

Tabs. 9.37a,b - Site V44 directional results.
a) Sample best representative directions. b) Site mean values.
*mean value obtained excluding sample 08A

b - *Lava flow mean value*

All the sites showed similar mean directions and statistically very well defined (Tab. 9.38a.) The lava flow mean obtained is shown in Tab.9.38b)

Sample	N samples	Dec	Inc	k	α_{95}
V042	7	347.2	59.0	1472.4	1.6
V043	8	347.2	56.6	4594.7	0.8
V044	8	349.9	56.7	2065	1.2

a)

Lava	N samples	Dec	Inc	k	α_{95}
1839	3	348.1	57.4	2570.8	2.4

b)

Tabs. 9.38a,b - AD 1839 lava flow directional results.
a) Sites best representative directions. b) Lava flow mean values.

9.8.2 - *Palaeointensities*

a - MTT

Sample V42.5 showed unacceptable high value of the palaeointensity at low temperature in both MTT A-B and C-D, while the values showed at medium and high temperature were acceptable in terms of reliability and statistically. Similar acceptable values were also obtained at high temperature in sample V43.13b and at low temperature in sample V44.6a (Tabs.9.39a,b). Best representative values for each sample were used to calculate the mean values (Tab.9.39c).

b- Microwave

Sample V443b-2 showed a very unacceptable high value at low power range. All the other at the same range, were quite similar (Tab.9.41a) and widely acceptable. One mean value for this lava flow was obtained value (Tab.9.41b,c)

9.9 - Comparison of Mean Magnetic Values with Rock Magnetic Properties

It is important to underline that the magnetic properties were obtained by analysing only a few samples (2 or 3) out of, generally, 15 from the same site, all of which were close to each other. However, all the samples used for magnetic mineral and grain size investigations were taken next to those used for thermal and microwave experiments. Therefore, the magnetic properties can be considered to be typical for each single site. The magnetic properties (Chapter 8) were identified as belonging to two main groups, A (which was divided in two slightly different sub-groups, A1 and A2) and B. Samples of A1/A2 groups, as already described in section 8.6, are characterized by the dominance of high coercivity Ti-poor titanomagnetite, while those of group B, are characterized by the dominance of titanomagnetites with relatively higher content of titanium and lower coercivity. The

V1839

a)

MTT A-B	low						medium						high						All					
Samples	T (°C)	F (µT)	N	g	q	σ_b	T (°C)	F (µT)	N	g	q	σ_b	T (°C)	F (µT)	N	g	q	σ_b	T (°C)	F (µT)	N	g	q	σ_b
V42.6b	300-440	248.7	6	0.76	0.36	0.85	440-535	65.0	6	0.68	7.03	0.06	420-595	42.2	7	0.36	16.45	0.01						
V43.13b							390-520	51.9	7	0.58	5.74	0.05	390-595	37.0	9	0.43	16.93	0.01						
V44.6a	250-460	37.4	5	0.48	2.48	0.08	460-535	5.9	4	0.60	0.82	0.02												

b)

MTT C-D	low						medium						high						all					
Samples	T (°C)	F (µT)	N	g	q	σ_b	T (°C)	F (µT)	N	g	q	σ_b	T (°C)	F (µT)	N	g	q	σ_b	T (°C)	F (µT)	N	g	q	σ_b
V42.6b	150-520	131.9	12	0.76	15.37	0.22	460-580	39.4	6	0.47	36.19	0.02	520-580	23.1	5	0.61	7.11	0.04						
V43.13b	150-500	100.8	11	0.82	2.97	0.18							480-580	32.1	7	0.68	9.27	0.03						
V44.6a	150-440	44.2	8	0.70	3.67	0.11							480-580	4.3	8	0.68	2.88	0.01						

V1839

c)

Samples	T (°C)	F (µT)	N	g	q	σ_b
V42.6b	460-580	39.4	6	0.47	36.19	0.02
V43.13b	390-595	37.0	9	0.43	16.93	0.01
V44.6a	250-460	37.4	5	0.48	2.48	0.08

mean value
d)

F (µT)	std
37.9	1.3

Tabs 9.39a,b,c,d - AD 1839: MTT palaeointensity results.
a,b) Palaeofield estimate grouped for temperature range.
c) Best site's representative values
d) Lava flow mean value

V 1806   Palaeointensity results from Microwave experiment

sample	sub sample	Power range (W)	N	f	g	q	b	σ_b	Fpalaeo (μT)	Uncertainty
v25	2-1	26 - 75	14	0.308	0.878	8.105	-1.198	0.040	**59.904**	7.391
	2-2	-	-	-	-	-	-	-	-	-
v24	3-2	20 - 27	4	0.145	0.656	0.376	-1.147	0.289	**57.337**	152.294

a)

Tab. 9.40 - AD 1806: Microwave paleointensity results.

V 1839   Palaeointensity results from Microwave experiment

sample	sub sample	Power range (W)	N	f	g	q	b	σ_b	Fpalaeo (μT)	Uncertainty
v42	13b-1	50-65	4	0.187	0.642	1.124	-1.099	0.118	**54.931**	48.869
v43	9c-2	42 - 80*	9	0.166	0.827	4.135	-1.061	0.035	**53.031**	12.826
		45 - 80	8	0.117	0.829	2.124	-1.066	0.049	**53.321**	25.109
v44	3b-1	29 - 60	6	0.214	0.778	1.369	-4.409	0.537	**220.455**	161.011
	3b-2	-	-	-	-	-	-	-	-	-

a)

sample	sub sample	Fpalaeo (μT)
V42	13b-1	**54.931**
V43	9c-2	**53.031**

b)

mean value

Fpalaeo (μT)	std
53.98	1.34

c)

Tabs. 9.41a,b,c - AD 1839: Microwave paleointensity results.
a) All possible palaeofield estimate.
b) Best site's representative values
c) Lava flow mean value

palaeointensity experiment always showed an inverse relationship between the temperature ranges and the palaeointensities estimated, with slightly concave curves or two clearly different slopes for temperature v. intensity. In contrast, the microwave experiments showed mostly convex curves for power v. intensity, when more then one slope was defined. (The two methods are compared later in section 10.3.)

9.9.1 -Thermal experiments

a -AD 79-1631

Palaeodirection - As described in section 7.7, all the sites from this very large lava flow showed magnetic properties that belong to three different groups (Tab. 8.2). All the sites (V27, V31, V36, V37) belonging to the A1 and A2 groups showed well defined mean directions (α_{95} <3°) for their high temperature components. The least well-defined results (α_{95} >3°) and most inconsistency were showed by the mean directions of V26 and V33, mostly calculated from their low/medium temperature component. Both of these sites had magnetic properties belonging to group B. Surprisingly site V30, referred to as Ex in Chapter 7 because of its exceptional behaviour, showed acceptable (α_{95}=2°) medium/high temperature directional results (Tabs 9.1a,b). These were also very consistent with all the other site results, despite being characterized by a titano-haematite magnetic carrier. .

Palaeointensity - Samples from sites V27, V31, V36 and V37 (groups A1/A2), showed unrealistically high values (>100 mT) at low temperature and acceptable values at high temperatures. Samples from sites V26 and V33 (group B) values at both low and high temperatures were clearly lower than those compared with the other samples; the low temperature range showed the more acceptable values. Sample V30 (Ex) showed a unique acceptable value of the palaeofield, during MTT A-B, while it behaved in the same way as the samples belonging groups A1/A2 during MTT C-D.

b - AD 1697, 1714(1906), 1754 & 1760

All the site magnetic properties belong to groups A1/A2 and samples showed the same palaeodirection and palaeointensity behaviour.

Palaeodirection - All sites showed very well defined mean directions obtained from high temperature components.

Palaeointensity - The Thellier experiment showed the highest values of the palaeofield at low temperatures. However in sites 1714(1906), 1754 and 1760 lava flows, the low temperature component seemed to be the most reliable and statistically acceptable.

c - AD 1806

Palaeodirection - Sites V24 and V25 belong to group B and showed mean directions very similar to each other. However, while the V24 mean value was from components that were very well defined mostly in the medium/high range of temperatures, the V25 mean direction was obtained from components less defined in the low/medium range.

Palaeointensity - In samples from site V25, the values obtained, at low and high temperature, were clearly lower, compared with all the samples from the other sites and consistent with all the other "B" behaviour samples. The low temperature range showed the more acceptable value. Sample from site V24 seemed to behave as the samples belonging to A1/A2 groups, showing a very high value at the low temperature range and a more acceptable, more precise value at high temperature.

d -AD 1839

Palaeodirection - Sites V42 and V43, belonging to the A1 and A2 groups, showed a very well defined mean directions (respectively $\alpha_{95} = 1.2°$ and $0.8°$) which were obtained from high temperature components. Although site V44 belongs to group B it also showed a well defined mean direction ($\alpha_{95}=1.6°$) that was very consistent with the other

two. The only difference was that its mean value was calculated from components identified both low/medium and medium/high temperature ranges.

Palaeointensity - Samples V42, V43 (groups A1/A2), showed very high values at low temperature and acceptable values at high range. In the sample from site V44 (group B), the values obtained, at low and high temperatures, were clearly lower compared with all the other samples. Furthermore the low temperature range showed the more acceptable values that appeared to be consistent with the other sample values.

9.9.2 - Microwave experiments

In general, one palaeofield estimate was obtained from the low range of the microwave power. As pointed out earlier, in the few samples that showed more than one value, both a direct and inverse relationships between microwave power and palaeointensity estimates were found, resulting in graphs that showed slightly convex/concave curves or two different slopes.

9.9.3 - Conclusion

a - Palaeodirection

The best results, in terms of precision and consistency within the same site, and also between sites within the same lava flow, appear to be obtained for samples belonging to groups A1 and A2, i.e. characterized by the dominance of high coercivity Ti-poor titanomagnetite. The most important general behaviour, which appeared clearly in all these samples, is that they showed very well defined components within high range of temperature (usually greater then 520°C). Samples of group B, characterized by higher Ti titanomagnetites and lower coercivity compared with A1/A2 groups, gave less defined results that were generally from a medium range of temperature (390-500°C). Sites V24 and V44 showed the best statistical results in this group, almost comparable with those obtained by the samples of groups A1/A2. After a further review of their magnetic

properties, they appeared to have intermediate characteristics lying between groups A1/A2 and B. In fact, sample V24.2 had K and K_{ARM} values (Tab. 8.1) comparable with the other of group B while their H_{CR} values were clearly more similar to groups A1/A2. In sample V44.4a all the values were comparable with those of group B but its mineralogy (see section 8.6c) showed the coexistence of high and low coercivity Ti-poor titanomagnetites. Site V30 (Ex) showed acceptable results although it seemed to be characterized by a titano-haematite magnetic carrier. The medium temperature (up to 460°C) components, identified within most samples, could be due to the presence of the titanomagnetite (x=2) observed in the soft coercivity fraction of the 3 axes IRM experiment (section 7.6d). A coexistence with a low percentage of titanomagnetite, with higher Tub, can only be hypothesised but not clearly affirmed, as an explanation of the source of the high temperature components identified within some samples.

b - Palaeointensity

All the samples belonging to groups A1/A2 showed very high values (sometime too high) over low temperature ranges and acceptable value at high temperature ranges. All the samples (except V24) belonging to group B showed clearly lower values at low and high temperature ranges. Sample V30 (Ex) behaved as samples of groups A1/A2. A closer analyses of the magneto mineralogical characteristics of these two apparent anomalous behaviours (V24, V30), showed that they had rock magnetic parameters that were different from all the others used to classify the different groups, except for H_{CR} which was comparable with all the values showed by A1/A2. Although more evidence is needed, this seems to suggest that, of the thermally analysed samples, the grain sizes were significantly influential on the palaeointensity determination. However, this behaviour could be due to the fact that in general the magneto-mineralogy was almost the same in all the samples, and the few exceptions may be untypical. No particular relationship was observed between magnetic property groups and microwave components behaviour.

Although Hill & Shaw (1999 and 2000) illustrate that the microwave method using the perpendicular field method is highly successful for recent lava, for Vesuvian lavas it was not possible to get very high quality results. Reasons for this results just acceptable, could be human error when the experiments were carried out (it is, in fact, very easy with the microwave equipment to change the direction of the applied field) or that the samples contained secondary components that were not removed. Furthermore the samples need to be isotropic (but this is usually the case for lava) and the primary direction of magnetisation should be stable, although almost all the thermal experiments and some microwave demagnetization showed that the sample analysed can be considered characterised by single component.

9.10 – Paleo-Secular Variation Curves

9.10.1 - Directions

All the sites mean values obtained have been plotted on a DEC/INC graph (Fig. 9.1) with their relative 95% probability error bars (δDec and δInc). All the sites define two clear trends: A) with a declination around 15° and B) with a declination around 350° (-10° on the graph). Sites of the AD 79-1631 lava flows lie very close to each other on the arc A, except sites V033 and V026. Both of these have poor statistical definitions (α_{95} and MAD). On this basis and for their magnetic properties (section 9.9), they will not be considered here. Site V028 and V029 (AD 1697) lie quite close to each other. The former will be considered, despite a large scatter, for several reasons. Its mean value has been calculated from only three samples but with very well defined components (see Tab. 9.11). Its mean value is consistent with V029 that has a good statistical definition. Finally, its magnetic properties did not show anomalous behaviour. Both sites lie on arc A at a lower inclination than that showed by sites belonging to AD 79-1631. Each of AD 1754,1760,1806 and 1839 lava flows has sites that lie very close to each other. In general, they lie on arc B, with a progressive decrease in inclination with age. Sample

V038 belongs to an uncertain lava flow (1714/1906), lies on the arc B with the lowest inclination and is therefore inconsistent with the 1714 age, but consistent with the alternative 1906 age. Consequently, all the lava flows seem to define two different arcs (A and B), with A having a clockwise trend with decreasing age, and B have an apparently anti-clockwise trend.

The lava flows mean values, with their relative error bars, are then compared with other results from a recent palaeomagnetic study on Mt. Etna, Mt. Arso (Ischia, Naples) and Mt. Vesuvius (Angelino et al., 1999, Incoronato, 1996, Gialanella et al., 1998). All the lava values of Dec and Inc, summarised on the South Italian Secular Variation Curve (SISVC), have been relocated to Vesuvius via the inclined geocentric dipole method (Noel and Batt, 1990) and will be referred to as V (for Vesuvius), E (for Etna) and A (for Arso). The curve, relocated to Vesuvius, will be referred to as VSVC.

The VSVC shows a clear clockwise trend (Fig. 9.2), starting from E1284/85 until E1983, and a medieval branch with an upward trend. The clearest result is that the lava flow mean value obtained from V79-1631 has exactly the same direction of the V1631 on the VSVC. Therefore, the mean value obtained from the directional study can be ascribed to that time. The age attributed in literature to V1697 lava flow seems to be wrong. In fact, its mean value, as described earlier, has a lower inclination than V1631, and lies between E1595 and E1537. Because of its high error in Dec and Inc it could also have a medieval age or even be attributed to V1631. However, as discussed earlier, site V29 (see Fig. 9.1) is much better defined and seems to suggest a mid XVI century (~AD1540). Both the mean values obtained from V1754 and V1760 lie very close to the previously identified V1760 lava flow. Furthermore, they follow the same clockwise trend. The age attributed in literature to these two lava flows seems, therefore, to be correct. The same observations can be made for V1806 and V1839. They both lie before V1858, very close to the VSVC, and following the same trend. The mean value from the site V038 seems to resolve the uncertainty on the age of this site (1906 or 1714). Although it lies far from V1910, a recent age seems much more realistic than AD 1714.
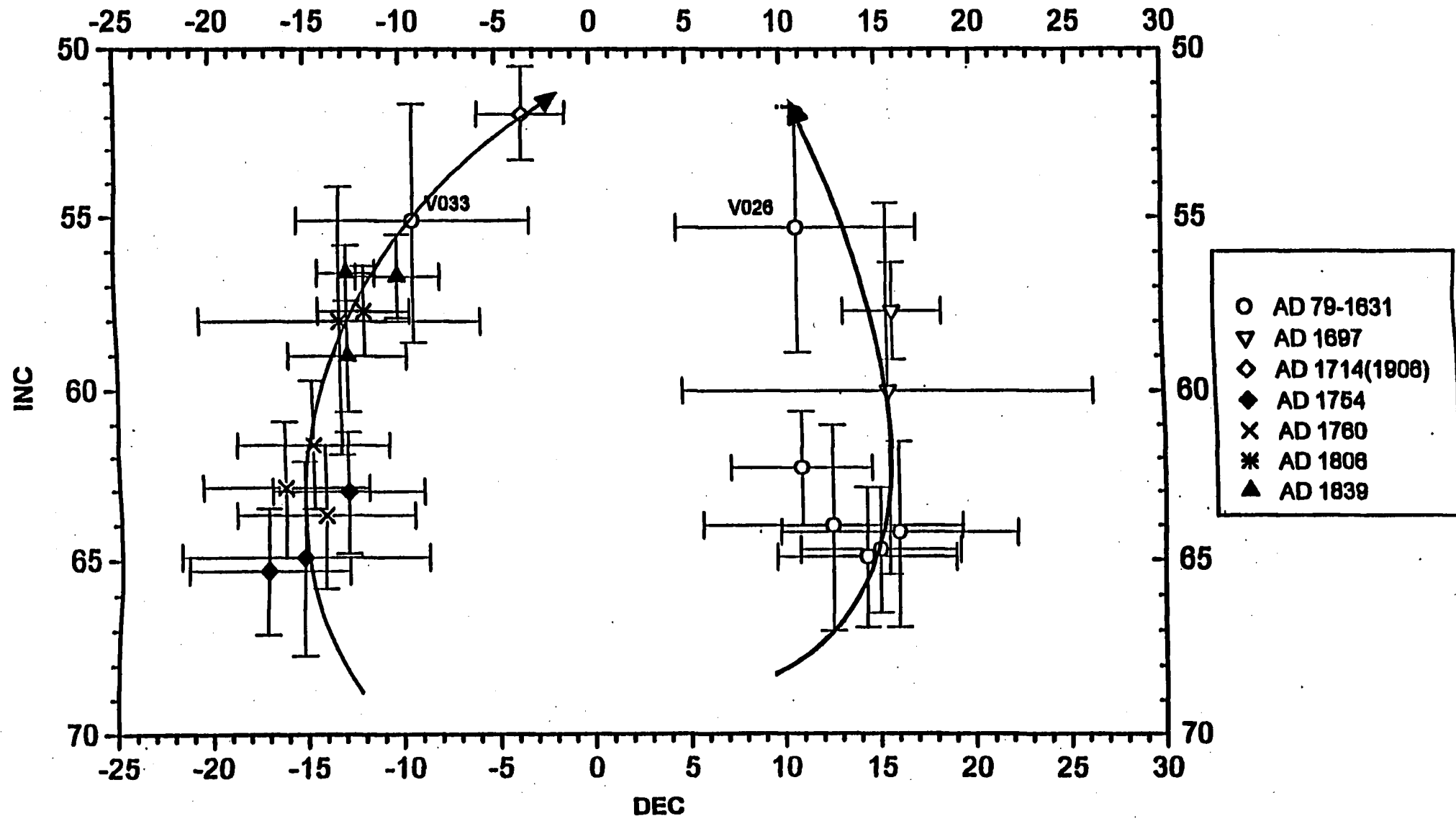
Fig. 9.1 - Dec/Inc graph with all the sites mean values.
All the values are plotted with their 95% probability error bars (δDec and δInc).
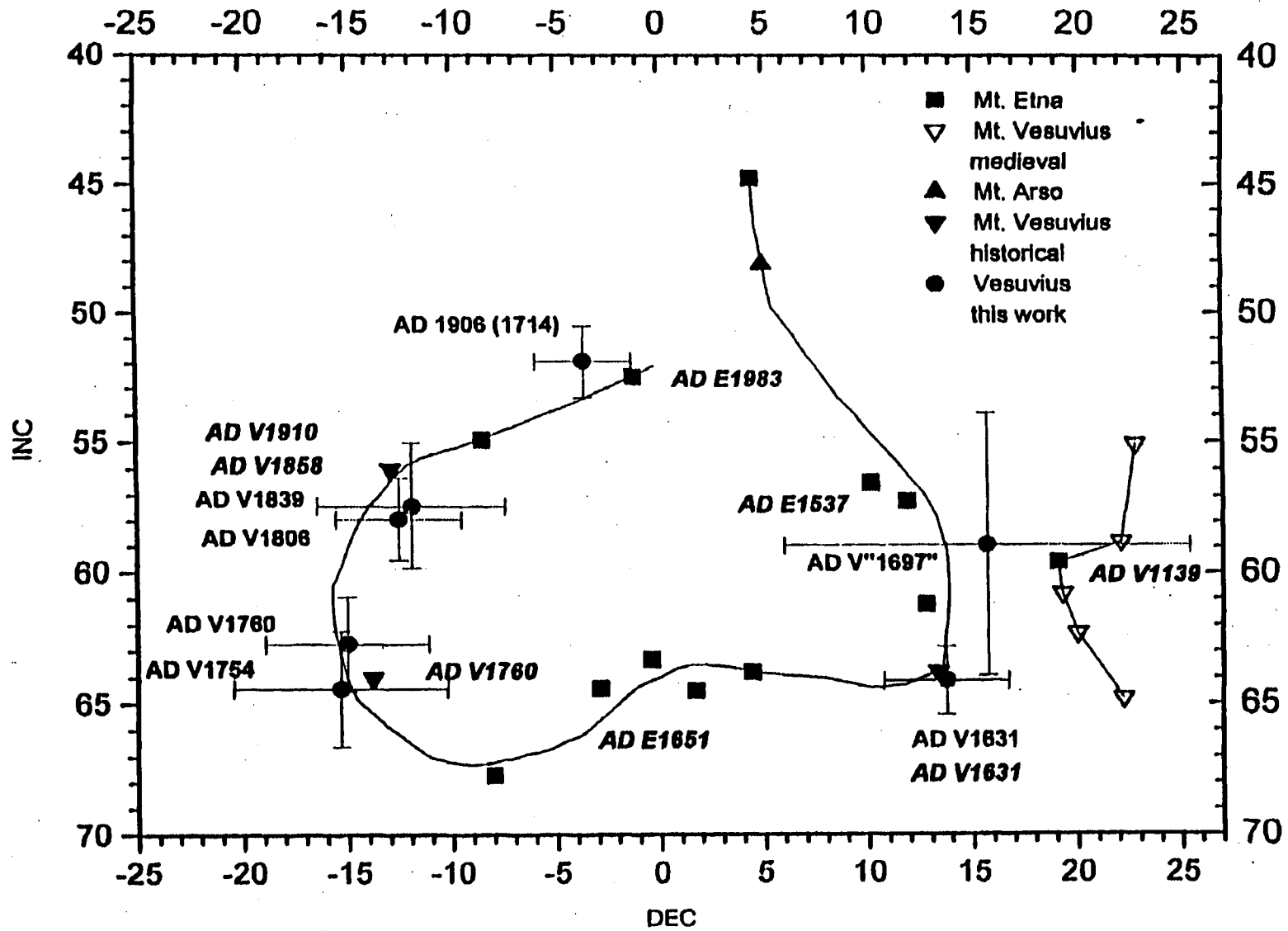
Fig. 9.2 - The Vesuvian Secular Variation Curve (VSVC).
In bold & italic characters some other results from Vesuvius and Etna (see section 9.10.1).

9.10.2 - Intensity

All the sites mean values have been plotted on time-dependent graphs with their relative standard deviations. On the basis of the ambiguous directional results obtained for the AD 1697 lava flow (section 9.10.1), two different ages are considered: the ages attributed in literature and that suggested by the directional data (~AD 1540). The mean value from the site V038 does not seems to resolve the uncertainty on the age of this site (1906 or 1714). However a high value of the palaeointensity (~85 μT from MTT and ~100 μT from microwave), appear unrealistic for the first option, therefore the older age will be considered.

The values of the palaeointensity obtained for AD 1631 from both MTT and microwave experiments are quite similar.

MTT experiment - As the palaeointensity results showed for both AD 1754 and AD 1760 two possible values (see Tabs. 9.23 and 9.29), both are considered. Starting from the last century the intensity plots seem to show a slight decrease until AD 1806 (Fig. 9.3a,b) or AD 1754/60 (Fig. 9.4a,b). This is followed by a quite rapid increase until the beginning of the XVIII century. If the correct age for V28 and V29 is AD 1697 (Figs. 9.3a and 9.4a) then the palaeointensity seems to stay fairly constant until AD 1631. If the age AD 1540 is considered correct then the palaeointensity shows a slight decrease (Figs. 9.3b and 9.4b)

Microwave experiment - The results seem to show a general but clear increase in intensity with the decreasing time. This trend is even clearer if sites V28 and V29 are considered to be of AD 1540 (Fig.9.5a,b).
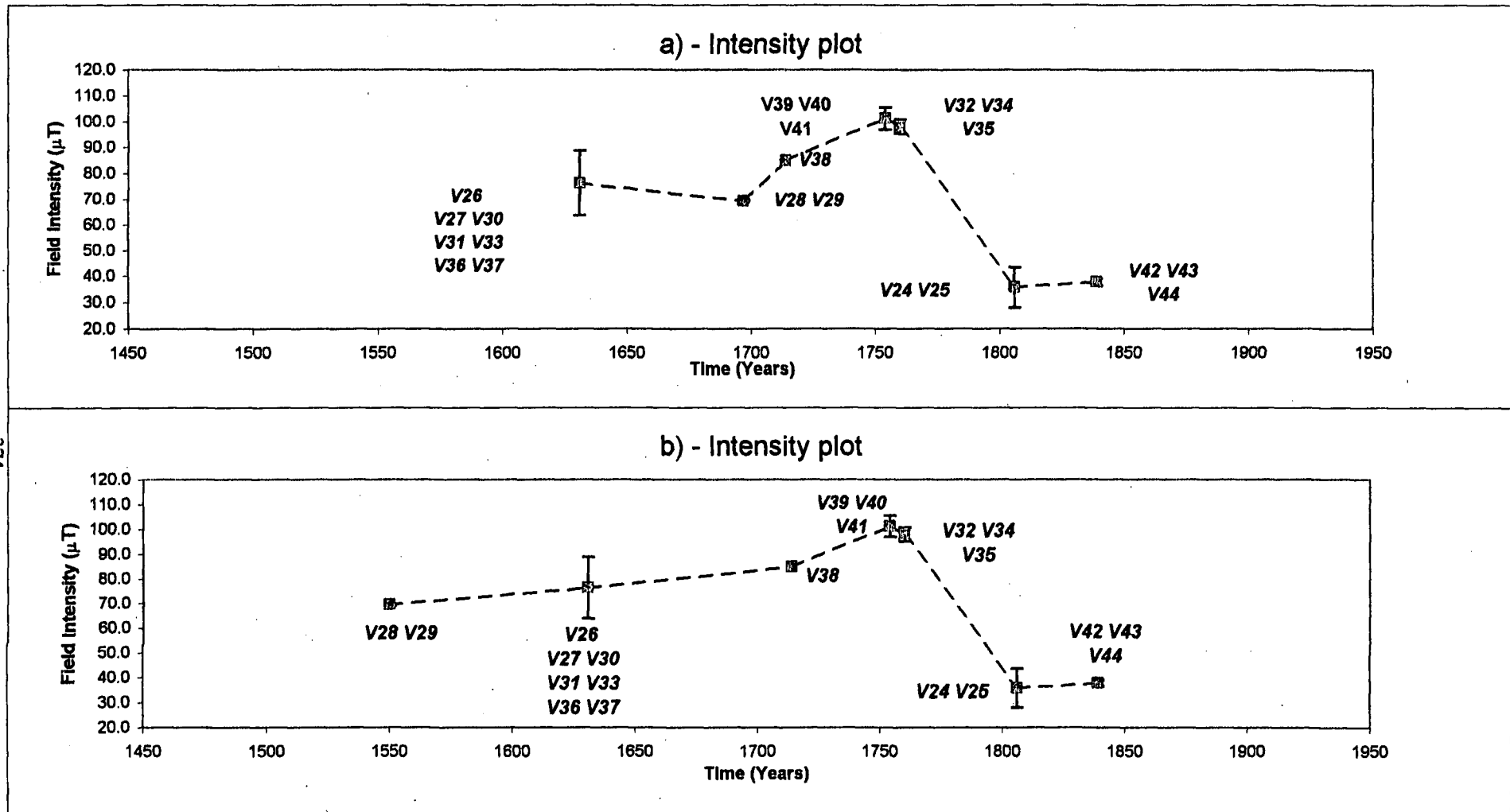
Fig. 9.3a,b - Time-dependent graph with all thermal palaeointensity results.
In a) and b) two different ages are considered for sites V28 and V29 (see section 9.10.2).
In both graphs the highest values obtained for sites V39,V40,V41 and V32,V34,V35 are shown.
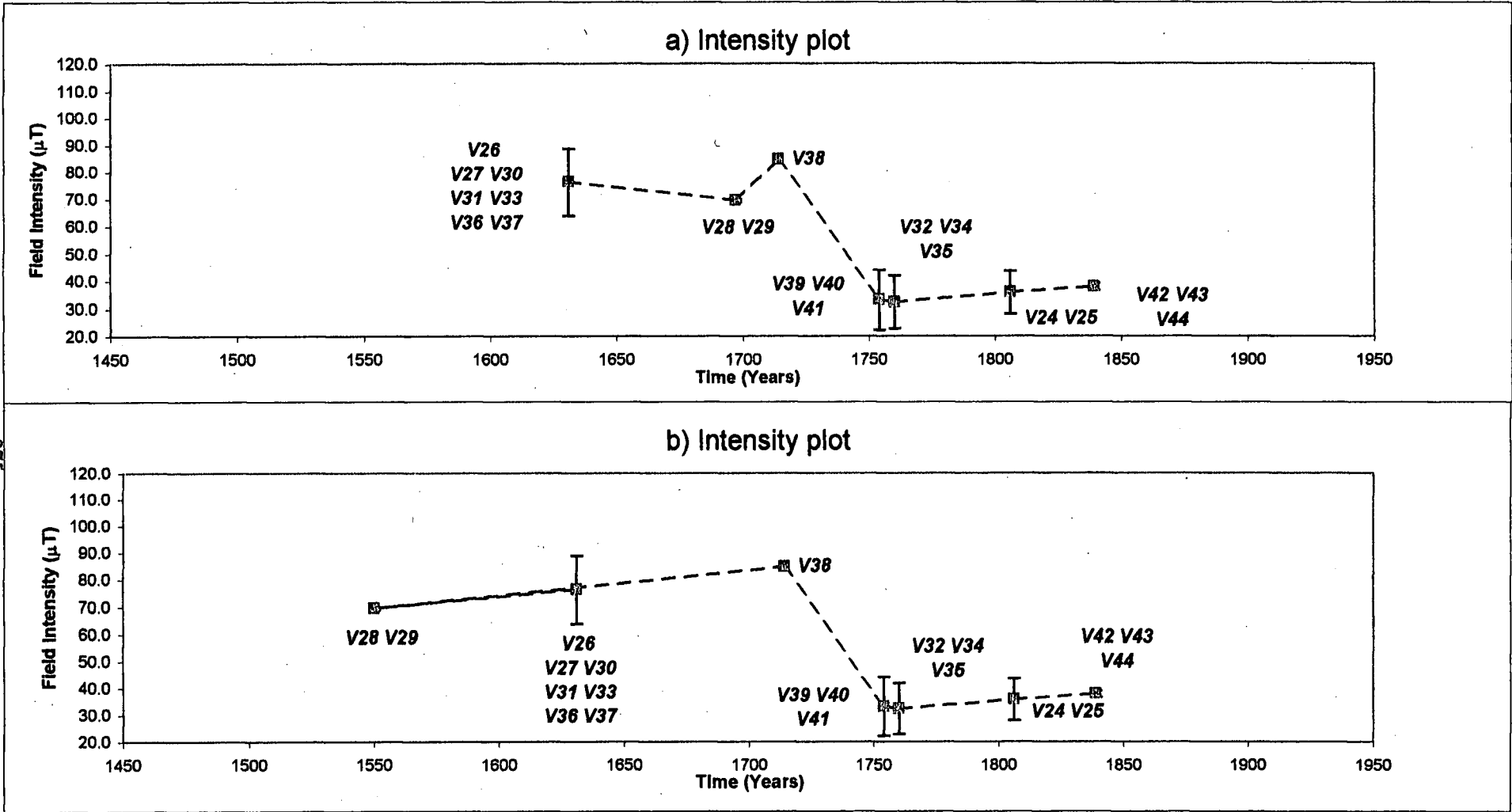
Fig. 9.4a,b - Time-dependent graph with all the thermal palaeointensity results.
In a) and b) two different ages are considered for sites V28 and V29 (see section 9.10.2).
In both graphs the lowest values obtained for sites V39,V40,V41 and V32,V34,V35 are shown.
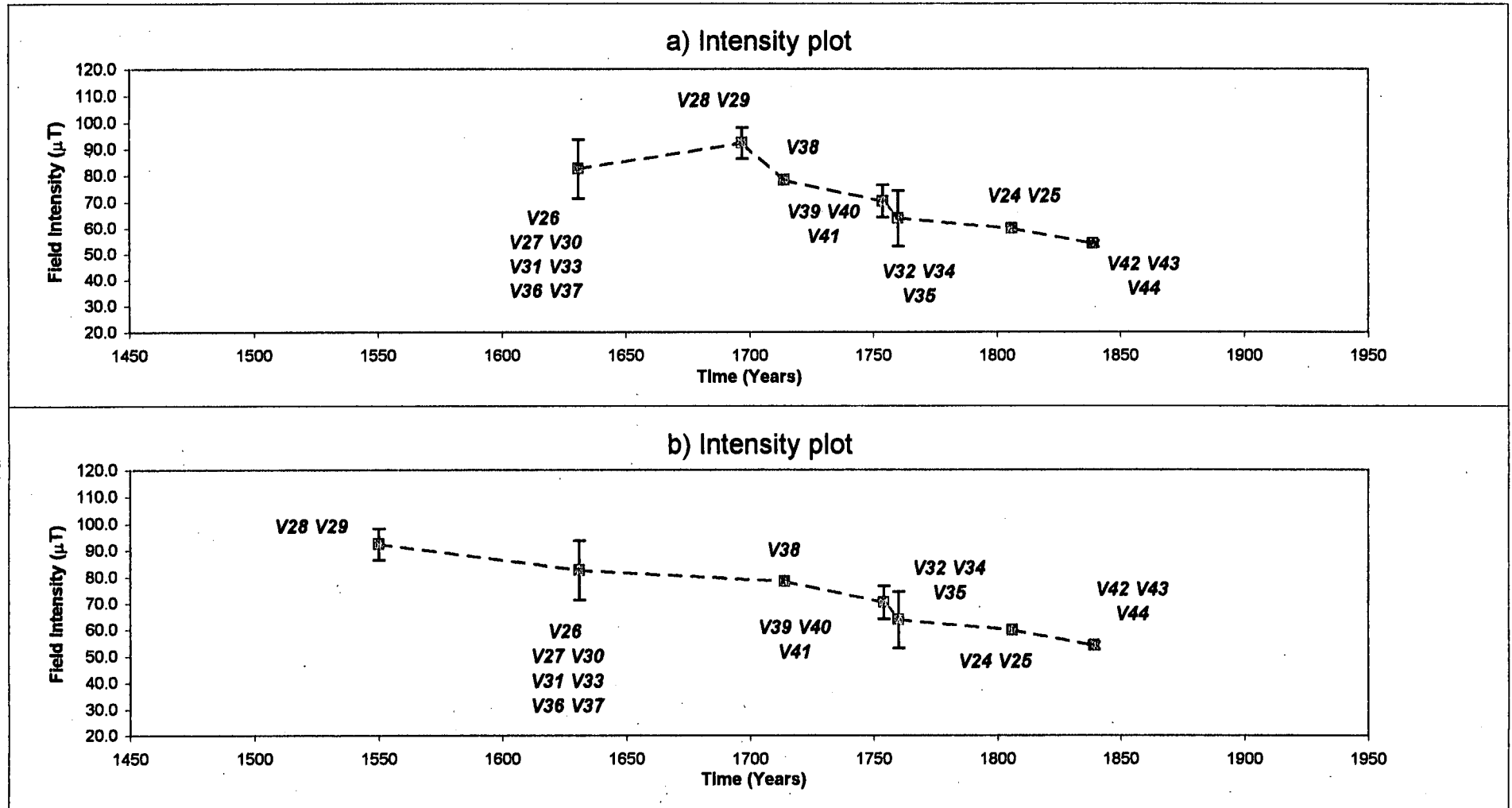
Fig. 9.5a,b - Time-dependent graph with all microwave palaeointensity results.
In a) and b) two different ages are considered for sites V28 and V29 (see section 9.10.2).

Chapter X

CONCLUSIONS

10.1 – Validity of historical reports

"L'ultimo rivo di fuoco allagando la campagna ne bruciava alcune, altre tralasciava senza far danno e per labirinti e per giri, in sembianze di un meandro, fiammeggiante, serpeggiante, diede finalmente nella strada regia" (from Recupito, 1635)

The recorded history of Vesuvius has been largely handed down through oral traditions and the writings of historians and chroniclers. Hundreds of papers have been written about its eruptive history and its products, although geo-volcanological mapping is surprisingly scarce (Johnston-Lavis, 1891, Ufficio Geologico d'Italia, 1910, Servizio Geologico d'Italia, 1971). The middle period, the A.D. 79-1631 time-span, has few and intermittent historical documentation (the most famous is certainly the description of the AD 79 eruption reported by Pliny the Younger), while the youngest period (1631-1944) is, on the whole, well documented. Reconstruction of the eruptive history of the volcano during this time span is mainly based on the collection, interpretation, and synthesis of historical documentation and has different approaches according to their reliability. Very detailed, but in part confusing or even misleading information is available about the AD 1631 eruption from contemporaneous or near-contemporaneous sources (Braccini, 1632, Danza, 1632, Falcone, 1632, Giuliani, 1632, Masculi, 1633, Mormile, 1635, Recupito, 1632, Naudet, 1632, De Contreras, 1633). [The opening sentence of this section is one of the numerous descriptions of the AD 1631 event. It describes a "river of fire" (*rivo di fuoco*) that, as meander, slowly reaches the main road (*strada regia*).] Most of the more or less recent works are mainly based on the same historical sources but end up with contrasting hypotheses. For example

Arno' et al., (1987) made a reconstruction of the 1631 event, underlining that the eruption was exclusively characterized by explosive behaviour. In fact they affirmed that no lavas connected with this event were recognised: all lava flows assigned to 1631 were said to be older, having probably been erupted during the period 968-1037. In contrast, Burri and Di Girolamo (1975) affirmed that the eruption was certainly characterized by a significant effusive component. Such a contrast can be due to subjective interpretations and it is possible that historical sources can report altered version of the real course of the eruption, especially if it was of wide proportion and rapidly changing. Braccini, who is one of the most accredited sources, together with many other contemporaneous authors, described the beginning of the 1631 eruption as a huge column about 30 miles high. Naudet inexplicably missed this unmistakable "particular". Detailed recent geo-volcanological observations (Rolandi et al., 1991) confirmed the hypothesis of the initial explosive eruption with a sustained column. On the other hand, Braccini does not mention any bountiful rains on the days of the eruptions and describes some "flows" as coming straight from the mountain. This could be interpreted as pyroclastic flows but all the other authors reported the same flows as results of very heavy rain, which gives a completely different volcanological picture. However the importance of historical sources is not in discussion, but it is equally important to verify, when possible, their truthfulness with field observation and/or all the modern sources. This study has shown that establishing whether or not different exposures or flows are contemporaneous can be established, in most, but not all, cases successfully using their magnetic remanences to define the geomagnetic field direction and intensity at the time of eruption.

10.2 – Nature and frequency of Vesuvian eruptions.

Vesuvius is probably the most famous volcano on Earth, and certainly one of the most, if not the most dangerous. It is particular for its unusual versatility, its activity ranging from Hawaiian-style emission of very liquid lava, with fountains and lava lakes, to Strombolian and Vulcanian violently explosive activity, including Plinian events that produce pyroclastic flows and surges. The eruptive activity of Vesuvius is widely considered to occur in cycles of several centuries, alternating with repose periods also of several centuries duration. Each of these repose periods ends with a major (Plinian) eruption, thus initiating an active cycle. One of the problems is that cycles apparently do not always repeat exactly the same patterns and phenomena. Thus, the cycle or cycles following the 79 A.D. eruption seem to have been quite different from the most recent one, lasting from 1631 until 1944. Critically since December 1944 Vesuvius has remained dormant. This long quiescent period departs from the 1631-1944 pattern of activity. Therefore, the mode of the future renewal of activity cannot be predicted at this stage.

Vesuvius is also well known for the high density of population living in the surrounding area. Almost half a million people live in towns and villages around the volcano, in the zone immediately threatened by future eruptions. Since the last eruption, occurred in 1944, the population has had an exponential increase that also increased the volcanic hazard. Basically the hazard is based on two principal parameters: the probability that a certain volcanic phenomenon can happen and the damages that it can cause. On this basis, although the next Vesuvian eruption cannot be predicted, the high density of population surrounding the volcano makes Vesuvius a very high hazard phenomenon. For this reason knowledge of the frequency and nature of events plays an important role in assessing the hazard of this volcanic area. As described above, it is still a matter of debate whether the AD 1631 eruption was a purely explosive or mixed explosive-effusive event. From this work all the

lava flow mean value obtained from V79-1631 had exactly the same direction as that of the V1631 on the VSVC (see section 9.10.1). Therefore, the mean value obtained from the directional study can be ascribed to that time and that lava flows were emitted during the AD 1631 event. Hence it cannot be considered entirely explosive. Another case is that the age attributed in the literature to V1697 lava flow is not consistent with the directional results. In fact, its mean value seems to suggest a very different age (between AD 1595 and AD 1537). Some poor historical sources do mention a minor event occurred in AD 1568 (Palmieri, 1880). Although more investigations are needed, it seems realistic that the age AD 1696 attributed in literature is wrong and that a small effusive event did occur during the XVI century, about 100 years before the last big eruption. This can be important as the eruptive activity of Vesuvius occurs in alternated cycles of activity and repose and that the cycle or cycles preceding the AD 1631 are considered to be quite different from the most recent one.

10.3 – Comparison of microwaves and MTT experiments

The types of lavas analysed are characterized by the dominance of high coercivity Ti-poor titanomagnetite (A1/A2 groups) and titanomagnetites with relatively higher content of titanium and lower coercivity (group B). The palaeointensity *thermal* experiment always showed an inverse relationship between the temperature ranges and the palaeointensities estimated, with slightly concave curves, or two clearly different slopes for temperature v. intensity. All the samples belonging to groups A1/A2 showed very high values (sometime too high) over low temperature ranges and acceptable value over high temperature ranges. All the samples (except V24) belonging to group B showed clearly lower values at low and high temperature ranges. As the magneto-mineralogy is almost the same in all the samples,

it seems possible that differences in grain sizes may be important (section 9.9.3). Although more evidence is needed, it seems that grain-size may be a more important factor in thermal experiments than has generally been recognised. No particular relationship was observed between magnetic property groups and *microwave* components behaviour. From microwave experiments one palaeofield estimate was, in general, obtained from the low range of the microwave power. For almost all the sample analysed, considering the entire spectrum of the microwave power, therefore considering also the unaccepted data where theta was tending to increase with the increasing power, a convex microwave power relationship to intensity (the inverse to the concave temperature relationship to intensity) was observed. At this stage, it is not clear why this relationship should exist. It may, for example, indicate that the microwave technique is even more sensitive to the grain size range or that the available microwave power range now exceeds that necessary for isolating meaningful palaeointensity determinations for Vesuvian lava.

In terms of results (Fig.10.1) those obtained for AD 1631 from both techniques are almost the same while those for AD 1714 are fairly consistent. All the others are significantly different. In general the thermal experiment gives palaeointensity estimate lower than the microwave (except for AD 1754 and 1760 which had two different estimates, one higher and one lower than the microwave value). Although the plots do not show clear trends for either techniques, it seems that the microwave results are more consistent with a linear decrease in intensity, while the thermal results gives higher and somewhat more variable time dependence of palaeointensity. In both methods, the geomagnetic intensity has been generally decreasing with increasing time, particularly if the older age (~AD 1540) is attributed to AD 1697. This general trend is similar to that one obtained for the last few century from other European, Mediterranean and Near East regions (Aitken et al., 1989).
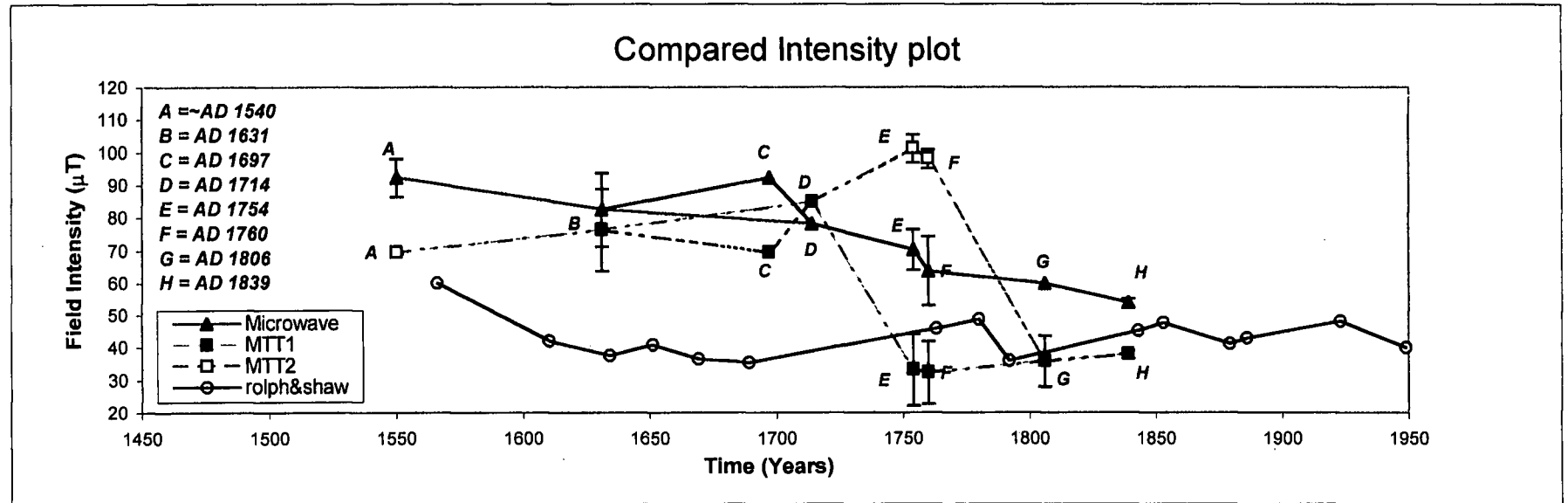
Fig. 10.1 - Comparison of thermal and microwave palaeointensity results.
Red line when the age 1540 is considered instead of 1697 (see section 9.10.2 and 10.3).
MTT1 and MTT2 (dashed lines) considering both the high and low values obtained for E and F.
With empty circle a set of palaeointensity values from Mt. Etna, Sicily (Rolph & Shaw, 1986).

10.4 – Palaeointensity and Palaeodirections as dating tools

It is well known that lava sequences can provide a series of readings of the geomagnetic field at the time of their extrusion. However, without time-markers, their directions and intensities can be used usefully only for correlation and discriminations between different lava flows. Normally one can date the rock when the palaeomagnetic field for that time has already been determined for another site accompanied by an absolute (usually radiometric) date. Potassium-argon (K-Ar) and Ar-Ar techniques are amongst the most common but, as with most dating tools, they are based on assumptions. In the case of K-Ar, for example, any original Ar must be lost from the magma prior to crystallisation and cooling, and all ^{39,40}Ar generated subsequent to cooling must remain trapped in the rock. Unfortunately both assumptions can fail since they are not immune from chemical alteration problems and, in particular circumstances, original ^{39}Ar and ^{40}Ar can coexist with those generated subsequently. In addition this technique is neither very sensitive for very young ages nor cheap. This study has shown that historic Vesuvian lava flows can record and retain palaeomagnetic information that can be successfully used to define the geomagnetic field direction and intensity at the time of eruption. This characteristic, in the case of Vesuvius that has erupted almost continuously for three centuries (AD 1631-1944) and for which most of the events are well documented, makes palaeomagnetic methods particularly valid as dating tools. From this study a better definition of the geomagnetic field has been obtained for the XVIII and XIX centuries, at least for directional data, while for the first time both palaeodirection and palaeointensity (the latter evaluated using two completely different techniques) identified lava flows emitted during the AD 1631 event. This result, so far, has not been obtained from any other dating tools, despite the volcanological importance of this

eruption. However, this result is the only one obtained from the combined direction and intensity determinations. For all the other lava flows, thermal and microwave palaeointensity determinations showed a low level of agreement and ambiguous age interpretations in some cases. Furthermore although directional data obtained from thermal experiments showed that they work extremely well on lava, no comparable directional studies have yet been made using microwave experiments to establish if the components isolated in this way have the same directional values as those determined thermally.

10.5 – Further work

Form this work it appears that Vesuvian lava flows can record and retain directional palaeomagnetic information somewhat more successfully than the intensity. This could be due to a particular characteristic of minerals involved in the process of acquisition of magnetic remanence in these particular lavas or it could be due to the current accuracy of techniques at this stage of development. It is also possible that the basic linear relationship hypothesised between NRM and TRM is not valid at least for Vesuvian lavas. In order to understand that more study are suggested on the following:

Vesuvian Magneto-mineralogy

More studies are suggested, especially on determining grain-sizes. In fact more evidence is needed to understand why this factor appears to be so influential on both thermal and microwave palaeointensity experiments. Furthermore it is not clear why this influence seems to be more evident in microwave technique than in thermal experiments. However, it is also not clear which technique is actually more valid as all comparisons, at this stage are with previous thermal methods or extrapolations of geomagnetic values, only made since 1835.

Palaeointensity experiments: thermal and microwave

The "acceptable" microwave values are all established at lower power ranges than the "unacceptable" values, indicating that the available microwave power range now exceeds that necessary for isolating meaningful palaeointensity determinations from these types of lava. The convex microwave power relationship to intensity, observed using all the data points, was the inverse of that of the concave temperature relationship to intensity. At this stage, it is not clear why this relationship should exist. It may be related to the fact (as pointed out above) that the microwave technique is even more sensitive to the grain size range, or to the high stability of the primary direction of magnetization which probably become less stable with the increasing power. Or it is simply too subject to human errors.

Vesuvian eruptions

As described earlier, the age attributed in the literature to V1697 lava flow is not consistent with the directional results. In fact, its mean value seems to suggest a very different age (between AD 1595 and AD 1537). On the base of the present work, it seems that the age of AD 1696 attributed in literature is wrong and that a small effusive event did occur during the XVI century. However, because of the importance of this information for the Vesuvius volcanic hazard, more evidence is needed and further investigations are recommended.

References

Aitken, M. J., Allsop, A.L., Bussel, G. D., Winter, M.B. (1989). "Geomagnetic intensity variation during the last 4000 years." Physics Earth Plan. Int. 56: 49-58.

Alfano, G.B. *Le eruzioni del Vesuvio tra il 79 ed ill 631, studio bibliografico - Voile di Pompei* (Roma, Tipografia 1st. Pio IX, 1924b).

Alfano, G.B. and Fiedlaender, L. << La storia del Vesuvio illustrata dai documenti coevi », *Vim. a.d Donau, K. Holm*, 1-69 (1929) (Bibl. Osserv., Vesuviano).

Angelino, A., Incoronato, A. and Sarno, P. (1996). "Magnetic stratigraphy of Etna products. I - medieval lavas." Studia Geoph. et Geod 40: 217-224.

Angelino, A., and Incoronato, A.. (1997). "Stratigrafia magnetica in aree vulcaniche: esperienze al Vesuvio e all' Etna." Atti GNGTS: 13-18.

Angelino, A., Cacciapuoti S., Incoronato A., Sauna R. and Tiano, P.. (1998). "Indagini di "palaeo- and rock-magnetism" in aree vulcaniche: un esempio di applicazione all'Etna." XIV convegno scientifico annuale del GNV.

Audunsson, H., Levi, S. and Hodges, F. (1992). "Magnetic property zonation in a thick lava flow." J. Geophys. Res. 97 N° B4: 4349-4360.

Baag, C., Helsley, C.E., Shi-zhe Xu and Lienert, B.R. (1995). "Deflection of palaeomagnetic directions due to magnetization of the underlying terrain." Journal Geoph. Res 100 N° b7: 10,013-10,027.

Banerjee, K. S. "Magnetic properties of Fe-Ti oxides." - Chapter 4: 107-128.

Barberi, F., Borsi, S., Ferrara, G. and Innocenti, F., (1967). Contribute alla conoscenza magmatologica e vulcanologica delle isole dell'Arcipelago Pontino », *Mem. Soc. Geol. Ital.*, 6,581-606.

Barberi, F., Navarro, J.M., Rosi, M., Santacroce, R. and Sbrana, A.: « Explosive interaction of magma with groundwater: insights from xenoliths and geothermal drillings », *Workshop on volcanic blast, Mount St. Helens, August, 1984* (abst).

Barton, C.E., Merrill, R.T. and Barbetti, M. (1979). Intensity of the earth's magnetic field over the past 10000 years. Phis. Earth Planet. Int. 20, 96-110.

Bernasconi, A., Bruni, P., Borla, L., Brincipe, C. and Sbrana, A.: (1981).« Risultati preliminari dell'esplorazionegeotermica profonda nell'area vulcanica del Somma-Vesuvio », *Rend. Soc. Geol. It.*, 4, 237-240

Bloch, F. (1930). "Zur theorie des ferromagnetismus, zeit. Phys., 61, 206-219

Briden, J.C., (1966) "Estimates of direction and intensity of the palaeomagnetic field from the Mugga Mugga Porphyry", Australia, Geophys. J. R. Astron. Soc., 11 267-278.

Braccini, G.C.: *Dell'incendio fattosi sul Vesuvio a 16 di Dicembre 1631 e delle sue cause ed effetti* (Napoli, Roncagliolo, 1632) (Bibl. Osserv. Vesuviano).

Bloxham, J. Gubbins, D. (1985). "The secular variation of Earth's magnetic field." Nature 317: 777-781.

Butler, F. R. (1992). Palaeomagnetism: Magnetic Domains to Geologic Terranes. Boston, Blackwell scientific Publications.

Capaldi, G., Civetta, L. and Gasparini, P.: (1976).« Volcanic history of the island of Ischia (South Italy) », *Bull. Volcanol.*, 40 (1), 1-12

Capaldi , G., Munno, R. and Rolandi, G.: « Volcanology, Geo-chronology and Geochemistry of Ventotene island (Ponza archipelago », *IAVCEI 1985 Scientific Assembly, Giardini Naxos (Italy), Sept. 1-21, 1985* (abst.).

Cafarella, L., De Santis, A. and Meloni, A. (1992). "Secular variation in Italy from historical geomagnetic field measurements." Phisics Earth Plan. Int. 73: 206-221.

Carracedo, J. C., Principe C., M. Rosi and Soler, V.. (1993). "Time correlation by palaeomagnetism of 1631 eruption of Mount Vesuvius. Volcanological and volcanic hazard implications." J. Volc. Geoth. Res. 58: 203-209.

Chevallier, R. (1925). "L'aimantation des laves de l'Etna et l'orientation du champ terrestre en Sicilie du XIIe au XVIIe siecle." Annales Phys. 4: 5-162.

Chvojka, R. (1990). "Computation of the palaeointensity of the geomagnetic field." Physics Earth Plan. Int. 63: 13--22.

Clark, D.A. (1984). "Hysteresis properties of sized dispersed monocinic pyrrhotite grains. Geophys. Res. Letters, 11, 173-176

Coe, R., S. (1978). "Geomagnetic Palaeointensities from radiocarbon-dated lava flows on Hawaii and the question of the pacific nondipole Low." J. Geophysic. Res. 83 N°B4: 1740-1756.

Coe, R., S. (1967). "The determination of the paleo-intensities of the earth's magnetic field with emphasis on mechanisms which could cause non-ideal behaviour in Thellier's method. Journal of Geomag. and Geoelect. 19(3): 157-179.

Collinson, W. (1983). Intensity of NRM. Methods in rock magnetism and palaeomagnetism. Techniques and Instrumentation. London, **Chapman and Hall: 418-447.**

Cundari, A.: (1979).« Petrogenesis of leucite-bearing lavas in the Roman Volcanic Region, Italy. The Sabatini lavas », *Contrib. Mineral. Petrol.*, 70, 9-21

Cundari, A. and Le Maitre, R.W.: (1970)« On the petrogeny of the leucite-bearing rocks of the Roman and Birunga volcanic regions », *J. Petrology*, 11, 33-47.

Danza, E., *Breve discorso dell'incendio succeduto a 16 di Dicembre 1631 nel monte Vesuvio e luoghi convicini et terremoti nella citta di Napoli* (Trani, Lorenzo Valeri, 1632) (Bibl. Osserv. Vesuviano).

Day, R., Fuller, M. and Schmidt (1977). "Hysteresis properties of titanomagnetites: grain-size and compositional dependence." Physycs Hearth Planet. Int. 13: 260-267.

Day, R. (1977). "TRM and Its Variation with Grain Size." J. Geomag. Geoelectr. 29: 233-265.

D'argenio, B., Pescatore, T. and Scandone P.: (1973). « Schema geologico dell'Appennino Campano - Lucano », *Accad. Naz. Lincei, Quad.*, 183, 49-72

Di Girolamo P.: (1978).« Geotectonic setting of Miocene-Quaternary volcanism in and around the eastern Tyrrhenian sea border (Italy) as deduced from major elements geochemistry », *Bull. Volcanol*, 41, 3

Dodson, M., H. and McClelland, E. (1980). "Magnetic blocking temperatures of single-domain grains during slow cooling." J. Geophys. Res. 85 N°B5: 2625-2637.

Dunlop, D., J. (1998). "Thermoremanent magnetization of nonuniformly magnetized grains." **J. Geophys. Res.** 103 N° B12: 30,561-30,574.

Falcone, S.: *Discorso naturale delle cause ed effetti causati nell'incendio del Monte Vesuvio con relazione di tutto* (Napoli, Ottavio Beltrano, 1632) (Museo Civico di Storia Naturale, Milano).

Finetti, I. and Morelli C.: « Esplorazione sismica a riflessione dei golfi di Napoli e Pozzuoli », *Boll. Geofis. Tear. Appl*, 16, 175-222 (Trieste, 1974).

Fisher, R. A. (1953). "Dispersion on a sphere." Proc. R. Soc. Ser. A. 217: 295-305.

Gauss, C. F. (1839). Algemaine Theorie des Erdmagnetismus

Gialanella, P. R., Incoronato, A., Russo, F. and Nigro, G.. (1993). "Magnetic stratigraphy of Vesuvius products. I. 1631 lavas." J. Volc. Geoth. Res 58: 211-215.

Gialanella, P. R., Incoronato, A., Russo, F., Sarno, P. and Di Martino, A.. (1998). "Magnetic stratigraphy of Vesuvius product II - medieval lavas." Quaternary International.

Giannetti, B., Nicoletti, M. and Petrucciani.C.: (1979). « Datazioni K-Ar di lave leucitiche dello strato-vulcano di Roccamonfina », *Rend. Soc. It. Mineral. Petrol.*, *35*, 349-354

Gilbert, W. (1600) - De magnete.

Gillot, P.Y., Chiesa S., Pasouare, G. and Vezzoli, L.: (1982). « 33,000 yr K-Ar dating of the volcano-tectonic horst of the Island of Ischia, Gulf of Naples », *Nature*, 299, 242-245.

Giuliani, G.B.: *Trattato del Monte Vesuvio e dei suoi incendi* (Napoli, Longo, 1632), (Biblioteca Osserv. Vesuviano).

Haag, M. Dunn, J., R. and Fuller, M. (1995). "A new quality check for absolute palaeointensities of the Earth magnetic field." Geophys. Res. Let. 22 N° 24: 3549-3552.

Hale, C., J., Fuller, M., Bailey, R.,C. (1978). "On the application of microwave heating to lunar palaeointensity determination." Proc. Lunar Planet. Sci. Conf. 9th: 3165-3179.

Hill, M. J. Shaw, J (1999). "Palaeointensity results for historic lavas from Mt Etna using microwave demagnetization/remagnetization in a modified Thellier-type experiment." Geophys. J. Int. 139: 586-590.

Hill, M. J. Shaw, J (2000). "Magnetic field intensity study of the 1960 Kilauea lava flow, Hawaii, using the microwave palaeointensity technique." Geophys. J. Int. 142: 487-504.

Hill, M. J. (2000)."The microwave palaeointensity technique and its application to lava." PhD Thesis, University of Liverpool

Hongre, L., Hulot, G., and Khokhlov, A. (1998). "An analysis of the geomagnetic field over the past 2000 years." Physics of the Hearth and Planetary Interiors 106: 311-335.

Hoye, G. S. (1981). "Archaeomagnetic secular variation record of Mount Vesuvius." **Nature** 291: 216-.

Imbo', G.: (1949). « L'attivita eruttiva vesuviana e relative osservazioni nel corso dell'intervallo intereruttivo 1906-1944 ed in particolare del parossismo del marzo 1944 », *Ann. Osserv. Vesuviano, Napoli* 5ᵃ serie, vol. unico celebrativo del 10 centenario dell'Osservatorio Vesuviano: p. 185-380

Imbo', G.: // *Vesuvio e la sua storia*, a cura di L. CASERTANO (Napoli, Ediz. Scient. Italiane, 1984).

Incoronato, A. (1996). "Magnetic stratigraphy procedures in volcanic areas: the experience at Vesuvius." Palaeomagnetic and Tectonics of the Mediterranean Region, Geological Society Special Publication 105: 367-371.

Jacobs, J., A. (1998). "Variations in the intensity of the earth's magnetic field." Surveys in Geophysics 19: 139-187.

Johnston lavis, H.J.: *Geological map of Monte Somma and Vesuvius (1:10,000) constructed during the years 1880-1888.* (London, Philips and son, 1891a).

Johnston lavis, H.J.: (1909)« The eruption of Vesuvius in April, 1906 », *Sc. Trans. R. Dublin Soc.*, 9/2, 139-200.

King, J.W., Banerjee, S.K., Marvin, J. And Özdemir, Ö. (1982). A comparison of different magnetic methods for determining the relative grain size of magnetite in different materials: Some results from lake sediments. Earth Planet. Sci. Lett., 59, 404-412

Kirschvink, J., L. (1996). "Microwave Absorption by Magnetite." Bioelectromagnetics 17: 187-194.

Kirschvink, J., L. (1980). "The least-squares line and plane and the analysis of palaeomagnetic data." Geophys. J. R. astr. Soc. **62**: 699-718.

Kono, M. and Ueno, N. (1977). "Palaeointensity determination by a modified Thellier method, Phys. Earth Planet. Int. 13, 305-314.

Lacroix A. (1906).« L'eruption du Vesuve en Avril 1906 », *Rev. Gen. Sci. Pures et Appliquees, Paris,* 20-21

Le Hon, H.: « Histoire complete de la grande eruption du Vesuve de 1631, with topographic map of Vesuvius lavas from 1631 till 1861 », *Bull. Acad. R. Belgique,* 2 (20), 8 (Bruxelles, 1865).

Lowrie, W. (1990). "Identification of ferromagnetic minerals in a rock by coercivity and unblocking temperature properties." Geophis. Res. Letters 17: 159-162.

Marinelli, G.: « Ily a 19siecles... Pompei, Herculanum », *Plurisciences,* p. 405-414 (1979) Encyclopaedia Universalis France S.A..

Masculi, I.B.: *De incendio Vesuviiex citato XVII kal. Ianuarii anno trigesimo primo saeculi decimiseptimi* (Napoli, Roncaglido, 1633).

Matteucci, R.V.: *Carta degli efflussi lavici 1885-1886 su base topografica 1:10.000, levata de 1872* (1886), (Bibl. Osserv. Vesuviano).

Matteucci, R.V.: *Carta degli efflussi lavici 1891-1894* (1894), (Bibl. Osserv. Vesuviano).

Matteucci, R.V.: *Carta degli efflussi lavici 1895-1899* (1899), (Bibl. Osserv. Vesuviano).

Matteucci, R.V.: Carta *delle colate laviche delperiodo effusivo 1903-1904* (1904), (Bibl. Osserv. Vesuviano).

Matteucci, R.V., Nasini.r., Casoria, E. and Fiechter, A.: (1906). « Appunti sull'eruzione vesuviana 1905-1906 », *Boll. Soc. Geol. It.*, 25, 3

McClelland, E., and Briden, J.C. (1996). "An improved methodology for Thellier-type palaeointensity determination in igneous rocks and its usefulness for verifying primary thermoremanence." J. Geoph. Res. 101 N°B10: 21,995-22,013.

Merril, R.T. and McElhinny, M.W. (1983) The Earth's Magnetic Field: Its History, Origin and Planeta.ry perspective. Academic Press, London and New York, 401 pp.

Metrich, N., Santacroce, R. and Savelli, C.: *Ventotene a Quaternary Potassic Volcano in Central Tyrrhenian Sea* (preprint, 1985).

Mormile, J.: *L'incendio del Monte Vesuvio e delle stragi e rovine che ha fatto ne tempi antichi e moderni infine alii 3 marzo 1632.* Con appendice: nota di tutte le relazioni stampate sino ad oggi del Vesuvio raccolte da VINCENZO BOVE (Napoli, Egidio Longo, 1632), (Bibl. Osserv. Vesuviano).

Nagata, T. (1979).: Rock Magnetism, 2ed, Maruzan, Tokyo, p.350

Nazzaro, A. (1985). "Il Vesuvio: storia naturale dal 1631 al 1944." Boll. Soc. Natural. 94: 1-26.

Nazzaro, A. (1997?). "Vesuvio: il vulcano. Storie, leggende, tradizioni." supplemento a: Il mattino di Napoli: 1-48.

Neel, L. (1948). Propriétés Magnétiques de Ferrites; Ferrimagnétism et Antiferromagnétisme. Ann. Physiques. 3, 137-198.

Ninkovich, D. and Hays, L.D.: (1972).« Mediterranean Island Arcs and Origin of High Potash Volcanoes », *E.P.S.L.*, 16, 331-345

Noel, M. a. Batt C.M. (1990). "A method for correcting geographically separated remanence directions for the purpose of archaeomagneting dating." Geophys. J. Int. 102: 753-756.

Palmieri, L. (1880). Il Vesuvio e la sua storia. Milano, Tipografia Faverio.

Palmieri, L. « Il Vesuvio dal 1865 al 1895 »,*AttiR. Accad. Sci. Fis. Mat.*, s. 2, 8, 5 (Napoli, 1896).

Perrin, M. (1998). "Palaeointensity determination, magnetic domain structure, and selection criteria." J. Geophys. Res. 103 N° B12: 30,591-30,600.

Pescatore, T. and Sgrosso, L: « I rapporti tra la piattafor-ma campano-lucana e la piattaforma abruzzese-campana nel Casertano », *Boll. Soc. Geol. It.*, 92, 925-938 (1973).

Principe, C., Rosi M., Santacroce, R. and Sbrana, A.: *Guidebook of the field excursion to Phlegren Fields and Vesuvius. Workshop on explosive volcanism, may 1982* (CNR, Italy and NSF, USA, 1982).

Recupito, T.C.: *De Vesuviano incendio nuntius* (Napoli, Egidio Longhi, 1632).

Rolandi, G. a. R., F. (1992). "L'eruzione del Vesuvio del 1631." Boll. Soc. Geol. It.: 1-17.

Rolandi G., Mastrolorenzo G., Barrella A.M., Borrelli A. (1993): "The Avellino plinian eruption of Somma-Vesuvius". Journal of Volcan. And Geoth. Res, 58.

Rolph, T. C., Shaw,J. and Guest,J.E. (1987). "Geomagnetic field variations as a dating tool: application to sicilian lavas." Journal of Archaeological Sciences 14: 215-225.

Rolph, T. C., Shaw,J. (1986). "Variations of the geomagnetic field in Sicily." J.

Geomag. Geoelectr. **38**: 1269-1277.

Rosi, M. and Santacroce, R: (1984).« The famous A.D. 1631 eruption of Vesuvius: a revised interpretation in light of historical and volcanological data », *Workshop on volcanic blast, Mount St. Helens, August, 1984,* abst.

Sabatini, V.: . (1906).« L'eruzione vesuviana dell'Aprile 1906 », *Boll. R. Com. Geol. It*

Santacroce, R.: (1983). « A general model for the behavior of the Somma-Vesuvius volcanic complex », *J. Volcanol. Geo-therm. Res.,* 17, 237-248

Scandone, R., and Cortini, M.. (1997). "Il Vesuvio: un vulcano ad alto rischio." Le Scienze quaderni 93: 73-80.

Scandone, P.: (1978).« Origin of the Tyrrehenian Sea and Cala-brian Arc », *Boll. Soc. Geol. It.,* 98, 27-34

Servizio Geologico D'ITALIA: (1971). *Carta Geologica d'Italia alia scala 1:100.000,* foglio 185, Salerno

Servizio Geologico D'ITALIA: (1971).*Carta Geologica d'Italia alia scala 1:100.000,* foglio 184-185, Napoli, Ischia, Campi Flegrei

Shaw, J., Yang, S., Rolph, T.C. and Sun, F.Y. (1999). "A comparison of archaeointensity results from Chinese ceramics using using microwave and conventional Thellier's and Shaw's methods." Geophys. J. Int. 136: 714-718.

Tanaka, H. and Turner G. M. (1995). "Palaeosecular Variation: Direction and Intensity." J. Geomag. Geoelectr. 47: 5-147.

Tanguy, J. C. (1975). "Intensity of the geomagnetic field from recent italian lavas using a new palaeointensity method." Earth Planet. Sci. Let. 27: 314-320.

Tarling, D. H. and Hrouda., F. (1993). The magnetic anisotropy of rocks. London, Chapman and Hall.

Tarling, D. H. (1983). "Palaeomagnetism". London and New York: Chapmann and Hall.

Thellier, E. (1937). "Sur l'aimantation dite permanente des basaltes. C.R. Acad. Sci., 204: 876-879.

Thellier, E. (1938). " Sur l'aimantation des terres cuites et ses applications géophysiques. Ann. Inst. Phys. Globe Univ. Paris, 16: 157-302.

Thellier, E. (1977). "Palaeomagnetic field intensity, its measurements in theory and practice." Phiscs Earth Plan. Int. 13: 241-339.

Thellier, E. and Thellier, O.(1952b). The intensity of the geomagnetic field in the historical and geological past. Akad, Nauk. SSR. Izv. Geophys. Ser., 1296-1331.

Thellier, E. and Thellier, O.(1959). "Sur l'intensitè du champ magnètique Terrestre dans le passè historique et géologique", Ann. Geophys. 15, 285.

Thomas, D. N., Rolph, T.C., Shaw, J., Gonzales de Sherwood, S. and Zhuang Z. (1998). "Palaeointensity studies of a late Permian lava succession from Guzhou province, South china: implications for post-Kiaman dipole field behaviour." Geophys. J. Int. 134: 856-866.

Tiano, P., Incoronato A. and Tarling D. H. (2000a). "Palaeomagnetic investigations of Vesuvius lava flows." VIII Workshop on Geo-Electromagnetism, October 12-14, Maratea, Italy 53.

Tiano, P., Tarling D. H. and Incoronato A. (2000b). "Palaeointensity determinations from Vesuvius lava flow specimens." VIII Workshop on Geo-Electromagnetism, October 12-14, Maratea, Italy 54.

Ufficio geologico d'ITALIA: (1910). *Fogti della Carta Geologica d'Italia alla scala 1:100.000*, foglio 185, Salerno

Ufficio geologico d'ITALIA: (1911). *Fogli della Carlo Geologica d'Italia alia scala 1:100.000:* foglio 184, Napoli

Verwey, E. J. W. and Haayman, P. W. (1941). Electronic conductivity and transition point in magnetite. Phisycs 8, 979-982.

Walton, D., Shaw, J.,Share, J. and Hakes, J. (1992). "Microwave demagnetization." J. Appl. Phys. 71: 1549-1551.

Walton, D., Share, J., Rolph, T., C. and Shaw, J. (1993). "Microwave magnetisation." **Geophys. Res. Let. 20 N° 2: 109-111.**

Walton, D., 1988. "The lack of reproducibility in experimentally determined intensities of the Earth's magnetic field, Rev. Geophys., 26, 15-22

Washington, H.S. (1906). "The Roman Comagmatic region", Carnegie Inst. Washington, publ. 57, 1-199.

Weiss, P. (1907). "L'hypothese du champ moleculaire et la propriete ferromagnetique. J. Phys. E4, 37-40.

Zijderveld, J. D. A. (1967). "A.C. demagnetization of rocks: analysis of results." D.W. colinson, K. M. Creer and S.K. Runcorn (eds) "Methods in Palaeomagnetisms", Elsevier, Amsterdam.: 254-286.